A Robust Surface Matching Technique for Coastal Geohazard Monitoring

Pauline Elizabeth Miller

BSc (Hons) Topographic Science

University of Glasgow

Thesis Submitted for the Degree of

Doctor of Philosophy

NEWCASTLE UNIVERSITY LIBRARY

206 53345 1

Thesis L8642

School of Civil Engineering and Geosciences

Newcastle University

August 2007

ABSTRACT

Coastal geohazards, such as landslides, mudflows, and rockfalls, represent a major driver for coastal change in many regions of the world, and often impinge on aspects of the human and natural environment. In such cases, there is a pressing need for the development of more effective monitoring strategies, particularly given the uncertainties associated with the impact of future climate change. Traditional survey approaches tend to suffer from limited spatial resolution, while contemporary techniques are generally unsuitable in isolation, due to the often complex coastal topography. To address these issues, this thesis presents the development and application of a strategy for integrated remote monitoring of coastal geohazards. The monitoring strategy is underpinned by a robust least squares surface matching technique, which has been developed to facilitate change detection through the reliable reconciliation of multi-temporal, multi-sensor datasets in dynamic environments.

Specifically, this research has concentrated on integrating the developing techniques of airborne and terrestrial laser scanning. In addition, archival aerial photography has been incorporated in order to provide a historical context for analysis of geohazard development. Robust surface matching provides a mechanism for reliable registration of DEM surfaces contaminated by regions of difference, which may arise through geohazard activity or vegetation change. The development of this algorithm has been presented, and its potential demonstrated through testing with artificial datasets.

The monitoring strategy was applied to the soft-cliff test site of Filey Bay, North Yorkshire. This highlighted the viability of the robust matching algorithm, demonstrating the effectiveness of this technique for absolute orientation of DEMs derived from archival aerial photography. Furthermore, the complementary qualities of airborne and terrestrial laser scanning have been confirmed, particularly in relation to their value for multi-scale terrain monitoring. Issues of transferability were explored through application of the monitoring strategy to the hard rock environment of Whitby East Cliff. Investigations in this challenging environment confirmed the potential of the robust matching algorithm, and highlighted a number of valuable issues in relation to the monitoring techniques. Investigations at both test sites enabled in-depth assessment and quantification of geohazard activity over extended periods of time.

ACKNOWLEDGEMENTS

The last four years of study have been immensely enjoyable and rewarding, and I look back with a tremendous sense of achievement. I have been fortunate enough to undertake a PhD which has closely matched my own interests, and there have been numerous highlights. The successful completion of this work would not have been possible however without the help of so many. Firstly, I am indebted to my supervisors, Jon Mills and Stuart Edwards for setting up the project, and for allowing me to develop the research in line with my own interests. I am also grateful for their support and encouragement, and for smoothing my way through the tricky parts. English Heritage and the British Geological Survey have funded and supported the work throughout, and I am extremely grateful to both Paul Bryan (EH) and Stuart Marsh (BGS) for their commitment to the project, and their unstinting enthusiasm and encouragement. I am also indebted to Ordnance Survey, for provision of photogrammetric data, NERC ARSF for acquisition of ALS data, and 3D Laser Mapping for supplying the Riegl laser scanner.

Some of the happiest and most enduring memories of the research relate to fieldwork, which is always a high point. This aspect would not have been possible without the help of Martin Robertson, to whom I am immensely grateful, and who has gone above and beyond the call of duty so many times. I would also like to thank Tuyuan (Shih-Yuan Lin), Ian Thomas and Simon Buckley, for sacrificing their time, and providing such willing and capable assistance. The last four years would have been so much harder had I not been able to share them with so many friends in Geomatics. There are too many to mention all, but special thanks go to Tuyuan, Henny Mills, Wiske Rotinsulu, Saad al-Hamlan, Ali Ford, Gobe Hobona, Yu-Ching Lin, Mike Lim, Ian Thomas and Dave Blauvelt. Thanks also go to Nikorn Mahawan and 'the Thais' for keeping me sane through badminton. To my friends Tracy Craddock, Jude MacDonald, Craig Inglis and Ian Woodard, I am eternally grateful for the distractions from work.

Finally, and most importantly, I thank my family – my brothers, Martin, Simon, and Christopher, for always managing to make me feel like the PhD was a million miles away, and Mum and Dad for helping me to keep things in perspective when the going got tough. Without your love and support I would never have got this far in life.

TABLE OF CONTENTS

ABSTRACT i

ACKNOWLEDGEMENTS ii

TABLE OF CONTENTS iii

LIST OF FIGURES x

LIST OF TABLES xv

LIST OF ABBREVIATION AND NOTATION xvii

CHAPTER ONE: INTRODUCTION 1

1.1 Research Background 1

1.1.1 Overview 1

1.1.2 Coastal Geohazards 2

1.1.3 Monitoring Studies 8

1.1.3.1 Overview 8

1.1.3.2 Scale and Accuracy 9

1.1.3.3 Temporal Frequency 10

1.1.3.4 Spatial Resolution 11

1.1.3.5 Further Considerations 13

1.1.3.6 Monitoring in the Coastal Zone 15

1.2 Aims and Objectives 18

1.3 Research Methodology 19

1.4 Thesis Structure 19

1.5 Summary 21

CHAPTER TWO: GEOMATICS MONITORING TECHNIQUES 23

2.1 Introduction 23

2.1.1 Geotechnical Monitoring Techniques 24

2.2 Basic Survey Approaches 26

2.2.1 Overview 26

2.2.2 Suitability for Coastal Monitoring 29

2.3 GNSS 30

2.3.1 Introduction 30

2.3.2 Technological Overview 31

2.3.3 Accuracy Considerations 33

2.3.4 Suitability for Coastal Monitoring 34
2.4 Photogrammetric Monitoring Techniques 35
2.4.1 Introduction 35
2.4.2 Digital Photogrammetric Workstations 38
2.4.3 Accuracy Considerations 39
2.4.4 Suitability for Coastal Monitoring 41
2.5 Airborne Laser Scanning 42
2.5.1 Introduction 42
2.5.2 Technological Overview 43
2.5.3 Terrain Reconstruction 46
2.5.4 Accuracy Considerations 48
2.5.5 Suitability for Coastal Monitoring 50
2.6 Terrestrial Laser Scanning 51
2.6.1 Introduction 51
2.6.2 Technological Overview 51
2.6.3 Terrain Reconstruction 53
2.6.4 Accuracy Considerations 56
2.6.5 Suitability for Coastal Monitoring 57
2.7 Additional Remote Sensing Techniques 58
2.7.1 Introduction 58
2.7.2 Overview 59
2.7.3 Suitability for Coastal Monitoring 61
2.8 Integrated Monitoring Approaches 63
2.8.1 Overview 63
2.8.2 Suitability for Coastal Monitoring 64
2.9 Summary 65

CHAPTER THREE: MONITORING STRATEGY 67

3.1 Introduction 67
3.2 Methodology Development 68
3.2.1 Background 68
3.2.2 Monitoring Strategy Overview 70
3.3 Primary Monitoring Components 72
3.3.1 Airborne Laser Scanning 72

3.3.1.1 Optech ALTM 3033 Airborne Laser Scanner 73
3.3.2 Terrestrial Laser Scanning 75
3.3.2.1 Leica HDS2500 Terrestrial Laser Scanner 77
3.3.2.2 Leica HDS3000 Terrestrial Laser Scanner 79
3.3.2.3 Riegl LPM-i800HA Terrestrial Laser Scanner 80
3.3.3 Archival Aerial Photography 82
3.3.3.1 Overview 82
3.3.3.2 Justifications for Inclusion 83
3.3.3.3 Coastal Monitoring Considerations 83
3.4 Digital Surface Modelling 85
3.4.1 Introduction 85
3.4.2 DEM Structure 87
3.4.2.1 Grid Structure 88
3.4.2.2 Triangulated Irregular Network 89
3.4.3 DEM Interpolation 90
3.4.3.1 Global Interpolation 91
3.4.3.2 Patchwise Interpolation 91
3.4.3.3 Pointwise Interpolation 92
3.4.4 Accuracy Considerations 94
3.4.4.1 Factors Influencing DEM Accuracy 94
3.4.4.2 Measures of DEM Quality 97
3.5 Surface Registration 100
3.6 Summary 101
CHAPTER FOUR: ROBUST INTEGRATION OF DIGITAL ELEVATION MODELS 103
4.1 Introduction 103
4.2 Surface Matching Overview 104
4.2.1 Introduction 104
4.2.2 Surface Matching in the Geomatics Domain 107
4.2.3 Suitability for Coastal Geohazard Monitoring 113
4.3 Least Squares Surface Matching 114
4.3.1 Introduction 114
4.3.2 Theoretical Basis 116
4.3.2.1 Three-Dimensional Conformal Coordinate Transformation 117

4.3.2.2 Surface Matching Theory 119
4.3.3 3DSurf Matching Algorithm 121
4.4 Robust Surface Matching Development 125
4.4.1 Problem Specification 125
4.4.2 Robust Estimation 127
4.4.2.1 Overview 127
4.4.2.2 Maximum Likelihood Estimators 129
4.4.3 Robust Algorithm Development 130
4.4.3.1 Iteratively Reweighted Least Squares 130
4.4.3.2 Computational Aspects of the Biweight M-Estimator 132
4.4.3.3 Algorithmic Implementation 135
4.4.4 Evaluation of Robust Matching Algorithm 138
4.4.4.1 Robust Matching of Artificial Surfaces 138
4.5 Summary 144

CHAPTER FIVE: INTEGRATED REMOTE MONITORING AT FILEY BAY 146
5.1 Introduction 146
5.2 Filey Bay Test Site 147
5.2.1 Overview 147
5.2.2 Previous Monitoring 150
5.2.3 Test Areas 150
5.3 Episodic Monitoring Campaigns 153
5.3.1 Overview 153
5.3.2 Campaign Specifics 154
5.3.2.1 Epoch 0 Monitoring Campaign 154
5.3.2.2 Epoch 1 Monitoring Campaign 155
5.3.2.3 Epoch 2 Monitoring Campaign 156
5.4 Acquisition and Processing of Airborne Datasets 157
5.4.1 Airborne Laser Scanning 157
5.4.1.1 Data Acquisition 157
5.4.1.2 Independent Quality Analysis 158
5.4.1.3 ALS Data Processing 160
5.4.2 Archival Aerial Photography 162
5.4.2.1 Data Acquisition 162

5.4.2.2 Processing of Archival Imagery 166
5.5 Acquisition and Processing of Terrestrial Datasets 169
5.5.1 GPS Control Data 169
5.5.1.1 Data Acquisition 169
5.5.1.2 GPS Data Processing and Analysis 169
5.5.2 Terrestrial Laser Scanning 171
5.5.2.1 Data Acquisition 171
5.5.2.2 TLS Data Processing 173
5.5.3 Profile Validation of Laser Scanning Datasets 175
5.5.3.1 Data Acquisition 175
5.5.3.2 Quality Assessment of Laser Scanning Datasets 176
5.6 Retrospective Analysis of Geohazard Activity 178
5.6.1 Introduction 178
5.6.2 Robust Matching of Photogrammetric DEMs 180
5.6.2.1 Surface Matching Procedure 180
5.6.2.2 Analysis of Matching Solutions 181
5.6.3 Validation of Surface Matching Results 185
5.6.3.1 Production of Validation Surface 185
5.6.3.2 Surface Matching Quality Analysis 187
5.6.4 Geohazard Assessment 1967 – 2005 191
5.6.4.1 Visualisation and Analysis of Change 191
5.6.4.2 Volumetric Assessment of Change 195
5.6.4.3 Rates of Change 196
5.7 Contemporary Analysis of Geohazard activity 199
5.7.1 Introduction 199
5.7.2 Dataset Integration 200
5.7.2.1 Multi-Sensor Dataset Fusion 200
5.7.2.2 Multi-Temporal Dataset Integration 204
5.7.3 Assessment of Contemporary Geohazard Activity 206
5.8 Summary 209

CHAPTER SIX: TRANSFERABILITY TESTING AT WHITBY EAST CLIFF 211
6.1 Introduction 211
6.2 Whitby Test Site 212

6.2.1 Overview 212
6.2.2 Previous Monitoring 215
6.3 Episodic Monitoring 217
6.3.1 Introduction 217
6.3.2 Data Acquisition and Processing 218
6.3.2.1 Airborne Laser Scanning 218
6.3.2.2 Archival Aerial Photography 219
6.4 Dataset Quality Analysis 224
6.5 Multi-Temporal Analysis of Geohazard Activity 227
6.5.1 Introduction 227
6.5.2 Robust Matching of Multi-Temporal DEMs 228
6.5.2.1 Surface Matching Procedure 228
6.5.2.2 Validation of Multi-Temporal Matching Solutions 233
6.5.3 Assessment of Geohazard Activity 1994 – 2006 237
6.5.3.1 Preparation and Pre-Analysis of Inter-Epoch Change Surfaces 237
6.5.3.2 Visualisation and Assessment of Inter-Epoch Change 240
6.5.3.3 Profile-Based Analysis of Change 243
6.5.3.4 Volumetric Analysis of Change 245
6.5.3.5 Rates of Change 250
6.5.4 Changes to Cliff Edge Position 1986 – 2006 251
6.5.4.1 Introduction 251
6.5.4.2 Analysis of Cliff-Edge Change 252
6.6 Summary 254

CHAPTER SEVEN: DISCUSSION AND CONCLUDING REMARKS 256
7.1 Introduction 256
7.2 Discussion of Research Outcomes 257
7.2.1 Suitability of Techniques 257
7.2.1.1 Airborne Laser Scanning 257
7.2.1.2 Terrestrial Laser Scanning 259
7.2.1.3 Archival Aerial Photography 262
7.2.1.4 Robust Surface Matching 264
7.2.2 Integrated Remote Monitoring Strategy 268
7.2.2.1 Overall Performance Assessment 268

7.2.2.2 Assessment of Transferability 270
7.2.3 Implications in Relation to Geohazard Monitoring 272
7.2.4 General Software Issues 275
7.3 Revisiting the Research Objectives 276
7.4 Recommendations for Future Work and Outlook 278
7.4.1 Robust Surface Matching Development 278
7.4.1.1 Software Development 278
7.4.1.2 Suitability for Alternative Applications 281
7.4.2 Upscaling to Wide-Area Monitoring of Coastal Change 282
7.4.3 Emerging Techniques and Technology 283
7.4.3.1 Continuous GNSS Monitoring 283
7.4.3.2 Unmanned Aerial Vehicles 285
7.4.3.3 Mobile Mapping Systems 285
7.4.3.4 Satellite Remote Sensing 286
7.5 Summary 287

REFERENCES 288

LIST OF FIGURES

Figure 1.1 Classification of major mass wasting processes (USGS, 2004). 3

Figure 1.2 The impact of soft-cliff retreat on human settlement in Pacifica, California (NASA JPL, 2003). 6

Figure 1.3 The receding Suffolk coastline, as illustrated by the location of the former churches of Dunwich (Pye and Blott, 2006). 7

Figure 1.4 Example of discrete geodetic monitoring network on the volcanic island of Stromboli, Italy (Puglisi et al., 2005). 12

Figure 1.5 Airborne laser scanning-derived DEM of a river environment in Northumberland (Charlton et al., 2003). 13

Figure 1.6 Real-time monitoring of slope failure (inset) in Hong Kong (Leung, 2003). 14

Figure 1.7 High water line, delineated from wet-dry sand boundary, indicating shoreline position on an aerial photograph (Klein and Lichter, 2006). 17

Figure 2.1 Wire extensometer for measuring displacement along a fault (Coe et al., 2003). 25

Figure 2.2 Holderness erosion rates, calculated from erosion post data (East Riding of Yorkshire Council, 2005) 27

Figure 2.3 Kinematic GPS surveys of cliffs, left (Buckley et al., 2002) and the swash zone, right (Seymour et al., 2005). 35

Figure 2.4 Photogrammetric monitoring of shore platform changes (Dornbusch et al., 2005). . 42

Figure 2.5 Typical ALS system (Wehr and Lohr, 1999). 43

Figure 2.6 Profile through waveform digitised dataset, with grey level indicating signal amplitude (Hug et al., 2004). 46

Figure 2.7 So-called 'grain noise' and other artefacts (indicated by arrows) arising due to improper system calibration, in what should be a smooth beach area (Huising and Gomes Pereira, 1998). 48

Figure 2.8 Erroneous ground point filtering due to steep terrain (left). Corrected DTM (right) (Ruiz et al., 2004). 50

Figure 2.9 Time-of-flight (left), and phase comparison (right) ranging principles (Wehr and Lohr, 1999). 52

Figure 2.10 TLS-derived, photo-textured digital geological outcrop model, with digitised stratigraphy (Bellian et al., 2005) 56

Figure 2.11 Interferogram of an active caldera in Long Valley, California (Newman et al., 2006). 60

Figure 2.12 Systematic error, highlighted through straightforward dataset combination (Buckley, 2003) 64

Figure 3.1 Occluded regions of ALS dataset (left) supplemented with TLS data (right) to provide complete coverage of mountainous terrain (colours represent flightlines) (Ruiz et al., 2004). 71

Figure 3.2 Basic outline of integrated coastal geohazard monitoring strategy, as developed and implemented in this research. 72

Figure 3.3 ALS first and last pulse return concept. 74

Figure 3.4 Optech ALTM 3033 system (left), and the ARSF research aircraft (right) (NERC ARSF, 2007). 75

Figure 3.5 Leica HDS2500 terrestrial laser scanner. 78

Figure 3.6 Leica Cyclone software, HDS2500 scanner control interface. 78

Figure 3.7 Leica HDS3000 terrestrial laser scanner. 80

Figure 3.8 Riegl LPM-i800HA terrestrial laser scanner. 81

Figure 3.9 Examples of the DEM grid structure (a), and TIN structure (b) (Zhu et al., 2005)... 88

Figure 3.10 Potential errors (E_b) at C, due to grid spacing (d) in linearly interpolated data (Li, 1993). 89

Figure 3.11 Illustration of the effect of different interpolation techniques on surface representation (Desmet, 1997). 96

Figure 3.12 Hybrid grid-based DEM, supplemented with breaklines and spot heights incorporated through triangulation (Kraus and Otepka, 2005). 97

Figure 3.13 Normal error distribution curve, indicating confidence intervals (Uren and Price, 2006). 99

Figure 4.1 Corresponding point selection concept of the ICP algorithm (Planitz et al., 2005). 105

Figure 4.2 2D point maps and corresponding spin images for a toy duck, in local object-centred coordinate system (α,β) (Johnson and Hebert, 1999). 106

Figure 4.3 Surface matching through selection of intensity-based interest points, a) & b), which are then triangulated, e.g. c), and matched, to recover the transformation and align the surfaces, d) (after Roth, 1999)). 107

Figure 4.4 TLS point cloud (left), and associated Z-Image (right), from which features such as walls can be extracted and used as registration primitives (Zhao and Shibasaki, 2001). ... 108

Figure 4.5 Accumulator array for estimation of the ω rotation parameter through the Hough transform approach. The peak value indicates the parameter solution. (Habib and Kelley, 2001). 109

Figure 4.6 TLS representations of a Buddha statue prior to alignment, left, and after feature-based registration, right (Bae and Lichti, 2004). 110

Figure 4.7 Curve to surface matching (Gruen and Akça, 2005). 112

Figure 4.8 3DSurf matching algorithm (Buckley, 2003). 123

Figure 4.9 Weight function for the biweight estimator, showing response to the standardised residuals (u), where the tuning constant c=4.685 has been applied (after Fox, 2002)) 130

Figure 4.10 Biweight weighting function, displaying the effect of different tuning constants (c) on the weights (w_b) derived from the standardised residuals (u). The default value of c=4.685 is shown in solid 134

Figure 4.11 Robust weighting incorporated at the least squares solution stage (refer to Figure 4.8 for overview of original 3DSurf algorithm). 136

Figure 4.12 3DSurf-*R* user interface. 137

Figure 4.13 Surfaces employed in artificial testing, *Base* and *Spikes*. 139

Figure 4.14 Test 2 post-match surface residuals, showing deteriorating results, as increasing weights are applied. Negative residual values indicate where the *Spikes* surface is above *Base*. 143

Figure 5.1 Northern end of Filey Bay, looking towards Filey Brigg. 148

Figure 5.2 Example of typical mudflow affecting the cliffs at Filey Bay. 149

Figure 5.3 Location of test areas within Filey Bay. 151

Figure 5.4 CPK north (left) and south (right) sub-areas, with validation profile locations, and control points indicated. 152

Figure 5.5 GLF and HUN test areas, with validation profile locations, and control points indicated. 152

Figure 5.6 SPT test area, with validation profile locations, and control points indicated. 153

Figure 5.7 Example of buried Feno marker used for control monumentation at Filey Bay 156

Figure 5.8 GPS test field, located at Filey Country Park. 158

Figure 5.9 Overlapping flightlines (left) cut by removing poorer quality points (centre, red) from landward flightline, and retaining points from seaward flightline only (right). 161

Figure 5.10 Coverage of archival imagery detailed in Table 5-4 164

Figure 5.11 1967 aerial imagery (67-254-32). 165

Figure 5.12 1980 aerial imagery (80-135-008). 165

Figure 5.13 *SocetSet* mass point extraction for the 1 m TIN DEMs for 1967 (left) and 1980 (right). 168

Figure 5.14 Specially adapted target for controlling the Leica HDS2500 scans. 171

Figure 5.15 Epoch 2 GLF1 profile. Area A highlights differing TLS and ALS surface representations in densely vegetated area; area B indicates break in total station data due to dense vegetation. 177

Figure 5.16 Reighton area highlighted in 2005 ortho-image. 179

Figure 5.17 Illustration of terrain change, with correct solution (A), and possible outcome of un-weighted matching algorithm (B). 181

Figure 5.18 Post-match level difference maps for 1967-2005 Reighton matching..... 183

Figure 5.19 Post-match level difference maps for 1980-2005 Reighton matching..... 184

Figure 5.20 Location of GPS GCPs acquired for rigorous orientation of 1980 imagery. Profiles and check area used in subsequent analysis are also indicated..... 186

Figure 5.21 Comparison of robust and un-weighted solution accuracies at profile locations. . 188

Figure 5.22 Comparison of matching and validation surfaces at Profile 2a (cliff-face). 189

Figure 5.23 Profile through camping field check area, illustrating DEM offsets. 190

Figure 5.24 Elevation differences over Reighton cliff-face, 1967-1980, with features of interest highlighted..... 193

Figure 5.25 Elevation differences over Reighton cliff-face, 1980-2005, with features of interest highlighted..... 194

Figure 5.26 Occluded scan regions in TLS dataset (A), and improved coverage, with merged ALS-TLS dataset after surface matching (B)..... 203

Figure 5.27 SPT profile RMSEs for TLS pre-match, post-match and final merged TLS-ALS surfaces. 206

Figure 5.28 Map of elevation differences, epoch 1 to epoch 2, for integrated ALS-TLS DEMs at Reighton, with regions of change highlighted, and indicated on corresponding epoch 2 ortho-image..... 208

Figure 5.29 Visualisation of cliff change between epochs 1 and 2 at Reighton, with SPT validation profiles indicated. Change is represented through same scale as for Figure 5.28.. 209

Figure 5.30 Elevation differences for SPT area using only ALS datasets (left), and with merged ALS-TLS datasets (right). Resolution differences are highlighted. 209

Figure 6.1 Location map (top), and overview of test site shown against backdrop of 1994 ortho-image (bottom). 213

Figure 6.2 Study site at Whitby East Cliff. 214

Figure 6.3 Coastal erosion affecting the cliff-top footpath. 215

Figure 6.4 EH mapping of cliff-edge position, 1940-2001, derived from aerial photographs (after Lyons, 2004, personal communication). 216

Figure 6.5 TLS-derived model of Whitby East Cliff (top), with 0.25 m contours indicating change between 2003 and 2004 (bottom) (Rosser et al., 2005). 217

Figure 6.6 ALS flightline coverage for Whitby test site and adjacent cliff-top region..... 219

Figure 6.7 1986 (red) and 1994 (blue) stereo coverage of the Whitby test site. 221

Figure 6.8 1986 archival imagery (86-253-2006). 221

Figure 6.9 1994 archival imagery (9872)..... 222

Figure 6.10 *SocetSet* FOM visualisation for 1986 grid-based DEM..... 224

Figure 6.11 Distribution of check points across Whitby Abbey Headland..... 225

Figure 6.12 Cross-sectional view of pre-match positions of 1986 and 1994 surfaces..... 226

Figure 6.13 ALS-derived elevation model of Whitby Abbey Headland, with matching extent delineated (red). Contours (2 m interval) indicate the relatively flat terrain..... 229

Figure 6.14 Pre- and post-match vertical check point discrepancies for April 2005 ALS surface..... 234

Figure 6.15 Post-match check point discrepancies for ALS datasets..... 235

Figure 6.16 Histograms of inter-epoch cliff-face change at Whitby East Cliff..... 238

Figure 6.17 Pre- and post-match cliff sections through ALS datasets, with the May 2006 pre-match dataset illustrating a potential planimetric offset..... 240

Figure 6.18 Multi-temporal change over Whitby cliff-face, with rendered model of cliff-face included (top) for reference..... 241

Figure 6.19 Profile locations depicted against 1994 ortho-image..... 243

Figure 6.20 Profiles illustrating cliff-face change at selected locations..... 244

Figure 6.21 Division of upper and lower cliff for volumetric change analysis..... 246

Figure 6.22 Inter-epoch volumetric change for lower cliff, upper cliff, and cliff-face as a whole..... 246

Figure 6.23 Map of cliff-face change, August 2005-May 2006, with primary failure area outlined (Miller et al., in review)..... 248

Figure 6.24 Debris from cliff failure highlighted in Figure 6.23..... 249

Figure 6.25 Large sandstone blocks jutting from the cliff-top..... 249

Figure 6.26 Cliff edge change at Whitby East Cliff, 1986-2006, with 1994 ortho-image as backdrop..... 253

Figure 7.1 Scan of cliff area at Filey Bay (acquired with Leica HDS2500), rendered according to point intensity..... 261

Figure 7.2 The detrimental influence of TLS sensor noise over a flat beach area, in an integrated ALS-TLS dataset..... 280

LIST OF TABLES

Table 1-1 Summary of the factors involved in sea cliff recession (after Komar, 1998). 4

Table 2-1 Summary of potential error sources in GPS measurements (after Misra and Enge, 2006). 33

Table 3-1 Primary characteristics of the Optech ALTM 3033 ALS instrument (Arnold et al., 2006; NERC ARSF, 2006)..... 74

Table 3-2 Summary of main characteristics of scanners utilised in the research (Point of Beginning, 2004; Leica Geosystems, 2006; Riegl, 2006a). 77

Table 3-3 Standard deviation multipliers for percentage probable errors of the normal distribution (after Wolf and Ghilani, 1997). 100

Table 4-1 Test 1 – transformations applied to *Base* matching surface to validate integrity of 3DSurf-*R*. Distance units are dimensionless. 139

Table 4-2 Test 1 results for the original program (a), and the robust version (b). Distance units are dimensionless. 140

Table 4-3 Test 2 mismatch statistics for differing weight values. Distance units are dimensionless. 143

Table 5-1 Annual cliff erosion rates within Filey Bay (after Elliot et al., 1991)). 150

Table 5-2 Summary of datasets acquired for episodic monitoring campaigns, including specifics of TLS instruments..... 154

Table 5-3 Summary of quality statistics for ALS check point analysis. 159

Table 5-4 Details of archival imagery acquired for Filey Bay test site..... 163

Table 5-5 Summary of solutions achieved from *SocetSet* bundle adjustment procedure. 167

Table 5-6 Summary of GPS-derived inter-epoch displacements at HUN1, 2000-2005. 170

Table 5-7 Summary of profile validation statistics for TLS datasets..... 176

Table 5-8 Summary of profile validation statistics for ALS datasets. 177

Table 5-9 Summary of surface matching parameters and results for matching of historical DEMs at Reighton. RMSE refers to final matching residuals (vertical surface differences).. 181

Table 5-10 Summary of level difference statistics for Reighton matching..... 182

Table 5-11 Summary of bundle adjustment results for GPS-controlled 1980 photography. 187

Table 5-12 Summary of level difference statistics over camping field area, with respect to the 2005 ALS DEM. 190

Table 5-13 Distribution of level difference values within confidence intervals derived from check area analysis..... 192

Table 5-14 Volumetric change analysis over Reighton cliffs. 196

Table 5-15 Rates of change across Reighton cliff-face, derived from volumetric analysis..... 197

Table 5-16 Rates of elevation change across Reighton cliff-face, derived from level differences. 198

Table 5-17 Summary of multi-sensor matching input parameters and results. RMSE refers to final matching residuals. 201

Table 5-18 Final transformation parameters for multi-sensor matching at SPT..... 201

Table 5-19 Profile validation analysis for multi-sensor matching at SPT. 202

Table 5-20 Summary of multi-temporal matching input parameters and results. RMSE refers to final matching residuals. 204

Table 5-21 Final transformation parameters for multi-temporal matching at SPT..... 205

Table 5-22 Profile validation analysis for multi-temporal matching of epoch 1 data at SPT... 205

Table 6-1 Details of archival imagery acquired for Whitby East Cliff test site. 220

Table 6-2 Summary of bundle adjustment results for 1986 and 1994 imagery. 223

Table 6-3 Summary of check point analysis for Whitby multi-temporal datasets. 225

Table 6-4 Summary of Whitby multi-temporal matching strategies and convergence details, for robust and un-weighted matching. 1994 DEM was used as reference in each case..... 231

Table 6-5 Final transformation parameters for multi-temporal matching at Whitby. 232

Table 6-6 Summary of post-match quality statistics for robust and un-weighted matching of multi-temporal datasets. 233

Table 6-7 Comparison of expected and attained heighting precisions. 236

Table 6-8 Level difference statistics for inter-epoch change across Whitby East Cliff. 239

Table 6-9 Rates of change across Whitby East Cliff, March 1994-May 2006, derived from volumetric analysis. 250

Table 6-10 Rates of change across Whitby East Cliff, March 1994-May 2006, derived from level differences. 251

LIST OF ABBREVIATIONS AND NOTATION

ALS	Airborne Laser Scanning
ARSF	Airborne Research and Survey Facility
b/H ratio	Base-height ratio
cm	Centimetre
CUCAP	Cambridge University Collection of Air Photos
CW	Continuous Wave
DEM	Digital Elevation Model
DOP	Dilution of Precision
DPW	Digital Photogrammetric Workstation
DSM	Digital Surface Model
DTM	Digital Terrain Model
EDM	Electronic Distance Measurement
EH	English Heritage
FOM	Figure of Merit
FOV	Field Of View
GCP	Ground Control Point
GIS	Geographical Information System
GNSS	Global Navigation Satellite Systems
GPS	Global Positioning System
HWL	High Water Line
Hz	Hertz
ICP	Iterative Closest Point
IDW	Inverse Distance Weighted
IMU	Inertial Measurement Unit
INS	Inertial Navigation System
InSAR	Interferometric Synthetic Aperture Radar
IRLS	Iteratively Reweighted Least Squares
kg	Kilogram
km	Kilometre
LAT	Lowest Astronomical Tide
LiDAR	Light Detection and Ranging
LMS-estimator	Least-Median-of-Squares estimator
m	Metre
mm	Millimetre
μm	Micron

MAD	Median Absolute Deviation
M-estimator	Maximum Likelihood estimator
MMS	Mobile Mapping System
NAPLIB	National Association of Aerial Photographic Libraries
NERC	Natural Environment Research Council
nm	Nanometre
NMR	National Monuments Record
OS	Ordnance Survey
OSGB36	Ordnance Survey Great Britain 1936
POS	Position and Orientation System
ppm	parts per million
PRN	Pseudo-Random Noise
RCAHMS	Royal Commission on the Ancient and Historical Monuments of Scotland
RMSE	Root Mean Square Error
RSPSoc	Remote Sensing and Photogrammetry Society
RTK	Real Time Kinematic
s	Scale
SAR	Synthetic Aperture Radar
SMP	Shoreline Management Plan
SSSI	Site of Special Scientific Interest
SVD	Singular Value Decomposition
TIN	Triangulated Irregular Network
TLS	Terrestrial Laser Scanning
T_x	Translation of the x axis
T_y	Translation of the y axis
T_z	Translation of the z axis
UAV	Unmanned Aerial Vehicle
ULM	Unit for Landscape Modelling
UTM	Universal Transverse Mercator
WGS-84	World Geodetic System 1984
ω	Rotation around the x axis
ϕ	Rotation around the y axis
κ	Rotation around the z axis
σ	Standard deviation

CHAPTER 1

INTRODUCTION

1.1 RESEARCH BACKGROUND

1.1.1 Overview

Coastal change is a naturally-occurring, irreversible global process which has been ongoing for hundreds of thousands of years, but which has only become a matter of concern in relatively recent times. With two-thirds of the world's population occupying the coastal margins, and this figure projected to continue to increase in the future (World Bank, 1996; Komar, 1998; Charlier and Bologa, 2003), there is real concern as to the capacity of the coastal environment to adjust to the pressures imposed by increased levels of development. This is further complicated by the projected effects of climate change, which although characterised by uncertainty (Lee and Clark, 2002), are generally acknowledged as likely accelerants of coastal change (Bray and Hooke, 1997 Komar, 1998).

Coastal geohazards represent a major driver for coastal evolution, and are prevalent on certain cliffed coastlines, particularly those which are susceptible to failure due to their geological composition. These phenomena directly impact on the human, natural and historic environments, and in order to effectively manage the associated risks, coastal managers and planners require timely and efficient coastal geohazard monitoring. Such information also contributes towards improved understanding of the underlying processes, and provides valuable input for the development and implementation of

wider-scale management policies. However, the coastal environment exhibits complex and hazardous topography, which has traditionally proved hostile to the straightforward implementation of many monitoring techniques. This research attempts to improve the effectiveness of current geohazard monitoring practices by adopting an integrated monitoring approach, and exploring the potential of the relatively new geomatics techniques of airborne and terrestrial laser scanning and the opportunities that these offer for enhanced monitoring – particularly in terms of resolution, and remote application. In addition, archival aerial photography is investigated in relation to its potential for retrospective analysis of geohazard activity. A key issue in relation to any monitoring study involving multi-sensor or multi-temporal datasets is accurate registration, which is a particular challenge in the dynamic coastal environment. This concern is often overlooked, but has the potential to introduce significant errors to the quantification of coastal change. In acknowledgement of the critical importance of this issue, a solution structured around robust surface matching of digital elevation models (DEMs) has been developed and implemented.

1.1.2 Coastal Geohazards

Geohazards include geological and associated geophysical phenomena such as earthquakes, volcanoes, subsidence, and landslides, which regularly cause mass destruction and loss of life around the world (IGOS, 2003). While the impact of geohazards tends to be most extreme in developing nations, where loss of life can be significant, the economic legacy often hits hardest in the industrialised world (Guzzetti et al., 1999). Mass movements, such as landslides, are perhaps the most common and widespread expression of geohazard activity, ranging hugely in scale and severity. Coastal geohazards represent a special case of instability, occurring where the incidence of land and sea results in cliffed terrain. Slope failure develops where the compressive strength of a material is exceeded by the load on it (Viles and Spencer, 1995; Masselink and Hughes, 2003). This encompasses a range of mass wasting processes, such as rockfalls, debris avalanches, and rotational slides, as illustrated in Figure 1.1. The development of such features is governed by a complex interaction of direct and indirect factors (Bray and Hooke, 1997), which essentially relate to the interplay of subaerial processes (such as mass movement and hydrological processes), and wave erosion at the

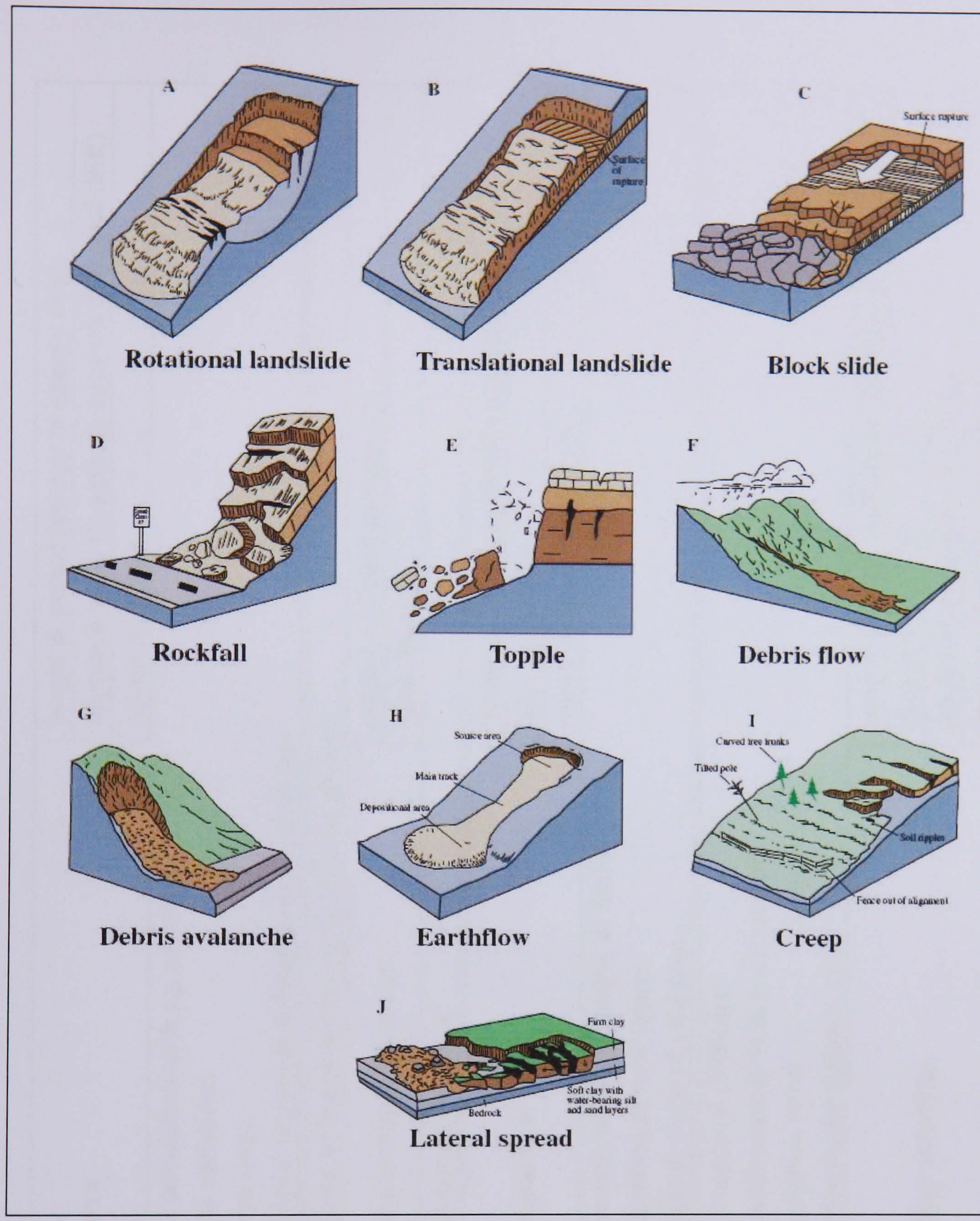

Figure 1.1 Classification of major mass wasting processes (USGS, 2004).

toe of the cliff (Viles and Spencer, 1995). Table 1-1 outlines some of the major factors influencing the development of coastal geohazards. While hard-rock coasts retreat relatively slowly, soft-rock cliffs are susceptible to additional weakening and slope failure (Bray and Hooke, 1997). Through analysis of a vast archive of cliff recession studies from around the world, Sunamura (1992) concluded that although granite cliffs may retreat by as little as 1 mm per year, the recession of glacial deposits can range from 1 m to as much as 10 m per year. Furthermore, Bird (2000) observes that in soft clays and glacial deposits, which are common along the south and east coasts of

MARINE FACTORS	Waves	height & period (energy or energy flux)
		approach angle (longshore currents & littoral drift)
		set-up & run-up
	Cell circulation with rip currents Tidal variations Storm surge Sea level (seasonal & long-term net changes)	
BEACH FACTORS	Volume of beach sediments (buffering ability)	
	Composition & grain size	control on beach morphology
		sand 'blasting'
	Presence of drift logs	
CLIFF FACTORS	Composition	'hardness' (e.g. compressive strength)
		talus production
		source of beach sediments
	Layering (bedding), joints, & faults Inclination of rock layers Height & slope of cliff face	
OTHER FACTORS	Rain wash on cliff-face Ground-water flow & pore pressure Vegetation cover Burrowing by rodents, etc.	
	Human activities	erosion through walking & climbing on cliff & talus
		excavation of cliff
		sea defences & other structures
		drainage channels – e.g. culverts

Table 1-1 Summary of the factors involved in sea cliff recession (after Komar, 1998).

England, cliffs recede through recurrent slumping, often following a period of wet weather. Despite the fact that individual failure events may be relatively insignificant, over time, the cumulative impact can be dramatic (Lee et al., 2001). Coastal geohazards therefore play a key role in driving coastal change, whether this is manifest through the irregular activity of spectacular and complex landslide features, or the gradual recession of hard rock cliffs through occasional rockfalls.

With cliffs occupying approximately 80 percent of the world's ocean coastline, and occurring at all latitudes (Emery and Kuhn, 1982), it is essential that geohazards are monitored and mitigated where appropriate, especially with uncertainties over the impact of global warming, and associated sea level rise. This is further necessitated by the increasing global population, which has seen the spread of human settlement and associated infrastructure (particularly in developing countries) to areas prone to slope failure or associated hazards (Guzzetti et al., 1999). In such cases, failure may be hastened or initiated through deforestation, road construction, excavation and the like (Chang and Slaymaker, 2002; Capra et al., 2003; Knapen et al., 2006; Sidle et al., 2006). This population expansion has incorporated a growing trend for migration towards the world's coastal fringes (World Bank, 1996; Komar, 1998; Moore, 2000), and as highlighted by Tralli et al. (2005), eleven of the world's fifteen largest cities are now located on coasts or estuaries. Increased development places mounting pressure on the coastal resource, with residential buildings and infrastructure often located close to eroding coastlines (Bray and Hooke, 1997). This is especially true of the west coast of the United States, and California in particular, where pockets of urbanisation coincide with actively-retreating soft-rock cliffs (Moore and Griggs, 2002), as illustrated in Figure 1.2. Here, existing weakness is often aggravated by seismic events, and severe storms.

As highlighted by Hall et al. (2002), 'Many coastlines suffer from an inheritance of communities built on eroding cliff tops'. This is illustrated in Figure 1.3, which indicates the reduction of Dunwich in Suffolk, from a thriving port of significant status in medieval times, to its current status as a small coastal village (Pye and Blott, 2006). A similar situation is to be found at Happisburgh in Norfolk, where erosion rates of 8 - 10 m per year have been reported (Poulton, 2004), and are evidenced by the loss of

Figure 1.2 The impact of soft-cliff retreat on human settlement in Pacifica, California (NASA JPL, 2003).

several residential cliff-top properties over recent years. On the south coast of England, the Ventnor Undercliff landslide complex on the Isle of Wight poses the greatest risk to an urban population in the UK, with ongoing instability responsible for significant cumulative damage to town of Ventnor, which has a population of more than 6,000 (Lee and Clark, 2002). However, in terms of more dynamic geohazard activity, one of the most spectacular and celebrated examples of recent times was the 1993 Holbeck Hall Hotel landslip on the outskirts of Scarborough, North Yorkshire, where more than 60 m of cliff collapsed overnight, and a further 35 m was lost over the next few days, leading to the eventual destruction of the hotel (Lee and Clark, 2002).

Coastal recession is more than just a nuisance of nature; over time, expenditure on repairs and measures of mitigation can amount to millions, even for short stretches of coastline, and perhaps of greater concern is the risk to human life. Furthermore, the coastal zone is a landscape of great cultural value, and for thousands of years humans have settled here in order to take advantage of natural resources (such as fishing and rich agriculture soils), to establish trading routes, and to exploit natural defensive situations. The physical remnants of this heritage include historical buildings, landscape features, and archaeological sites, which provide an invaluable record of human activity

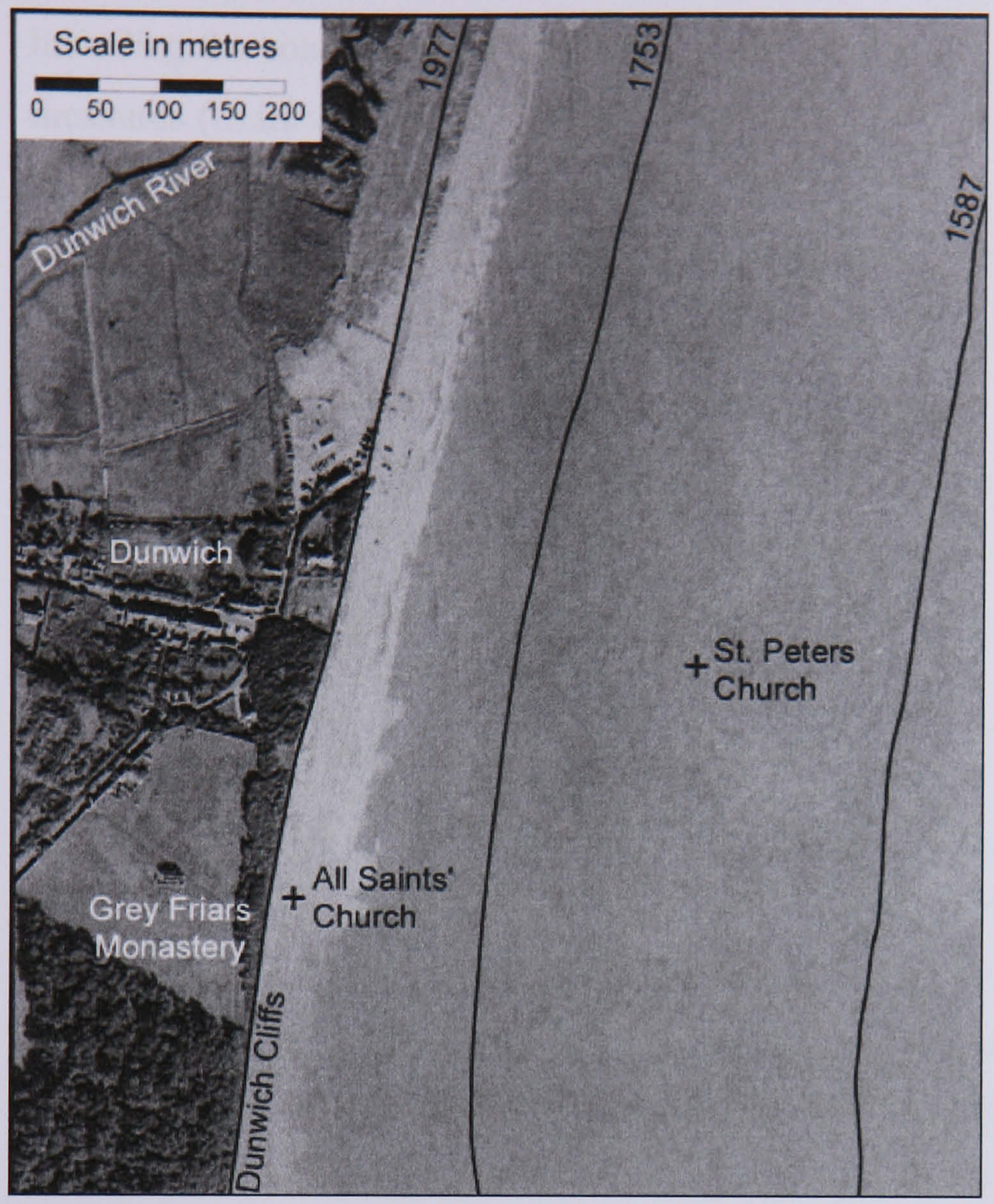

Figure 1.3 The receding Suffolk coastline, as illustrated by the location of the former churches of Dunwich (Pye and Blott, 2006).

over time, but which are vulnerable to coastal change, and cannot be replaced once damaged or destroyed (English Heritage, 2003). In relation to such issues, the National Trust has recently expressed concern for the implications of coastal recession with respect to its assets on the Welsh coast (BBC, 2007). Coastlines are also rich in flora and fauna, and more than a third of England's 5496 km of coastline is designated for its natural or scenic value, and is recognized as supporting a diverse range of nationally and internationally important natural habitats (DEFRA, 2006a).

As focus increasingly shifts towards the impacts of climate change, and the potential for associated sea level rise, consideration must be given to the most appropriate course of action in terms of mitigation. The coastal zone represents a complex interaction of systems which act over a range of temporal and spatial scales. As a component of this, coastal change is a difficult issue to manage. Where a serious threat to population and infrastructure exists, coastal defences are commonplace, and can take various forms,

including the construction of sea walls, rock armour, and slope drainage or stabilisation measures (Clark and Guest, 1991; Lee and Clark, 2002). England is protected by some 860 km of coastal defences (Lee et al., 2001). However, coastal defences can prove detrimental to coastal ecosystems, and can significantly impact on the sediment budget, limiting the supply of beach-building material (Lee and Clark, 2002). This is supported by Runyan and Griggs (2003), who found that the construction of coastal armouring structures along the Californian coastline reduced the supply of sediments from cliff erosion sources by as much as 20 percent. Therefore, prior to construction, the impacts of this form of intervention must be fully assessed and justified.

UK government policy has seen a recent shift away from hard defensive measures, towards adoption of a longer-term, sustainable approach to coastal management, working with, rather than against, coastal processes wherever possible. A key aspect of this relates to holistic management, with a more integrated approach aimed at harmonising the activities and goals of the various management bodies involved (DEFRA, 2006a). In England and Wales, Shoreline Management Plans (SMP) provide the basis for implementation of this policy. SMPs, first introduced in 1995, are designed to provide an assessment of the risks to the human and natural environment for particular stretches of coastline (originally based on sediment cell boundaries), and guidance on best practice for sustainable management of such risks (DEFRA, 2006b). Production of a second generation of SMPs is currently underway; these are designed to provide a longer-term outlook on sustainable coastal management, through incorporation of the latest research on coastal change.

1.1.3 Monitoring Studies

1.1.3.1 Overview

Given the impact of coastal geohazards on society and the natural environment, and coupled with uncertainty over the influence of current and future climate change, there is an unequivocal requirement for monitoring of such phenomena. In addition, it is becoming increasingly important to establish which types of action are most appropriate for particular locales (Bray and Hooke, 1997).

In terms of landslide hazards in general, monitoring serves several important purposes (National Research Council, 2004b):

- it enables the identification of fresh or increased landslide activity, thus providing a geohazard early warning capability;
- it enables the morphological analysis of landslide features in order to assist in landslide susceptibility mapping;
- it facilitates improved understanding of landslide mechanisms and triggering factors;
- it allows for evaluation of the effectiveness of mitigation measures.

The requirement for monitoring is further supported by Lee and Clark (2002), who stress the key role this plays in relation to coastal risk assessment, and the formation and review of coastal defence policy, which must be founded on a sound understanding of cliff behaviour. Furthermore, Pethick and Crooks (2000), observe that monitoring plays a vital role in assessing progressive coastal change, and in managing response to such variations, both natural and manmade.

Monitoring studies can take many different forms depending on the nature of the entity under observation, and the purpose of the monitoring activity. Consequently, there are a number of associated factors which influence the selection of a particular technique, and the nature of its implementation.

1.1.3.2 Scale and Accuracy

Scale and accuracy are fundamental considerations, which are likely to exert a strong influence on the design of the monitoring strategy. In relation to geomorphological monitoring, Lane et al. (1998) define three scales:

- the micro-scale (extents of up to 10 km^2);
- the meso-scale (extents of less than 100 km^2);
- the macro-scale (extents ranging to the global level).

This provides a convenient classification for monitoring scales, particularly with regards to geohazard monitoring, which has close association with geomorphological processes. In terms of more general monitoring activities however, scale can range from ultra close-range (or ultra micro-scale) activities to applications at the global scale. Examples of ultra close-range monitoring activities are to be found in the fields of medicine and dentistry, where high-precision, non-contact methods may be a requirement. Close-range photogrammetry has long been utilised for such purposes, and is particularly suitable due to the instantaneous acquisition of the subject, and the non-invasive nature of this approach (Newton and Mitchell, 2001). However, more recently, research has been undertaken to evaluate emerging techniques, such as laser scanning. An example of this is provided by Rosin et al. (2002) who studied the development of gum swelling by scanning casts of patients' mouths over a 40-day period. In their conclusions, they remark on the high (μm) levels of precision and accuracy achieved, and the benefits this provides for quantification (particularly in volumetric terms) of the anomaly.

It is important to note however, that considerations of accuracy and precision will not necessarily degrade with scale. For example, high precision is also a requirement for Global Positioning System (GPS) monitoring of regional plate tectonics, where annual deformation rates may be at the mm-level. Conversely, regional- or global-scale monitoring of environmental processes may concentrate more on the synoptic capabilities of techniques such as satellite remote sensing (Gorman et al., 1998; White and El Asmar, 1999), and consequently may only achieve metre-level accuracy (Bayram et al., 2004).

1.1.3.3 Temporal Frequency

The temporal frequency of the monitoring will be dictated by the rate of deformation expected, and may be influenced by considerations relating to measurement precision. Firstly however, it is necessary to differentiate between episodic and continuous monitoring. Episodic monitoring involves repeated measurements, often at regular temporal intervals, but with a time-lag between successive monitoring epochs, whereas continuous monitoring normally involves high-frequency measurements, with the measuring instrument permanently located at the monitoring site. For example, monitoring of a landslide through airborne techniques such as photogrammetry or

airborne laser scanning may be carried out on a regular basis, or through the utilisation of irregular historical datasets, as demonstrated by Brückl et al. (2006), who compared photogrammetric DEMs from 1962 and 1996, to analyse the development of a landslide in Austria. Fraser and Riedel (2000) provide an example of continuous monitoring, for a study with a relatively short lifetime. This example demonstrates the utilisation of digital close-range photogrammetric techniques for monitoring the thermal deformation of steel beams, in order to validate the integrity of their mathematically-modelled behaviour. Due to the rapid change of state, measurements were carried out at 70 – 80 epochs over a period of two hours, as the beam cooled, essentially providing a continuous deformation time-series.

However, relatively slow displacement rates do not always translate to episodic measurements, as illustrated by continuous GPS monitoring techniques, which have become established as a standard means for analysis of long-term regional- and global-scale crustal deformations (Langbein and Bock, 2004). Here, processes often operate at the mm-level, and continuous monitoring can bring several advantages, as the identification and removal of daily and seasonal signals is often required, and a continuous deformation time-series may result in more meaningful analysis, given the restricted spatial sampling approach.

1.1.3.4 Spatial Resolution

Spatial resolution is closely associated with the selection of technique. A distinction can be made between discrete and continuous data. Discrete datasets concern measurements acquired at specific, isolated point locations, and generally relate to applications such as geodetic, geotechnical, and structural monitoring, where high levels of accuracy and precision may be a requirement. Furthermore, as the techniques employed may necessitate measurement at pre-defined locations, the use of continuous datasets is often not an option. Examples of discrete monitoring include the use of GPS for continuous monitoring of crustal deformation (as described above), and the monitoring of structures such as dams (Behr et al., 1998), and bridges (Lennartz-Johansen and Ellegaard, 2002; Roberts et al., 2005). In a similar vein, Puglisi et al. (2005) report on deformation monitoring of the volcanic island of Stromboli in Italy using a monitoring strategy comprised of a combination of automated Electronic Distance Measurement (EDM) and

GPS measurements at discrete point locations (Figure 1.4). Their results stress the usefulness of such an approach for real-time monitoring and early-warning of hazard, as well as for improved understanding of volcanic processes.

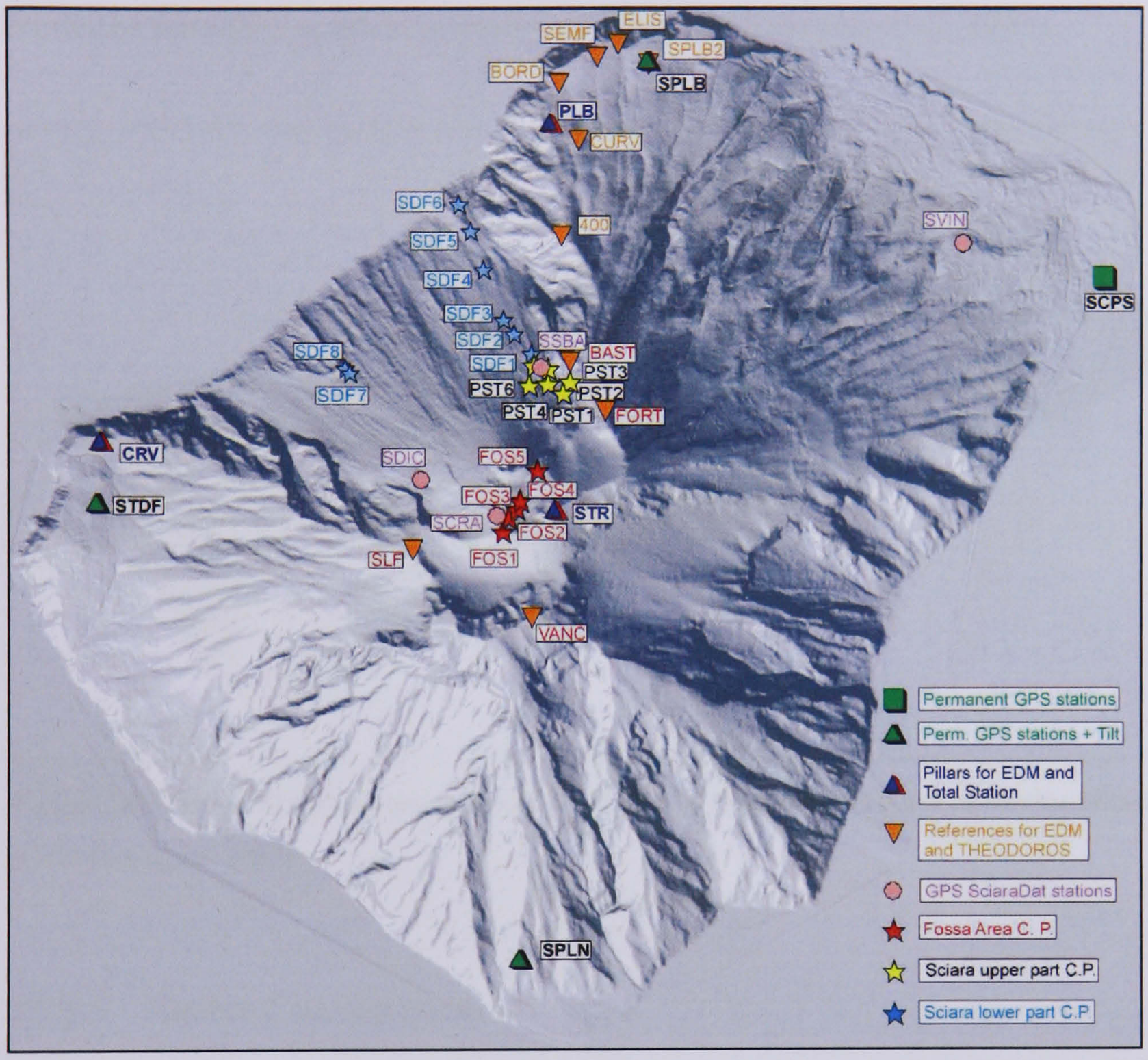

Figure 1.4 Example of discrete geodetic monitoring network on the volcanic island of Stromboli, Italy (Puglisi et al., 2005).

As an alternative, continuous datasets are able to offer several advantages, primarily in relation to the three-dimensional representation of surfaces through DEMs, or the use of imagery data, as acquired by satellite remote sensing systems. As noted by Lane et al. (1998), recent technological advances have allowed for DEMs to be acquired more easily, and via an increasing range of techniques. In particular, this relates to developments in digital photogrammetry, and techniques such as laser scanning and radar interferometry, which will be discussed more thoroughly in Chapter 2. While discrete point data may be more applicable for certain applications, it can be argued that continuous data is more suited to terrain monitoring, particularly where early-warning is not the first priority, and this approach is often implemented through episodic

monitoring campaigns. Continuous data enables advanced quantification and analysis of changes to terrain morphology in three dimensions, and over a range of scales (Dixon et al., 1998). Figure 1.5 shows an airborne laser scanning-derived digital elevation model (DEM) of a river environment, illustrating how subtle topographic undulations can be modelled through the use of a continuous dataset (Charlton et al., 2003).

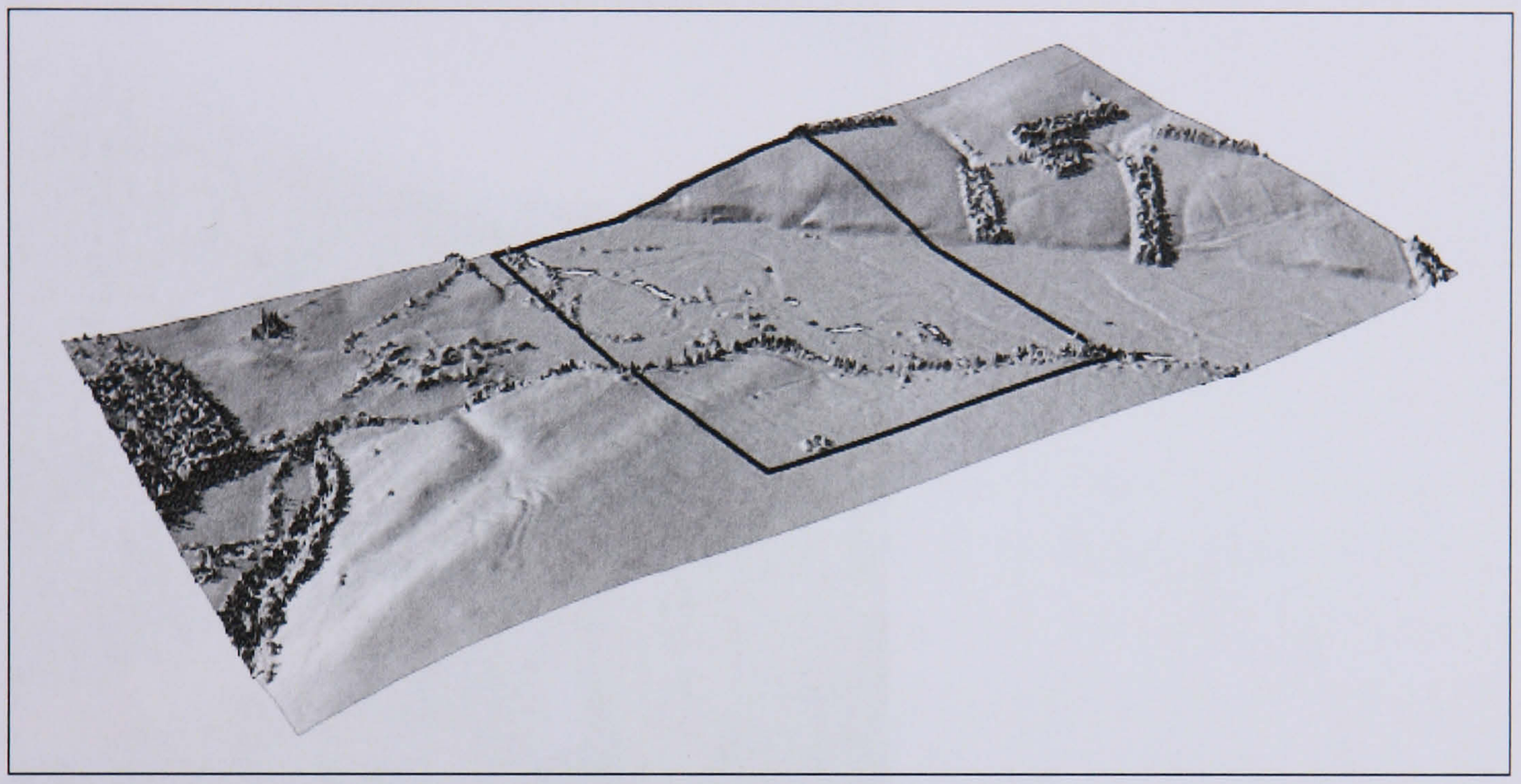

Figure 1.5 Airborne laser scanning-derived DEM of a river environment in Northumberland (Charlton et al., 2003).

1.1.3.5 Further Considerations

There are a range of additional considerations which must also be evaluated. The nature of the monitoring environment may place particular constraints upon the monitoring approach. For example in the study by Fraser and Riedel (2000) which was presented earlier in this section (photogrammetric monitoring of the thermal deformation of steel beams), the authors noted that photogrammetry was the most feasible option for the application in question, as the high temperature environment ruled out the use of a total station, and there was a requirement for all points to be measured instantaneously for each epoch. In addition, special ceramic targets had to be constructed to withstand temperatures exceeding 1100°C. In terms of the natural environment, numerous factors can complicate the monitoring strategy, including access to the site, and weather conditions. Time constraints may also exist, and in relation to this, some degree of automation may be required in order to ensure rapid delivery of monitoring data. This may relate to the highly automated acquisition of measurements, and also the processing

workflow. An example of this is provided by Leung (2003), who describes the development of an automated robotic total station system for real-time monitoring of slope displacements in Hong Kong (Figure 1.6). In this configuration, regular monitoring and autonomous data transfer enabled on-line analysis and notification when a pre-defined displacement threshold was exceeded.

Figure 1.6 Real-time monitoring of slope failure (inset) in Hong Kong (Leung, 2003).

Other considerations may be specific to the monitoring technique employed. For example, Saadatseresht et al. (2004) and Fraser (2001) discuss issues of network design in relation to close-range photogrammetry, noting the important influence of camera station geometry on the overall accuracy of the photogrammetric measurement process. Saadatseresht et al. (2004) highlight potential constraints in this regard, including those which are related to range, visibility, and accessibility, and hence are strongly influenced by the nature of the working environment. Saadatseresht et al. (2004) then go on to detail a method for enhancing network design through modelling of existing visibility weaknesses, promoting improved network design.

A major issue, which should not be overlooked, is the availability of resources, including access to equipment or data, the experience and availability of personnel, and perhaps most importantly, financial constraints. These details are discussed by Moore (2000), and must be thoroughly considered in order to select the most appropriate monitoring technique, and structure its successful implementation.

1.1.3.6 Monitoring in the Coastal Zone

The motivation for coastal geohazard monitoring has been outlined in Section 1.1.2, and general monitoring considerations have been discussed in the preceding section; however, given the unique nature of the coastal environment, it is necessary to devote further attention to geohazard monitoring in this particular context. The coastal zone presents certain challenges to the successful implementation of geohazard monitoring schemes. Both terrestrial and airborne monitoring techniques are affected by the dynamic nature of this environment; tidal conditions generally exert significant restrictions on the length of available, continuous survey time, and can prove especially problematic for airborne monitoring approaches (Pethick and Crooks, 2000), as it is generally desirable to capture data at low tide. Furthermore, in an actively eroding environment, the integrity of control points cannot be guaranteed over time, and in relation to this, coastal environments are often relatively featureless in terms of suitable control points for aerial photographic surveys (Dixon et al., 1998; Brown and Arbogast, 1999). Poor weather conditions are frequently associated with coastal regions, particularly in the UK, with high winds, poor visibility, and precipitation all contriving (often simultaneously) to hamper spaceborne, airborne and terrestrial monitoring efforts. Further difficulties may relate to access, which can prove impossible by vehicle, and even on foot may be difficult and dangerous, especially where steep cliffs are present, and when heavy, expensive equipment also has to be transported. In extreme cases, access for terrestrial surveys may prove impossible.

Historical datasets (usually maps and/or aerial photographs) can provide a valuable source of information on past geohazard behaviour and coastal change, and provide a useful context for present-day monitoring trends. The incorporation of such data is always desirable where available. Additionally, it often forms a necessary input for numerical modelling of future cliff evolution (Hall et al., 2002). However, an over-

reliance on historical datasets must be avoided. Due to uncertainties associated with climate change, the straightforward prediction of future coastal behaviour from the limited historical record (which can incorporate unrepresentative short-term variations) may prove inaccurate (Bray and Hooke, 1997). Moreover, it can be extremely difficult to quantify uncertainties associated with historical data sources (Thieler and Danforth, 1994a).

A long-standing issue in coastal zone monitoring and management worldwide, is the lack of standardisation in relation to the use of a common geospatial reference system, and the difficulty this poses for seamless integration of digital datasets (National Research Council, 2004a). This situation exists partly as a result of the traditional separation of topographic and bathymetric mapping activities. In the UK for instance, the Ordnance Survey (OS), in their role as providers of national topographic mapping, utilise mean sea level (Newlyn Datum) as the vertical reference frame, whereas the UK Hydrographic Office, with responsibility for bathymetric mapping, defines chart datum with respect to lowest astronomical tide (LAT) observations. At some coastal locations, this can result in a gap of as much as 6.5 m between datum levels (National Tidal & Sea Level Facility, 2006). Where coastal monitoring incorporates historical datasets, this situation is often exacerbated by a confusion of horizontal and vertical reference systems which must be reconciled to a common datum, projection, and scale before meaningful comparisons can be made (Camfield and Morang, 1996; Gorman et al., 1998; Moore, 2000).

A further concern is often the selection of a suitable reference feature from which shoreline change can be mapped. Again, this is an issue which has suffered from a lack of standardisation, with a number of different approaches employed. Historically, most attempts have concentrated on utilising a visibly-identifiable feature, which can be readily delineated from maps or photography. For this reason, traditionally the high water line (HWL) has been favoured (Figure 1.7). However, errors are introduced through the short-term fluctuation of the HWL due to seasonal and tidal variations, and difficulties in interpreting its exact location on aerial photographs (Camfield and Morang, 1996; Moore, 2000). Further uncertainty can arise from inaccuracies associated with early topographic mapping of the HWL (Gorman et al., 1998). However, alternative approaches, which have focussed more keenly on cliff processes as opposed

to general shoreline change, may have utilised the main cliff-top, or back-scar, as this is seen to provide a more relevant indicator of risk for management purposes (Bray and Hooke, 1997). Although the latter approach may provide a more reliable definition, Bray and Hooke (1997) go on to caution against the use of this as the sole datum, as changes to this may not be typical of the cliff-face as a whole.

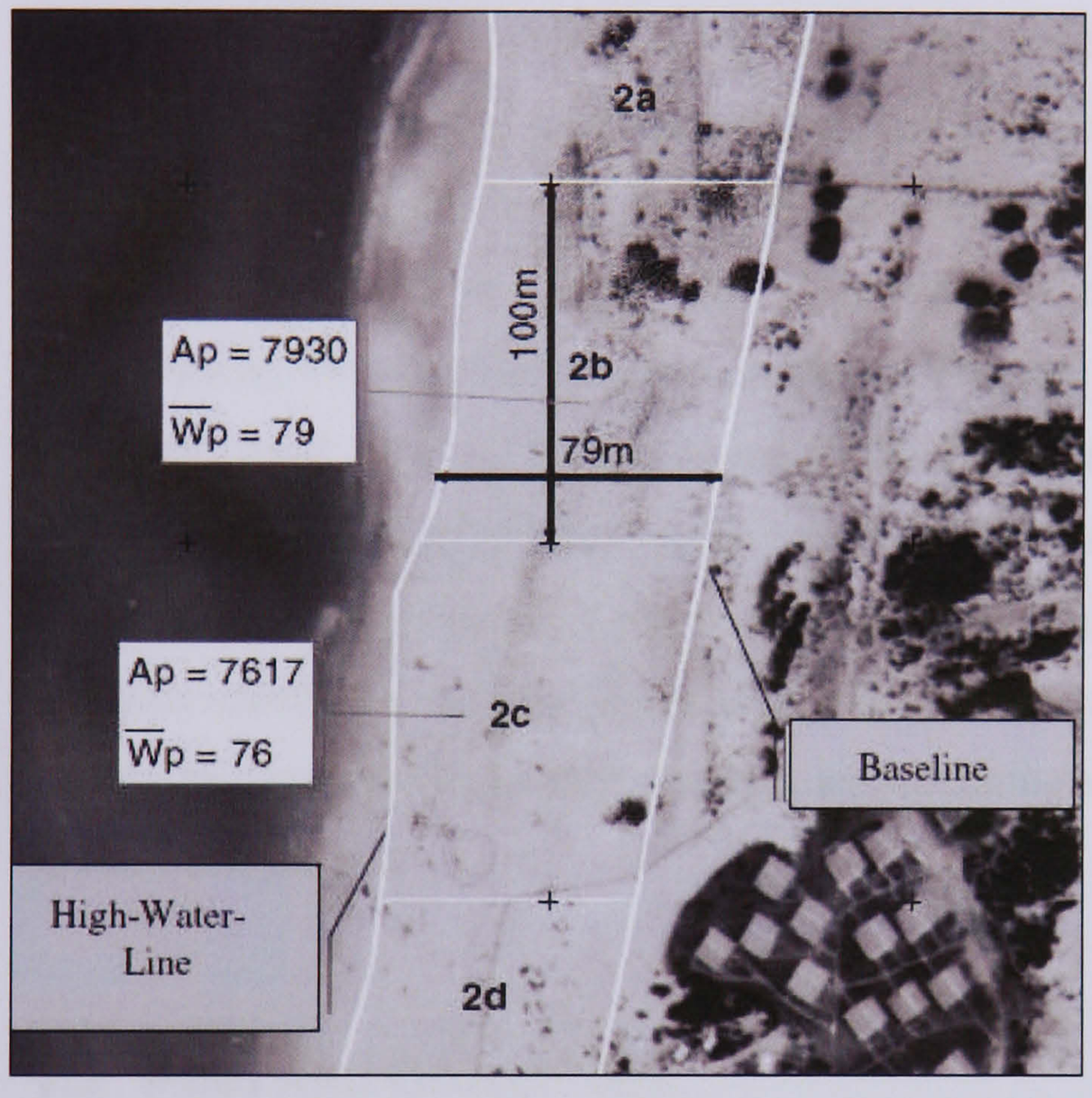

Figure 1.7 High water line, delineated from wet-dry sand boundary, indicating shoreline position on an aerial photograph (Klein and Lichter, 2006).

With respect to coastal geohazard monitoring, there are significant weaknesses in adopting such measures in isolation. While the use of erosion rates in relation to cliff-top retreat may provide an indication of short-term trends, and may offer a tangible measure for coastal planners, managers, and local residents (and in this sense they are certainly useful), they do not provide a reliable reflection of coastal geohazard activity, which generally acts across the cliff-face as a whole (Pethick, 1996). The mechanisms involved are important to understand, as these govern the nature and rate of retreat, and most approaches fail to treat the beach, cliff and shoreface as an integrated process system (Bray and Hooke, 1997). Therefore, provision of recession rates as the sole product of a monitoring strategy by-passes the opportunity to further understanding, particularly with the increasing availability of continuous (as opposed to discrete)

datasets, and their capability for high resolution quantification of geomorphological change.

Coastal change arises as the result of a complex interaction of systems which operate over a range of spatial and temporal scales, and so it is important to acknowledge that coastal geohazards cannot be considered as isolated processes, solely responsible for change. However, they do represent a significant mechanism for coastal evolution, and as Bitelli et al. (2004) note in relation to landslides in general, monitoring is a fundamental requirement for improved knowledge of potential spatial and temporal development. However, given the complex and dynamic nature of the coastal environment, the selection of an effective and efficient monitoring technique is far from straightforward, and is further complicated by issues relating to effective dataset registration, which affects both present-day and historical datasets. Coastal geohazard processes primarily operate at the micro- and meso-scale (as defined in Section 1.1.3.1), and thus monitoring at these levels is of greatest relevance in this research, subsequently influencing monitoring strategy design, and dictating issues of temporal frequency and spatial resolution.

1.2 Aims and Objectives

Section 1.1 has set the background for this research, detailing the motivations for coastal geohazard monitoring, and highlighting a number of important design-related monitoring considerations. In this context, this research aims to develop a strategy which improves the effectiveness of coastal geohazard monitoring, and in doing so, addresses the inadequacies of existing approaches, particularly in relation to issues of spatial and temporal resolution. Of particular importance is the critical and often troublesome dataset registration task, which is a fundamental pre-requisite for reliable and effective change detection. Ultimately, it is anticipated that this research will facilitate improved understanding of coastal geohazards, enabling more effective coastal management and planning. In order to achieve the above aim, a number of objectives have been identified:

- assess existing and emerging geomatics techniques, both in isolation and combination, in relation to suitability for coastal geohazard monitoring;

- develop a software-based solution, enabling the robust integration of multi-temporal, multi-sensor datasets in dynamic environments;
- implement and evaluate the monitoring strategy through application to coastal test sites, examining issues of accuracy, effectiveness and transferability;
- undertake quantitative assessment of coastal geohazard activity, and through this determine the potential of the monitoring strategy in relation to enhancing understanding of coastal geohazard processes.

1.3 Research Methodology

In order to evaluate current geomatics monitoring techniques, and their potential in relation to coastal geohazard monitoring, the first stage involved carrying out an extensive literature review. This exposed the relative strengths and weaknesses of existing and emerging approaches, and provided justification for the subsequent design and development of an integrated remote monitoring strategy. Following this, efforts were focussed on practical aspects, primarily involving the development of an existing least squares-based surface matching algorithm, in order to incorporate robust outlier handling capabilities, essential for the successful fusion of disparate datasets, contaminated by change. The robust algorithm was validated through experimental testing, involving the matching of artificial surfaces with simulated outlier effects. The integrated monitoring strategy was then applied to real-world test sites on the North Yorkshire coast, allowing rigorous assessment of the monitoring strategy, including evaluation of the component techniques, and the performance of the robust surface matching algorithm. This facilitated quantitative analysis of coastal geohazard activity over historical periods, and more recent time intervals.

1.4 Thesis Structure

This thesis is structured around seven chapters. Chapter One and Two are primarily literature-based, discussing the motivations for coastal geohazard monitoring, reviewing monitoring considerations, and assessing the suitability of existing and emerging geomatics techniques for coastal geohazard monitoring. Chapter Three and Four present the development of the monitoring methodology, while Chapter Five and Six provide a real-world implementation of the integrated remote monitoring strategy. In conclusion,

Chapter Seven presents a general discussion of the research outcomes and details suggestions for future work. The chapters can be summarised as follows:

- **Chapter One** introduces the motivation for coastal geohazard monitoring, and provides a definition of the issue. Following this, general monitoring considerations, including issues of scale and accuracy, temporal frequency, and spatial resolution are discussed. More specific concerns related to the coastal zone are then presented.
- **Chapter Two** presents a comprehensive literature review of geomatics techniques for coastal geohazard monitoring. Established and emerging techniques are considered, and for each technique, a general overview is presented, before considering suitability in relation to coastal geohazard monitoring. In conclusion, the value of an integrated monitoring approach is considered.
- **Chapter Three** details the monitoring methodology, providing an in-depth description of the individual components, and the motivations for selecting these. A detailed overview of DEMs is presented, in recognition of their fundamental importance in relation to the dataset integration technique developed in Chapter Four.
- **Chapter Four** provides an overview of surface matching as a dataset integration technique, highlighting the advantages of this in relation to coastal monitoring. The development of a robust least squares-based surface matching algorithm is then outlined in detail, with the results of experimental testing presented.
- **Chapter Five** describes the implementation of the integrated remote monitoring strategy to the soft-cliff test site of Filey Bay, North Yorkshire. The application of the robust matching algorithm for the reconciliation of disparate topographic datasets is detailed, with results validated. Quantitative analysis of geohazard activity is carried out.
- **Chapter Six** examines the transferability of the monitoring strategy through application to a hard rock test site located at Whitby East Cliff. The application of the robust matching algorithm for absolute orientation of multi-temporal DEMs is presented, and assessment of geohazard activity is carried out. Issues of transferability are highlighted.

- **Chapter Seven** revisits the research objectives, discussing the effectiveness of the monitoring strategy, with detailed examination of the specific components, including the dataset fusion technique. A number of recommendations for future work are presented.

1.5 SUMMARY

This chapter has introduced the research topic, providing an overview of coastal geohazards, and highlighting the requirement for effective monitoring. In the context of a globally increasing coastal population and uncertainties over future climate change, coastal geohazard monitoring is an issue which requires urgent attention. Focussing specifically on the UK, a number of examples of coastal change and cliff failure have been highlighted. Monetary implications and the impact upon natural and cultural heritage have been briefly considered. A recent shift in UK government policy away from hard defensive measures towards a longer-term, sustainable approach is evident.

A number of important considerations have been raised in relation to monitoring strategy design. These have examined issues of scale and accuracy, themes which are closely inter-linked, and temporal frequency, which is likely to be influenced by the anticipated magnitude of the processes under study. Spatial resolution has also been considered, and this is a factor which is often closely associated with the capabilities of the monitoring technique. A range of further considerations also exist, and many of these are related to the constraints of a particular site. This can include access restrictions, and time limitations dictated by the environment. Specific issues relating to coastal monitoring have also been discussed. Tidal conditions have been identified as exerting a significant limitation on the timing of survey work. Furthermore the dynamic nature of the coastal environment, both in relation to tides, and active geohazard processes, may threaten the short- and long-term integrity of control points. The potential of historical datasets has been emphasised, and it has been highlighted that the incorporation of such datasets is generally desirable wherever possible. The use of reference features, such as the high water line, for monitoring of shoreline change has been discussed. However, this suffers from drawbacks, due to seasonal fluctuations, and the difficulties associated with accurately identifying this feature. More importantly, the use of this approach to communicate erosion rates is generally undesirable, particularly

in cliffed coastal environments, as this fails to communicate the variability of geohazard activity across the cliff-face as a whole, and contributes little to improving understanding of the underlying processes.

The discussion presented in this chapter has specified the context for this research, and established the motivations. The review of key monitoring considerations has focussed attention on the requirements for this research. With this background, the closing sections of this chapter have outlined the research objectives and methodology. Chapter Two will provide an overview of established and emerging geomatics techniques, and review their suitability for purposes of coastal geohazard monitoring.

CHAPTER 2

GEOMATICS MONITORING TECHNIQUES

2.1 INTRODUCTION

Chapter One introduced the issue of coastal change, and the associated, influential phenomena of coastal geohazards, outlining the threat that these can pose, and consequently, highlighting the requirement for effective management of this issue, where appropriate. In addition, the concept of monitoring was introduced, and issues specific to implementation of this in the coastal arena were presented and discussed. However, there are a number of complex factors at play in this dynamic environment, confusing the selection of an appropriate monitoring approach. Therefore, it is necessary to undertake a comprehensive assessment of available techniques, and their suitability in relation to coastal monitoring. As Moore (2000) notes, due to the diverse motivations for monitoring of coastal evolution, and the variety of equipment, funds, and expertise of those involved, there is no standardised method for shoreline change monitoring. Accurate spatial referencing is fundamental to ensuring the success of most monitoring schemes, particularly where terrain change over time is a consideration (Cooper, 1998), and consequently geomatics techniques have an important role to play, given their capabilities for provision of metric information. This may simply relate to coordinating the location of geotechnical sensors, or may involve more direct application through the use of techniques such as photogrammetry and GPS (Lee and Clark, 2002). Moreover, Moore (2000) highlights that 'Erosion rates can only be as accurate as the data from which they are derived and the methods by which they are

calculated'. However, it is important to recognise that this may often involve a trade-off between accuracy and cost-effectiveness.

Since the inception of organised national mapping agencies in the late 18th and early 19th centuries, continuous technological advancement has seen the refinement of traditional techniques, and the introduction of a diverse range of new technologies and instruments, offering increasingly sophisticated capabilities, particularly in terms of output. The field of surveying and mapping has now broadened to encompass these new developments, some of which essentially provide the same fundamental services as were necessary in ancient times, and others which offer revolutionary new capabilities. This modern-day field of geomatics, makes available techniques with tremendous potential for a range of monitoring applications, and through advanced computational solutions, these techniques are now becoming more readily accessible to experts from other disciplines, such as geomorphology. While certainly a welcome trend, as Chandler (1999) emphasises, there is a need to ensure that the basic principles of such techniques are adequately appreciated by all who exploit them in pursuit of high quality metric information.

Chapter Two presents an examination of techniques – including a brief discussion of historical approaches -- which are applicable for coastal geohazard monitoring. Discussion here is primarily restricted to geomatics techniques, but for completeness, passing consideration is also given to geotechnical approaches, as these are extensively utilised in geohazard monitoring, often nowadays in combination with geomatics techniques. Considering the strengths and weaknesses of these various approaches, and the complex demands of the coastal arena, the merits of an integrated approach are also considered in conclusion.

2.1.1 Geotechnical Monitoring Techniques

Geotechnical monitoring techniques are of significance here in relation to their value in assessment of geohazards, such as landslide phenomena, and the emerging trend for integration with geomatics techniques. The range of potential applications and relevant instrumentation is long and diverse, and consequently, discussion here is restricted to those of relevance to geohazard monitoring. Although this work is concerned

specifically with coastal geohazards, often the monitoring practices differ little to those applied in more general slope-stability monitoring.

Geotechnical monitoring is the traditional approach employed by geotechnical engineers in order to examine and monitor ground deformation, and the processes contributing to this. This includes the use of a range of in-situ devices, such as piezometers for measurement of ground water; extensometers (Figure 2.1), and inclinometers for surface displacement measurements; and settlement cells for measurement of ground settlement. These sensors are often equipped with automated logging and data transfer capabilities, thus enabling continuous remote monitoring and early-warning of failure (Lee and Clark, 2002).

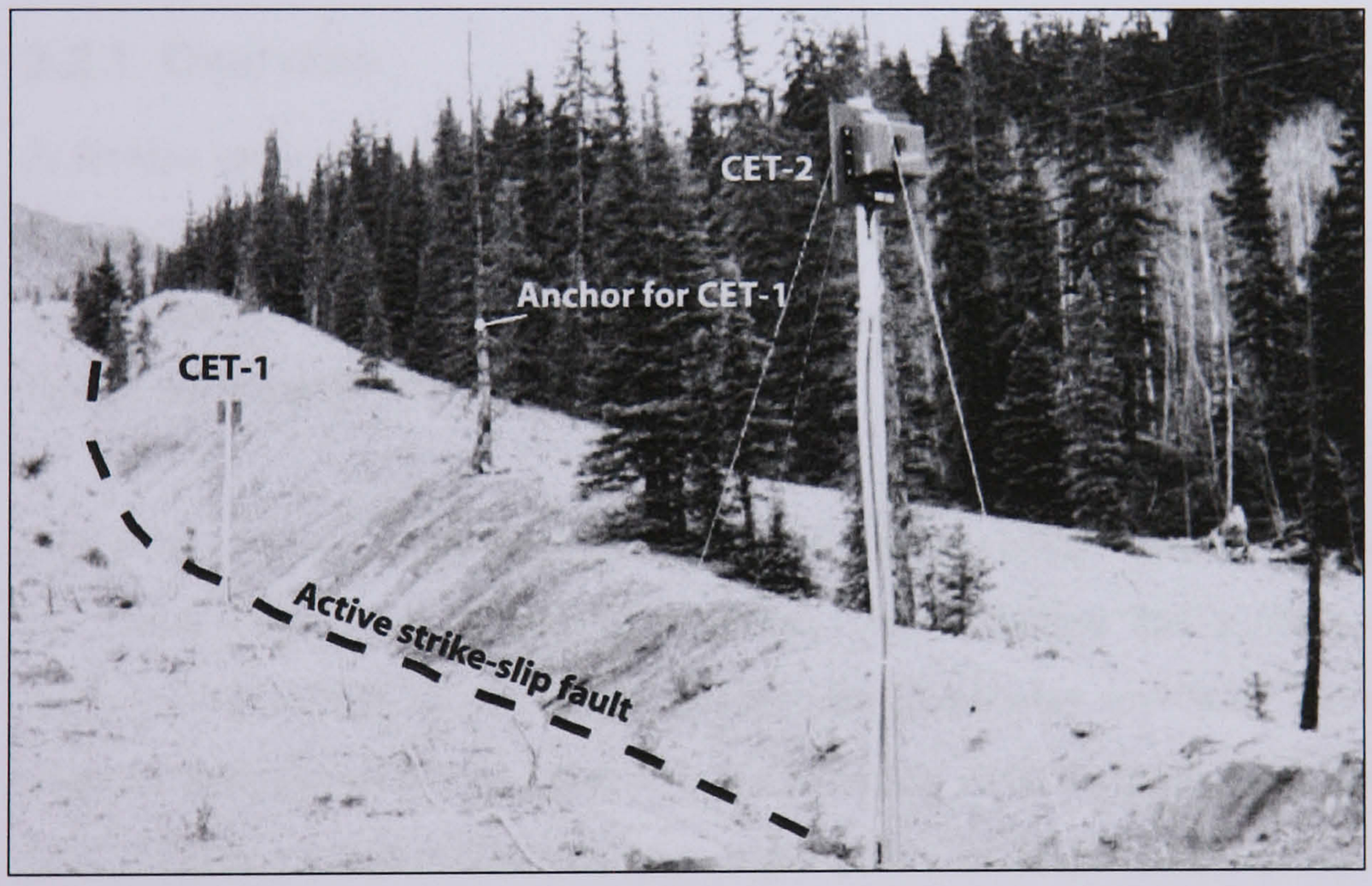

Figure 2.1 Wire extensometer for measuring displacement along a fault (Coe et al., 2003).

Geotechnical sensors can provide valuable and highly accurate information on rates and types of ground deformation, and it is important to note that such techniques may play an important role in assessing sub-surface processes. Lee and Clark (2002) provide the example of an inclinometer system specifically designed for measuring the rate of movement of landslides, and for detecting pre-cursor processes such as creep in coastal slopes. However, crucial to success is appropriate selection and distribution of the instruments (Angeli et al., 2000; Hill and Sippel, 2002). By their very nature, geotechnical sensors provide data which is limited in resolution to a selected number of

discrete locations. As a consequence, it can be difficult to interpret underlying behaviour patterns, particularly where the failure is extensive and/or complex (Petley et al., 2005). As a result of such difficulties, it is often therefore necessary to augment geotechnical datasets with information from a range of additional sensors, and as Hill and Sippel (2002) observe, 'The combination of sensors of various types provides the key to successful monitoring'. There are several well-documented examples of the use of geotechnical techniques alongside a range of geomatics techniques, such as GPS, automated total station measurement, and aerial photography, for deformation monitoring (Hill and Sippel, 2002; Coe et al., 2003; Corsini et al., 2005).

2.2 Basic Survey Approaches

2.2.1 Overview

A diverse range of approaches have been employed for geohazard monitoring over time. Those discussed here are essentially concerned with measurement of positional change and recession rates. These methods range in accuracy, but are all relatively straightforward in their approach.

One of the earliest, systematic examples of coastal change monitoring can be found on the Holderness coast of eastern England. This coastline has a extensive history of retreat, with the loss of 26 villages listed in the Domesday survey of 1086, reflecting the inland migration of the coastline by around 2 km over the past 1000 years (Lee et al., 2001). Pethick (1996) describes how, since 1957, the local authority has monitored this retreat through the use of 'erosion posts' - markers which were installed at 500 m intervals along 40 km of coastline, with measurements made between the posts and the cliff edge on an annual basis, thus enabling calculation of erosion rates (Figure 2.2). While Pethick (1996) acknowledges the unique value and foresight of this long-term monitoring campaign, he also highlights some of the drawbacks of such an approach:

- annual measurements fail to detail higher temporal frequency erosion events;
- the spatial resolution of the monitoring is limited;

- while measurements were initially designed to be coast-normal, non-uniform erosion may have altered local coastal orientation, thus introducing random error;
- only changes to cliff-top position are considered, which may not be representative of processes across the rest of the cliff-face.

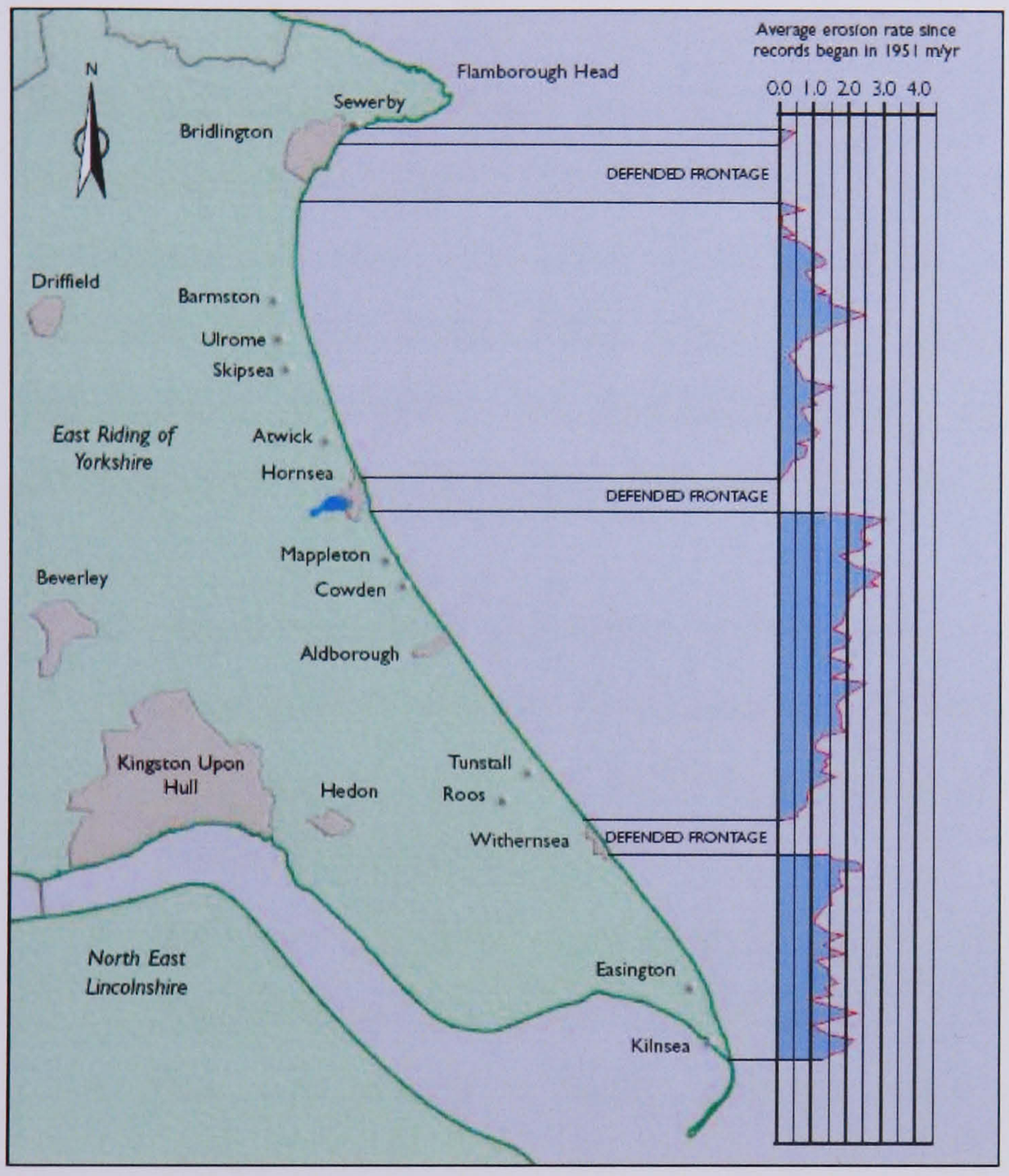

Figure 2.2 Holderness erosion rates, calculated from erosion post data (East Riding of Yorkshire Council, 2005).

Determination of a reliable historical recession rate is essential for prediction of future rates (Bray and Hooke, 1997). Historical rates can be derived from a number of sources, for instance, the erosion post measurements described above. However, this type of historical dataset is extremely rare. As Thieler and Danforth (1994a) remark, 'Maps and aerial photographs comprise the two basic sources of data used in historical shoreline change studies'. Increasingly, satellite datasets are also being utilised, but these typically offer only restricted snapshots of the last thirty years or so. The serious exploitation of metric information from aerial photography and satellite remote sensing will be considered more fully in Sections 2.4 and 2.7 respectively. Historical maps are

commonly used to extend the coastal change record beyond the era of stereo aerial photography (typically pre-World War II), with a number of researchers providing an overview of this data source, and its limitations (Thieler and Danforth, 1994a; Camfield and Morang, 1996; Moore, 2000), as will be discussed further in Section 2.2.2. An example of such an approach is presented by Robinson (2004), who utilised maps dating from 1804 in order to analyse shoreline changes in southern Jamaica.

Basic land survey techniques are traditionally one of the most commonly-employed methods for measurement of coastal terrain, and can take the form of occasional surveys in response to a major recession event, or systematic monitoring surveys, often at fixed locations (Lee and Clark, 2002). Despite the existence of more comprehensive and sophisticated approaches (as discussed in the remainder of this chapter), such techniques are still commonplace. This is perhaps due to the following factors:

- they require little investment in comparison to many of the more sophisticated measurement techniques which are discussed in the remainder of this chapter;
- they deliver a tangible and simple means of assessing change (even if not particularly appropriate);
- the historical legacy of their use is often difficult to overcome, particularly in organisations such as local authorities;
- they can provide a highly accurate means of verifying other techniques (although in this sense, they do not strictly fall into the context of monitoring).

Although some survey experience is desirable, with practice, the non-expert can quickly become relatively conversant with basic survey practices. Beach profiling methods are a typical example, often involving the use of a total station for measuring points along a pre-defined transect line, generally normal to the coast, with profiles spaced at regular intervals along the shore (Saye et al., 2005). With the use of control markers for orientation (located a safe distance inland from the eroding cliff edge), such profiles can be repeated at regular temporal intervals, thus enabling the evaluation of coastal change, and with time, the calculation of erosion rates. Simplified versions of this approach include taping and levelling. Komar (1998) reviews some techniques for measurement of beach profiles, including those extending into deep water. Some of these are more

advanced and novel than others, but most would now have to be regarded as of historical interest only.

2.2.2 Suitability for Coastal Monitoring

Historical datasets offer a means for addressing (to some extent) biases introduced by short-term events, and provide an indication of the significance of such events (Lee and Clark, 2002). However, there are a number of major issues associated with the utilisation of historical data, particularly concerning accuracy, and the quantification of error. Camfield and Morang (1996) and Moore (2000) highlight the complications associated with reconciling historical maps from a range of sources to a common projection, ellipsoid, and datum in order to enable direct comparison of coastline position. In relation to this, alterations to datums or projections can prove a source of error – for instance, when the OS County Series mapping was upgraded from county-based projections to the National Grid projection in the 1950s, positional inaccuracies propagated into subsequent map products; an issue which was not addressed in any concentrated manner until 2001. Camfield and Morang (1996) and Moore (2000) discuss further difficulties in relation to identification of suitable control points, and the introduction of errors through map shrinkage, and pen-line width. Satisfactory evaluation and quantification of such errors can be extremely challenging, and is often overlooked altogether (Thieler and Danforth, 1994a).

The primary drawback of basic survey approaches, such as profiling, is their limited spatial resolution, which severely restricts their usefulness in terms of understanding of the processes influencing coastal change and geohazard development. A further disadvantage is the labour-intensive nature of many basic techniques, and the requirement for prolonged direct contact with the survey environment, which can be a particular hindrance in the hazardous and dynamic coastal zone (Göpfert and Heipke, 2006). While such techniques may have formed the sole monitoring input in the past, ideally they are now best suited to act in supplement to the main monitoring effort, perhaps in order to maintain a historical record of change from particular reference points, or to provide accurate validation of more sophisticated techniques (Morton et al., 1993; Mills et al., 2003; Tarchi et al., 2003).

2.3 GNSS

2.3.1 Introduction

GNSS (Global Navigation Satellite Systems) is the umbrella term for satellite positioning systems. Formerly, discussion of this technology would have largely been confined to GPS, which for around the last fifteen years has been the only globally available, reliable satellite-based positioning system. However, the term GNSS has now been extensively adopted in order to reflect not only GPS, but also the anticipated rejuvenation of the Russian system GLONASS, and the soon-to-be-realised European venture, GALILEO. GPS is operated by the United States (US) military, and was declared fully operational for commercial use in 1995 (Misra and Enge, 2006). Although primarily designed for military purposes, its exploitation for a diverse range of non-military applications has seen continuing expansion ever since. GLONASS, also a military system, reached its full operational capability not long after GPS, but financial difficulties associated with the dissolution of the USSR led to an almost immediate degradation of capabilities. However, from 2001 onwards, the Russian government has committed towards continued investment, with a view to a return to reliable, global positioning (Polischuk and Revnivykh, 2004). The development of GALILEO, a joint initiative of the European Union and the European Space Agency, was motivated by the requirement for an independent European-controlled system, which was also fully interoperable with GPS (Trautenberg et al., 2004). It is anticipated that GALILEO will be fully operational by 2010. The potential integration of these GNSS systems over the coming years promises significant advances in terms of accuracy, robustness, and integrity of service (Misra and Enge, 2006).

It can be argued that no field has been revolutionised by GNSS technology more so than surveying, which has seen the introduction of a technique allowing for high-accuracy positioning, without the requirement for intervisibility between survey locations. GNSS techniques are now utilised for almost every aspect of modern-day surveying, and have become a standard control method. In this respect, GNSS technology is increasingly providing an alternative or complement to the basic land survey techniques outlined in Section 2.2.

2.3.2 Technological Overview

Discussion here will concentrate on GPS, as conceptually this is very similar to both GLONASS and GALILEO, and represents the current standard for satellite positioning. Classically, GPS is described as being composed of the space segment, the control segment, and the user segment. The *space segment* refers to aspects of the satellite constellation. Presently, this is composed of a nominal 24 satellites arranged in six, near-circular orbital planes, inclined at 55°. The satellites orbit at an altitude of about 20,200 km with a period of approximately twelve hours. This is designed to ensure optimal global coverage, with most users able to receive upwards of four satellites, assuming a clear sky-view. The GPS satellite signal transmits two L-band radio frequencies, and a navigation message, which are generated from a fundamental frequency. The L1 signal is modulated with the C/A-code, while the P-code is modulated on both L1 and L2. The codes are pseudo-random noise (PRN) sequences, which allow precise ranging measurements and also possess particular mathematical properties which enable satellites to transmit at the same frequencies without interference (Misra and Enge, 2006). In its encrypted form, the P-code is referred to as the Y-code. This encryption is referred to as anti-spoofing, and denies access to the P-code to all but authorised military users. Effectively, this means that civilian users are relegated to utilising only the C/A code. The final aspect of the satellite signal is the navigation message. The navigation message is a binary-coded signal which provides information on satellite health, ephemeris, clock bias parameters, and includes an almanac, providing low-precision orbital details of all satellites in the constellation (Leick, 2004).

The *control segment* is tasked with ensuring the maintenance and smooth performance of the system. As well as the master control station, there are also monitor stations and ground control stations distributed globally. The main functions of the control segment includes, the monitoring of satellite orbits; the monitoring and maintenance of satellite health; the maintenance of GPS time; the prediction of satellite emphemerides and clock parameters; and updating of the satellite navigation messages (Misra and Enge, 2006).

In considering the *user segment*, only civilian users are of relevance here. For non-survey related applications, position is often calculated by code pseudoranging,

whereby correlation of the satellite PRN code with an identical version generated in the receiver, allows for determination of signal travel time, and thus calculation of range. Measurements to four or more satellites enable the computation of unambiguous position. In surveying however, position is generally determined through the relative GPS technique, with measurements made using the L1 and L2 carrier waves, thereby allowing for higher precision positioning. Relative positioning allows for determination of the baseline vector between a reference receiver located at a known point, and the rover receiver located at the position to be determined (Hofmann-Wellenhof et al., 2001). Distance to the satellite is a function of the number of whole wavelengths, and the measured fractional phase portion. However, the number of whole cycles, commonly referred to as the integer ambiguity, is unknown. Relative GPS measurement attempts to resolve this all-important integer ambiguity through the execution of simultaneous observations at two locations, thus enabling phase differencing techniques to be employed in order to eliminate errors arising as a result of satellite and receiver clock biases, and time-dependant ambiguities. Subsequently, relative positioning, at cm-level accuracy is achievable through post-processing, under normal circumstances. Hofmann-Wellenhof et al. (2001) and Misra and Enge (2006) provide a comprehensive overview of the computational aspects of relative GPS positioning.

A number of differing surveying practices, such as static, rapid static, real time kinematic (RTK) and others, have been developed in order to maximise the potential of GPS for a range of requirements. The most accurate means of positioning is by static surveying, with post-processing of the observations. This would be applicable for geodetic purposes, where mm-level accuracy is required. A variation of this is the rapid static technique, whereby the rover receiver is static for a period of five minutes or so, and can then be moved on to the next position. This is often employed as a highly efficient means of establishing a control network. Kinematic GPS refers to a moving rover receiver, with a static reference station, with results produced either by post-processing, or in real-time – i.e. RTK, where differential corrections are transmitted from the reference station to the rover by means of a radio link. Kinematic GPS has become particularly useful for accurately positioning an aircraft in order to provide georeferencing information for photogrammetric, ALS, or other surveys. Misra and Enge (2006) provide an overview of current GPS surveying practices.

2.3.3 Accuracy Considerations

GPS is essentially a point positioning technique, and there are a large number of factors affecting the quality of an individual GPS position fix, with the main error sources summarised in Table 2-1. These error effects must be addressed through post-processing, or minimised through other means, such as the use of real-time differential corrections, in order to optimise positioning quality.

Source	**Potential Error**
Satellite clock model	2 m (rms)
Satellite ephemeris prediction	2 m (rms)
Ionospheric delay	2 - 90 m
Tropospheric delay	2.3 – 25.0 m
Multipath	0.5 – 1.0 cm ('clean' environment)
Receiver noise	1 – 2 mm (rms)

Table 2-1 Summary of potential error sources in GPS measurements (after Misra and Enge, 2006).

Additional external effects can influence the quality of GPS positioning. As a surveying technique, GPS is subject to the same requirements as traditional techniques in terms of centring and levelling the receiver over a station. Perhaps one of the most crucial elements of the GPS measurement process relates to the task of correctly measuring the antenna height, as a small error in this can propagate into a systematic height bias.

Good reconnaissance and planning is particularly important in optimising the quality of GPS observations, and there are a number of factors to be considered. Firstly, mission planning software should be utilised in order to determine if there are likely to be any windows of poor satellite coverage for the survey location. At least four satellites are required at all times to ensure determination of position, although normally up to eight or more may be visible at any one time. A closely related consideration is satellite geometry. Generally expressed in terms of DOP (Dilution of Precision), this is particularly important for achieving high quality results, especially in the case of kinematic or single-point positioning (Hofmann-Wellenhof et al., 2001). Both of these factors must be evaluated in terms of the survey location, as the presence of hills, trees, buildings or other obstacles may partly obscure portions of the sky, or cause issues associated with loss of signal lock and cycle slips. Although these considerations may seem laborious, and the error budget complex, the use of standardised off-the-shelf

processing software has made GPS an accessible and highly productive tool for even the most inexperienced of surveyors.

2.3.4 Suitability for Coastal Monitoring

Given the high accuracies achievable with GPS, this technique has seen much uptake for monitoring applications. There are also a number of additional factors influencing this trend. Previously, the use of traditional surveying methods for establishing control stations would have required line-of-sight observations. However, GPS overcomes this, in turn offering significant savings in terms of cost and labour. This is particularly useful for monitoring applications concerning natural features such as landslides, which are often located in remote, mountainous terrain. Furthermore, GPS is a true all-weather, 24-hour technique, making it suitable for both episodic and continuous monitoring applications.

Since its inception, GPS has been utilised in coastal monitoring not only for the purpose of simplifying control measurements, but also for more elaborate monitoring approaches generally utilising kinematic techniques (Morton et al., 1993; Baptista et al., 2002; Mitasova et al., 2004). Mills et al. (2005) describe the use of kinematic GPS in order to collect DEM data for monitoring of beach and cliff areas. In this approach, a GPS receiver was mounted on an all-terrain vehicle for beach surveys, and then fixed to a surveyor's detailing pole attached to a mountain-bike wheel for capturing cliff areas (Figure 2.3). A similar approach was adopted by Seymour et al. (2005), where, in addition to kinematic beach surveys, sub-aqueous surveys were also conducted, utilising a jet-ski equipped with GPS and an acoustic depth sounder (Figure 2.3). Although possible to utilise GPS in this manner to create a highly-accurate wireframe DEM, this can be a rather time-consuming approach, which must be justified by the application. In addition, this can be subject to drawbacks associated with the subsequent structure of the surface model, as noted by Buckley (2003), who highlighted triangulation issues associated with the presence of mass point clustering and long, thin triangles. Although not insurmountable, such difficulties require additional processing effort. One further issue which must be borne in mind with regards to GPS, is that this is not a truly remote technique, as direct contact with the survey environment is generally a requirement.

Figure 2.3 Kinematic GPS surveys of cliffs, left (Buckley et al., 2002) and the swash zone, right (Seymour et al., 2005).

The use of continuously-operating GPS for high-precision monitoring of structures, and natural phenomena such as crustal motion and volcanoes is well-established, and has been discussed in Chapter One. Recently, this form of monitoring has also been the subject of investigation for the study of slope instability in mountainous regions, such as the Alps, and this technique is potentially equally applicable to coastal geohazard monitoring, where slope stability is often a fundamental consideration in terms of cliff evolution. Through this approach, a network of continuously-operating GPS receivers can be deployed in order to provide a monitoring network across a landslide body, with reference points located elsewhere on stable ground. While Malet et al. (2002) notes that this approach allows for quantification of three-dimensional flow kinematics, and investigation of behavioural rhythms, most researchers have chosen to implement continuous GPS monitoring alongside episodic monitoring (Mora et al., 2003; Chadwick et al., 2005; Brückl et al., 2006), either through kinematic GPS, or airborne remote monitoring, and highlight that the real value of this technique lies in the provision of early-warning information. Continuous GPS monitoring will be discussed further in Section 7.4.3.1.

2.4 Photogrammetric Monitoring Techniques

2.4.1 Introduction

The first practical experiments into the use of photographs for topographic mapping took place in France in the mid-19th century, following the development of photography. As cameras and instrumentation evolved, and with the invention of the

aeroplane in 1902, photogrammetry became an established technique, to the extent that by the inter-war years, it had become the standard means for topographic mapping. With the advent of the computer age heralding continuous advancement in instrumentation, and increased efficiency in workflow and production, the relevance of photogrammetry as a core geomatics technique was sustained, and is further supported in present times by the increasing shift towards a complete end-to-end digital photogrammetric workflow. Photogrammetry lends itself to an immense diversity of applications beyond topographic mapping, and in this respect, the close range field should not be overlooked. Close range photogrammetry generally refers to applications where object distances are less than about 100 metres (Cooper and Robson, 2001), and applications are to be found in areas including archaeology, engineering, forestry, geology, forensics, oceanography, medicine and dentistry (Wolf and Dewitt, 2000).

At the core of metric photogrammetry lies the collinearity condition, where under ideal conditions, a ray of light passing through object point, camera perspective centre, and image point, will travel in a straight line. On a pair of overlapping photographs, light rays from an object travelling under such conditions will intersect in a manner which enables calculation of three-dimensional object space position from two-dimensional image space coordinates. However, this relationship is complicated by a number of factors, which leads to consideration of the classical photogrammetric stages of interior, relative, and absolute orientation.

Interior orientation is the process by which the camera geometry at time of exposure is recreated (Wolf and Dewitt, 2000). Central to interior orientation is the concept of camera calibration, which involves determination of the elements of interior orientation, the main ones being, the principal distance; the principal point of autocollimation; the fiducial origin; and the radial and decentring components of lens distortion. Camera calibration can be performed by a number of methods. For traditional metric frame mapping cameras, laboratory calibration is the norm. However, self-calibration is a popular method where non-metric cameras are concerned, and allows the recovery of interior orientation elements through the use of a least-squares bundle adjustment (Fryer, 2001).

Once interior orientation has been completed, an image coordinate system, determined through measurement of the fiducial marks and taking into account the camera geometry, will have been established. The next phase is *relative orientation*, which involves establishing the relative attitude and positional displacements between adjacent images at the time of exposure. Through analytical orientation, this is often done by fixing the orientation parameters of the left photo, and resolving the relative orientation parameters of the right photo through measurement of tie points in the imagery. A minimum of five corresponding points are required, but six tie points should enable an improved solution through the use of least squares. This is outlined further by (Wolf and Dewitt, 2000).

As a result of successful relative orientation, a model coordinate system will exist for each stereomodel. This may be useful in some circumstances, particularly perhaps in close range photogrammetry. However, for topographic mapping, and other applications concerning aerial photography, it is usually necessary to carry out *absolute orientation*. This allows the model coordinate system to be related to a ground system for derivation of useful measurements, which can be related to existing surveys. To achieve this, a three-dimensional conformal coordinate transformation can be implemented, requiring a minimum of two horizontal control points, and three vertical control points, for which coordinates are known in both model and ground systems (Wolf and Dewitt, 2000). Additional control points are normally utilised in order to provide redundancy, enabling the implementation of a least squares solution. Once solved, the transformation parameters can be applied to convert all model coordinates to the ground coordinate system, enabling progression towards the end photogrammetric product. This is described in some detail by McGlone (2004). Where more than one stereomodel exists, and the images are in strip and/or block formation, it is possible to apply *aerial triangulation*, a technique which has had a large contribution towards increasing the feasibility of photogrammetric mapping (Mikhail et al., 2001). In the semi-analytical approach, which stemmed from increased computational capabilities, simultaneous processing of multiple stereo-models is made possible, thus facilitating a reduction in ground survey effort, as control can be distributed throughout the block. A further extension of this approach is fully-analytical aerial triangulation, which can be implemented through the *bundle adjustment*. This maximises the benefits of modern computing power to enable simultaneous exterior (relative and absolute) orientation of

large blocks of photography, and is a technique which is heavily utilised in modern digital photogrammetric workstations.

2.4.2 Digital Photogrammetric Workstations

As previously implied, the development and progression of computing capabilities has had a direct impact on photogrammetric developments. In the analogue era, the photogrammetric workflow was reliant on bulky optical-mechanical instruments, requiring highly skilled operators. The introduction and integration of computers, heralded the arrival of the analytical era, allowing the enforcement of rigorous mathematical calculations via semi-analytical, and then fully-analytical approaches (Wolf and Dewitt, 2000). Today, the digital photogrammetric workstation (DPW) is common-place, demonstrating full implementation of analytical principles. DPWs offer a fully digital workflow, which although following the basic photogrammetric principles outlined in Section 2.4.1, offer increased levels of automation and efficiency (McGlone, 2004).

DPWs place particular demands on computing hardware, and although the cost of such a system far outstrips that of a standard computer workstation (particularly when photogrammetric software costs are considered), this approach is more economical and versatile than analytical photogrammetry (Wolf and Dewitt, 2000). DPWs handle imagery in purely digital form, with the input coming either from scanned film, or increasingly, from digital sensors – thus rendering the workflow entirely digital. Digital photogrammetry has enabled the automation of several key stages, including that of interior orientation, where pattern matching algorithms enable the automated location and measurement of camera fiducial marks to a high degree of accuracy (Lue, 1997). Such techniques can also be exploited at the relative orientation stage, where image matching is employed in order to identify corresponding tie points in overlapping images.

Digital elevation models (DEMs) form one of the key products of digital photogrammetry, and underpin another, the orthophoto. Central to DEM extraction, is the process of image matching, which has many applications throughout the digital photogrammetric workflow, including the pattern matching procedures mentioned

above. Image matching requires the accurate determination of conjugate points in overlapping images. This can be achieved by either area-based, feature-based, or hybrid matching techniques (Wolf and Dewitt, 2000). Image matching has revolutionised photogrammetry, particularly in terms of efficiency, automation, and the range of possible outputs. By matching and retrieving the image coordinates of regularly or irregularly distributed points in the left and right images, collinearity equations can be written for each location, and corresponding three-dimensional ground coordinates computed, thus allowing the creation of a DEM. Perhaps the most valuable digital photogrammetric product is the orthophoto – i.e. orthorectified imagery exhibiting the geometric properties of a map. This can be produced as a matter of routine by a DPW, through application of the collinearity condition to calculate necessary photo-coordinates of each DEM point, which are then converted to a regular array, and resampled to produce suitable grey level values (Wolf and Dewitt, 2000). The orthophoto is of potential use in a wide range of applications, from straightforward feature extraction and mapping in the DPW environment, to its many uses within a Geographical Information System (GIS), or on the Web. DPWs typically offer many digital outputs, including 'fly-throughs', perspective views, line-of-sight analysis, and others, with applications in visualisation, environmental impact assessment, military reconnaissance, and many more.

2.4.3 Accuracy Considerations

The accuracy of measurements derived from digital photogrammetry is influenced by a number of factors, some of which are related to the nature of the photography, some which relate to external factors, and yet more, which are associated with the quality of processing carried out.

In additional to the obvious considerations, such as the use of a calibrated camera with a high quality lens, Wolf and Dewitt (2000) highlight that wide or super-wide angle photography is generally preferable for quantitative measurement, in order to ensure a high base-height ratio (b/H). Large b/H ratios indicate low flying heights and large x-parallaxes, promoting higher accuracy (Wolf and Dewitt, 2000). In this respect, flying height, focal length, and airbase all require consideration when planning a photogrammetric survey, particularly in respect to scale, resolution, and desired

accuracies. If images are acquired on film, then digitisation is necessary, preferably with a photogrammetric-quality scanner. These variables can be utilised to determine the expected heighting precision, σ_h, of subsequent photogrammetric measurements, through the following equation (after Kraus, 2000):

$$\sigma_h = \frac{H}{f} \times \frac{H}{b} \times \sigma_P$$

Eqn. 2-1

Where H is the flying height above ground level, f is the calibrated focal length of the camera, b is the airbase (the displacement between the exposure stations), and σ_P is the measurement precision of the photogrammetric instrument. This equation is applied in Sections 5.4.2.1 and 6.3.2.2 for evaluation of the photogrammetric datasets acquired for this research.

The quality of processing in the DPW is another factor affecting overall accuracy. The success in accurately modelling the behaviour of light passing into the camera will depend partly on the quality of the camera calibration, and also on the quality of the interior orientation procedure. Errors introduced at this stage will propagate into subsequent stages, in turn influencing the success of relative orientation, and absolute orientation. Poor ground control geometry, as well as accuracy, in both the terrain coordinates, and the performance of the operator in locating the corresponding imaged points, will influence the absolution orientation. Although on-board position and orientation systems now present opportunities for the direct orientation of imagery, a recent study by Mills et al. (2006) concluded that in order to achieve expected levels of accuracy, there is currently still a requirement for the inclusion of ground control points.

In consideration of a DEM product, as well as positional errors introduced through the processing issues detailed above, further degradation can result due to the effects of occlusions, and image matching difficulties in shadow regions, or featureless expanses such as beaches and glaciers (Hapke and Richmond, 2000; Baltsavias et al., 2001; Buckley, 2003; Würländer et al., 2004). Such effects can lead to the introduction of blunders. Additional considerations relate to DEM-specific issues. For example, a grid-based DEM is recognised as being susceptible to error, as it forces measurements to be

made in areas prone to the type of problems mentioned above, thus leading to the interpolation of unreliable points, and systematic errors. DEM-specific issues are discussed further in Section 3.4.

2.4.4 Suitability for Coastal Monitoring

Aerial photography has, for several decades, been one of the most heavily utilised techniques in monitoring of coastal change worldwide (El-Ashry and Wanless, 1967; Thieler and Danforth, 1994a; Moore, 2000). This is primarily due to the ready archive of vertical aerial photography, which for many locations stretches back to the World War II era. Not only does this resource offer provision of metric information, but the inherent imagery content presents an unrivalled opportunity for interpretation of landscape change, and this asset remains one of the core advantages of photogrammetry. The following benefits can also be identified:

- rapid acquisition of extensive tracts of coastal terrain is possible;
- the photogrammetric workflow, and issues of standards are well-established (Baltsavias, 1999b);
- photogrammetry has become increasingly accessible to the non-specialist, given the introduction of digital photogrammetry (Chandler, 1999).

However, photogrammetry is not without its drawbacks, which can often be exacerbated in coastal regions. Specifically, photogrammetry is particularly sensitive to poor weather, and cloud cover in particular, which by unfortunate coincidence can often be a feature of coastal regions, particularly in the UK. In relation to this point, photogrammetry is not well suited to provision of rapid response surveys in reaction to major storm events or similar. Another feature of coastal regions which is unfavourable to photogrammetry is the homogeneous nature of land cover types, which can result in poor image texture, as was discussed in Section 2.4.3.

Nevertheless, photogrammetry remains a popular coastal monitoring tool, and has been widely utilised to this end for some time (e.g. Thieler and Danforth, 1994a; Smith and Waldram, 1996; Brown and Arbogast, 1999; Hapke and Richmond, 2000; Moore, 2000; Moore and Griggs, 2002; Mills et al., 2005). Dornbusch et al. (2005) present an

interesting example of the use of digital photogrammetric techniques to measure the erosion of a shore platform on the south coast of England, and report the reliable detection of vertical changes less than 0.2 m in magnitude (Figure 2.4). Although not a coastal example, useful parallels can be drawn from Casson et al. (2003), who detail photogrammetric analysis of a landslide in eastern France between 1983 and 1999, allowing for the extraction of displacement rates over this period. In addition, it is worth mentioning the special case of close range photogrammetry, which has also been the subject of coastal monitoring research (Adams et al., 2003; Gulyaev and Buckeridge, 2004; Lim et al., 2005). This allows for terrestrial measurement from the beach or shore-platform in order to image a selected section of coast, and consequently, differs markedly from the airborne case, in that it allows for higher resolution monitoring, particularly suited to more vertical sections of cliff, but conversely, is restricted to much smaller spatial extents.

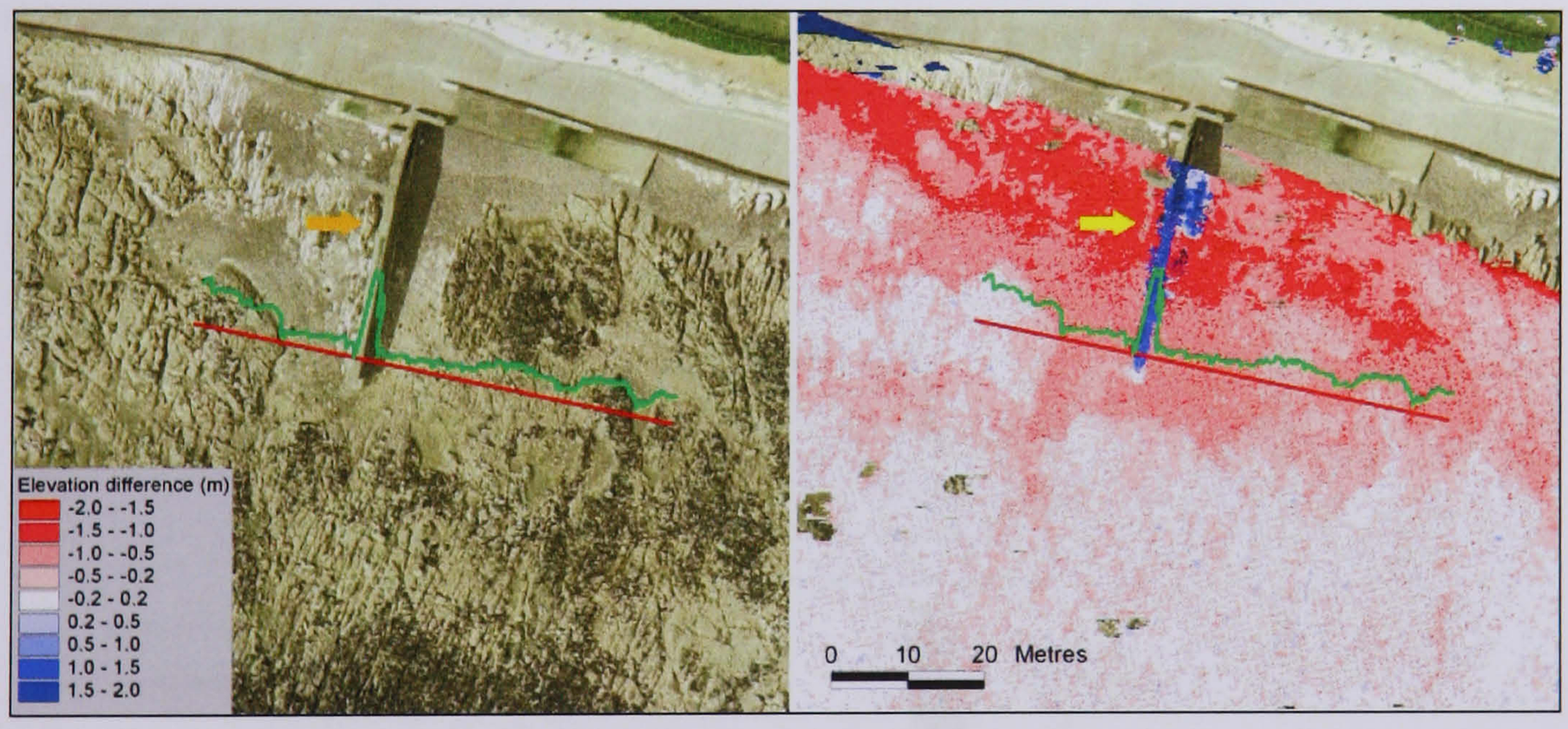

Figure 2.4 Photogrammetric monitoring of shore platform changes (Dornbusch et al., 2005).

2.5 Airborne Laser Scanning

2.5.1 Introduction

Airborne laser scanning (ALS), also commonly termed LiDAR (*Li*ght *D*etection *A*nd *R*anging) in the commercial sector, is an active sensing technique which utilises a laser ranging mechanism to rapidly scan the terrain from either a fixed, or rotary wing aircraft. In this manner, it is possible to rapidly construct dense and accurate digital topographic models (Flood, 2001). Although ALS did not become a commercial reality

until the mid-1990s, its development can be traced back to the 1970s and early 1980s, with particular regards to experimental NASA ventures (Ackermann, 1999; Flood, 2001). The development of ALS has largely been technology-driven, initially governed by the availability of pulsed laser technology, then, and perhaps more crucially, the reality of accurate positioning was realised through GPS, thus enabling accurate reference of laser measurements to an external coordinate system (Ackermann, 1999). From the mid-1990s onwards, commercial exploitation gathered pace – a trend which is continuing in present-times alongside technological advancements, which are enabling the utilisation of this technique for an increasing range of applications.

2.5.2 Technological Overview

A typical ALS system is illustrated in Figure 2.5, and is composed of three primary components: (i) laser ranging unit; (ii) scanning mechanism; and (iii) position and orientation system. The *laser ranging unit* consists of the emitting laser source and the electro-optical receiver (Wehr and Lohr, 1999).

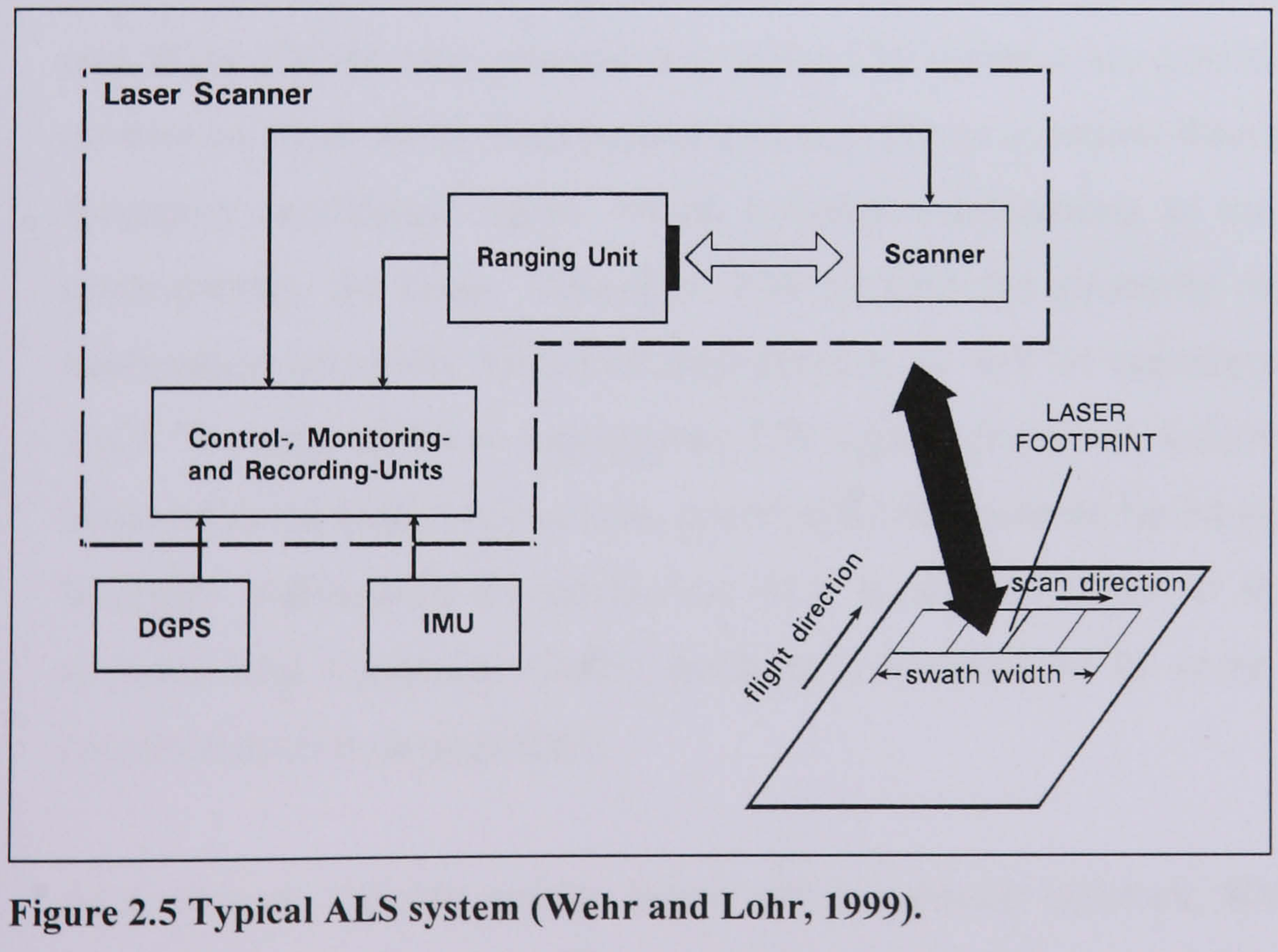

Figure 2.5 Typical ALS system (Wehr and Lohr, 1999).

ALS systems generally utilise either a pulsed laser or a continuous-wave (CW) laser, both ultimately determining position through the principle of ranging (hence why ALS is sometimes referred to as airborne laser ranging). However, these two systems differ in the manner by which range is determined. CW systems can be modulated with a

sinusoidal signal (Wehr and Lohr, 1999), allowing signal travel time to be calculated by the phase difference between transmitted and received signals, which in turn allows for calculation of range. This approach is also referred to as phase comparison. However, most ALS systems currently work on the pulsed laser principle, commonly referred to as time-of-flight ranging. This allows for the output of a very powerful, collimated signal, over very short time intervals, and with high pulse repetition rates – highly suitable characteristics for range imaging (Wehr and Lohr, 1999). Through this approach, range is measured as a function of the time lag between transmitted and received signals, and in its most basic form, can be described by the following:

$$R = \frac{1}{2}ct$$

Eqn. 2-2

Where, R is the range from the laser source to the target; $c = 3 \times 10^8 ms^{-1}$, the velocity of light travelling in a vacuum; and t is the time delay between transmitted and received pulses, as measured by a time interval counter. The reasons for the almost total dominance of pulsed ranging techniques in ALS is discussed in some depth by Thiel and Wehr (2004), who observe that while CW systems are capable of attaining higher accuracies more easily than pulsed systems, this is achieved through the use of a high frequency modulated signal, which introduces limitations to the power output, and consequently, the range. Therefore, CW systems are generally restricted to relatively short-range, primarily terrestrial applications, as will be considered briefly in Section 2.6.2. The only airborne topographic CW system for which information can be readily obtained is the ScaLARS system, operated by the Institute for Navigation, University of Stuttgart. Subsequent discussion on ALS generally relates to time-of-flight ranging systems, and Lemmens (2007) presents a comparison of some of the mainstream sensors currently in operation.

ALS systems largely utilise lasers which operate between 800 nm and 1600 nm. Systems offering longer ranging capabilities (e.g. greater than 1500 m) make use of the upper end of this wavelength spread, as they require the implementation of higher powered pulses which are only eye-safe at these longer wavelengths (Wehr and Lohr, 1999). The reflection characteristics of the laser must also be considered, as different

wavelengths interact differently with the terrain. As Wehr and Lohr (1999) note, a laser of wavelength 1535 nm would be a poor choice for measurement of glacial surfaces, as reflectance from ice and snow at such wavelengths is weak; in this case, an 810 nm laser system would be more suitable. This consideration is closely related to intensity of the returned signal, which is often provided to the end-user as an attribute for each laser range. While intensity information can provide an 'image' of the scanned terrain, this is often rather coarse in resolution.

The *scanning mechanism* exerts an important influence on the structure of the raw point cloud, and naturally, is a crucially important element of any ALS system. Common mechanisms include, the oscillating mirror (producing a zigzag line pattern); Palmer scan (elliptical pattern); fibre scanner (parallel line scan); and rotating polygon (parallel line pattern) (Wehr and Lohr, 1999). Alongside scan pattern, pulse repetition rate, flying height, flying speed (and in relation to these), laser footprint size and swath width, influence the resultant point distribution and density, and such aspects must be carefully evaluated during survey planning. Typically, ALS surveys are acquired in relatively long, narrow strips, with adjacent, overlapping strips flown to build up areal coverage.

The *position and orientation system* (POS), is primarily composed of kinematic differential GPS and an inertial measurement unit (IMU), and together with navigational software, is often referred to as an INS (Inertial Navigation System). The POS facilitates georeferencing of laser ranges to an external reference frame, and requires the precise synchronisation of the laser instrument, GPS, and IMU in both time and space (Wehr and Lohr, 1999). The quality of the POS solution exerts an important influence on the overall quality of the ALS measurements, as is discussed further in Section 2.5.4. Detailed treatment of ALS fundamentals can be found in Wehr and Lohr (1999) and Baltsavias (1999a).

An evolving aspect of ALS technological development relates to processing and analysis of the returned signal. While systems offering multiple return echoes for a single laser pulse – typically first and last returns – are commonplace (Hug et al., 2004; Jutzi and Stilla, 2006), recent advances have focussed on high frequency digital sampling of the returned analogue waveform in order to fully characterise each pulse (Gutierrez et al., 2005). This process is known as waveform digitising, and although not

a new concept, its implementation to date has generally been restricted to experimental and research situations. However, recent advances in processing power and storage capacity, have brought about the commercial realisation of waveform digitising (Hug et al., 2004). Waveform digitising offers several advantages over the discrete echo based approach. It overcomes the issue of ambiguity in the pulse detection algorithms implemented by individual manufacturers, and the associated accuracy concerns (Hug et al., 2004). Additionally, detailed characterisation of complex targets is made possible (Hug et al., 2004; Gutierrez et al., 2005; Persson et al., 2005), and consequently, this technique is causing particular excitement in the forestry and vegetation research communities. This is illustrated in Figure 2.6, which shows detailed structural characterisation of objects including trees and buildings.

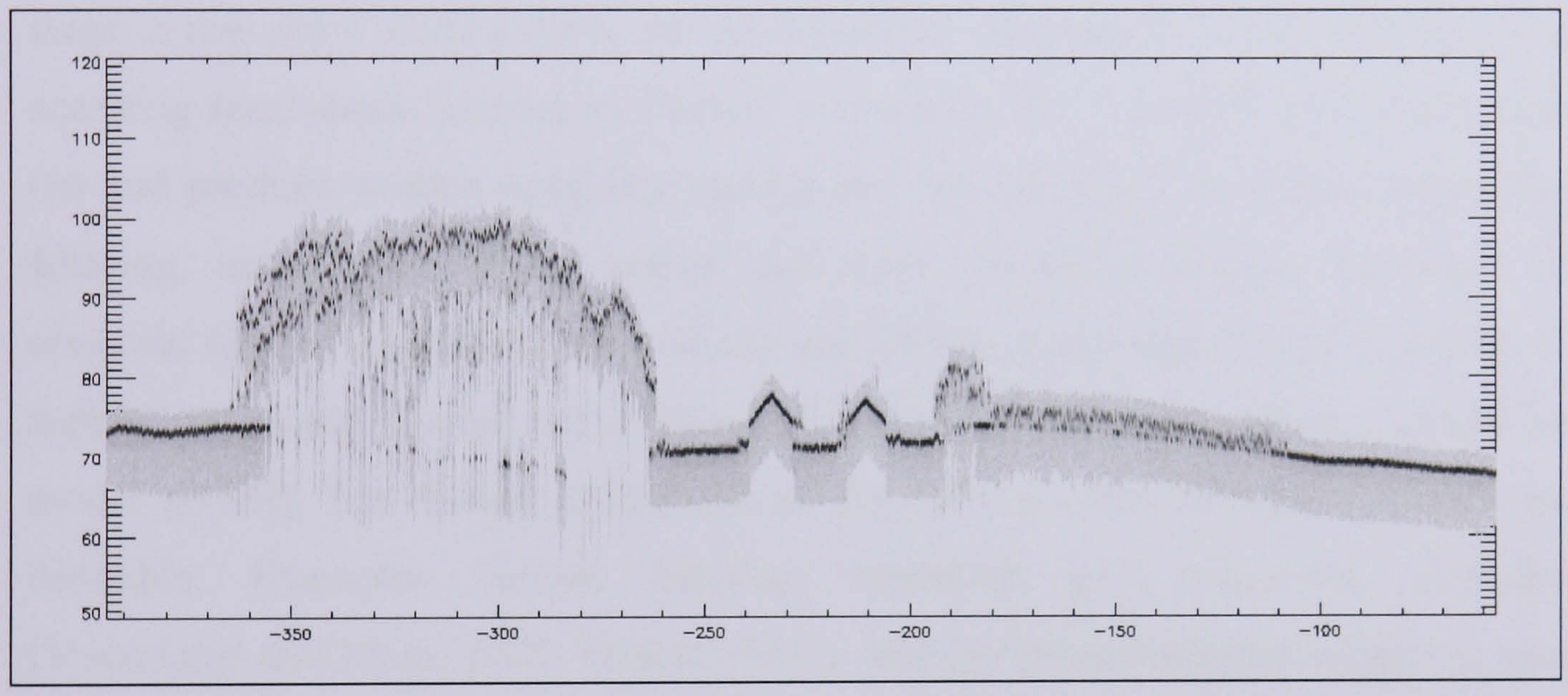

Figure 2.6 Profile through waveform digitised dataset, with grey level indicating signal amplitude (Hug et al., 2004).

2.5.3 Terrain Reconstruction

Whereas photogrammetry is traditionally based upon perspective geometry, ALS systems are reliant on polar geometry (Baltsavias, 1999b), resulting in conceptually simpler georeferencing and terrain reconstruction. During post-mission processing, data can be georeferenced through combination of the laser ranges and instantaneous scan angles with calibration and POS data. Skaloud and Lichti (2006) define ALS calibration as relating to two aspects, these being:

- the calibration of individual sensors, particularly the laser ranging unit;

- the calibration of system-specific configuration parameters, namely the relative orientations of the laser, GPS and IMU sensors (bore-sight parameters), and the spatial offsets between these same sensors (lever-arm parameters).

Calibration is often carried out through a combination of ground- and flight-based procedures (Skaloud and Lichti, 2006). In commercial systems, in-flight calibration is often carried out by flying cross-strips over test fields, which are usually flat, and offer good reflectivity. The relative discrepancies between overlapping strips enables the determination of bore-sight calibration values (Wehr and Lohr, 1999).

Georeferencing will initially lead to World Geodetic System 1984 (WGS-84) coordinates, which can then be transformed as required to a local projection. At this stage, a raw point cloud results, the configuration of which is largely dependant on the scanning mechanism employed. Further processing, the nature of which is dictated by the end-product, is then normally carried out. This is likely to include some form of filtering, usually to remove spikes and other erroneous returns. Axelsson (1999) observes that in most cases, one of the most basic processing functions relates to the separation of non-ground points from the DEM in order to produce a digital terrain model (DTM). For further refinement of the dataset, other filtering routines may be desirable. Examples include building extraction and vegetation classification (Vosselman and Maas, 2001; Sithole, 2005), and algorithms tailored to specific markets, such as classification of powerlines (Axelsson, 1999). Due to the size of ALS datasets, and the limitations of generic commercial software packages, thinning, such as interpolation to a gridded DEM, is often necessary (Wehr and Lohr, 1999; Smith et al., 2003).

ALS has proved useful in a wide range of applications, including forestry (Lim et al., 2003); corridor mapping (Tao and Hu, 2002; Akel et al., 2005); river and floodplain mapping (Charlton et al., 2003; French, 2003; Thoma et al., 2005; Lohani et al., 2006); geohazard monitoring (Hudnut et al., 2002; Conforti, 2004; McKean and Roering, 2004; Scaioni et al., 2004); building extraction (Haala and Brenner, 1999; Zhou et al., 2004); and glacial monitoring (Würländer et al., 2004; James et al., 2006). A major application of ALS relates to bathymetry, with several bathymetric ALS systems capable of both

topographic and bathymetric measurements, in operation (Irish and Lillycrop, 1999; Wozencraft and Lillycrop, 2002).

2.5.4 Accuracy Considerations

Error sources in ALS datasets are complex and numerous. Filin (2005) and Katzenbeisser (2003) identify the primary system-related error sources as:

- Laser range error, which can be caused by system electrical biases and atmospheric conditions;
- Beam deflection errors, due to mechanical misalignment or electrical biases;
- Mounting bias, which can be due to in-flight laser – INS bore-sight instability;
- IMU errors;
- GPS errors.

The first three error types can be minimised through rigorous system design (Katzenbeisser, 2003) and calibration – although they cannot be completely eliminated. Issues of system calibration continue to attract much attention and debate, as there are no standard procedures in place, and current practices are widely acknowledged as being sub-optimal (Flood, 2001; Schenk, 2001; Skaloud and Lichti, 2006). Figure 2.7 illustrates data artefacts arising as the result of improper system calibration.

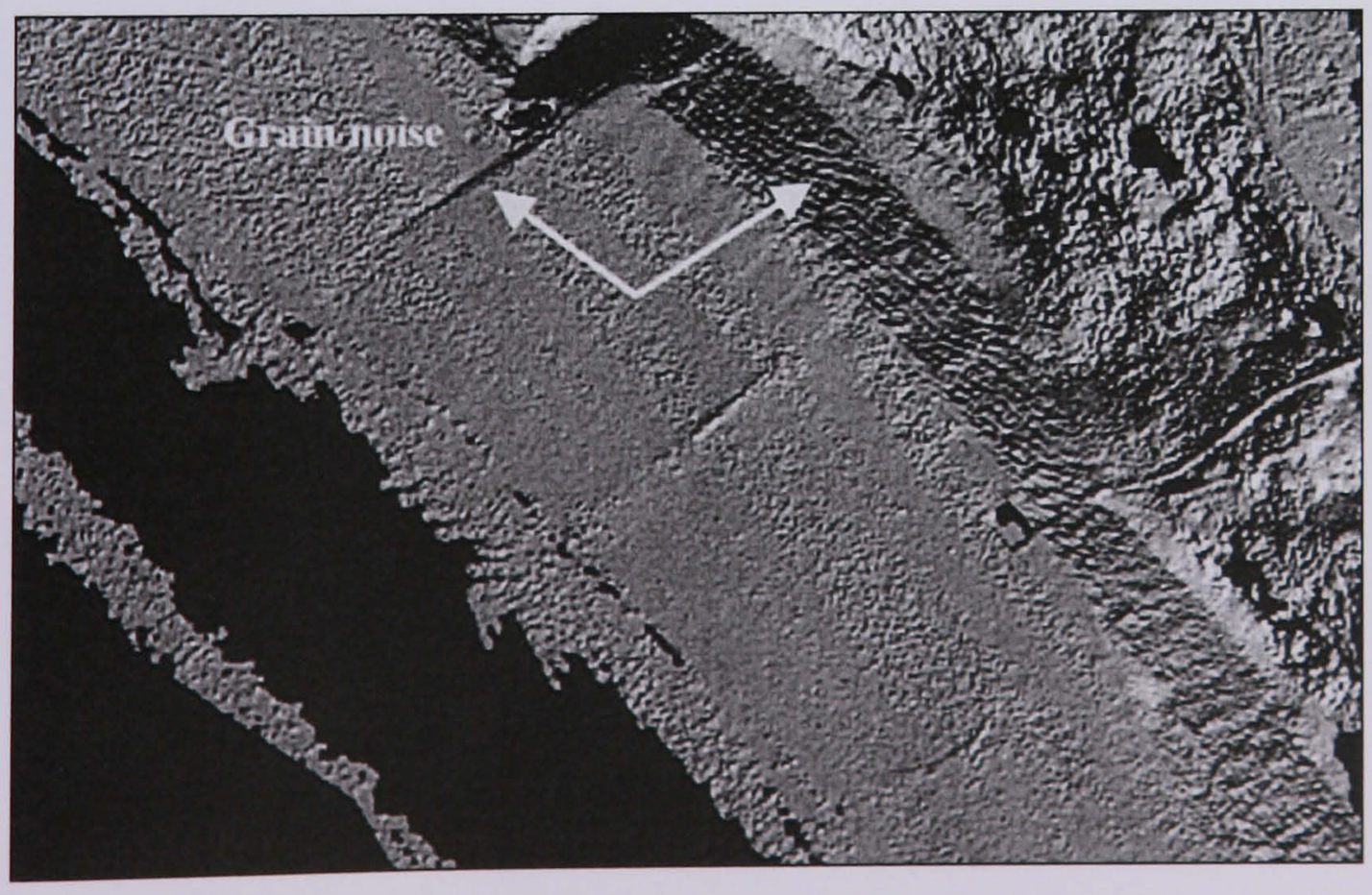

Figure 2.7 So-called 'grain noise' and other artefacts (indicated by arrows) arising due to improper system calibration, in what should be a smooth beach area (Huising and Gomes Pereira, 1998).

GPS and IMU errors have a major influence on the overall error budget, (Maas, 2002), and are often manifest in the form of systematic shifts, tilts, and vertical offsets, which can affect the strip for several kilometres (Crombaghs et al., 2002). IMU errors are dependant on a number of factors, including hardware quality, post-processing methodology, and integration with GPS (Baltsavias, 1999a). GPS-specific issues include satellite constellation geometry, distribution of GPS base stations, and quality of post-processing. Although vertical discrepancies are often most noticeable, particularly in strip overlap areas, Filin (2005) has shown that planimetric errors are equally, if not more, significant, and as such, any error recovery approach must treat this as a three-dimensional problem.

Issues of ALS accuracy have been examined by a number of researchers, and from several different perspectives. Filin and Vosselman (2004) describe most approaches as being either system-driven, whereby efforts are made to recover the main error components based on, and with knowledge of, the system design, or data-driven, where overlapping laser strips are transformed in order to remove systematic effects (e.g. the application of least squares based strip matching by Maas (2002)).

In addition, errors in the final ALS DEM are also attributable to factors associated with terrain characteristics and processing methodology. There is also a great deal of variation in the reflectance characteristics of different terrain materials, both natural and man-made, and optimisation of returns from particular surfaces is closely related to laser wavelength. Areas of low reflectivity can result in fewer returns and lower point density in particular regions of the DEM. As is the case with all DEM-generation techniques, the processing routines employed also exert a significant influence on the quality of the final product. Issues related to georeferencing have been discussed above, but in addition, filtering error and misclassification can introduce significant blunders to a dataset, as is illustrated in Figure 2.8, while any form of interpolation (such as to a regular grid) is likely to result in a loss of accuracy.

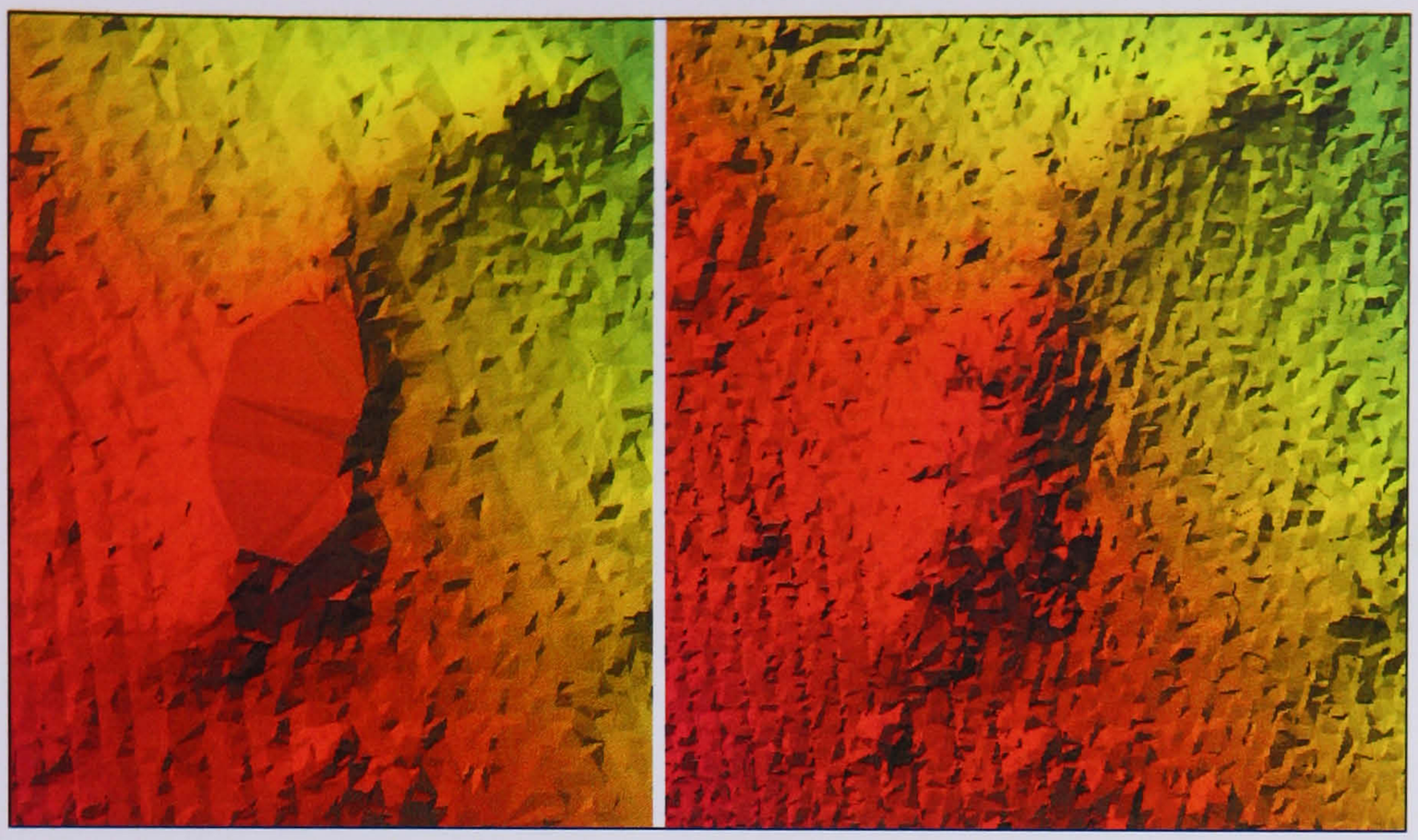

Figure 2.8 Erroneous ground point filtering due to steep terrain (left). Corrected DTM (right) (Ruiz et al., 2004).

2.5.5 Suitability for Coastal Monitoring

ALS offers a range of benefits which combine to make this a highly suitable technique for coastal monitoring purposes. Like photogrammetry, ALS enables rapid, remote coverage over wide areas. However, a number of additional advantages can be identified; in comparison to photogrammetry, ALS can be operated in comparatively poorer weather conditions (Baltsavias, 1999b; Würländer et al., 2004). In addition, as an active sensing technique, ALS is not subject to the correlation difficulties which can afflict photogrammetry in areas such as beaches, or regions of shadow, and instead is capable of producing a rapid, reliable representation of coastal terrain (Göpfert and Heipke, 2006), making it particularly suited not just to coastal, but a range of other monitoring applications.

However, ALS also suffers from a number of drawbacks. As discussed in Section 2.5.4, rigorous, standardised calibration procedures are thus far lacking. Furthermore, there is also a requirement (which is starting to be addressed) for standardisation of survey practices, and a more comprehensive quality assessment. Although ALS lacks the inherent imagery of photogrammetry, and the added interpretational advantages this offers, most commercial operators simultaneously capture imagery as standard practice.

Despite the current drawbacks, ALS is undoubtedly a valuable DEM acquisition technique, and there are increasing examples of its uptake for coastal monitoring (Krabill et al., 2000; Brock et al., 2001; Saye et al., 2005; Shrestha et al., 2005; Lohani et al., 2006). Adams and Chandler (2002) evaluated ALS and aerial photogrammetry, for monitoring of a soft-cliff geohazard, the Black Ven mudslide, on the south coast of England, and concluded that in their case, ALS was able to offer superior vertical accuracy. With regards to the future, the evolving technique of waveform digitising promises new possibilities and extended capabilities, particularly for monitoring of vegetated coastal areas.

2.6 TERRESTRIAL LASER SCANNING

2.6.1 Introduction

A further laser-based measurement technique, which is becoming increasingly commonplace for a range of applications, is terrestrial laser scanning (TLS). Like its airborne counterpart, TLS makes use of an active laser profiler to scan and record features. However, the primary difference is that TLS is a static, ground-based technique. The diversity of TLS systems in existence stems from the various application areas from which they have originated, and in relation to this, the specific purposes for which they are designed. TLS systems are used widely, both indoors and out, and generally are composed of the scanner head, a laptop running proprietary software for controlling the instrument, and a power supply.

2.6.2 Technological Overview

Like ALS, TLS systems are fundamentally composed of a laser ranging unit, supported by a scanning mechanism, which allows the dataset to be acquired. The *laser ranging unit* generally employs one of three basic measurement principles: time-of-flight, phase comparison, or triangulation scanning (Boehler and Marbs, 2002), and these provide a convenient classification approach for TLS systems, corresponding to range and accuracy characteristics. The time-of-flight, and phase comparison approaches are both essentially timing-based, and have been introduced in the discussion on ALS ranging in Section 2.5.2. These two approaches are reiterated in Figure 2.9.

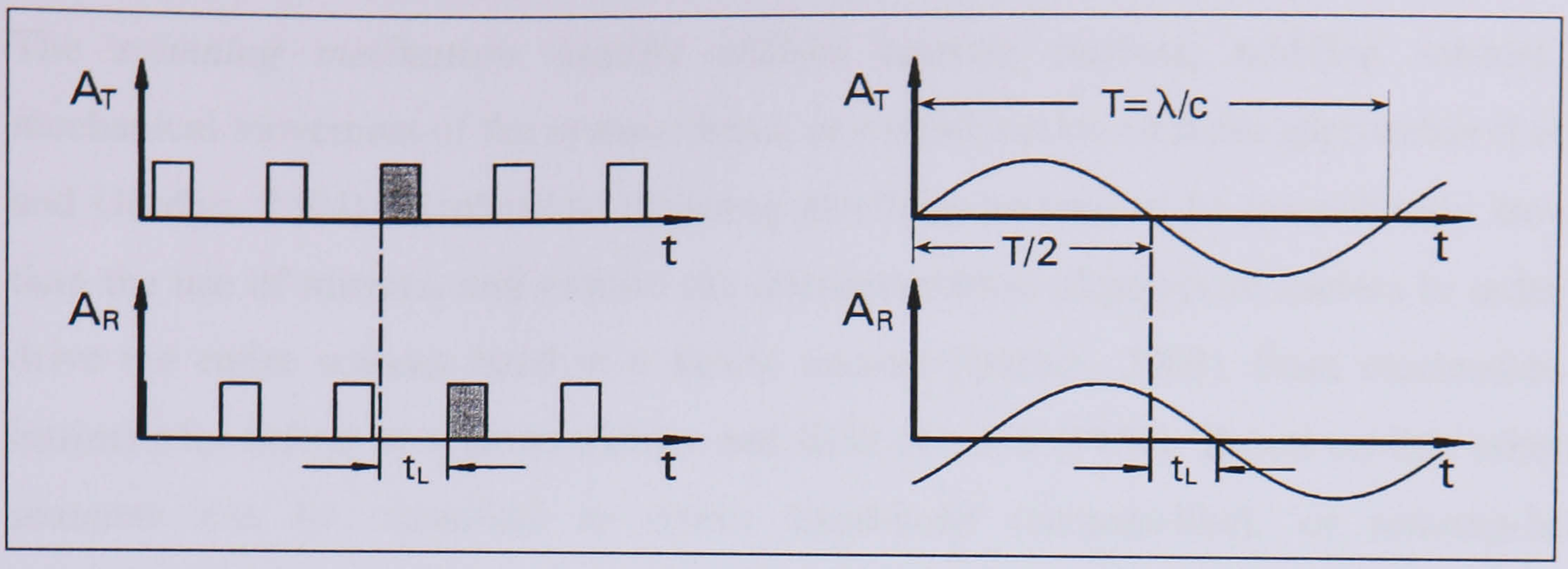

Figure 2.9 Time-of-flight (left), and phase comparison (right) ranging principles (Wehr and Lohr, 1999).

The triangulation method is based on an entirely different approach, modelled around the geometry of the instrument. While triangulation scanners are capable of extremely precise (sub-millimetre), high resolution measurement, they tend to be limited to short-range applications – typically less than two metres (Boehler et al., 2001; Mills and Barber, 2004), and for geohazard monitoring at the scale defined in Section 1.1.3.6, are of no further relevance here.

As was discussed in Section 2.5.2, ALS systems are generally restricted to operating under the time-of-flight (pulsed) measurement technique in order to achieve the power necessary for efficient ranging from an airborne platform. However, TLS is more amenable to the implementation of phase comparison approaches, as there is not necessarily the same requirement for ranging over such great distances. In TLS, time-of-flight and phase comparison scanners show some overlap in terms of capabilities. However, there are also some notable differences; while time-of-flight scanners are capable of ranging up to 1500 m (Optech, 2006; Riegl, 2006b), phase comparison scanners tend to be limited to around 100 m (Schulz and Ingensand, 2004; Sgrenzaroli, 2005), but are capable of achieving higher measurement precision, for the reasons outlined in Section 2.5.2. Most medium- to long-range scanners are based on the time-of-flight principle, perhaps because this offers greater flexibility for a wider range of applications. As with ALS, many TLS systems also record the intensity of the returned signal, which, due to the high spatial resolutions achievable with TLS, can often be a valuable interpretational aid in the absence of imagery – although many systems do also incorporate digital cameras in order to provide textural information (Boehler and Marbs, 2002).

The *scanning mechanism* usually utilises rotating mirrors, nodding mirrors, a mechanical movement of the scanner head, or a combination of these approaches (Lichti and Gordon, 2004). Mechanical scanning mechanisms tend to be considerably slower than the use of mirrors, and require the implementation of powerful motors in order to drive the entire scanner head in a steady manner (Barber, 2003). Scan mechanism is intrinsically linked to scanner design and field of view (FOV). Based on this criteria, scanners can be classified as either fixed-head (camera-like), or rotating-head (panoramic) (Wunderlich, 2003; Gordon and Lichti, 2004). Fixed-head scanners generally use mirrors to deflect the beam horizontally and vertically, and are associated with a limited FOV. Rotating-head scanners offer an extended FOV (often 360° in the horizontal) by combining a mechanical movement to drive the horizontal motion, with a mirror to provide the vertical scan. Scan resolution is determined by the angular scanning increment, which normally can be defined by the user, up to the instrumental limitations.

2.6.3 Terrain Reconstruction

TLS is usually underpinned by some form of control method, enabling registration of the point clouds. In order to fully capture the target scene, it is often necessary to carry out scanning from multiple locations, or scan stations. This is especially true if the object is complex or multi-faceted – for example, a building or a monument. For each scan station, measurements will initially exist in an internal Cartesian coordinate system, derived from the angular deflections and range of each individual laser return, and with origin at the scanner location (Gordon and Lichti, 2004). Consequently, registration can be considered as a two-stage process: (i) the registration of multiple point clouds to a common coordinate system; then (ii) registration to an external reference frame (if desired).

The registration of multiple point clouds can be approached in a number of ways. If sufficient control points are available in each cloud, then it is possible to independently register each scan to an external reference frame (Scaioni, 2003). Alternatively, control points or clearly identifiable features in the overlapping portion of adjacent scans can be used as tie points in order to register all scans to an arbitrary reference frame (Scaioni, 2003; Gordon and Lichti, 2004). The final possibility is point cloud matching of

overlapping scans in order to achieve the same goal as described in the previous approach. This typically employs a method such as the iterative closest point algorithm (ICP) (Besl and McKay, 1992), which negates the requirement for control points, and instead establishes the necessary transformation parameters by deriving control information from mathematical analysis of the overlapping point clouds. A number of researchers, including Roth (1999); Zhao and Shibasaki (2001); Akça (2003); and Bae and Lichti (2004), have proposed alternative TLS point cloud matching strategies. Surface matching is introduced and discussed more fully in Chapter Four.

The second aspect to be considered is absolute registration. Gordon and Lichti (2004) identify two distinct approaches. The first is the indirect, or 3D resection method, where scanner location is determined by resection through the use of control points located in the target scene. This requires a minimum of three points, but in practise more are normally used in order to provide redundancy. The control points are usually planar retro-reflective targets, which are placed in the scene, and can be automatically identified from their intensity signature, or sometimes are shape-based (often spherical) targets whose centre can be mathematically fitted (Scaioni, 2003; Ullrich et al., 2003; Gordon and Lichti, 2004). The coordinates of the targets can be fixed by total station, or similar, for registration to an external reference frame through the three dimensional conformal transformation (Wolf and Dewitt, 2000).

The alternative registration approach, as defined by Gordon and Lichti (2004), is the direct method. This applies to scanners which have the capability to be oriented, centred and levelled over a known point, thus providing direct registration of the point cloud. There is an increasing move towards this approach, as the potential of TLS for traditional surveying applications is being recognised, with scanners becoming increasingly 'surveyor-friendly'. This is reflected by the acquisition of several independent TLS manufacturers by mainstream surveying companies in recent years.

The registration process results in a controlled point cloud, often made up of several sub-scans. One of the most important pre-processing steps is filtering, to remove noise from the dataset (Bornaz and Rinaudo, 2004). Given the relatively high spatial resolutions achievable, TLS datasets often consist of millions of points. For most applications, this level of detail in unnecessary, and therefore, as with ALS, some form

of data classification and thinning may be required. Some off-the-shelf software packages are equally capable of handling both ALS and TLS datasets, with the same basic classification or filtering algorithms suitable for either. Often the only difference will be the initial filter settings – for example, a higher terrain steepness setting may be required for a TLS dataset. As TLS is commonly used for the capture of buildings, monuments, industrial plant, and other man-made structures, a common post-processing step is the fitting of geometric primitives such as cylinders for the modelling of pipes, or planes for representation of building facades (Wunderlich, 2003). Consequently, TLS datasets are often imported to CAD systems for further treatment. An overview of current TLS software is presented by Lemmens (2006).

Some possible TLS applications have been hinted at above, including cultural heritage recording (Bornaz et al., 2003; Alshawabkeh and Haala, 2004; Mills and Barber, 2004), which is a major application area, given the relatively high accuracies and spatial resolutions achievable with TLS. For the same reasons, TLS is often viewed as a competitor, and complement to close range photogrammetry (Kadobayashi et al., 2004). However, it is only in the last few years, as scanners have become more robust, and as manufacturers have become more attuned to fulfilling the requirements of an increasingly diverse market, that there has been increased uptake amongst those concerned with applications in the natural environment. Examples include the use of TLS for surveying of volcanoes (Hunter et al., 2003; Jones, 2006), fluvial environments (Heritage and Hetherington, 2007), soil erosion (Schmid et al., 2004), and tree stands (Watt and Donoghue, 2005). Bellian et al. (2005) examine the potential of TLS for creation of digital outcrop models, and highlight its value in providing rapid quantitative assessment, and enabling direct geological interpretation (Figure 2.10). Nagihara et al. (2004) present an interesting example of the use of TLS for monitoring of dynamic sand dunes in a desert environment in New Mexico, USA. While the increasing uptake of this technology is certainly a positive trend, as with ALS, there remains uncertainty over issues of calibration, standards, and understanding of the error budget.

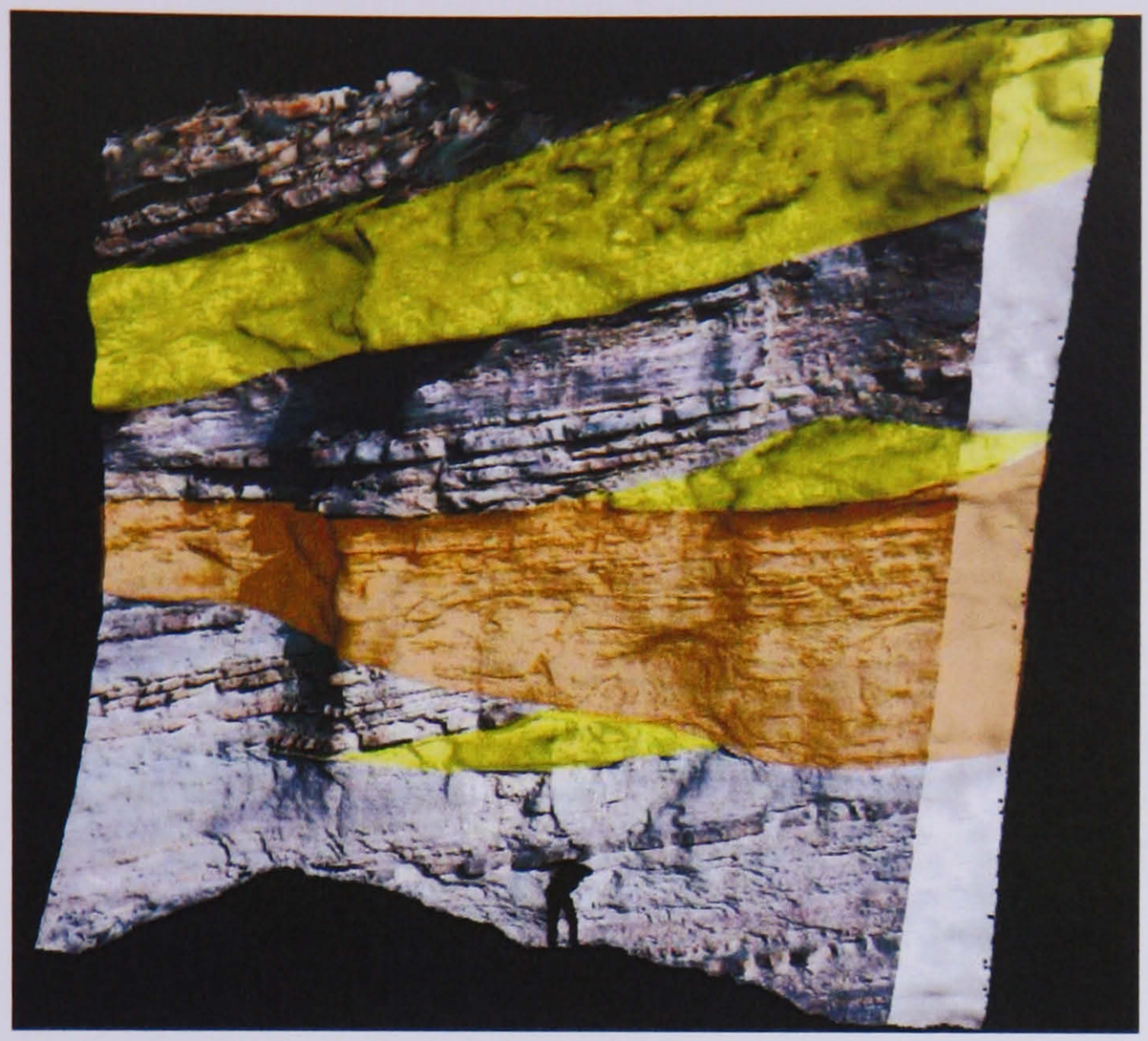

Figure 2.10 TLS-derived, photo-textured digital geological outcrop model, with digitised stratigraphy (Bellian et al., 2005).

2.6.4 Accuracy Considerations

There are a number of factors influencing the accuracy of a TLS dataset. Some of these relate to external factors, while others are associated with the instrument itself. Gordon and Lichti (2004) and Lichti et al. (2005) carried out investigations into the error budgets of TLS scanners utilising indirect and direct registration approaches, respectively. Their findings indicate that while the geometry of control points exerts a major influence on scanners employing the indirect registration method, direct georeferencing scanners are affected by a number of factors, including instrument and backsight station setup errors, and location of the backsight target. There are a number of additional external influences on TLS accuracy, including atmospheric conditions, and ambient radiation, which can interfere with the signal detection procedure (Boehler et al., 2003). The reflectance properties of the target scene also exert a strong influence on accuracy, and are known to cause systematic range errors (Schulz and Ingensand, 2004). Lichti et al. (2005), provide an overview of data artefact errors.

The errors discussed thus far, arise as a result of external factors, but it is also necessary to examine those associated with the instrument itself. One of the major influences on point cloud resolution and uncertainty is the laser beamwidth (Lichti et al., 2005), which

equates to the laser footprint in ALS. Laser light diverges over increasing distance, and the location of the return target will be interpreted as the centre of the outgoing beam. This produces uncertainty in the actual location of a return, especially in the vicinity of edges (Mills and Barber, 2004; Lichti et al., 2005). There are additional accuracy concerns relating to angular and range errors (Boehler et al., 2003). However, assessing the accuracy of a TLS instrument is far from straightforward, as the proprietary nature of scanners hinders understanding of systematic errors associated with design (Reshetyuk, 2006). Furthermore, most TLS manufacturers have not approached instrument design and manufacture from a surveying perspective, and therefore the advantages that this would bring in terms of reliable performance and ease of calibration cannot be exploited (Schulz and Ingensand, 2004).

As with ALS, further errors will propagate into the TLS dataset through insufficient treatment of errors or noise in the point cloud, and indeed, this can be a relatively serious issue in TLS, where datasets can contain high levels of noise, arising from some of the issues discussed above. Furthermore, blunders can be introduced through filtering procedures, and these are often harder to detect.

2.6.5 Suitability for Coastal Monitoring

While ALS has been widely investigated for coastal monitoring, the full potential of TLS for this application remains largely unexamined. However, by investigating the capabilities of TLS, its potential as a coastal monitoring tool can be assessed. TLS offers rapid, accurate acquisition of dense datasets, thereby achieving a level of data capture which would outstrip the time, and effort requirements of traditional surveying approaches. There are also additional advantages; TLS brings the benefits of a non-contact methodology to this hazardous environment, and in comparison to airborne approaches, is not only less costly, but can also be deployed at short-notice in response to an extreme event. Additionally, given the high spatial resolutions achievable, TLS enables detailed characterisation and analysis of terrain. While TLS is apparently highly-suited to coastal monitoring, it is also necessary to consider some of the drawbacks. Coverage is restricted to relatively limited extents, and it is not feasible to consider acquisition of extensive areas through TLS alone, and like any terrestrial techniques, TLS remains vulnerable to local environmental conditions and hazards.

Furthermore, Bitelli et al. (2004) highlight the difficulties posed by vegetation, and suggest that in many cases, extensive interactive editing may be required in order to produce a satisfactory DTM. A typical TLS system can be relatively costly, although equipment sharing and extensive utilisation can justify the necessary investment (Nagihara et al., 2004). However, while TLS is often marketed as a portable tool for operation by a lone individual, this is generally not the case, due to the weight of the scanner head and power supply alone (Tucker, 2002).

The use of TLS for monitoring of geohazards, particularly unstable slopes, has seen increasing investigation by a number of researchers in recent times (Rowlands et al., 2003; Hsiao et al., 2004; Ruiz et al., 2004; Scaioni et al., 2004; Abellán et al., 2006). In application to the study of a landslide in the northern Apennines, Italy, Bitelli et al. (2004) note the advantages that TLS can offer over traditional topographic surveys, particularly with respect to rapid, high resolution acquisition over large areas. In an application such as this, a further, important benefit must also be the largely remote nature of this technique. Recently, some researchers have also begun to explore the use of TLS for coastal geohazard monitoring (Lim et al., 2005; Rosser et al., 2005; Collins and Kayen, 2006), which in many cases can be considered as a variation on the general case of slope stability monitoring, with the added complication of tidal fluctuations.

2.7 Additional Remote Sensing Techniques

2.7.1 Introduction

This section is intended to provide a brief overview of various additional monitoring techniques which could be considered for coastal monitoring. This includes satellite-borne and aircraft-mounted sensors, as well as brief consideration of emerging ground-based techniques. Primary amongst these approaches is satellite remote sensing, which encompasses a diverse range of sensors, and could be considered worthy of more detailed consideration. However, as will be discussed, for monitoring at the scale under consideration here, as defined in Chapter One, satellite remote sensing is still rather limited by issues of resolution and availability.

2.7.2 Overview

Satellite remote sensing is a well-established technique, which began in earnest with developments stemming from military reconnaissance research, and the refinement of early meteorological satellite imaging in the 1960s (Lillesand and Kiefer, 2004). In terms of satellite-based earth imaging in the visible spectrum, the first notable venture which was to have prolonged value to non-military users came with the early Landsat missions in the 1970s, which have continued to present times, with Landsat-7 launched in 1999. Although this suite of sensors has provided the earth science community with an incredibly valuable tool for assessment of the state of the earth's natural resources stretching back over the last thirty years, spatial resolutions of 15 m at best, effectively mean that this technology is realistically only appropriate for monitoring of wide-area processes. The French SPOT programme has provided further opportunities for global monitoring since the first launch in 1986, and also boasts stereoscopic capabilities through its pointable optics. The latest sensor, SPOT-5, is capable of achieving spatial resolutions up to 2.5 m. Recently, commercial high resolution visible remote sensing has gained real momentum, with the introduction of systems such as IKONOS (1 m), QuickBird (0.61 m), and OrbView-3 (1 m). OrbView-5, scheduled for launch in 2007 should offer spatial resolution in the panchromatic band of 0.41 m. Campbell (2002) and Lillesand and Kiefer (2004) provide a comprehensive overview of optical remote sensing, including full details of these and other sensors. A range of multispectral, hyperspectral, and thermal sensors, gathering data in the visible and non-visible portions of the electromagnetic spectrum are also in operation, on both satellite-, and aircraft-based platforms.

Synthetic Aperture Radar (SAR) offers great value to monitoring applications due to its change detection capabilities through the application of interferometric radar, often referred to as InSAR. A major advantageous property of microwave energy is its ability to penetrate the atmosphere even in poor weather conditions, as is reflected in the early origins of active radar remote sensing, where the technique was applied experimentally for aircraft-based wide-area mapping of remote tropical regions in the late 1960s and 1970s (Lillesand and Kiefer, 2004). This nurtured advances leading to the development of InSAR, which analyses the phase of radar signals received from two antennas located in different positions in space. The phase difference in the received signals can then be

used to calculate the elevation of a point on the terrain, a process analogous to the exploitation of parallax for height determination in photogrammetry (Campbell, 2002). Repeat-pass interferometry is an extension of this approach, often employing repeat passes of the sensor in close to the same track (orbit), but separated temporally by several days or weeks. The extracted phase differences can then be combined with knowledge of the topography, for example through a previously-acquired interferometric DEM, in order to asses the residual phase differences which should largely be due to terrain change. Through the known radar wavelength, this can be converted to line-of-sight positional change, with possibilities for resolving mm-level changes, thus allowing for use in high-precision monitoring applications such as ground subsidence studies (Chatterjee et al., 2006), and monitoring of volcanic processes (Massonnet et al., 1995; Fernández et al., 2003) (Figure 2.11). However, as noted by Lillesand and Kiefer (2004), this approach is most successful for spatially-correlated changes acting over large areas, such as glacier surging. The ERS-2, Envisat, RADARSAT-1, and ALOS sensors offer global SAR coverage, and are utilised for InSAR operations, alongside archive imagery from the likes of ERS-1. Rosen et al. (2000) and Hanssen (2001) provide comprehensive overviews of InSAR, detailing the fundamental concepts, and discussing some common applications.

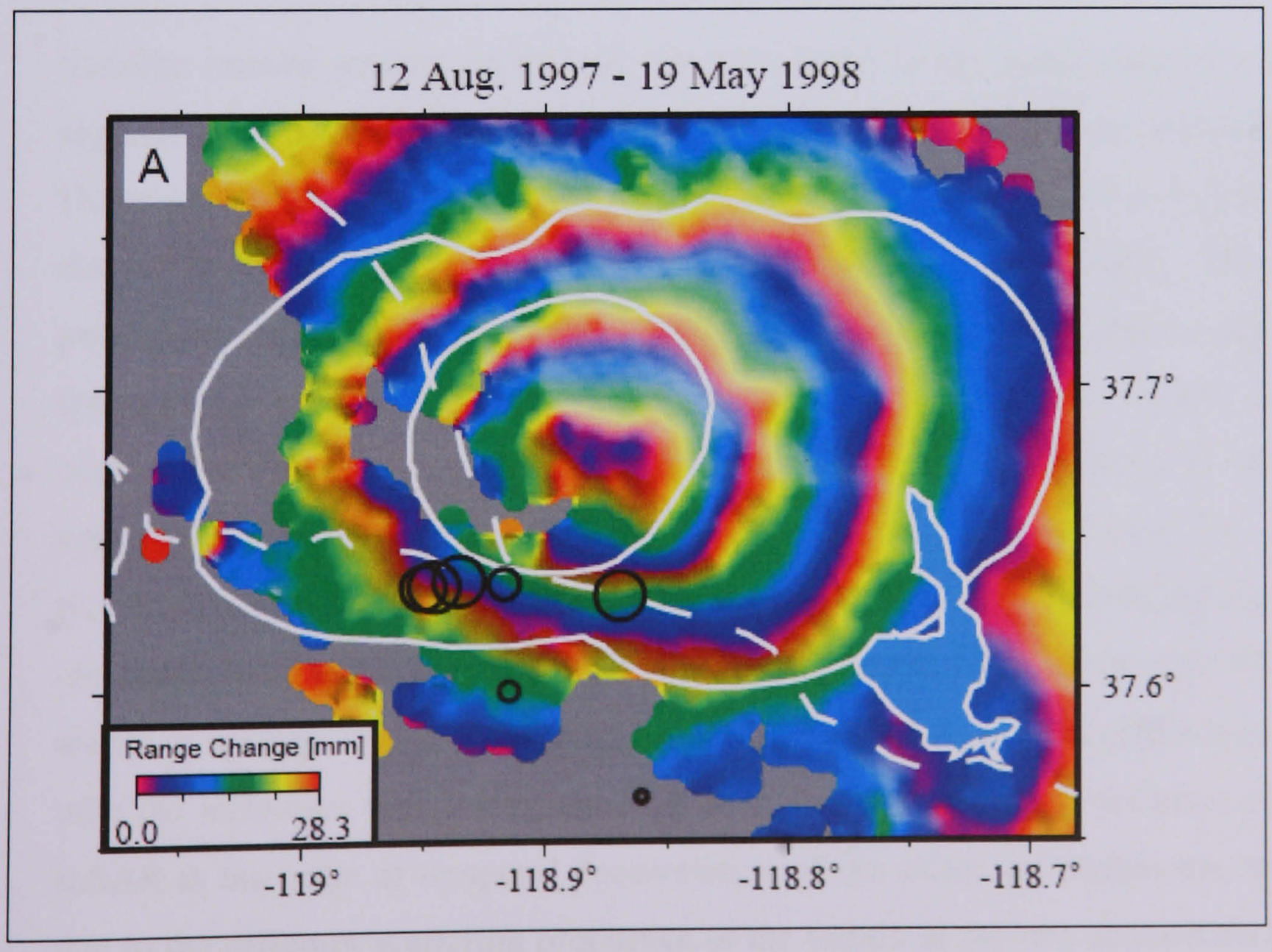

Figure 2.11 Interferogram of an active caldera in Long Valley, California (Newman et al., 2006).

The InSAR technique has recently been investigated from the terrestrial perspective through the use of portable ground-based sensors, particularly in relation to monitoring of landslides (Leva et al., 2003; Tarchi et al., 2003; Luzi et al., 2006). This approach employs the same principles as conventional spaceborne or aircraft-mounted SAR, but repeat measurements can be made from the same ground position, and displacements calculated and analysed over short time periods.

2.7.3 Suitability for Coastal Monitoring

At first glance, it would appear that satellite remote sensing, and associated airborne remote sensing techniques have a great deal to offer to coastal monitoring, and indeed, there has been much exploration of a range of sensors to this end (White and El Asmar, 1999; Lee and Shan, 2003; Nayak, 2004). Niedermeier et al. (2005), working at the regional scale, present research into the extraction of waterlines from SAR datasets in order to carry out analysis of morphological changes in the German Bight. Their findings seem to indicate that even at this relatively large scale, applications of the work are limited by current sensor resolution. Li et al. (2003) describe the use of high-resolution IKONOS imagery for extracting shoreline position, and notes that positional accuracies of 2 - 4 m were achieved.

Satellite remote sensing techniques are well-suited to the monitoring of wide-area, or regional processes, and consequently, may be of value to planners and policy-makers. However, there remain a number of drawbacks associated with this technique, which detract from its value in the context of coastal geohazard monitoring. The return-visit period may be quite lengthy (for example 35 days for Envisat), and in coastal regions (particularly the UK and northern Europe), cloud cover can be a major issue for the optical sensors which are otherwise potentially very well suited to this type of application. In addition, previously-discussed techniques such as ALS and photogrammetry have the means to offer superior resolution, despite the capabilities of the current and emerging set of high-resolution visible satellite sensors. While InSAR would seem appropriate for coastal monitoring, there are several difficulties associated with the technique which severely limit its effectiveness. One of the main afflictions of InSAR is the issue of temporal decorrelation of the phase measurements, which arises due to the different scattering properties of the terrain at the two acquisition times. This

may result due to natural topographic changes, such as deformation, which can be desirable if resolving these changes is the goal of the study; however, the added influence of factors such as atmospheric conditions, vegetation changes, and other anthropogenic effects can result in extreme decorrelation to the extent that it is no longer possible to successfully carry out phase unwrapping (Hanssen, 2001). This can be a particular problem in coastal areas, where the presence of moisture and vegetation can both contribute to this effect (Buckley, 2003), with temporal decorrelation becoming an issue over periods shorter than the repeat pass of the satellite. Furthermore, tropospheric delays can be a significant source of uncertainty (Xu et al., 2006), and geometric decorrelation severely limits applications in areas of steep terrain (Hanssen, 2001).

However, despite such issues, there are some positive considerations. Ground-based InSAR would seem to be a technique worthy of further exploration, particularly given its potential for continuous monitoring and early-warning capability (Luzi et al., 2006). In terms of spaceborne InSAR, the permanent scatterers technique (Ferretti et al., 2000, 2001) has shown a great deal of success in overcoming issues of decorrelation. This approach works through the use of strong radar reflectors, including man-made features, such as buildings, which are stable over time. These essentially act as a network of geodetic monitoring points, and allow for identification and removal of decorrelation effects such as the atmospheric contribution, leaving only residual motion due to ground instability (Meisina et al., 2006). However, in relation to landslide monitoring, Meisina et al. (2006) note a lack of suitable permanent scatterers in landslide areas, as the density of such features is closely related to land-use, with greatest concentrations found in urban areas (Farina et al., 2006), a factor which is likely to also hinder the extensive use of this technique in coastal regions.

To summarise, it would seem that satellite remote sensing techniques in particular, have a great deal of potential in terms of coastal monitoring, but at present they can perhaps be considered as most useful at the regional scale, and do not facilitate detailed examination of the micro- or meso-scale geomorphological processes often driving cliff recession. In this context, and considering current capabilities, satellite remote sensing is perhaps of greatest use for acquiring a coarse indicator of change over extensive

areas, possibly in order to invoke higher resolution monitoring techniques, as suggested by White and El Asmar (1999).

2.8 Integrated Monitoring Approaches

2.8.1 Overview

While each of the techniques outlined above can offer strengths in its own right, there is an increasing trend towards an integration of approaches, often facilitated by the co-location of several airborne sensors in a single aircraft, alongside an INS system. While some techniques are strongly established for particular applications (e.g. the use of GPS for crustal deformation monitoring), other applications call for more challenging requirements to be fulfilled. Dowman (2004) states that 'Data fusion exploits the synergy of two or more data sets to create a new data set which is greater than the sum of the parts', and a number of researchers have advocated the benefits of integrating data from various sensors, particularly in relation to the effective creation of surface models. The disadvantages of a particular technique can often be overcome by the complementary features of another, leading to a synergistic effect (Schiewe, 2000; Buckley et al., 2002; Schenk and Csathó, 2002). Furthermore, Buckley and Mitchell (2004) highlight the potential of DEM integration for identification and elimination of errors and occlusions. Figure 2.12 illustrates how even a straightforward combination of datasets can be useful in highlighting the presence of systematic error. Recently, there has been significant research into the fusion of laser scanning and photogrammetry (McIntosh and Krupnik, 2002; Schenk and Csathó, 2002; Demir et al., 2004; Würländer et al., 2004), as these two techniques can be considered as being particularly complementary, and Böhm and Haala (2005) describe the use of TLS datasets in order to supplement ALS data for city modelling. Hudak et al. (2002) integrated ALS and satellite remote sensing datasets for forest canopy height mapping, noting that while ALS can provide detailed structural characterisation over specific extents, its integration with (in this case) Landsat datasets, allows for measurements to be modelled over much wider areas. Gamba et al. (2003) present an example of the integration of ALS and InSAR in urban areas, utilising ALS to refine the planimetric accuracy of the InSAR dataset.

However, it is important to note that integration also presents new challenges, such as the treatment of conflicting surface representations (Schiewe, 2000), and, as emphasised by Schenk and Csathó (2002), registration to a common reference frame, which is of fundamental importance.

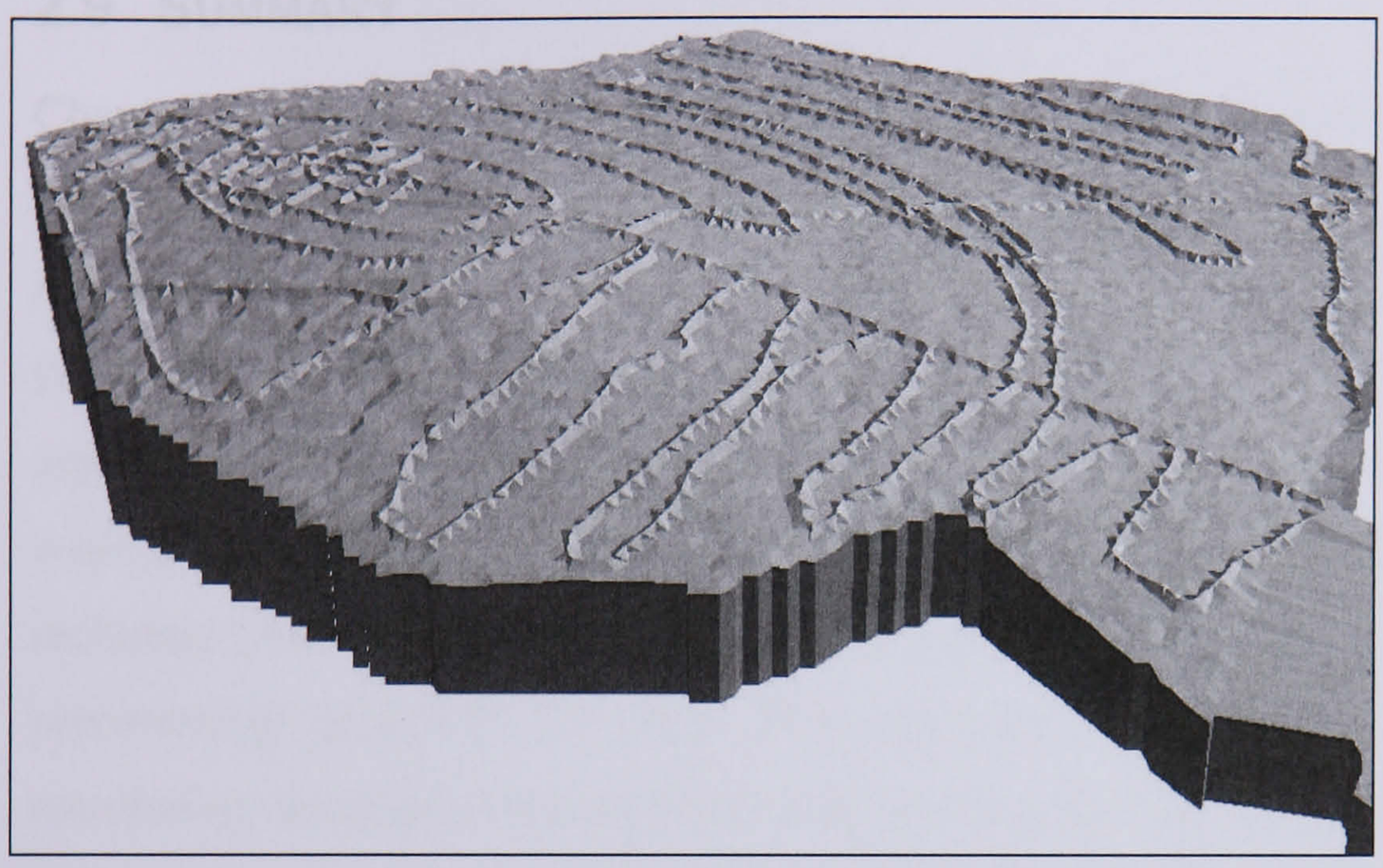

Figure 2.12 Systematic error, highlighted through straightforward dataset combination (Buckley, 2003).

2.8.2 Suitability for Coastal Monitoring

Due to the complex and varying nature of the coastal arena, there is no one technique which could be considered as an optimum monitoring solution - a fact reflected by examination of the literature, where the only clear trend is the lack of a consistent approach. Coastal processes act over a range of both temporal and spatial scales, thus pointing towards a requirement for a multi-scale monitoring strategy, which would be difficult to fulfil without the implementation of a combination of techniques. Furthermore, the coastal zone is often a morphologically-complex environment, further supporting the requirement for adoption of an integrated methodology. A number of researchers have adopted an integrated approach to coastal monitoring (Lee and Shan, 2003; Lohani et al., 2006). In consideration of soft-cliff coastal monitoring on the North Yorkshire coast of England, Mills et al. (2005) noted that no single geomatics technique provided an optimum solution. Instead, they report a synergistic effect was achieved through the integration of photogrammetry and GPS. Likewise, Lim et al. (2005) combined the benefits of TLS and photogrammetry for monitoring of hard rock cliffs.

Given these considerations, it was decided that adoption of an integrated monitoring strategy would be most appropriate in this case, particularly considering the complex nature of the coastal environment. This approach is outlined explicitly in Chapter Three.

2.9 SUMMARY

Chapter Two has presented a review of geomatics monitoring techniques, focussing on application to coastal monitoring, and citing examples where appropriate. For completeness, this has included a brief discussion of geotechnical monitoring techniques, in view of their relevance to slope stability monitoring. A range of basic approaches have been presented and discussed, particularly with regards to the acquisition of historical monitoring datasets. Well-established geomatics techniques, including photogrammetry, and GNSS have also been considered, with photogrammetry representing probably the most thoroughly-examined and widely-applied coastal monitoring technique for analysis of both modern-day and historical datasets.

In addition, the maturing technology of laser scanning has also been examined, with reference to both airborne (ALS) and terrestrial (TLS) approaches. The potential, of laser scanning is evident, presenting many exciting new possibilities, and recently has seen increasing investigation for monitoring of the coastal zone, particularly with regards to ALS. On a cautionary note, issues of error budgets and standards require more comprehensive treatment in relation to both ALS and TLS. Some attention has also been devoted to the current status of the field of satellite remote sensing, primarily in relation to high resolution visible remote sensing, and InSAR techniques. It would seem that while many promising developments are in hand, current sensors still remain limited by spatial resolution, and are further hindered by data availability. Section 7.4.3 includes some discussion on the potential of newly emerging techniques likely to play a significant role in future monitoring of the coastal zone.

These observations have highlighted the advantages and disadvantages of the techniques presented here, leading to the conclusion that for efficient and effective monitoring of coastal geohazards, an integration of techniques may be most suitable. This allows for the shortcomings of individual techniques to be overcome, and addresses issues presented by the complexity of the coastal environment. Therefore,

integrated coastal monitoring is the approach which has been adopted in this research, and which will be developed and implemented throughout the remainder of this thesis. Chapter Three introduces and details the monitoring methodology, focussing on technique-specific considerations, and examining issues related to digital surface modelling, which represents a fundamental aspect of the strategy applied in this research.

CHAPTER 3

MONITORING STRATEGY

3.1 INTRODUCTION

As detailed in Chapter One, the requirement for monitoring of coastal geohazards is of increasing importance due to the potential for accelerated coastal recession instigated by climate change. Monitoring of this hazardous environment serves numerous purposes, including assisting towards policy development and risk management; improving understanding of the underlying failure mechanisms; modelling of future behaviour; and facilitating early warning of geohazard activity. Chapter One discussed some generic considerations in relation to monitoring, and underlined some of the specific barriers to implementation of a successful coastal geohazard monitoring strategy. In response to these constraints, the potential of a range of both traditional and emerging geomatics techniques was reviewed in Chapter Two. Existing inadequacies were highlighted, and it was concluded that integrated monitoring would provide the most effective solution, by allowing for synergistic exploitation. This chapter briefly reviews some further constraints introduced by the unique character of the coastal zone, and in response, introduces an integrated remote monitoring strategy, composed of airborne and terrestrial laser scanning techniques, supplemented by archival aerial photography. These techniques are examined in detail, and the characteristics of the instrumentation utilised in this research are presented. Attention is then devoted to digital surface modelling which is of fundamental importance to the successful integration of multiple datasets. In conclusion, the core issue of dataset registration is discussed, with regard to the specific challenges of the coastal zone, and the particular techniques selected.

This chapter essentially addresses technique-related aspects of the monitoring strategy, and considers the key issue of digital surface modelling. The following chapter, Chapter Four, will investigate the crucial requirement for reliable dataset registration, and will address this through the development and testing of a robust surface matching algorithm.

3.2 Methodology Development

3.2.1 Background

Many of the specific challenges relating to effective coastal monitoring have been outlined in Chapter One. In terms of direct environmental factors, these include complications associated with the dynamic, tidal environment, and issues surrounding the integrity of control points in an actively-eroding landscape. Further difficulties are associated with weather conditions, and restricted access. The reconciliation of data from a multitude of sources, particularly in relation to effective registration, is also a central issue. There are a number of additional constraints which are directly related to the characteristics of geohazards and cliffed coastal terrain in particular. As discussed in Section 1.1.2, coastal geohazards often occur in areas of cliffs. Sea cliffs can range extensively in character, from gentle coastal slopes, to towering vertical cliffs composed of more resistant materials (Viles and Spencer, 1995). Between these extremes lies an extensive range of coastal topography, encompassing slopes of varying degrees of steepness and complexity, which exhibit a range of geohazard processes. This diversity of coastal landform presents one of the main impediments to efficient coastal monitoring, as even short stretches of coastline can exhibit great diversity in terms of topography. In relation to this, a major challenge is the development of an approach which is applicable to a range of geohazard scenarios, and which is equally effective for monitoring at scales ranging from major rotational landslides, to relatively minor rockfall events.

Airborne monitoring approaches provide exceptional benefits in terms of efficiency and extent of acquisition, and are able to capture areas that are inaccessible from the ground (Gorman et al., 1998). However, due to their vertical perspective they are best suited to capturing relatively flat areas of terrain, such as beaches or cliff-tops. Conversely,

terrestrial techniques often suffer from the occlusion of such regions, and instead their value increases alongside the verticality of the terrain, particularly in areas of cliffs (Adams et al., 2003). The rationale for a multi-scale monitoring strategy was briefly introduced in Section 2.8.2. As coastal geohazard processes operate over a range of scales, it is important that any monitoring strategy is able to respond in a manner which is both spatially and temporally sensitive. While some geohazard features may be particularly active, others could be lying dormant, or may be in the early stages of development. This further justifies the requirement for an integrated approach, as no single monitoring technique is currently capable of simultaneously tracking the status of activity over extensive coastal tracts, while providing highly detailed analysis of active pockets of failure. Again, there is a clear correlation with the capabilities of airborne and terrestrial approaches. Terrestrial techniques may prove more labour intensive, but ultimately are capable of providing increased levels of resolution and accuracy, ideally suited to detailed monitoring of high risk areas. This is supported by Adams et al. (2003) who observe that terrestrial approaches offer opportunities for the capture of more detailed information and at higher-temporal frequencies. Alternatively, airborne techniques allow for rapid, cost-effective acquisition of wide areas, but generally the resolution is more appropriate for a coarser level of monitoring.

The hazardous nature of the coastal environment has already been stressed in Chapter One, and it is important to consider safety and risk reduction in relation to carrying out coastal monitoring surveys. While basic land survey techniques may have been the mainstay of monitoring in the past, these approaches are costly and labour intensive, and often involve direct contact with hazardous coastal terrain (Göpfert and Heipke, 2006). Hence, where possible, it is desirable to apply non-contact methods.

It can be difficult to successfully tailor a monitoring strategy for a particular section of coastline without some knowledge of past behaviour, as this can provide an indication of the processes at work, thus facilitating refinement of specifications for suitable spatial and temporal resolutions. Historical datasets are particularly relevant in this regard, and can provide valuable background details relating to the evolution of coastal geohazards, even where the information may be sparse, or of limited quality.

3.2.2 Monitoring Strategy Overview

The discussion in Section 3.2.1, leads to identification of a number of key criteria which should be fulfilled, where possible, in order to formulate an effective coastal geohazard monitoring strategy. These can be summarised as:

- a capability for high quality quantitative assessment of change;
- flexibility in terms of spatial resolution, thus allowing for multi-scale monitoring;
- a capability for minimising occlusions arising as a result of the complex nature of the coastal terrain;
- remote data acquisition in order to minimise risk, and reduce the opportunity for further destabilisation of the terrain;
- adaptability to a range of geohazard environments;
- incorporation of historical datasets wherever possible.

Traditional geomatics approaches offer relatively limited solutions, which cannot address all of the above criteria. However, over the last ten years, a number of fresh techniques have emerged with the potential to meet these specifications, particularly when applied in an integrated manner. This relates specifically to laser scanning, including both airborne and terrestrial approaches, which have been described and assessed in detail in Sections 2.5 and 2.6. These techniques offer exciting possibilities for integrated remote geohazard monitoring, both in the coastal arena and elsewhere, and there is a requirement for a more comprehensive investigation of their capabilities and limitations in this respect. Furthermore, from the issues discussed in Section 3.2.1, it is clear that a combined aerial-terrestrial approach is required in order to satisfy the complex requirements imposed by the coastal environment, and the geohazard processes under consideration. This further supports the application of ALS and TLS, and a number of recent studies from the geohazard domain lend further credence to this combinational approach. Abellán et al. (2006) carried out a study to evaluate the use of TLS for analysis of rockfalls on steep slopes in the Pyrenees, Spain. Their findings highlight the value of TLS for rapid acquisition of extremely dense point datasets, and the possibilities these offer for rockfall inventory and detailed three-dimensional characterisation. However, they also remark on the occurrence of occluded terrain, and

suggest that combination with aerial data would allow for this issue to be overcome. In a similar rockfall-analysis application, Ruiz et al. (2004) explored this route more fully by acquiring TLS data in order to overcome occlusions in an ALS dataset (Figure 3.1), noting in conclusion the synergistic achievements of such an approach.

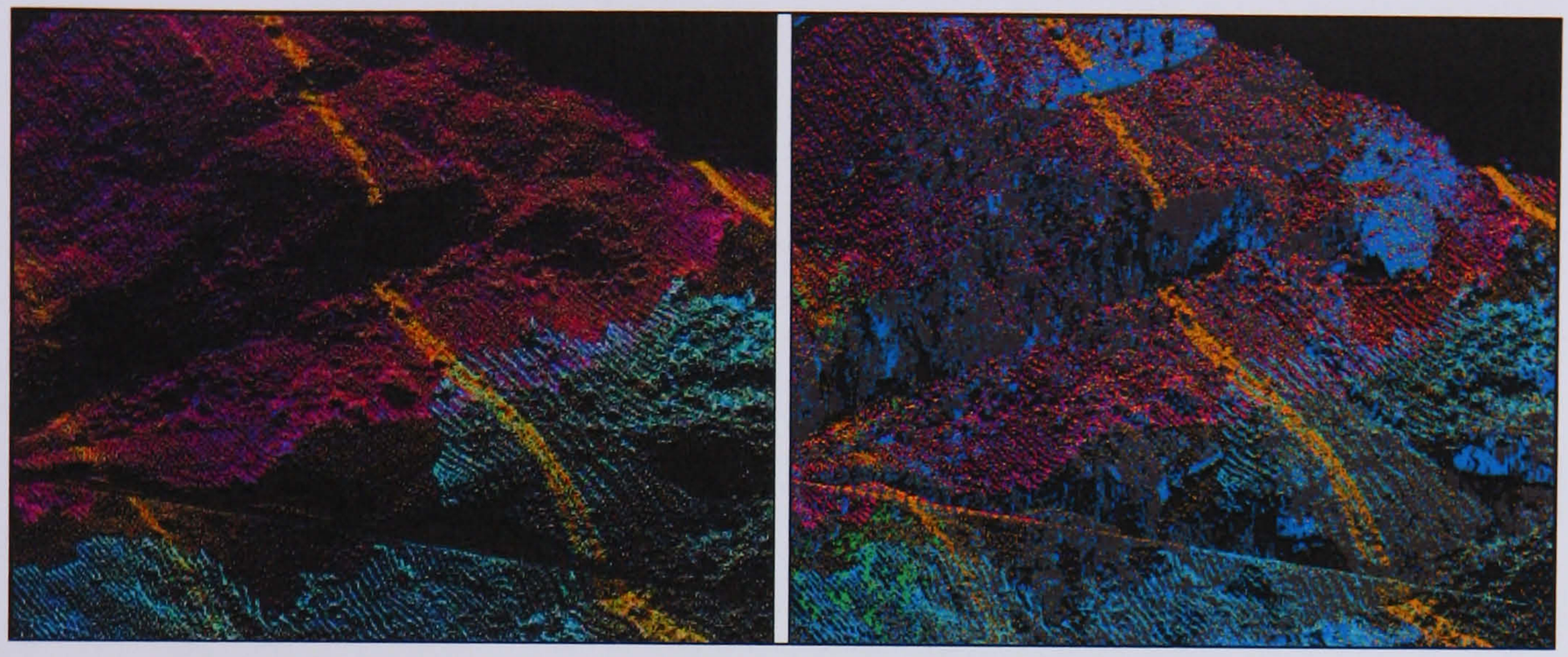

Figure 3.1 Occluded regions of ALS dataset (left) supplemented with TLS data (right) to provide complete coverage of mountainous terrain (colours represent flightlines) (Ruiz et al., 2004).

The research presented here has therefore seen the development, implementation and assessment of a coastal monitoring strategy based upon ALS and TLS. These present-day monitoring datasets have been supplemented by archival aerial photography, in order to provide a historical perspective on geohazard evolution, and explore more fully the challenges associated with the successful incorporation of such data, particularly in relation to accurate dataset registration, and change detection. The integrated remote monitoring strategy is outlined in Figure 3.2.

Continuous monitoring of geohazard activity can be extremely valuable. However, on the downside, it requires relatively high levels of investment, but can provide analysis of only a discrete number of locations. The approach developed and implemented in this research is based on episodic monitoring, which is more practical for monitoring over wide areas, and is capable of offering high temporal frequency measurements where required. This strategy will be detailed in the remainder of this chapter, with careful consideration given to each of the individual components. Digital surface modelling will also be considered, as this is a key concern with respect to dataset registration, and successful detection and quantification of change over time.

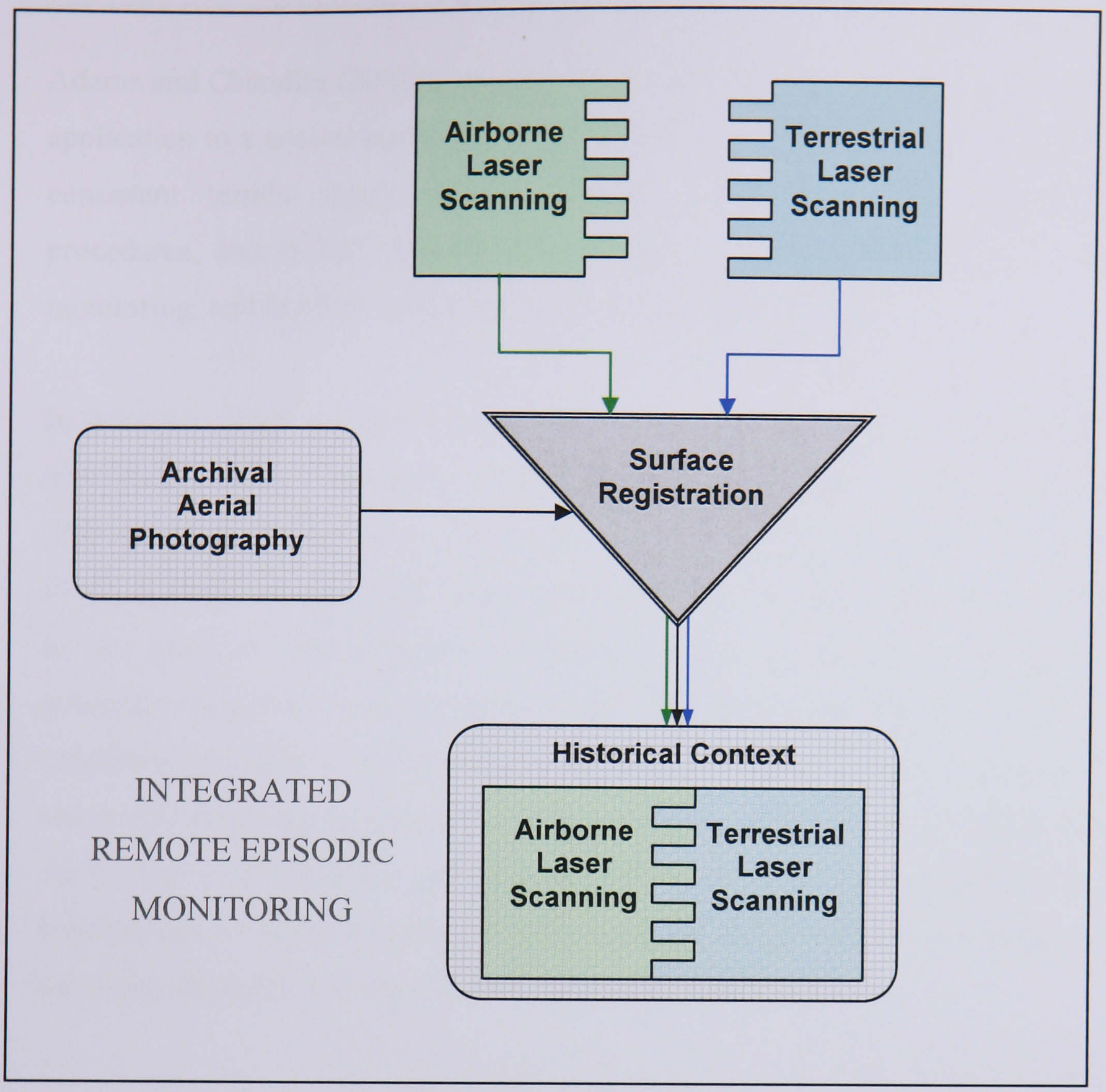

Figure 3.2 Basic outline of integrated coastal geohazard monitoring strategy, as developed and implemented in this research.

3.3 Primary Monitoring Components

3.3.1 Airborne Laser Scanning

The principles of ALS were presented in Section 2.5, where some fundamental considerations in relation to its suitability for coastal monitoring were also discussed. These advantages primarily relate to the ability of ALS to offer rapid, remote acquisition of extensive tracts of coastal terrain (Shrestha et al., 2005). Whereas aerial photogrammetric surveys can also provide such advantages, photogrammetry is afflicted by image matching difficulties, which are accentuated by the often-featureless coastal terrain, especially in areas such as beaches, and regions of deep shadow. As an active sensing technique, ALS is not affected by terrain texture (Würländer et al., 2004), and is able to return a reliable and consistent surface representation. Furthermore,

Adams and Chandler (2002) compared the capabilities of photogrammetry and ALS for application to a coastal landslide, and determined that ALS was able to provide a more consistent terrain representation. Although ALS lacks standardised calibration procedures, and is still maturing as a technique, it offers great promise for terrain monitoring, and requires continuing evaluation in this regard.

In terms of coastal geohazard monitoring, ALS survey planning is of prime importance, as it is essential that appropriate temporal and spatial frequencies are selected. Issues of both temporal and spatial resolution are dictated by the expected rates and magnitudes of the deformation processes under study. Furthermore, spatial resolution is influenced by the particular characteristics of the ALS system, including parameters such as scanning frequency and scanning angle. In turn, these specifics will influence considerations such as flying height, and flightline spacing, and with these issues in mind, it is necessary to ensure that data gaps are avoided through adequate overlap of ALS strips. An additional consideration is the provision and configuration of GPS basestations to enable accurate positioning of the aircraft along its complete trajectory, by means of post-processing of the GPS and attitude data.

3.3.1.1 Optech ALTM 3033 Airborne Laser Scanner

The Optech ALTM 3033 instrument was utilised for all ALS acquisitions presented in this thesis. The main characteristics of the ALTM 3033 are summarised in Table 3-1. This is a discrete return instrument, consisting of first and last pulse returns, supplemented with intensity information. The first and last pulse return concept is illustrated in Figure 3.3, which highlights the capability of this system for limited discrimination between features such as vegetation, and the ground surface.

The ALTM 3033 system is operated by the Natural Environment Research Council's (NERC) Airborne Research and Survey Facility (ARSF), where it is mounted in a Dornier 228-101 research aircraft (Figure 3.4). The ARSF utilise an Applanix POS-AV system to determine aircraft position and attitude. Accurate georeferencing is carried out through post-processing, where this data is combined with local GPS basestation measurements. Where possible, the ARSF utilise data from one or more of the OS Active Network GPS stations, acquired at a rate of 1 Hz (this was the case for the ALS

data utilised in this research), in order to minimise field effort. This initial processing was carried out by the ARSF, with data delivered in ASCII first and last pulse return format, supplemented with intensity information, on a flightline, by flightline basis.

Optech ALTM 3033	
Scanning method	rotating mirror
Pulse frequency	33 kHz
Maximum scanning angle	± 20°
Wavelength	1064 nm
Return characteristics	first and last return, intensity
Vertical accuracy	< ± 15 cm
Planimetric accuracy	< 1 / 2000 × flying height
Platform	fixed wing

Table 3-1 Primary characteristics of the Optech ALTM 3033 ALS instrument (Arnold et al., 2006; NERC ARSF, 2006).

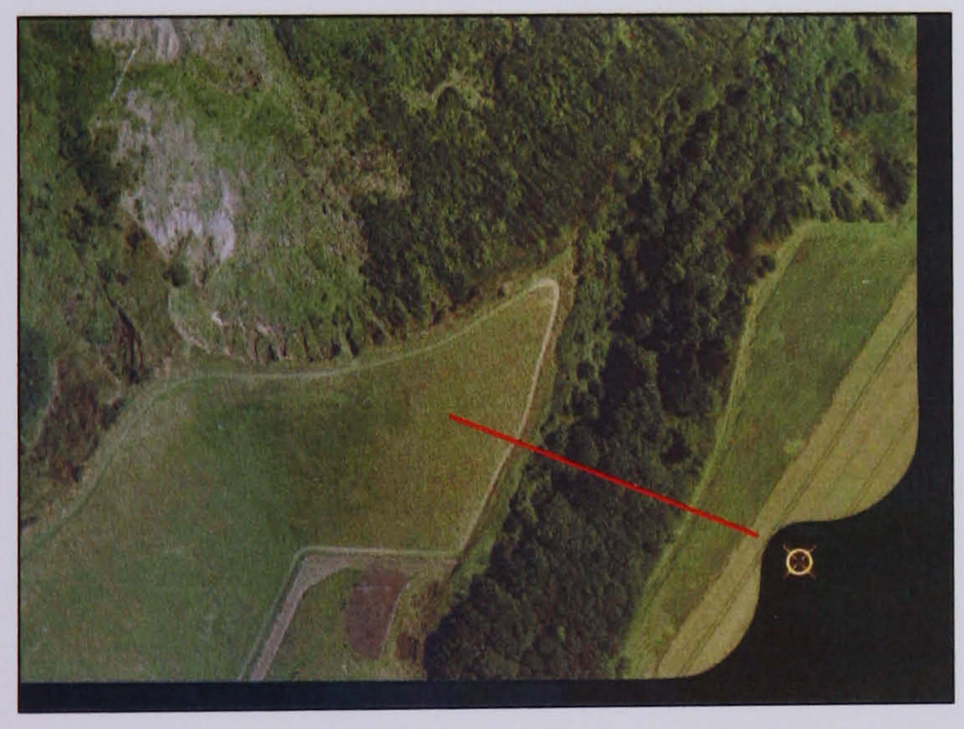

Transect through wooded valley.

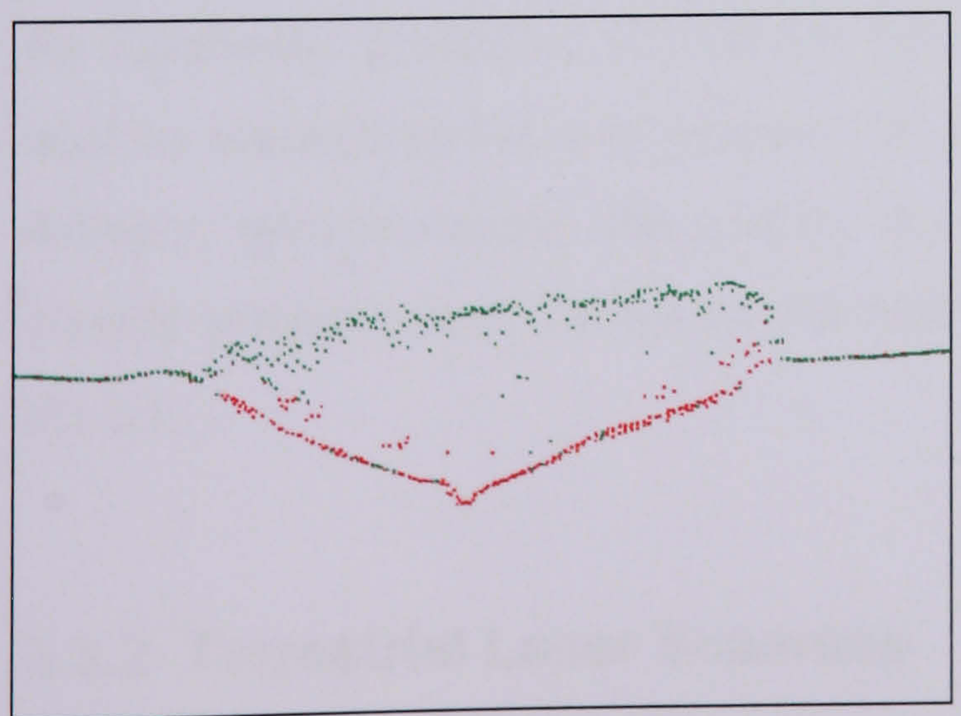

Corresponding profile through ALS dataset. First pulse return (green) from top of canopy. Last pulse return (red), which generally represents the best approximation of the ground surface.

Figure 3.3 ALS first and last pulse return concept.

Figure 3.4 Optech ALTM 3033 system (left), and the ARSF research aircraft (right) (NERC ARSF, 2007).

Table 3-1 details the accuracy specifications for the ALTM 3033, where the manufacturers claim a vertical accuracy of better than ± 0.15 m, and a planimetric accuracy of better than $1/2000 \times$ *flying height* . At a typical ALTM 3033 flying height of 1000 m, this translates to a planimetric accuracy of better than ± 0.50 m. ALS datasets were acquired for the research project in April 2005, August 2005, and May 2006, and independent assessments of ALS dataset quality were carried out. However, as ALS errors are known to vary between and even within flightlines (Latypov, 2002) – primarily as a result of the GPS-IMU errors as discussed in Section 2.5.4 – the results will be presented in Sections 5.4.1 and 6.4, in the context of the individual study sites. As stated above, georeferencing of the ALS data was carried out by the ARSF. It should be noted that the April 2005 data was captured by the University of Cambridge's Unit for Landscape Modelling (ULM), on behalf of the ARSF. The same instrument was used in acquisition, but was mounted on a Piper Navajo Chieftain aircraft. After data delivery, post-processing was carried out in order to remove erroneous points, and classify ground points. Details of this will be presented in Section 5.4.1.3 and Section 6.3.2.1.

3.3.2 Terrestrial Laser Scanning

Terrestrial laser scanning forms the second component of the monitoring strategy. The principles of TLS, and general issues of suitability for coastal monitoring, have been discussed in detail in Section 2.6. The primary benefits of TLS include its capability for

rapid, accurate acquisition of dense datasets (Abellán et al., 2006). Furthermore, like ALS, the non-contact methodology is especially important in an active geohazard setting such as the coastal zone. As a terrestrial technique, TLS provides excellent coverage of more vertical components of the landscape, thus presenting the opportunity to operate in harmony with ALS to minimise occlusions in critical areas. Additionally, although it is not practical to monitor extensive sections of coastline through TLS, as this is essentially a static terrestrial technique, TLS can offer considerably higher levels of accuracy and spatial resolution in comparison to ALS, and thus when considering a multi-scale monitoring approach, is a highly suitable choice. ALS can provide reliable coarse-level monitoring over large areas, allowing for identification of pockets of increased or renewed geohazard activity, thus instigating the TLS component for fine-scale monitoring, which can be implemented at a higher temporal frequency if deemed necessary. TLS also offers the potential to provide a more rapid assessment of geohazard risk, as with suitable organisation, the scanner could be deployed to the field relatively quickly and easily in comparison to the airborne approach. Also, airborne surveys are likely to be more restricted by weather conditions, and will incur higher costs, which may not be justifiable for surveying of relatively small extents. As reviewed in Section 2.6, although TLS has been extensively applied to applications such as cultural heritage, its development in terms of monitoring of the natural environment is rather less mature, and it would appear that only a limited number of researchers (e.g. Adams et al., 2003; Lim et al., 2005) have investigated the potential of TLS for coastal geohazard monitoring. However, parallels can be drawn from landslide monitoring in mountainous regions, an application which recently has seen notable examination of this technique, and in practice, the phenomena under study differ little from many coastal geohazard processes.

TLS instrument selection is especially important, as issues of range, resolution and accuracy are crucial with respect to acquisition of a dataset which will be sensitive to the rate and nature of the deformation processes. In this research, three different scanners, demonstrating a variety of capabilities, were evaluated over the monitoring period. Their main characteristics are summarised in Table 3-2, and discussed in greater depth in the following sections.

Characteristics	**Leica HDS2500**	**Leica HDS3000**	**Riegl LPM-i800HA**
Measurement Principle	Time-of-flight	Time-of-flight	Time-of-flight
Range (m)	100	100	800
Precision (mm)	± 6 at 50 m	± 6 at 50 m	± 15 at 800 m
Resolution (mm)	0.25	1.25	1.00
Measurement Rate (Hz)	1000	1800	1000
Laser Wavelength (nm)	532	532	904
FOV (H° x V°)	40 x 40	360 x 270	360 x 150
Scanner & Power Supply Weight (kg)	42	29	34

Table 3-2 Summary of main characteristics of scanners utilised in the research (Point of Beginning, 2004; Leica Geosystems, 2006; Riegl, 2006a).

3.3.2.1 Leica HDS2500 Terrestrial Laser Scanner

The majority of TLS data was acquired with a Leica HDS2500 scanner (Figure 3.5), which is essentially a re-branded Cyrax 2500 scanner. This scanner is based on the time-of-flight ranging principle, and is a fixed-head (camera-like) scanner, as defined in Section 2.6.2, with the laser beam deflected through the horizontal and vertical by the use of dual oscillating mirrors. Georeferencing is carried out via the 3D resection approach; control points located in the scene provide absolute reference to an external coordinate system, and can also act as tie points to register adjacent, overlapping scans. The HDS2500 system is comprised of the scanner head, tripod, power supply, and a laptop running Leica Cyclone software to the control scanner operation. A low-resolution digital camera is incorporated in the scanner head, and through the Cyclone interface, the user is supplied with an image of the scene (Figure 3.6). As well as enabling refinement of the pointing of the scanner head, the imagery also allows the user to define the region to be scanned. Furthermore, the image can be used to enhance visualisation of the post-processed point cloud, but generally is of rather coarse resolution for this purpose. Once the region of interest has been defined, the user can specify the spatial resolution of the scan. The HDS2500 is capable of producing relatively high resolution scans, with up to 0.25 mm point spacing (Table 3-2).

Figure 3.5 Leica HDS2500 terrestrial laser scanner.

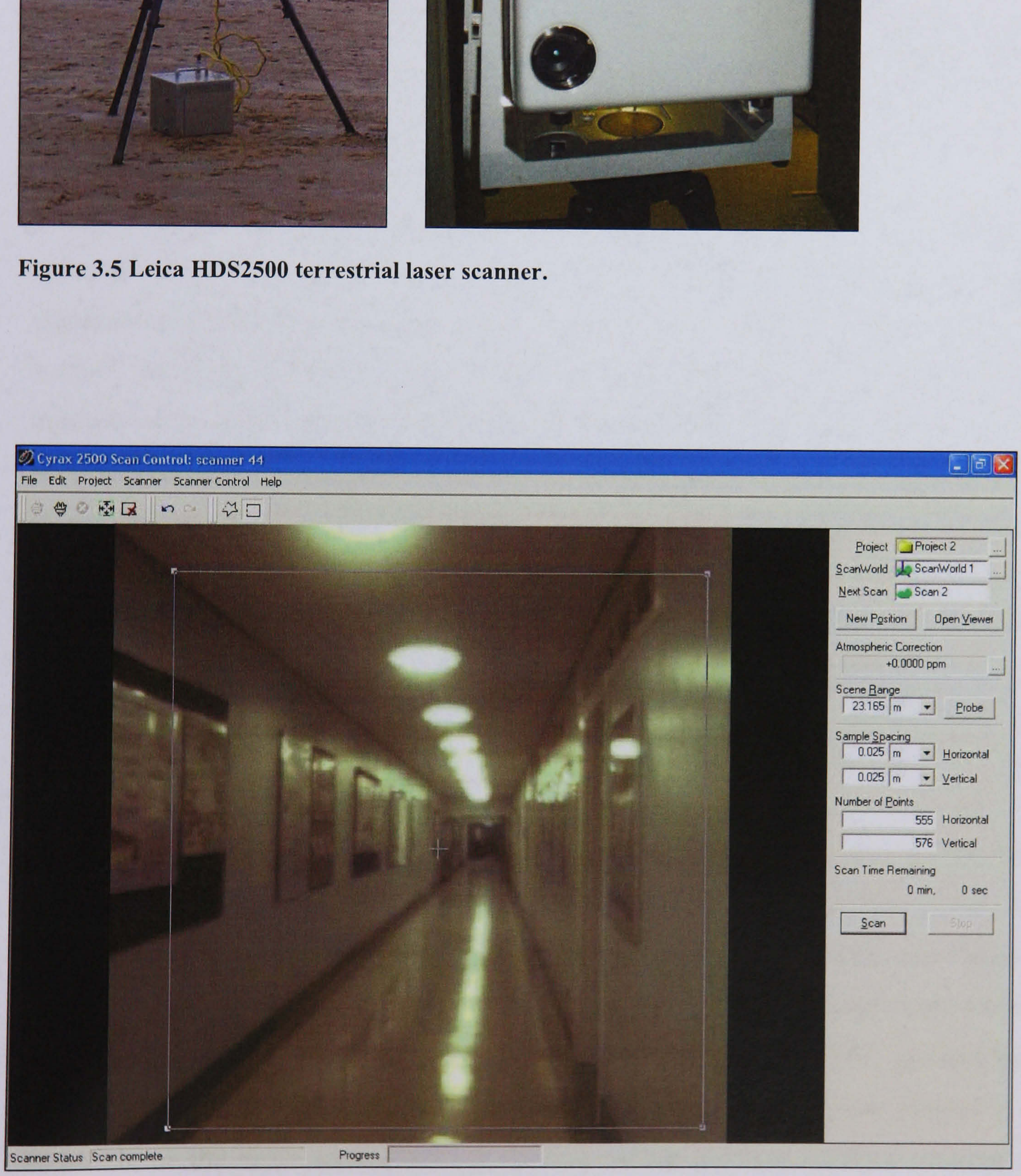

Figure 3.6 Leica Cyclone software, HDS2500 scanner control interface.

Although the HDS2500 is no longer in production, it has been utilised extensively worldwide, being employed for a range of purposes, including heritage applications (Allen et al., 2003; Takase et al., 2003; Wunderlich, 2003), structural deformation analysis (Gordon et al., 2004; Su et al., 2006), and geomorphological analysis (Nagihara et al., 2004). The HDS2500 is generally acknowledged as a highly flexible scanner, offering high precision (specified $\sigma = \pm 6$ mm) for its medium-range capabilities. Testing by a number of researchers (Tucker, 2002; Barber, 2003; Boehler et al., 2003; Santala and Joala, 2003; Reshetyuk, 2006) would indicate that the HDS2500 is capable of performing within this specification, although importantly, it must be noted that such findings were generally achieved under laboratory conditions.

The Cyclone software is also utilised in order to register adjacent scans, and to provide reference to an external coordinate system. This software offers a number of different registration options, including those based on the use of control points, or alternatively, a cloud matching approach which permits the alignment of overlapping portions of adjacent scans. The latter approach may also be combined with a limited number of control points to permit absolute orientation. Additionally, Cyclone offers a toolset which enables the modelling of sections of the point cloud through the fitting of geometric primitives such as planes and cylinders to represent features such as walls and pipes. Such objects can then be exported to CAD systems if desired. Particulars of data processing carried out in relation to this research are discussed in Section 5.5.2.

3.3.2.2 Leica HDS3000 Terrestrial Laser Scanner

The Leica HDS3000 (Figure 3.7), which has recently been superseded by the Leica ScanStation, shares similar technical characteristics with the HDS2500 (Table 3-2). However, there are two important features which set this instrument apart from its earlier counterpart; firstly, the HDS3000 is a rotating-head/panoramic type scanner, which translates to a 360° horizontal FOV, and a 270° vertical FOV; and secondly, georeferencing can be implemented through either the 3D resection control point approach, *or* the direct georeferencing method, which involves accurate centring and levelling of the scanner over a known point, and orientation to a backsight target. The HDS3000 may incorporate a higher resolution digital camera than the HDS2500, but in this regard, the only real advantage over the HDS2500 is that more realistic scene

rendering is possible. The HDS3000 also utilises Cyclone for controlling the scanner during field operations. As with the HDS2500, Cyclone provides the platform for point cloud registration, with details presented in Section 3.3.2.1 above. Like the HDS2500, the HDS3000 has also been utilised for heritage applications (Achille et al., 2005; Dorninger and Briese, 2005), and other documented studies include the analysis of tunnel deformation (Lindenbergh et al., 2005) and integration with ALS data for 3D city modelling (Böhm and Haala, 2005).

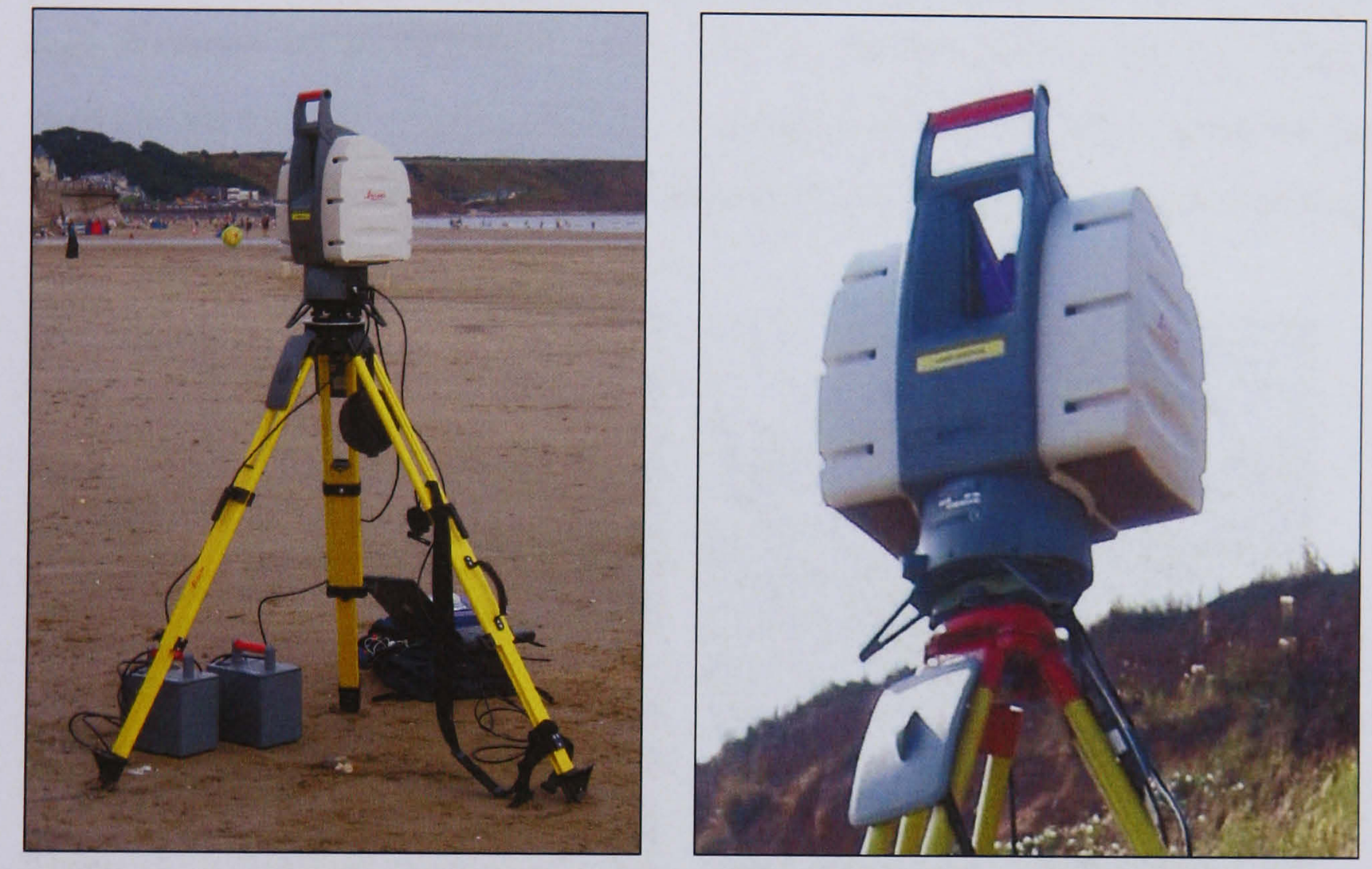

Figure 3.7 Leica HDS3000 terrestrial laser scanner.

3.3.2.3 Riegl LPM-i800HA Terrestrial Laser Scanner

The Riegl LPM-i800HA (Figure 3.8) is also a time-of-flight scanner, but offers distinctly different capabilities to the two Leica instruments. Whereas the Leica scanners offer flexibility for a wide range of applications, Riegl scanners are noted for their rugged design (Afshar et al., 2002), and are highly suited to applications in the geosciences (Hunter et al., 2003; Jones, 2006). With respect to coastal geohazard monitoring, the main feature of the LPM-i800HA is its range, which is specified as up to 800 m (standard). This contrasts with the 50 - 100 m range of both the HDS2500 and HDS3000. Furthermore, the LPM-i800HA optionally incorporates a high-quality digital SLR camera, mounted externally next to the scanning optics. Like the HDS3000, the LPM-i800HA is a rotating-head/panoramic scanner, and offers a 360° horizontal FOV

and 150° vertical FOV. The manufacturers quote a measurement precision of ± 15 mm at a range of 800 m. Although this is poorer than that achievable with the Leica instruments, this is still suitable for coastal geohazard monitoring, given the magnitudes of change which are of interest, and which can be interpreted as meaningful in the context of coastal change. The LPM-i800HA can be mounted on a standard survey tripod via a tribrach, and centred and levelled over a point for direct georeferencing (although alternatively, 3D resection can be carried out with control points located in the scan). A telescope mounted on the scanner head assists in orientation, permitting measurement of a backsight target. In a similar manner to the HDS3000, the configuration of this system allows for interchange with standard survey targets or GPS receivers for fixing the scanner location and backsight, before or after scanning.

Figure 3.8 Riegl LPM-i800HA terrestrial laser scanner.

The LPM-i800HA field system consists of the scanner head (and camera), survey-grade tripod, power supply, and laptop computer for controlling data acquisition, through the Riegl RiPROFILE software. This software is also utilised upon return from the field to carry out point cloud registration, and enables visualisation and manipulation of the data, image registration, rendering, modelling and export of the point cloud. The LPM-i800HA has been utilised for applications including rockfall hazard mapping (Alba et al., 2005), landslide hazard monitoring (Basili et al., 2004), and spatial snow depth analysis (Prokop, 2006).

3.3.3 Archival Aerial Photography

3.3.3.1 Overview

The value of incorporating historical datasets in a coastal monitoring strategy has been discussed in Section 1.1.3.6, where both advantages and disadvantages were noted. However, it was emphasised that the inclusion of historical datasets is generally advantageous, providing an indication of coastal evolution, and facilitating calculation of annual rates of change (Lee and Clark, 2002). Although such datasets may provide a restricted perspective, Bray and Hooke (1997) identify the value of this information in establishing likely future trends in coastal change. In this sense, historical data often forms a necessary input for modelling of future cliff behaviour. Although the uncertainties associated with historical datasets can be difficult to quantify, they can be minimised through careful decision making. For the monitoring strategy presented in this thesis, archival aerial photography was identified for inclusion. This data resource was hinted at briefly in Section 2.2.1, and will be considered in greater depth here.

El-Ashry (1977) observes how the value of aerial photography for topographic mapping had been established by the inter-war years, and indeed, by 1930, a programme for complete coverage of the whole of the US was underway. Furthermore, by the onset of World War II, aerial photography was routinely being flown for military reconnaissance purposes. Such activities have resulted in a rich legacy of archival aerial photography for many regions of the world, including the UK. As an island nation, the UK's coastline is of great importance – it acts as a natural border, provides the first line of defence against attack, and is of interest for scientific purposes and for the development of coastal policies. For these reasons, there have long been motivations for mapping and monitoring the coastal zone, and as a consequence, there exists a relatively rich archive of historical photography, from both civilian and military sources. This data is held in a number of repositories, including English Heritage's National Monuments Record (NMR), the Cambridge University Collection of Air Photos (CUCAP), the Royal Commission on the Ancient and Historical Monuments of Scotland (RCAHMS), and the Central Register of Air Photography for Wales. In addition, the OS maintains vertical imagery dating back to 1980, and BLOM Aerofilms Ltd. also hold an extensive collection of historical images. The National Association of Aerial Photographic Libraries (NAPLIB), a Special Interest Group of the UK Remote Sensing and

Photogrammetry Society (RSPSoc), promotes the use and preservation of aerial photography, and is a useful source of information in relation to collections in the UK.

3.3.3.2 Justifications for Inclusion

Not only does the use of aerial photography allow for quantification of coastal change, but perhaps just as importantly (especially in the historical sense), it provides a visual snapshot of the landscape at a certain point in time. This is useful for assessment of the ecological and anthropogenic influences on the environment, such as vegetation colonisation (Hugenholtz and Wolfe, 2005) or human settlement, which can have significant impacts upon slope stability. The incorporation of archival photography also provides some context for present-day monitoring schemes by allowing for assessment of how geohazards have developed over time, and indicating types of behaviour, and rates of deformation. Information such as this is vital to the monitoring strategy design, as it provides some loose constraints for the nature and scale of activity which can be expected, thus enabling initial determination of suitable temporal and spatial resolution. Furthermore, as discussed in Section 1.1.3.6, historical aerial photography is able to indicate rates of shoreline change or cliff evolution, which may provide a practical, if somewhat limited, measure of risk for coastal managers and policy-makers.

3.3.3.3 Coastal Monitoring Considerations

With regards to utilising archival aerial photography for coastal geohazard monitoring, there are a number of specific issues which must be borne in mind. Although a vast archive of aerial photography exists in the UK, this is of variable quality, both in metric terms, and general image quality. For this reason, a number of important issues have to be considered. It is desirable that the imagery has been acquired from a vertical perspective and with suitable stereoscopic overlap. In a similar vein, acquisition with a calibrated metric camera is important, as is access to the camera calibration certificate. In order to permit high quality measurements in a digital environment, it is important to obtain photogrammetric-quality scans of contact diapositives (Chandler and Clark, 1992; Brown and Arbogast, 1999). Furthermore, to facilitate the quantification of changes to individual geohazard features, and changes in the position of the cliff-top, the photography must be of a large enough scale – scales larger than 1:20,000 are

generally recommended for coastal change analysis (Thieler and Danforth, 1994b; Moore, 2000). Furthermore, consistency in resolution (or ground sample distance of the scanned image) is desirable when considering images from different sources or imagery acquired at different periods in time. Additionally, the nature of solar illumination is especially important in this environment, as the presence of near-vertical sections of cliff can introduce extensive areas of deep shadow which may render the photography useless for the purpose of this work (refer to discussion on image matching in Section 2.4.3). Imagery acquired at, or near to, low tide is most suitable for assessment of coastal change (Gorman et al., 1998) and if possible, it is best to utilise photography from a similar time of year in order to minimise short-term seasonal fluctuations (Moore, 2000). In practice however, it is difficult, if not impossible to satisfy all of the aforementioned criteria, and unfortunately it is often necessary to make the best of what is available. Setting aside metric concerns, archival photography is often simply poor in quality, and may be grainy, scratched and overexposed. This is often compounded by decades of neglect, and such material is usually prone to natural deterioration over time in any case.

Furthermore, a lack of accessible and suitable ground control points in many coastal regions can prove problematic in terms of controlling the photography (Brown and Arbogast, 1999), and further control difficulties can arise through extensive landscape changes due to both human and natural activities since time of capture (Thieler and Danforth, 1994a). In relation to these points, Stylianidis et al. (2003) observes that while archival photography is of great value in evaluating terrain changes over long periods of time, the primary restriction of the archival technique relates to identifying suitable control points on stable ground.

While these concerns may do much to communicate the difficulties associated with the exploitation of archival photographic datasets (and indeed these are not to be underestimated), the inclusion of such material is highly beneficial, as has been demonstrated through a number of applications to coastal change analysis. Adams and Chandler (2002) evaluated historical aerial photogrammetry for examining changes to a coastal mudslide on the south coast of England, comparing imagery from 1976 to ALS data acquired in 1998. Although this study focussed on a relative assessment of the performance of these techniques, results also indicated the potential of such an approach

for detecting soft-cliff coastal change at a level suitable for analysis of individual geohazard features. Brown and Arbogast (1999) examined changes to sand dunes on the shores of Lake Michigan, USA, by comparing DEMs derived from archival aerial photography from 1965 and 1987. While the quality of their results was limited by the use of paper prints, and low-accuracy ground control points, their conclusions emphasised the potential of the archival photogrammetric technique for monitoring of dynamic coastal terrain.

The uptake of digital photogrammetry has greatly increased the possibilities for utilising archival photogrammetric datasets, offering exciting opportunities for the exploitation of what remains a largely untapped metric resource, often extending over periods of 50 years or more. The acquisition and processing of archival aerial photography for this research was carried out with consideration for the issues described in this section, and the observations of this experience, and the outcomes are discussed in full in Section 5.4.2 and Section 6.3.2.2.

3.4 Digital Surface Modelling

3.4.1 Introduction

Kennie and Petrie (1990) define surface modelling as the process by which a physical or artificially-created surface is represented through a mathematical expression. Although applications are numerous and diverse, this research is specifically concerned with surface modelling in the context of the natural environment, and at the scales defined in Section 1.1.3.6 – i.e. the micro- and meso-scales. In this sense, digital surface modelling hinges on the acquisition of three-dimensional coordinates of the Earth's surface (Kennie, 1990), often through one or more of the techniques presented in Chapter Two. The real value of surface modelling is encapsulated by Kidner (2003), who comments that this solves the problem of how to best represent the Earth's surface through a limited number of observations. There are important distinctions to be made with regards to terminology, and the following terms should not be (but often are) confused:

- a Digital Elevation Model (DEM) is the most general form of surface model, comprising all of the acquired points, including those representing both natural

and man-made features. In this sense, it is heavily reliant on *surface* characteristics, and is sometimes referred to as a Digital Surface Model (DSM);

- in contrast, a Digital Terrain Model (DTM) is concerned only with those features relating to *terrain* or *ground*, which as Kennie and Petrie (1990) emphasise, relates to the solid surface of the Earth. Hence, surface features such as buildings and trees are stripped away.

Although alternative definitions and terms may exist, DEM and DTM are the two most widely applied, and are of greatest relevance here. It is important to highlight that a DTM is usually derived from a DEM, through filtering out non-ground points, and hence the characteristics and quality aspects of the DTM are heavily dependant on those of the original DEM. In this section, and indeed throughout the remainder of this thesis, the term DEM is used for consistency. However, it is acknowledged that some of the surface models referred to in Chapters Five and Six may be more accurately described as DTMs.

DEMs have become an increasingly important product in recent times. Digital photogrammetry has had much to do with this, as dense DEMs can be produced in an automated manner at little or no extra cost (Huang, 2000). In addition, the realisation of techniques such as ALS and InSAR has offered increased possibilities for the availability of high-quality DEMs (Chang et al., 2004). DEMs are now seen as a core product of national mapping agencies (Gong et al., 2000), and as a consequence, relatively high-resolution continuous three-dimensional datasets are readily available for many regions of the world. As the availability of this data has increased, the benefits of such information are being recognised by an increasing number of specialists, and DEMs are now commonly incorporated in flood risk analysis, civil engineering applications (e.g. cut and fill analysis), land use planning (e.g. line of sight analysis and transport route planning), military analysis, visualisation, and many more applications.

Surface modelling is an important concept in relation to mathematical analysis of the terrain, and modelling of surface processes (Desmet, 1997). Lane et al. (1998) identify the importance of digital terrain data in describing topography, thus facilitating the identification of different slope processes, and examination of how these processes in turn drive the development of topography. Consequently, DEMs are fundamental in the

monitoring and evaluation of terrain instability, allowing for analysis of deformation over time, and calculation of volumetric change (IGOS, 2003). Lane and Chandler (2003) observe that as a result of techniques such as digital photogrammetry and ALS, it is becoming possible to analyse geomorphological processes at increasingly larger spatial scales. High resolution terrain models are particularly important for monitoring of small scale landslides, as they facilitate detailed landform analysis (IGOS, 2003). This is an especially pertinent observation with regards to coastal geohazard monitoring, where processes often operate over relatively restricted extents, and the detection of pre-cursor deformation processes can provide a valuable indication of an increased susceptibility to failure. Surface modelling is therefore a key concept with regards to the geohazard monitoring techniques identified earlier in this chapter – namely ALS, TLS, and photogrammetry. ALS and TLS are capable of high density sampling of the terrain surface, producing data of a continuous nature which is ideally suited to the derivation of DEMs at resolutions suitable for analysis of the processes under study here. Likewise, digital photogrammetric procedures offer the opportunity for highly automated extraction of high resolution DEMs from archival photography, provided the issues discussed in Section 3.3.3.3 can be addressed. The techniques of ALS, TLS and digital photogrammetry have been introduced and discussed in Chapter Two, where issues pertaining to terrain reconstruction were also briefly outlined, primarily in relation to the specific characteristics of the techniques under consideration. However, it is also necessary to consider some fundamental and generic aspects of DEMs, which influence all datasets, irrespective of the means by which the source data has been acquired.

3.4.2 DEM Structure

DEM structure is one of the most fundamental concepts in relation to surface modelling. As the source dataset is only capable of providing discrete samples of the real-world terrain, there will always be discrepancies between the surface model and the actual terrain. In order to optimise the faithfulness of the model, DEM structure must be carefully considered. However, it is also important to acknowledge that there is likely to be a trade-off between the most efficient representation (in terms of cost and data volume), and the most accurate representation. In the domain of terrain modelling, there

are two DEM structures in widespread use – the grid structure, and the triangulated irregular network (TIN) (Shi et al., 2005), as illustrated in Figure 3.9.

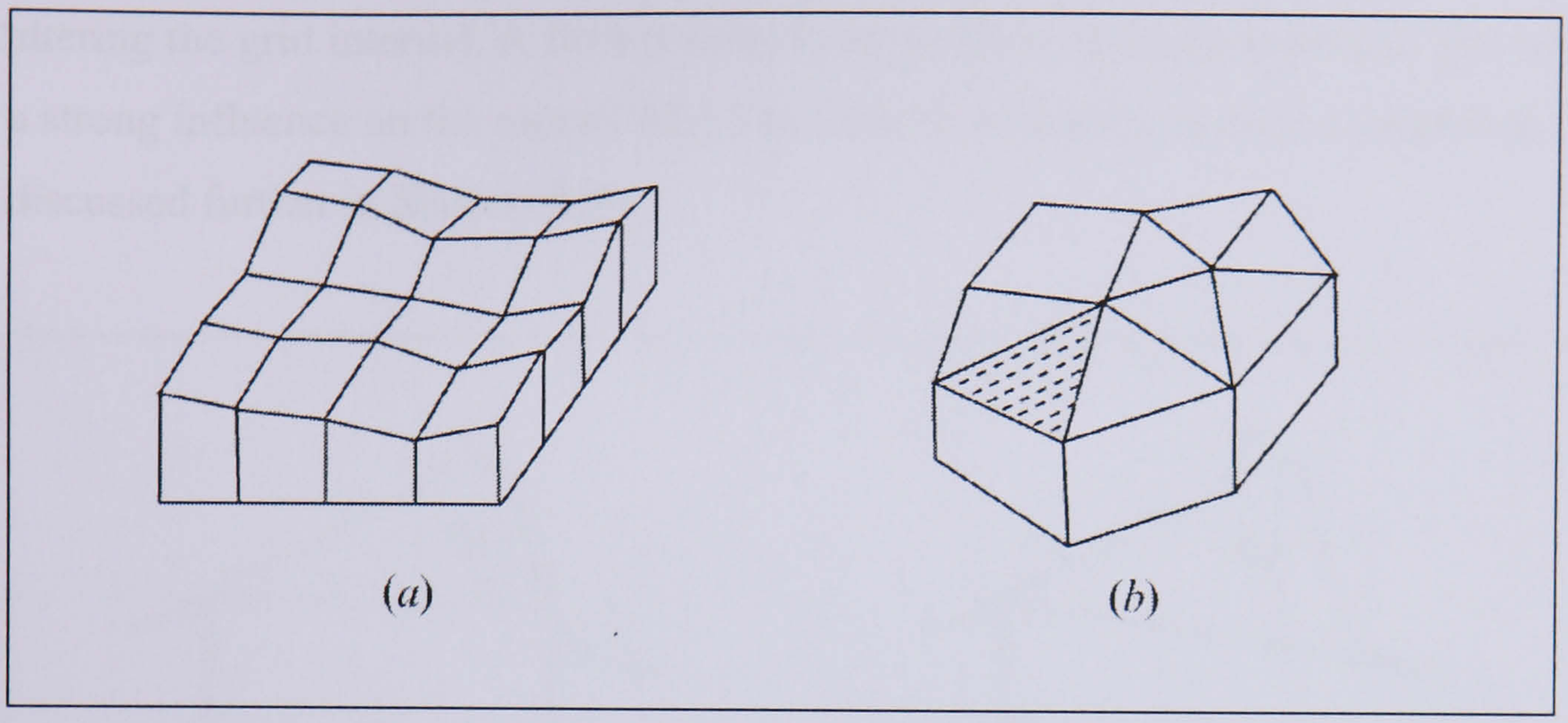

Figure 3.9 Examples of the DEM grid structure (a), and TIN structure (b) (Zhu et al., 2005).

3.4.2.1 Grid Structure

The grid structure is the simplest and most commonly utilised approach for digital surface modelling (Kidner, 2003), with the square grid being the most dominant manifestation of this. Although the source data may have been acquired in this manner, more commonly some form of interpolation will be involved. The grid structure is popular for a number of reasons. In many software packages this is an efficient representation, as if the grid interval and extents are known, then the DEM can easily be stored as a matrix of elevation values. In raster-based software, particularly GIS, spatial analysis operations can easily be carried out on a grid DEM (Shi et al., 2005), thus increasing the potential value of the dataset. This structure also facilitates calculation of surface attributes such as slope and aspect which are useful in many environmental applications (Skidmore, 1989; Bolstad and Stowe, 1994; Barringer and Lilburne, 1997; Kienzle, 2004).

However, grid structures suffer from a number of drawbacks. As the sampling strategy is restricted to pre-determined locations, this can lead to poor representation of the surface, as illustrated in Figure 3.10. To some extent, this issue can be offset by applying a higher grid sampling interval, but this in turn can prove problematic in terms of data volumes, especially when considering DEMs at the national level. Burrough and

McDonnell (1998) also highlight two further disadvantages: firstly, the significant data redundancy in areas of relatively uniform terrain; and secondly inflexibility in the sense that areas of differing relief complexity cannot be adequately represented without altering the grid interval. A further issue is the process of interpolation, as this exercises a strong influence on the overall faithfulness with which the surface is modelled. This is discussed further in Section 3.4.3.

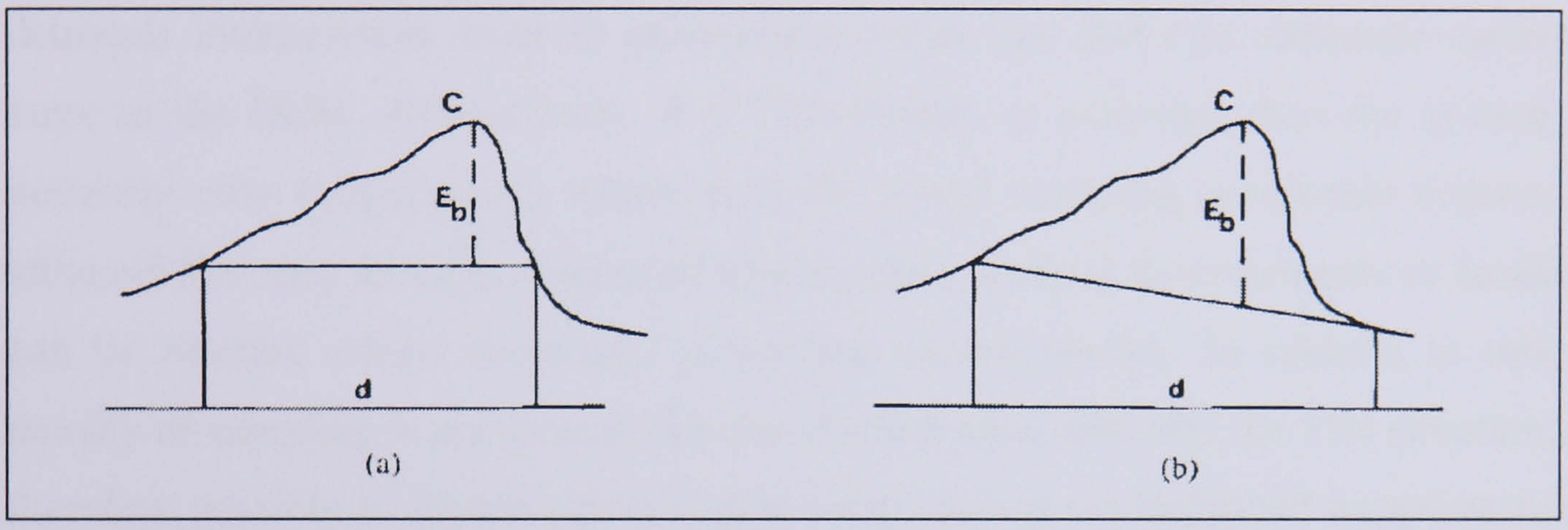

Figure 3.10 Potential errors (E_b) at *C*, due to grid spacing (*d*) in linearly interpolated data (Li, 1993).

3.4.2.2 Triangulated Irregular Network

As computing capabilities have advanced in recent years, the use of irregular point structures for surface modelling has become increasingly feasible. In the scope of terrain modelling, the triangulated irregular network (TIN) is applied almost exclusively for irregular surface representation, and hence discussion here will be restricted to this. A TIN is a highly versatile surface description, which is usually comprised of planar triangular facets (Jones, 1997), as depicted in Figure 3.9. It is important to establish a unique triangulation, composed of triangles which are as equilateral as possible, and with minimum side lengths (Petrie, 1990; Jones, 1997), and in order to achieve this, Delaunay triangulation is frequently employed. Delaunay triangulation is associated with the Thiessen polygon or Voronoi diagram strategy which defines the geometric region of influence for each point. An important condition is that the circumcircle through the vertices of a Delaunay triangle will contain no other points from the dataset (Petrie, 1990; Hessami et al., 2001). The Delaunay algorithm searches clockwise around each data point attempting to identify neighbouring points (Thiessen neighbours) which satisfy this condition, and which will form the basis for the triangulation.

The TIN structure can offer a number of advantages over the grid approach. The TIN structure is capable of directly honouring the source data, and hence uncertainty introduced by interpolation is avoided (McCullagh, 1988; Jones, 1997). This can be demonstrated in the case of digital photogrammetry, where the extraction of a DEM is a relatively routine process. As has been discussed in Section 2.4.3, image matching procedures can be subject to failure in areas of poor image texture. If the user has specified the extraction of a grid DEM however, then the nature of the grid structure demands interpolation, even in problematic areas, and this can introduce systematic error to the DEM. Alternatively, if a TIN strategy is enforced, then the system will normally only extract points which meet the image matching correlation criteria, and although this may result in regions of sparse points, manual measurements or breaklines can be inserted where necessary, preserving overall quality. In relation to this, the density of sampling is associated with the original data, and with the TIN structure, it is therefore possible to incorporate a higher point density for improved representation of complex regions of terrain, alongside sparse, but effective, sampling of areas which are relatively flat or of constant slope (Jones, 1997). This is encapsulated by Zhu et al. (2005) who observe that the TIN is a more efficient model for representing terrain characteristics; regular grids will always be subject to some degree of over- and under-sampling of the surface. Furthermore, as noted by McCullagh (1988), the incorporation of breaklines and other discontinuities is a relatively straightforward process in a TIN.

3.4.3 DEM Interpolation

Issues of DEM interpolation have been alluded to in the preceding sections. Interpolation is generally dependant on the application of mathematical functions, and the importance of these are summarised by Jones (1997), who observes that, 'they provide methods of inferring the presence of phenomena at all locations in space, even though they may only have been measured originally at particular discrete locations.'. Interpolation can be applied to triangulated surface structures, but is more commonly associated with grid DEMs, where it represents a fundamental issue, controlling the nature by which the modelled surface is created from the original source data.

Petrie (1990) identifies three basic types of interpolation:

- global interpolation;
- patchwise interpolation;
- pointwise interpolation.

3.4.3.1 Global Interpolation

In global interpolation methods, a single, mathematical surface is fitted to all of the original data points, and this can then be used to derive points on a regular grid. The global surface usually takes the form of a polynomial function, and is sometimes referred to as a polynomial trend surface (Jones, 1997). This surface will not pass directly through all of the source data points, but a best-fit solution is usually obtained through least-squares. However, Jones (1997) observes that the global approach is not best-suited to the accurate representation of surfaces (other than those which are relatively simple), as it requires the use of high-order polynomial functions, which are computationally intensive, and tend to incorporate significant errors towards the edge of the surfaces.

3.4.3.2 Patchwise Interpolation

Patchwise interpolation provides a compromise to the global approach of forcing a single mathematical surface through all measured data points. Instead, the surface is divided into patches, which are normally either square or rectangular, and then individual patches are modelled independently by a polynomial function (Petrie, 1990). Each patch will usually contain several grid nodes, the values of which can be derived from the surface function. The advantage of this local interpolation approach is that lower-order polynomials are usually sufficient for most surface patches, and hence this method is less computationally-intensive than the global approach. Additionally, and perhaps of greater importance in terrain modelling, the modelled surface should be of a higher accuracy. However, as the polynomial functions may vary for each patch, this introduces complexities in data storage and organisation (Jones, 1997).

In a similar manner, splines are piece-wise functions which are fitted to a small number of data points in a smooth manner (Burrough and McDonnell, 1998). However, they are sometimes regarded as global in the sense that adjacent splines can be modelled to be continuous with their neighbours, hence ensuring a smooth representation of the entire surface (Jones, 1997). Spline functions are useful for modelling gentle terrain and smooth slopes, as reported by Desmet (1997). However, this technique is less suitable for discontinuous surfaces, where features such as cliffs and buildings may be poorly represented (Aguilar et al., 2005).

3.4.3.3 Pointwise Interpolation

Point-based methods interpolate surface heights based on the values of the surrounding measured points (Petrie, 1990), and are popular in terrain modelling applications, as they are well-suited to representing natural surfaces, which are often characterised by local terrain complexities. Numerous methods have been developed and implemented, but discussion here will be restricted to a selection of the most-common approaches.

Nearest Neighbour

Nearest neighbour interpolation is not a particularly sophisticated approach. In its simplest form, the value of the closest measured value is assigned to the point being interpolated (Burrough and McDonnell, 1998), usually on the basis of Thiessen polygons (introduced in Section 3.4.2.2), which define the region of influence for each data sample. However, as Jones (1997) points out, this approach is not well-suited to gradually-varying phenomena, and fails to account for spatial correlations. Hence the nearest neighbour interpolator is poorly suited to DEM interpolation.

Linear Interpolators

Linear interpolation techniques calculate values of unknown points in the DEM on the basis of the neighbouring, measured points. These methods tend to be most appropriate where the original data is densely spaced (Lloyd and Atkinson, 2002). Bilinear interpolation is a basic implementation of this technique, which linearly calculates an unknown value from the values of the surrounding grid nodes (where existing data is distributed in a grid pattern). A similar approach can be implemented for triangulated data. The bilinear approach is popular for image resampling and data visualisation, but

can lead to artefacts such as rectangular discontinuities (Schneider, 2001). Other point-based linear interpolation techniques involve calculating the average of points within a given radius. In order to offset smoothing, a weighted average, based on distance is usually employed to ensure that the closest points exert the greatest influence (Jones, 1997). The inverse distance weighted (IDW) interpolator is one of the most widely implemented strategies for surface modelling (Aguilar et al., 2005), and is commonly utilised in GIS software in order to interpolate raster datasets from irregularly distributed observations (Burrough and McDonnell, 1998).

Geostatistical Interpolation

Spatial autocorrelation in the sense of DEMs, relates to the fact that a height value is likely to be influenced strongly by the values of the surrounding heights – i.e. that height values are correlated in space. While this consideration has already been exemplified by the IDW strategy described above, some approaches tackle this issue through the adoption of a more mathematically rigorous approach, utilising geostatistical surface modelling techniques (Jones, 1997). A primary example of this is kriging, which is popular in the geosciences community. Like IDW, kriging works on the principle of determining values through locally weighted averaging, but in this case, the weights are a measure of the spatial variance of the neighbouring samples (Desmet, 1997). Kriging performs a preliminary analysis of the dataset, producing a semi-variogram, which is an expression of half the mean of the squared height differences between the samples, as a function of their distance separation. The semi-variogram provides an indication of the spatial variance of the data, illustrating the distance (range) at which the semi-variogram levels out (the sill) and samples can be said to be independent of one another. An analytical function can then be fitted to the semi-variogram, and this can be used to derive weights for the data points in order to facilitate interpolation at unknown locations (Mason et al., 1997). A major advantage of kriging over the alternative approaches outlined above, is the stochastic properties of the technique, which allow for the variance of each interpolated point to be calculated from the weighted sample values, thus providing a measure of confidence (Burrough and McDonnell, 1998). However, for natural surfaces which incorporate discontinuities due to geological or geomorphological features, the semi-variogram may not yield an adequate representation of spatial correlation (Jones, 1997), and as McCullagh (1988)

observes, in order to attain good quality results, a clear understanding of the kriging technique is required.

3.4.4 Accuracy Considerations

3.4.4.1 Factors Influencing DEM Accuracy

DEM accuracy and the factors influencing this must be fully assessed when considering the methods to be employed for derivation of the model, and in view of the ultimate applications of the DEM (Shearer, 1990). Accuracy is the product of errors from a number of sources. Shearer (1990) and Li (1992) identify the following issues (in no particular order of importance) as being especially influential in this respect:

1. the data acquisition technique;
2. the accuracy, distribution, and density of the source data;
3. the characteristics of the terrain surface;
4. the methods employed for creating the surface model.

Factors 1 and 2 above are intrinsically linked, as the method of data acquisition will naturally influence the characteristics of the source data. However, it is possible that accuracy, distribution and density could be modified independently through post-processing; for example data thinning could be employed prior to DEM creation, and classification of ALS data for instance, may influence these aspects also. In any case, quality issues associated with particular techniques have been discussed separately in Chapter Two. It is important to recognise however, that the density of the original data is perhaps one of the most important aspects in terms of accuracy, particularly when interpolation is required (Li, 1993).

The characteristics of the terrain surface are known to exert a major influence on DEM quality. The deterioration of DEM accuracy with increasing relief has been observed by a number of researchers (Torlegård et al., 1986; Li, 1992; Gong et al., 2000; Adams and Chandler, 2002; Fabris and Pesci, 2005). Su and Bork (2006) carried out a study to examine the influence of slope, vegetation, and sampling angle on ALS DEM accuracy. Their most notable finding was a strong relationship between accuracy and slope angle,

with accuracy decreasing as slope gradient increased. Aguilar et al. (2005) examined the influence of topography, sampling density and interpolation technique on DEM accuracy, and concluded that the nature of the topography exerted the greatest influence on overall accuracy. Vegetation is also known to degrade the quality of the DEM, influencing the accuracy with which the source measurements represent the true ground surface, even after filtering and manual editing. This affects DEMs derived from both photogrammetry (Lane et al., 2000; Fabris and Pesci, 2005) and laser scanning techniques (Göpfert and Heipke, 2006). To address this issue in the context of ALS, Raber et al. (2002) have proposed an adaptive filtering algorithm which is based on vegetation characteristics derived from the raw ALS dataset.

Finally, the importance of the techniques employed for DEM creation must not be underestimated, as they represent a crucial factor in accuracy. Associated issues have already been discussed to some extent in Section 3.4.3, where the relative merits of the various interpolation approaches was discussed. Figure 3.11 illustrates the varying surface representations which can be achieved through the use of different interpolation techniques. It is important to acknowledge however, that the best representation of the terrain will always be achieved through direct utilisation of the source data, avoiding interpolation. Therefore TIN DEMs can provide a more faithful surface representation than grid-based models. However, as noted by Shearer (1990), '... the absolutely accurate terrain model does not exist.', and all DEMs will contain error to some extent. Errors introduced through the surface modelling procedure are termed as 'information loss' by Huang (2000), who also observes that these can form the dominant component of the DEM error budget. Huang (2000) investigated this issue in the context of digital photogrammetry by comparing a series of interpolated DEMs to a densely sampled reference DEM which was assumed to be free of information loss. It was observed that regions of difference between the DEMs could direct users towards areas requiring manual editing, and that this approach was useful and cost-effective in assessing quality, particularly where check points are lacking (Huang, 2000).

Chaplot et al. (2006) examined the performance of various interpolation techniques, including kriging, IDW, and spline functions for DEM generation, comparing results in terrain which ranged from relatively gentle to mountainous. Their findings indicated that particularly for low levels of data sampling, the choice of interpolation technique

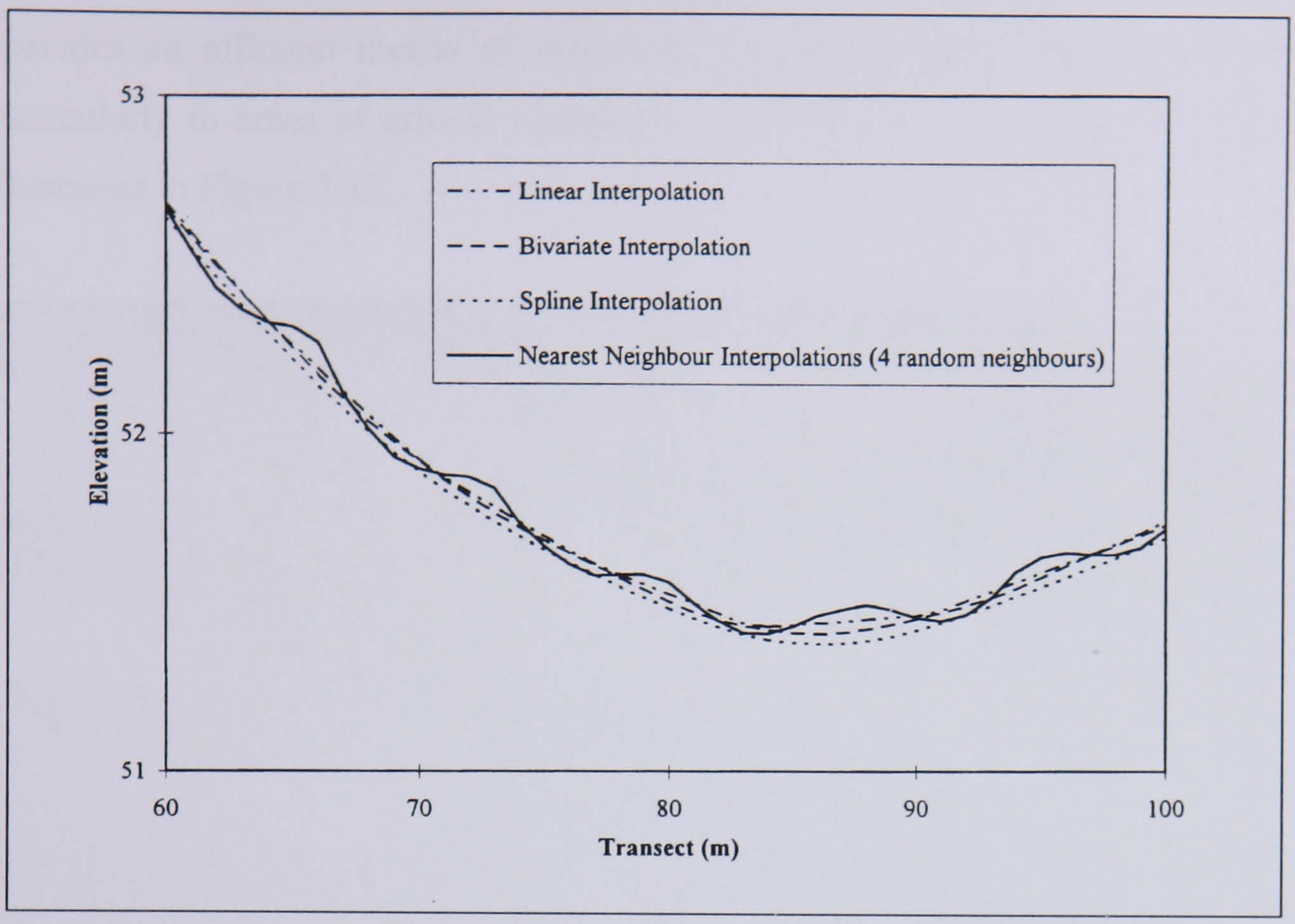

Figure 3.11 Illustration of the effect of different interpolation techniques on surface representation (Desmet, 1997).

has an important influence on the accuracy of the resultant DEM. Furthermore, they observe that the performance of individual interpolation techniques is highly dependant on specific terrain characteristics, and in conclusion they stress the need to select an interpolation technique which will perform well across the entire DEM area (Chaplot et al., 2006). Review of the literature would seem to indicate that no single interpolation technique can be classed as being optimal for all situations. For example, Su and Bork (2006) remark on the effective performance of IDW for interpolation of a DEM from ALS data, noting that this was most likely as result of the high density of the raw ALS points (better than 0.75 points per m^2). In contrast, other studies have noted that this technique produces relatively poor results, indicating that it may be limited in terms of general applicability (Aguilar et al., 2005; Chaplot et al., 2006).

Unsurprisingly, sampling density has also been noted for exerting a strong influence on accuracy (Li, 1992; Takagi et al., 2002). Kienzle (2004) reported that as DEM grid resolution decreased, so too did the accuracy of terrain derivatives, including slope, aspect and plan and profile curvature. This is an important consideration as these are often core products for terrain analysis applications. Several researchers have highlighted that the inclusion of feature-specific or breakline points in a grid DEM,

provides an efficient means of increasing the quality of the surface representation, particularly in areas of critical topography (Li, 1992; Kraus and Otepka, 2005), as is illustrated in Figure 3.12.

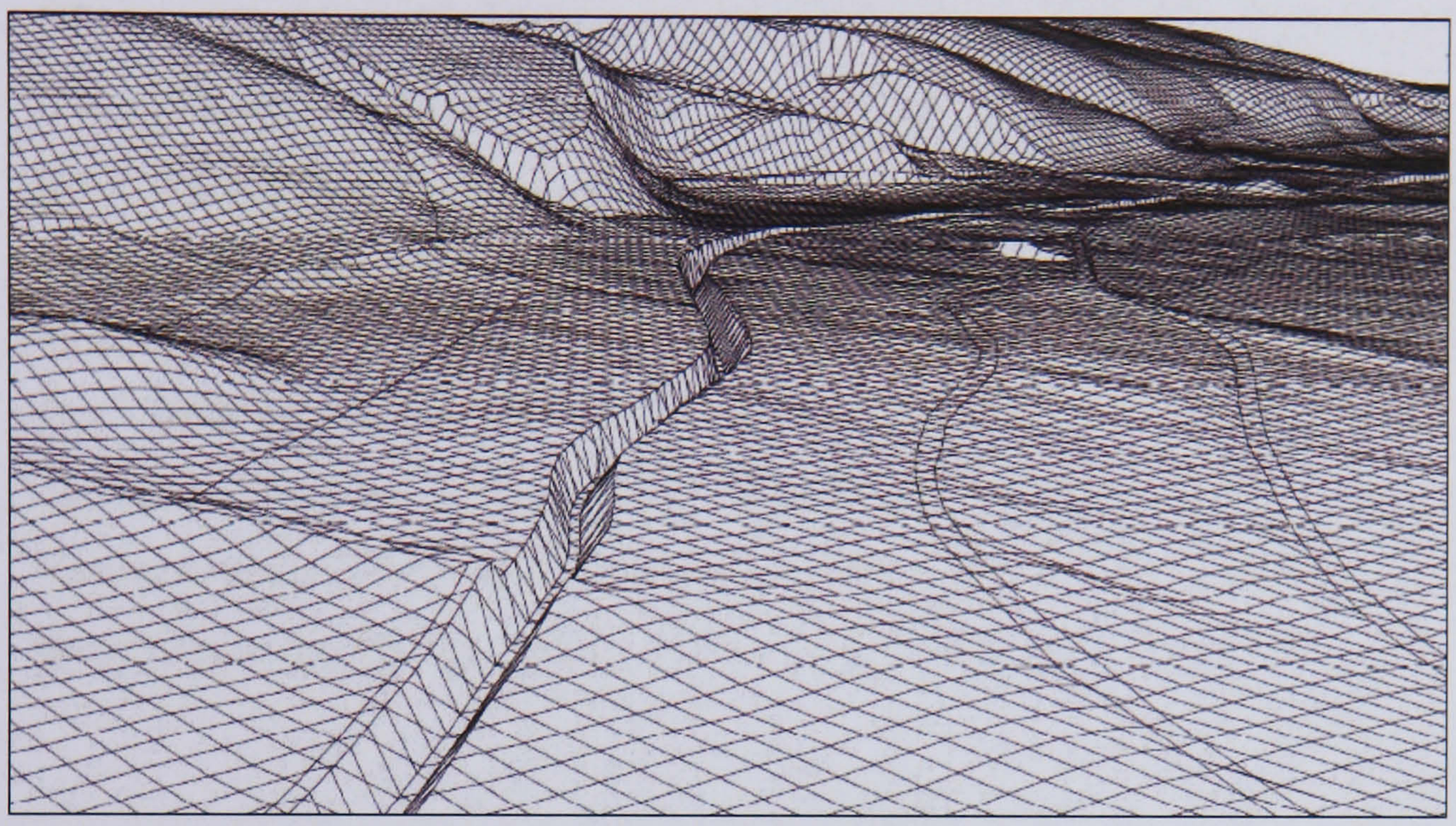

Figure 3.12 Hybrid grid-based DEM, supplemented with breaklines and spot heights incorporated through triangulation (Kraus and Otepka, 2005).

3.4.4.2 Measures of DEM Quality

In the fields of surveying and photogrammetry, errors are identified as falling into one of three categories – gross, systematic, or random. Gross errors, sometimes also referred to as blunders, mistakes, or outliers, are not really errors in the statistical sense. Such errors are often introduced through human failure; for example misreading the scale on a level or total station, or point misidentification in photogrammetric measurement. In the past, when manual data collection and processing were more prevalent, gross errors could be identified and eliminated relatively easily; however through automated procedures, this process is more challenging (Cooper and Cross, 1988). Systematic errors are introduced through the use of poorly-calibrated equipment or an erroneous functional model (Cooper, 1998). However, as systematic error follows physical laws, it can generally be corrected for (Wolf and Ghilani, 1997). The final type is random error, which relates to those errors which remain after gross and systematic errors have been removed. Random errors arise due to measurement variations, which can be introduced through human or instrumental imperfections. These are relatively small in magnitude,

unavoidable, and must be dealt with through probability statistics (Wolf and Ghilani, 1997).

In digital surface modelling, it is necessary to define a rigorous means of assessing DEM quality. The root mean square error (*RMSE*) is an established measure of accuracy (Li, 1988), and its use is widespread (Desmet, 1997; Fisher, 1998; López, 2002; Aguilar et al., 2005; Su and Bork, 2006). In order to calculate *RMSE*, DEM height values can be compared against heights obtained from a higher order source, which may be a DEM which is known to be of superior quality (Huang, 2000), or preferably, data obtained from field survey (Shearer, 1990). Consequently, *RMSE* provides a measure of the deviation of observed values from what can be considered as their true values. The resultant height differences, *dH*, allow for *RMSE* to be calculated as follows, where *n* is the number of observations (check points) (Li, 1988):

$$RMSE = \sqrt{\frac{\sum_{1}^{n} dH^2}{n}}$$

Eqn. 3-1

Despite the ubiquitous usage of *RMSE*, this is a rather selective measure of accuracy, which can be unduly influenced by the distribution of check points, thereby failing to provide a true reflection of overall DEM performance (Gooch and Chandler, 2001). The algebraic mean can provide a useful indication of systematic bias (Wise, 1998) and its use is advocated by Li (1988). The algebraic mean ($\overline{X}$) can be defined as:

$$\overline{X} = \frac{\sum_{1}^{n} dH}{n}$$

Eqn. 3-2

Where *dH* and *n* are as defined previously. Furthermore, Li (1988) emphasises the importance of assessing the dispersion of the height discrepancies, and recommends that additional statistical measures should be considered in this regard. Primary amongst these is the standard deviation, although the maximum and minimum differences (range) are also suggested. Standard deviation (σ), calculated on the assumption that all

systematic and gross errors have been removed, gives an indication of the precision of the measurements and the level of random error present in the dataset, and can be expressed as:

$$\sigma = \sqrt{\frac{\sum_{1}^{n}\left(dH - \overline{X}\right)^2}{(n-1)}}$$

Eqn. 3-3

Where dH, n, and $\overline{X}$, are as defined previously. Random error is usually assessed through the use of probability statistics, where it is assumed that the data are normally distributed about the mean, in a Gaussian manner. On this basis, the normal error distribution curve (Figure 3.13) is used to estimate the probability of an error of a particular size arising (Wolf and Ghilani, 1997).

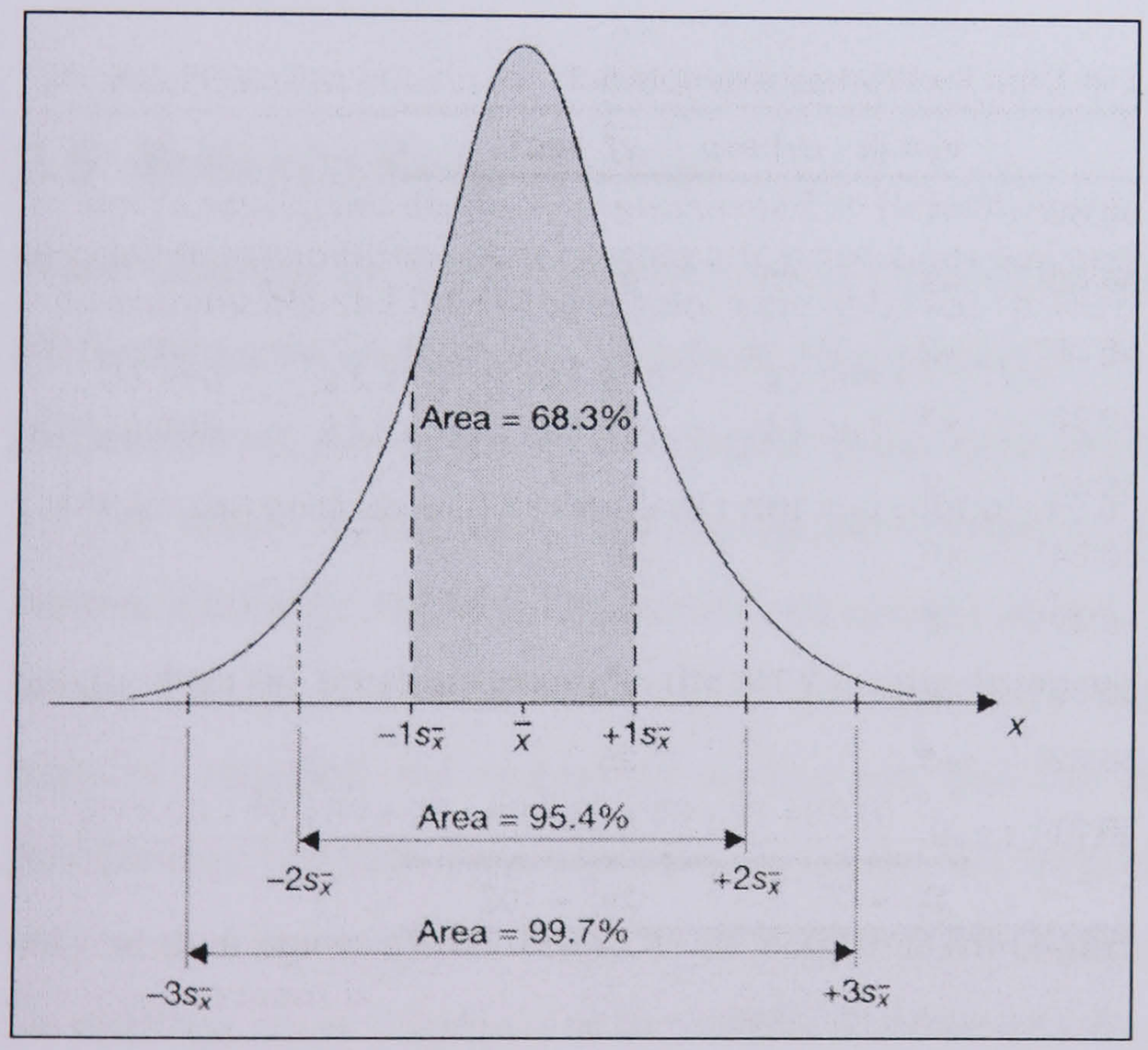

Figure 3.13 Normal error distribution curve, indicating confidence intervals (Uren and Price, 2006).

Approximately 68.3% of all measurements are expected to fall between $\pm\ \sigma$, and approximately 99.7% are expected to lie within $\pm\ 3\sigma$. The latter value is generally regarded as a critical measure of precision in surveying and photogrammetry, with measurements falling outside of this range ($\pm\ 3\sigma$) classified as outliers (Wolf and

Ghilani, 1997; Bannister et al., 1998). Specific percentage probabilities, as defined by Wolf and Ghilani (1997) (Table 3-3) have been utilised where appropriate in Chapters Five and Six. In this manner, the standard deviation of the measuring technique or DEM provides a useful measure for assessing the confidence with which observed terrain changes can be attributed to geohazard activity, as opposed to measurement error.

Multiplier	Percentage Probable Error (%)
0.6745 σ	50.0
1.0000 σ	68.3 ($\pm 1\sigma$)
1.6449 σ	90.0
1.9600 σ	95.0 ($\sim \pm 2\sigma$)
2.5760 σ	99.0
2.9650 σ	99.7 ($\sim \pm 3\sigma$)
3.2900 σ	99.9

Table 3-3 Standard deviation multipliers for percentage probable errors of the normal distribution (after Wolf and Ghilani, 1997).

3.5 Surface Registration

When adopting an integrated approach to monitoring, successful dataset registration is of fundamental importance. However, this procedure is far from straightforward. The difficulties of surveying in the coastal zone have already been discussed in Section 1.1.3.6, where it was noted that the dynamic nature of this environment often poses a serious challenge to the establishment of control points. This is related to two separate issues. Firstly, tidal conditions affect the short term stability of control points which may be required for terrestrial survey on the foreshore, and this is particularly problematic in beach environments. Secondly, the transient nature of the coastal terrain may pose a threat to the integrity of higher-order control points, such as those located on cliff-top areas (Gorman et al., 1998). Further concerns, relating in particular to the exploitation of archival aerial photography have already been outlined in Section 3.3.3.3. To recap, these relate to the initial problem of identifying suitable ground control points in an environment which can often prove relatively featureless in terms of hard detail, and the subsequent issue of ensuring that these points exist in the archival imagery, and have remained stable over the intervening time period.

Provided datasets are registered to a common reference frame, multi-temporal DEMs can be compared in order to identify regions of deformation, and quantify physical changes due to mass movement processes (Fabris and Pesci, 2005). However, the critical issue here relates to successful registration, and this introduces significant challenges. Böhm (2005) describes the integration of TLS and ALS for city modelling applications, and highlights reconciliation of the datasets to a common reference frame as a crucial step in facilitating data fusion. Cooper (1998) notes that changes to coordinates over time arise not only because of changes to the terrain itself, but also as a result of measurement errors and datum differences, and that as only the first effect is of interest in monitoring applications, it is necessary to minimise the effects of the latter. Exhaustive reconnaissance, redundant measurements, and incorporation of rigorous checks, carried out by experienced surveyors, will ensure that control errors are minimised. However, issues relating to the identification and integrity of control points in the dynamic coastal environment are difficult, if not impossible to overcome, as observed by Buckley (2003) in the context of photogrammetry. Furthermore, when considering the techniques of ALS, TLS and archival photogrammetry, the possibility of systematic error must always be considered. Such concerns highlight the importance of dataset registration, and the requirement for an effective and robust means of tackling this issue. To overcome the drawbacks of traditional approaches, particularly in relation to their dependence on physical ground control points, an alternative technique employing least squares-based surface matching has been implemented and further developed in this research. This approach offers a robust and efficient means of integrating multi-sensor, multi-temporal datasets, providing not only a registration mechanism, but also an inherent capability for change detection. Surface matching is introduced and discussed in detail in Chapter Four, where the specifics of the algorithm will be outlined. Additionally, further software developments will be presented, and the results of experimental testing assessed.

3.6 SUMMARY

Chapter Three has presented a strategy for integrated remote monitoring of coastal geohazards, and has detailed the associated methodology. While general concerns with regards to coastal zone monitoring were discussed in Chapter One, Chapter Three has introduced some specific constraints in relation to geohazard monitoring, highlighting

the requirement for a combined airborne-terrestrial approach in order to minimise terrain occlusions and permit remote, multi-scale monitoring. Furthermore, the importance of a historical component has also been noted, as this can provide an record of past geohazard activity, and an indication of the required spatial and temporal sensitivity of the present-day monitoring programme.

Following these discussions, an integrated remote coastal geohazard monitoring strategy, comprised of airborne and terrestrial laser scanning, and archival aerial photography has been presented. Photogrammetry is a well-established technique and represents the most accessible archive of metric information pertaining to coastal change over extended time periods. In contrast, the techniques of ALS and TLS, introduced in Sections 2.5 and 2.6 respectively, are still maturing, and there is a continuing requirement to fully asses the exciting potential which they offer for a range of applications, including that of coastal geohazard monitoring. However, their inclusion is also fully justified by their technological capabilities, particularly with regards to the remote nature of these techniques, and their ability to rapidly capture mass point cloud datasets over a range of scales. Chapter Three has thus included in-depth discussion on the individual monitoring components, including specifics of the particular sensors used for ALS and TLS acquisition.

Digital surface modelling has been introduced and discussed, particularly in relation to factors influencing DEM structure and accuracy. In conclusion, the challenges relating to dataset registration have been considered. These two topics are central to the monitoring strategy, as ultimately the individual datasets are analysed through their surface representations, and without successful dataset registration, there is a danger that the effects of mis-registration may be wrongly interpreted as genuine terrain change.

This chapter has introduced an integrated strategy for remote monitoring of coastal geohazards, based upon the techniques of ALS, TLS and archival aerial photography. This monitoring strategy will be further developed in Chapter Four, where robust surface matching will be introduced as a solution to the essential issue of dataset registration. The surface matching technique resides at the core of the monitoring strategy, and is designed to facilitate reliable reconciliation of disparate datasets.

CHAPTER 4

ROBUST INTEGRATION OF DIGITAL ELEVATION MODELS

4.1 INTRODUCTION

Chapter Three introduced a methodology for integrated monitoring of coastal geohazards, specifically focussing on the techniques of airborne and terrestrial laser scanning, with incorporation of retrospective analysis through aerial photography. The concept of digital surface modelling was also presented, and in relation to this, the importance of successful dataset registration was emphasised. From this discussion, it has become evident that effective integration of multi-sensor, multi-temporal datasets is highly dependant on the effectiveness of the registration technique. However, this in itself presents a major challenge, due in particular, to the dynamic nature of the coastal environment, which has proved largely problematic with respect to the implementation of traditional surveying methodology, as discussed in Section 2.2.

Successful and accurate dataset registration is of fundamental importance in any monitoring strategy, as this is a prerequisite for reliable change detection (Cooper, 1998). Any registration error introduced at this early stage can propagate into subsequent analysis, with the potential to contaminate measures of volumetric change, cliff recession rates, the interpretation of geohazard behaviour, and any ensuing actions based on such information. In conclusion to Chapter Three, Section 3.5 briefly introduced the concept of surface matching, and presented this as a potential solution to overcoming the difficulties associated with establishing reliable control points for dataset registration in the coastal zone. This technique is the sole focus of this chapter,

and will be introduced at some length, in reflection of its core importance in facilitating efficient and accurate coastal geohazard monitoring. The latter portion of the chapter will concentrate on the development of a robust surface matching algorithm, which, as will be subsequently explained, is crucial for the work proposed in this thesis, and which is also potentially valuable for a range of alternative terrain monitoring applications. Experimental testing of the robust algorithm will be presented, prior to its full-scale application to topographic datasets in Chapters Five and Six.

4.2 Surface Matching Overview

4.2.1 Introduction

The comparison of two or more surfaces is a common task in many applications, including the following (Habib and Schenk, 1999):

- sensor calibration (for example in ALS or photogrammetry), which often requires the comparison of an acquired surface, and the known surface (test field);
- change detection, which usually involves comparing two surfaces acquired at different times;
- merging of multiple datasets (fusion), where quality control is crucial;
- reconciliation of data acquired in local coordinate systems to a common, global reference system.

Surface matching is therefore introduced as an alternative, highly appropriate technique, which is beneficial for a number of reasons in the context of geohazard monitoring, as will be discussed in Section 4.2.3.

Surface matching is a relevant technique not only in geomatics, but also in the field of computer vision, where it has been described as a 'fundamental issue' (Zhang and Hebert, 1999). In the most general sense, the goal of surface matching is to determine the optimal transformation which aligns, or registers, two free-form 3D point sets, establishing the correspondence between them (Besl and McKay, 1992). It is important to recognise that one surface is usually treated as the 'template' or fixed reference

surface, while the other is regarded as the unfixed matching surface, with the objective being to determine the transformation required to align the matching surface with the reference surface. In computer vision, research into surface matching, which is also commonly referred to as the correspondence problem (Chen and Medioni, 1992; Dorai et al., 1997), has been driven by a number of issues. One of the prime applications is that of 3D object recognition (Johnson and Hebert, 1999), which can be of use, for instance, in the quality control of manufactured objects. This was a major motivation for the work of Besl and McKay (1992), who proposed the Iterative Closest Point (ICP) matching algorithm, which has subsequently become well-established. The ICP algorithm searches for pairs of closest points between two surfaces (Figure 4.1), and through least squares-based iterative minimisation of the mean squared distance metric, determines the six-parameter rigid transformation relating the two surfaces. A variation of this approach is presented by Chen and Medioni (1992) who instead of searching for point to point correspondence between the two surfaces, minimise point to tangent plane distances in the direction of the surface normal, in order to recover the transformation parameters. The ICP approach is discussed further in Section 4.3.1.

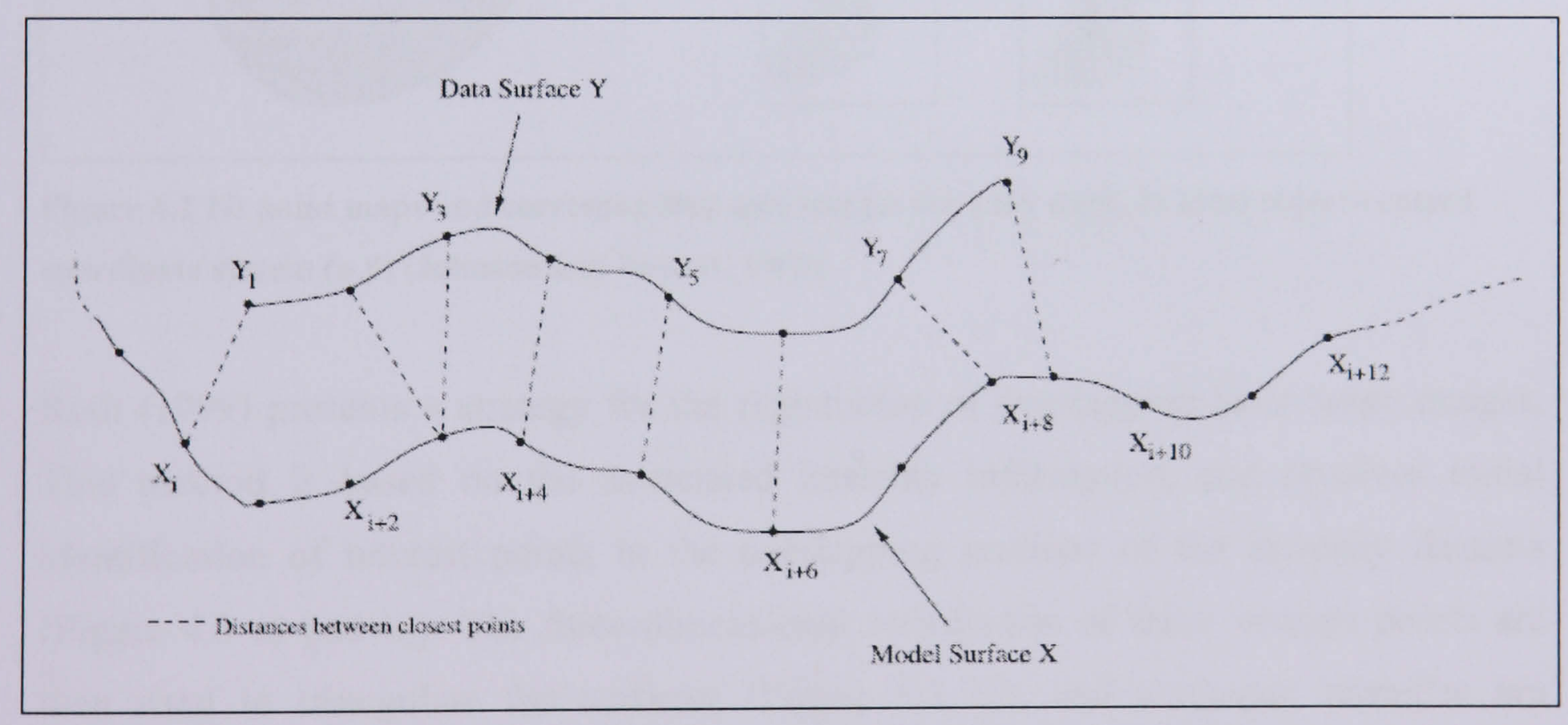

Figure 4.1 Corresponding point selection concept of the ICP algorithm (Planitz et al., 2005).

Johnson and Hebert (1998, 1999) introduce the concept of spin images for surface matching and 3D object recognition. Through this approach, surface shape is described via triangulated surface points, and their associated surface normals. For each point, the relative positions of other points on the same surface can be described as a two-dimensional image representation – referred to as the spin image, as is illustrated in

Figure 4.2. In this manner, the three-dimensional surface matching problem can be simplified to a two-dimensional image matching task, and by matching images between two surfaces, point correspondences can be established in order to determine the global transformation relating the two surfaces. The final transformation is then refined through application of a modified version of the ICP algorithm.

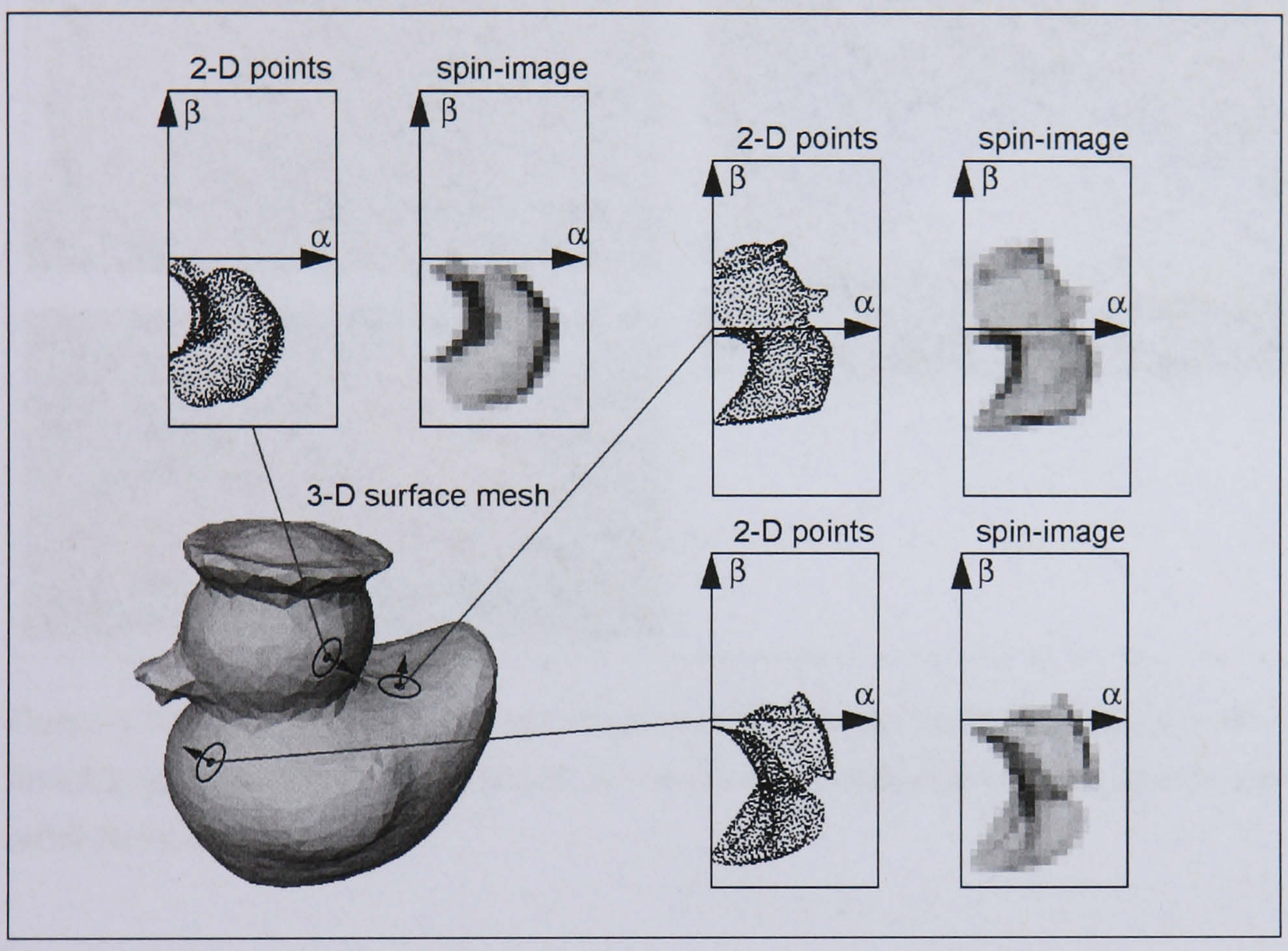

Figure 4.2 2D point maps and corresponding spin images for a toy duck, in local object-centred coordinate system (α,β) (Johnson and Hebert, 1999).

Roth (1999) presents a strategy for the registration of overlapping laser range images. This method is based on the associated intensity information, and involves initial identification of interest points in the overlapping portions of the intensity datasets (Figure 4.3 a) and b)). The three-dimensional coordinates of these interest points are then used to triangulate the surfaces (Figure 4.3 c)), and conjugate triangles are identified, and aligned to determine the transformation parameters, allowing for the surfaces to be registered (Figure 4.3 d)). While this technique reportedly produced encouraging results in application to experimental datasets, one of the major limitations would appear to be a dependence on intensity (or image) information, which may restrict its more general applicability.

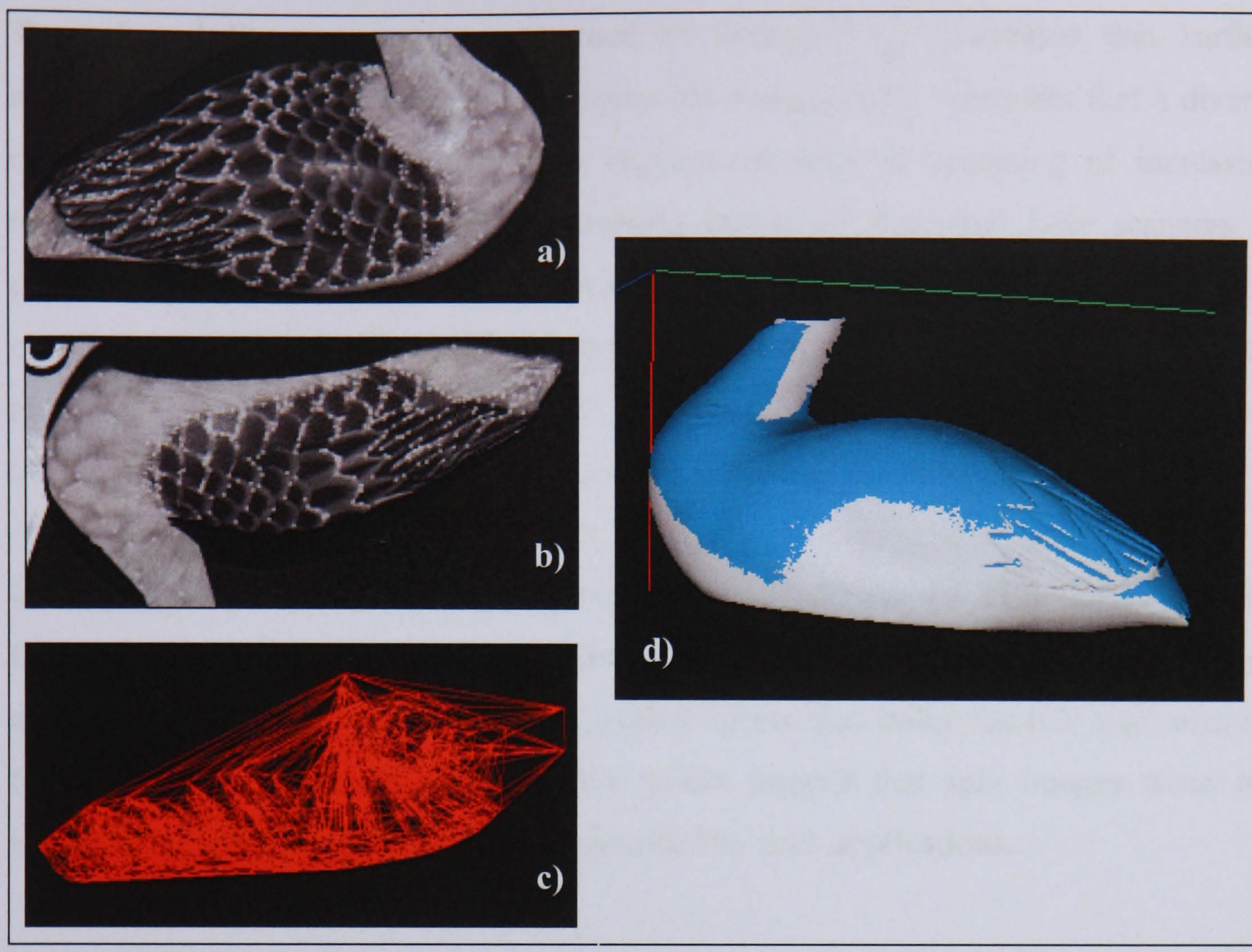

Figure 4.3 Surface matching through selection of intensity-based interest points, a) & b), which are then triangulated, e.g. c), and matched, to recover the transformation and align the surfaces, d) (after Roth, 1999)).

4.2.2 Surface Matching in the Geomatics Domain

The transformation of point data from one coordinate system to another is a fundamental task in surveying and mapping (Wolf and Ghilani, 1997). The requirement for this may arise, for example, where photogrammetrists initially working in some convenient arbitrary coordinate system require to transform their measurements to a national or global reference frame (Wolf and Dewitt, 2000), perhaps to permit integration with data from other sources. However, for a number of reasons, this task may prove to be far from trivial. Difficulties associated with carrying out successful registration in the coastal context have already been discussed, and in other settings it may be impossible or unethical to establish control markers (e.g. industrial and medical applications). Hence, the registration task addressed by surface matching is of great relevance to geomatics applications.

The selected literature review presented in Section 4.2.1 illustrated that surface matching is an active research area in computer vision, and it is evident that a diverse range of approaches exist. The basic registration issue is becoming of increasing relevance in geomatics also. The increasing uptake of terrestrial laser scanners in particular, has led to renewed interest in techniques for improving and automating point cloud registration (e.g. Zhao and Shibasaki, 2001; Akça, 2003; Scaioni, 2003). In this regard, it is interesting to note that much of the original research into surface matching in computer vision was based on data acquired from laser scanning devices.

Guarnieri et al. (2003) utilise spin images for registration of TLS datasets, while Carmichael et al. (1999) investigate this approach for matching of terrain datasets acquired from laser scanning. However, as both approaches utilise the ICP algorithm for final refinement of the registration, this would suggest that spin images alone are incapable of achieving the accuracies demanded by such applications.

Zhao and Shibasaki (2001) present a technique for registration of TLS datasets. This firstly establishes a 'Z-Image' for each scan, where all range points are projected onto a two-dimensional X-Y plane, under the assumption that the scanner is level (Figure 4.4). Features such as walls will be represented as lines in the Z-Image, and the matching algorithm proceeds by extracting these line segments and analysing intersection angles and distances in order to establish a coarse alignment. Fine adjustment is performed through an ICP-based approach. While the authors report encouraging results, this strategy targets urban datasets, and is unlikely to work in natural terrain, where the Z-Image may lack the necessary geometric features.

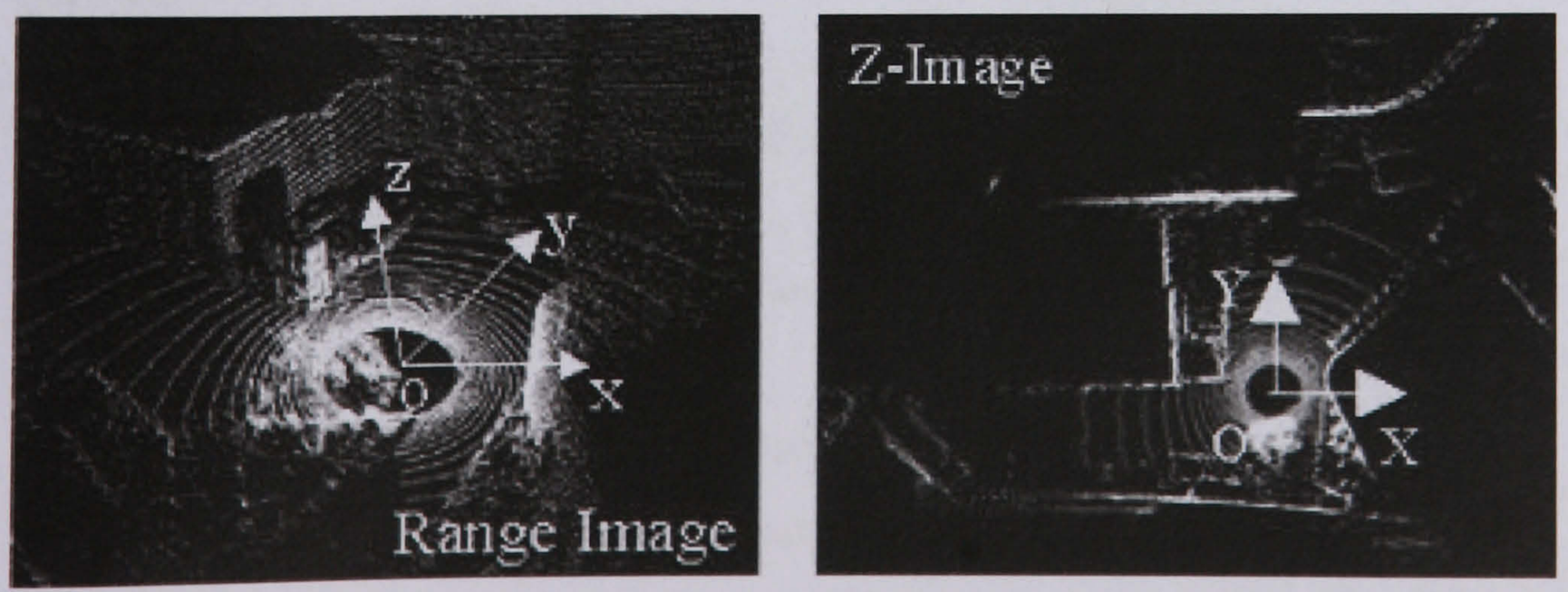

Figure 4.4 TLS point cloud (left), and associated Z-Image (right), from which features such as walls can be extracted and used as registration primitives (Zhao and Shibasaki, 2001).

Habib and Schenk (1999) propose a method to determine the initial approximations of the unknown transformation parameters based on the Hough transform, which introduces an accumulator array and voting scheme for parameter determination. Through this approach, surfaces are compared in the direction of the surface normal between points on the matching surface and the corresponding surface patch in the reference point set. In order to determine the values of the transformation parameters, an accumulator array is used to record the possible solutions for each parameter individually, while the remaining parameters are held fixed. Once this parameter has been estimated for each point on the matching surface, and all possible combinations of corresponding surface patches, a distinct peak in the accumulator array should reveal the true parameter value (Figure 4.5), and the procedure can be repeated for the next parameter until all parameters have been solved for. As a final step, the precise transformation can be determined simultaneously through a least-squares adjustment. In a development of this approach, Habib and Kelley (2001) implemented this technique for tackling the automatic relative orientation task in digital photogrammetry.

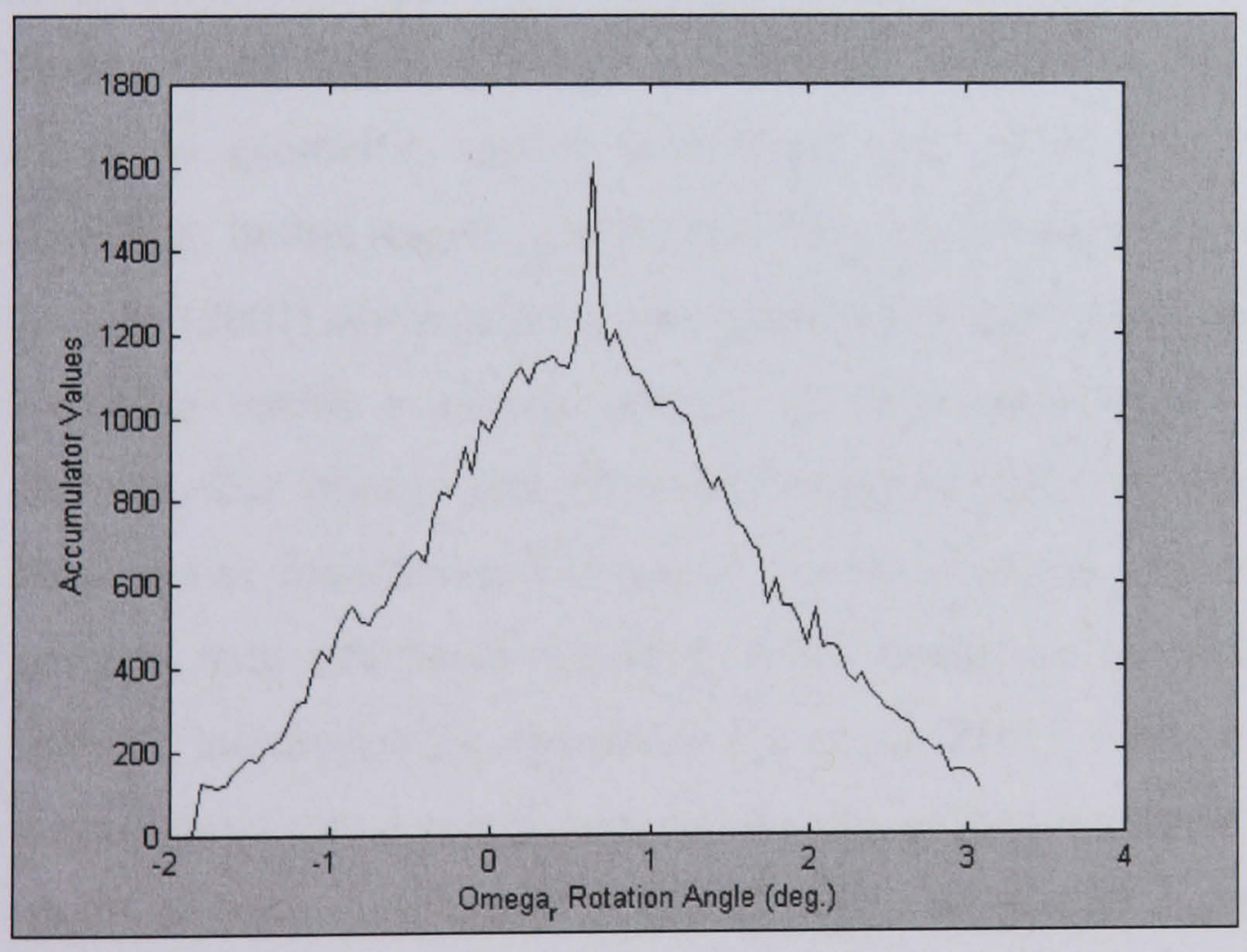

Figure 4.5 Accumulator array for estimation of the ω rotation parameter through the Hough transform approach. The peak value indicates the parameter solution. (Habib and Kelley, 2001).

Bae and Lichti (2004) and von Hansen (2006) present feature-based approaches to matching of TLS datasets, utilising surface normal vectors and changes of curvature (Bae and Lichti, 2004, Figure 4.6), and planar surfaces (von Hansen, 2006). However, both of these strategies provide only approximate solutions, which require further

refinement through other means (such as the ICP) in order to determine a more precise set of transformation parameters. However, feature-based approaches such as these are likely to be poorly-suited to unstructured natural scenes (Kweon and Kanade, 1992), such as those found in the coastal zone.

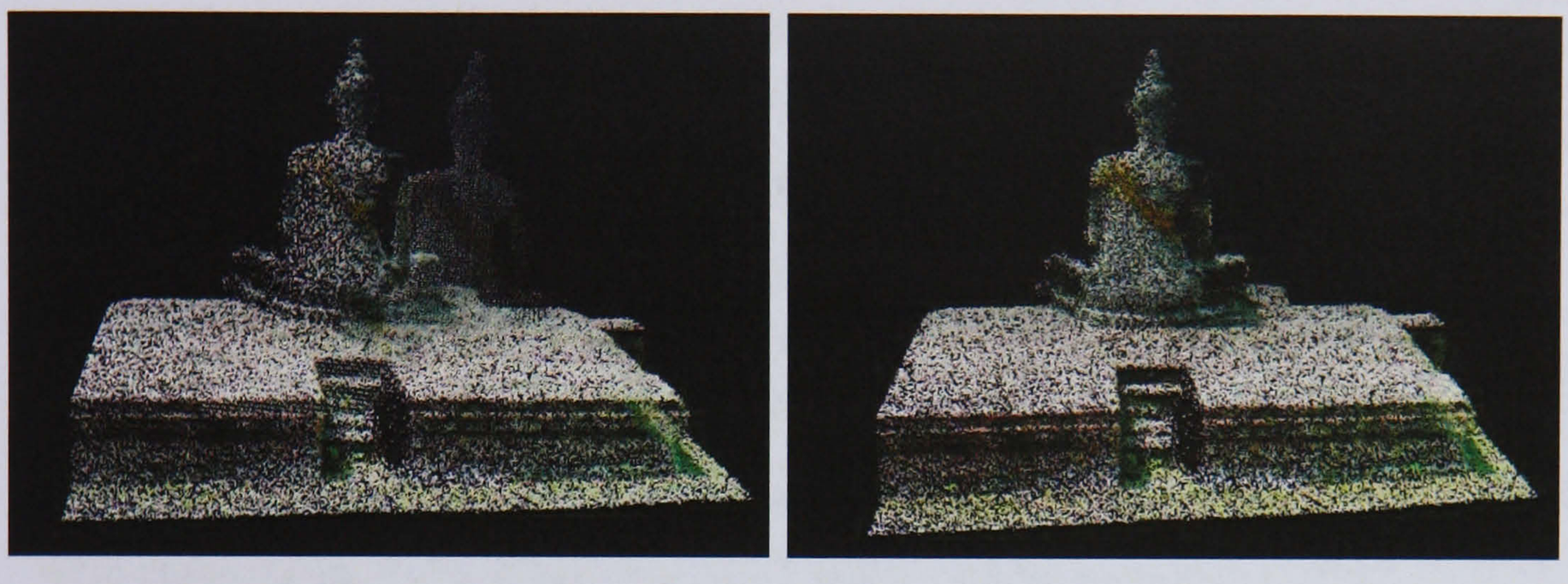

Figure 4.6 TLS representations of a Buddha statue prior to alignment, left, and after feature-based registration, right (Bae and Lichti, 2004).

In general, most approaches to surface matching fall into one of two categories: the feature-based approach, which is reliant on establishing the correspondences between extracted geometric surface primitives; and the alternative strategy of area-based matching. In this respect, surface matching is perhaps not dissimilar to image matching. Li et al. (2001) compare these two fundamental approaches, noting that as feature-based matching entails a certain amount of pre-processing in order to identify suitable features, this strategy can often be computationally intensive. Furthermore, although large initial orientation differences can be tolerated, ultimately, this method is less accurate than area-based matching, which avoids the accumulation of error introduced through pre-processing operations (Li et al., 2001). However, area-based approaches require good initial approximations for the unknown transformation parameters. These observations are reflected in the examples presented earlier in this section, which concentrate on the application of feature-based matching for pre-alignment of the surfaces, before utilising area-based procedures (such as the ICP algorithm) in order to refine this transformation and achieve a more accurate solution. The following discussion assumes that pre-alignment has already been achieved, and focuses on resolving the higher order registration problem which is of primary importance for most geomatics applications.

While some of the more recent research into surface matching in geomatics has focussed on laser scanning-related applications, much of the groundwork concentrated on photogrammetric aspects, and the application of least squares-based matching, where DEMs are utilised as control surfaces. Ebner and Strunz (1988) were amongst the first to implement least squares surface matching, in their research into the use of DEMs for the absolute orientation of photogrammetric blocks. At the same time, this approach was also being developed by Rosenholm and Torlegård (1988). In their study, datasets had been measured through analytical techniques in a regular grid fashion, and matching was carried out by minimisation of the vertical distances between the two surfaces, allowing for determination of the seven-parameter conformal coordinate transformation required to absolutely orient the stereo model. Rosenholm and Torlegård (1988) reported that for the elevation component, results of the absolute orientation were comparable, if not superior to those obtained through conventional means. Karras and Petsa (1993) present an excellent overview of their application of this technique to close-range photogrammetry for medical applications, highlighting the potential of surface matching for overcoming the expense and challenges which are often associated with establishing suitable control schemes. This point is also emphasised by Rosenholm and Torlegård (1988). Additionally, Karras and Petsa (1993) draw attention to a number of salient issues, including the requirement for gross error treatment. Further investigation has also been carried out by Pilgrim (1996a, 1996b), who examines least squares matching as a tool for deformation detection (refer to Section 4.4.2 for further discussion). Mitchell and Chadwick (1999) introduce a further close-range application, this time with respect to dental erosion analysis. Tooth replicas for the study were sampled in regular grid manner by a mechanical measuring device, and the surfaces were matched through minimisation of vertical distances.

Regular grid-based data structures have formed the basis for all of the least squares matching studies highlighted above. However, Maas (2000, 2002) implements matching in irregular TIN-based ALS datasets, through minimisation of vertical surface differences, with the goal being to recover the three-dimensional discrepancies (only the three translation parameters were considered) between overlapping portions of ALS strips. Gruen and Akça (2005) present a variation of this approach which instead of minimising the vertical distance, minimises the Euclidian distance. Their decision to focus on the Euclidian distance may be reflective of the application area, which

primarily focuses on TLS acquisition of building facades, and heritage artefacts. Such scenes would be poorly suited to minimisation of vertical differences, as these surfaces are largely vertical in composition. In this investigation, Gruen and Akça (2005) also explored curve to surface matching (Figure 4.7), and the possibility of matching based on sub-patches rather than the entire dataset, in order to reduce computational cost. Buckley (2003) also developed a least squares matching algorithm for application to irregular point datasets. This particular research is highly relevant, as it considers the matching of multi-sensor datasets – specifically the matching of small-format aerial photogrammetric DEMs to those acquired through kinematic GPS, and for the purposes of difference detection in coastal areas. The details of this specific implementation will be described more fully in Section 4.3.3 as this forms the basis for the developments presented in this thesis.

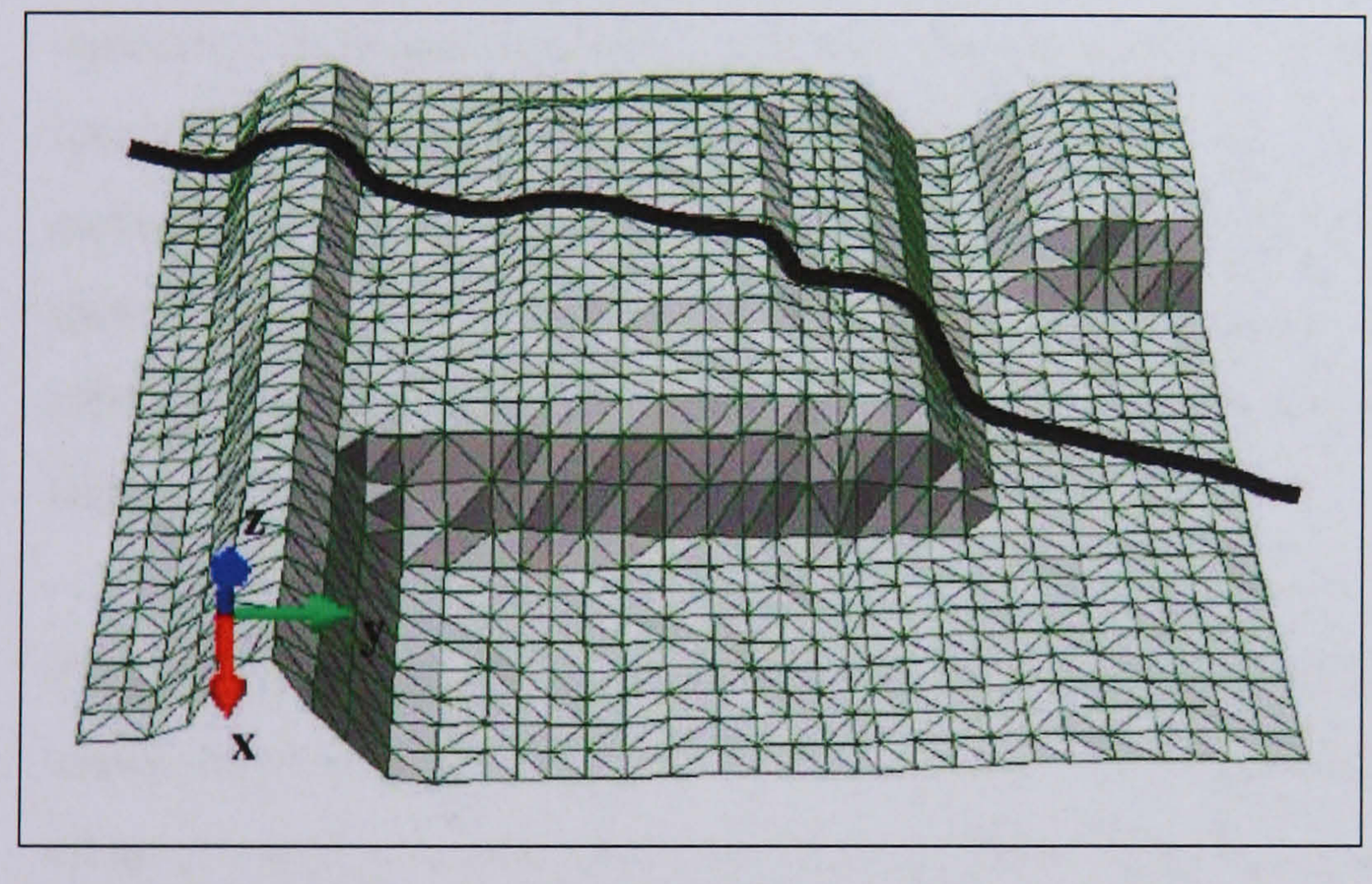

Figure 4.7 Curve to surface matching (Gruen and Akça, 2005).

Particulars of least squares-based matching are discussed more fully in Section 4.3. It is important to note however, that while the examples discussed above include slight variations in the implementation of the general least squares matching algorithm, there may in effect be no significant difference between the final results (Mitchell and Chadwick, 1999).

4.2.3 Suitability for Coastal Geohazard Monitoring

There are a number of factors supporting the decision to employ surface matching in coastal geohazard monitoring. Several researchers have highlighted the difficulties associated with identifying and establishing control points in the coastal zone (Dixon et al., 1998; Brown and Arbogast, 1999), an issue which has been discussed already. Moreover, the expense associated with such a procedure can be significant (Rosenholm and Torlegård, 1988; Karras and Petsa, 1993). Surface matching offers the possibility to overcome this reliance on physical control points, and instead exploit the geometry of the DEM surfaces in order to perform the essential registration task.

A prominent theme to-date has been the investigation of surface matching for change detection and deformation analysis (Pilgrim, 1996b; Mitchell and Chadwick, 1999; Li et al., 2001; Mills et al., 2003). Difference detection is an inherent feature of least squares matching, as examination of the post-match surface residuals directly reveals the location and magnitude of discrepancies between the two surfaces. Least squares surface matching is therefore a particularly appropriate technique for coastal geohazard monitoring, as multi-temporal surfaces can be registered in an efficient and cost-effective manner, which is simultaneously capable of revealing terrain change over time.

Finally, the flexibility of least squares matching for handling irregular point data is important to consider, and the benefits that TIN data structures can offer over grids has already been discussed. Moreover, Maas (2000, 2002) notes that in the context of laser scanning data, interpolation to a regular grid may degrade the dataset by introducing systematic errors, especially in occluded regions. This is certainly undesirable for change detection studies, where it is important to avoid introducing any effects which may lead to erroneous change detection, or reduce the confidence with which genuine change can be detected.

Buckley (2003) applied least squares surface matching for detection of change in the coastal zone, and consequently, the findings of this investigation are highly relevant. Buckley (2003) highlighted the following specific benefits of the surface matching technique:

- as a data fusion technique, surface matching is semi-automated and offers inherent quality control through the least squares statistics, and final surface differences;
- the quality of individual datasets can be examined through the matching precision, and possible areas of error will be highlighted through the residuals;
- surface matching offers an inherent capacity for change detection;
- surface matching provides a superior means of recovering systematic error in comparison to conventional registration approaches.

However, Buckley (2003) cautions that the final solution is dependant on the quality and distribution of the source data, and also reiterates the importance of surface gradients, which can be thought of as a form of surface texture. A lack of suitable texture may result in erroneous minimisation of surface differences, resulting in a poor transformation (Buckley, 2003). Ultimately however, Buckley (2003) notes that not only does surface matching provide an efficient means of overcoming photogrammetric control difficulties in the coastal zone, but it also enables synergistic dataset fusion, with an in-built capacity for change detection.

4.3 Least Squares Surface Matching

4.3.1 Introduction

Least squares based surface matching was introduced in Section 4.2.2, where a number of examples of its use in relation to geomatics were presented. As the technique adopted for dataset registration and integration in the research presented here, the motivations behind selecting this particular surface matching technique will now be discussed, and fundamentals of this approach will be outlined in greater detail.

It is evident from the review of surface matching literature, as presented in Section 4.2, that the ICP algorithm is widely utilised, both in computer vision and geomatics. However, the ICP approach suffers from a number of drawbacks, which renders it inappropriate here. The ICP strategy attempts to minimise the distance from each point in one dataset to the corresponding closest point of the other dataset, and hence is reliant on a local operator, which can cause the solution to converge to a local minimum rather

than the most suitable global minimum (Besl and McKay, 1992; Roth, 1999; Bae and Lichti, 2004). A further important weakness is that the ICP algorithm is unsuited to datasets containing regions of outliers, where portions of one dataset do not directly correspond to the other (Besl and McKay, 1992) – a situation which is likely to exist in change detection studies, such as the one presented here. Instead, an alternative least squares-based technique, as outlined in the following sections, will be utilised.

The examples presented in the latter half of Section 4.2.2 demonstrated the successful application of least squares matching as an alternative registration technique in the geomatics domain. While a number of these studies have focussed on close-range applications (Karras and Petsa, 1993; Pilgrim, 1996a; Mitchell and Chadwick, 1999), others have utilised topographic surfaces, similar to those of relevance in this research (Ebner and Strunz, 1988; Rosenholm and Torlegård, 1988; Maas, 2000, 2002; Buckley, 2003). In such cases, least squares matching is highly suitable, as DEMs of natural terrain can be considered as continuous surfaces, which are normally 2.5D in nature – that is to say, that height is effectively considered as an attribute of planimetric position. This scenario is highly favourable to minimisation of vertical surface differences, and does not warrant implementation of the more complex ICP algorithm (Mitchell and Chadwick, 1999), which in any case, may be susceptible to the failings outlined above. Pilgrim (1996b) draws attention to the following favourable characteristics of matching through least squares minimisation of surface differences:

- least squares adjustment techniques are well established;
- the least squares technique facilitates statistical analysis of the final solution and the individual transformation parameters;
- least squares matching is based on slope calculations, which are relatively straightforward to implement;
- least squares matching is flexible in a number of ways – the number of transformation parameters can be altered; the parameters can be weighted; and the solution can be made robust to outliers;
- the datasets utilised for least squares matching generally contain a high degree of redundancy, thus improving the quality of the solution.

In addition, Cooper and Cross (1988) note that the least squares procedure is capable of attaining a unique solution, and that least squares estimates are the minimum variance, best estimates. As the observation equations for least squares matching are non-linear, good initial approximations of the unknown parameter values must be supplied (Schenk, 1999; Mills et al., 2003). While this is often highlighted as an inconvenience, in geomatics this requirement generally does not present a significant difficulty, as often a coarse alignment will be available as a matter of course, or can be obtained with little inconvenience. Indeed surface matching is highly suited to the refinement of registration solutions, or removal of systematic error, as observed by Rosenholm and Torlegård (1988) and Maas (2002).

In this research, the surface matching algorithm developed and implemented by Buckley (2003) has been utilised, and further developed, as detailed in Section 4.4, and summarised in Miller et al. (2006); Miller et al. (2007) and Miller et al. (in review). This algorithm minimises vertical differences between the two surfaces, and is capable of handling datasets structured in grid or TIN fashion. Further details of the initial development of this algorithm, and its application to coastal change monitoring can be found in Buckley (2003); Mills et al. (2003) and Mills et al. (2005). However, the mathematical foundations, and issues relating to practical implementation of this approach will be outlined in the following section.

4.3.2 Theoretical Basis

Least squares surface matching of DEMs is effectively a registration problem, typified by the requirement to transform a surface of poorer orientation (the matching surface) into the coordinate system of the fixed reference surface. This situation may also arise where surfaces existing in different coordinate systems must be reconciled for purposes of comparison or integration. The challenge relates to recovering the transformation parameters required to perform this operation. This issue can be tackled from the surface matching perspective by firstly considering the conventional means of addressing such a problem.

4.3.2.1 Three-Dimensional Conformal Coordinate Transformation

The three-dimensional conformal coordinate transformation, also referred to as the similarity transformation, provides a means of converting from one three-dimensional coordinate system to another, and is a standard procedure in surveying and photogrammetry (Wolf and Ghilani, 1997). In total, seven parameters are required: three rotations (ω, ϕ, κ), three translations (T_x, T_y, T_z), and a scale parameter (s). In matrix notation, the 3D conformal coordinate transformation can be expressed as:

$$\overline{X} = sM^T X + T$$

Eqn. 4-1

Where the initial coordinates of a point (X), are modified through application of the scale factor (s), the rotations, as defined by the rotation matrix (M), and the translation vector (T), in order to obtain the final transformed coordinates ($\overline{X}$). These matrices are defined in full below.

$$\overline{X} = \begin{bmatrix} X \\ Y \\ Z \end{bmatrix}$$

Eqn. 4-2

$$X = \begin{bmatrix} x \\ y \\ z \end{bmatrix}$$

Eqn. 4-3

$$T = \begin{bmatrix} T_x \\ T_y \\ T_z \end{bmatrix}$$

Eqn. 4-4

$$M = \begin{bmatrix} m_{11} & m_{12} & m_{13} \\ m_{21} & m_{22} & m_{23} \\ m_{31} & m_{32} & m_{33} \end{bmatrix}$$

Eqn. 4-5

Where, the terms of M are combinations of the rotations around the x, y and z axes as follows:

$$
\begin{aligned}
m_{11} &= \cos\phi\cos\kappa \\
m_{12} &= \sin\omega\sin\phi\cos\kappa + \cos\omega\sin\kappa \\
m_{13} &= -\cos\omega\sin\phi\cos\kappa + \sin\omega\sin\kappa \\
m_{21} &= -\cos\phi\sin\kappa \\
m_{22} &= -\sin\omega\sin\phi\sin\kappa + \cos\omega\cos\kappa \\
m_{23} &= \cos\omega\sin\phi\sin\kappa + \sin\omega\cos\kappa \\
m_{31} &= \sin\phi \\
m_{32} &= -\sin\omega\cos\phi \\
m_{33} &= \cos\omega\cos\phi
\end{aligned}
$$

Eqn. 4-6

By conventional means, the seven transformation parameters can be solved for if the coordinates of at least two horizontal and three vertical control points are available in both systems. However, in practice, additional control points would usually be utilised in order to provide redundancy and thus permit a least squares solution to be obtained (Wolf and Dewitt, 2000). For each control point, the following set of equations can then be formed:

$$
\begin{aligned}
X &= s(m_{11}x + m_{21}y + m_{31}z) + T_x \\
Y &= s(m_{12}x + m_{22}y + m_{32}z) + T_y \\
Z &= s(m_{13}x + m_{23}y + m_{33}z) + T_z
\end{aligned}
$$

Eqn. 4-7

In order to obtain a solution, these equations must be linearised with respect to the seven unknown parameters. This can be carried out through application of a Taylor series expansion, evaluating first-order terms only. This then leads to the following linearised transformation for the height term Z of a point, P:

$$
\begin{aligned}
Z_P = (Z_P)_0 &+ \left(\frac{\partial Z_P}{\partial s}\right)_0 \Delta s + \left(\frac{\partial Z_P}{\partial \omega}\right)_0 \Delta\omega + \left(\frac{\partial Z_P}{\partial \phi}\right)_0 \Delta\phi \\
&+ \left(\frac{\partial Z_P}{\partial \kappa}\right)_0 \Delta\kappa + \left(\frac{\partial Z_P}{\partial T_x}\right)_0 \Delta T_x + \left(\frac{\partial Z_P}{\partial T_y}\right)_0 \Delta T_y + \left(\frac{\partial Z_P}{\partial T_z}\right)_0 \Delta T_z
\end{aligned}
$$

Eqn. 4-8

Where the subscript 0 refers to terms evaluated at their initial approximations. For further details, refer to Wolf and Dewitt (2000). Corresponding linearised equations can be written for X_P and Y_P. Equation 4-8 is now in a form suitable for solving through least squares, and can be expressed in matrix notation as:

$$AX = L + V$$

Eqn. 4-9

Where A is the design matrix (the partial derivative terms of the unknowns); X is the vector of parameter corrections; L is the vector of discrepancies between start values and current values; and V is the vector of residuals.

4.3.2.2 Surface Matching Theory

Having outlined the mathematical basis for converting between two 3D coordinate systems, namely the 3D conformal coordinate transformation, it is necessary to consider how this concept can be applied to the surface matching problem. Instead of utilising conventional control points, the points on one surface are used to derive control information, and in this manner, a solution is achieved through minimising the vertical surface separations in order to attain a best-fit position (Mitchell and Chadwick, 1999). The development of the mathematical model for surface matching can be found in Rosenholm and Torlegård (1988); Karras and Petsa (1993); Mitchell and Chadwick (1999) and Gruen and Akça (2005), with slight variations. The salient details of the strategy implemented by Buckley (2003) are revisited here.

Two points, P_1 at (X_1, Y_1, Z_1) on the reference surface *S1*, and P_2 at (X_2, Y_2, Z_2) on the matching surface *S2*, can be introduced. These points can be considered as true conjugates, such that P_2 should equal P_1 when transformed by a set of unknown parameters, $p = \{p_i\}$, where $p_i = p_i^0 + \Delta p_i$. Consequently, the vertical discrepancy (δZ) between P_1 and P_2 should be zero, as follows:

$$\delta Z = Z_2^{Trans} - Z_1 = 0$$

Eqn. 4-10

Where the superscript *Trans* indicates P_2 transformed by parameters $p = \{p_i\}$. Corresponding expressions exist for the X and Y components. However, random and systematic errors in the datasets, compounded by parametric errors, may dictate that this condition is not achieved. Consequently, discrepancies ΔX, ΔY and ΔZ will be introduced to the transformed point, P_2^{Trans}, where the Z component (Z_2^{Trans}) can be expressed as:

$$Z_2^{Trans} = Z_2\left(p_i^0\right) + \Delta Z = Z_2\left(p_i^0\right) + \frac{\partial Z}{\partial p_1}\Delta p_1 + ... + v$$

Eqn. 4-11

Where $Z_2\left(p_i^0\right)$ is the current approximation for Z_2^{Trans} and the discrepancy ΔZ is evaluated through the parameter corrections, Δp_i, ignoring higher order terms. v is the remaining residual error. Corresponding expressions exist for X_2^{Trans} and Y_2^{Trans}, with errors ΔX and ΔY respectively. Furthermore, these discrepancies in P_2^{Trans} mean that the erroneous Z_2^{Trans} is no longer being compared with the correct Z_1 value, but with the value located at $X_1 + \Delta X$, $Y_1 + \Delta Y$. This gives rise to an error, ΔZ_e in Z_1:

$$\Delta Z_e = -\frac{\partial Z}{\partial X}\Delta X - \frac{\partial Z}{\partial Y}\Delta Y$$

Eqn. 4-12

where $\Delta X = \left(\frac{\partial X}{\partial p_1}\right)\Delta p_1 + ...$ and, $\Delta Y = \left(\frac{\partial Y}{\partial p_1}\right)\Delta p_1 + ...$

Consequently, Equation 4-10 must be re-evaluated as:

$$\delta Z = \left[Z_2(p_i^0) + \Delta Z\right] - \left[Z_1 - \Delta Z_e\right]$$

Eqn. 4-13

Where terms are as defined in Equations 4-11 and 4-12. With residual term, v, included, Equation 4-13 can be expanded, rearranged, and written in full as:

$$\delta Z = \left[Z_2(p_i^0) - Z_1\right] + \frac{\partial Z}{\partial s}\Delta s + \frac{\partial Z}{\partial \omega}\Delta\omega + \frac{\partial Z}{\partial \phi}\Delta\phi + \frac{\partial Z}{\partial \kappa}\Delta\kappa + \frac{\partial Z}{\partial T_x}\Delta T_x + \frac{\partial Z}{\partial T_y}\Delta T_y$$
$$+ \frac{\partial Z}{\partial T_z}\Delta T_z - \frac{\partial Z}{\partial X}\frac{\partial X}{\partial s}\Delta s - \frac{\partial Z}{\partial X}\frac{\partial X}{\partial \omega}\Delta\omega - \frac{\partial Z}{\partial X}\frac{\partial X}{\partial \phi}\Delta\phi - \frac{\partial Z}{\partial X}\frac{\partial X}{\partial \kappa}\Delta\kappa - \frac{\partial Z}{\partial X}\frac{\partial X}{\partial T_x}\Delta T_x$$
$$- \frac{\partial Z}{\partial X}\frac{\partial X}{\partial T_y}\Delta T_y - \frac{\partial Z}{\partial X}\frac{\partial X}{\partial T_z}\Delta T_z - \frac{\partial Z}{\partial Y}\frac{\partial Y}{\partial s}\Delta s - \frac{\partial Z}{\partial Y}\frac{\partial Y}{\partial \omega}\Delta\omega - \frac{\partial Z}{\partial Y}\frac{\partial Y}{\partial \phi}\Delta\phi - \frac{\partial Z}{\partial Y}\frac{\partial Y}{\partial \kappa}\Delta\kappa$$
$$- \frac{\partial Z}{\partial Y}\frac{\partial Y}{\partial T_x}\Delta T_x - \frac{\partial Z}{\partial Y}\frac{\partial Y}{\partial T_y}\Delta T_y - \frac{\partial Z}{\partial Y}\frac{\partial Y}{\partial T_z}\Delta T_z + v$$

Eqn. 4-14

This gives the full, linearised observation equation, suitable for solving through least squares. With reference to Equation 4-9, this allows the design matrix (A) to be evaluated, through the partial derivatives with respect to the unknown parameters; X is the vector of parameter corrections; L is the vector describing the surface separations; and finally, the vector, V, is populated by the residual terms (v). Buckley (2003) describes in detail the formation of the design matrix from the above observation equation. It should be noted that the terms $\partial Z / \partial X$ and $\partial Z / \partial Y$ represent the surface gradients, and form a core aspect of the design matrix. Furthermore, they are essential for achieving a successful solution (Karras and Petsa, 1993; Mitchell and Chadwick, 1999; Schenk, 1999), as will be explained more fully in the following section.

4.3.3 3DSurf Matching Algorithm

The development of the surface matching software utilised and then developed in this research, 3DSurf, is detailed by Buckley (2003). Primary aspects are outlined here. The main task in surface matching relates to identifying conjugate points on both surfaces. Whereas such information is inherent in the conventional control point-based transformation, this is not so with surface matching. In surface matching, each point effectively provides a control point in height (Ebner and Strunz, 1988). Where data is sampled in an irregular manner, the search for conjugate points is complicated, and no true conjugate points may exist (Buckley, 2003). This scenario will also occur where datasets have been acquired through different techniques, and in this situation, surface

discrepancies will always exist, thus introducing minor errors or parameter deviations to the matching algorithm (Mills et al., 2003).

In least squares matching of TIN-based data, the conjugate point issue is addressed through the interpolation of surface patches (Maas, 2000; Mills et al., 2003). Through this process, triangulation of the reference surface (*S1*) is carried out, and can be stored and used to determine the enclosing triangle for a point on the matching surface. The surrounding *S1* points are then used to interpolate a direct *S1* conjugate height value, Z_1, thus allowing minimisation of the vertical distances between the two surfaces in a global least squares fashion, permitting recovery of the transformation parameters. This is explained in greater detail below.

The quality of the interpolation is critical to the success of the matching algorithm (Buckley, 2003). Interpolation error will introduce inaccuracies to the vertical surface difference observations. However, Buckley (2003) observes that the trade-off between improved solution accuracy, and increased computational expense, does not justify the implementation of higher order interpolation techniques, such as polynomial fitting. Furthermore, Mitchell (1994) reports that planar interpolation appears to produce more reliable results than the polynomial approach. Consequently, the 3DSurf algorithm relies on planar interpolation, although an option for kriging interpolation is also available (refer to Section 3.4.3 for discussion on interpolation strategies).

As stated in Section 4.3.2.2, surface matching is heavily reliant on the gradients in the X and Y directions. However, these gradients can only be approximated, as the DEM is comprised of discrete samples, and thus is merely an approximation of a continuous surface (Mills et al., 2003). As the gradients are utilised directly in the design matrix, then any errors will propagate into this, and affect the quality of the subsequent match (Rosenholm and Torlegård, 1988). Karras and Petsa (1993) observe that the gradient values directly influence the precision of the parameter solutions, with the determination of the T_x and T_y translations exclusively dependant on the respective gradients in these directions. Rosenholm and Torlegård (1988); Schenk (1999); Habib and Lee (2001) and Buckley (2003) discuss the importance of these surface slopes, and further considerations with regards to ensuring that the surfaces are suitably

constrained. The least squares surface matching algorithm, as developed by Buckley (2003), is illustrated in diagrammatic form in Figure 4.8.

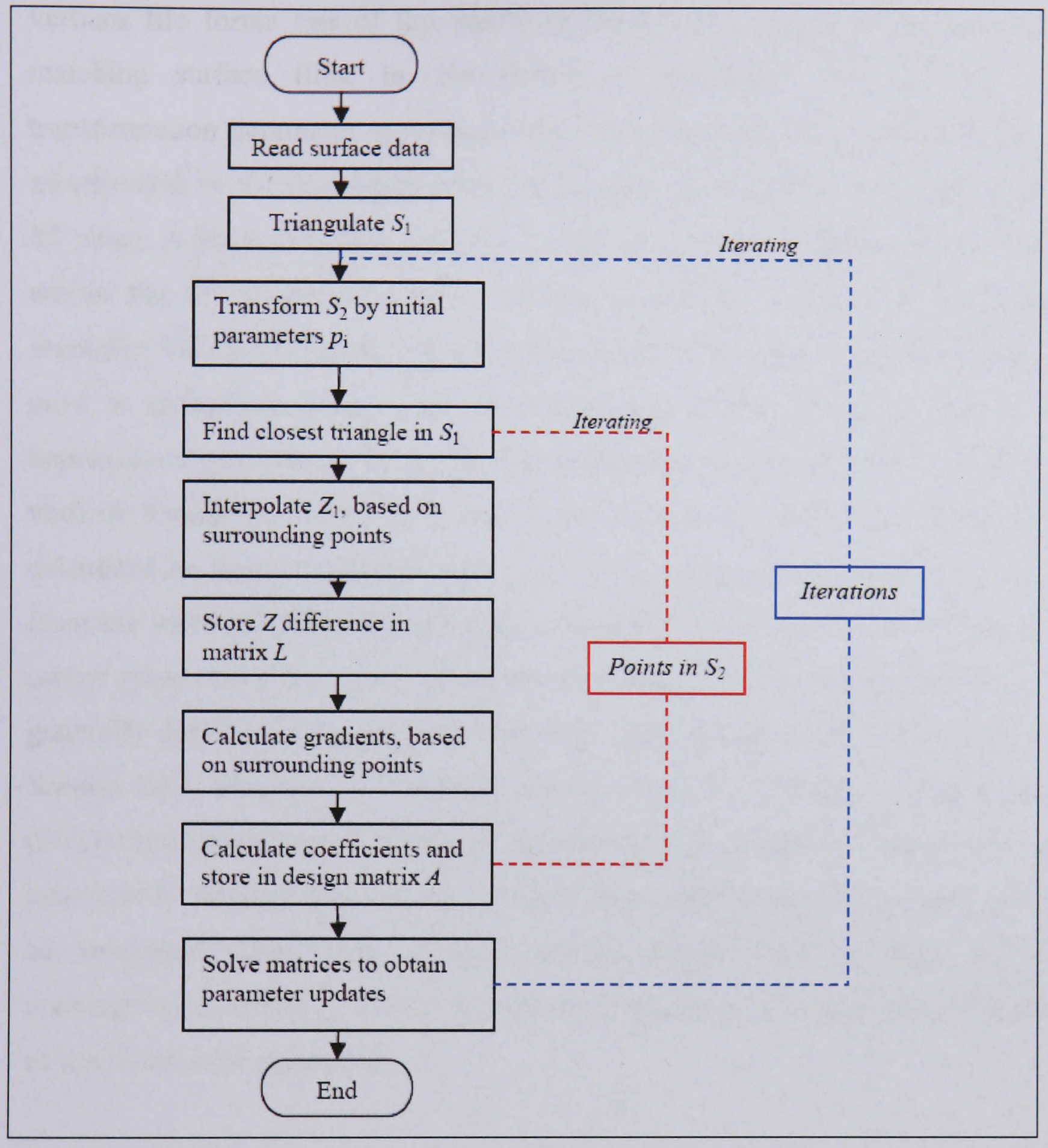

Figure 4.8 3DSurf matching algorithm (Buckley, 2003).

The matching algorithm which lies at the core of the 3DSurf software originated at the University of Newcastle, Australia, and was initially designed for grid-based data structures (Buckley, 2003), primarily for close-range photogrammetric applications. This algorithm was developed by Buckley (2003), making it compatible with irregular topographic point datasets, and resulting in the 3DSurf software. The 3DSurf algorithm was implemented through Microsoft Visual Basic 6.0, and the program runs in a Windows environment.

The program proceeds as outlined in Figure 4.8. Firstly, the reference surface is triangulated using *Triangle* (a freely available Delaunay triangulation algorithm developed at Carnegie Mellon University, USA (Schewchuk, 1996)). The triangle vertices file forms one of the inputs to the program, along with the reference and matching surface files, in *xyz* format. A parameter file specifies the initial transformation parameter approximations. The points on the matching surface, *S2*, are transformed by the initial parameter values, and the algorithm then loops through each *S2* point. A point-in-polygon search is used to determine firstly whether the point is within the *S1* surface boundary and thus should be included in the solution, and secondly, which *S1* triangle the point falls inside. The vertices of this triangle are then used to interpolate a Z_1 value at the location of the *S2* point, and to determine approximate gradients in X and Y. The difference between Z_2 and Z_1 gives the current vertical separation, which is stored in the matrix, *L*, while the coefficients can be calculated to form the design matrix, *A*. At this stage, some points may be excluded from the solution if they exceed a user-specified cut-off value which is used to reject outlier points (as these could otherwise contaminate the solution). The cut-off value is generally defined on an experimental basis, and this approach is discussed further in Section 4.4.1. This process is repeated for all points in *S2*. Singular value decomposition (SVD) then allows for the parameter corrections to be computed, and for the covariance matrix to be formed (Press et al., 1992). Following this, the least squares residuals can be computed. This entire process is then repeated for the next iteration, until convergence is achieved, at which point the *S2* points are transformed using the final set of transformation parameters.

Gruen (2001) observes that in least squares matching, it is sometimes the case that the solution vector converges very slowly, oscillates, or converges to an erroneous solution. It is essential therefore, that convergence criteria are selected with careful consideration. In the 3DSurf program, convergence is evaluated by monitoring a combination of the reference standard deviation, and the parameter corrections, as together these are considered to provide a suitably robust indication of convergence status (Buckley, 2003). When these values change insignificantly between subsequent iterations, convergence is achieved. However, if these criteria are not met, then the program may continue to run, ultimately failing to converge.

After convergence, the 3DSurf program outputs a log file, detailing the final transformation parameters and their standard deviations, and aspects relating to the quality of the match, including details of the final surface residuals, and the correlation matrix. In addition, the final transformed point file is output in *xyz* format.

4.4 Robust Surface Matching Development

4.4.1 Problem Specification

Least squares surface matching has been outlined in some detail above. However, for successful implementation of this technique, the nature and quality of the input surfaces must be carefully considered. Pilgrim (1996a) summarises the four possible relationships which can exist between two matching surfaces:

- the surfaces may represent the same object, but may have been acquired at different epochs, thus introducing time-related surface differences;
- the surfaces may represent the same object, but may have been acquired through different techniques, giving rise to differing surface representations;
- the surfaces may represent two different objects, which nevertheless are similar, with only slight differences;
- the surfaces may represent two different objects, where the level of difference determines if the objects can be considered as distinctly different.

While the two latter cases primarily relate to applications such as object recognition and quality control, the first two situations are of direct significance in this research. It is evident from the above list, that in each situation (and indeed every situation involving topographic datasets) differences will exist between the two surface representations.

As previously stated, deformation detection has been the basis for a number of studies which have employed surface matching in the geomatics domain. However, the introduction of local surface deformation will influence the estimation of the transformation parameters, and where the effects are significant, conventional least squares approaches may fail, or converge to an erroneous solution (Pilgrim, 1996a; Li et al., 2001). Although minor differences between the surfaces can be tolerated by the least

squares matching procedure, the assumption that the surfaces are overwhelmingly similar is critical for attaining a successful solution. The application at hand is very much concerned with difference detection, and the processes under study – geohazard activity and coastal change – have the potential to introduce significant discrepancies to multi-temporal datasets. Additionally, multi-sensor datasets lie at the heart of the monitoring strategy, and surface discrepancies will certainly arise as a result of the differing acquisition techniques. Furthermore, differing surface representations are likely to arise due to issues associated with vegetation, such as seasonal growth, and the effectiveness of any vegetation removal (filtering) routines. Despite these complications, one of the major advantages of least squares surface matching is that mechanisms for difference detection can easily be incorporated (Li et al., 2001).

Such differences can effectively be considered as gross errors or outliers (Pilgrim, 1996b; Li et al., 2001). However, least squares performance is optimal for the normal distribution (Rousseeuw and Leroy, 1987), which follows the assumption that only random, normally-distributed errors remain. Hence, the effect of any outliers must be mitigated in order to prevent the matching surface from being 'pulled' into an erroneous position, which could lead to terrain change being incorrectly quantified.

Outliers are a feature of real datasets (Rousseeuw and Leroy, 1987), and conventionally are handled through either outlier detection methods or robust estimation (Rousseeuw and Leroy, 1987; Li et al., 2001). Outlier detection approaches rely on diagnostic examination of the data in order to identify and then remove suspect observations prior to fitting the data using the remaining observations. For example, Karras and Petsa (1993) employ a data snooping technique in their application of least squares matching for deformation detection in medical photogrammetry. However, this approach is limited to the identification of a single outlier at a time, and as Karras and Petsa (1993) acknowledge, the detection of spatially concentrated deformations (such as those which may arise through geohazard processes), is more complex than the detection of isolated outliers. In the original 3DSurf algorithm developed by Buckley (2003), outliers are excluded by means of a user-controlled cut-off value. While this mechanism offers some basic protection against outlying observations, there are two main drawbacks. Firstly, the use of a cut-off value for outlier exclusion assumes that the user possesses basic knowledge of the quality of the surfaces and the influence of any pre-processing

operations. This could prove particularly problematic with inexperienced users, and in practice, the value is often determined through a trial and error approach, which is inefficient and may lead to sub-optimal performance. Secondly, geohazard activity is likely to vary in extent and magnitude across the surfaces, and the use of a single, fixed rejection value, is likely to prove deficient. Therefore, in order to meet the challenges posed by the application at hand, and to increase the general robustness of the 3DSurf algorithm, a more sophisticated outlier-handling routine must be implemented.

Robust estimation, also referred to as robust regression, takes an alternative approach to outlier detection routines, and instead embraces the outliers in the least squares estimation procedure, while mitigating their influence through down-weighting. The effectiveness of robust estimation for deformation detection in least squares surface matching has been demonstrated by a number of researchers, including Pilgrim (1996a, 1996b) and Li et al. (2001). The findings of these studies are examined in context below.

4.4.2 Robust Estimation

4.4.2.1 Overview

Robust estimation refers to regression techniques which are resistant to the contaminating effects of outlying observations (Rousseeuw and Leroy, 1987). In ordinary least squares, although no weighting is applied, this effectively equates to a situation where observations are equally weighted in order to obtain parameter estimates. However, by introducing weighting, and modifying the weights of individual observations, robust estimation can be applied (Draper and Smith, 1998). In essence, weights are derived from a weighting scheme, which is defined through the choice of robust estimation function. This allows those observations which produce large residual values to be down-weighted accordingly (Draper and Smith, 1998). This is encapsulated by Pilgrim (1996a), who states that 'robust estimation is used to detect outlying observations by improving the stochastic model'. A comprehensive overview of the influence of outliers and robust regression theory can be found in a numbers of texts, including Cook and Weisberg (1982); Hoaglin et al. (1983); Rousseeuw and Leroy (1987); and Draper and Smith (1998).

Investigation of robust surface matching in the field of geomatics has been relatively limited to-date. It would appear that of the studies which have been presented, most have been very much limited to applications involving simulated datasets, or as in the case of Gruen and Akça (2005), applications involving fairly regular, geometric objects. However, applications such as terrain monitoring would seem ideally suited to robust surface matching techniques, and the research presented here will attempt to drive forward this aspect, evaluating the feasibility of such an approach where topographic surfaces are concerned.

Pilgrim (1996a) applies robust estimation to least squares matching through the implementation of a modified Maximum Likelihood Estimator (M-estimator). Focussing on medical applications using close-range photogrammetric data, outliers are introduced in the form of simulated growths and swelling. Pilgrim (1996a) reports markedly improved performance over the non-robust algorithm, noting however, that there is a trade-off between the extent of contamination tolerable and the 'pull-in' range (the initial misalignment between the surfaces). Xu and Li (2000) and Li et al. (2001) evaluate the performance of several robust functions, including the M-estimator and a Least-Median-of-Squares Estimator (LMS-estimator), for matching of simulated datasets, again noting improved performance over the non-robust version. Gruen and Akça (2005) apply a simplified form of robust estimation, based on a multiple of the standard deviation of the residuals, for matching of laser scanning datasets, as was introduced in Section 4.2.2. However their research does not concern difference detection, and hence the effectiveness of this technique in the presence of concentrated regions of contamination cannot be evaluated.

Further examples of the use of robust regression can be drawn from a range of fields. Wager et al. (2005) present an example of the use of robust least squares regression for neuroimaging analysis, reaching the important conclusion that while robust estimation offers significant advantages over ordinary least squares when outliers exist, no deterioration in performance is evident when outliers are not present. Hence, this points towards the general applicability of a robust approach. Robust regression has also been applied in the context of geophysical data (Chave and Thomson, 2003), medical model registration (Ma and Ellis, 2003), and spectroscopy (Ruckstuhl et al., 2001).

4.4.2.2 Maximum Likelihood Estimators

Robust estimation can be regarded as a modified version of least squares regression (Mirza and Boyer, 1993). This technique makes use of a robust estimation function, which generalises the least squares estimation. There are several different classes of robust estimator, each of which possesses differing characteristics. In this research, a robust function from the M-estimator family has been selected and implemented. M-estimators are a popular class of robust estimator, offering flexible performance (Goodall, 1983), and permitting straightforward incorporation in least squares routines. The generalised form of the M-estimator can be defined as (Pilgrim, 1996a):

$$\sum_{i=1}^{n} f(v_i) = \min$$

Eqn. 4-15

Thus, M-estimators attempt to minimise a function of the residuals, $f(v)$. From Equation 4-15 it is evident that the most familiar M-estimator is in fact the least squares procedure, which minimises:

$$f(v_i) = v_i^2$$

Eqn. 4-16

A detailed overview of M-estimators is provided by Goodall (1983), and Mirza and Boyer (1993) compare the relative performance of different M-estimators for noisy range data. In this research, Tukey's biweight was selected as a suitable M-estimator. The biweight is one of the most commonly-utilised M-estimators, and as noted by Goodall (1983) is difficult to surpass in terms of delivering good overall performance in most situations. In the evaluation of robust surface matching carried out by Li et al. (2001), the biweight was the M-estimator selected for inclusion, and was cited as possessing '…desirable properties of robustness'. As intimated in the previous section, the M-estimator is embedded in the least squares routine through weighting, and therefore the M-estimator weight function is of greatest interest here.

Figure 4.9 illustrates the weight function of the biweight, which can be defined as:

$$w_b(u) = \begin{cases} (1-u^2)^2 & |u| \leq 1 \\ 0 & |u| > 1 \end{cases}$$

Eqn. 4-17

Where the weights, w_b, ranging from 0 to 1, are calculated from u, the standardised least squares residuals.

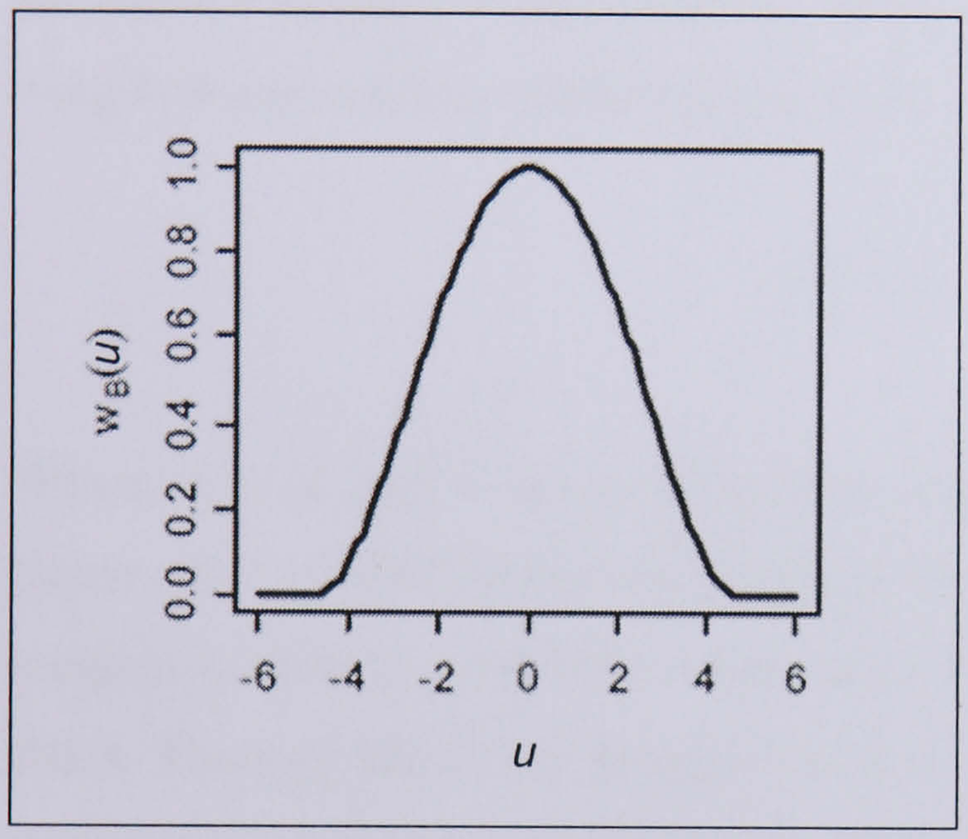

Figure 4.9 Weight function for the biweight estimator, showing response to the standardised residuals (u), where the tuning constant c=4.685 has been applied (after Fox, 2002)).

The weights, often referred to as bisquare weights in the case of the biweight estimator, are used to modify the observations, thus mitigating the influence of outlier data points. In practice, this is implemented through a technique known as Iteratively Reweighted Least Squares (IRLS), which is explained further in Section 4.4.3.1.

4.4.3 Robust Algorithm Development

4.4.3.1 Iteratively Reweighted Least Squares

The inclusion of a weight matrix is a extension to standard least squares, and is widely utilised in order to reduce the contribution of less reliable observations (Draper and Smith, 1981).

The weighted least squares condition can be expressed as (Wolf and Ghilani, 1997):

$$\sum_{i=1}^{n} w_i v_i^2 = \min$$

Eqn. 4-18

Where w are the weights, and v, the least squares residuals. The weights range between 0 and 1, where the value is lowered in order to reduce influence, although if all weights are set equal than this has the same effect as if no weighting was applied. Therefore it is the relative weights of observations which controls their influence. In matrix notation, weighted least squares can be expressed as:

$$AX = L + V, \quad W$$

Eqn. 4-19

Where A, X, L and V are as defined in Equation 4.9, and W is the associated weight matrix. This weight matrix can therefore be populated with the corresponding bisquare weights in order to establish an appropriate stochastic model, and implemented through IRLS. Through IRLS, the weight matrix is computed as a function of the scaled least squares residuals after each iteration of the adjustment (Coleman et al., 1980; Goodall, 1983), and in this manner, the robust estimator is embedded in the estimation procedure. This allows for high leverage observations, corresponding to outliers, to be identified and down-weighted accordingly. Wager et al. (2005) summarise robust estimation through the IRLS procedure as follows:

- select a suitable robust weighting scheme;
- obtain initial residuals from un-weighted least squares (first iteration);
- apply the M-estimator weight function to compute robust weights, and place these on the diagonal of the least squares weight matrix, W;
- re-evaluate the least squares estimation (next iteration) using the new weight matrix, W, to obtain updated residuals.
- repeat steps 3 and 4 until convergence.

The IRLS technique therefore provides a mechanism for automated robust estimation, where the weights are not held fixed, but alter in response to the changing residuals. The

robust matching investigations carried out by Li et al. (2001) and Pilgrim (1996a, 1996b), as detailed in Section 4.4.2.1, were implemented through IRLS. Rousseeuw and Leroy (1987) and Heiberger and Becker (1992) provide further details of robust estimation with M-estimators using IRLS. Having outlined the basic approach for robust least squares, it is now necessary to consider some of the practicalities associated with calculating the bisquare weights and incorporating these in the 3DSurf algorithm.

4.4.3.2 Computational Aspects of the Biweight M-Estimator

The weight function for Tukey's biweight was defined in Equation 4-17, with the weights, w, calculated as a function of the standardised least squares residuals, u. It is necessary therefore to consider how the least squares residuals are standardised. Firstly, the least squares residuals v, calculated after each iteration, are adjusted in order to account for high-leverage points. Leverages can be obtained from the diagonal elements, h_{ii}, of the 'hat matrix', H, which is a projection of the design matrix, A (Cook and Weisberg, 1982; Rousseeuw and Leroy, 1987). This is defined as:

$$H = A(A^T A)^{-1} A^T$$

Eqn. 4-20

The leverages relate to the influence that an individual observation exerts on the overall fit of the data, and can be used to diagnose likely outliers (Cook and Weisberg, 1982; Wager et al., 2005). However, computing H in this manner is extremely computationally expensive. Initial testing, using typical ALS and TLS topographic datasets, comprised of upwards of ten thousand points, suggested that this approach would prove impractical. Instead, as Hoaglin and Welsch (1978) suggest, it is possible to compute H from SVD, the approach implemented in 3DSurf for solving the least squares problem. Although explanation of SVD is beyond the scope of this work, this can be summarised as a technique for solving least squares, which involves decomposition of the design matrix A, into the matrices U, W, and V, as defined by Press et al. (1992), with matrix dimensions as indicated here:

$$\underset{mxn}{A} = \underset{mxn}{U} \quad \underset{nxn}{W} \quad \underset{nxn}{V}^T$$

Eqn. 4-21

It is then possible to compute H as follows (Hoaglin and Welsch, 1978):

$$H = UU^T$$

Eqn. 4-22

In practice, a simplified version can be programmed such that a column vector containing only the relevant elements, the h_{ii} diagonal values is calculated. From a computational aspect, this approach is efficient, and was observed to have little effect on the overall processing budget for the existing 3DSurf algorithm.

Following this, the next step is to adjust the least squares residuals, v, in order to account for the different leverages of the observations (Hoaglin and Welsch, 1978):

$$r_i = \frac{v_i}{\sqrt{(1 - h_i)}}$$

Eqn. 4-23

Thus producing r_i, the adjusted residuals. The next stage is related to scaling of the sample. A number of alternative scale estimators are in common usage, including the standard deviation, the interquantile range, and the median absolute deviation (*MAD*). Of these, the standard deviation is the least robust and is not applied in the case of M-estimators, as it is susceptible to outlier contamination (Goodall, 1983). The *MAD* has gained the greatest popularity, as this is capable of achieving the best overall performance in terms of robustness (Goodall, 1983). The *MAD* is therefore implemented here. The *MAD* of the adjusted residuals, *r,* is calculated as:

$$MAD = med\left|r_i - med(r_i)\right|$$

Eqn. 4-24

Following this, the *MAD* is normalised in order to determine *S*, the robust variance, which provides an outlier-robust estimation of the spread (Li et al., 2001; Wager et al., 2005):

$$S = \frac{MAD}{0.6745}$$

Eqn. 4-25

M-estimators usually require the use of one or more tuning constants, which exert an important influence on performance, by controlling the shape and rejection limits of the weighting functions (Mirza and Boyer, 1993). This is illustrated in Figure 4.10, which shows the effects of different tuning constants on the biweight weighting function. This capability therefore allows the function to be fine-*tuned* to meet the necessary robustness requirements (Goodall, 1983). The final expression for the standardised least squares residuals, u_i is thus given by:

$$u_i = \frac{r_i}{c \cdot S}$$

Eqn. 4-26

Where r and S are as defined above, and c is the tuning constant for the biweight estimator. In this research, the tuning constant was fixed to $c = 4.685$ which is the default value for the biweight, providing 95% efficiency at the normal distribution (Mirza and Boyer, 1993). A comprehensive overview of robust estimation is provided by Hoaglin et al. (1983).

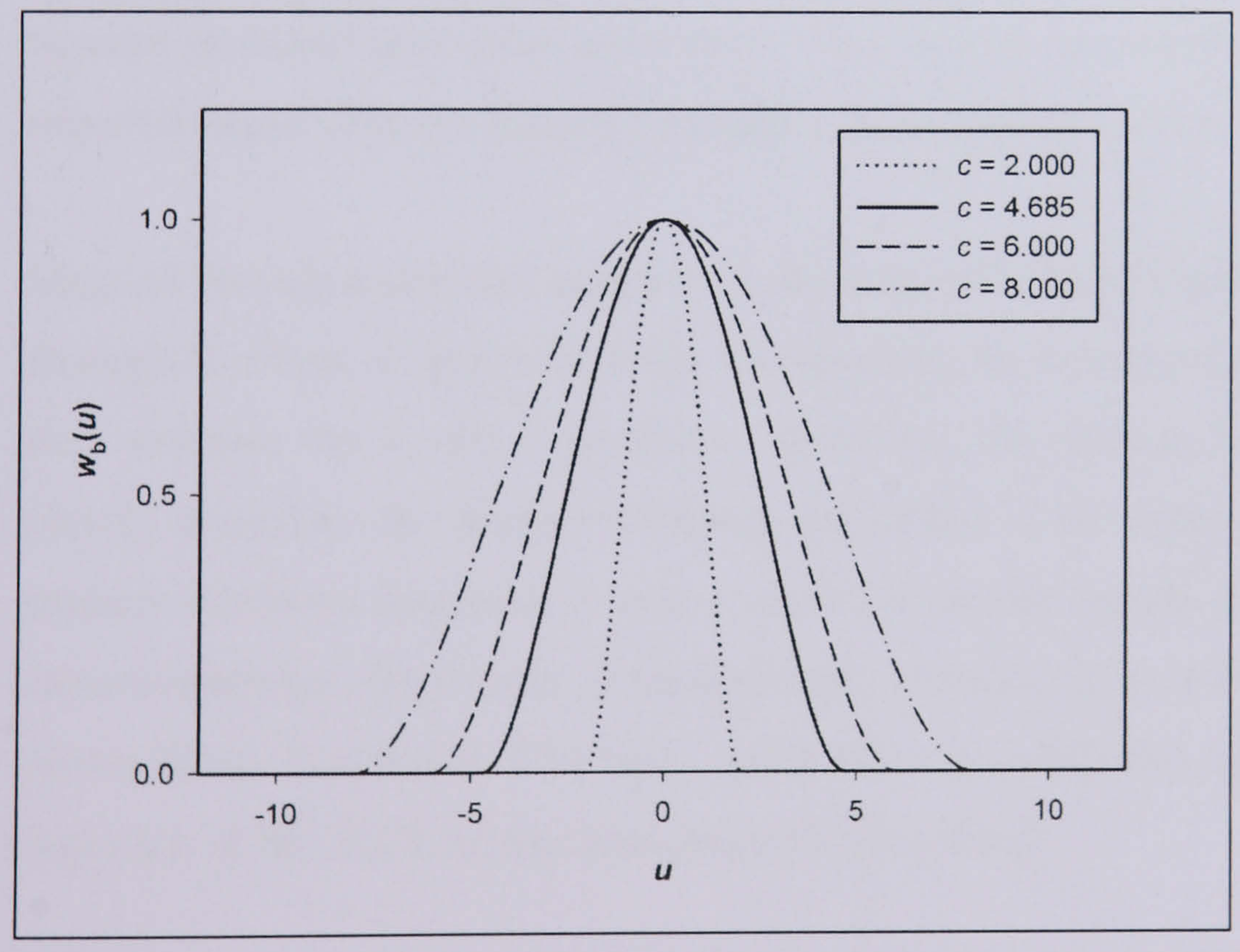

Figure 4.10 Biweight weighting function, displaying the effect of different tuning constants (c) on the weights (w_b) derived from the standardised residuals (u). The default value of c=4.685 is shown in solid.

4.4.3.3 Algorithmic Implementation

This section considers the practicalities associated with implementing the biweight estimator in the 3DSurf software through the IRLS procedure. The main steps required for realisation of this have been described above, and from this, it is evident that the most crucial requirements involve incorporation of a weight matrix, and development of a routine for computing the bisquare weights. Figure 4.11 illustrates how these features have been integrated in the existing algorithm, at the least squares solution stage – refer to Figure 4.8 (after vertical separations have been calculated and design matrix formed). Programming was carried out using Visual Basic 6.0, in order to ensure compatibility with the existing 3DSurf code. The existing 3DSurf convergence criteria were retained (monitoring a combination of the reference standard deviation and the parameter corrections). From examination of Figure 4.11 it can be seen that an option has been built-in to by-pass the capability for robust estimation, and instead invoke un-weighted least squares, by applying equal weights of 1 to all observations. A major advantage of the IRLS technique is that it requires minimal alterations to the existing code, as the fundamental least squares calculations are maintained. The bisquare weighting function is completely contained within an additional module, which is called after the least squares residuals have been calculated. This module essentially implements the steps required to calculate the bisquare weights, as outlined in Section 4.4.3.2.

Most of the computational expense of the original 3DSurf algorithm relates to looping through all of the *S2* points in order to interpolate a corresponding *S1* height value, and thus evaluate the A and L matrices. Therefore, the running time of the software is closely related to the number of points contained in the input surfaces, and the least squares solution component is only a small part in this regard. Although integrating the robust estimator added some computational elements, these were relatively minor, and observations confirmed that any additional computational effort incurred through inclusion of the IRLS routine was insignificant overall.

There were a number of minor computational aspects which had to be addressed when implementing the robust weighting function through IRLS. Not all *S2* points will necessarily be included in the least squares solution, as some may fall outside of the *S1* boundary, and can therefore be excluded. However, this will vary from iteration to iteration, as the surface is transformed into slightly different positions each time.

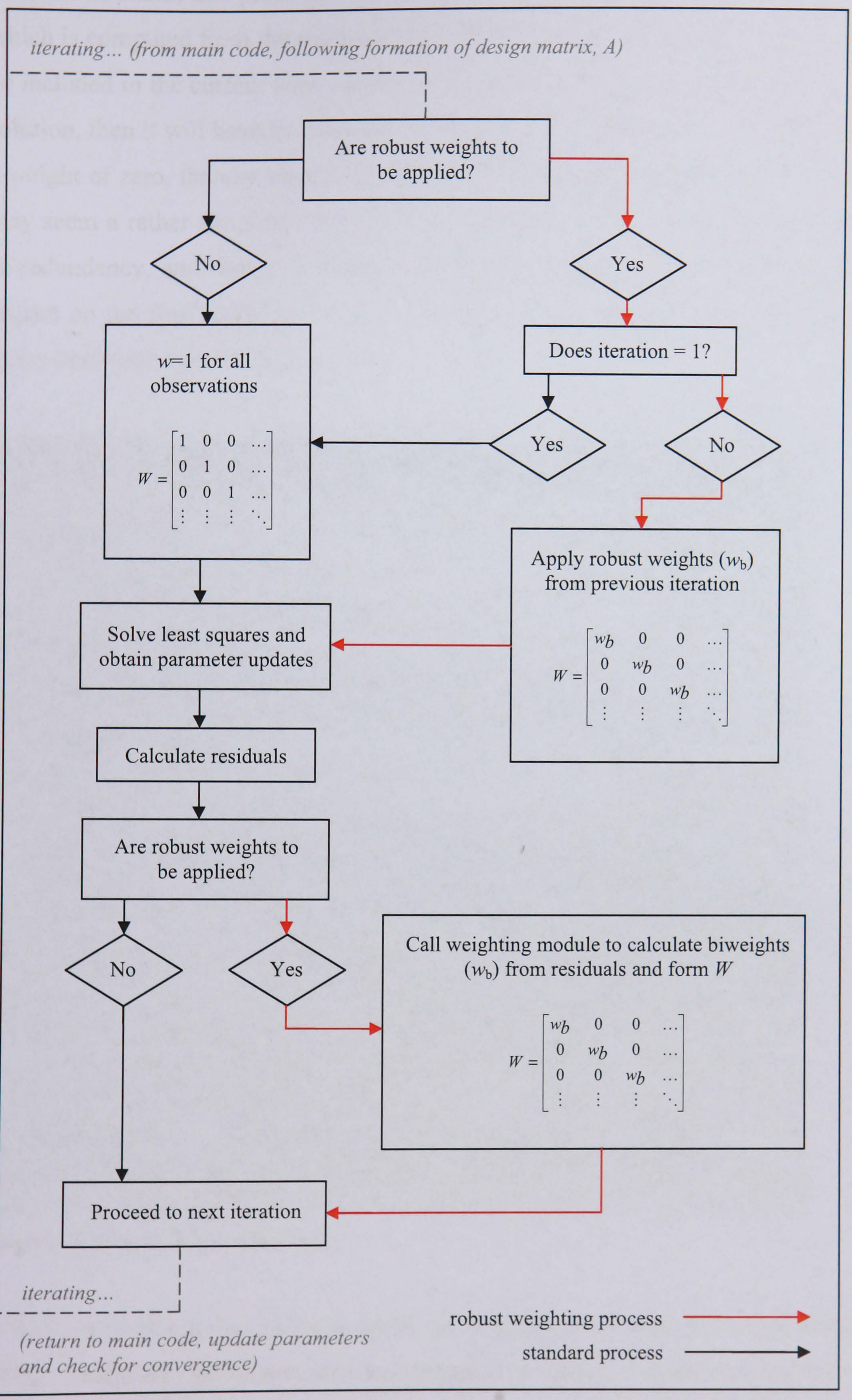

Figure 4.11 Robust weighting incorporated at the least squares solution stage (refer to Figure 4.8 for overview of original 3DSurf algorithm).

In terms of IRLS, this presents a complication, as each point has an associated weight, which is computed from the residuals derived from the previous iteration. If a point is to be included in the current least squares estimation, but was not included in the previous solution, then it will have no associated weight. In this situation, it was decided to apply a weight of zero, thereby effectively excluding the influence of these points. While this may seem a rather simplistic approach, the datasets will generally contain a high level of redundancy, and thus it is highly unlikely that this course of action will have any impact on the final solution. Figure 4.12 illustrates the modified user interface, which incorporates the robust functionality.

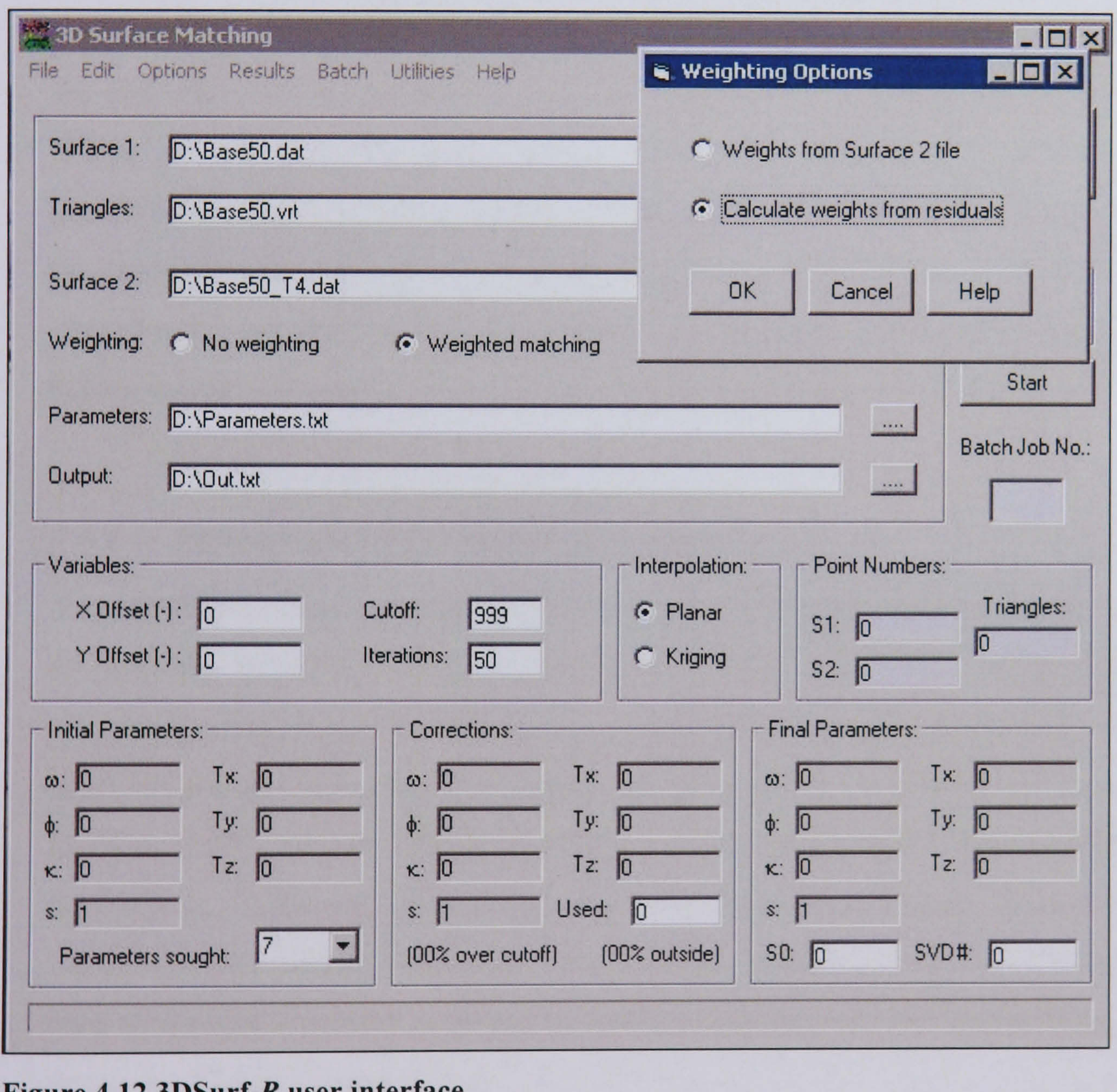

Figure 4.12 3DSurf-*R* user interface.

As well as retaining the ability to apply un-weighted least squares surface matching, a further weighting option was also incorporated, in order to maximise flexibility. This allows users to apply a manual weighting scheme to the observations, by reading these in through the *S2* file. This may be a useful feature if an area of the surface is known to be unreliable or of poor quality, and the user wishes to directly eliminate the effects of

this from the surface matching. Furthermore, this capability proved useful in early testing, as it allowed the potential of a robust matching approach to be evaluated in a basic manner prior to implementation of robust weighting through IRLS (refer to Section 4.4.4.1). The robust surface matching software will be referred to as 3DSurf-*R* from this point forwards, in order to distinguish this version from the original version, 3DSurf.

4.4.4 Evaluation of Robust Matching Algorithm

The original 3DSurf algorithm was extensively tested by Buckley (2003) using both artificial and topographic surfaces. These investigations demonstrated the integrity of the algorithm and the potential of this approach for multi-temporal monitoring studies. While the fundamental performance of the least squares matching algorithm can therefore be accepted, it is necessary to rigorously evaluate performance with respect to the developments outlined in the above sections. Initially, this was carried out through testing with simulated surfaces (as detailed in Miller et al. (2006), and described below), before testing and application to the coastal datasets (Chapters Five and Six).

4.4.4.1 Robust Matching of Artificial Surfaces

Testing of the robust matching algorithm using artificial datasets offers the opportunity to examine behaviour under carefully controlled conditions. This approach has previously been adopted in the field of surface matching by a number of researchers in order to validate their adopted strategies (Pilgrim, 1996b; Mitchell and Chadwick, 1999; Li et al., 2001; Pâquet, 2003). A number of artificial datasets were implemented for testing here. These datasets were all derived from a single surface, *Base* (Figure 4.13), which was also utilised by Buckley (2003) for controlled testing. This surface is derived from sinusoidal functions in X and Y, and is comprised of 2500 points, being of size 50 ×50 posts (dimensionless units).

The first test involved validating the integrity of the newly-developed 3DSurf-*R* program. It was decided that the most appropriate course of action would be to match outlier-free surfaces using the IRLS approach, and compare the results to those obtained through identical testing with the original version, 3DSurf. Therefore, the surface *Base*

was simply duplicated, and then transformed by varying amounts, as detailed in Table 4-1 in order to provide a number of idealistic, uncontaminated matching scenarios.

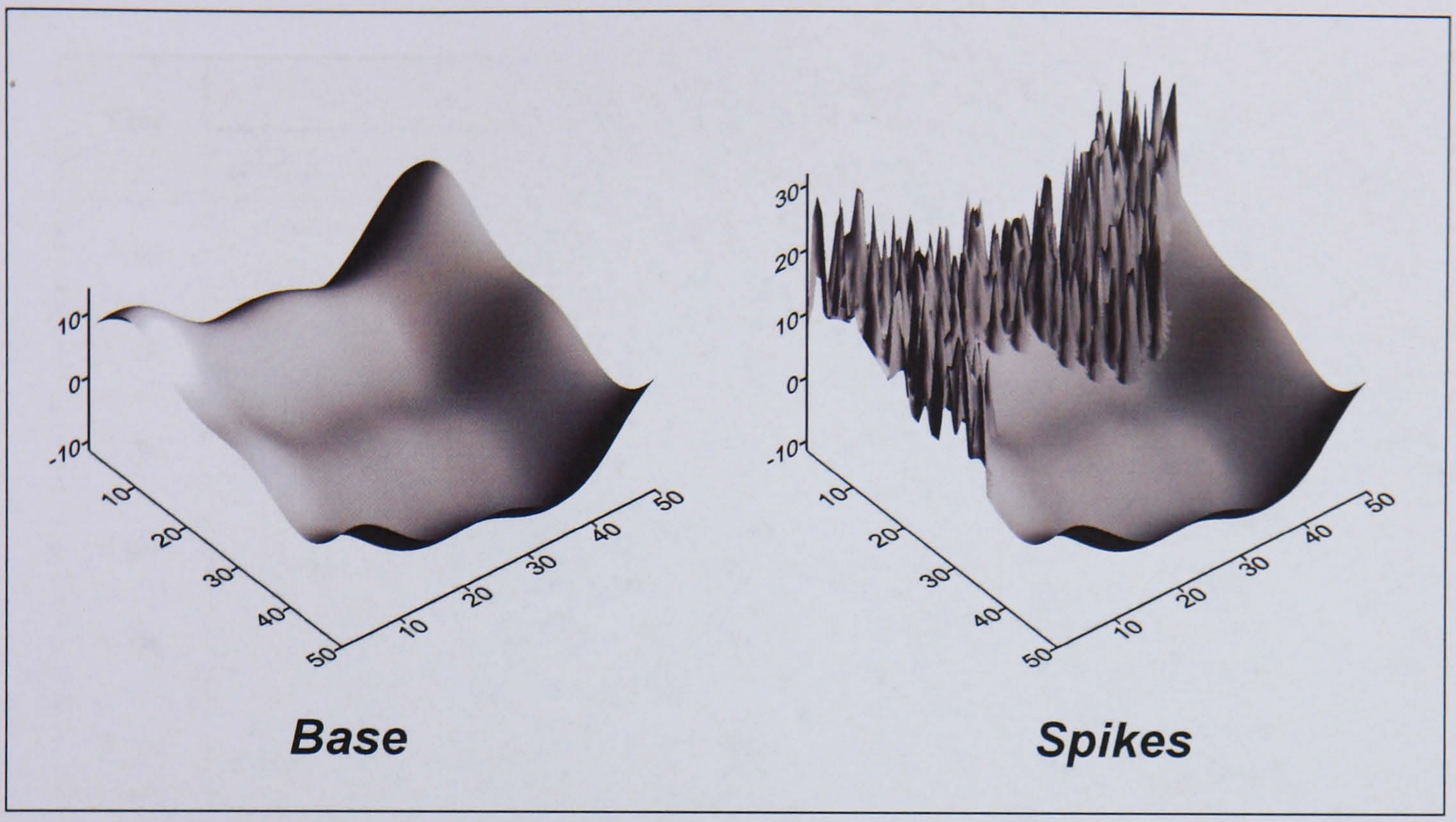

Figure 4.13 Surfaces employed in artificial testing, *Base* and *Spikes*.

Test	S1	S2	ω°	ϕ°	κ°	T_x	T_y	T_z	s
1-1	*Base*	*Base-T_1*	0	0	0	0.5	0.5	0.5	1.000
1-2	*Base*	*Base-T_2*	1	1	1	1.0	1.0	1.0	1.006
1-3	*Base*	*Base-T_3*	2	2	2	3.5	3.5	3.5	1.004
1-4	*Base*	*Base-T_4*	5	5	5	5.0	5.0	5.0	0.996

Table 4-1 Test 1 – transformations applied to *Base* matching surface to validate integrity of 3DSurf-*R*. Distance units are dimensionless.

The results of Test 1 are detailed in Table 4-2, where 'a' denotes the results obtained using the original program, and 'b' refers to the 3DSurf-*R* software, with robust weighting applied. With each subsequent run (1-1, 1-2, etc.) the initial alignment of the surfaces was degraded by the values specified in Table 4-1. In general, all of the returned parameter solutions were close to their original values. However, with the exception of Test 1-1 where perfect solutions were achieved, the other tests returned slightly different results for the two alternative program versions. This is most likely due to the fact that in 3DSurf-*R*, initial observations will be down-weighted due to the surface differences introduced through misalignment, and as evidenced by the results in Table 4-2, this is likely to have an increasing effect on the results as the initial

misalignment increases. Effectively, this will cause the surfaces to be transformed in a slightly different manner than through the un-weighted software.

Test	Final Transformation Parameters						
	$\omega^\circ \pm \sigma$	$\phi^\circ \pm \sigma$	$\kappa^\circ \pm \sigma$	$T_x \pm \sigma$	$T_y \pm \sigma$	$T_z \pm \sigma$	$s \pm \sigma$
1-1a	0.000000 ± 0.000000	0.000000 ± 0.000000	0.000000 ± 0.000000	-0.500 ± 0.000	-0.500 ± 0.000	-0.500 ± 0.000	1.000 ± 0.000
1-1b	0.000000 ± 0.000000	0.000000 ± 0.000000	0.000000 ± 0.000000	-0.500 ± 0.000	-0.500 ± 0.000	-0.500 ± 0.000	1.000 ± 0.000
1-2a	-1.017463 ± 0.000044	-0.982171 ± 0.000040	-1.017507 ± 0.000036	-0.994 ± 0.000	-0.994 ± 0.000	-0.994 ± 0.000	0.994 ± 0.000
1-2b	-1.017466 ± 0.000052	-0.982166 ± 0.000043	-1.017498 ± 0.000041	-0.994 ± 0.000	-0.994 ± 0.000	-0.994 ± 0.000	0.994 ± 0.000
1-3a	-2.069775 ± 0.000044	-1.927741 ± 0.000040	-2.069753 ± 0.000037	-3.490 ± 0.000	-3.486 ± 0.000	-3.482 ± 0.000	0.996 ± 0.000
1-3b	-2.069619 ± 0.000058	-1.927644 ± 0.000051	-2.069359 ± 0.000053	-3.490 ± 0.000	-3.486 ± 0.000	-3.482 ± 0.000	0.996 ± 0.000
1-4a	-5.433227 ± 0.000044	-4.525203 ± 0.000040	-5.433323 ± 0.000037	-5.060 ± 0.000	-5.017 ± 0.000	-4.984 ± 0.000	1.004 ± 0.000
1-4b	-5.432974 ± 0.000087	-4.525174 ± 0.000079	-5.432428 ± 0.000087	-5.060 ± 0.000	-5.017 ± 0.000	-4.984 ± 0.000	1.004 ± 0.000

Table 4-2 Test 1 results for the original program (a), and the robust version (b). Distance units are dimensionless.

A further two aspects must be examined in relation to Test 1. The first issue relates to establishing whether or not these slightly different results (for the alternative program versions) are of any significance, and the second relates to the recovered transformation values. With regard to this latter concern, it can be seen from Table 4-2 that particularly for the final run (Test 1-4), the results (especially the rotations), differ from the user-induced transformation outlined in Table 4-1. However, this does not necessarily indicate an erroneous solution (Pâquet, 2003). This observation is further supported by Buckley (2003), who notes that slightly different sets of parameter combinations, arising in part through the effects of interpolation, can lead to the same, correct solution. Instead, Buckley (2003) suggests that the most effective means of evaluating matching success may be through a visual inspection of the two surfaces in their final relative positions. However, although this approach may be valuable for the appraisal of field datasets, it lacks the rigorous and quantifiable qualities required for formal testing. An alternative strategy is to evaluate the success of the match through the use of

'mismatch' statistics – a method of analysis advocated by Pâquet (2003). In order to explain this approach, it is firstly necessary to reiterate the method for artificial testing of the surface matching algorithm. This proceeds as follows:

1. create the matching surface by replicating the reference surface;
2. apply user-defined transformations in order to alter the matching surface orientation and position, thus providing a suitable basis for testing the surface matching algorithm;
3. carry out the surface matching, obtaining final transformation parameters, and the post-match transformed surface.

The original position of the matching surface (at stage 1), including the original coordinate values of every point, is known, as this surface has been artificially created. As the surface matching procedure is attempting to return the matching surface to this original pre-match position, then it is possible to exploit this knowledge of original surface position in order to assess the quality of the solution. This can be achieved by comparing the post-match transformed coordinate values (at stage 3) to their original values at stage 1, thus allowing the significance of any discrepancies to be assessed. This mismatch technique therefore provides a means of assessing the ability of the matching program to return the individual points to their correct positions (Pâquet, 2003).

A small Visual Basic .NET program was written to perform this analysis, by comparing the two *xyz* point files, and then calculating and reading out relevant statistics (mean, standard deviation, and root mean square error). A mismatch evaluation for Test 1 was carried out, with the results indicating that the surfaces had been successfully returned to their original locations in all cases, with no significant differences between the solutions obtained for the different program versions. It should be noted that further testing was carried out with increasingly poor initial surface misalignments, but when rotations exceeded 5° (the status in Test 1-4), convergence could not be achieved. This gives an indication of the quality of the initial parameter approximations which are generally required for least squares matching.

After verifying the integrity of the 3DSurf-*R* algorithm in terms of general matching performance, the next phase involved examination of its robust qualities. Again, *Base* provided a suitable reference surface, and acted as a template for the matching surface. However, this time, disturbances were introduced to produce a further matching surface, *Spikes*, which is shown alongside *Base* in Figure 4.13. The *Spikes* surface is intended to represent the potential extreme effects of unfiltered vegetation or similar, and was created by randomly incrementing Z values over a restricted portion of the original *Base* dataset. The *Spikes* surface was then transformed by rotating 2° in ω, ϕ, κ, translating by 2 (dimensionless) units in T_x, T_y, T_z, and preserving scale. This surface was then matched to *Base* in order to recover the transformation parameters, and thus gauge the success of the match.

Test 2 compared the effects of three different approaches to outlier handling. Firstly, the surfaces were matched using the original 3DSurf algorithm (no weighting, and no cut-off for outlier rejection), to ascertain how the software would behave when the outlier effects were permitted unmitigated influence on the solution. The second strategy saw the *Spikes* surface weighted manually by applying the same weight to all outlier points, and then gradually incrementing the weighting for each subsequent program run (all non-outlier points were given a weight of 1 each time). Although this was a rather rudimentary approach, the objective was to gain some understanding of the influence of different weights, and to establish if there was a requirement for a more sophisticated strategy. Finally, the 3DSurf-*R* software, with robust weights, was applied.

The mismatch statistics for Test 2 are detailed in Table 4-3. These indicate the effects of the different weighting approaches. Where outliers were completely weighted out, by assigning weights of zero, and where they were down-weighted through robust weighting (Tests 2-2 and 2-8 respectively), the software was successfully able to transform the matching surface to its correct original position. However, as the weights were incremented to gradually increase the influence of the outliers, the quality of the corresponding solutions steadily deteriorated, until no convergence could be achieved at the 0.9 weight level (Test 2-7). Likewise, the software failed to achieve a solution in Test 2-1 where the 3DSurf algorithm was applied. These effects are illustrated through plots of the final residuals in Figure 4.14, where it can be seen that the application of increasing weights to the outliers in *Spikes* serves to 'pull' this surface downwards until

some portions lie beneath the reference surface *Base*. Although this may establish the best overall fit between the surfaces, this deviates from the correct solution, IRLS / w=0.00, as shown uppermost left.

Test	**Outlier Weighting**	**Mismatch**		
		Mean	***σ***	***RMSE***
2-1	None	*No Convergence*		
2-2	$w = 0.0$	0.000	0.000	0.000
2-3	$w = 0.1$	0.589	0.255	0.642
2-4	$w = 0.3$	1.766	0.765	1.925
2-5	$w = 0.5$	2.778	1.217	3.033
2-6	$w = 0.7$	4.055	1.726	4.408
2-7	$w = 0.9$	*No Convergence*		
2-8	Robust	0.000	0.000	0.000

Table 4-3 Test 2 mismatch statistics for differing weight values. Distance units are dimensionless.

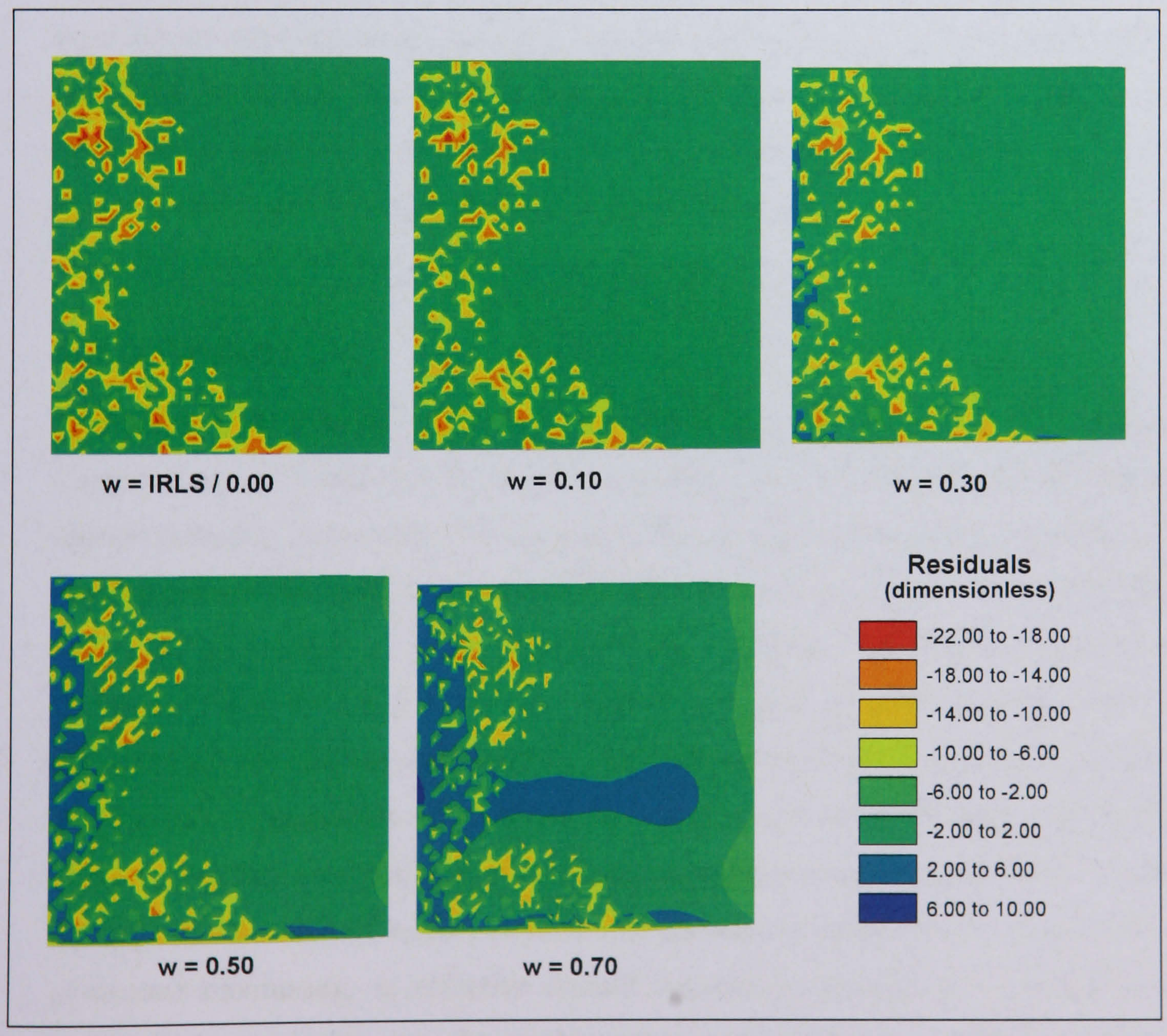

Figure 4.14 Test 2 post-match surface residuals, showing deteriorating results, as increasing weights are applied. Negative residual values indicate where the *Spikes* surface is above *Base*.

These findings illustrate that in the case of severe outliers, such as those present in the *Spikes* surface, even low levels of weighting can still fail to return a completely correct match. Furthermore, it is not feasible to control down-weighting through a manual approach such as this. While the location and severity of the outliers is known in the case of controlled testing, this is not so for natural topographic datasets which may be unpredictable in terms of noise level, and the existence and extensiveness of any concentrated areas of change or isolated gross errors. Therefore, the requirement for an automated weighting mechanism is evident, and particularly essential in an environment such as the dynamic coastal zone, where surface differences are to be expected.

Tests were also carried out on other matching surfaces (e.g. Miller et al., 2006), in order to examine the influence of a number of different contaminating effects. These responded in a similar manner to the *Spikes* surface, and application of the robust weighting strategy confirmed the effectiveness of this approach. However, these tests were carried out using ideal, noise-free surfaces, with artificially-induced outlier effects, and while these tests delivered encouraging performances, coastal datasets present a much more challenging prospect, as will be evaluated in the following chapter, alongside the results of the geohazard monitoring strategy.

4.5 Summary

Through a review of literature from the fields of computer vision, and geomatics, Chapter Four has introduced the concept of surface matching for dataset registration and change detection. It has emerged that a diversity of approaches, which generally can be categorised as either feature-based or area-based have been applied. Surface matching is driven by a number of different motivations, ranging from object recognition to deformation detection, and surface registration, and these considerations may ultimately dictate which approach is most suitable. In the geomatics domain, establishing the set of transformation parameters which aligns one dataset with another is generally the prime concern, and for some years, this has drawn attention to least squares surface matching through minimisation of surface separations. Surface matching is well suited to coastal geohazard monitoring, as effective dataset registration through conventional control point-based approaches can be problematic in the dynamic coastal environment.

Furthermore, surface matching offers an inherent capacity for change detection. This technique therefore holds much potential for terrain monitoring applications.

The surface matching software 3DSurf, developed by Buckley (2003) has been further investigated here. This software is compatible with irregular point structures, and was developed for the matching of coastal datasets, thus making it well-suited to this research. 3DSurf implements least squares matching through minimisation of vertical surface differences, and the corresponding mathematical theory has been presented. However, this software is not optimised for datasets affected by significant terrain change, or other contaminating features, such as discrepancies introduced through different acquisition techniques, or vegetation change. Such anomalies effectively introduce outliers into the datasets, which can contrive to return an erroneous matching solution. The crux of Chapter Four therefore relates to addressing and overcoming this issue through the development and implementation of a robust matching algorithm.

A review of robust surface matching research in the context of geomatics applications has been presented. From this two issues are evident; firstly, research into this aspect of surface matching has been relatively limited to-date; and secondly, the existing studies have effectively restricted their scope to testing with simulated datasets. This research therefore aims to drive forward this aspect and evaluate the potential of robust surface matching in the context of terrain monitoring applications concerned with difference detection.

A robust matching algorithm has been developed on the basis of robust regression theory. This utilises a maximum likelihood estimator to compute and assign robust weights, based on the magnitude of the least squares residuals. This is implemented through the iteratively reweighted least squares technique, which effectively provides an automated form of robust weighting, where weights are updated following each iteration of the software. Testing of this robust software, 3DSurf-*R*, using simulated datasets has provided encouraging results, which indicate the effectiveness of the algorithm for mitigating the influence of outlier data points. While the development of the 3DSurf-*R* software offers much potential for matching of coastal geohazard datasets, application to noisy, topographic surfaces is likely to present a significant challenge, and will be examined further in Chapters Five and Six.

CHAPTER 5

INTEGRATED REMOTE MONITORING AT FILEY BAY

5.1 INTRODUCTION

An integrated strategy for remote monitoring of coastal geohazards has been introduced and developed in Chapters Three and Four. This strategy involves the fusion of datasets derived from airborne and terrestrial laser scanning, and archival aerial photogrammetry, thus facilitating both present-day, and retrospective analysis of geohazard activity. At the core of this approach lies a robust surface matching algorithm, which has been designed to enable the reliable reconciliation of multi-temporal, multi-sensor datasets in dynamic environments. Chapter Four demonstrated the potential of the robust algorithm through experimental testing with artificial datasets. However, the application of this technique to real-world topographic geohazard surfaces is likely to prove a much more challenging exercise, and will be explored at length in this chapter. Real-world surfaces may be unpredictable, and are likely to vary due to differing terrain representations, random error, the effects of vegetation, and importantly, geohazard activity. This chapter will explore a number of aspects critical to the effectiveness of the coastal monitoring strategy, and through this will establish the potential of the overall approach.

Here, the monitoring strategy is applied to a soft-cliff geohazard environment located on the North Yorkshire coast, at Filey Bay. This offers a range of active geohazard processes, which present a tangible threat to natural and human aspects of the local environment. Attention is initially devoted to introducing the ALS, TLS and archival

aerial photography datasets acquired for the monitoring, with particular focus on issues of data acquisition, processing and quality analysis. The next phase concentrates on examining the effectiveness of the robust algorithm for the matching of surfaces which are extensively contaminated by geohazard activity. This is delivered through archival photogrammetric DEMs from 1967 and 1980, and ALS data from 2005. Following this, contemporary monitoring, utilising ALS and TLS is presented. This allows the integrated terrestrial-airborne approach to be evaluated with respect to multi-scale monitoring, and the minimisation of data occlusions. Furthermore, this enables the potential of the specific techniques of ALS and TLS to be assessed in relation to soft-cliff coastal geohazard monitoring. Quantitative analysis of geohazard activity occurring over extended periods of time is presented and evaluated.

5.2 Filey Bay Test Site

5.2.1 Overview

Parts of the east coast of England are particularly dynamic and susceptible to coastal change. This includes sections of the North Yorkshire coastline, which is characterised by cliff instability, weathering, and erosion of the cliff-toe (Crosby, 1995). The soft glacial deposits which occupy portions of this coastline give rise to some of the most advanced erosion rates in the UK (Lee and Clark, 2002). It is on this coastline that the primary test site for the research, Filey Bay (Figure 5.1), is located. This nine kilometre-long bay, which lies eleven kilometres south of the resort town of Scarborough, is fronted by a broad, flat expanse of sand, and is backed by moderately-steep cliffs, which rise to between 30 m and 50 m in height. The cliffs are largely composed of soft glacial tills, which are vulnerable to erosion, and prone to failure (Elliot et al., 1991). Filey Bay represents a soft-cliff geohazard environment. Soft-cliff coasts are shaped through the exposure of rocks of low resistance, such as clays, shales or sandstone, or unconsolidated materials such as sand (Lee and Clark, 2002). Consequently, while a variety of geohazards are found within the bay, these primarily involve landslides, earthflows, and creep processes. Although average erosion rates for this area are relatively low, this conceals significant local variation, with some locales retreating by up to 2 m per year (Symonds Group, 1998).

Figure 5.1 Northern end of Filey Bay, looking towards Filey Brigg.

At its northern, extreme, Filey Bay is protected by the protruding headland of Filey Brigg, which is primarily composed of resistant sandstones (Wright, 2000). Where this outcrop meets the sandy beach in the northern corner of the bay, the steep glacial till cliffs are heavily gullied and eroded. Moving southwards, the cliffs become more variable in profile, and as observed by Crosby (1995), are prone to gullying and rotational landslides. The middle and upper portions of the slopes are frequently vegetated with rough grass, and occasionally shrubs and small trees. However, some steeper sections are vegetation-free, and are affected by runoff, which can lead to small mudflows (Figure 5.2), particularly during winter months. At the southern end of the bay, south of Reighton Gap, the cliffs are composed of Speeton Clay, which is particularly prone to instability, and extensive cliff failures are evident (Wright, 2000). South of this, resistant chalk formations emerge, rising to the sheer cliffs of Flamborough Head.

The main settlement is the town of Filey, which has a permanent population of around 6,500, and is located at the northern end of the bay. In addition, there are a number of small villages, and several large caravan parks occupying the cliff-tops. This latter feature is reflective of the importance of tourism to the local economy, particularly during the summer months. In addition to the bay's natural wealth, tourists

Figure 5.2 Example of typical mudflow affecting the cliffs at Filey Bay.

are also attracted by the diverse range of recreational opportunities. This includes a variety of watersport and beach activities, and Filey Country Park, which occupies the Brigg and cliff-tops immediately north of the town. Filey Bay also provides a valuable habitat for a range of flora and fauna, and locally, there are two Sites of Special Scientific Interest (SSSI), the first at Filey Brigg, and the second south from Reighton Gap to Flamborough Head. Both sites are designated for their noteworthy geology and ornithology. Geohazard activity, and the broader effects of coastal change, will naturally impact upon the varied assets of the bay, and in terms of the human ramifications, the central section of the bay is presently the most directly affected. Here, there are a number of small, informal communities which are threatened by recurrent slumping and landslips. This is typical of a problem which Hall et al. (2002) describe as '… an inheritance of communities built on eroding cliff tops and bluffs'. The struggles of one local householder attempting to protect his property from the encroaching cliff edge was described in a recent television documentary (BBC, 2006). The variety of geohazards within Filey Bay, and the importance of the natural and man-made environment to the local economy, renders this a highly suitable test site for application of the integrated remote monitoring strategy.

5.2.2 Previous Monitoring

Filey Bay provided the test site for an earlier Newcastle University coastal monitoring research project, which is detailed by Buckley (2003). This involved the application of small format aerial photogrammetry and kinematic GPS for episodic monitoring of coastal change. Buckley (2003) reports slumping of the cliffs in the test areas identified in Section 5.2.3 below, suggesting that Filey Bay is an active geohazard environment, containing a sufficient degree of terrain complexity to warrant the application of an integrated airborne-terrestrial monitoring approach. Furthermore, it is desirable to maintain this existing monitoring regime, which incorporates datasets stretching back to 2000.

Elliot et al. (1991) highlight monitoring carried out at Filey Bay through the erosion post technique introduced in Section 2.2.1. The average rate of 0.25 m per annum, appears to mask a degree of variability for different locations within the bay (Table 5-1).

Post No.	Location	Annual erosion rate (m)
1A	Reighton Gap	1.300
1	Reighton Gap	0.150
2	Hunmanby Gap	0.140
3	Primrose Valley	nil
4	Muston	0.110
5	Lifeboat House	0.033
6	Horn Dale	0.033
Average annual erosion rate:		0.250

Table 5-1 Annual cliff erosion rates within Filey Bay (after Elliot et al., 1991)).

5.2.3 Test Areas

Although the full length of Filey Bay is of interest, efforts were concentrated on four test areas. This approached permitted efficient incorporation of the terrestrial laser scanning component, and also provided a basis for concentrated validation of the robust matching approach, with pairs of check profiles measured by total station at each test area. The test areas are distributed along the length of the bay (Figure 5.3) and are

representative of the variety of soft-cliff environments found locally. Three of these areas (CPK, GLF and HUN) correspond to sites which were utilised in the earlier Newcastle University coastal monitoring research project (Section 5.2.2). The first of these test areas, CPK, is located to the north of the town of Filey, adjacent to Filey Country Park. CPK is actually composed of two sub-areas (Figure 5.4), divided by a wooded ravine and Filey Sailing Club. The northern area is comprised of steep slopes, which are vegetated with grass on their upper portion, before dropping off sharply to a near vertical scarp slope at the cliff-toe. The section south of the ravine is primarily vegetated with grass. Moving southwards, the second test area, which is located adjacent to Filey Golf Club, is composed of gentler slopes which are heavily vegetated, particularly around the GLF1 profile (Figure 5.5, left).

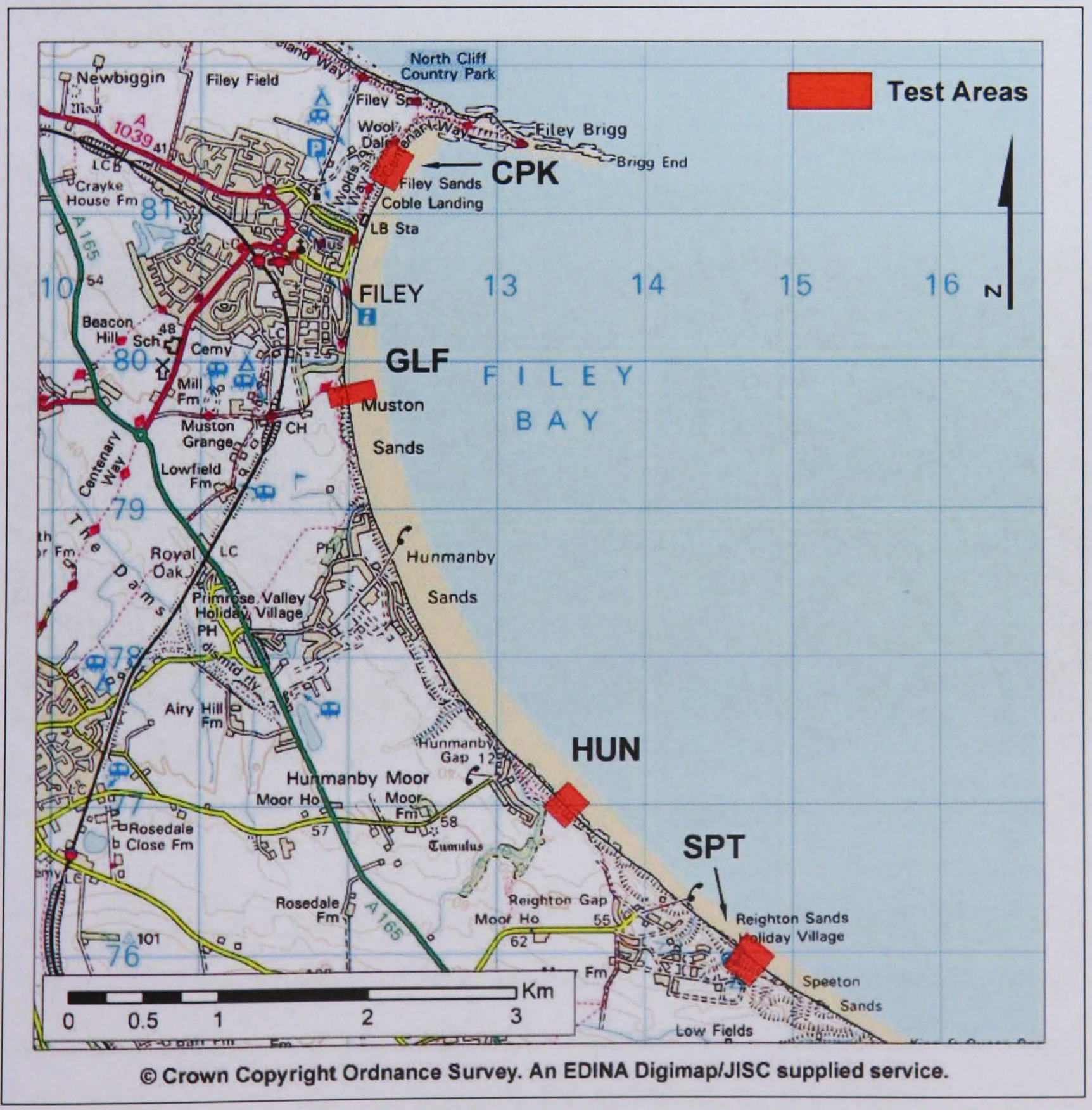

Figure 5.3 Location of test areas within Filey Bay.

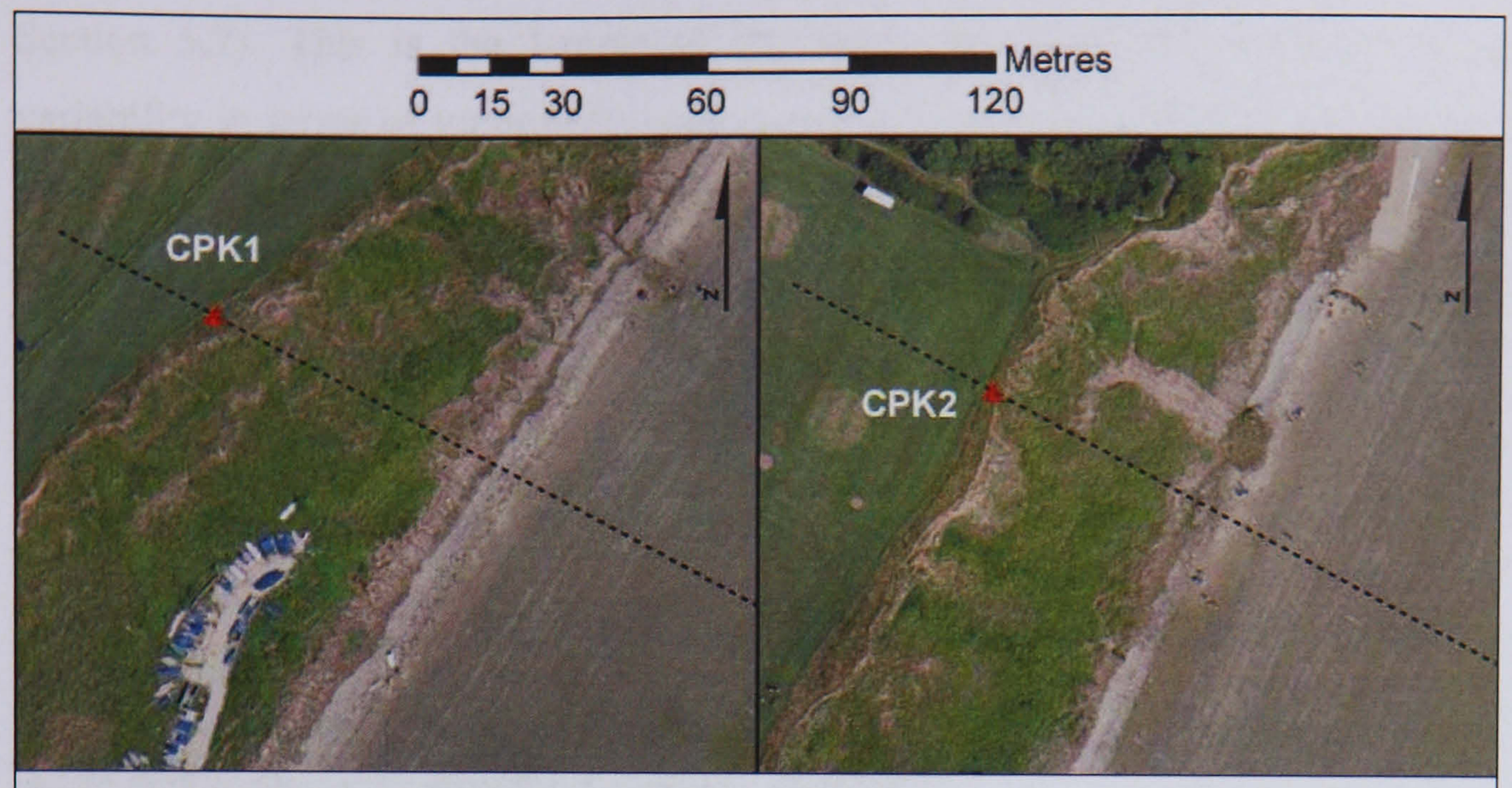

Based on digital spatial data licensed from the Natural Environment Research Council ©NERC (2005).

Figure 5.4 CPK north (left) and south (right) sub-areas, with validation profile locations, and control points indicated.

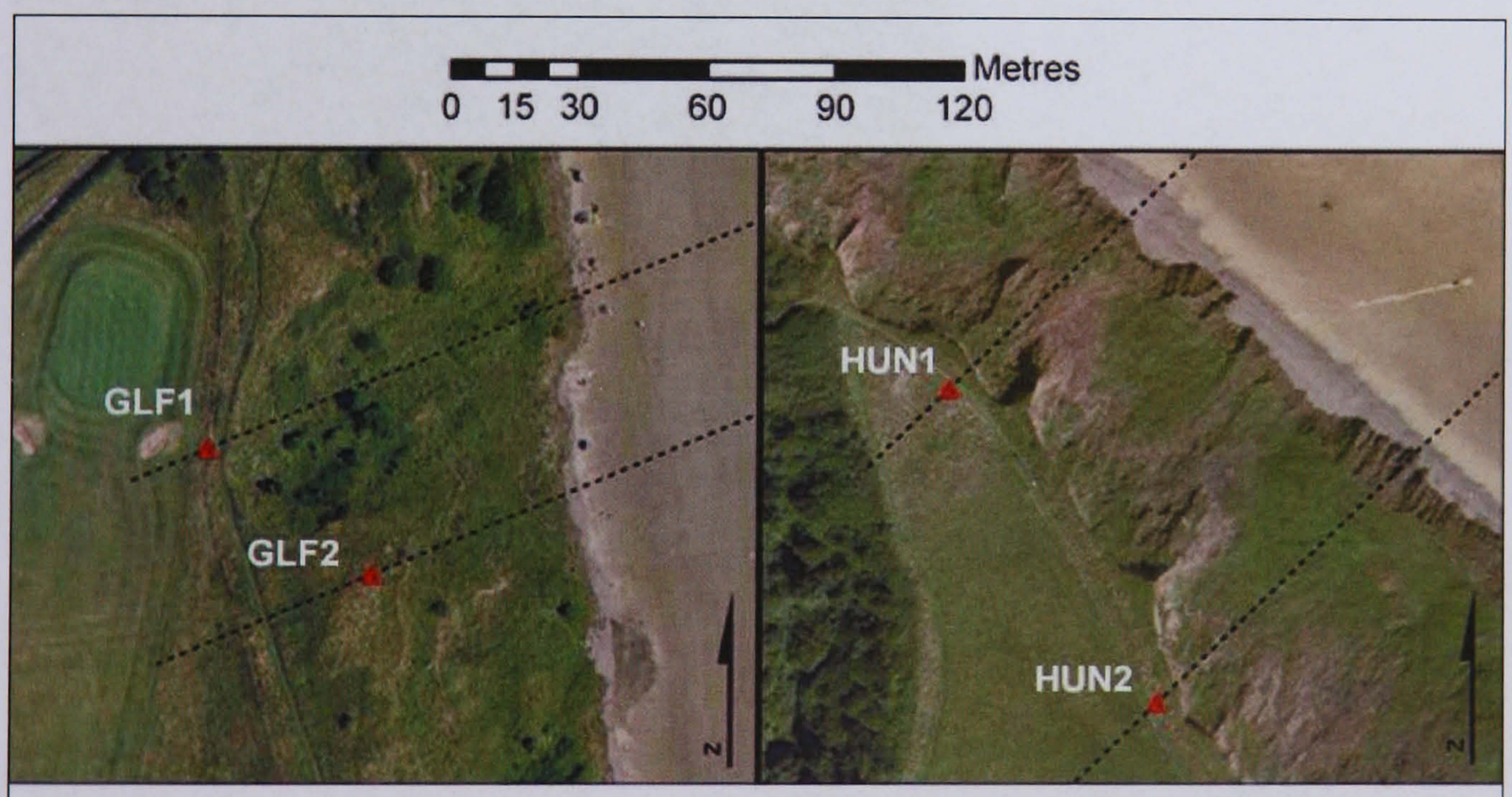

Based on digital spatial data licensed from the Natural Environment Research Council ©NERC (2005).

Figure 5.5 GLF and HUN test areas, with validation profile locations, and control points indicated.

The HUN test area lies to the south of the small settlement of Hunmanby Moor, and displays a variety of slope profiles (Figure 5.5, right), with many of the steeper sections exhibiting evidence of active erosion. The SPT test area (Figure 5.6) lies a further 1.5 km south. This site was selected for inclusion, as it comprises an extensive and moderately-active landslide complex, which provides an excellent opportunity for both retrospective and present-day assessment of geohazard activity (refer to Section 5.6 and

Section 5.7). This is the largest of the four test areas, and contains the greatest variability in terms of topography and vegetation. Whereas the three existing test areas of CPK, GLF, and HUN are primarily utilised in assessing and analysing the quality of the ALS and TLS datasets, the SPT test area forms the core site for application and evaluation of the integrated remote monitoring strategy at Filey Bay.

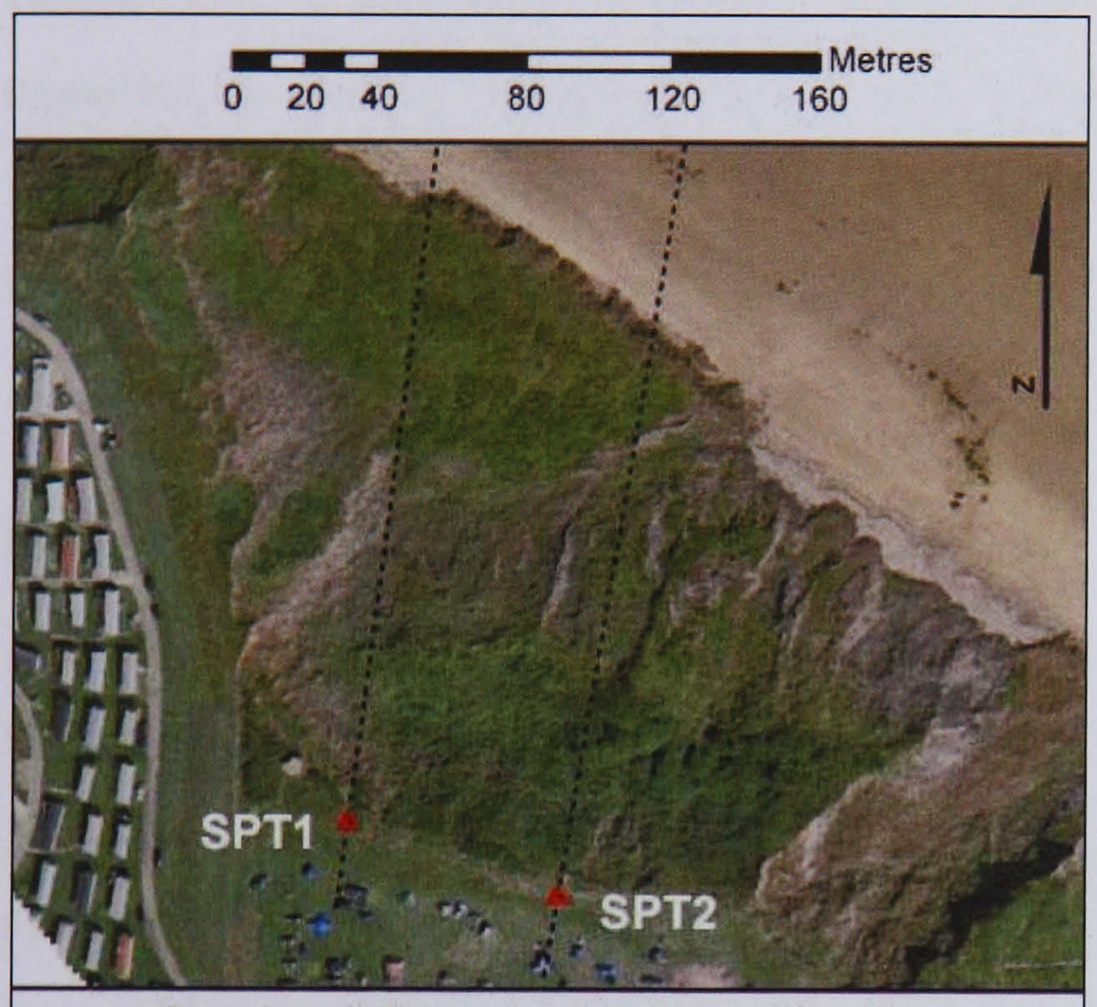

Figure 5.6 SPT test area, with validation profile locations, and control points indicated.

5.3 Episodic Monitoring Campaigns

5.3.1 Overview

The datasets for the monitoring strategy were acquired through a number of episodic campaigns. Initially, these were designed to permit four epochs of data collection at six-monthly intervals over a two year period spanning 2004 and 2005. However, due to major technical problems with the ALS instrument, and subsequent delays to the ARSF's acquisition schedule, the planned ALS sorties had to be rescheduled. This affected the timing of the monitoring campaigns, as concurrent acquisition of TLS and ALS data was crucial. Ultimately, episodic monitoring datasets were acquired in September 2004, April 2005, August 2005 and May 2006. The final acquisition is only utilised in the analysis at Whitby Abbey Headland (Chapter Six), as the ARSF delivered poor coverage of Filey Bay during this sortie, with regions of the cliff-face missing.

Therefore, this latter epoch of data is not referred to further in this chapter. With datasets for Filey Bay spanning September 2004 to August 2005, there were good opportunities for observing geohazard activity. Although it was impossible to anticipate the scale of any changes, the high spatial resolutions of the techniques being applied (particularly TLS), and the approximate six-monthly monitoring intervals, gave cause for optimistic expectation that meaningful quantitative analysis could be performed. Furthermore, a number of archival datasets were acquired, and these in particular were expected to permit thorough evaluation of the robust surface matching approach. Acquisition of the archival datasets is discussed in Section 5.4.2.1, while the following section presents a detailed overview of the contemporary acquisitions.

5.3.2 Campaign Specifics

The datasets acquired during each monitoring epoch are summarised in Table 5-2. It can be seen that there is some variability between the datasets captured at different epochs. Although undesirable in some respects, this was unavoidable, as will be explained in the following discussion.

Epoch	Date	Test Areas											
		CPK			GLF			HUN			SPT		
0	Sept. 2004	TLS o	-	V	TLS o	-	V	TLS o	-	V	TLS o	-	V
1	Apr. 2005	-	ALS	-	-	ALS	-	-	ALS	-	TLS +	ALS	V
2	Aug. 2005	TLS * o	ALS	V	TLS *	ALS	V	TLS o	ALS	V	TLS *	ALS	V
V: validation data; o: Leica HDS2500; *: Leica HDS3000; +: Riegl LPM-i800HA													

Table 5-2 Summary of datasets acquired for episodic monitoring campaigns, including specifics of TLS instruments.

5.3.2.1 Epoch 0 Monitoring Campaign

The epoch 0 monitoring campaign took place between the 19th and the 24th of September 2004. As Table 5-2 indicates, only TLS and validation datasets were acquired for this epoch. As explained in Section 5.3.1, major difficulties were encountered with the original ALS acquisition schedule, and the initial sortie,

timetabled for spring 2004, had been postponed. It remained unclear as to whether an autumn acquisition would take place during 2004, and so it was decided to acquire the necessary terrestrial datasets before the onset of winter, in anticipation that ALS data would be acquired within a number of weeks. However, this did not transpire, resulting in a terrestrial-only dataset for epoch 0. While this situation was unfortunate, it was beyond the control of the project team, and nevertheless, the TLS data proved to be of use (Section 5.5.3).

Scanning was carried out at each test area using the Leica HDS2500 scanner, with efforts made to ensure that the whole extent of the cliff-face was acquired, as well as adjacent areas of beach and cliff-top. Validation was carried out by measuring two profiles at each test area by total station, thus providing a source of ground-truth. These profiles were measured shore-normal, and so traversed the cliff-face, from landwards of the cliff-top, down the cliff-face, extending across the beach into the inter-tidal zone. In addition, the existing cliff-top control points at each test area were surveyed by static GPS in order to monitor their stability. As the SPT test area was newly-defined, a pair of control points had to be established on the cliff-top. As for the other sites, these control points provide an accessible source of primary control for the terrestrial surveys, but are particularly important for the validation profiles, as they facilitate orientation. Suitable locations were identified adjacent to the cliff-edge – close enough to provide line-of-sight to the foot of the cliff, and to each other, but far enough inland so as they were not thought to be in any immediate danger of erosion. The points were established with Feno markers (Figure 5.7), which are comprised of a resistant resin head and steel anchor, offering favourable ageing and stability characteristics in an environment such as this. Processing and analysis of the validation datasets is discussed further in Section 5.5.3. Weather conditions were largely dry and sunny throughout the week. However, strong winds made the surveys particularly difficult and uncomfortable, especially around the beach areas.

5.3.2.2 Epoch 1 Monitoring Campaign

The next epoch of terrestrial monitoring took place seven months later, between the 25th and the 27th of April 2005. As Table 5-2 shows, on this occasion, ALS data was

Figure 5.7 Example of buried Feno marker used for control monumentation at Filey Bay.

acquired, and was flown on the 19th of April. While this was certainly a welcome improvement, the unpredictability of the ARSF schedule meant that the corresponding fieldwork had to be arranged at very short notice, with a shortage of personnel. For this reason, it was decided that terrestrial efforts would be focussed on the SPT test area at the southern end of the bay. Of the four test areas, this is the largest and most active in terms of geohazard activity, and therefore was deemed as being of highest priority for terrestrial acquisition. A Riegl LPM-i800HA terrestrial laser scanner, as described in Section 3.3.2.3, was used in this survey. Validation profiles were measured in the same manner as for the epoch 0 survey, but were restricted to the SPT site. Weather conditions were overcast for most of the week, although there was no significant rainfall.

5.3.2.3 Epoch 2 Monitoring Campaign

ALS data for the epoch 2 monitoring campaign was captured on the 2nd of August 2005. Corresponding terrestrial surveys were carried out between the 14th and the 19th of August. As Table 5-2 indicates, this time it proved possible to acquire TLS, ALS and validation data for all of the test areas. In addition, aerial imagery was also acquired, and this later proved useful for interpretation purposes. The initial application to the ARSF had requested that concurrent imagery be captured with each ALS acquisition, but ultimately this only proved possible in this case. Terrestrial laser scanning was carried out using the Leica HDS3000 scanner for the first occasion. However, while this scanner proved to be flexible and easy to use, unfortunately it developed a fault towards

the end of the week, and had to be replaced with the HDS2500 instrument. The characteristics of the three different scanners used throughout the fieldwork are contrasted in Section 5.5.2.1. Validation profiles were measured for all test areas, and analysis of this aspect is presented in Section 5.5.3. Weather conditions were excellent throughout the week.

5.4 Acquisition and Processing of Airborne Datasets

5.4.1 Airborne Laser Scanning

5.4.1.1 Data Acquisition

ALS data was acquired for Filey Bay in April 2005 and August 2005, by NERC ARSF, using an Optech ALTM 3033 first and last pulse return instrument. Details of the ARSF operations, and specifications of the instrument, are provided in Section 3.3.1.1. Data was acquired from a flying height of around 1000 m in all cases, resulting in a ground resolution of approximately 1 point/m^2. The flightlines were designed to ensure adequate coverage of the inter-tidal zone, the beach, the cliff-face, and the cliff-top, in recognition of the fact that the coastal zone should be treated in its entirety, as a set of inter-related processes.

All aspects of georeferencing were performed internally by the ARSF. For all flights, 1 second GPS data acquired from the Scarborough (SCAR) OS Active Reference Station, provided reference data for processing of the in-flight GPS measurements, before further integration with IMU data to permit calculation of accurate flightline trajectories. Given the resultant, relatively short GPS baseline lengths of around 12 km, it was anticipated that this should contribute towards provision of good quality GPS solutions. However, after data delivery, it emerged that the epoch 1 dataset for Filey Bay contained a systematic height offset of around +3.80 m. Following quality assurance reporting back to the ARSF, it was discovered that the ARSF had carried out the original processing using GPS data from a local basestation, which had been set-up for another ARSF flight in the same area on the day of collection. The dataset was returned to the ARSF, where it was re-processed using the SCAR basestation, which rectified the issue.

5.4.1.2 Independent Quality Analysis

As the ALS data was acquired and georeferenced by the ARSF, it was desirable to carry out an independent quality analysis, especially in light of the systematic error discovered in the epoch 1 dataset. This was achieved by comparing the datasets to a test field of GPS check points, which had been acquired in 2001 by kinematic GPS for the purposes of the earlier Newcastle University monitoring research. The test area consisted of a hard-surfaced, level road circuit (Figure 5.8) located in Filey Brigg Country Park, close to the CPK study area.

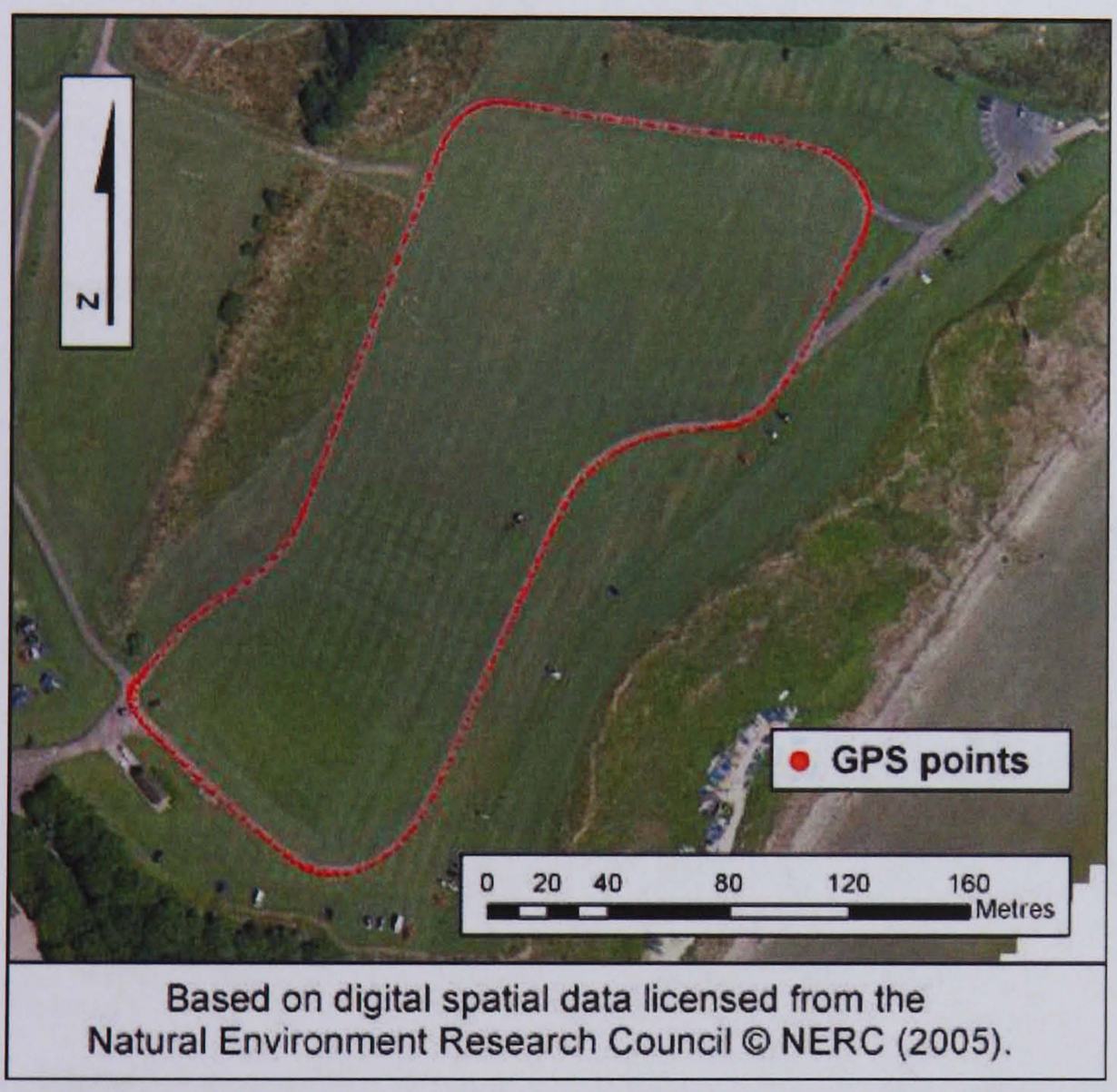

Figure 5.8 GPS test field, located at Filey Country Park.

These measurements had been made in order to evaluate the precision of kinematic GPS mounted on an all-terrain vehicle (Buckley, 2003). During testing, the 600 m long circuit was surveyed six times by the kinematic GPS system, resulting in a mean standard deviation of 0.018 m in height (Buckley, 2003). Although no measure of absolute accuracy was available, this can be anticipated as being in the region of 0.01 m for kinematic GPS (Hofmann-Wellenhof et al., 2001). Given the fact that this is markedly better than the expected accuracy of the ALS system, and combined with the verified high precision of the dataset, it was decided to use all 845 points measured from the six GPS circuits as check measurements in assessing the accuracy of the ALS

datasets. It was assumed that the road had not been resurfaced over the intervening time period, and there was no evidence to suggest otherwise.

The analysis was performed in *TerraSolid's TerraScan* software, a package running under *MicroStation*, which is capable of handling both airborne and terrestrial laser scanning datasets, and which is described further in Section 5.4.1.3. *TerraScan* provides a useful facility for performing check point analysis, allowing vertical discrepancies to be determined between known points, and corresponding points interpolated on a triangulated surface model – in this case derived from ALS. In order to minimise the effects of vegetation and other non-terrain features, analysis was performed using the last pulse return data only. The results of the check point analysis are presented in Table 5-3. The manufacturer's specifications state that the Optech ALTM 3033 can be expected to achieve a vertical accuracy of better than ± 0.15 m from a flying height of 1000 m. While the April 2005 dataset is comfortably within specification, with an RMSE of 0.070 m, the accuracy of the August 2005 dataset is poorer, at 0.168 m. However, this latter figure could not be considered as falling significantly outwith the specified accuracy.

ALS Dataset	Mean (m)	σ (m)	RMSE (m)	Max. (m)	Min. (m)
Apr. 2005	-0.062	0.033	0.070	0.034	-0.161
Aug. 2005	-0.161	0.049	0.168	0.237	-0.299

Table 5-3 Summary of quality statistics for ALS check point analysis.

While this approach provided a means of assessing the vertical component of accuracy, planimetric quality is more difficult to assess (Schenk et al., 2001; Vosselman, 2002; Csanyi and Toth, 2007). The manufacturer's specifications state that for this dataset, a planimetric accuracy of better than ± 0.50 m could be anticipated (refer to Section 3.3.1.1). However, due to repeated delays and uncertainties over the timing of the ALS surveys, it was not possible to carry out any field-based assessment of data quality, such as through the use of artificial check points (e.g. Csanyi and Toth, 2007). The resolution of the ALS data proved too low to permit any post-acquisition analysis of planimetric accuracy through inspection of manmade features such as gable roofs, and for the same reason, ruled out the use of intensity data for this purpose. However, no significant

shifts could be detected between the datasets or flightlines at the Filey Bay test site, and this was supported by the lack of any associated artefacts in subsequent geohazard analysis. The Filey ALS datasets were deemed suitable for inclusion in the monitoring strategy, although it was suspected that accuracy values would be poorer over the cliff-face areas due to the effects of vegetation and slope, as suggested by the investigations of Göpfert and Heipke (2006) and Su and Bork (2006). This is analysed further in Section 5.5.3.

5.4.1.3 ALS Data Processing

The ALS data was delivered by the ARSF in ASCII *xyz* format on the basis of flightlines. These files contained both first and last pulse returns for each laser shot, as well as intensity information, which proved helpful for interpretive purposes, especially for the April 2005 dataset, where concurrent imagery was unavailable. The flightlines consisted of up to eight million points (considering both pulses), and therefore were initially cumbersome to handle, as computer memory limitations made it difficult to even just examine the raw text data. The data was delivered in British National Grid coordinates, Ordnance Survey Great Britain 1936 (OSGB36), and the first step involved transforming to the Universal Transverse Mercator (UTM) projection system (Zone 30 North). UTM was used for all data processing and analysis, as this offers the benefits of a global projection system, potentially permitting the integration of observations with datasets such as models of sea level change, thus facilitating inferences to be drawn in relation to wider-scale processes. The use of UTM coordinates also ensured that the data could be directly compared to the previous Newcastle University monitoring datasets.

Once the ALS datasets had been transformed, they were imported to *TerraScan*. The *TerraScan* software offers a range of functions; in addition to visualisation of point datasets using the standard *MicroStation* interface, a number of routines are available for data classification. This includes algorithms to classify low points and ground points, and consequently allows points to be exported on the basis of these classifications for further processing elsewhere. A wide range of input and output file formats are supported, and various forms of *xyz* datasets can be imported and manipulated. This therefore makes *TerraScan* particularly valuable for general DEM

manipulation, and consequently, this software was utilised extensively throughout the research.

As it was desirable to remove the effects of vegetation, and restrict analysis to the terrain surface as far as possible, the first pulse returns were discarded for all flightlines. The next issue which required treatment was the handling of strip (flightline) overlap areas. A number of the test areas were covered by overlapping flightlines, giving rise to concerns over possible systematic strip offsets arising as a result of GPS-IMU errors, as discussed in Section 2.5.4. The overlap regions were visually inspected with this concern in mind. However, no shifts could be detected, and it was decided that no further course of action was necessary in this respect. However, where two or more flightlines overlap, there is likely to be increased surface noise, which could lead to poor representation of the terrain in such areas. It was therefore desirable to take action in order to reduce these effects. The options in this regard were rather limited, as no trajectory information was provided, which ruled out the possibility of directly determining if one flightline was of superior quality, or removing points on the basis of scanning angle. A solution was found by exploiting *TerraScan's* capability to manually assign relative quality values to flightlines. This then allowed removal of points from the poorer quality flightline in the overlap regions. Most of the relevant overlaps occurred in the vicinity of the coastal slopes, and these areas were of greatest importance for analysis purposes. Generally, on the cliff-faces the ALS incidence angle was near perpendicular for the seaward flightline, but oblique for the landward flightline. Therefore, the seaward flightlines were assigned higher quality values, and points from these were retained, resulting in an improved surface representation for these areas. This procedure is illustrated in Figure 5.9.

Figure 5.9 Overlapping flightlines (left) cut by removing poorer quality points (centre, red) from landward flightline, and retaining points from seaward flightline only (right).

For cliff-top overlaps, where terrain was relatively flat, and there was no obvious difference in quality, the overlaps were cut manually down the centre, to retain half of the points from either side. The next pre-processing stage related to filtering out non-ground points over the cliff-top areas. Although, as already stated, the first pulse returns had been removed, some non-terrain features such as buildings and walls still remained in the datasets. Therefore, non-ground features had to be eliminated in order to minimise subsequent multi-temporal change issues in these regions. The *TerraScan* ground classification routine was invoked in order to remove non-ground points. This routine works on the basis of identifying initial low points, and then triangulating these and searching for new ground points within the resultant triangles. This procedure is iterated, and the triangulation and subsequent ground model become increasingly refined. The algorithm is particularly sensitive to the user-defined terrain angle parameter. The *TerraScan* ground classification routine is based on the algorithm developed by Axelsson (1999) (Elmqvist, 2002). This has been found to perform favourably in comparison to alternative routines, particularly over steep slopes (Sithole and Vosselman, 2003), and visual inspection suggested that the resultant terrain models were of high quality.

The DEMs were generally thinned prior to surface matching. The *TerraScan* 'Model Keypoints' classification routine was used in preference to the 'Thin Points' tool. The Thin Points algorithm implements a straightforward reduction in point density by applying user-defined horizontal and vertical tolerances for point culling. However, the Model Keypoints classification applies a more sophisticated approach in order to identify and retain critical points, thus ensuring a faithful representation of the terrain, while enabling high levels of point reduction over relatively flat areas.

5.4.2 Archival Aerial Photography

5.4.2.1 Data Acquisition

A visit was made to the National Monuments Record (NMR) in Swindon in order to identify suitable archival aerial imagery for the research. The NMR holds around 2,000,000 vertical aerial photographs, and as discussed in Section 3.3.3.1, coverage is often relatively good in coastal regions. This proved to be the case for the North

Yorkshire coastline, and paper prints were ordered for the frames of interest, enabling the selection to be refined. It was decided not to include earlier imagery from the 1940s and 1950s, as investigations revealed that no camera calibration information existed for these, and they appeared to have been acquired with non-metric cameras. While it would have been interesting to investigate if DEMs of suitable photogrammetric quality could have been extracted from this imagery, unfortunately time did not permit.

Acquiring suitable photogrammetric scans of the selected images proved to be a time-consuming procedure. The first difficulty related to copyright restrictions. Of the original imagery investigated, copyright was held by a number of parties, including the OS, North Yorkshire County Council, and an aerial photography company which no longer existed. Contacting and gaining permission from the necessary departments required a great deal of perseverance, and in some cases had to be abandoned. This was one of the reasons why the imagery which was ultimately selected (Table 5-4) was restricted to OS photography.

Characteristics	**1967**	**1980**
Source	NMR (OS copyright)	NMR (OS copyright)
Media	Scanned diapositives	Scanned diapositives
Acquisition Date	28th June 1967	4th September 1980
Sortie No.	67-254	80-135
Frames	32, 33	008, 009
Flying Height (m)	1500	2360
Focal Length (mm)	152.240	305.379
Scale	1:10,000	1:7,800
b/H ratio	0.6	0.3
Scanning resolution (μm)	21	14
Ground sample distance (m)	0.21	0.11

Table 5-4 Details of archival imagery acquired for Filey Bay test site.

The second hurdle concerned acquiring suitable photogrammetric scans. The NMR only had access to a standard desktop scanner, which could not be considered as geometrically stable, and initially, NMR staff were loathe to release films for external scanning. Fortunately, a solution emerged, as photogrammetric scanning was able to be

arranged through OS, who were copyright holders. The relevant rolls of film were therefore released to OS, who scanned the necessary stereopairs for the two epochs, as detailed in Table 5-4. These provide coverage of the SPT test area at the southern end of Filey Bay, as shown in Figure 5.10. Examples of the imagery are show in Figure 5.11 (1967), and Figure 5.12 (1980).

The information presented in Table 5-4 was utilised to calculate the expected heighting precision of subsequent photogrammetric measurements, by applying Equation 2-1 (refer to Section 2.4.3). This resulted in anticipated precision values of 0.175 m for the 1967 imagery, and 0.182 m for the 1980 imagery. These values provided an approximate indication of the likely measurement quality (in terms of height) which could be expected through subsequent photogrammetric processing and DEM extraction, as described in Section 5.4.2.2. Unfortunately however, check point data could not be acquired for either the 1967 or 1980 imagery (as explained in Section 5.6.3.2), and therefore, it was not possible to assess how closely these precision estimates corresponded to those actually achieved. Alternative quality evaluation procedures are presented in Section 5.6.3.

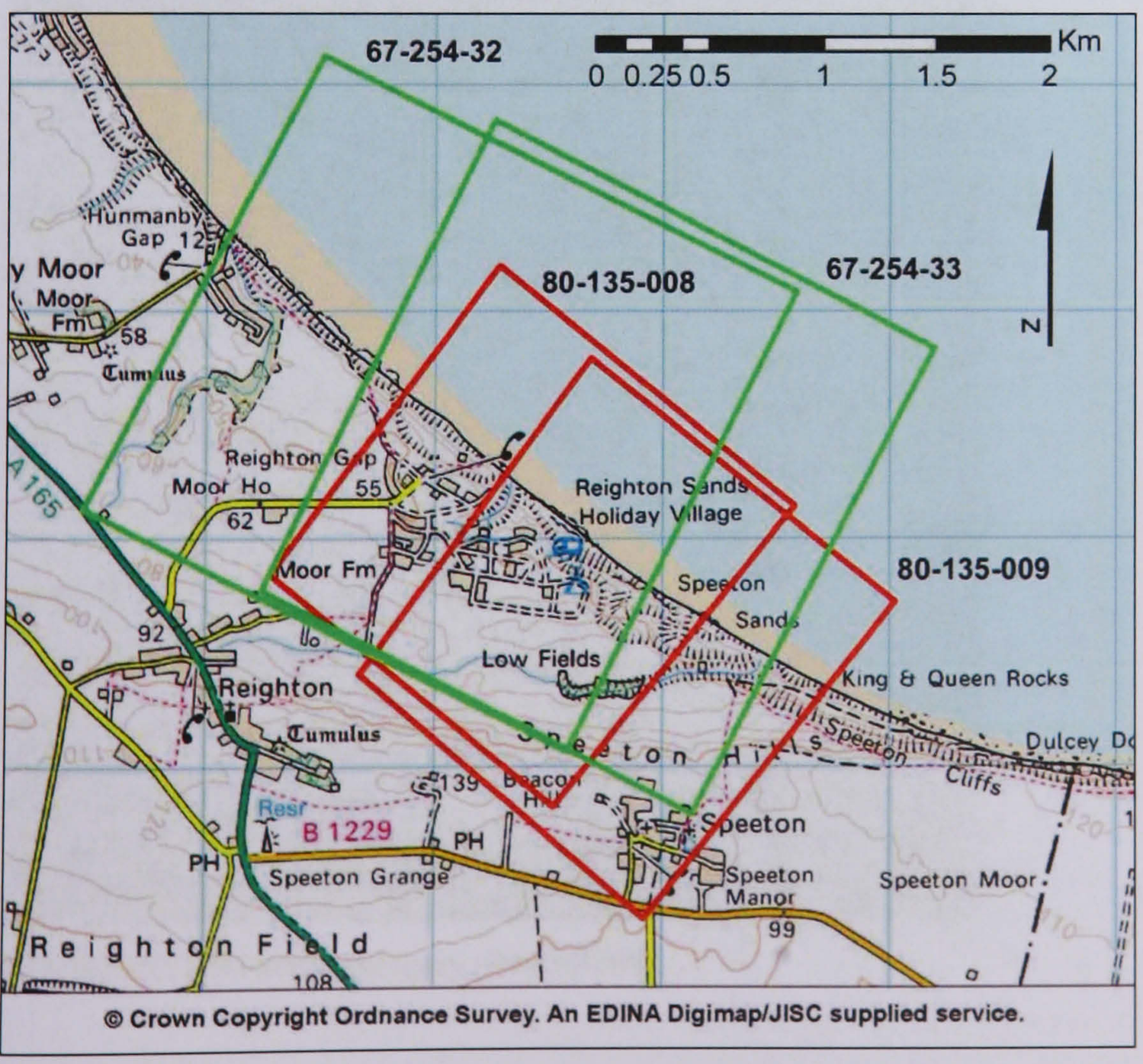

Figure 5.10 Coverage of archival imagery detailed in Table 5-4.

Figure 5.11 1967 aerial imagery (67-254-32).

Figure 5.12 1980 aerial imagery (80-135-008).

5.4.2.2 Processing of Archival Imagery

Measurement of Fiducial Coordinates

The first processing stage related to preparation for interior orientation. Calibrated focal lengths were available for the two epochs of imagery, 1967 and 1980. However, OS were unable to locate any camera calibration certificates, which was somewhat surprising, especially in the case of the 1980 imagery. This lack of calibration data is a common problem amongst those utilising archival aerial photography (e.g. Moore and Griggs, 2002; Dornbusch et al., 2005; Schiefer and Gilbert, 2007), and usually represents the primary challenge to successful photogrammetric exploitation of such datasets (Chandler and Clark, 1992). In order to perform photogrammetric interior orientation, it was therefore necessary to specify a camera coordinate system for the two sets of images, and identify and manually measure the coordinates of substitute or existing fiducial marks in this reference system. The 1980 imagery had standard fiducial marks in the corners and sides, and the 1967 imagery was exposed on a reseau grid, thus providing suitable reference features for this purpose. However, as the original film could not be directly accessed, this made for a less than ideal situation, as the camera coordinate system had to be defined on the basis of the scanned imagery, rather than through measurement of the original film. *Adobe PhotoShop* was utilised for this purpose. The centre of the images, determined as the intersection of lines connecting opposite pairs of fiducial marks, was defined as the origin for the camera coordinate systems. Seven fiducial marks were identified in the 1980 imagery (the eighth fiducial could not be determined due to poor image contrast), while nine were utilised in the case of the 1967 images. The selected fiducial marks were measured ten times each, to ensure high precision. Measurements were made on both the left and right images for each epoch, and any discrepancies were averaged in order to provide the best possible estimate. Although it must be acknowledged that this approach is not ideal, under the circumstances (particularly in relation to the lack of access to the original film), this was deemed to be the most appropriate course of action. Similar approaches have been adopted by other researchers who have encountered this situation (e.g. Dornbusch et al., 2005; Walstra, 2006).

Digital Photogrammetric Processing in *SocetSet*

A *BAE Systems SocetSet* digital photogrammetric workstation (versions 5.2.0 and 5.3.0) was used to carry out all photogrammetric processing, in accordance with the standard

DPW workflow. As the robust matching technique was to be used to provide absolute orientation for the archival photogrammetric DEMs, essentially only a relative orientation was required in *SocetSet*. However, as the surface matching software requires good initial parameter approximations, the most appropriate solution was to perform an approximate absolute orientation of the stereo-model. In order to achieve this, the *SocetSet* user manual recommends the inclusion of a number of pseudo control points (BAE Systems, 2006). This procedure was carried out by obtaining the approximate coordinates of four ground control points (GCPs) per stereopair, from large scale digital mapping.

Interior orientation was then performed using the fiducial coordinates determined through measurements in *PhotoShop*. Following this, the GCPs were located on the imagery, and *SocetSet* performed automated tie point measurement. These measurements formed inputs for the bundle adjustment procedure, which enabled an approximate absolute orientation of the stereo-model to be produced, with results as indicated in Table 5-5. Low image RMSE values were obtained for both epochs, suggesting that the internal quality of the models was strong. The relatively large ground RMSE values reflect the use of approximate GCPs.

Epoch		1967	1980
No. Control Points		4	4
No. Tie Points		11	10
Image RMSE (pixels)		0.075	0.067
Ground RMSE (metres)	x	0.881	0.858
	y	0.859	0.720
	z	0.173	0.087
	Total	1.242	1.124

Table 5-5 Summary of solutions achieved from *SocetSet* bundle adjustment procedure.

The next phase involved DEM extraction. DEMs were extracted using the *SocetSet* Automatic Terrain Extraction module, and application of the adaptive extraction strategy. This performs image correlation by attempting to automatically adapt to the terrain type across the DEM area. The DEMs were extracted as TINs to avoid the undesirable effects of interpolation (refer to Section 3.4.2). A resolution of 1 m was specified (this is a nominal value, as gaps exist in areas where correlation was not

achieved). As the photogrammetric DEMs were only approximately oriented, then it was not possible to asses quality through the conventional check point based approach. Ultimately the quality of the DEMs is analysed at the surface matching-based registration stage (Section 5.6.3). However, in this section, inspection of the extracted DEM mass points suggests that the terrain extraction procedure was largely successful. Figure 5.13 shows the extracted points for the 1967 and 1980 DEMs. It can be seen that while few notable gaps appear in the 1980 DEM, correlation failure has led to sparse regions in the lower-left of the 1967 DEM, corresponding to poor image texture in agricultural fields. The 1967 imagery also appeared to be over-exposed, and this may have contributed to these problems. However, these issues did not affect terrain extraction over the cliff-face, and had no impact on subsequent processing and analysis.

Figure 5.13 *SocetSet* mass point extraction for the 1 m TIN DEMs for 1967 (left) and 1980 (right).

DEM Refinement

Following terrain extraction in *SocetSet*, the DEMs were exported in ASCII format for the final stage of processing. This involved the removal of non-ground points. It was decided that *TerraScan* should be used for this procedure, in order to maintain consistency with the ALS DEMs. Therefore the ASCII DEMs were imported to *TerraScan*, where ground classification and point thinning (where necessary) were performed in the same manner as described in Section 5.4.1.3.

5.5 Acquisition and Processing of Terrestrial Datasets

5.5.1 GPS Control Data

5.5.1.1 Data Acquisition

As already discussed in Section 5.3.2.1, pairs of cliff-top control points at each test site provided a source of control and orientation for the validation profiles and the TLS surveys. The coordinates of the six stations at CPK, GLF and HUN had already been established through the earlier Newcastle monitoring work (refer to Buckley, 2003)). However, as these were located close to actively eroding cliffs, it was necessary to re-observe these points during each monitoring campaign in order to assess their stability. This also enabled comparisons with the existing archive of measurements (2000 – 2002). In addition, the locations of the new control points at SPT had to be determined and monitored over the course of the study.

The position of the control markers was determined through static GPS observations. During the epoch 0 survey, *Leica System 500* receivers were utilised, while for the later surveys, *Leica GPS1200* receivers were used. These models are both standard survey-grade receivers, permitting dual frequency measurement. At least one hour (and frequently closer to two hours) of continuous observations were acquired for the stations during each field campaign, using a sampling rate of 30 seconds. It should be noted that only stations SPT1 and SPT2 were surveyed during epoch 1, as terrestrial acquisitions were limited to this test site, as discussed in Section 5.3.2.2.

5.5.1.2 GPS Data Processing and Analysis

Leica Geo Office, and its predecessor, *SKI-Pro*, were used to process all GPS datasets for the research. These packages enabled the observations to be processed relative to reference station data in order to facilitate accurate positioning. The OS Active Network Station at Scarborough (SCAR), some 12 km away was used as the reference station. Data for SCAR spanning the relevant time periods was downloaded from the OS website (Ordnance Survey, 2007), and in order to optimise accuracy, precise ephemerides were downloaded from the International GNSS Service website

(IGS, 2007). Processing was carried out using a 10° elevation mask, and the final WGS-84 coordinates were converted to UTM Zone 30 North.

As already stated, in addition to the three epochs of control station measurements computed for the purposes of this research, the locations had also been observed over the period 2000 to 2002. This permitted an extended analysis of the stability of the control monuments. The epoch-to-epoch variations at each point were generally in the region of 1-2 cm or less. No significant displacement trends could be identified at any of the points, suggesting that the source of the discrepancies was most likely associated with the precision of the measurements.

Table 5-6 presents a summary of inter-epoch discrepancies at HUN1, which is representative of the magnitudes of change observed at the other sites. Interestingly, while Buckley (2003) notes a consistent positive increase in the height component at all stations between 2000 and 2002, this trend is reversed over the current monitoring, with consistent downwards movement. However, the displacements cannot be considered significant in relation to measurement precision, and so without longer-term monitoring it is impossible to asses whether this is representative of any underlying processes.

Monitoring Study	**Epoch**	**HUN1 Displacement (m)**		
		ΔE	**ΔN**	**Δh**
Buckley (2003)	Aug. 2001 – Aug. 2000	+ 0.013	+ 0.011	+ 0.030
	Mar. 2002 – Aug. 2001	+ 0.022	- 0.009	+ 0.027
Results determined through this research	Sept. 2004 – Mar. 2002	- 0.042	+ 0.009	- 0.021
	Aug. 2005 – Sept. 2004	+ 0.011	- 0.002	- 0.013
Net displacement 2000-2005:		+ 0.004	+ 0.009	+ 0.023
HUN1 E: 678478.711 m N: 6006605.715 m h: 74.597 m (August 2000)				

Table 5-6 Summary of GPS-derived inter-epoch displacements at HUN1, 2000-2005.

5.5.2 Terrestrial Laser Scanning

5.5.2.1 Data Acquisition

In total, three different terrestrial scanners were used to acquire data during the survey campaigns. The key characteristics of these instruments have already been introduced in Section 3.3.2, and Table 5-2 details which scanners were used for each epoch of monitoring. The distinctly different features of the three scanners meant that differing survey strategies were required on each occasion. The Leica HDS2500 was the most heavily utilised instrument, as this was readily accessible throughout the research. As a fixed head scanner with a range of 50 m to 100 m, scans had to be acquired from several different positions in order to ensure acceptable coverage of the cliffs.

Furthermore, as the HDS2500 relies on the resection-based orientation approach, targets had to be placed within the scans, and observed by total station. Specially adapted targets were devised by gluing the standard scanner targets to a slightly larger square of foamboard (which provided some additional stability), and then mounting these on wooden stakes which could be driven into the relatively soft tills of the cliff-face (Figure 5.14). Field testing prior to the fieldwork confirmed that these were fit for purpose.

Figure 5.14 Specially adapted target for controlling the Leica HDS2500 scans.

Four well-distributed targets were positioned in each scan. The cliff-top control point pairs were used to establish temporary survey stations on the beach (although in some cases temporary points were established directly, using rapid-static GPS), and from these, a total station was used to observe the scanner targets on the cliff-face. This procedure had to be well-coordinated to ensure rapid observation of the targets, while scanning was being carried out, before the targets were repositioned and had to be re-observed for the next scan position.

The Leica HDS3000 scanner offers direct georeferencing capabilities (refer to Section 3.3.2), which altered and reduced the control exercise in comparison to the HDS2500. In practice, it was often possible to use the same orientation point for all scans, and furthermore, in comparison to the HDS2500, fewer scan positions were required, as the HDS3000 is a panoramic scanner, with a 360° horizontal FOV. Rapid-static GPS proved the fastest method for establishing the reference points in this case. However, the HDS3000 offers the same range capabilities as the HDS2500 and therefore, a number of scan positions were required to fully capture the whole cliff-face. Both Leica scanners facilitated the acquisition of data at high spatial resolutions, with point densities ranging between 40 and 80 points/m^2.

The third scanner, the Riegl LPM-i800HA, is capable of scanning over ranges up to 800 m. This feature made it well-suited to the application at hand, and effectively meant that scanning could be carried out from a single station on the foreshore. In contrast, the Leica scanners typically necessitated scanning from four to five different positions in order to ensure good coverage at each test site. However, the extended range of the LPM-i800HA translated to lower resolution scans in comparison to the Leica instruments, with a point spacing of 20 cm in the vicinity of the cliff-top (refer to Table 3-2 for comparison of instrument specifications). Like the HDS3000, the LPM-i800HA is a rotating head instrument, and again, the direct georeferencing approach was used. It should be noted that for both the HDS3000 and the LPM-i800HA, control can be provided via the resection approach. However, for the application at hand, direct georeferencing, through rapid-static GPS, offered a more suitable strategy. This was primarily due to the time restrictions imposed by incoming tides.

In comparing and contrasting the suitability of the three scanners, each offered a number of advantages and disadvantages. The LPM-i800HA is a ruggedised instrument, designed for challenging outdoor conditions, and from this perspective, was well suited to coastal monitoring. Neither of the Leica instruments could be considered as being designed for operation in an environment such as this. However, the HDS2500 performed exceptionally well in this regard, and was found to be capable of consistent, reliable performance. Despite the restricted FOV, which necessitated multiple scan stations, with systematic and well-drilled survey routines, this approach was found to be as fast as that of the LPM-i800HA. None of the scanners were fully-optimal for this application: the LPM-i800HA offered excellent range, but relatively low resolution and slow speed of acquisition; the HDS3000 provided a full 360° FOV, but relatively limited range; and the HDS2500 offered excellent resolution, but required the positioning of control points within the scene. It should also be noted that both of the Leica scanners necessitated some scanning from the cliff-face. Positions had to be carefully selected so as to ensure good coverage, while minimising risk. This approach was of course undesirable, but ultimately unavoidable, as a consequence of instrument availability. However, it is important to highlight that this did not disadvantage the monitoring strategy. In an ideal situation, it would be preferable to ensure continued application of an instrument with ranging capabilities similar to the LPM-i800HA. However, all of the TLS survey techniques employed here ensured the provision of datasets representative of terrestrial acquisition, including the presence of occluded terrain, as highlighted in Section 5.7.2.1.

5.5.2.2 TLS Data Processing

Processing of TLS Control Data

Where control had been acquired through rapid-static GPS, *Leica Geo Office* was used in processing, as described in Section 5.5.1.2. This facilitated the determination of control points for directly-georeferenced scans.

For the HDS2500 scanner, ultimately control was provided through total station observations of the scanner targets. *LSS* is a terrain modelling and visualisation software package which is heavily utilised in the land survey sector for processing survey observations, and performing quantitative analyses on the basis of these. The final GPS-

derived positions of the cliff-top control points were input to the *LSS* software for each monitoring epoch, as these provided a source of reference and orientation for the raw survey observations. This subsequently enabled the positions of the scanner targets to be determined.

Registration of TLS Datasets

The various approaches to registration of TLS datasets have already been discussed in Section 2.6.3. In this research, the most efficient strategy was to globally register each scan independently. This was due to the fact that it would have been difficult and prohibitively time-consuming to adopt any approach which necessitated a requirement for scan overlaps. Instead, the terrain was scanned with minimal overlaps, ensuring that each scan contained sufficient control to enable independent registration in the survey coordinate system (UTM). While this may not necessarily conform to the most accurate approach, this was deemed suitable for the application at hand, and it was anticipated that any mis-registration could be addressed through surface matching, which as it transpired, proved to be the case, as explained below.

Leica Cyclone software, as introduced in Section 3.3.2.1 was used to register scan data from the HDS25000 and HDS3000 scanners. For the HDS2500, the final positions of the scanner control targets, determined in *LSS*, were imported to *Cyclone*, facilitating registration to the project coordinate system. Registration of the HDS3000 data required final coordinates and heights of the scan stations and backsight stations. *Riegl RiPROFILE* software (refer to Section 3.3.2.3) was utilised for registration of the LPM-i800HA datasets in a similar manner. However, some difficulties were encountered with this dataset (epoch 1), as processing revealed that one of the scans had 'swung' by 4° around its origin, most likely as a result of a blunder during acquisition in the field. This was successfully rectified by surface matching the erroneous TLS dataset to overlapping portions of the epoch 0 TLS, and epoch 1 ALS datasets.

For each scan (in both *Cyclone* and *RiPROFILE*), final editing was carried out in order to eliminate error points, such as those arising through interference caused by people walking in front of the instrument during scanning – an unavoidable complication, as parts of the beach were particularly busy with holidaymakers. The point clouds were then exported in ASCII *xyz* format for further processing.

Refinement in TerraScan

The point clouds were then imported into *TerraScan* for further processing. This effectively involved the same steps as described in Section 5.4.1.3 in relation to ALS processing. In comparison to ALS processing, the ground classification procedure was more time-consuming, and required greater manual intervention in the case of the TLS data. This is an issue which has been previously highlighted by Bitelli et al. (2004). The reasons for this can be attributed to two factors; firstly, the high resolution of the datasets, and the oblique scanning angles, meant that the scans contained a large number of vegetation points; and secondly, the complex cliff topography introduced a range of slope angles over relatively short distances. As a result of these issues, it was initially more difficult to determine optimal settings for the ground classification routine, which is particularly sensitive to the terrain angle parameter. It was also necessary to perform some targeted ground classification of the back-scarp at the cliff-top, and the toe-scarp at the foot of the cliff. These areas contained slopes which were often vertical or overhanging. The targeted classification involves a form of semi-manual classification, which can be applied over localised areas (e.g. two metres), by setting the parameters, and then clicking (using the mouse) for repeated application to the desired regions. The quality of these final ground models is evaluated in Section 5.5.3.2.

As the TLS data for a single study site could amount to 250,000 points for just one survey epoch, it was necessary to carry out data reduction prior to surface matching. This involved application of the Model Keypoints routine as described in Section 5.4.1.3. The datasets were generally restored to full resolution at the analysis stage.

5.5.3 Profile Validation of Laser Scanning Datasets

5.5.3.1 Data Acquisition

As outlined in Section 5.3.2, two validation profiles were measured at each study site for every epoch of monitoring (with the exception of epoch 1, where data was only acquired for the SPT site). The profile locations are shown in Figures 5.4, 5.5 and 5.6. The profiles were set out from the cliff-top control points, which also provided a source of orientation, therefore allowing each profile to be re-occupied during subsequent surveys. Each profile extended from the inter-tidal zone, up the cliff-face, and several

metres inland. *Leica TCRA1103*, *TCR303* and *TCR307* total stations, with angular precisions of 3", 3" and 7" respectively, and a distance precision of ± 2 mm + 2 ppm, were used to acquire the profile data. The profiles were each measured three times in order to ensure precision, and the final merged profiles for each epoch resulted in an average along-profile point spacing of 0.5 m.

5.5.3.2 Quality Assessment of Laser Scanning Datasets

The validation profiles enabled the quality of the TLS and ALS datasets to be assessed over the cliff-face test areas, and also provided a means for comparing the relative accuracies of these two techniques. *LSS* was used to calculate the vertical differences between each of the laser scanning datasets and the profile point measurements. As explained in Section 5.4.1.3, the ALS first pulse returns were discarded in order to minimise vegetation and non-ground effects as far as possible, and consequently, last pulse data only was utilised in the quality analysis. The results for the TLS and ALS datasets are summarised in Table 5-7 and Table 5-8 respectively.

Epoch	Site	TLS - Profile Vertical Differences (m)				
		Mean	σ	RMSE	Max.	Min.
0	CPK2	0.493	0.471	0.681	2.273	-0.225
	GLF1	0.615	0.428	0.747	1.501	-0.361
	HUN2	0.107	0.172	0.202	0.615	-0.459
	SPT1	0.233	0.349	0.419	1.523	-0.313
1	SPT1	0.600	0.799	0.995	3.244	-0.093
	SPT2	0.236	0.448	0.502	1.272	-1.102
2	CPK1	0.232	0.247	0.337	0.741	-0.071
	CPK2	0.161	0.237	0.285	0.716	-0.550
	GLF1	0.294	0.328	0.440	1.192	-0.791
	HUN2	0.161	0.272	0.300	1.397	-0.214
	SPT1	0.218	0.427	0.478	1.856	-0.258

Table 5-7 Summary of profile validation statistics for TLS datasets.

The outcomes are rather surprising, with the ALS data displaying consistently lower RMSE values than the TLS datasets. This is in contrast to expectation, as TLS should theoretically offer considerably higher accuracy in all cases. The relatively poor performance of TLS here is likely due to the effects of vegetation, combined with oblique scanning angles. This is reflected in the mean positive offset of the TLS

datasets. ALS is generally able to offer a more perpendicular angle of incidence, which may have resulted in improved penetration of the vegetation cover. This is illustrated in Figure 5.15 which shows ALS and TLS profiles for epoch 2 at GLF1, a particularly heavily vegetated site.

Epoch	Site	ALS - Profile Vertical Differences (m)				
		Mean	σ	RMSE	Max.	Min.
1	SPT1	0.011	0.316	0.314	1.315	-0.608
	SPT2	0.049	0.393	0.393	1.341	-0.660
2	CPK1	-0.123	0.138	0.184	0.315	-0.534
	CPK2	0.022	0.255	0.255	1.077	-0.403
	GLF1	0.033	0.180	0.182	0.528	-0.294
	GLF2	-0.040	0.165	0.169	0.407	-0.440
	HUN1	-0.014	0.261	0.260	0.925	-0.370
	HUN2	0.051	0.167	0.174	0.510	-0.368
	SPT1	-0.007	0.147	0.147	0.558	-0.368
	SPT2	0.036	0.232	0.234	1.555	-0.496

Table 5-8 Summary of profile validation statistics for ALS datasets.

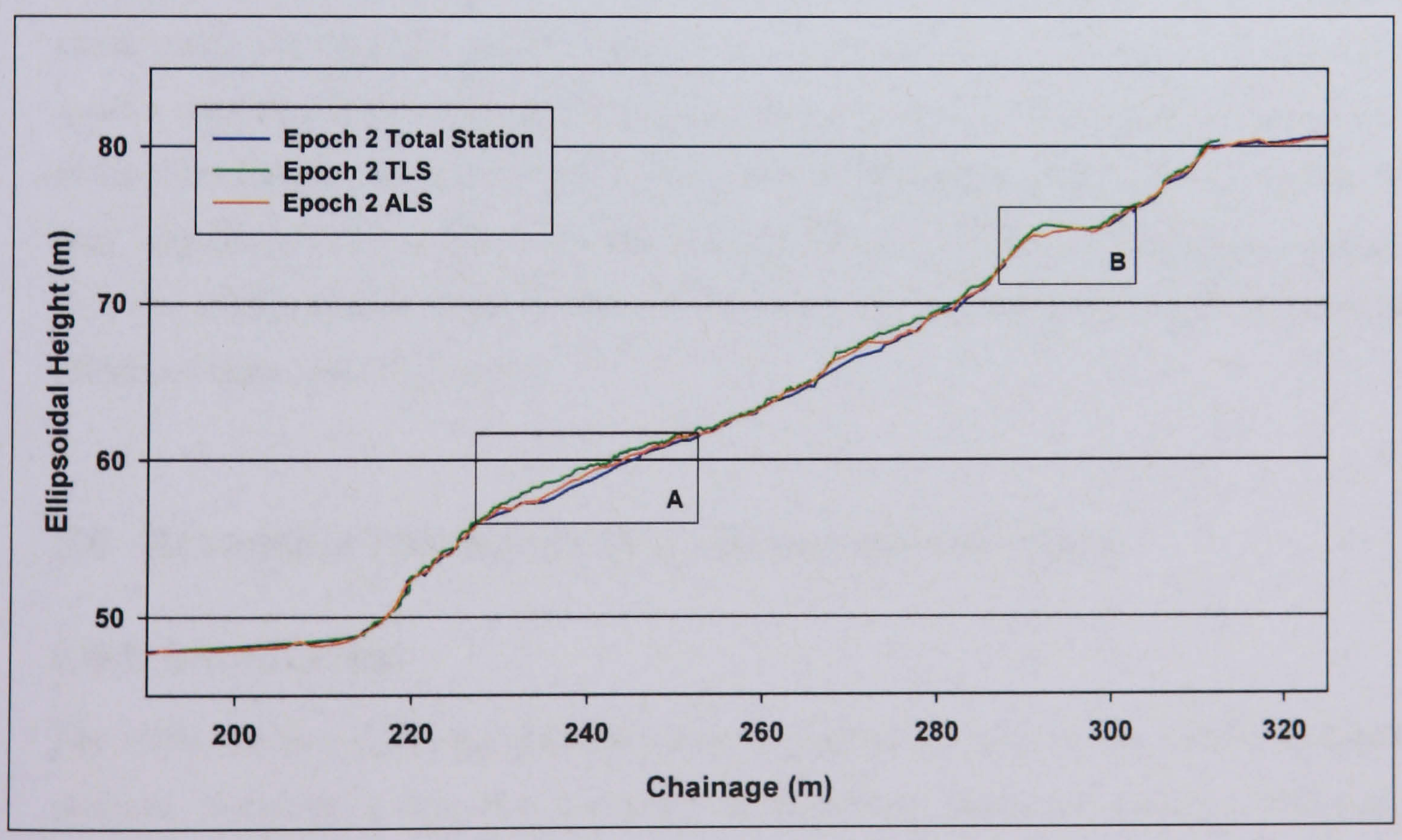

Figure 5.15 Epoch 2 GLF1 profile. Area A highlights differing TLS and ALS surface representations in densely vegetated area; area B indicates break in total station data due to dense vegetation.

The GLF test site displays the largest mean discrepancies for both the epoch 0 and epoch 2 TLS datasets. Differing terrain representations are evident in areas of particularly dense vegetation (e.g. area A), while area B indicates a break in the total station profile, due to an impenetrable area of brambles which prevented measurement (Figure 5.15).

There is a great deal of variability in terms of TLS dataset quality for the different test areas, and between the different survey epochs. Again, this is most likely due to the effects of vegetation; for instance, the HUN2 site is relatively sparsely vegetated, and this appears to be reflected in correspondingly lower RMSE values. Furthermore, although scanning was carried out in such a manner so as to ensure good coverage along the profiles, it is likely that some minor occlusions may have occurred, thus leading to gaps in the TLS datasets, where the subsequent surface triangulation is less reliable. These results serve to highlight the unpredictable effects of vegetation and scanning angle, and suggest that TLS data quality is considerably hindered as a result. The epoch 1 TLS datasets are generally of the poorest accuracy, in keeping with the lower resolution and precision of the LPM-i800HA scanner. ALS appears to offer greater consistency, although the results indicate that the epoch 2 ALS dataset is of a higher quality than the epoch 1 dataset. However, this is in contrast to the analysis carried out at the Filey Country Park test field (Table 5-3), and perhaps suggests that ALS accuracy may vary between flightlines. As expected, the accuracy of the ALS datasets is poorer over the cliff-face than at the Country Park test field, most likely due to the combined effects of slope and vegetation.

5.6 Retrospective Analysis of Geohazard Activity

5.6.1 Introduction

The robust surface matching algorithm was evaluated in Section 4.4.4, using simulated surfaces. However, it was also necessary to rigorously assess the software with real topographic datasets, in order to determine how it would handle issues such as noise, and geohazard activity. Surface matching with archival datasets offered a good opportunity in this regard, not only providing the chance to assess the robust matching

algorithm, but also facilitating quantitative assessment of geohazard activity (Miller et al., 2007; Miller et al., in review).

The aerial imagery from 1967 and 1980 provides historical coverage of the SPT test area at the southern end of Filey Bay, while ALS provides corresponding coverage over more recent temporal periods. Visual inspection of the photography indicated that the cliff-face in this vicinity had been active over this period, with significant change evident. It was decided to broaden the extent of interest beyond the SPT area, to include the section of cliff-face depicted in Figure 5.16, as it was anticipated that this should provide ample opportunity for evaluation of the robust matching algorithm. Elliot et al. (1991) observe that the highest erosion rates occur in this area of the bay, around Reighton Gap. This section of cliffs is formed from boulder clay and Speeton Clay, with the latter noted for its instability (Wright, 2000). As Figure 5.16 illustrates, this portion of cliff is bordered by a large caravan park, with parts of the camping field only ten metres from the receding cliff edge. The area is popular with holidaymakers, walkers, and paragliders (who launch from the cliff edge adjacent to the tent field). The actively-eroding cliff poses a threat not only to those enjoying recreational activities, but also to the longer-term viability of the caravan park.

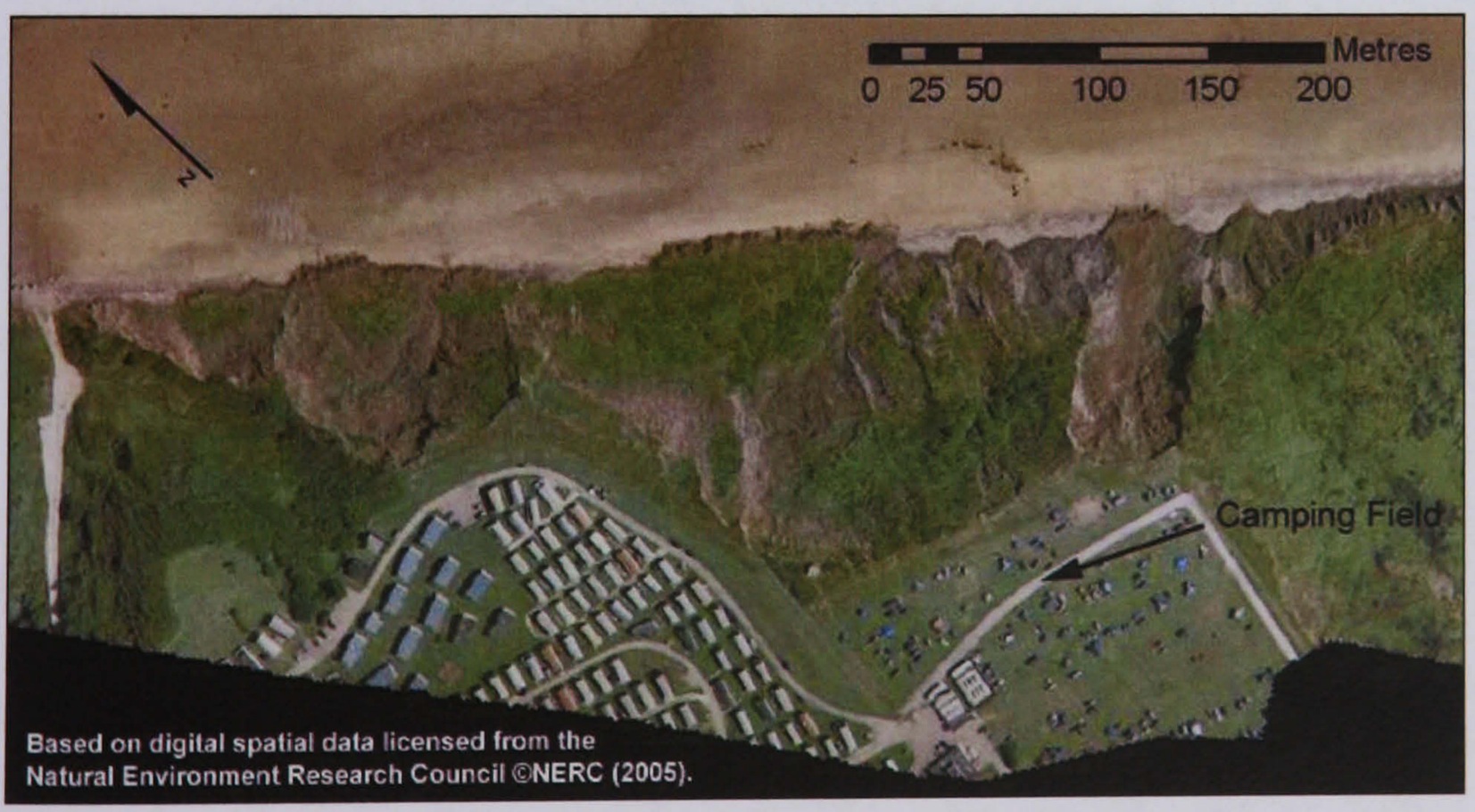

Figure 5.16 Reighton area highlighted in 2005 ortho-image.

5.6.2 Robust Matching of Photogrammetric DEMs

5.6.2.1 Surface Matching Procedure

To recap, the photogrammetric DEMs had only been approximately orientated (in an absolute sense) using points derived from large scale mapping, and therefore the surface matching provided a mechanism for reconciling these datasets to a common reference system – in this case provided by an ALS DEM – for comparison. The epoch 1 ALS dataset from April 2005 was selected as the reference surface in the matching. The RMSE of this dataset over the cliff-face area was in the region of 0.35 m (refer to Section 5.5.3.2). An alternative approach would have been to match the 1980 surface to the 2005 ALS DEM, and then to use the transformed 1980 DEM as the reference surface for matching of the 1967 DEM. However, this strategy was rejected, as the photogrammetric DEMs were relatively noisy in comparison to the ALS DEM, which also offered a more continuous representation of the terrain.

It is necessary to ensure that the input matching surfaces contain sufficient areas which are uncontaminated by surface differences, otherwise the performance of the robust algorithm may become sub-optimal (Li et al., 2001). For this reason, matching was carried out over the entire DEM surface areas for both the 1967 and 1980 datasets (725 m × 825 m and 950 m × 870 m respectively). Matching was applied in both robust and un-weighted modes in order to assess the relative performance of the different approaches.

Table 5-9 summarises the matching parameters and results from the 3DSurf-*R* software. These results indicate that in the case of the historical datasets, the robust algorithm converged to a solution more slowly than when un-weighted matching was applied. The RMSE values, which are calculated from the final least squares residuals, are lower in the case of un-weighted matching. This is to be expected, as the un-weighted algorithm utilises all observations, and in attempting to minimise the residuals globally, will effectively find the best adjustment to 'balance' the differences between the surfaces, as illustrated in Figure 5.17 (B). Therefore, the differences should be truly minimised, leading to lower RMSE values than in the case of the robust algorithm. This is also mirrored in the mean differences between the matching surfaces (Table 5-10). The robust approach mitigates the influence of outliers on the solution, theoretically

producing a solution which is closer to the real terrain (Figure 5.17, A), and where surface differences are reflected more truthfully through larger RMSE values.

Match	Input Parameters			Outputs	
	Weighting	**Parameters**	**Interpolation**	**Iterations**	**RMSE (m)**
2005/1967	Robust	7	Planar	35	2.842
2005/1967	None	7	Planar	14	2.353
2005/1980	Robust	7	Planar	23	1.535
2005/1980	None	7	Planar	12	1.339

Table 5-9 Summary of surface matching parameters and results for matching of historical DEMs at Reighton. RMSE refers to final matching residuals (vertical surface differences).

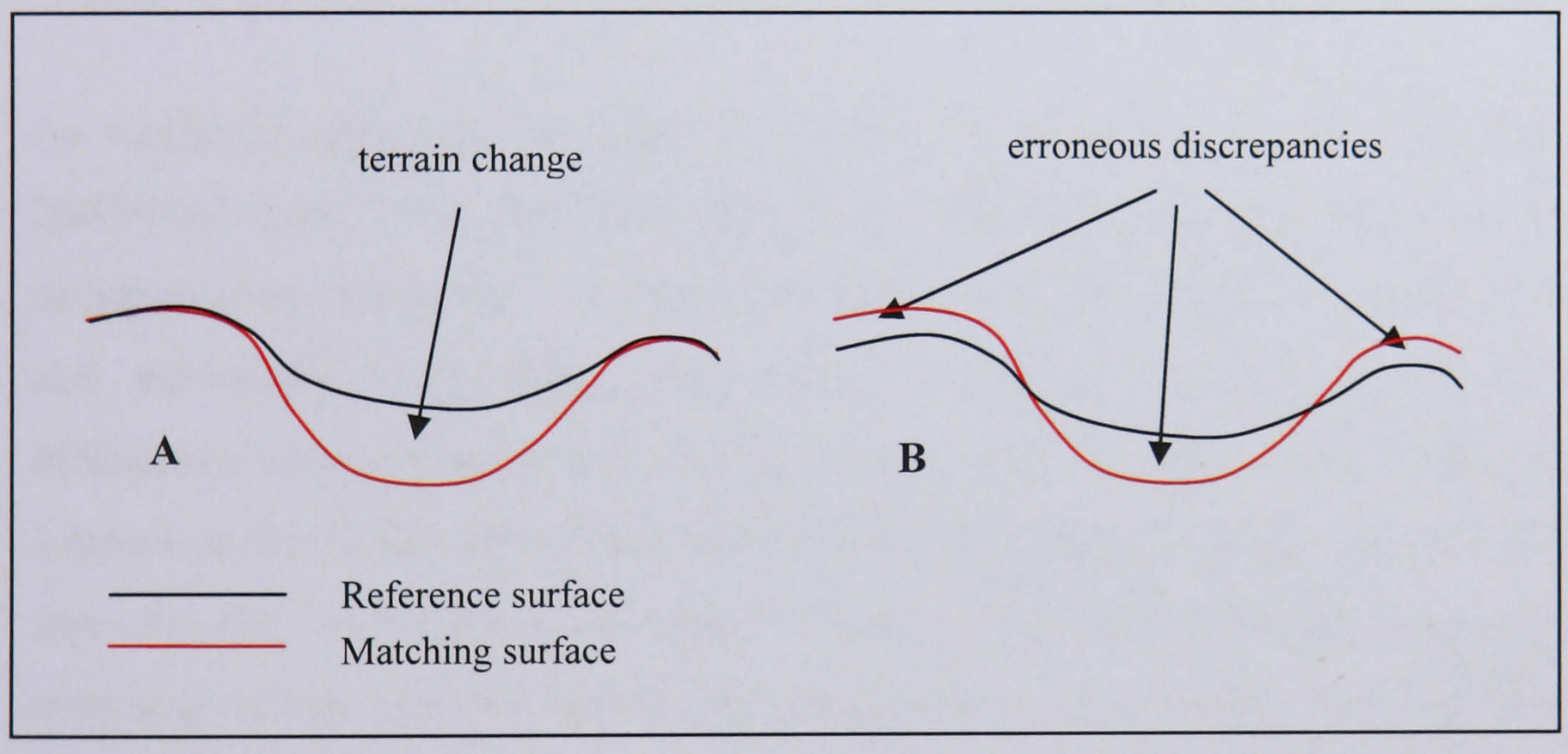

Figure 5.17 Illustration of terrain change, with correct solution (A), and possible outcome of un-weighted matching algorithm (B).

5.6.2.2 Analysis of Matching Solutions

Following surface matching, the post-match transformed DEMs for 1967 and 1980 were compared to the 2005 DEM. The surfaces were imported to *LSS*, where level differences were computed between the surfaces, 1967-2005 and 1980-2005. *LSS* offers the opportunity to calculate the differences using points from *both* surfaces, rather than just points from the matching surface (as the 3DSurf-*R* matching residuals would provide). This allows the higher point density of the ALS matching surface to be exploited when analysing and visualising the differences. Furthermore, if point reduction was carried out in *TerraScan* prior to surface matching, then the DEMs can

also be restored to full resolution (if appropriate), prior to analysis in *LSS*. The level differences were then imported to *Microsoft Office Excel* for statistical analysis. The results of this analysis are presented in Table 5-10 for both robust and un-weighted matching solutions for the 1967 and 1980 surfaces.

Surface Comparison	**Level Difference Statistics (m)**				
	Mean	**σ**	**RMSE**	**Max.**	**Min.**
2005/1967r	-0.851	2.675	2.807	15.896	-20.973
2005/1967	0.047	2.375	2.375	16.325	-17.101
2005/1980r	-0.477	1.592	1.662	5.219	-12.523
2005/1980	-0.045	1.494	1.495	5.331	-12.763
r: robust solution					

Table 5-10 Summary of level difference statistics for Reighton matching.

As would be expected, the statistics suggest that larger differences exist between the 2005/1967 match, than the 2005/1980 match, indicating that greater terrain change has occurred over this period. As discussed above, in comparing the results of the robust and un-weighted algorithms, the robust matching statistics suggest that larger differences exist between the surfaces, with larger RMSE values. Furthermore, in support of the earlier discussion, the mean surface differences are concentrated around zero for the un-weighted solutions, indicating that the algorithm has adjusted the matching surface to best 'balance' the discrepancies. In contrast, the robust mean values are clearly negative, implying that net erosion has occurred over the matching periods. The higher standard deviations of the 2005/1967 results would seem to suggest that a larger range of change has occurred over this period, and this is supported in part by the relatively large maximum and minimum difference values. The level differences maps for the 2005/1967 match (Figure 5.18), and the 2005/1980 match (Figure 5.19) support these observations.

Figure 5.18 reveals greater positive change across the cliff-top area for the un-weighted algorithm, in comparison to the robust solution, and less negative change across the cliff-face. This suggests that the un-weighted approach has raised the 1967 DEM in an attempt the balance the large negative changes across the cliffs. In contrast, the robust solution highlights a patchwork of minor changes across the cliff-top which closely

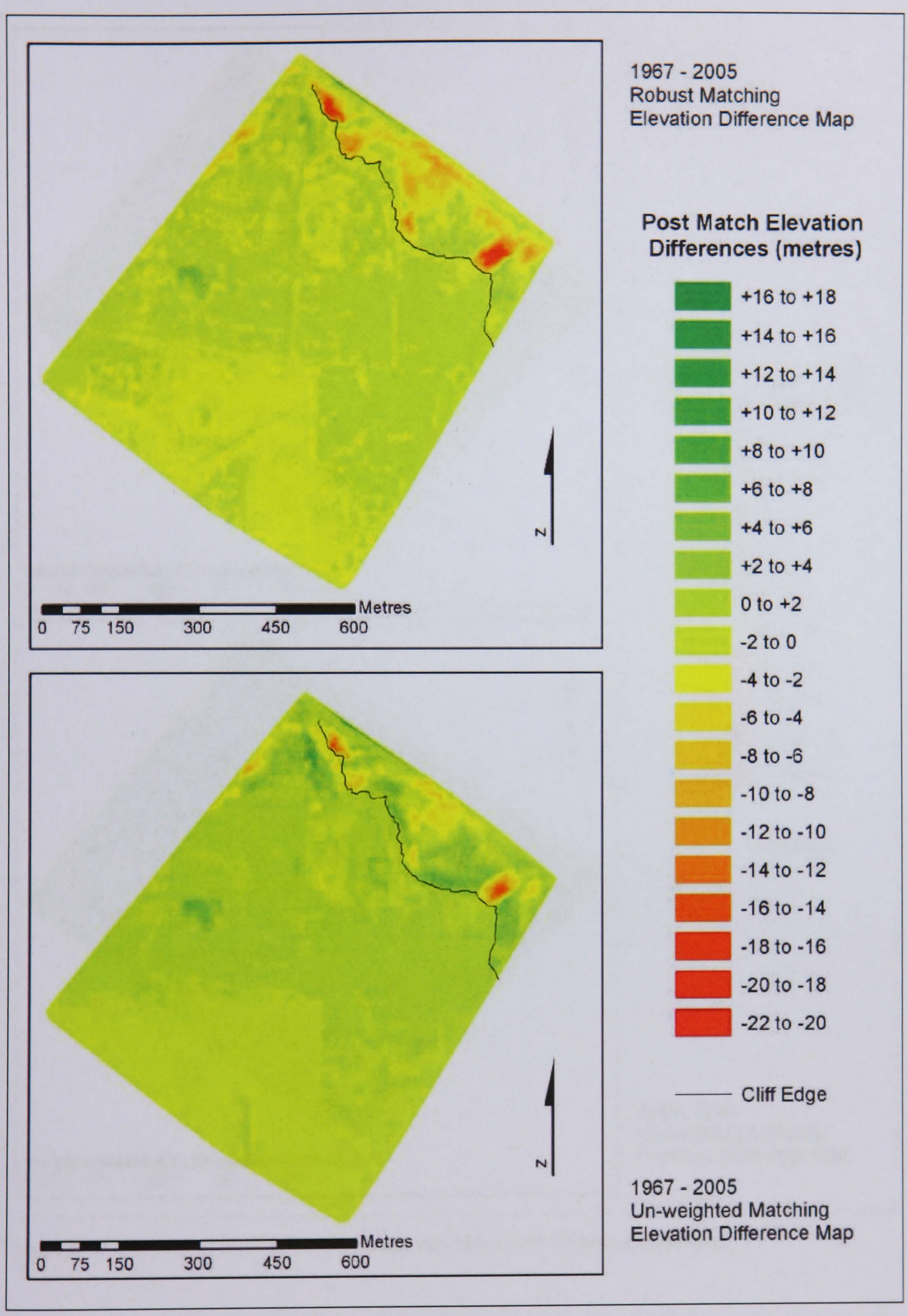

Figure 5.18 Post-match level difference maps for 1967-2005 Reighton matching.

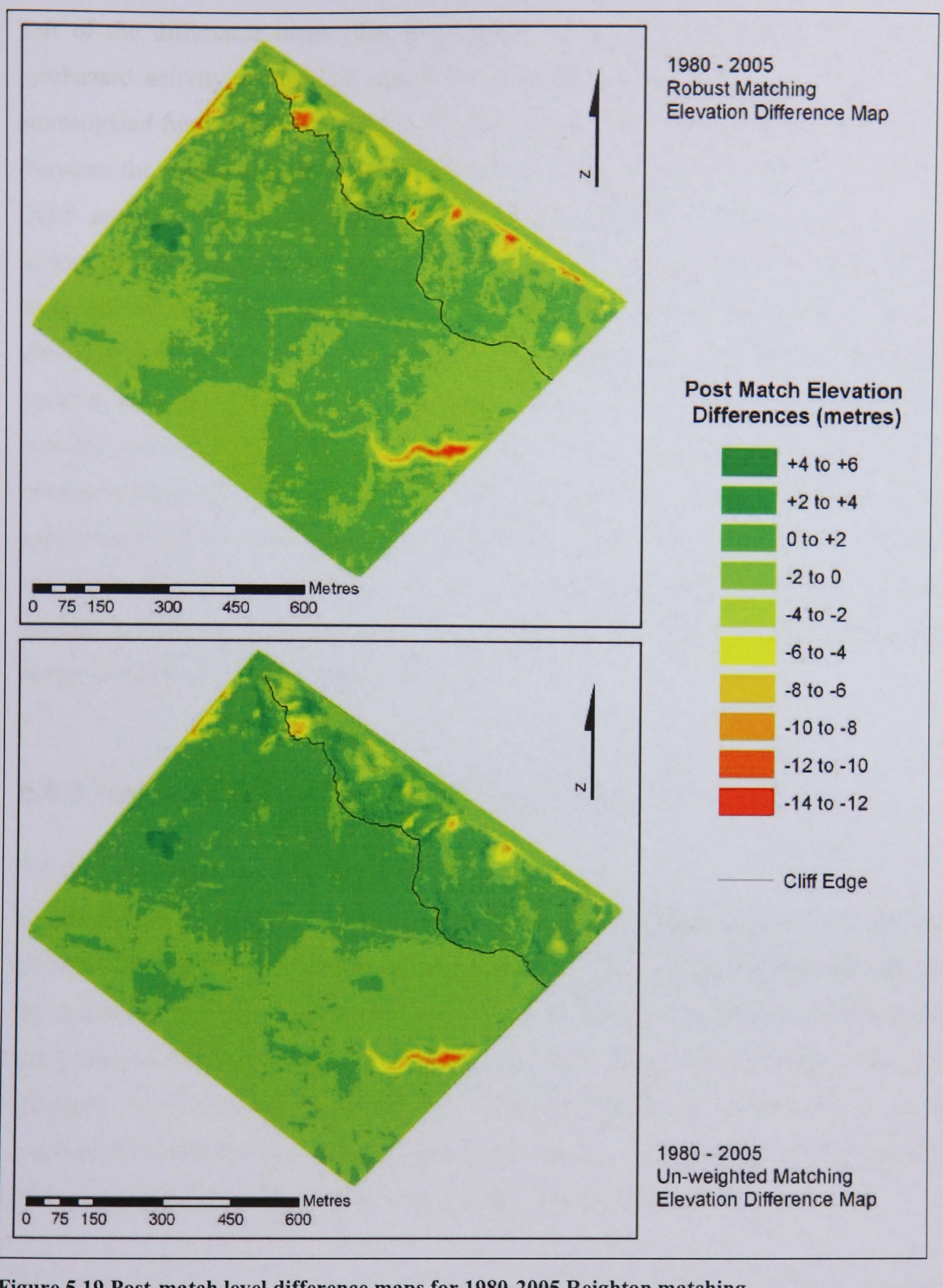

Figure 5.19 Post-match level difference maps for 1980-2005 Reighton matching.

correspond with field boundaries, and the caravan park area. This would indicate that the robust strategy is more successful in reflecting these subtle regions of difference, which are largely obscured in the un-weighted results. The construction of a large recreation centre for the holiday park is evident as a large positive change in the centre-

left of the difference maps (this also appears in Figure 5.19). Strong signatures of geohazard activity are evident across the cliff-face for this period, and this aspect is investigated further in Section 5.6.4. In general, Figure 5.19 reflects similar differences between the robust and un-weighted matching approaches as observed for the 1967 to 2005 analysis. Again, the un-weighted algorithm indicates greater positive change across the cliff-top, and is suggestive of an slight upwards rotation of the 1980 DEM over the cliff-face, thus causing the most landward portion of the surface to be titled down in order to compensate for the areas of negative change across the cliff-face. The snaking area of negative change on the south-east of the cliff-top corresponds to a wooded ravine. This highlights the differing surface representations of ALS and photogrammetry, as the difference is caused by photogrammetric extraction of the tree tops (which the *TerraScan* ground classification was unable to eliminate), while ALS will have been more successful in penetrating the canopy and returning a ground surface. In fact, this is the area depicted in Figure 3.3, illustrating the first and last pulse return capability of the ALS instrument.

5.6.3 Validation of Surface Matching Results

5.6.3.1 Production of Validation Surface

In order to assess the success of the surface matching technique, an absolute orientation of the 1980 DEM was carried out in *SocetSet* using GPS ground control points, thus facilitating production of a DEM which would correspond to that produced through the conventional orientation approach. Although it would have been desirable to also have assessed the quality of the 2005/1967 matching results in this manner, it proved impossible to obtain any suitable photo-control for the 1967 imagery, as the landscape had undergone significant change over the intervening period.

The 1980 stereo-pair were examined in order to identify suitable ground control points. This proved to be an extremely time-consuming and challenging exercise, for two reasons; firstly, the caravan park proved to be the only part of the overlap area which contained suitable photo-control points; and secondly, the caravan park had undergone extensive change and development between 1980 and the present, making the selection of suitable points problematic. Although this made for poor control point distribution,

there was little alternative, and so a number of points were identified and surveyed by rapid-static GPS in June 2006. Ten points were used in total, with most corresponding to road corners. Figure 5.20 shows the distribution of these control points within the overlap area.

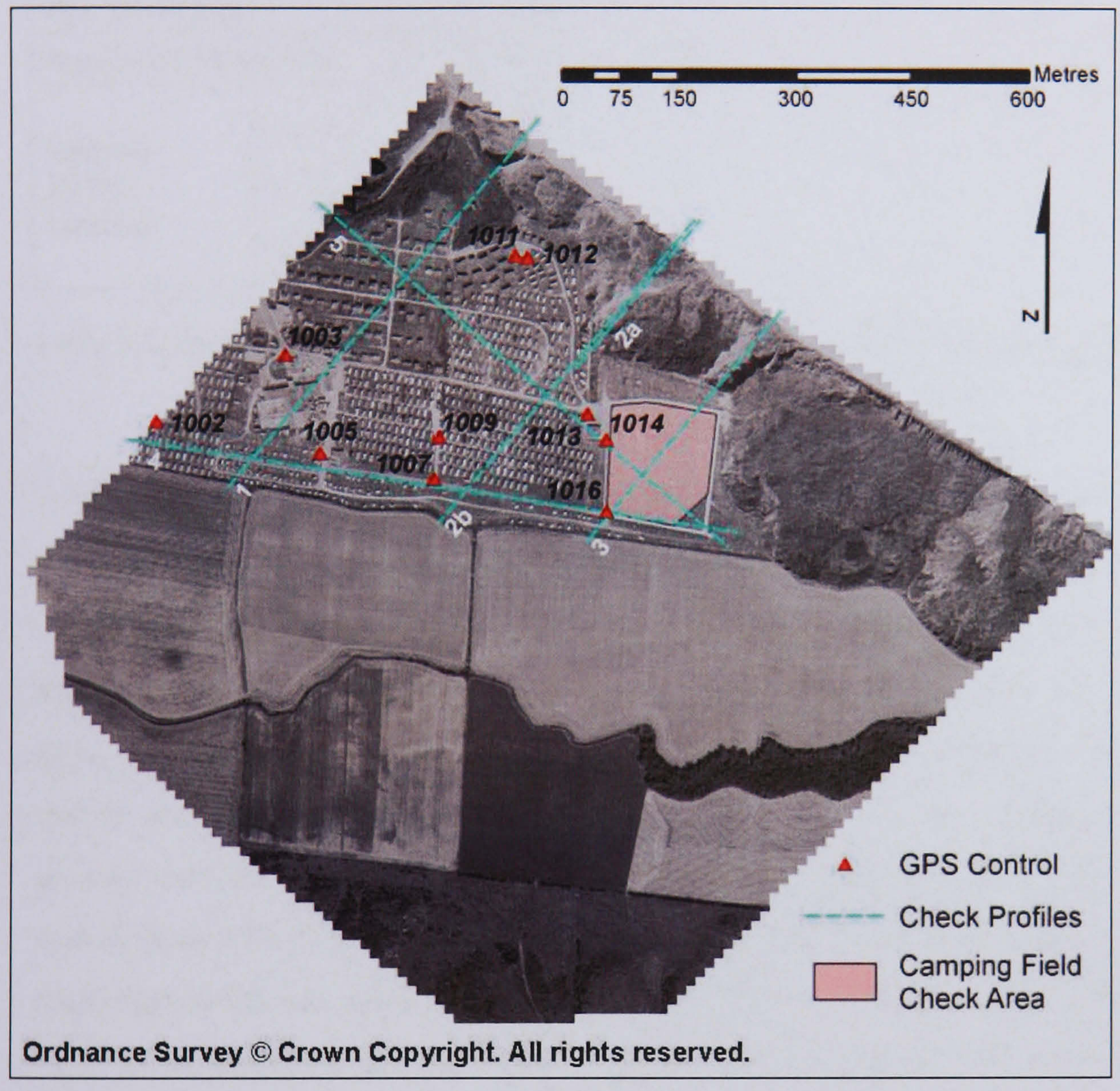

Figure 5.20 Location of GPS GCPs acquired for rigorous orientation of 1980 imagery. Profiles and check area used in subsequent analysis are also indicated.

As many of the road corners were rather indistinct on the imagery, this introduced a degree of uncertainty in locating the corresponding points in *SocetSet*. It was therefore decided to utilise all ten points as control, providing increased redundancy, and exterior orientation was performed, as described in Section 5.4.2.2. The results of this procedure are detailed in Table 5-11. Comparison of these results against those obtained through approximate orientation (Table 5-5), indicates that this approach was able to produce an improved absolute orientation of the model, with markedly lower ground RMSE values. A DEM was extracted as before, and identical surface preparation (ground classification

and point thinning) was carried out in *TerraScan*. This DEM was considered to provide a suitable benchmark for evaluation of the surface matching results.

Epoch		1980
No. GPS Control Points		10
No. Tie Points		16
Image RMSE (pixels)		0.097
Ground RMSE (metres)	x	0.162
	y	0.055
	z	0.046
	Total	0.177

Table 5-11 Summary of bundle adjustment results for GPS-controlled 1980 photography.

5.6.3.2 Surface Matching Quality Analysis

The next stage involved comparing the post-match transformed 1980 surfaces to the validation DEM in order to assess the quality of the robust and un-weighted matching solutions. As the GPS photo-control had been restricted to the area around the caravan park, it was decided that the validation DEM could only be considered reliable for this region. Fortunately the caravan park bordered the section of cliff-face which was of greatest interest (the area which directly overlapped with the 1967 DEM). Validation was performed by comparing the surfaces along selected profile lines which provided good representation across the cliff-top and cliff-face (Figure 5.20). Level differences were calculated between the 1980 validation DEM, and the two post-match surfaces (robust and un-weighted) at these profile locations. Figure 5.21 displays the profile RMSEs in graphical form.

These results highlight the higher accuracy of the robust matching solution. The largest RMSE values correspond to those profiles which transect significant portions of the cliff-face, suggesting that the slightly different positions of the surfaces may be exacerbated by the effects of slope, and possibly vegetation, over these areas.

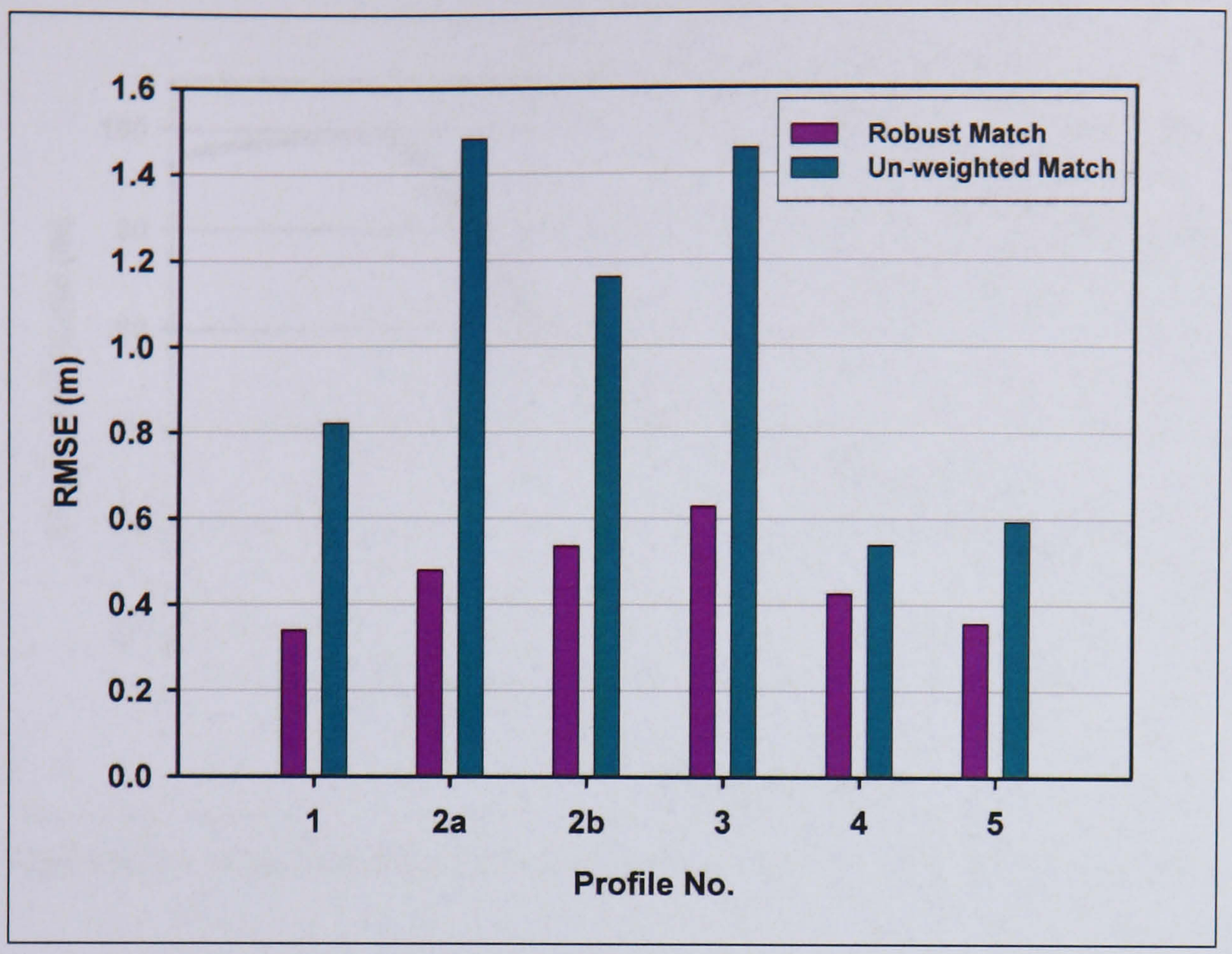

Figure 5.21 Comparison of robust and un-weighted solution accuracies at profile locations.

Figure 5.22 depicts the surface differences at Profile 2a, illustrating how the robust solution is consistently closer to the validation surface than the un-weighted solution. The un-weighted surface displays particularly large discrepancies towards the top of the cliff-face, falling below the 2005 ALS surface. Moreover, at the cliff-toe, the robust surface appears better able to cope with the large changes which have occurred between 1980 and 2005, remaining in good agreement with the validation surface, while its un-weighted companion is drawn downwards towards the 2005 DEM. However, it is important to acknowledge that although the robust matching produced consistently better results for all profiles, a discrepancy still exists between this surface and the validation DEM. This is most likely due to the fact that the 2005 ALS surface was used as the reference in the matching. Consequently, this will have led to a slightly different surface registration for the 1980 approximately-oriented DEM than that which was obtained via rigorous orientation using GPS ground control. It was decided to further investigate this matter.

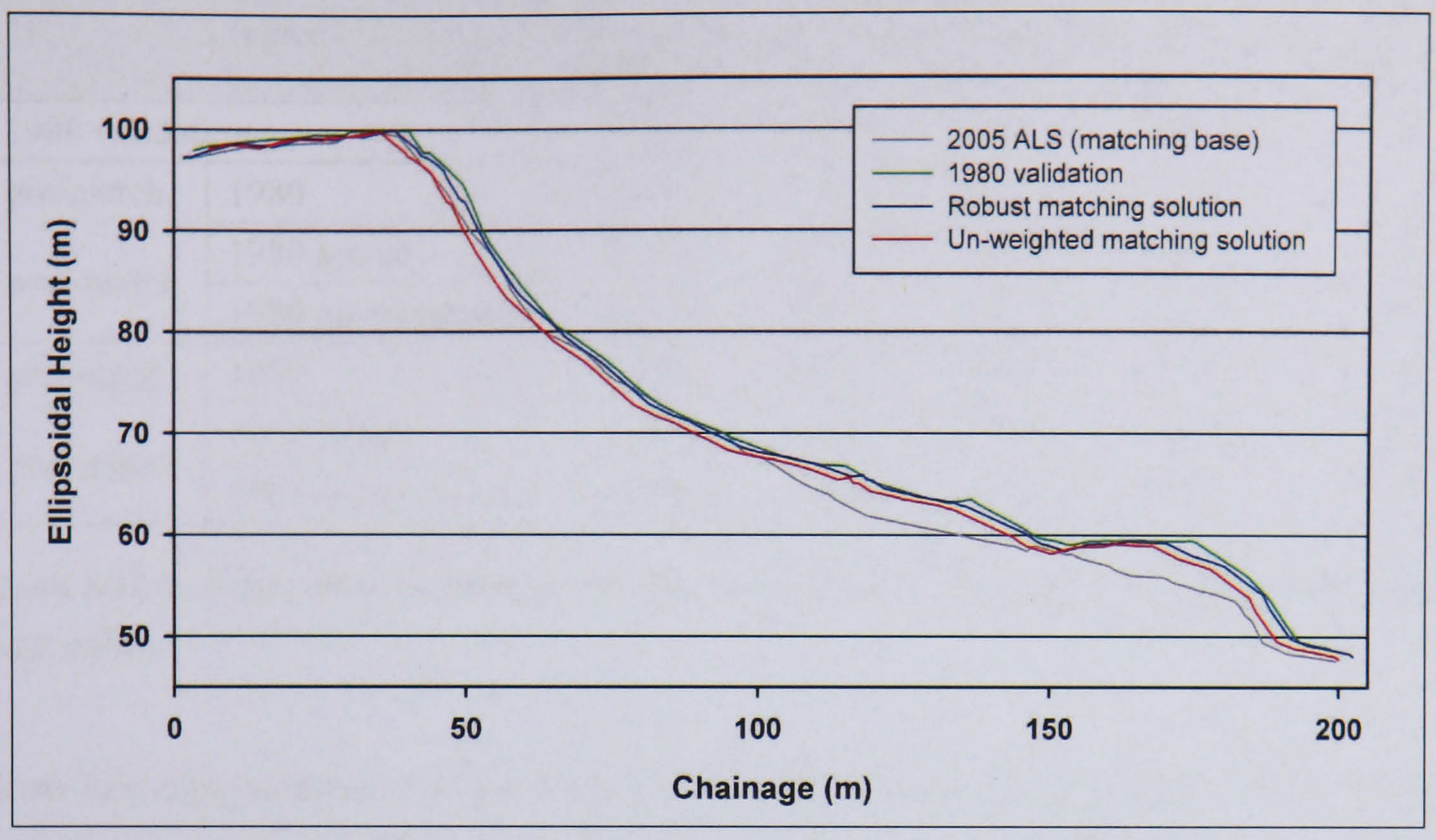

Figure 5.22 Comparison of matching and validation surfaces at Profile 2a (cliff-face).

The conventional approach for assessing the quality of the post-match historical DEMs would have been to compare the surfaces to independent check points acquired in the field. However, it was not possible to identify enough suitable points for this purpose, due to the lack of hard detail, and extensive landscape changes. An alternative strategy is advocated by De Rose et al. (1998); Betts et al. (2003) and Schiefer and Gilbert (2007), who recommend the use of check point areas for assessing the quality of photogrammetrically-derived DEMs, where it proves difficult to acquire check points in the field. Through this approach, multi-temporal DEMs can be compared across stable areas of terrain, facilitating the identification of systematic and random errors which may arise through poor quality exterior orientation solutions, or image matching difficulties (Schiefer and Gilbert, 2007). This approach was adopted here, and the camping field, indicated in Figure 5.16, was selected as a suitable area. This covers an area of 19,675 m^2 (approximately 135 m x 150 m), is relatively flat, and is vegetated with short grass. Level differences were calculated over this area in *LSS*, and in each case, the differences were calculated relative to the 2005 ALS DEM, using points from both surfaces (an average of 15,475 points for each comparison). This strategy also enabled the quality of the 1967 matching solutions to be evaluated. The results of this analysis are detailed in Table 5-12.

Surface		Level Differences (m)				
		Mean	**σ**	**RMSE**	**Max.**	**Min.**
1980 validation		0.307	0.133	0.335	1.014	-0.385
pre-match	1980	-1.487	0.174	1.497	-0.673	-2.360
post-match	1980 robust	-0.178	0.133	0.222	0.651	-0.811
	1980 un-weighted	-0.375	0.167	0.410	0.421	-0.928
pre-match	1967	-1.971	0.342	2.001	-0.593	-3.236
post-match	1967 robust	-0.507	0.287	0.582	0.757	-1.442
	1967 un-weighted	-0.888	0.486	1.012	0.797	-2.105

Table 5-12 Summary of level difference statistics over camping field area, with respect to the 2005 ALS DEM.

Two key observations can be made; firstly, the RMSE values indicate that the post-match 1980 DEM for the robust solution lies closer to the 2005 surface than the 1980 validation DEM; and secondly, the mean values suggest that while the post-match 1980 surfaces lie slightly below the 2005 DEM, the validation surface lies *above* this. This was confirmed through visual inspection of the data (Figure 5.23).

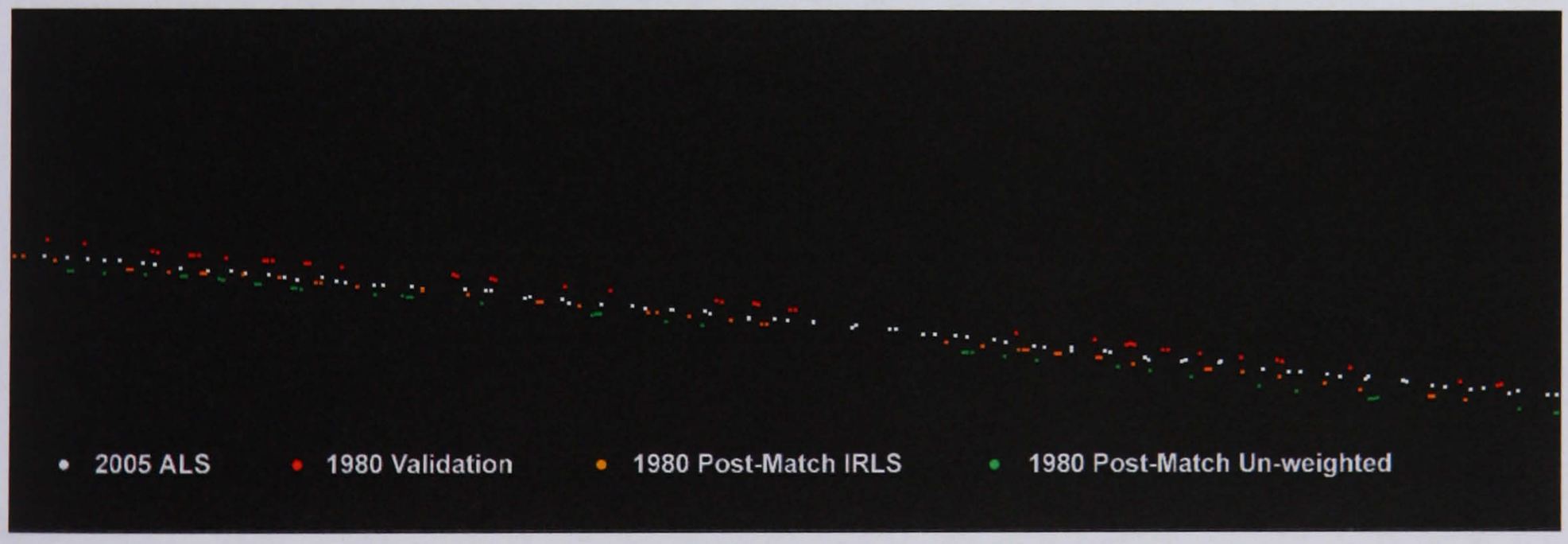

Figure 5.23 Profile through camping field check area, illustrating DEM offsets.

In combination, these two factors support the theory that the differences between the 1980 post-match surfaces and the 1980 validation DEM have partly arisen because an offset exists between the 2005 ALS (matching reference surface) and the 1980 validation surface. Table 5-12 also presents statistics for the 1980 and 1967 pre-match, approximately oriented DEMs, illustrating the effectiveness of the robust matching technique in improving their absolute orientation. The post-match statistics for the 1967 DEM indicate a greater disparity in relation to the 2005 DEM, than in the case of the 1980 surfaces. However, this is to be expected, as the 1967 surface appeared to be

noisier than the 1980 DEM, and in addition, the track surrounding the camping field had been re-routed between 1967 and 1980, which is likely to have introduced some terrain change.

5.6.4 Geohazard Assessment 1967 – 2005

5.6.4.1 Visualisation and Analysis of Change

Surface matching of the DEMs from 1967 and 1980 provided a valuable opportunity for retrospective analysis of geohazard activity across the cliff-face at Reighton. Due to the relatively high spatial resolutions, and continuous nature of the surfaces involved, it was possible to visualise change and perform quantitative assessment of targeted areas. Having established the superiority of the robust matching solution, these surfaces were used in the following analysis, and level differences were calculated between the 1967 and 1980 post-match surfaces in *LSS*, in order to provide relevant data over this period.

In analysing inter-epoch terrain change, it is necessary to consider DEM quality, as this places important limitations upon the confidence with which DEM differences can be classified as arising as a result of real surface change, as opposed to DEM error. A DEM is incapable of providing an exact replica of the terrain. In practice, even if blunders and systematic errors can be completely eliminated – a challenge in itself – uncertainty will still remain, due to the nature of the terrain, and sensor noise (random error). As discussed in Section 3.4.4.2, measurement precision is a frequently-applied measure of DEM quality, and is commonly expressed through the standard deviation statistic (Equation 3-3). This allows uncertainty to be communicated through critical values, which indicate the probability of an error of a certain size occurring within the dataset (Li, 1988; Cooper, 1998).

As discussed in Section 5.6.3.2, no absolute measures of accuracy or precision (i.e. check points) were available for the Reighton DEMs. As matching was carried out using the 2005 DEM as the control surface, the standard deviations of the 1980 and 1967 DEMs calculated over the camping field check area with respect to the 2005 DEM (Table 5-12), were used as precision measures for the purposes of change analysis. The standard deviation of the 1967-1980 dataset ($\pm$ 0.316 m) was determined through error

propagation theory, while the value of ± 0.133 m associated with the post-match 1980 dataset, was applied directly for the period 1980-2005. Critical values are usually based upon multiples of the standard deviation on the assumption of an underlying normal distribution, and in this research the multiples detailed in Table 3-3, as defined by Wolf and Ghilani (1997) have been applied, leading to the confidence intervals presented in Table 5-13. Inspection of the level difference distributions (1967-1980 and 1980-2005) over the matching extents, instantly reveals that fewer than 68.3 % of the observations fall within ± 1σ, suggesting the presence of error or terrain change, with the latter effect particularly likely, due to the lengthy inter-epoch time periods. The distributions suggest that the datasets contain marked positive and negative changes, with the 1980-2005 dataset exhibiting a particularly large negative tail, suggesting net erosion over this period.

1967-1980 (σ = ± 0.316m)				
Confidence Intervals	**+ %**	**- %**	**Total %**	**Cumulative Total %**
Within ± 1σ (68.3 %)	19.6	18.3	37.8	37.8
Within ± 95.0 %	13.6	11.1	24.7	62.5
Within ± 99.7 %	7.6	4.2	11.8	74.3
> ± 99.7 %	10.0	15.7	25.7	100.0
1980-2005 (σ = ± 0.133 m)				
Confidence Intervals	**+ %**	**- %**	**Total %**	**Cumulative Total %**
Within ± 1σ (68.3 %)	15.9	12.3	28.2	28.2
Within ± 95.0 %	11.2	8.9	20.1	48.3
Within ± 99.7 %	6.5	5.1	11.6	59.9
> ± 99.7 %	13.3	26.9	40.1	100.0

Table 5-13 Distribution of level difference values within confidence intervals derived from check area analysis.

ESRI ArcGIS software was used to convert the point-based level difference datasets to TINs, in order to visualise change across the cliff-face in a continuous manner. Figure 5.24 and Figure 5.25 illustrate these elevation differences, with reference to the corresponding epochs of ortho-imagery. It should be noted that visualisation is based upon the *ArcGIS* 'standard deviation' class-break option, which assigns colouring on the basis of the standard deviations of the datasets. Experimentation revealed that this provided the most suitable basis for presenting the level difference maps, as extreme

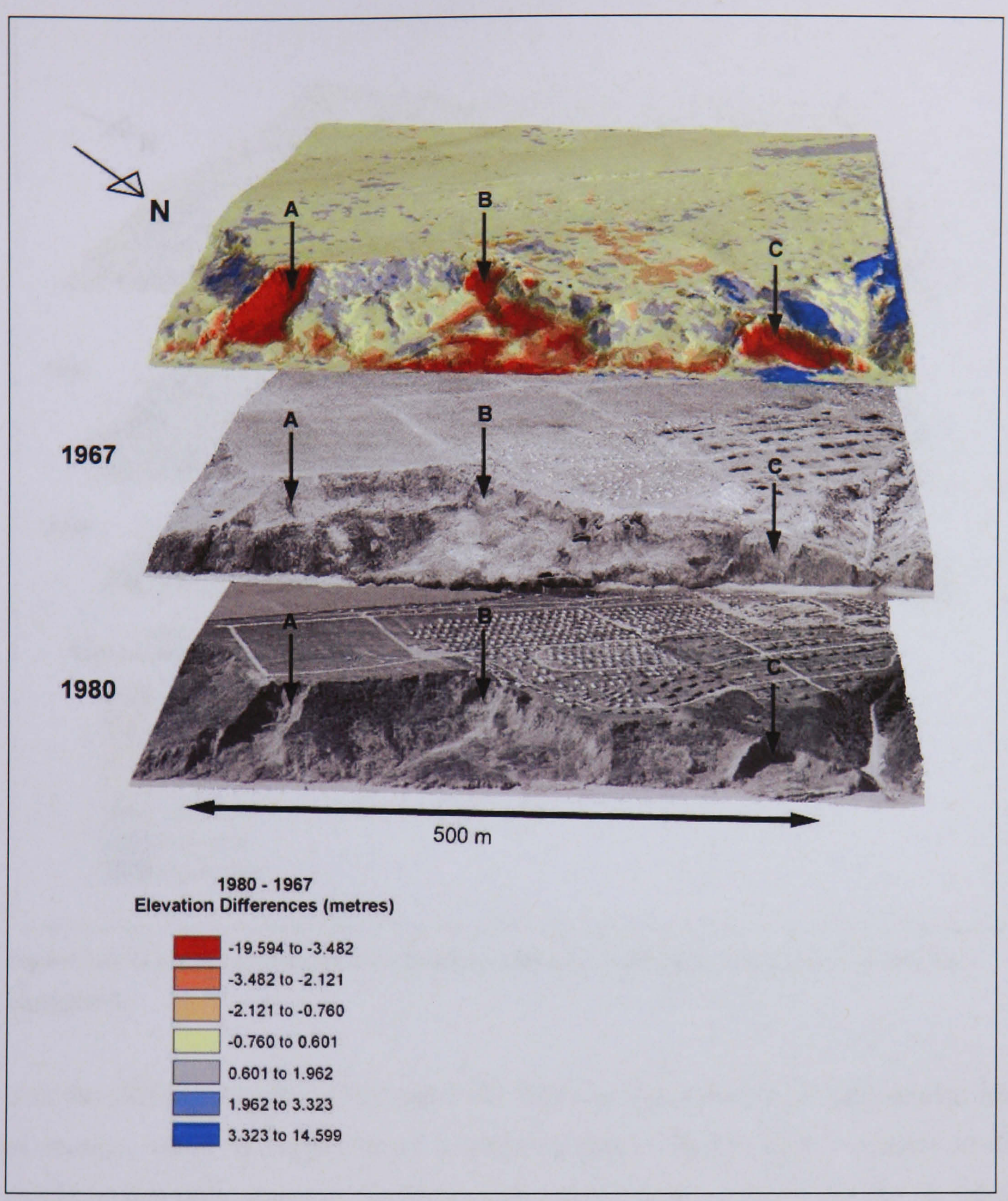

Figure 5.24 Elevation differences over Reighton cliff-face, 1967-1980, with features of interest highlighted.

areas of change are clearly represented, and do not become absorbed in more minor areas of difference. However, it is important to note that this classification scheme does not correspond to the confidence intervals described above, and presented in Table 5-13, and is thus should not be considered as an index of significance. However, examination of Table 5-13 leads to the conclusion that the more extreme regions of difference presented in Figure 5.24 and Figure 5.25 can be considered as genuine terrain change. Inspection of Figure 5.24 indicates that a large amount of change has occurred

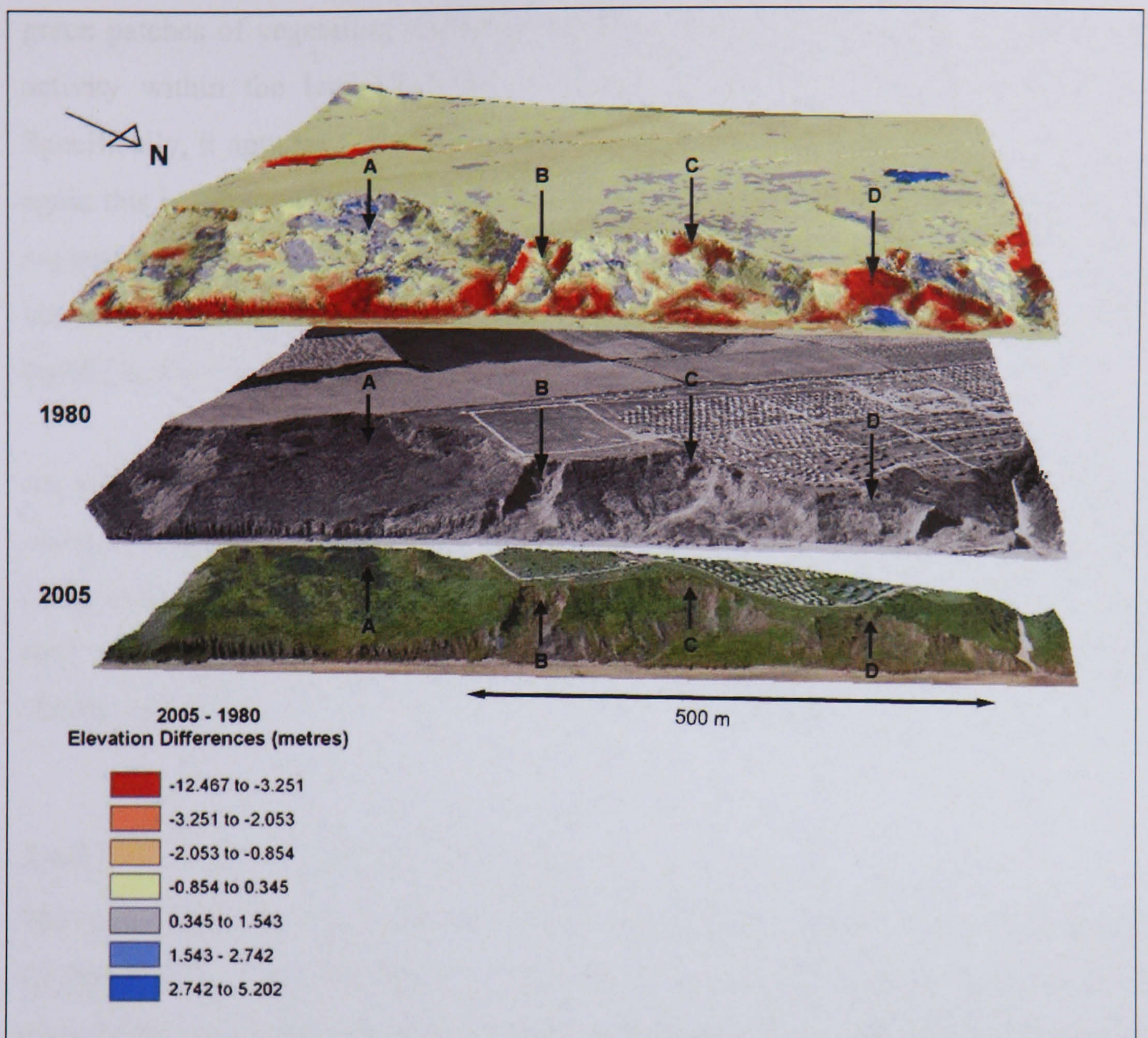

Figure 5.25 Elevation differences over Reighton cliff-face, 1980-2005, with features of interest highlighted.

over the cliff-face between 1967 and 1980. Most notable is area A, a concentrated area of erosion, which is suggestive of a major landslide. This is clearly evident in the corresponding ortho-imagery. Further erosion appears to have occurred at area B, which corresponds to the SPT test area, while area C indicates landslide activity, with a corresponding area of deposition at the foot of the cliff. Again, inspection of the imagery corroborates these observations, with the accumulation at area C especially clear on the 1980 imagery.

Figure 5.25 indicates that the Reighton cliff-face has also been active over the twenty-five year period between 1980 and 2005, with further indications of geohazard activity. Close scrutiny of area A suggests that significant vegetation growth has occurred over this period, manifest through regions of positive change, which correspond to the darker

green patches of vegetation visible in the 2005 ortho-image. Area B represents further activity within the large landslide scar highlighted in discussion of Figure 5.24. Specifically, it appears that the side-scarps have widened between 1980 and 2005, and again this is supported by examination of the corresponding imagery. Net loss at area C suggests continued erosion of the back-scarp within the SPT test area, while area D indicates further erosion and corresponding deposition at the site of the existing failure highlighted in Figure 5.24, as area C.

An additional observation which can be made with regards to Figure 5.25 is that the southern section of the cliff appears vulnerable to erosion of the cliff-toe. This is most likely as a result of wave attack, as the beach is particularly narrow at this end of Filey Bay, exposing the cliffs to greater marine erosion, particularly during storm periods (Elliot et al., 1991).

5.6.4.2 Volumetric Assessment of Change

The next phase involved carrying out a quantitative analysis of terrain change at Reighton. This was performed by calculating volumetric change over the periods spanned by the archival datasets. Volumetric calculations are commonly employed by geomorphologists for analysis of terrain change over a range of scales, particularly where DEM datasets are available (Dixon et al., 1998). In this research, *LSS* was utilised for volume computations. *LSS* employs a triangulation-based technique which is capable of utilising the full resolution of the dataset, and avoiding inaccuracies which may be introduced though the traditional cross-section-based approach. Initially analysis was performed over the cliff-face as a whole, for the periods 1967-1980 and 1980-2005, and then specific investigation of the large landslide area highlighted in Figure 5.24 and 5.25 (areas A and B respectively), was carried out. The results of this analysis are summarised in Table 5-14.

Volumetric analysis indicates a trend of net loss over the period under investigation. It is evident that a large amount of net erosion occurred over the cliff-face as a whole during both time periods. The larger volumetric quantities related to the 1980-2005 period are directly attributable to the fact that analysis was carried out over a much

Volumetric Change	Cliff-Face Extent		Landslide Feature	
	1967-1980	**1980-2005**	**1967-1980**	**1980-2005**
Total area (m^2)	88637	184501	7928	8260
Cut volume (m^3)	-113125	-190443	-37281	-15285
Fill volume (m^3)	46784	39765	1231	774
Net volume (m^3)	-66341	-150678	-36050	-14511

Table 5-14 Volumetric change analysis over Reighton cliffs.

larger extent. However, in relation to this, it is interesting to note that a greater fill volume is associated with the 1967-1980 elevation differences, despite the fact that this analysis was performed over an area less than half the size of the 1980-2005 dataset. This can be partly explained through examination of Figure 5.24, which shows evidence of large areas of positive change at the northern extreme of the cliff-face. Inspection of the corresponding datasets suggested that this was due to a combination of two factors; firstly, there was some evidence of vegetation growth around the wooded ravine; and secondly, it was discovered that a relatively poor ground model had been obtained for the 1980 DEM in this area, with vegetation points remaining. This latter point also explains the corresponding negative change over this region of the 1980-2005 elevation difference dataset (Figure 5.25), and is an important reminder of the dangers of accepting results at face value.

Table 5-14 also presents analysis of the landslide feature, confirming that most of the material was lost sometime between 1967 and 1980. However, the volumetric assessment also indicates that further erosion took place between 1980 and 2005, and the larger surface area associated with this period supports the earlier evidence (Figure 5.25) for lateral development of this feature through erosion of the side-scarps. The lack of fill volume for the landslide (and it should be noted that analysis included the adjacent beach area) supports the theory that marine erosion is particularly active in this part of the bay.

5.6.4.3 Rates of Change

The data presented in Table 5-14 also enabled rates of elevation change to be derived for the two inter-epoch periods. However, as these two periods span differing extents of

cliff-face, the volumetric change data was normalised, and is presented as change per square metre in order to enable direct comparison (Table 5-15). These results reveal that the annual rate of elevation change for the thirteen year period 1967-1980 was twice that for the twenty-five year period 1980-2005. This can most likely be attributed to the development of the major landslide feature, with initial failure occurring sometime between 1967 and 1980. This failure would appear to be the single most dominant geohazard event affecting the cliff-face during the entire monitoring period, 1967-2005. However, it is also important to acknowledge that other failures, such as those highlighted at B and C in Figure 5.24, are likely to have contributed to the higher rate of loss over the 1967-1980 period. While net loss has also occurred over the period 1980-2005, the scale of this is less severe than over the earlier period, perhaps as a result of lower magnitude cliff failures. While it is always desirable to derive associated confidence estimates for analysis such as this, in this case this proved impossible. Although the standard deviations associated with the vertical components of the 1967-1980 and 1980-2005 datasets have been derived in Section 5.6.4.1, assessment of the planimetric quality of these datasets was not possible, and therefore this precluded computation of volumetric uncertainty, and subsequent propagation of this uncertainty into the rates of change presented in Table 5-15.

Period	Total Area (m^2)	Net Volumetric Change (m^3)	Change per m^2 (m)	Annual Change per m^2 (ma^{-1})
1967-1980	88637	-66342	-0.75	-0.06
1980-2005	184501	-150677	-0.82	-0.03

Table 5-15 Rates of change across Reighton cliff-face, derived from volumetric analysis.

Vertical rates of change derived directly from the *LSS* level difference calculations (refer to Section 5.6.4.1) were also examined. Analysis was restricted to the cliff-face extent of the 1967-1980 dataset in both cases (i.e. for the 1980-2005 dataset also), in order to ensure that the results would be directly comparable. As Table 5-16 indicates, the mean elevation change (and associated uncertainty) was calculated for the two inter-epoch periods, facilitating derivation of annual rates of change over the cliff-face area. The resultant values (-0.071 ma^{-1} for 1967-1980, and -0.047 ma^{-1} for 1980-2005) broadly agree with the corresponding values presented in Table 5-15, which were derived from volumetric change analysis. The slight discrepancies between the two sets

of results can most likely be attributed to the fact that the rates derived in Table 5-15 were normalised from data which covered a larger extent of cliff-face (in the case of the 1980-2005 dataset), and hence this may have introduced some discrepancy. Also, *LSS* employs a vertical prism, triangulation-based technique to calculate volumetric differences, and although this offers improved accuracy over conventional volumetric computation approaches (such as cross-sectional analysis), such methods remain relatively sensitive to boundary delineations, as will be discussed further in Section 6.5.3.4. The uncertainty estimates presented in Table 5-16 may be rather overly-optimistic, being at the mm-level. This is due to the fact that error propagation in the mean is directly influenced by the number of observations, which in the case of the two inter-epoch surfaces, was in the region of 50,000 points. Ultimately however, the rates of elevation change calculated through the two different approaches, and reported in Table 5-15 and Table 5-16 are in relatively close agreement.

Period	**Mean Elevation Change (m) (95% confidence level)**	**Mean Annual Elevation Change (ma^{-1}) (95% confidence level)**
1967-1980	-0.921 ± 0.003	-0.071 ± 0.003
1980-2005	-1.164 ± 0.001	-0.047 ± 0.001

Table 5-16 Rates of elevation change across Reighton cliff-face, derived from level differences.

As explained above, the higher rate of change associated with the 1967-1980 period (Table 5-16) is most likely due to the major landslide which occurred during this time interval. It is important to note that individual cliff-failures are likely to result in localised instantaneous loss of a much greater magnitude than the rates presented in Table 5-15 and Table 5-16. The thirteen and twenty-five year periods over which analysis has been carried out, will likely mask shorter-term fluctuations in rates of erosion and volumetric change. Unfortunately, in the case of historical analysis, it is difficult to overcome this restriction, due to limited temporal resolution, dictated by dataset availability. Furthermore, the effects of deposition and vegetation growth are likely to offset rates of erosion to a certain extent.

Section 5.2.2 briefly discussed previous monitoring efforts at Filey Bay, and highlighted the results of a study which had utilised the erosion post technique to determine cliff edge retreat rates. This provided two values for annual retreat measured at Reighton

(Table 5-1): 1.30 m (post 1A) and 0.15 m (post 1). The location of these two posts is unknown. Such values cannot and should not be directly compared to those presented in Table 5-16, as cliff edge retreat is effectively a planimetric measure, whereas the analysis carried out here has considered vertical change across the cliff-face as a whole. Rates of retreat calculated through the erosion post technique represent the conventional approach to quantifying erosion, and are widely utilised by those responsible for managing and mitigating erosion risk. While the use of this approach may be of some relevance in communicating the direct threat to cliff-top infrastructure, it fails to account for the spatial variability of erosion, and the effects of deposition and vegetation change. The approach adopted here overcomes this weakness, taking into account change over the cliff-face as a whole. These issues will be discussed further in Section 7.2.3.

5.7 Contemporary Analysis of Geohazard activity

5.7.1 Introduction

Chapter Three introduced an integrated remote monitoring strategy for coastal geohazard assessment, emphasising the importance of the combined airborne-terrestrial approach for minimisation of occlusions and exploration of a multi-scale approach to coastal change monitoring. The acquisition, preparation, and quality analysis of TLS and ALS datasets has already been presented earlier in this chapter. This section focuses on the integration of these datasets through robust surface matching, in order to facilitate contemporary analysis of geohazard behaviour. As discussed in Section 5.3.2, the difficulties and uncertainties associated with the ALS acquisitions meant that no ALS data was available for the epoch 0 survey, and the epoch 1 terrestrial survey was restricted to the SPT test area. As a consequence, the SPT test area once again proved to be the most suitable site, and in any case, as the largest and most active of the test areas, this is an appropriate site for evaluation of the integrated monitoring approach.

5.7.2 Dataset Integration

5.7.2.1 Multi-Sensor Dataset Fusion

The first phase required reconciliation of the ALS and TLS datasets for each survey epoch, in order to optimise the final surface representations. The quality of the laser scanning datasets was examined in Section 5.5.3.2 through comparison to the total station check profiles. This revealed that, contrary to expectation, the ALS datasets were of consistently higher accuracy than the TLS surfaces. Consequently, the ALS datasets were selected as the reference surfaces, enabling subsequent matching of the TLS DEMs. This approach offers the advantage that, whereas the TLS coverage is concentrated in specific geohazard locales, the ALS datasets offer continuous coverage over large extents. Therefore, theoretically, the ALS DEMs make for a better continuous, extended reference surface, facilitating the integration of numerous TLS datasets covering smaller sub-sections of terrain. A region of the ALS datasets was defined for use in assessing the integrated monitoring approach. This area corresponded closely the section of cliff-face utilised in the retrospective analysis of change at Reighton (Figure 5.16), with the SPT test area and TLS datasets occupying an approximately central position within this area.

The multi-sensor matching strategy is outlined in Table 5-17, with relevant input parameters, and solution details provided. As Gruen and Akça (2005) observe, the scale parameter is particularly sensitive to poor initial parameter approximations or weak point distributions along the primary axes, and may converge to an erroneous solution in such cases. This has been observed in a small number of cases over the course of this research, and therefore, as no scale variations were anticipated between the laser scanning datasets, it was decided to hold scale fixed, and employ a six parameter transformation (rotations and translations). Examination of Table 5-17 reveals that the algorithm obtained convergence in less than twenty iterations in each case. This is faster than in the case of the archival datasets, and may be reflective of the fact that the laser scanning surfaces contained less noise overall, and could be partly related to the exclusion of the scale parameter. The matching RMSE refers to the RMSE of the final matching residuals, as presented in the 3DSurf-*R* output. These values are relatively low, suggesting that reliable solutions have been achieved by the software, and that little

difference exists between the ALS and TLS datasets. This is to be anticipated, as the ALS and TLS datasets were acquired concurrently in time.

Match (ref./match)	**Input Parameters**			**Outputs**	
	Weighting	**Parameters**	**Interpolation**	**Iterations**	**RMSE (m)**
Epoch 1 (ALS/TLS)	Robust	6	Planar	16	0.544
Epoch 2 (ALS/TLS)	Robust	6	Planar	13	0.266

Table 5-17 Summary of multi-sensor matching input parameters and results. RMSE refers to final matching residuals.

The final transformation parameters, determined by 3DSurf-*R* for each of the matches, are detailed in Table 5-18. The results indicate that relatively minor transformations were applied in order to register these DEMs to their respective ALS datasets. The parameter standard deviations are also relatively low, indicating strong solutions. The negative T_z values imply that the TLS surfaces have been shifted downwards to match the ALS datasets.

Match (ref./match)	**Final Transformation Parameters**					
	$\omega^\circ \pm \sigma$	$\phi^\circ \pm \sigma$	$\kappa^\circ \pm \sigma$	T_x (m) $\pm \sigma$	T_y (m) $\pm \sigma$	T_z (m) $\pm \sigma$
Epoch 1 (ALS/TLS)	0.092689 ± 0.003336	0.040780 ± 0.003921	0.220619 ± 0.003889	0.203 ± 0.012	0.511 ± 0.010	-0.352 ± 0.005
Epoch 2 (ALS/TLS)	0.039617 ± 0.001251	-0.017835 ± 0.004006	0.087082 ± 0.002825	0.140 ± 0.010	0.546 ± 0.006	-0.275 ± 0.003

Table 5-18 Final transformation parameters for multi-sensor matching at SPT.

Following multi-sensor surface matching, the TLS and ALS datasets were merged to provide multi-resolution coverage of the SPT area for April 2005 and August 2005. The quality of the matching solutions was then validated through comparison to the corresponding total station profiles, SPT1 and SPT2. This followed an identical process to that outlined in Section 5.5.3.2, with level differences calculated in *LSS* between the profile data and the laser scanning datasets, at the location of the total station measurements. Comparisons were made for both the post-match TLS datasets and the

merged ALS-TLS datasets. Results are presented in Table 5-19, with pre-match TLS analysis included for comparison.

Epoch	Surface	Profile	Level Difference Statistics (m)				
			Mean	σ	RMSE	Max.	Min.
1	TLS pre-match	SPT1	0.600	0.799	0.995	3.244	-0.093
		SPT2	0.236	0.448	0.502	1.272	-1.102
	TLS post-match	SPT1	0.297	0.879	0.922	2.953	-0.794
		SPT2	0.010	0.326	0.323	0.773	-0.640
	TLS-ALS merged	SPT1	-0.074	0.315	0.322	0.932	-0.788
		SPT2	-0.056	0.260	0.264	0.667	-0.641
2	TLS pre-match	SPT1	0.218	0.427	0.478	1.856	-0.258
	TLS post-match	SPT1	0.055	0.393	0.395	1.576	-0.409
	TLS-ALS merged	SPT1	-0.028	0.196	0.198	0.766	-0.413

Table 5-19 Profile validation analysis for multi-sensor matching at SPT.

There are a number of trends evident through this evaluation. Firstly, the post-match RMSE values of the TLS datasets show a slight improvement in each case over their corresponding pre-match values. However, these values markedly improve through merger with the ALS datasets. For instance the epoch 1 SPT1 RMSE has improved from 0.922 m to 0.322 m following matching and fusion with the ALS DEM. Furthermore, the accuracies of the merged datasets are approaching those of the ALS surfaces validated in isolation (refer to Table 5-8). These findings would suggest that the true cause of the poor TLS dataset accuracies, as determined in Section 5.5.3.2, is in fact due to regions of occlusion, resulting in weak triangulations over these areas. One further observation, from inspection of Table 5-19, is that the mean differences for the merged ALS-TLS datasets are negative, suggesting that the contribution of the TLS dataset lies slightly below the total station profiles.

Examination of the final merged datasets revealed that this procedure had been particularly important with regards to the TLS datasets. Due to the nature of the terrain at the SPT site, the TLS datasets suffered from numerous occlusions, generally corresponding to relatively flat sections of slope, located mid-cliff. Furthermore, TLS

instruments acquire data in a radial manner from a central point, which generally means that while multiple scans enable good overlaps at far-range, there may be gaps at near-range. These difficulties are illustrated in Figure 5.26 (A), where occlusions in the epoch 1 TLS DEM are evident through inspection of the surface triangulation. This reveals large and long, thin triangles in occluded areas. Conversely, Figure 5.26 (B) depicts the same area with merged TLS-ALS data after surface matching.

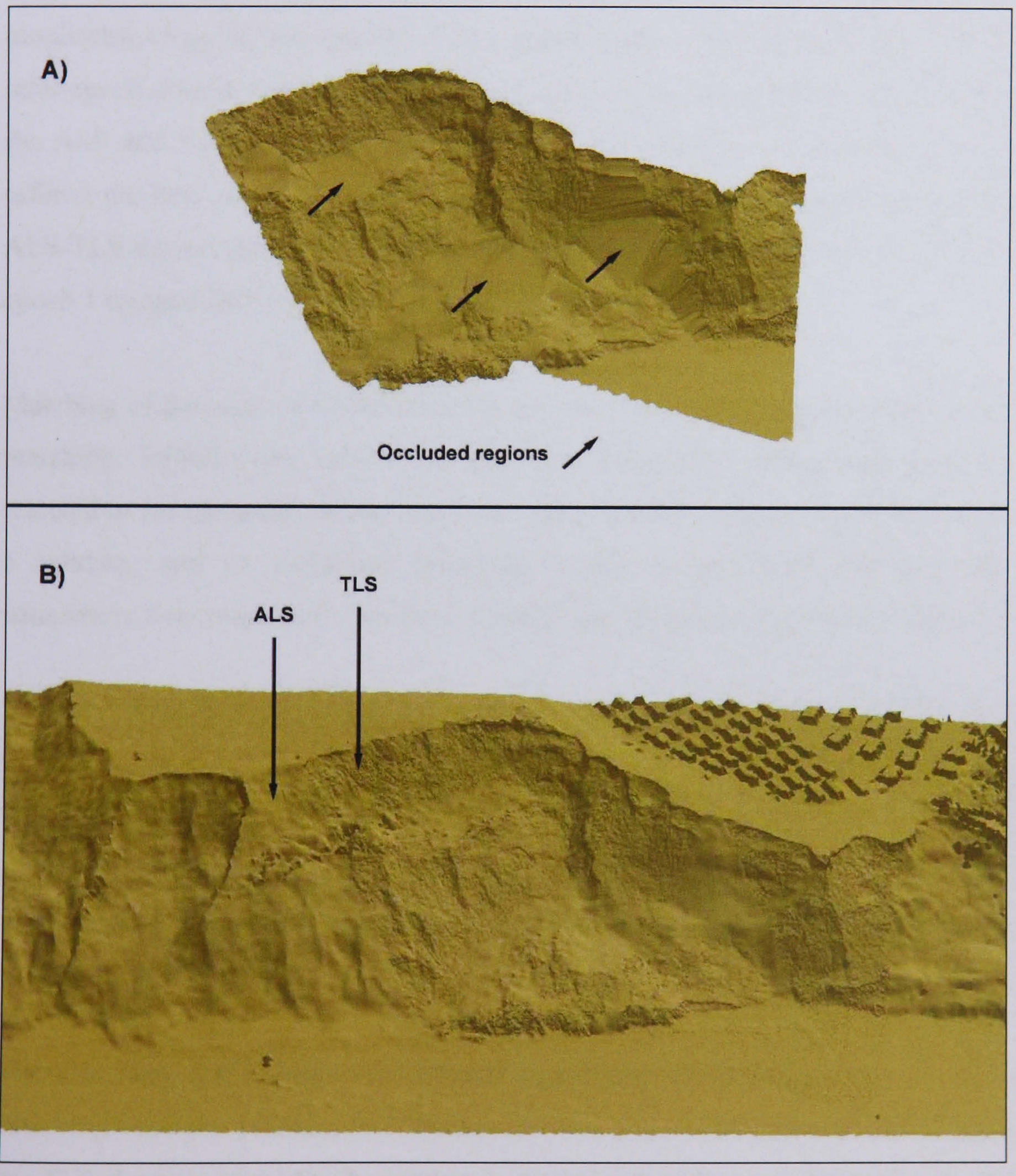

Figure 5.26 Occluded scan regions in TLS dataset (A), and improved coverage, with merged ALS-TLS dataset after surface matching (B).

The differing resolutions of the two datasets are clearly visible through changes in surface texture. However, the ALS has provided continuous coverage, enabling effective in-filling of the occluded TLS regions.

5.7.2.2 Multi-Temporal Dataset Integration

Following successful multi-sensor fusion for the epoch 1 and epoch 2 surveys, the next stage involved multi-temporal analysis of the merged ALS-TLS DEMs for multi-scale monitoring of geohazard activity. Again, robust surface matching provided the basis for inter-epoch dataset registration and change detection. Investigations into the quality of the ALS and TLS datasets in Section 5.5.3.2 revealed that the epoch 2 ALS surface offered the best accuracy over the SPT cliff-face. Consequently, the merged epoch 2 ALS-TLS dataset (epoch 2-m) was selected as the matching reference surface, with the epoch 1 merged DEM (epoch 1-m) matched to this.

Matching of the multi-temporal datasets proved more challenging than the multi-sensor matching. Initially, the same strategies (six parameters, planar interpolation) were selected as for the multi-sensor matching. However, the software was unable to achieve a solution, and so variations involving kriging interpolation and the full seven parameters were attempted. The final strategy and solution is detailed in Table 5-20.

Match (ref./match)	**Input Parameters**			**Outputs**	
	Weighting	**Parameters**	**Interpolation**	**Iterations**	**RMSE (m)**
Epoch 2-m/ Epoch 1-m	Robust	7	Kriging	21	0.571

Table 5-20 Summary of multi-temporal matching input parameters and results. RMSE refers to final matching residuals.

The matching difficulties were slightly surprising considering that the multi-senor matching had been problem-free. However, one possible explanation is that inclusion of the TLS datasets undoubtedly renders both merged surfaces (reference and matching) somewhat noisier than the ALS DEMs alone, and the software has been observed as having greater difficulty in converging where random errors are large. This is supported by the investigations of Gruen and Akça (2005), who note that convergence behaviour

is strongly influenced by dataset quality. Re-introducing the scale parameter (which proved successful) may have afforded the transformation a greater degree of flexibility.

The final set of transformation parameters are detailed in Table 5-21, where it can be seen that relatively minor transformations were required in order to register the epoch 1-m dataset to the epoch 2-m DEM. Although scale has been modified, again, this is relatively minor, and the low parameter standard deviations, supported by a visual inspection of the datasets, suggested that a strong matching solution had been achieved. This was further assessed by comparing the post-match epoch 1 surface to the validation profiles in the same manner as before. The results are summarised in Table 5-22, which includes the pre-match epoch 1 merged surface statistics for comparison. The inter-epoch surface matching resulted in a further improvement to the quality of the epoch 1 surface, as reflected in particular through improved RMSE values.

Match (ref./match)	**Final Transformation Parameters**						
	$\omega^\circ \pm \sigma$	$\phi^\circ \pm \sigma$	$\kappa^\circ \pm \sigma$	T_x (m) $\pm \sigma$	T_y (m) $\pm \sigma$	T_z (m) $\pm \sigma$	$s \pm \sigma$
Epoch 2-m/ Epoch 1-m	-0.014328 ± 0.001279	0.010356 ± 0.001106	0.013938 ± 0.001080	-0.388 ± 0.003	0.255 ± 0.003	0.054 ± 0.003	0.9996 ± 0.0000

Table 5-21 Final transformation parameters for multi-temporal matching at SPT.

Surface	**Profile**	**Level Difference Statistics (m)**				
		Mean	**σ**	**RMSE**	**Max.**	**Min.**
Epoch 1-m pre-match	SPT1	-0.074	0.315	0.322	0.932	-0.788
	SPT2	-0.056	0.260	0.264	0.667	-0.641
Epoch 1-m post-match	SPT1	-0.025	0.207	0.208	0.602	-0.664
	SPT2	0.002	0.227	0.226	0.651	-0.303

Table 5-22 Profile validation analysis for multi-temporal matching of epoch 1 data at SPT.

Figure 5.27 summarises the effects of the multi-sensor, multi-temporal dataset integration on the surface RMSE values, with the marked improvement through fusion of the airborne and terrestrial datasets particularly notable. Following surface matching, which had facilitated robust registration of the epoch 1 DEM to the epoch 2 surface, it was possible to proceed with multi-temporal change analysis.

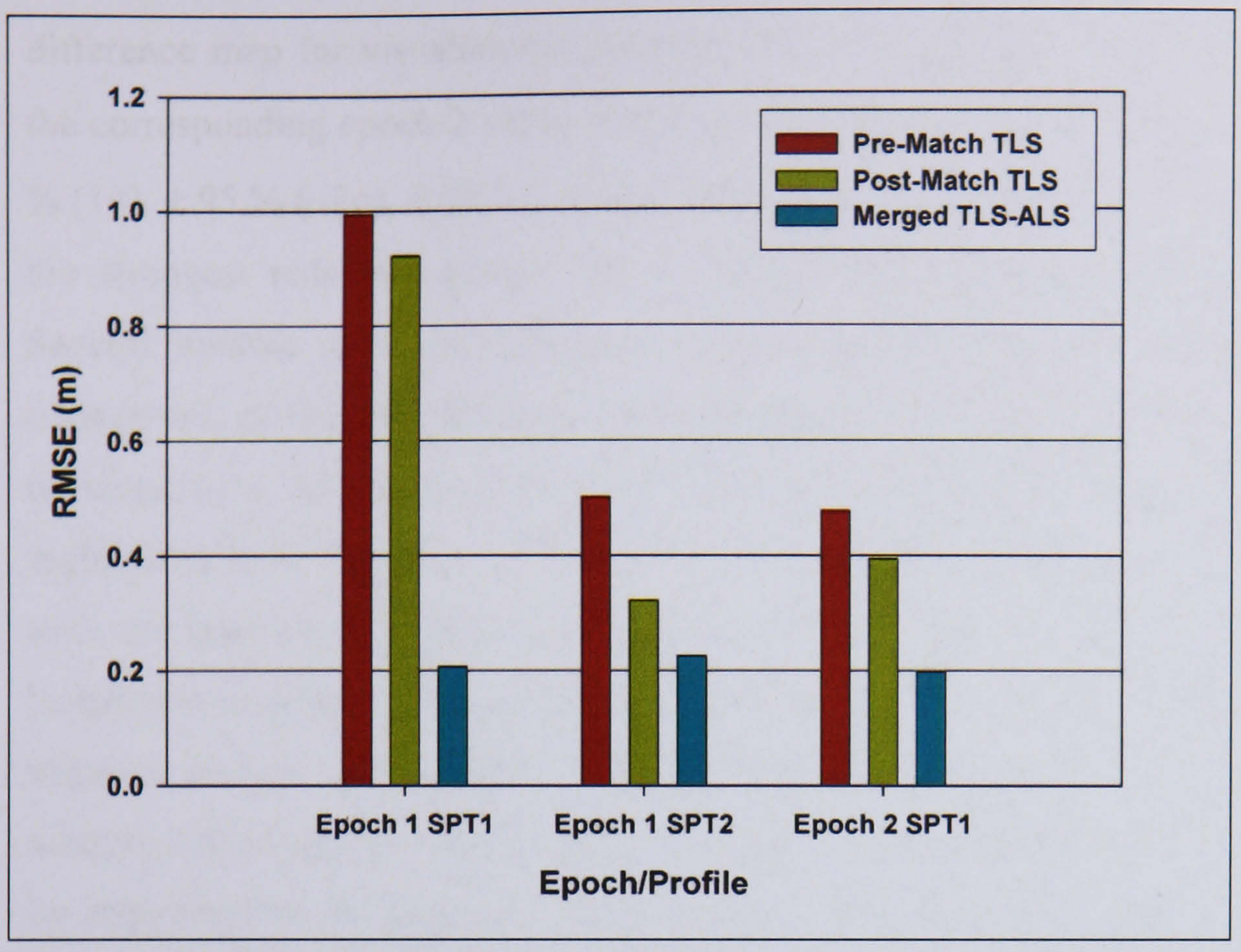

Figure 5.27 SPT profile RMSEs for TLS pre-match, post-match and final merged TLS-ALS surfaces.

5.7.3 Assessment of Contemporary Geohazard Activity

Implementation of the integrated remote monitoring strategy, as described in the previous section, offers an opportunity to investigate the potential of this approach, and the techniques of ALS and TLS, for multi-scale monitoring of change in a coastal geohazard environment. In order to facilitate this analysis, *LSS* was used to calculate level differences between the epoch 1 and epoch 2 surfaces. The resultant output was subsequently imported to *ArcGIS* where the point dataset was converted to a TIN structure for representation as a continuous surface of elevation differences. In the region of the TLS acquisitions, these datasets were of an extremely high resolution, with the level difference surface totalling 754,923 points. Although the resolution of the TLS datasets could have been degraded to speed up processing in *LSS* and *ArcGIS*, it was decided to retain all points in order to explore the full potential of TLS for geohazard monitoring.

As discussed in Section 5.6.4.1, the standard deviation of the datasets provides a useful measure of confidence for analysis of surface change. Therefore, the standard deviation of the post-match epoch 1 merged DEM, ± 0.227 m, was utilised in classifying the level

difference map for visualisation purposes. This is presented in Figure 5.28, alongside the corresponding epoch 2 ortho-image. Specifically, class breaks correspond to ± 68.3 % (1σ), ± 95 % (~2σ), ± 99.7 % (~3σ), and ± > 99.7 %. Therefore, the areas depicted by the strongest reds and greens can be considered as being of greatest significance. Several notable areas of difference are highlighted. Negative change at point A corresponds to sections of steep, vegetation-free cliff-face, suggesting that erosion has occurred here. In contrast, positive change appears to have occurred over the area highlighted at B. This is a region of dense gorse bushes, which are likely to have grown over the intervening spring and summer months. Area C is consistent with the large landslide scar which has been analysed previously in Section 5.6.4, and the patterns of negative change here suggest continued geohazard activity, particularly across the western side-scarp, and within the central part of the landslide body. This is supported by inspection of the imagery, which indicates that the central and western flanks are predominantly comprised of bare earth slopes, while the eastern flank appears to be vegetated, and thus is likely to be more stable. The beach appears to have been relatively active over this period, with areas of erosion and deposition (D) apparent. Patterns of negative change at E suggest that erosion of the cliff-toe has occurred towards the south of the SPT test area.

The *ArcScene* component of *ArcGIS* was then utilised to visualise the elevation differences in 3D. This enabled the elevation difference map to be draped over a TIN constructed from the epoch 2 merged DEM. This is depicted in Figure 5.29, which also shows the locations of the SPT1 and SPT2 validation profiles. The features highlighted in Figure 5.28 are visible in the 3D view, with areas of positive change generally corresponding to gentler slopes, while erosion is associated with the steeper back-scarp area, and cliff-toe.

Figure 5.30 illustrates the benefits of the multi-scale analysis provided through integration of the ALS and TLS datasets. Change is represented using the same scale as for Figure 5.28. While the image on the left depicts inter-epoch elevation differences calculated using only the ALS datasets, the right-hand image shows the merged ALS-TLS differences. It should be noted that the TLS datasets occupy the central part of the SPT site, closely following the course of the validation profiles.

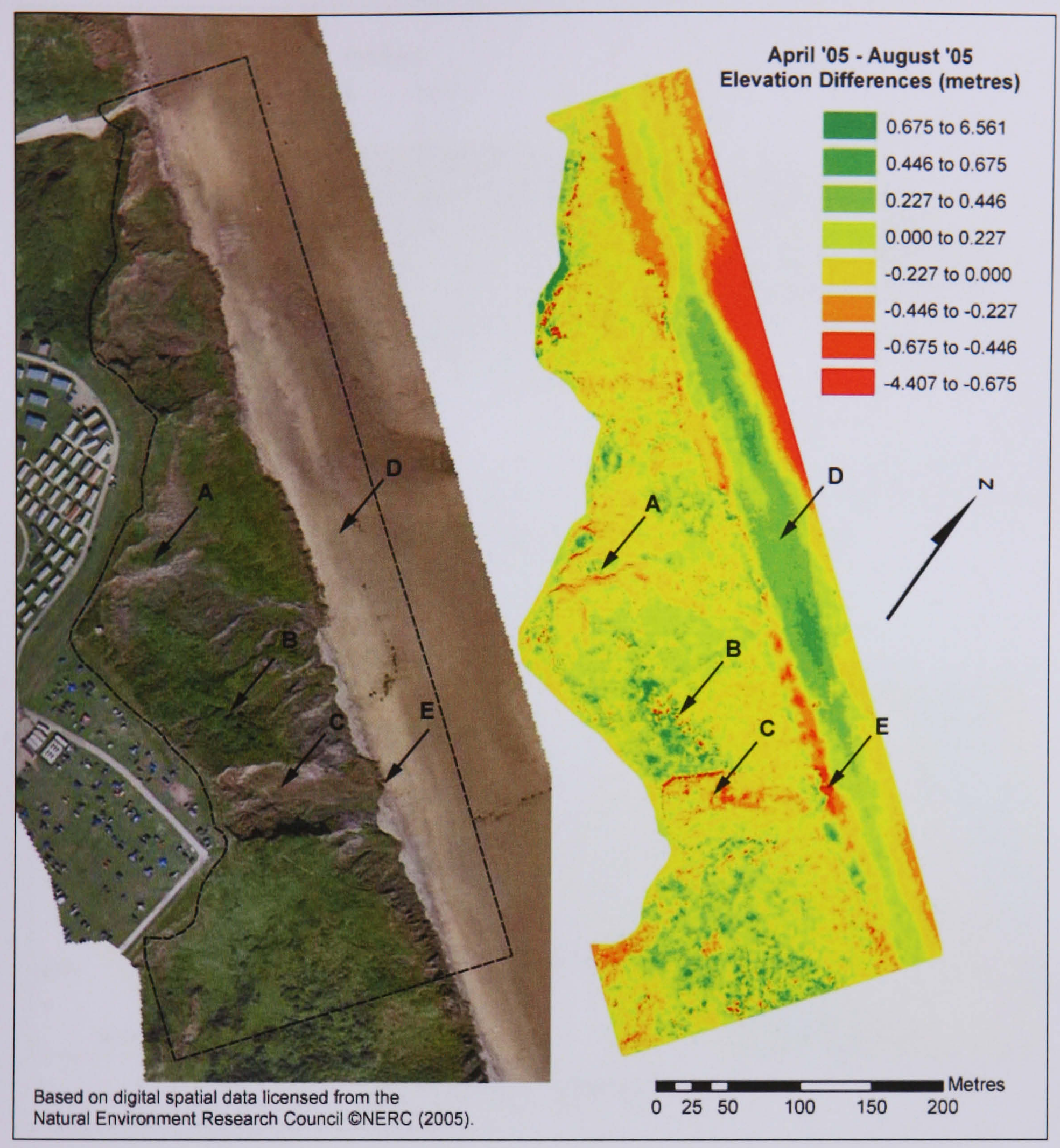

Figure 5.28 Map of elevation differences, epoch 1 to epoch 2, for integrated ALS-TLS DEMs at Reighton, with regions of change highlighted, and indicated on corresponding epoch 2 ortho-image.

Resolution differences are evident, as highlighted in Figure 5.30. In particular, erosion of the back-scarp is more clearly defined in the merged datasets, while linear patterns of positive change, closely associated with areas of vegetation along ridges in the cliff-face, are apparent in the merged dataset (right), but cannot be identified in the lower resolution ALS-derived change map.

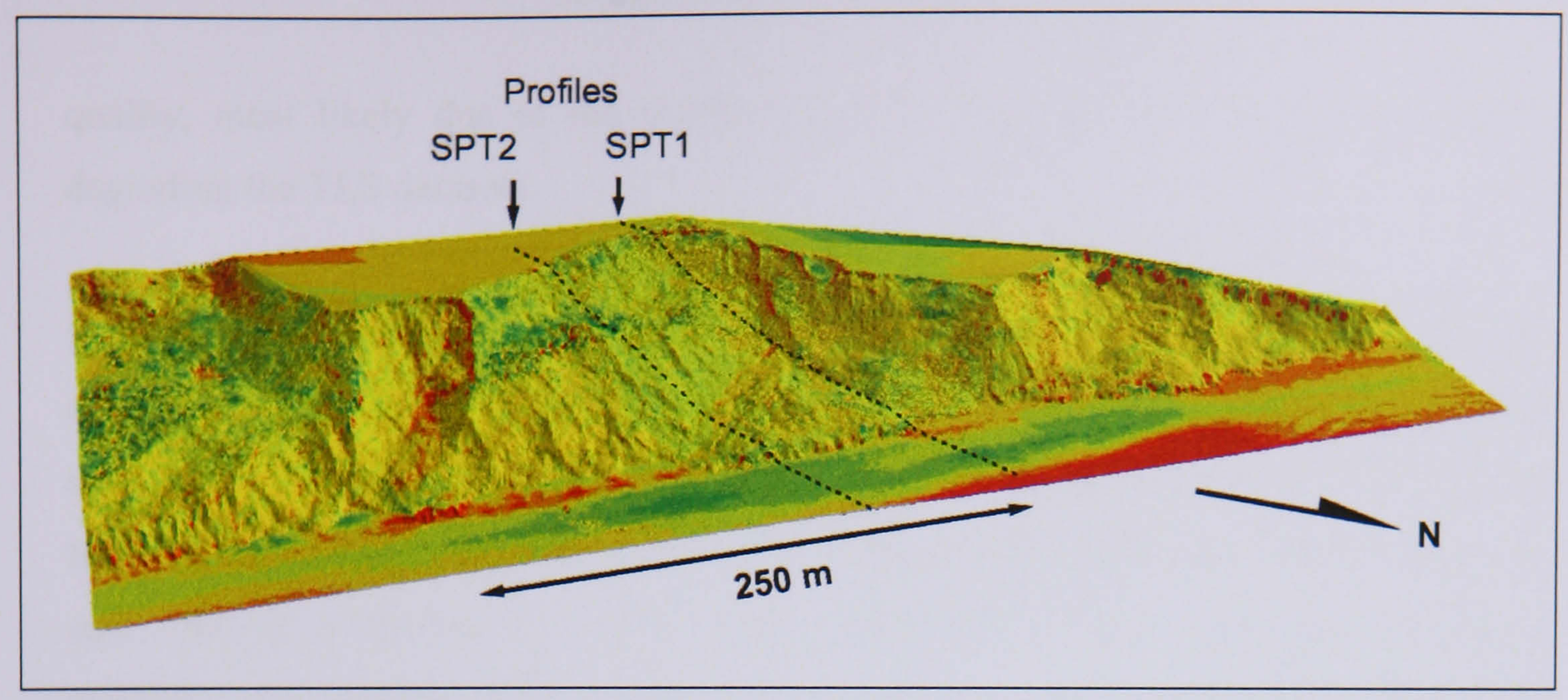

Figure 5.29 Visualisation of cliff change between epochs 1 and 2 at Reighton, with SPT validation profiles indicated. Change is represented through same scale as for Figure 5.28.

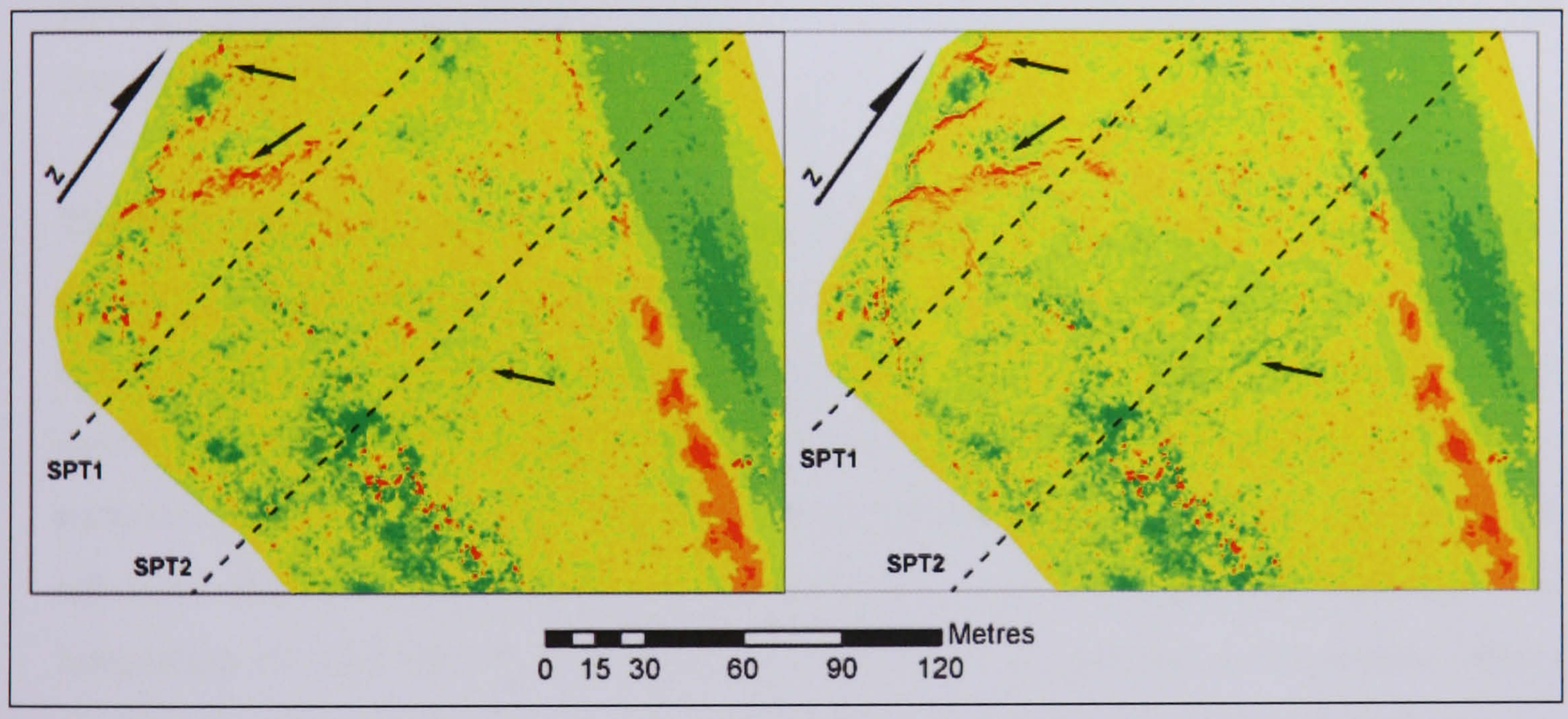

Figure 5.30 Elevation differences for SPT area using only ALS datasets (left), and with merged ALS-TLS datasets (right). Resolution differences are highlighted.

5.8 Summary

This chapter has applied the integrated remote monitoring strategy introduced in Chapters Three and Four to a soft-cliff test site located at Filey Bay on the North Yorkshire coast. After outlining the primary characteristics of the site, details of data collection and processing have been presented in relation to the airborne and terrestrial datasets. This has included investigations into the quality of the laser scanning datasets, and unexpectedly, the ALS datasets were determined to be of consistently higher

quality, most likely due to the combined effects of vegetation and data occlusions degrading the TLS datasets.

Retrospective assessment of geohazard activity has been carried out for the Reighton area at the southern end of Filey Bay, where archival datasets presented an excellent opportunity for rigorous testing of the robust matching technique with real-world topographic datasets. This has involved matching photogrammetric DEMs from 1967 and 1980 to a present day ALS dataset acquired in 2005. Following successful matching, the quality of the 1980 solution was assessed through comparison to a validation DEM. Further analysis has confirmed that surface matching is capable of producing a reliable and robust absolute orientation solution, and has also established the superiority of the robust matching strategy over the un-weighted algorithm. These findings permitted retrospective analysis of geohazard activity at Reighton over the periods 1967-1980 and 1980-2005.

The final section of Chapter Five has been devoted to evaluating the integrated remote monitoring strategy through contemporary assessment of geohazard activity. This has involved two stages; firstly multi-sensor fusion of the TLS and ALS datasets for each monitoring epoch; and secondly, multi-temporal integration of the subsequent merged surfaces. Robust surface matching has been successfully applied in both cases, with the solutions shown to offer marked improvements in surface quality. In particular, the integration of ALS and TLS datasets has been found to produce a synergistic effect, resulting in increased DEM accuracy, and facilitating multi-scale analysis of change.

The analysis presented in this chapter has demonstrated the applicability of the integrated remote monitoring strategy for both retrospective and contemporary assessment of geohazard activity in a soft-cliff geohazard environment. Robust surface matching has proved particularly valuable for the reconciliation of multi-sensor, multi-temporal datasets. Furthermore, the combined airborne-terrestrial approach, implemented through the techniques of ALS and TLS, has demonstrated potential for multi-scale monitoring, and the synergistic qualities of this approach have been highlighted. The following chapter will investigate the transferability of the monitoring strategy through application to a hard rock environment, located at Whitby, North Yorkshire.

CHAPTER 6

TRANSFERABILITY TESTING AT WHITBY EAST CLIFF

6.1 INTRODUCTION

Chapter Five successfully demonstrated the suitability of the integrated remote monitoring strategy for application to the soft-cliff geohazard environment of Filey Bay. However, as stated in Section 3.2.2, it is desirable that this monitoring strategy incorporates the flexibility which will permit its application to a range of coastal geohazard scenarios. This chapter therefore concentrates on exploring this aspect by examining the transferability of the monitoring approach through application to the hard rock geohazard setting of Whitby East Cliff, North Yorkshire. The nature of geohazard activity at Whitby and characteristics of the local topography combine to produce a challenging test site, which is distinctly different to Filey Bay. Cliff recession at Whitby East Cliff poses an immediate threat to existing cliff-top infrastructure, and a medium- to long-term risk to adjacent elements of the human environment and historic landscape. In this regard, Whitby is a site which presents a strong case for implementation of an effective coastal monitoring strategy.

One of the primary outcomes of Chapter Five was the successful application of robust surface matching for absolute orientation of DEMs derived from archival aerial photography. In the absence of terrestrial datasets, this element will be further evaluated here, in combination with ALS. These investigations facilitate multi-temporal assessment of geohazard activity at Whitby East Cliff over the twenty-year period 1986 to 2006. The potential of aerial photography and ALS is thoroughly assessed by the

characteristics of the test site, and a number of relevant issues are discussed. Cliff-face retreat is then further evaluated through examination of cliff-normal profiles, and volumetric change analysis. Finally, rates of retreat are assessed, and the role of these as a means of quantifying coastal change is discussed.

6.2 WHITBY TEST SITE

6.2.1 Overview

Whitby, a historic coastal town with a population of around 13,500, is situated on the North Yorkshire coast, 40 km north of Filey. Traditionally important as a port, its main economic activities are now related to tourism and fishing. The test site is located at Whitby East Cliff, which lies immediately east of the harbour entrance, and forms the seaward portion of Whitby Abbey Headland (Figure 6.1). Whereas Filey Bay represents a soft-cliff environment, with cliffs composed of soft glacial tills, Whitby consists of a hard rock geology. However, hard rock cliffs vary extensively in terms of resistance (Bird, 2000), and Whitby is largely composed of relatively weak rock types, which are prone to instability.

The test site is comprised of near-vertical cliffs, which rise to around 60 m in height. The sub-horizontal bedding of the cliff is clearly evident (Figure 6.2), and a detailed description of the geology of this stretch of coast is provided by Rawson and Wright (2000), summarised as follows. The cliff-toe is comprised of around 12 m of Alum Shales, which are part of the Whitby Mudstone Formation. These are overlain by a thin bed of the sandstone Dogger Formation. Erosion of these cliff-toe shales has resulted in a series of small embayments, referred to locally as bights. The upper cliff section is primarily composed of the fine sandstones, siltstones, and carbonaceous clays of the Saltwick Formation, which are overlain by the Ellerbeck sandstone interval at the top of the cliff, capped in turn by glacial tills (Rawson and Wright, 2000). Whitby East Cliff is fronted by a shallow-angled wave-cut platform, which extends to around 300 m from the base of the cliff, and which can be submerged by up to six metres of water at high tide (Rosser et al., 2005). This makes access to the foot of the cliff particularly difficult and hazardous.

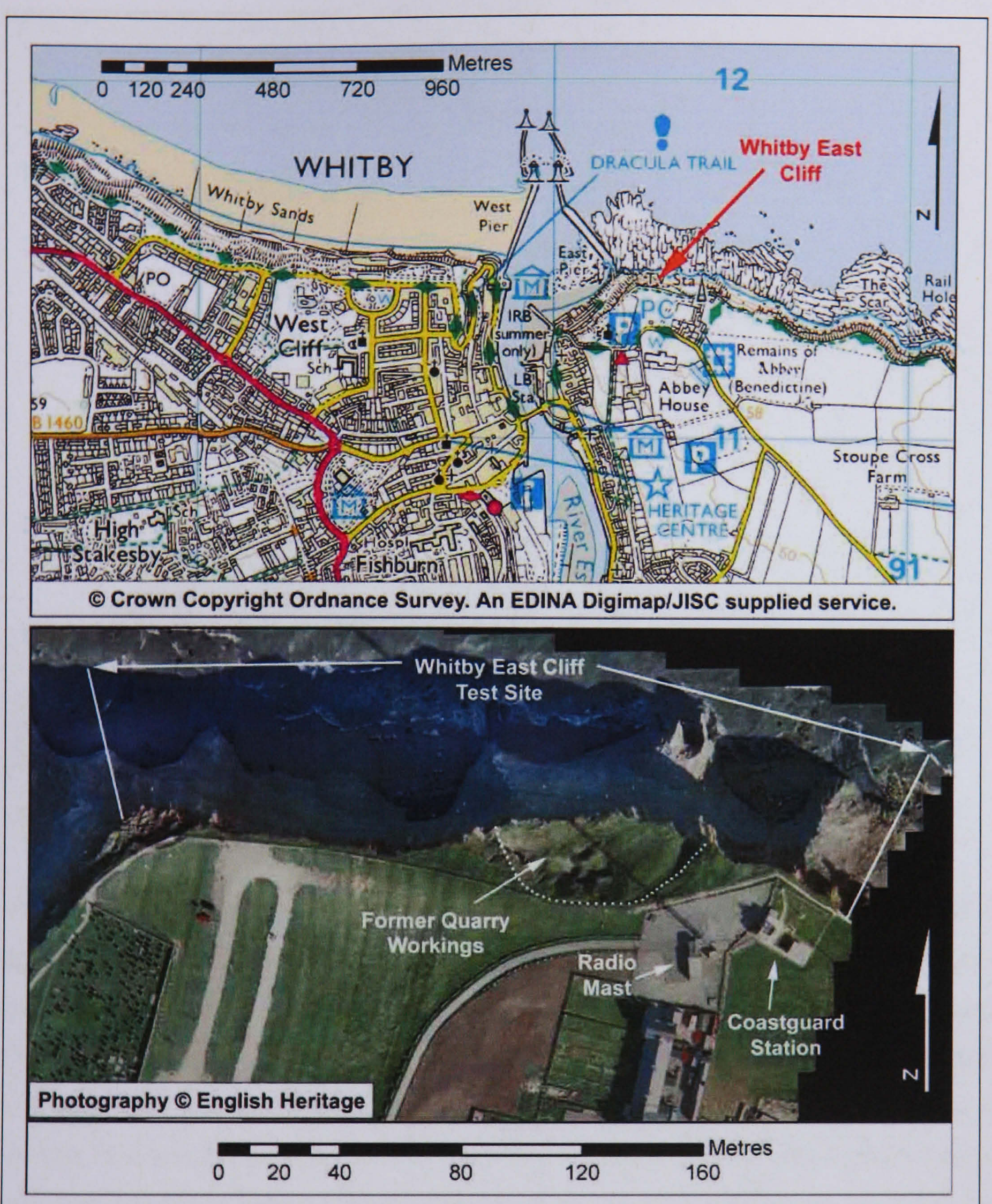

Figure 6.1 Location map (top), and overview of test site shown against backdrop of 1994 ortho-image (bottom).

Unlike Filey Bay, Whitby is affected in a much more direct manner by wave attack, which leads to marine erosion of the cliff-toe. However, as Clark and Guest (1991) observe, this is exacerbated by groundwater seepage from within the cliffs, which results in additional instability and erosion. Consequently, geohazard activity at Whitby East Cliff generally takes the form of rock- and debris-falls, which result in continued retreat of the cliff-face.

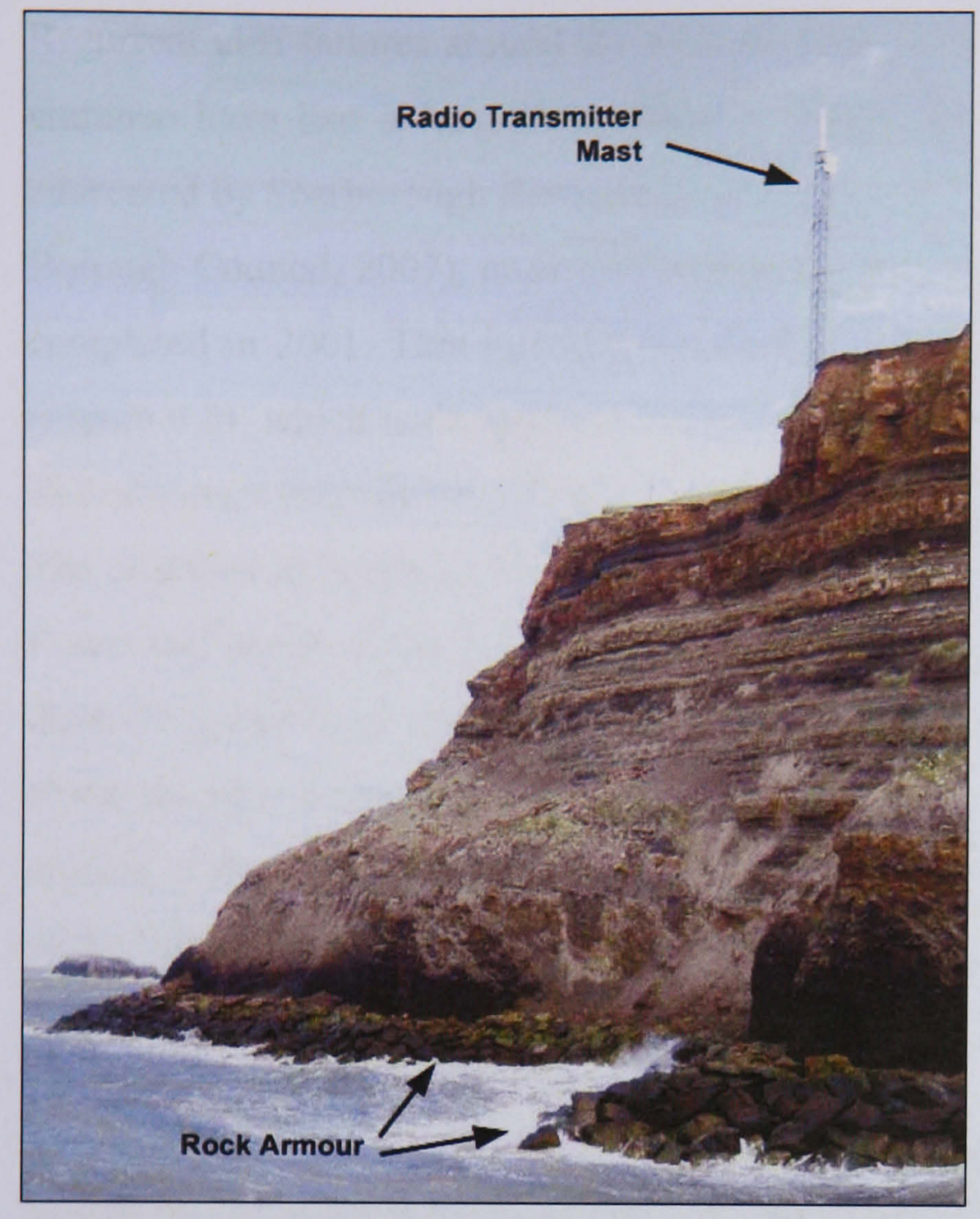

Figure 6.2 Study site at Whitby East Cliff.

This has had a prolonged effect on the human environment. Whitby East Cliff is particularly important in terms of local infrastructure, with the town's coastguard station and 45 m-high TV/radio transmitter mast located on the cliff-top, a matter of metres from the cliff-edge (Figure 6.1). As a direct result of cliff erosion, the TV/radio transmitter is currently in the process of being relocated to a new site, located inland at Whitby Business Park. Furthermore, the headland is an important cultural and historical site, and includes St Mary's Church, and the ruins of Whitby Abbey, parts of which date from the 7th century. English Heritage (EH), the body responsible for the preservation and management of the Abbey site, are keenly aware of the threat posed by coastal erosion. Although the Abbey is not at immediate risk, the headland contains artefacts from prolonged human settlement associated with the Abbey. Following a major cliff failure in October 2000, a salvage excavation had to be undertaken near the cliff-edge in order to prevent valuable archaeology from being lost to the sea (Jennings et al., 2002).

Recurrent cliff failures around the western extreme of Whitby East Cliff at the harbour entrance have had a long-term effect on access to the East Pier. This was recently addressed by Scarborough Borough Council who, at a cost of £1.6 million (Scarborough Borough Council, 2007), undertook a slope stabilisation and coastal protection scheme, completed in 2001. This included installing a four metre high rock armour revetment (Figure 6.2), which is designed to reduce the impact of marine erosion on the cliff-toe. This structure extends for 300 m east from the pier along the foot of Whitby East Cliff. The coastline at Whitby also forms part of the North Yorkshire and Cleveland Heritage Coast, and is part of the North York Moors National Park. The Cleveland Way, a long-distance footpath which traverses the Yorkshire Moors and Coast for 176 km, runs along the top of Whitby East Cliff, and has had to be continuously re-routed due to erosion of the cliff edge, as illustrated in Figure 6.3. Furthermore the test site forms part of the Whitby to Saltwick SSSI, which is considered as being of international geological significance (English Nature, 2007).

Figure 6.3 Coastal erosion affecting the cliff-top footpath.

6.2.2 Previous Monitoring

Due to the proximity of Whitby East Cliff to the town of Whitby, and the important infrastructure and historical assets located on the cliff-top, the site has been the subject

of previous monitoring studies. Following the October 2000 cliff collapse which initiated the emergency archaeological excavations of the cliff-edge, as referred to in Section 6.2.1, EH undertook historical analysis of cliff change at Whitby East Cliff through investigation of historical maps and aerial photographs (Lyons, 2004, personal communication). The overall retreat of the cliff-top is evident through examination of Figure 6.4 which depicts change to the cliff-edge, as derived from aerial photographs spanning the period 1940 to 2001. This suggests that the cliff-edge retreated by a maximum of 25 m (approximately) over this period.

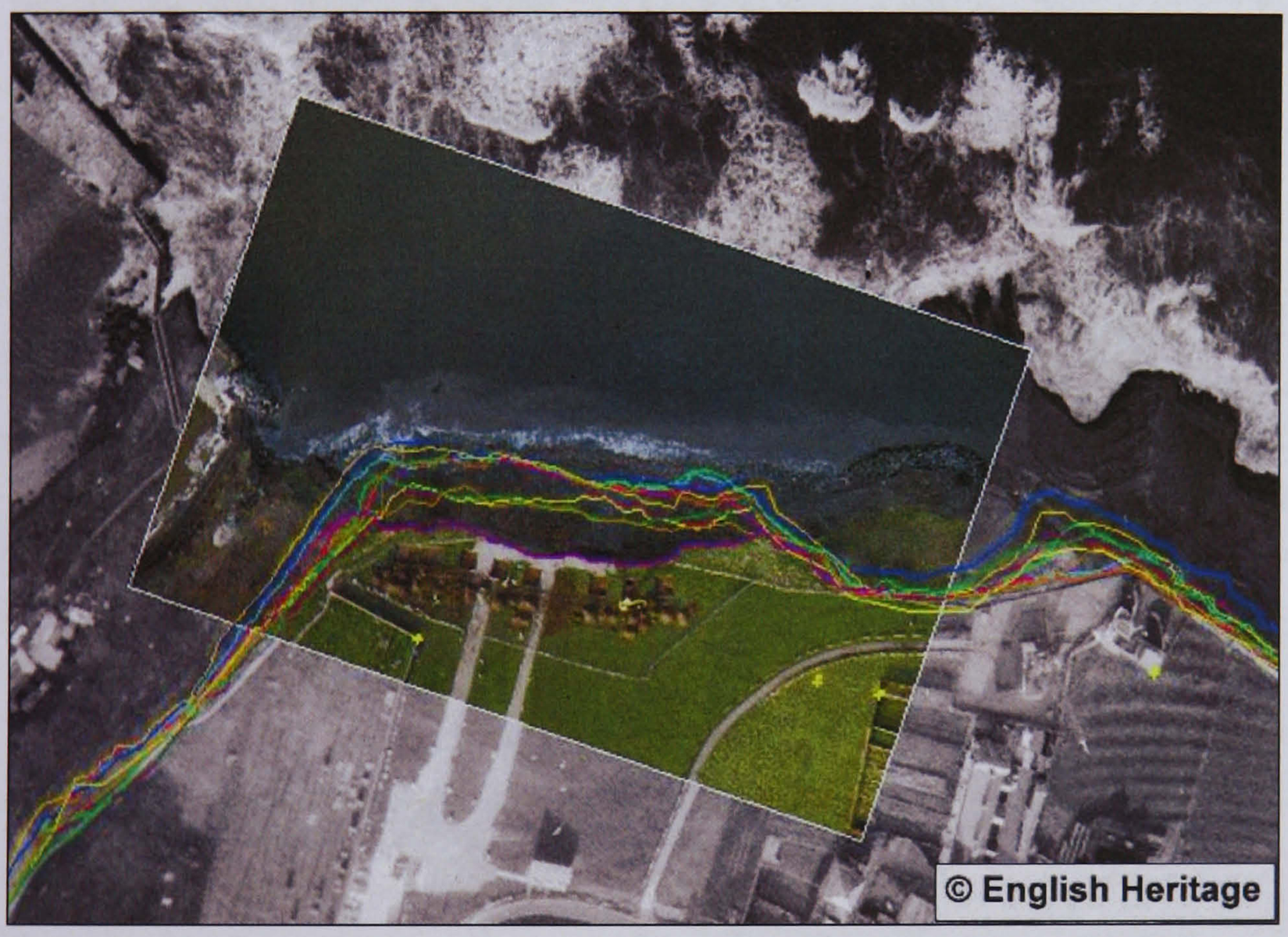

Figure 6.4 EH mapping of cliff-edge position, 1940-2001, derived from aerial photographs (after Lyons, 2004, personal communication).

More recently, Rosser et al. (2005) investigated the potential of TLS for monitoring rockfall activity at Whitby East Cliff, presenting results from surveys carried out on a monthly basis between 2003 and 2004 (Figure 6.5). Rosser et al. (2005) observe the value of TLS for quantitative assessment of rockfall events, and note that cliff-face geology appears to exert a strong influence on the development and propagation of such failures. The findings of this study would seem to indicate that TLS is a highly suitable technique for monitoring of a hard rock environment such as this. Furthermore, as discussed in Section 3.3.2, TLS can be exploited for monitoring at high temporal frequencies, as demonstrated by this study, which consequently facilitated the detection

of rockfalls of varying magnitudes. Rosser et al. (2005) also conducted analysis of historical maps and aerial photographs dating back to 1895, and from these determined an annual erosion rate of -0.18 m for the cliff-top.

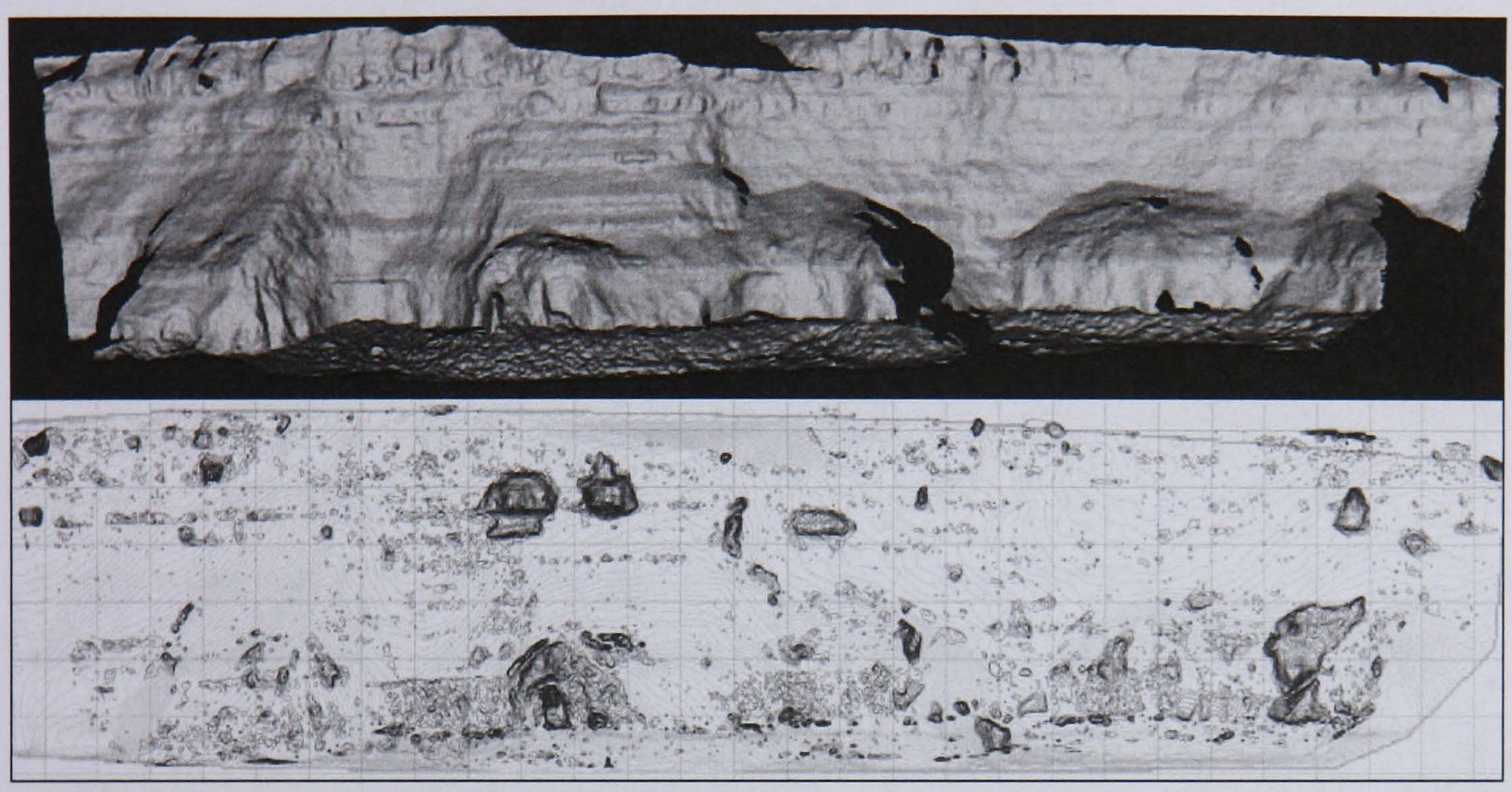

Figure 6.5 TLS-derived model of Whitby East Cliff (top), with 0.25 m contours indicating change between 2003 and 2004 (bottom) (Rosser et al., 2005).

6.3 Episodic Monitoring

6.3.1 Introduction

In a similar vein to the monitoring carried out at Filey Bay, episodic datasets covering extended historical periods were acquired. ALS datasets were collected at the same time as the acquisitions at Filey Bay. Specifically, this corresponded to April 2005, August 2005, and May 2006. Whereas terrestrial acquisition represented a major component of the investigations at Filey Bay, unfortunately it was not possible to undertake any terrestrial fieldwork at Whitby. This was primarily related to the delays and unpredictability associated with the ARSF's acquisition schedule (refer to Section 5.3.1). As a result, it proved difficult to organise and coordinate fieldwork at both the Filey Bay and Whitby sites, and efforts were therefore concentrated on carrying out terrestrial fieldwork at Filey Bay. This was regrettable, but ultimately, a range of airborne datasets provided ample opportunity for matching-based multi-temporal dataset integration, and subsequent analysis of geohazard activity at Whitby. In addition to the ALS datasets, two epochs of archival photography, from 1986 and 1994, were

acquired for incorporation in the episodic monitoring programme. Acquisition and processing of the ALS and photogrammetric datasets is described in Sections 6.3.2.1 and 6.3.2.2 respectively. The UTM Zone 30 North coordinate system was again applied throughout, for the reasons explained in Section 5.4.1.3.

6.3.2 Data Acquisition and Processing

6.3.2.1 Airborne Laser Scanning

ALS datasets were acquired for the research on the 19th April 2005, the 2nd August 2005, and the 3rd May 2006. These datasets were collected at the same time as the Filey Bay datasets, and specifications are identical to those presented in Section 5.4.1.1. To briefly recap, data was acquired with an Optech ALTM 3033 first and last pulse return instrument, operating from a flying height of approximately 1000 m, which resulted in a ground resolution of around 1 point/m^2. Initially there were concerns as to possible shadowing of the near-vertical cliff-face. However, examination of the datasets revealed that good coverage of the cliff-face had been achieved in the case of all three epochs.

Data processing followed the same procedure as described in Section 5.4.1.3 in relation to the Filey Bay ALS data. Figure 6.6 depicts the ALS flightline coverage for the test site, and the adjacent areas of Whitby Abbey Headland over which surface matching was carried out (refer to Section 6.5.2). Although the test site occupies a relatively small extent in comparison to the available ALS coverage (Figure 6.6), analysis was restricted to this area in order to match the coverage of the photogrammetric datasets (refer to Section 6.3.2.2) As explained in Section 5.4.1.3, flightline overlaps were cut in *TerraScan* in order to reduce surface noise in these regions. Where the test site was covered by more than one flightline (August 2005), the seaward flightline was utilised in analysis of the cliff-face (refer to Section 5.4.1.3). A ground classification was then carried out, followed by point reduction in preparation for surface matching. No major difficulties were encountered in relation to data acquisition and processing. However, the Whitby dataset was found to contain a large number of spikes, which had not been observed in the Filey Bay ALS datasets. Examination of the data led to the conclusion that these were mainly a result of returns from seabirds, which are found in large numbers in and around Whitby harbour, and the adjacent cliffs. An independent

analysis of ALS dataset quality is presented in Section 6.4, where all airborne datasets are analysed together in context.

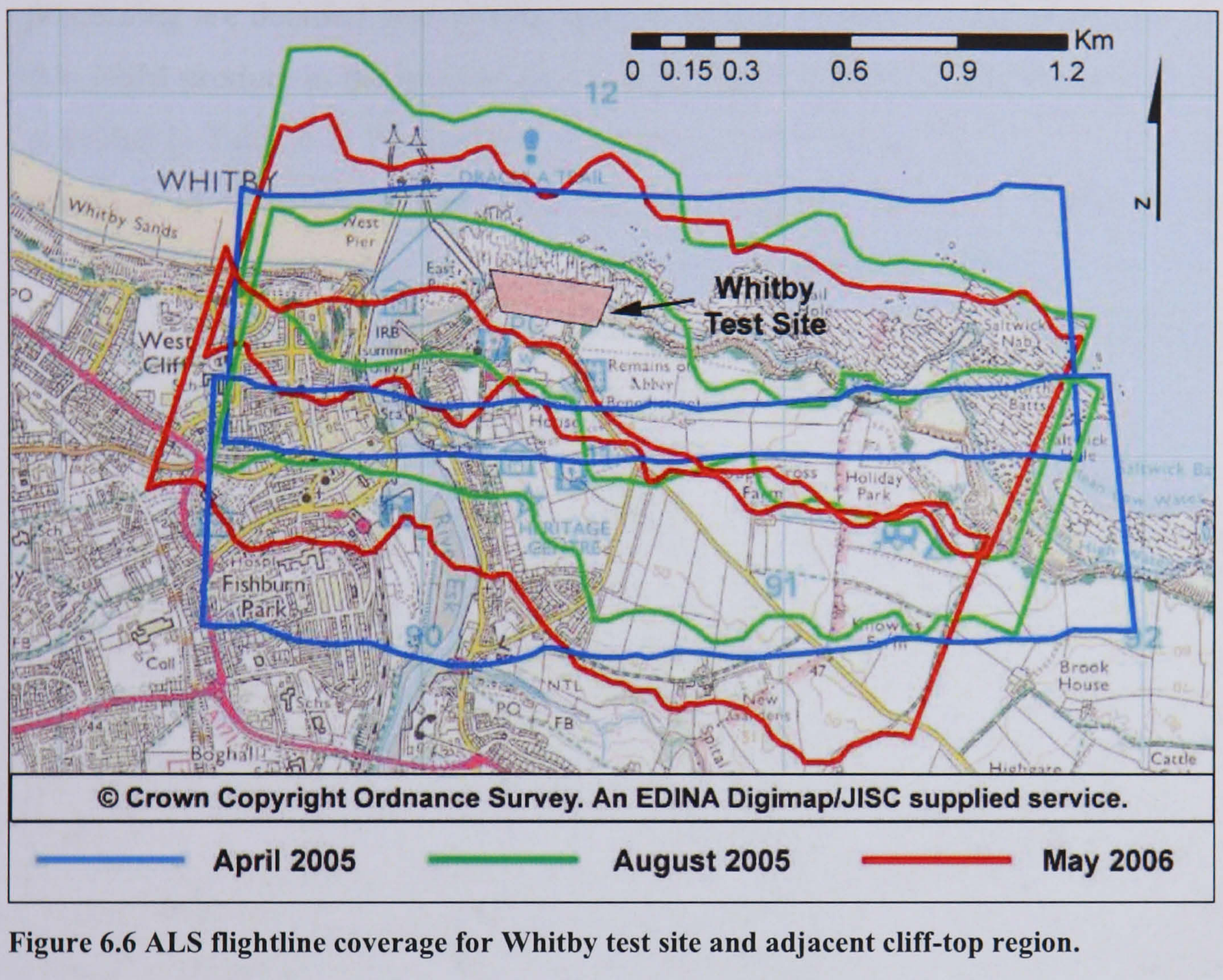

Figure 6.6 ALS flightline coverage for Whitby test site and adjacent cliff-top region.

6.3.2.2 Archival Aerial Photography

Data Acquisition

As explained in Section 5.4.2.1, a visit was made to the NMR in order to identify suitable archival aerial photography for the monitoring research. A number of possible epochs of vertical photography providing coverage of Whitby East Cliff existed. However, similar problems in relation to copyright permission and photogrammetric scanning were encountered as before (refer to Section 5.4.2.1). Eventually, an epoch of photography from March 1986 was selected, and photogrammetric scanning was carried out by the copyright holders, OS.

In addition, colour aerial photography from March 1994 was available from EH. This photography was of a particularly large scale (1:1,600), having been acquired for a topographic mapping project, and offered good coverage of Whitby Abbey Headland,

including Whitby East Cliff. The imagery had been processed by a professional EH photogrammetrist, and a resultant 1 m grid-based DEM was available. Due to the large scale of the imagery, the DEM was of excellent quality (results of EH photogrammetric processing are detailed later in this section). It was therefore decided to directly utilise this DEM product in the monitoring strategy. Details of the 1986 and 1994 imagery are provided in Table 6-1. The stereo coverage of the test site is depicted in Figure 6.7, and examples of the images are shown in Figure 6.8 and Figure 6.9. It should be noted that the 1994 EH photography and DEM offered coverage of the wider headland area (the full extent is utilised for surface matching, as detailed in Section 6.5.2.1). However, for clarity, only the frames relevant to the test area are depicted in Figure 6.7.

Characteristics	**1986**	**1994**
Source	NMR (OS copyright)	English Heritage
Media	Scanned diapositives	Scanned diapositives (colour)
Acquisition Date	19th March 1986	6th March 1994
Sortie No.	86-253	AF/94C/756
Frames	2005, 2006	9871-9873; 9883-9887; 9829-9833; 9856-9858
Flying Height (m)	812	488
Focal Length (mm)	153.19	303.90
Scale	1:5,300	1:1,600
b/H ratio	0.6	0.3
Scanning resolution (μm)	14	25
Ground sample distance (m)	0.07	0.04

Table 6-1 Details of archival imagery acquired for Whitby East Cliff test site.

From the details presented in Table 6-1, the anticipated heighting precisions were calculated using Equation 2-1 (refer to Section 2.4.3). This produced expected precision values of 0.062 m for the 1986 imagery, and 0.067 m for the 1994 photography. These values provided an indication of the quality of height measurements which were potentially achievable through subsequent photogrammetric processing, and this issue is revisited in Section 6.5.2.2, where the expected precisions are compared to those determined through check point analysis.

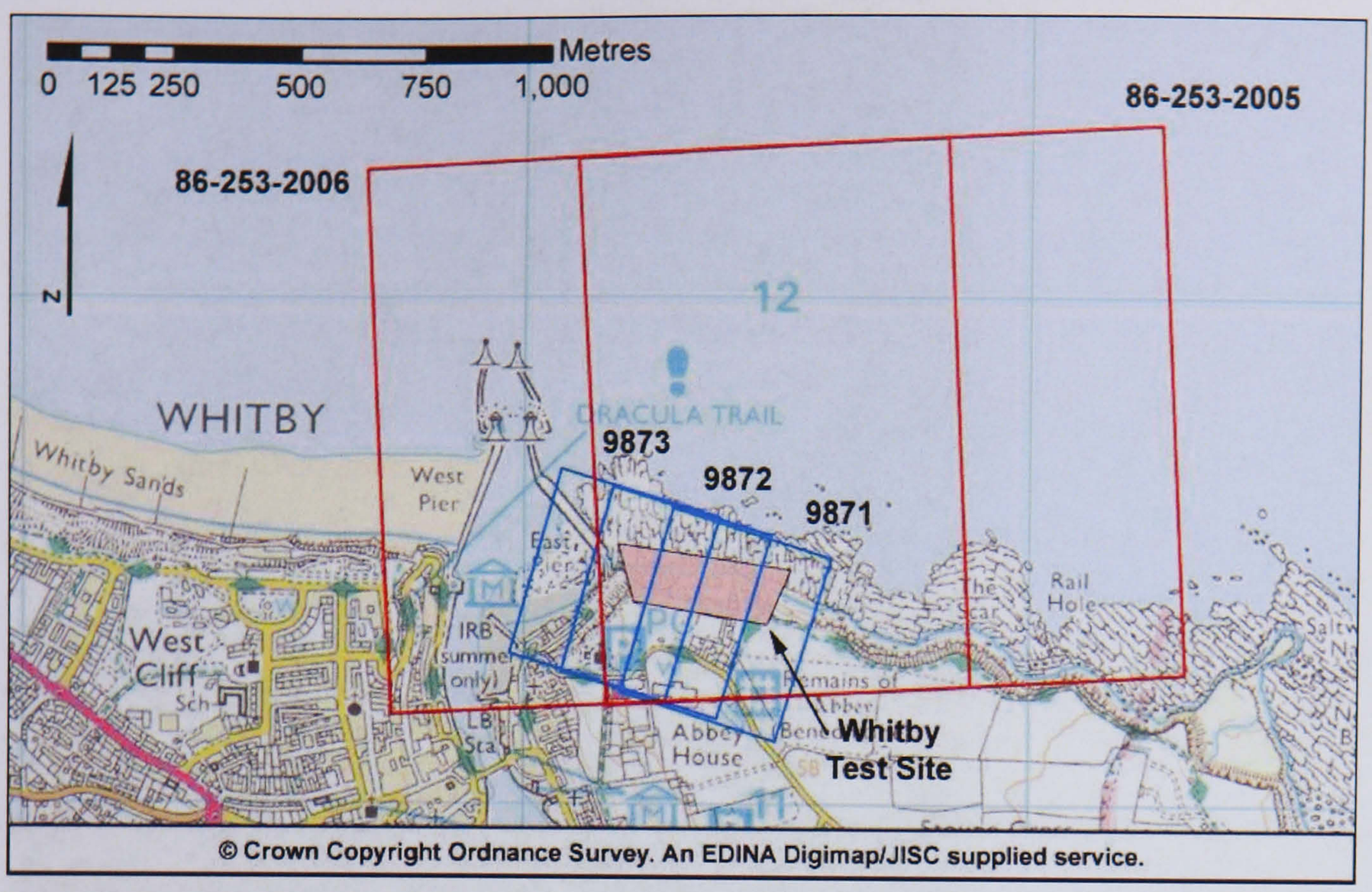

Figure 6.7 1986 (red) and 1994 (blue) stereo coverage of the Whitby test site.

Figure 6.8 1986 archival imagery (86-253-2006).

Figure 6.9 1994 archival imagery (9872).

Processing of Archival Imagery

As was the case for the 1967 and 1980 archival imagery of Filey Bay, OS were only able to provide a calibrated focal length for the 1986 photography, and so fiducial coordinates had to be determined in the same manner as before (refer to Section 5.4.2.2). The digital images were then imported to *SocetSet* where interior orientation was performed. As explained in Section 5.4.2.2, in order to obtain an approximate absolute orientation solution, it was necessary to supply *SocetSet* with pseudo GCPs. Three GCPs measured from large scale digital mapping were used. Due to the coverage of the stereo-pair, and the lack of hard detail, this proved a rather challenging procedure. As Figure 6.8 indicates, the image is primarily occupied by sea, with Whitby East Cliff forming a narrow strip along the top of the image. Unfortunately, the 1986 coverage of the study site was limited to this stereo-pair, and so the GCPs had to be located within this restricted area of land.

Once this procedure was completed, automatic tie point measurement was performed, and a bundle adjustment was carried out in order to determine the exterior orientation parameters. The results are detailed in Table 6-2. A *SocetSet* DPW was also employed by EH for processing of the 1994 photography (Clowes, 2007, personal

communication). EH were able to supply the results of the associated bundle adjustment procedure, and these are presented alongside the 1986 values in Table 6-2.

Epoch		1986	*1994
No. Control Points		3	7
No. Tie Points		13	15
Image RMSE (pixels)		0.131	0.222
Ground RMSE (metres)	x	5.742	0.039
	y	3.193	0.030
	z	0.088	0.022
	Total	6.571	0.054
* Source: Clowes (2007), personal communication.			

Table 6-2 Summary of bundle adjustment results for 1986 and 1994 imagery.

The outcome of the 1986 bundle adjustment reflects the difficulties associated with selecting suitable GCPs. While a satisfactory image RMSE value has been obtained, the ground RMSE values are poor, particularly in x and y. This is unsurprising however, given the poor quality of the selected GCPs, and the limited redundancy provided by the use of only three points (with no redundancy in z, hence the small and misleading RMSE value). The robust surface matching software was subsequently applied in order to derive an improved absolute orientation (Section 6.5.2). The 1994 bundle adjustment results indicate that a high quality solution was obtained by EH for exterior orientation, with low image and ground RMSE values. The results presented in Table 6-2 highlight the difference in the quality of absolute orientation solutions achieved through the use of a minimum number of approximate GCPs (1986), and through the use of high quality GCPs, incorporating redundancy (1994).

Initially, A TIN DEM was extracted from the 1986 stereo-model, using the *SocetSet* Automatic Terrain Extraction module, as described in Section 5.4.2.2. However, inspection of the resultant surface model revealed that the algorithm had been unable to extract elevations over large portions of the overlap area, particularly over parts of the upper cliff-face where image contrast was relatively poor due to shadowing. Consequently, it was decided to instead revert to grid-based measurement, and the adaptive strategy was applied to extract a 1 m DEM. The quality of grid-based DEMs can be examined in *SocetSet* through visualisation of Figure of Merit (FOM) values.

which are assigned to each DEM node as an indicator of the correlation success. FOM values also flag any manual editing procedures or specific error conditions encountered during image matching (e.g. high slope, spike post). Figure 6.10 depicts the FOM map for the 1986 DEM. Although successful correlation has been achieved for parts of the cliff-top (particularly around the cliff-top infrastructure), the elevations of large areas of the DEM, including most of the cliff-face, have had to be interpolated due to correlation failure. Consequently, manual editing was performed in order to improve elevation measurements around the cliff edge (light blue regions in Figure 6.10).

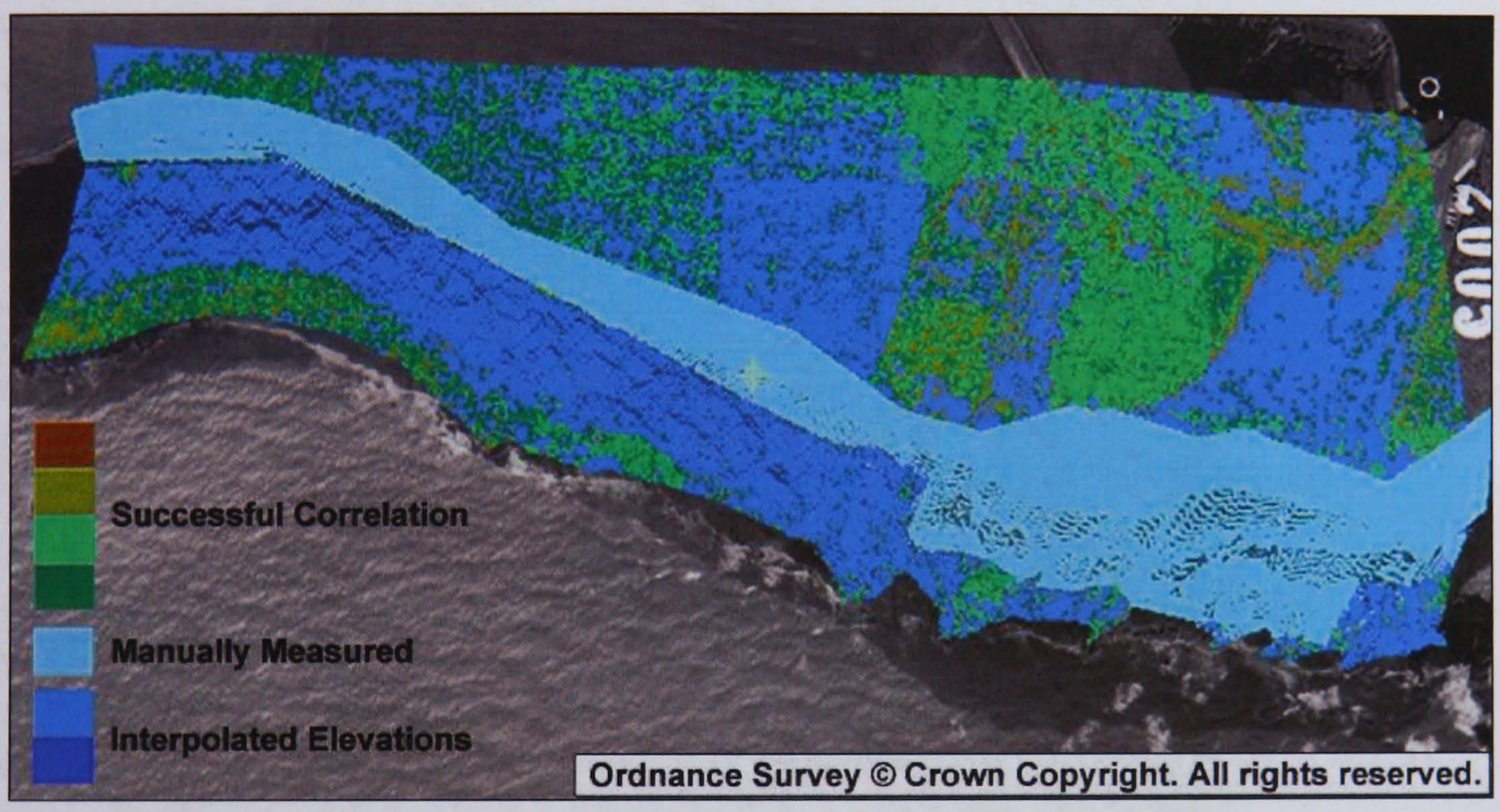

Figure 6.10 *SocetSet* FOM visualisation for 1986 grid-based DEM.

The *TerraScan* software was then used to perform a ground classification on the 1986 DEM, permitting the removal of cliff-top buildings and non-terrain features. The 1986 and 1994 datasets were then thinned using the Model Keypoints filter, as described in Section 5.4.1.3, in preparation for surface matching.

6.4 Dataset Quality Analysis

Prior to carrying out surface matching to facilitate integration of the multi-temporal DEMs, it was necessary to establish the quality of the datasets, in order to select a suitable surface as reference in the matching. The coordinates of a number of check points, measured by static GPS for topographic surveys of the headland in 1994 and 1999, were provided by EH. These points were well distributed across the headland, as

shown in Figure 6.11, and were located in areas which had undergone minimal change over the monitoring period. Check point analysis was carried out in *TerraScan*, as explained in Section 5.4.1.2. This enabled vertical discrepancies to be determined between the check points and the photogrammetric and ALS DEMs. The discrepancies were then analysed and summary statistics produced (Table 6-3).

Figure 6.11 Distribution of check points across Whitby Abbey Headland.

Surface	No. Check Points	Check Point Vertical Quality Statistics (m)				
		Mean	σ	RMSE	Max.	Min.
Mar. 1986	5	-3.403	2.072	3.875	-0.194	-5.141
Mar. 1994	17	0.023	0.132	0.130	0.260	-0.250
Apr. 2005	18	-0.314	0.152	0.347	-0.098	-0.625
Aug. 2005	18	-0.255	0.206	0.324	0.126	-0.654
May 2006	18	-0.060	0.155	0.162	0.142	-0.374

Table 6-3 Summary of check point analysis for Whitby multi-temporal datasets.

Due to the differing extents of the multi-temporal DEMs, the numbers of check points utilised in the analysis varied. Furthermore, some points were automatically excluded where they exceeded the slope tolerance defined by *TerraScan* (effectively an outlier exclusion mechanism). As the 1986 surface only covered a narrow strip of land adjacent to the cliff-face, only five check points could be utilised in the evaluation of this dataset. While the 1986 results should therefore be regarded as less reliable than those pertaining to the remaining datasets, they still provide an indication of the quality of the approximately oriented DEM, suggesting that this is the least accurate of the five surfaces. This is not surprising given the relatively poor quality of the GCPs used to orient the photography in *SocetSet*. This situation is confirmed by Figure 6.12, which depicts the relative positions of the 1986 and 1994 DEMs at this stage. This suggests that the 1986 DEM is affected by both translational and rotational offsets.

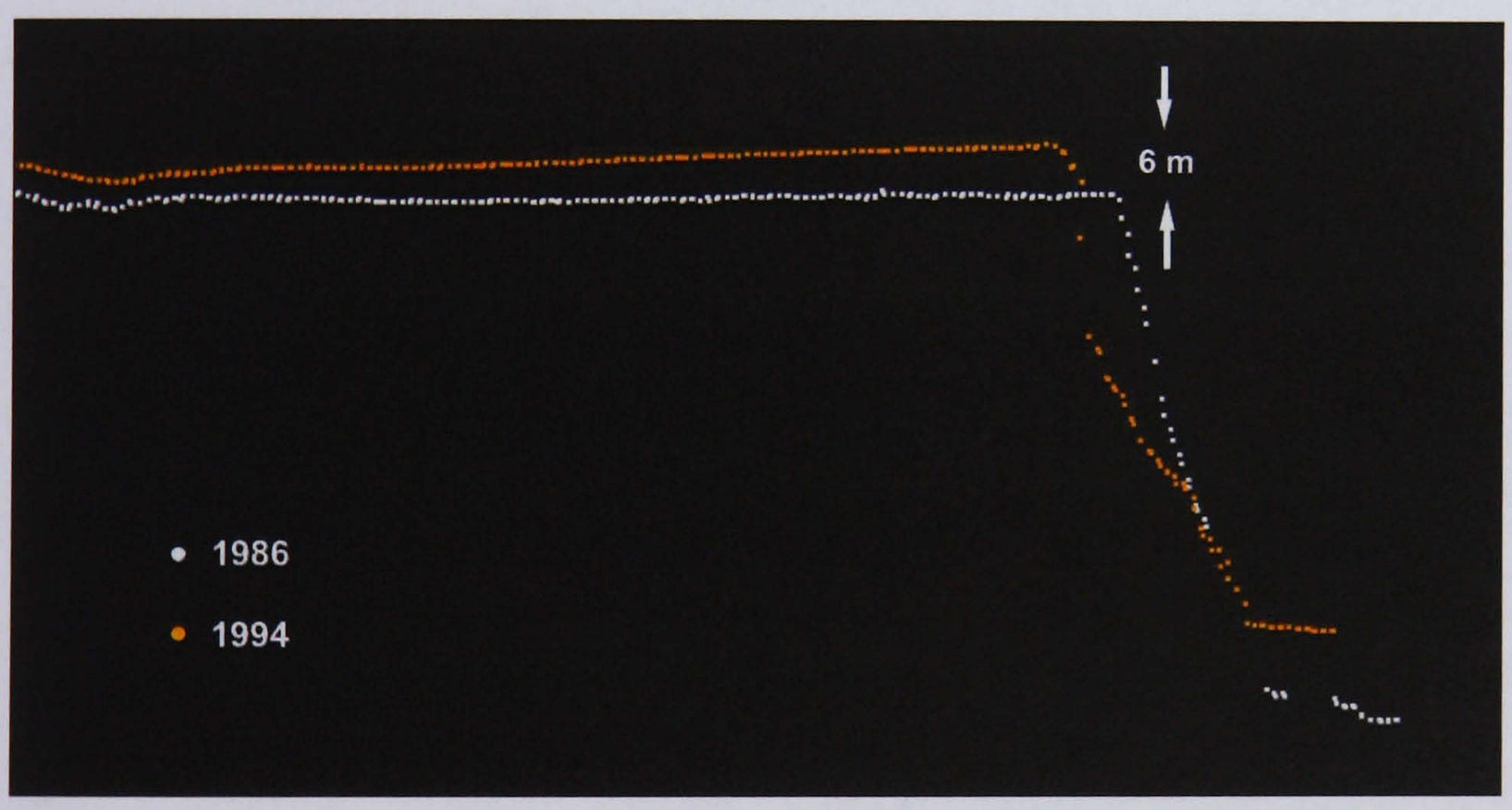

Figure 6.12 Cross-sectional view of pre-match positions of 1986 and 1994 surfaces.

Analysis of the mean discrepancies in Table 6-3 indicates that with the exception of the 1994 DEM, the other surfaces all lie slightly below the level of the GPS check points. The 1994 photogrammetric DEM is in best overall agreement, with an RMSE of 0.130 m. In terms of the ALS surfaces, the May 2006 ALS surface appears to be most accurate, and with an RMSE of 0.162 m, is approaching the accuracy of the 1994 DEM. However, the RMSE values of the April 2005 and August 2005 datasets are lower, at around 0.30 m. As the ALS surfaces lie below the check points, then these discrepancies cannot be accounted for through vegetation growth. Nevertheless, as the majority of the GPS check points were acquired at around the same time as the 1994 imagery, then it is

not possible to entirely discount the possibility that these discrepancies may be time-related to some extent. It is worth noting however, that although the independent check point analysis carried out in Section 5.4.1.2 in relation to the Filey Bay ALS data concluded that these datasets were within specification, the mean level of these surfaces was also below the GPS check points, suggesting that the ALS system may have a systematic tendency to underestimate terrain elevation.

However, these results do indicate that the 1994 photogrammetric DEM is of high quality, and consequently, this was adopted as the reference surface for subsequent surface matching.

6.5 Multi-Temporal Analysis of Geohazard Activity

6.5.1 Introduction

The episodic datasets acquired for the Whitby East Cliff test site provided an opportunity to extend the investigations carried out at Filey Bay, and further evaluate the performance of the robust matching algorithm. It was anticipated that this should enable rigorous absolute orientation of the multi-temporal DEMs, providing a reliable platform for assessing geohazard activity over the twenty-year period, 1986 to 2006.

In addition, the Whitby test site presents a distinctly different topography to Filey Bay, which formed the basis for testing in Chapter Five. The cliffs at Filey Bay vary greatly in steepness, but the average slope is around 35°. In addition, although the cliff-faces and cliff-tops are not consistently vegetated, in some regions, coverage is dense, with a number of wooded ravines. Sections 5.6 and 5.7 confirmed that the robust matching algorithm was able to accommodate this environment, facilitating reliable detection of terrain change through analysis of multi-sensor, multi-temporal datasets. Whitby is distinctly different. Whitby Abbey Headland is largely covered in short grass, and is almost completely devoid of more substantial vegetation, possibly due to its exposed location. Of greater relevance is the nature of the topography, particularly in relation to the near-vertical cliffs, and the flat cliff-top, whose local name, Abbey Plain, provides an apt description. As discussed in Section 4.3.3, the surface matching algorithm requires strong surface gradients in order to constrain the matching solution, and the

Whitby test site was identified as being likely to provide a rigorous challenge in this respect. These issues are investigated thoroughly in the following sections.

6.5.2 Robust Matching of Multi-Temporal DEMs

6.5.2.1 Surface Matching Procedure

Following assessment of dataset quality, as presented in Section 6.4, the 1994 photogrammetric DEM was selected as the most suitable reference surface for multi-temporal matching of the remaining DEMs. As the ALS datasets had been directly georeferenced through in-flight GPS-IMU, the main objective of surface matching in this regard was to provide a refined registration, which would facilitate reliable assessment of geohazard activity. Conversely, the 1986 photogrammetric DEM had only been approximately oriented in *SocetSet* and therefore, as evidenced in Table 6-3, was in relatively poor overall alignment. In this case, it was anticipated that surface matching should facilitate registration at a more fundamental level.

As discussed in Section 5.6.2.1 in relation to multi-temporal surface matching at Filey Bay, the issue of matching sequence had to be addressed. This related to whether all surfaces should be independently matched to the 1994 DEM (in keeping with the strategy adopted at Filey Bay), or whether the surfaces should be matched in temporal sequence to the 1994 DEM. For example, in the latter case, this would require matching of the April 2005 ALS dataset to the 1994 DEM, followed by matching of the August 2005 dataset to the transformed April 2005 DEM, and so on. Again, it was decided to independently match each surface to the selected reference surface, the 1994 DEM. This was mainly because the ALS surfaces generally appeared noisier than the 1994 DEM, and it was suspected that matching through temporal sequence may have resulted in a degradation of the registration solution. Given more time, it would have been desirable to explore this theory further.

Due to the vertical nature of the cliffs, matching was performed over the headland area only (Figure 6.13). The algorithm minimises vertical surface differences, and although generally well-suited to topographic applications, difficulties may arise where vertical surfaces, which have undergone change, occupy a significant portion of the input

surfaces. In order to facilitate further validation of the robust matching algorithm, matching was carried out in both robust and un-weighted modes. As already discussed, the headland area is relatively flat, and this is further illustrated by the contours in Figure 6.13. However, the western extreme of the matching area does include some steeper slopes.

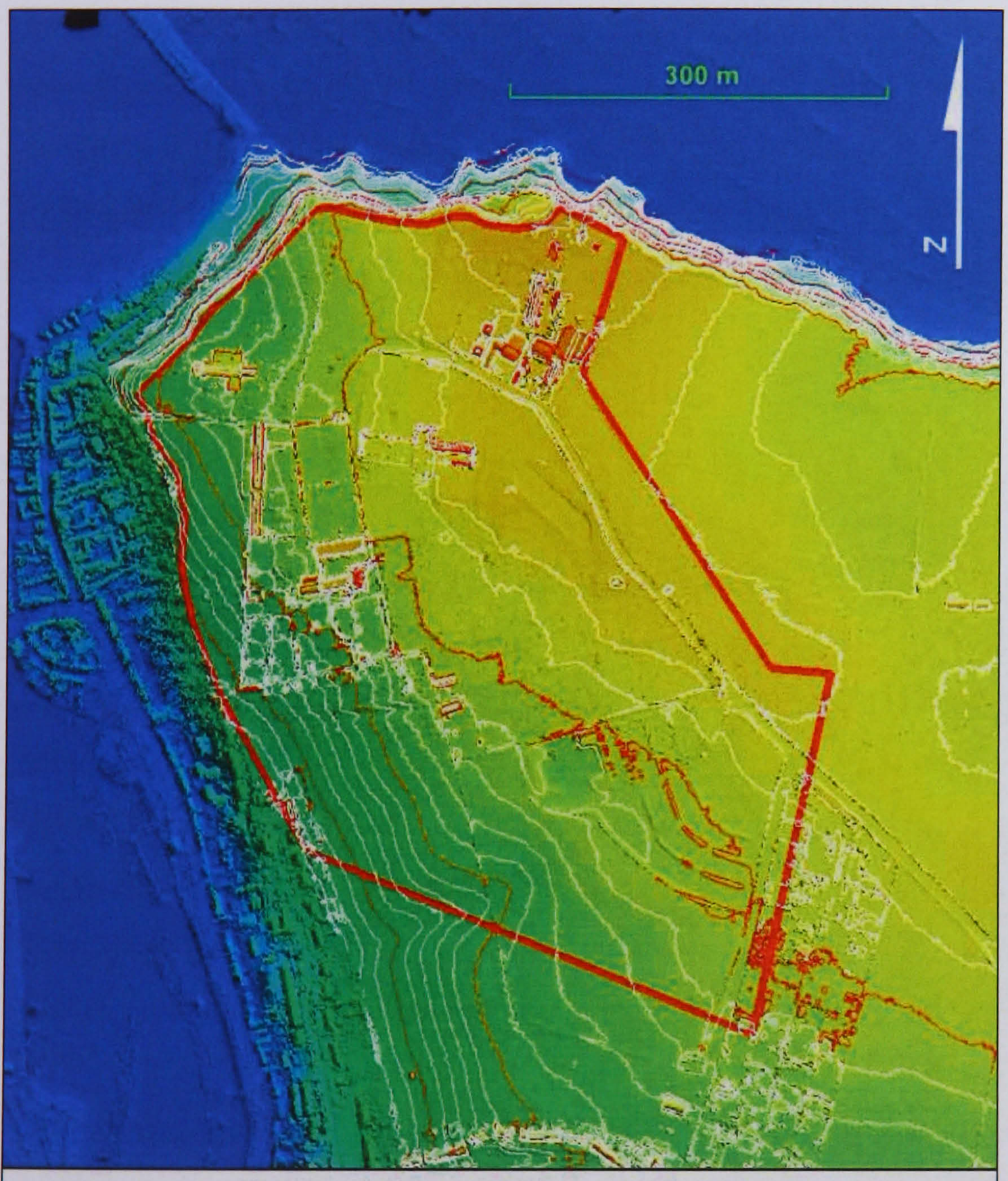

Figure 6.13 ALS-derived elevation model of Whitby Abbey Headland, with matching extent delineated (red). Contours (2 m interval) indicate the relatively flat terrain.

In the case of the ALS surfaces, surface matching proved to be relatively straightforward. However, the 1986 photogrammetric surface was initially rather troublesome, and attempts to match using the full seven-parameter transformation proved unsuccessful. However, inspection of the datasets suggested that some scale variation existed between the DEMs, and therefore, inclusion of the scale parameter was

imperative. It was decided to attempt to overcome the difficulties by adopting a two-stage approach, comprised of two separate matches. Firstly, the 1986 DEM was matched to the 1994 reference surface using six parameters (holding scale fixed), and secondly the post-match 1986 surface was matched to the 1994 DEM, applying the full seven-parameter transformation. In addition, as highlighted in Miller et al. (in review), cliff-top buildings were re-introduced to the DEMs in an attempt to incorporate improved surface gradients. This approach proved successful, and inspection of the final datasets suggested that an acceptable result had been obtained. This is analysed further in Section 6.5.2.2. The scale deficiency in the 1986 DEM may be connected to the initial poor approximate orientation in *SocetSet*. The scale error was confirmed in *SocetSet* by making comparative measurements of well-defined features in the 1986 and 1994 models.

Through their investigations into least squares surface matching, Gruen and Akça (2005) observe that in the case of poor initial approximations, the scale parameter in particular may converge to an erroneous solution. This may explain the behaviour observed here. Although the 1986 surface was initially in poor agreement with the 1994 dataset, the supplied initial approximations for the transformation parameters were all zero, and possibly these were not initially close enough to the correct values to permit a successful match to be obtained directly using all seven parameters. Instead, the overall alignment and orientation of the 1986 surface was improved through the first matching stage, allowing the scale parameter to be recovered in the second matching stage. The final matching strategies and solution details for all surfaces are provided in Table 6-4.

As discussed in Section 4.3.3, 3DSurf-*R* offers the possibility to perform either planar- or kriging-based point interpolation. In general, planar has been found to offer the most consistent results, and so was applied again here. However, where convergence could not be achieved through planar interpolation, the kriging option was used as an alternative. Kriging interpolation enabled successful un-weighted matching of the 1986 DEM at stage one (six parameters). However, an un-weighted solution could not be achieved for the August 2005 ALS surface through either interpolation strategy. This may be due to the fact that the August 2005 surface was observed as being slightly noisier than the other ALS surfaces, and this fact is reflected through the higher standard deviation of the check point discrepancies (Table 6-3). However, this

convergence failure was still rather unexpected, especially given the fact that no difficulties were encountered with the other ALS datasets.

Matching Surface	Input Parameters			Outputs	
	Weighting	**Parameters**	**Interpolation**	**Iterations**	**RMSE (m)**
1986 (6 par.)	Robust	6	Planar	19	1.688
1986 (6 par.)	None	6	Kriging	16	1.539
1986 (7 par.)	Robust	7	Planar	26	1.589
1986 (7 par.)	None	7	Planar	22	1.384
Apr. 2005	Robust	7	Planar	13	0.428
Apr. 2005	None	7	Planar	9	0.424
Aug. 2005	Robust	7	Planar	23	0.451
Aug. 2005	None	7	Planar; Kriging	No Convergence	
May 2006	Robust	7	Planar	12	0.435
May 2006	None	7	Planar	7	0.431

Table 6-4 Summary of Whitby multi-temporal matching strategies and convergence details, for robust and un-weighted matching. 1994 DEM was used as reference in each case.

As was observed in Section 5.6.2.1, the robust algorithm converged to a solution more slowly than the un-weighted version. However, this generally translated to only three or four iterations difference. As would be expected, the matching RMSE values are slightly higher for the robust solutions than the un-weighted solutions, reflecting the inclusion of outlying points. The notably larger RMSEs for the 1986 matching are a result of the re-introduction of buildings to the matching surfaces to increase surface gradients. The 1994 DEM, which was supplied by EH did not incorporate all cliff-top buildings, but only a select number. Therefore, in some areas there is a disparity between the 1986 and 1994 DEMs, where buildings exist in one surface but not the other. The final transformation parameters and associated standard deviations are detailed in Table 6-5.

Inspection of the final transformation parameters reveals that relatively large corrections were applied to the 1986 dataset at both stages in order to register this to the 1994 DEM. In particular, large translations are evident. Pâquet (2003) notes that the

Match		Final Transformation Parameters						
		$\omega^\circ \pm \sigma$	$\phi^\circ \pm \sigma$	$\kappa^\circ \pm \sigma$	T_x (m) $\pm \sigma$	T_y (m) $\pm \sigma$	T_z (m) $\pm \sigma$	$s \pm \sigma$
1986 (6 par.) Stage 1	r	1.491346 ± 0.023336	0.272480 ± 0.015879	1.004918 ± 0.042246	7.365 ± 0.462	-14.166 ± 0.740	-8.258 ± 0.377	–
	u	1.945109 ± 0.019148	0.461191 ± 0.012587	-0.517335 ± 0.049780	-9.886 ± 0.514	14.753 ± 0.935	-9.251 ± 0.302	–
1986 (7 par.) Stage 2	r	-0.057259 ± 0.024328	-0.001449 ± 0.015965	-0.296410 ± 0.076927	76.381 ± 1.323	49.787 ± 1.613	8.790 ± 0.366	0.925 ± 0.001
	u	0.507926 ± 0.018784	0.292471 ± 0.011934	-0.863317 ± 0.056107	81.972 ± 0.883	67.562 ± 1.200	8.958 ± 0.277	0.914 ± 0.001
Apr. 2005	r	0.005873 ± 0.001194	0.022419 ± 0.001627	-0.052524 ± 0.004519	0.415 ± 0.075	1.147 ± 0.098	0.639 ± 0.034	0.999 ± 0.000
	u	0.026865 ± 0.001055	0.023111 ± 0.001344	-0.062860 ± 0.002306	0.408 ± 0.049	1.201 ± 0.042	0.501 ± 0.028	0.999 ± 0.000
Aug. 2005	r	0.016824 ± 0.001417	0.012147 ± 0.001721	0.026954 ± 0.009689	0.034 ± 0.149	-0.411 ± 0.155	0.296 ± 0.039	1.000 ± 0.000
	u	No Convergence						
May 2006	r	0.015596 ± 0.001303	0.011715 ± 0.001666	0.184769 ± 0.007738	0.599 ± 0.151	-3.257 ± 0.136	0.054 ± 0.038	1.001 ± 0.000
	u	0.036322 ± 0.001086	0.011429 ± 0.001369	0.181709 ± 0.003299	0.430 ± 0.046	-3.275 ± 0.067	-0.109 ± 0.028	1.001 ± 0.000
r: robust; u: un-weighted								

Table 6-5 Final transformation parameters for multi-temporal matching at Whitby.

interactions of the transformation parameters are difficult to interpret, and the situation is complicated here by the application of the two stage transformation. While these values may seem nonsensical, inspection of the datasets indicated that good solutions had been achieved. The particularly large transformations applied in the second stage may be related to the scale alteration. The translations applied to the ALS datasets were lower, reflecting the fact that these datasets had been directly georeferenced. It is interesting to note that the standard deviations of the translations are larger in x and y, than they are in z. This is most likely due to the lack of strong surface gradients to constrain the matching in these directions. Furthermore, the robust results display slightly higher standard deviations than the un-weighted results. It is also worth noting that in relation to surface matching of ALS datasets, Maas (2002) observes that parameter standard deviation estimates are generally too low, as noise in the datasets propagates into the design matrix.

6.5.2.2 Validation of Multi-Temporal Matching Solutions

Following surface matching, the multi-temporal DEMs were transformed using the solutions presented in Table 6-5, in order to derive post-match transformed surfaces for both the robust and un-weighted matching solutions. The GPS-derived check points utilised in Section 6.4 provided an opportunity to independently assess the quality of these solutions. *TerraScan* was again used to determine the vertical check point discrepancies, and the resultant quality statistics are summarised in Table 6-6, which includes the pre-match values for reference.

Surface		No. Check Points	Check Point Vertical Quality Statistics (m)				
			Mean	σ	RMSE	Max.	Min.
Mar. 1994	Reference	17	0.023	0.132	0.130	0.260	-0.250
Mar. 1986 (final)	Pre-Match	5	-3.403	2.072	3.875	-0.194	-5.141
	Un-weighted	5	-0.009	0.396	0.354	0.569	-0.494
	Robust	4	-0.046	0.165	0.150	0.099	-0.194
Apr. 2005	Pre-Match	18	-0.314	0.152	0.347	-0.098	-0.625
	Un-weighted	19	0.004	0.178	0.173	0.436	-0.365
	Robust	20	-0.010	0.159	0.156	0.386	-0.365
Aug. 2005	Pre-Match	18	-0.255	0.206	0.324	0.126	-0.654
	Un-weighted	No Convergence					
	Robust	18	-0.003	0.211	0.205	0.399	-0.394
May 2006	Pre-Match	18	-0.060	0.155	0.162	0.142	-0.374
	Un-weighted	19	-0.037	0.158	0.158	0.217	-0.295
	Robust	19	-0.060	0.139	0.148	0.167	-0.295

Table 6-6 Summary of post-match quality statistics for robust and un-weighted matching of multi-temporal datasets.

The 1986 DEM has particularly benefited from application of surface matching, with the RMSE improving from a pre-match value of 3.875 m to a post-match (robust) value of 0.150 m. In each case, the robust algorithm has returned slightly improved results over the un-weighted version, most notably in the matching of the 1986 DEM. This is in agreement with the comparison of robust and un-weighted matching presented in Section 5.6.3.2 in relation to the Filey Bay datasets. The surface matching results are encouraging, particularly in the case of the robust algorithm, indicating that the post-match surfaces are approaching the quality of the 1994 reference DEM, with the RMSE values displaying discrepancies of only a few centimetres in nearly all cases. However, it is also important to note that these results are most likely influenced in a positive

manner by the flat topography of Whitby Abbey Headland. Nevertheless, the results serve to illustrate the value of the robust surface matching technique for absolute orientation of DEMs.

Figure 6.14 presents the check point discrepancies at each point for the April 2005 ALS pre-match and post-match surfaces. The data are plotted as linear series, as this clearly displays the relative variations between the different registration solutions, but it should be noted that the check point distribution is not continuous in manner. As explained in Section 6.4, the check points included in the analysis varied for different matching solutions and data epochs, and as a consequence the data series contain some breaks. Figure 6.14 indicates that the pre-match April 2005 ALS surface lies consistently below the level of the true ground surface.

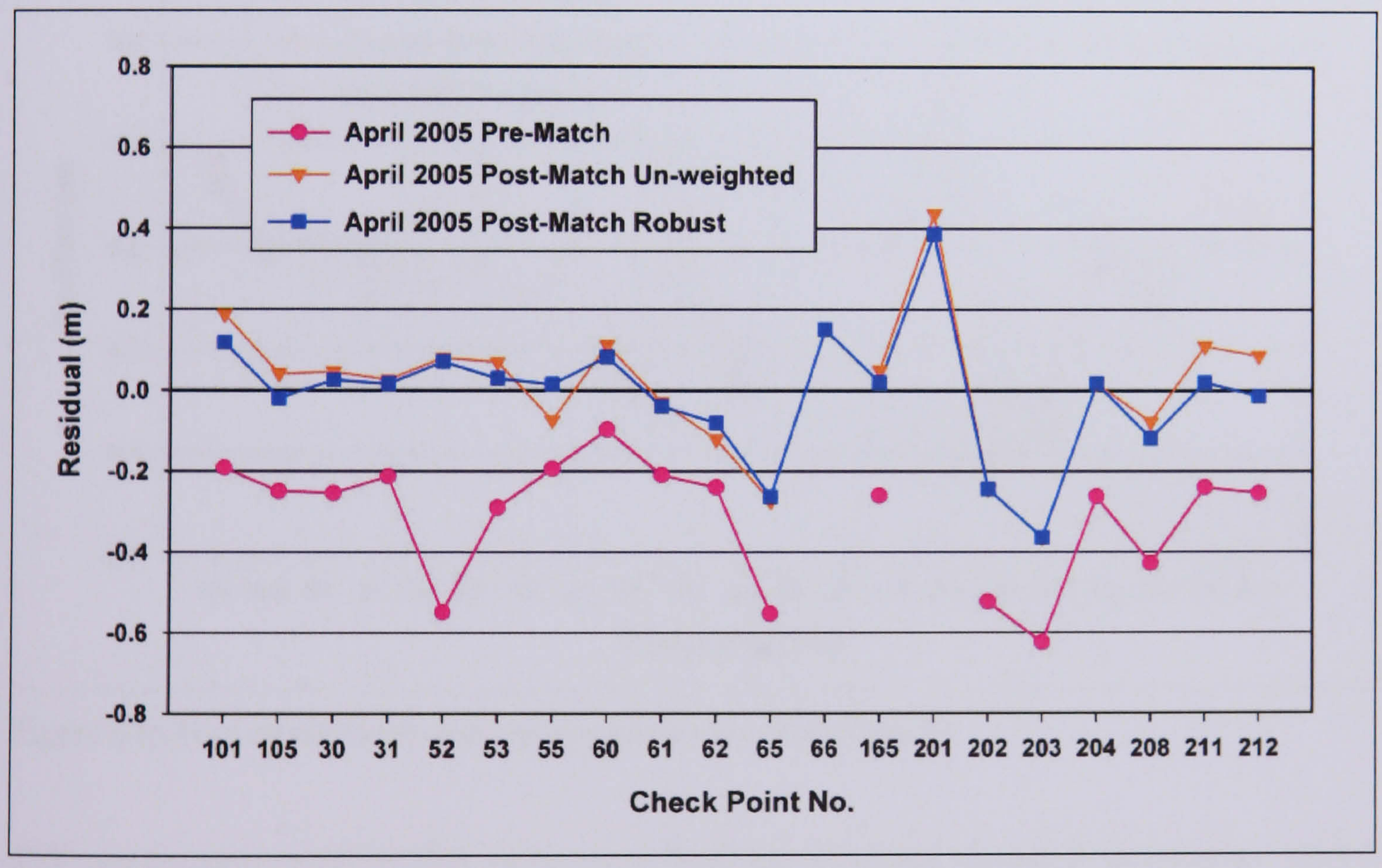

Figure 6.14 Pre- and post-match vertical check point discrepancies for April 2005 ALS surface.

The registration improvement achievable through surface matching is evident, with the DEM clearly shifted upwards, providing good overall agreement at the majority of check points, through both un-weighted and robust matching. The superiority of the robust matching algorithm over the un-weighted algorithm is also demonstrated, although at most locations, this is relatively minor in comparison to the overall improvement from the pre-match discrepancies.

Figure 6.15 details the post-match check point discrepancies for the three epochs of ALS data. This provides an indication of the discrepancies at different check points, and the consistency of the ALS DEM representations over time. The three epochs of data follow the same general trend, indicating that the surfaces are capable of delivering consistent representations of the terrain. However, certain check points, such as 201, 202, and 203, exhibit relatively large discrepancies in all three cases. This can most likely be attributed to their location, which is adjacent to the perimeter wall of Whitby Abbey (Figure 6.11). Although a ground classification was performed on the ALS datasets (refer to Section 6.3.2.1), the resultant surface model is likely to be poorer in the vicinity of structures such as high walls.

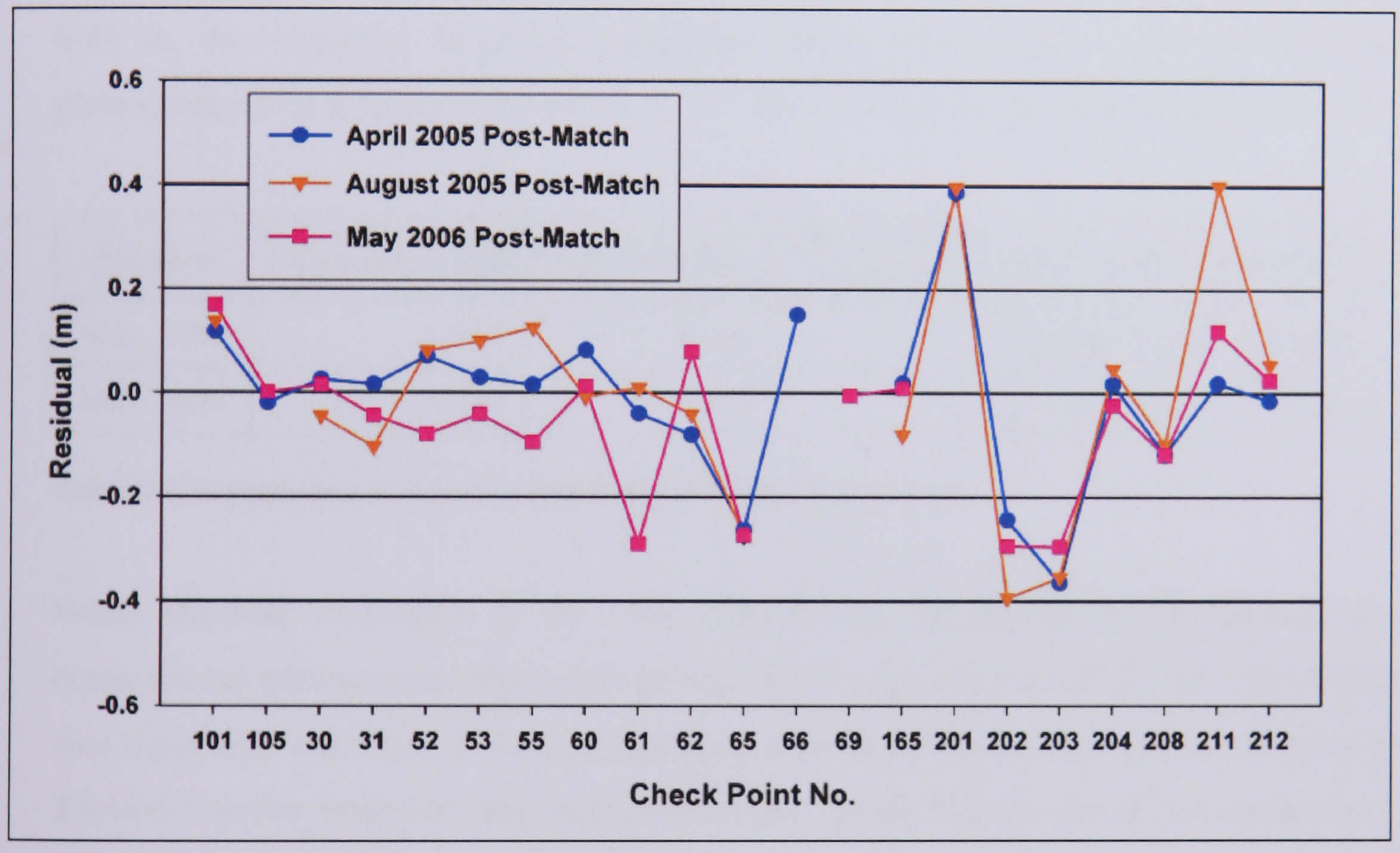

Figure 6.15 Post-match check point discrepancies for ALS datasets.

The results presented in this section confirm the findings reported in Section 5.6.3.2, demonstrating the superiority of the robust matching algorithm. In addition, it should be noted that whereas the Filey Bay historical DEMs contained extensive areas of geohazard activity over the cliff-face, the Whitby surfaces included only minor discrepancies, as matching was restricted to the cliff-top. This verifies the more generally applicability of the robust matching algorithm.

However, analysis thus far has been restricted to assessing the vertical component of ALS data quality. The difficulties associated with assessing the planimetric quality of ALS data – particularly in relation to the datasets acquired for this research – have been discussed already in Section 5.4.1.2. As the cliff-top at Whitby contained a number of buildings, it was initially hoped that this may provide a viable means of assessing planimetric quality, through comparison of features such as roofs or walls. However, once again, the resolution of the datasets prevented this. Consequently, evaluation was restricted to analysis of vertical quality only, reaffirming the difficulties associated with retrospective assessment of planimetric error in ALS datasets.

At this juncture, it is possible to compare the results of the check point analysis (Table 6-6) to the expected heighting precision values which were calculated for the photogrammetric datasets in Section 6.3.2.2. These values are summarised in Table 6-7.

Surface	Expected σ_h (m)	Actual σ_h (m)	No. of Check Points	Orientation Method
Mar. 1986	0.062	0.165	4	robust surface matching
Mar. 1994	0.067	0.132	17	conventional GCP-based

Table 6-7 Comparison of expected and attained heighting precisions.

While absolute orientation of the 1994 dataset was carried out by EH through the conventional photogrammetric route (using GCPs acquired via GPS), the 1986 DEM was rigorously oriented via surface matching (the robust matching value is reported in Table 6-7 as this represents the highest precision value). The results of this comparison (Table 6-7) indicate that in both cases, the achieved precisions are lower than the expected values. However, the theoretical values represent the ideal case, and the relatively large scale of the imagery – 1:5,300 (1986) and 1:1,600 (1994) – has resulted in relatively high estimates. In reality however, it would be difficult to attain this level of precision, and this has proved to be the case here. A further observation is that the attained precision of the 1986 DEM is slightly poorer than that of the 1994 DEM. However, for the reasons explained in Section 6.4, only a limited number of check points (four in this case) were available for assessment of the 1986 dataset, and consequently, this value must be treated with caution, and regarded only as an approximate indicator of quality.

6.5.3 Assessment of Geohazard Activity 1994 – 2006

6.5.3.1 Preparation and Pre-Analysis of Inter-Epoch Change Surfaces

Following analysis of the quality of the post-match surfaces, the transformed surfaces arising from robust matching were utilised for evaluation of geohazard activity. Although surface matching had only been performed over the cliff-top areas, the post-match transformations were applied to the complete surfaces, including the cliff-face region comprising the test site.

During visual inspection of the surfaces in their post-match, registered positions, it became apparent that the 1986 surface exhibited inconsistencies over the cliff-face in relation to the other surfaces. While the manually edited region around the cliff edge in the 1986 DEM appeared to deliver a faithful representation of the terrain, parts of the upper cliff-face for which elevations had been interpolated in *SocetSet* (refer to Section 6.3.2.2), were less reliable. Consequently, it was decided that the 1986 dataset should be excluded from analysis of inter-epoch change across the cliff-face. However, this dataset is utilised in Section 6.5.4 for assessment of cliff-edge change.

In the case of the Filey Bay datasets, change was examined through computation of vertical surface differences. However, due to the vertical nature of Whitby East Cliff, this approach would have been meaningless, and it was deemed more appropriate to examine multi-temporal change in the direction normal to the cliff-face. This also corresponds to the general direction of cliff retreat at the site. However, this approach presented some difficulties in terms of data handling. *LSS* was used to perform this change analysis, through calculation of level differences between the multi-temporal surfaces (as described in Section 5.6.2.2). However, initially, the y and z axes had to be swapped, and the cliff-face then had to be rotated to align it with the x-axis, in order to ensure that the 'vertical' differences computed by *LSS* were in the direction which was approximately normal to the cliff-face. Following the surface difference calculations, the data was then transformed from this local reference system back to the original UTM coordinates. This was a rather convoluted procedure, and highlighted some of the difficulties associated with analysis of coastal datasets – an issue which is discussed further in Section 7.2.4.

Inter-epoch change was examined in a sequential manner between surfaces adjacent in time, and histograms were produced in order to further analyse the differences (Figure 6.16). As would be anticipated, the histograms indicate that the greatest amount of change occurred over the longest time period, March 1994–April 2005. Negative change dominates this inter-epoch change period (March 1994–April 2005), and it is likely that some of this corresponds to the major cliff failure referred to in Section 6.2.1.

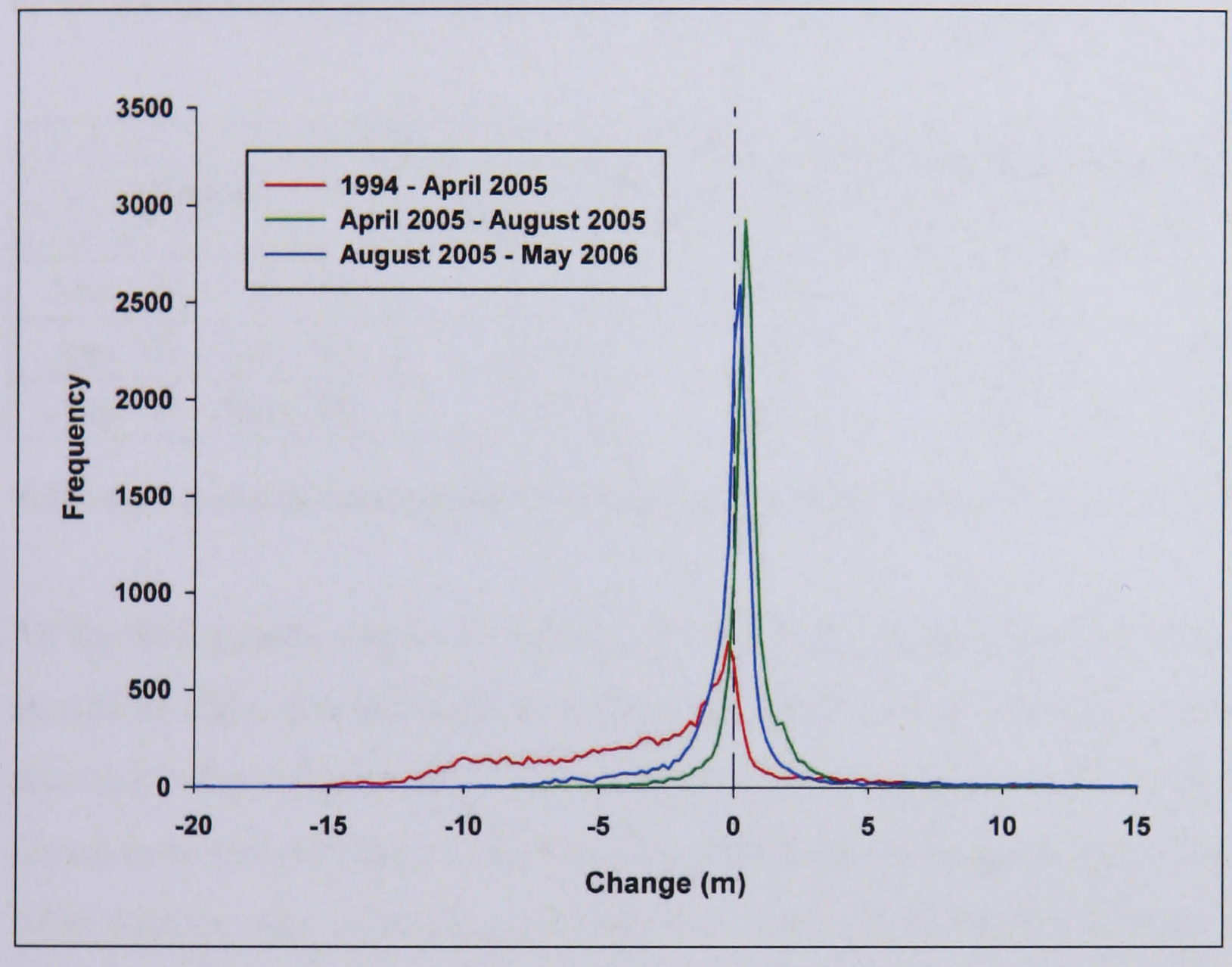

Figure 6.16 Histograms of inter-epoch cliff-face change at Whitby East Cliff.

The April 2005–August 2005 and August 2005–May 2006 histograms of change suggest that the majority of change has occurred at a relatively minor level, primarily clustered around zero. However, upon close inspection of Figure 6.16, it can be seen that in the case of the April 2005–August 2005 histogram, most of the change is positive, including the data peak. This suggests that positive change has occurred across extensive areas of the cliff-face. However, this is unlikely, as the cliff-face is near vertical, devoid of vegetation, and composed of hard rock. Although minor pockets of positive change may occur where eroded debris is deposited on rock ledges or at the cliff-toe, over a relatively short four month period such as this, it would be expected that most areas of the cliff-face will remain unchanged. This suggests the presence of planimetric error.

For the April 2005–August 2005 histogram, the peak value is 0.40 m, suggesting that this may correspond to the approximate mean magnitude of planimetric error between the datasets. This is further supported through examination of the level difference statistics for the inter-epoch surfaces (Table 6-8), which indicates that the mean difference between the April 2005 and August 2005 surfaces is 0.504 m. The peak of the August 2005–May 2006 histogram lies at 0.06 m, indicating that the planimetric registration for these two surfaces may be considerably better. This corresponds closely to the mean difference value of 0.037 m, as detailed in Table 6-8.

Period	Level Difference Statistics (m)				
	Mean	σ	RMSE	Max.	Min.
Mar. '94 – Apr. '05	-3.072	4.710	5.624	35.547	-20.251
Apr. '05 – Aug. '05	0.504	1.262	1.359	12.945	-16.166
Aug. '05 – May '06	0.037	2.630	2.630	17.675	-12.429

Table 6-8 Level difference statistics for inter-epoch change across Whitby East Cliff.

As the histograms and level difference statistics evaluate relative change between two epochs of data, it is difficult to determine which surface is in error, and the possibility also exists that both surfaces may contain error. However, as the August 2005 DEM is common to two epochs of change, and appears to be in good agreement with the May 2006 dataset, this would suggest that the April 2005 surface is most likely to be the primary source of the discrepancy. This implies that the March 1994–April 2005 dataset may also be affected to some extent.

Further inspection of the datasets suggested that possible planimetric offsets also existed in the pre-match datasets, as illustrated in Figure 6.17. In particular, the May 2006 pre-match dataset exhibits a possible seaward shift in relation to the two earlier epochs of data. This at least suggested that planimetric offsets had not necessarily been induced by the application of surface matching, and visual analysis suggests that surface matching may actually have reduced, although not necessarily eliminated, this offset.

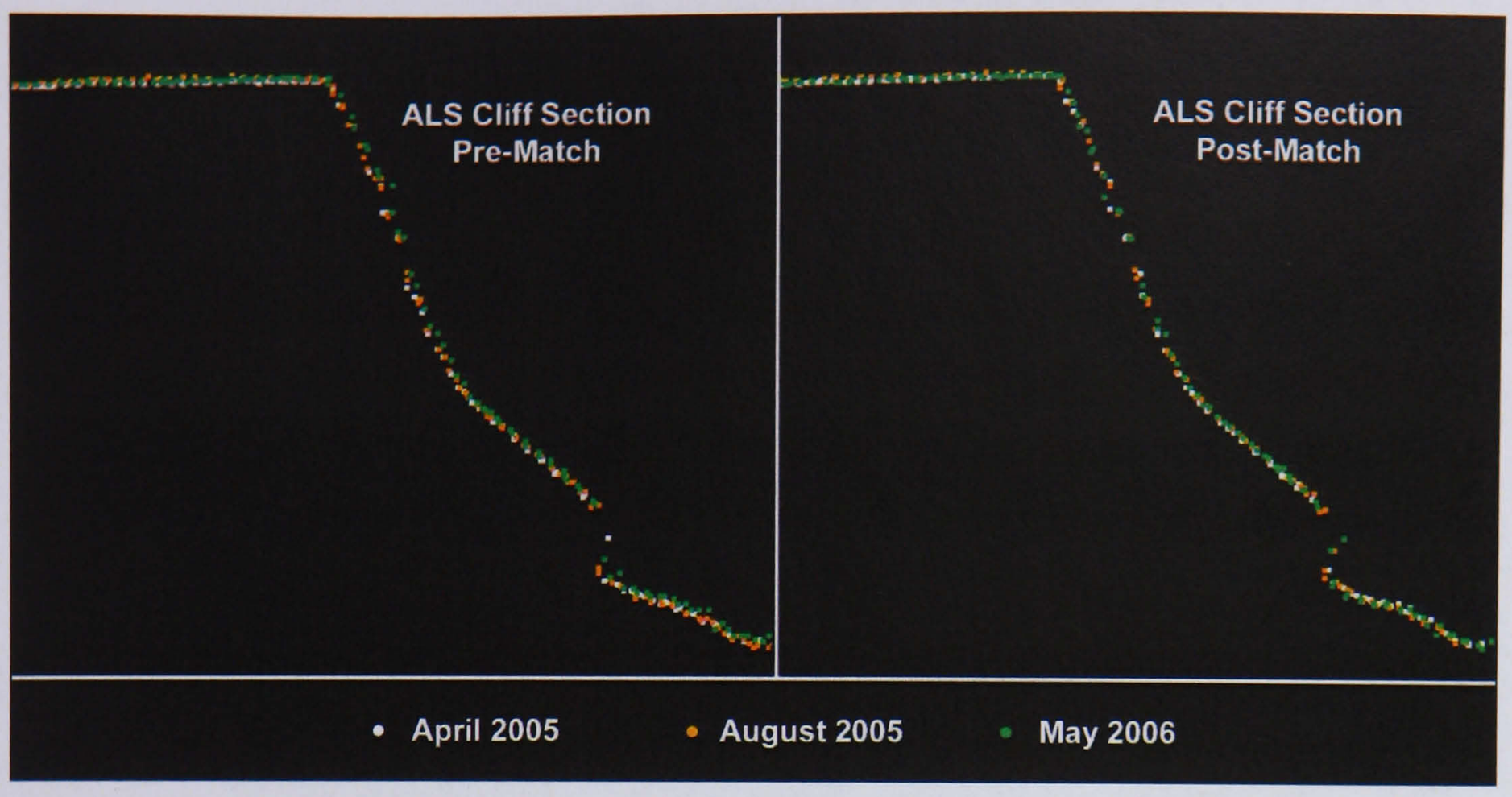

Figure 6.17 Pre- and post-match cliff sections through ALS datasets, with the May 2006 pre-match dataset illustrating a potential planimetric offset.

As detailed in Section 3.3.1.1, the manufacturer's specified planimetric accuracy is $< 1/2000 \times$ *flying height*. For the Whitby datasets, this translates to a value of < 0.50 m. Although it was not possible to rigorously evaluate the planimetric quality of the ALS datasets either at this site, or indeed at Filey Bay, visual inspection suggested that the accuracy was markedly better than 0.50 m, as no offsets were immediately evident between flightlines or multi-temporal datasets. However, this accuracy specification does convey the limitations in terms of the potential planimetric quality of ALS datasets. Surface matching may have improved the overall planimetric quality of the three epochs of ALS data, but the lack of strong surface gradients over the cliff-top may have limited improvements in this regard.

6.5.3.2 Visualisation and Assessment of Inter-Epoch Change

ESRI ArcGIS software was used to visualise inter-epoch change over the cliff-face at Whitby (refer to Section 5.6.4.1). Maps of change are presented in Figure 6.18. Classification is based on the *ArcGIS* standard deviation option, which provides an effective means of highlighting the regions of greatest difference, which in this case, are most significant. As the planimetric quality of the datasets could not be quantitatively assessed, it was not possible to determine confidence limits for change analysis. However, given the analysis of the probable planimetric shifts discussed in Section 6.5.3.1 in relation to the histograms of change, it is likely that all but the most minor of

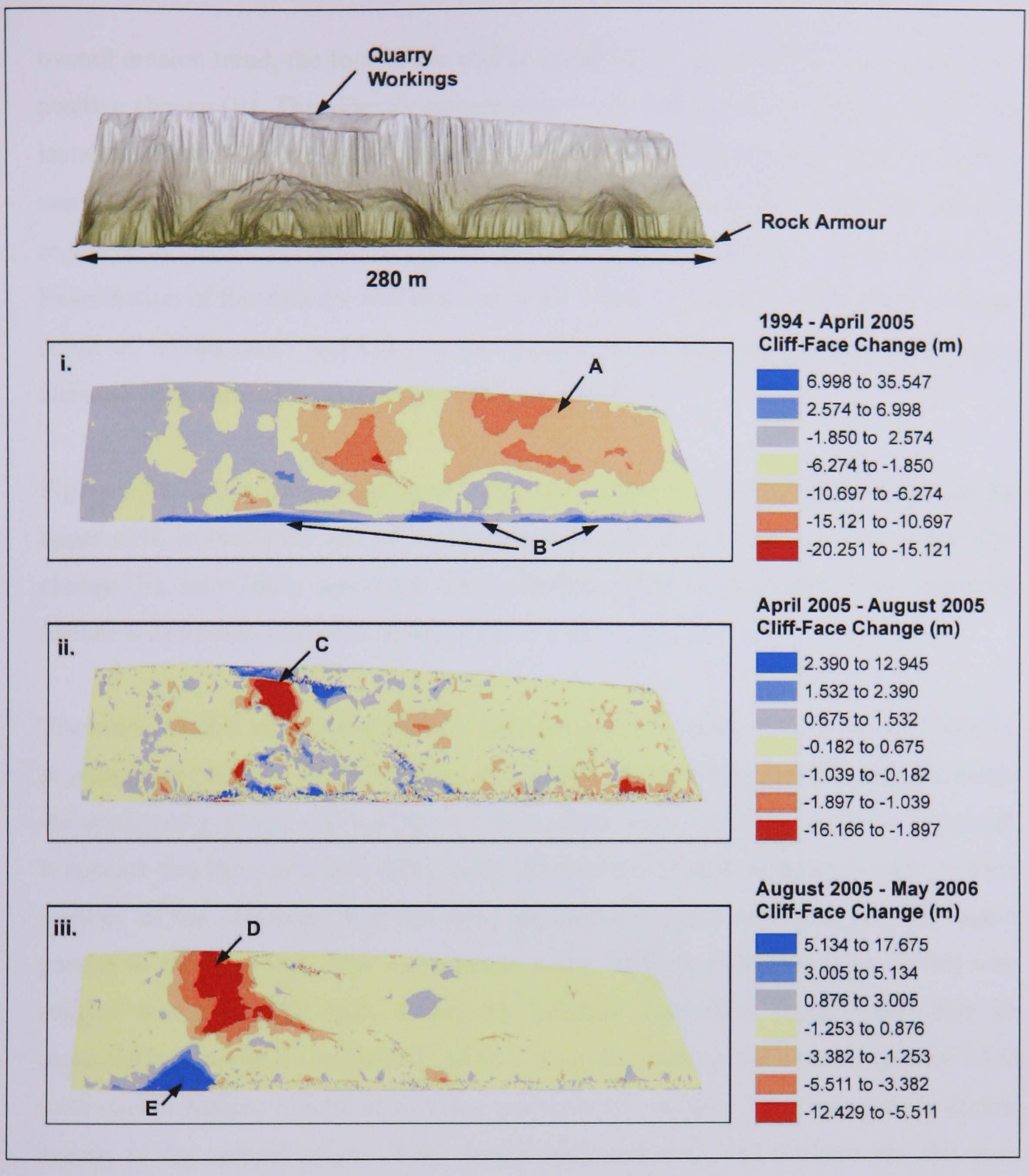

Figure 6.18 Multi-temporal change over Whitby cliff-face, with rendered model of cliff-face included (top) for reference.

difference classes in Figure 6.18 correspond to real areas of geohazard activity. This is further supported by the systematic spatial concentrations of change across the cliff-face. Figure 6.18 (i) depicts change between March 1994 and April 2005, revealing net loss over nearly the entire cliff-face during this period. A number of features are particularly notable. Firstly, loss over the extended region indicated at 'A', corresponds to the location of the major cliff failure which is documented as occurring in October 2000 (Jennings et al., 2002) (refer to Section 6.2.1). In addition, another large region of erosion is evident immediately beneath the old quarry workings. In contrast to the

overall erosion trend, the foot of the cliff is occupied by a narrow horizontal section of positive change (B). This directly corresponds to the rock armour revetment which was installed in 2001. Figure 6.18 (ii) and (iii), reveal more fragmented patterns of change, associated with shorter-term activity. Between April and August 2005, the primary region of difference is concentrated beneath the quarry workings (C), on the upper cliff. Examination of the datasets revealed that some of the more minor differences were the result of 'shadowing', highlighting the weaknesses of change detection based upon airborne-only datasets in an environment such as this.

Figure 6.18 (iii) is dominated by a significant region of erosion (D), located on the upper cliff, immediately left of the quarry workings. Below this, an area of positive change (E), most likely represents corresponding debris accumulation. This geohazard feature is examined further in Section 6.5.3.3 and Section 6.5.3.4.

The rendered cliff model (Figure 6.18, top), produced from the May 2006 ALS dataset, provides some context for the patterns of cliff-face change. Most notably, this illustrates the small embayments and headlands, which characterise the lower portion of the cliff. It appears that there is a link between the distribution of cliff recession events, and the geology of the cliff-face, with the most significant erosion occurring over the upper portion of the cliff-face. This corresponds to the findings of Rosser et al. (2005) who suggest that individual beds within the Saltwick Formation (upper cliff) may be particularly susceptible to failure, with a zone of bedding between 41 m and 52 m (orthometric height) identified as being particularly unstable. This corresponds almost exactly to the vertical extent of the failure indicated at C, and furthermore, this may have initiated the subsequent adjacent collapse at D. Again, this is in agreement with the observations of Rosser et al. (2005), who suggest that failure events are spatially linked, with the removal of a particular block detrimentally affecting the stability of an adjacent region.

Although Figure 6.18 (i) provides an indication of the scale of geohazard activity affecting Whitby East Cliff over this eleven year period, the shorter inter-epoch periods, corresponding to Figure 6.18 (ii) and (iii) are possibly more useful for investigating individual geohazard events, and may offer a more meaningful contribution towards understanding the failure mechanisms associated with this environment. However, as

highlighted in Section 6.5.3.1, there remain issues associated with the planimetric accuracy of ALS data, and these will be discussed further in Section 7.2.1.1.

6.5.3.3 Profile-Based Analysis of Change

Cliff-normal profiles were derived for the locations indicated in Figure 6.19 in order to examine the nature of cliff retreat in these areas. The resultant profiles are illustrated in Figure 6.20. Profile 1 transects the cliff failure and associated debris pile shown in Figure 6.18 (iii) at D and E. This indicates that this area remained relatively stable between March 1994 and August 2005, with the only discernable sign of change being that which is associated with the instalment of rock armour at the cliff-toe. Between August 2005 and May 2006 however, there has been a failure of the upper cliff, with the cliff-face retreating by up to 6 m. It appears that the resultant debris has accumulated over the base of the cliff.

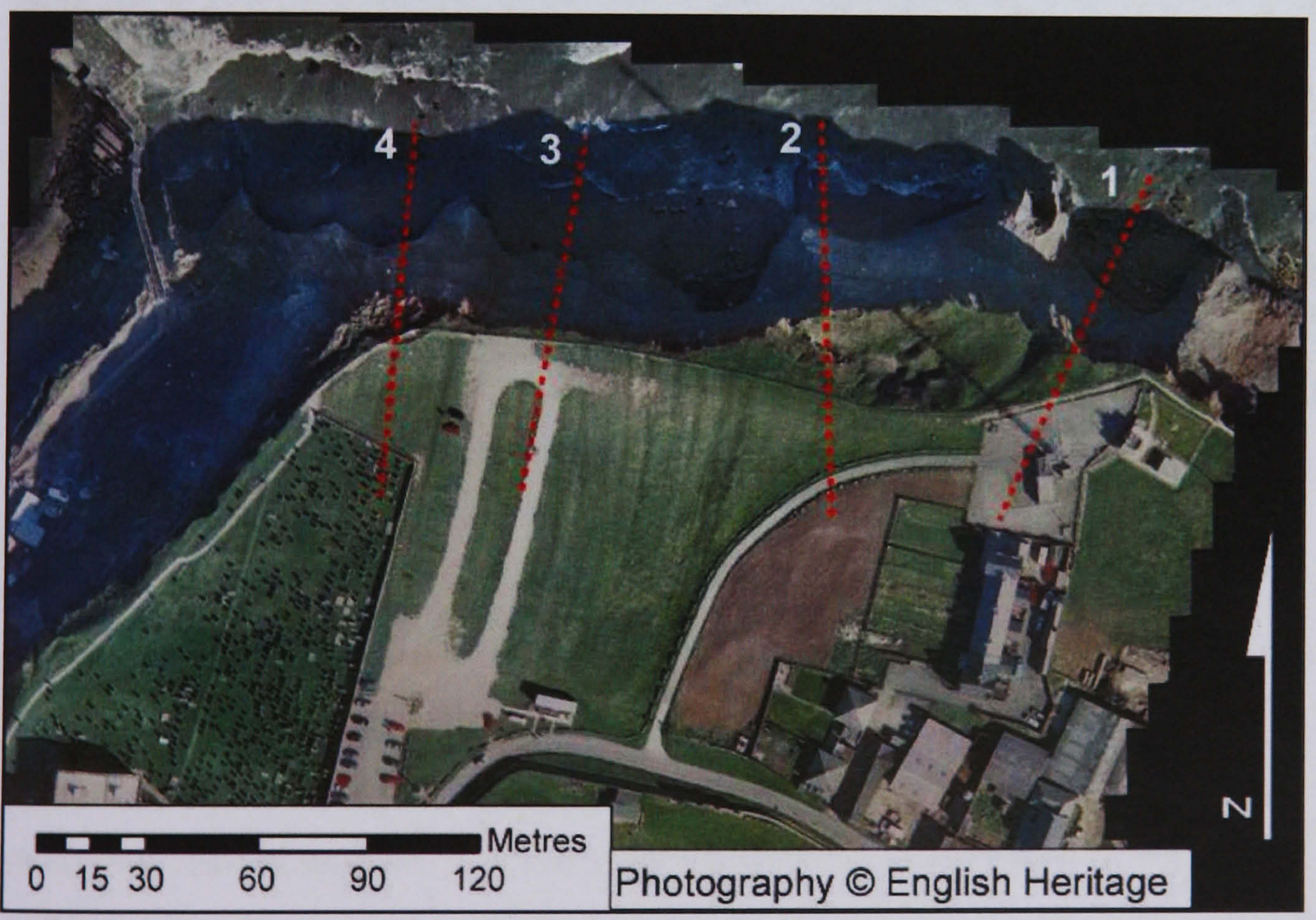

Figure 6.19 Profile locations depicted against 1994 ortho-image.

Profile 2 (Figure 6.20) passes through the western edge of the abandoned quarry workings on the cliff-top, and it is evident that while this area has been relatively dormant between April 2005 and May 2006, considerable retreat occurred between March 1994 and April 2005. This has resulted in a near parallel recession of the upper

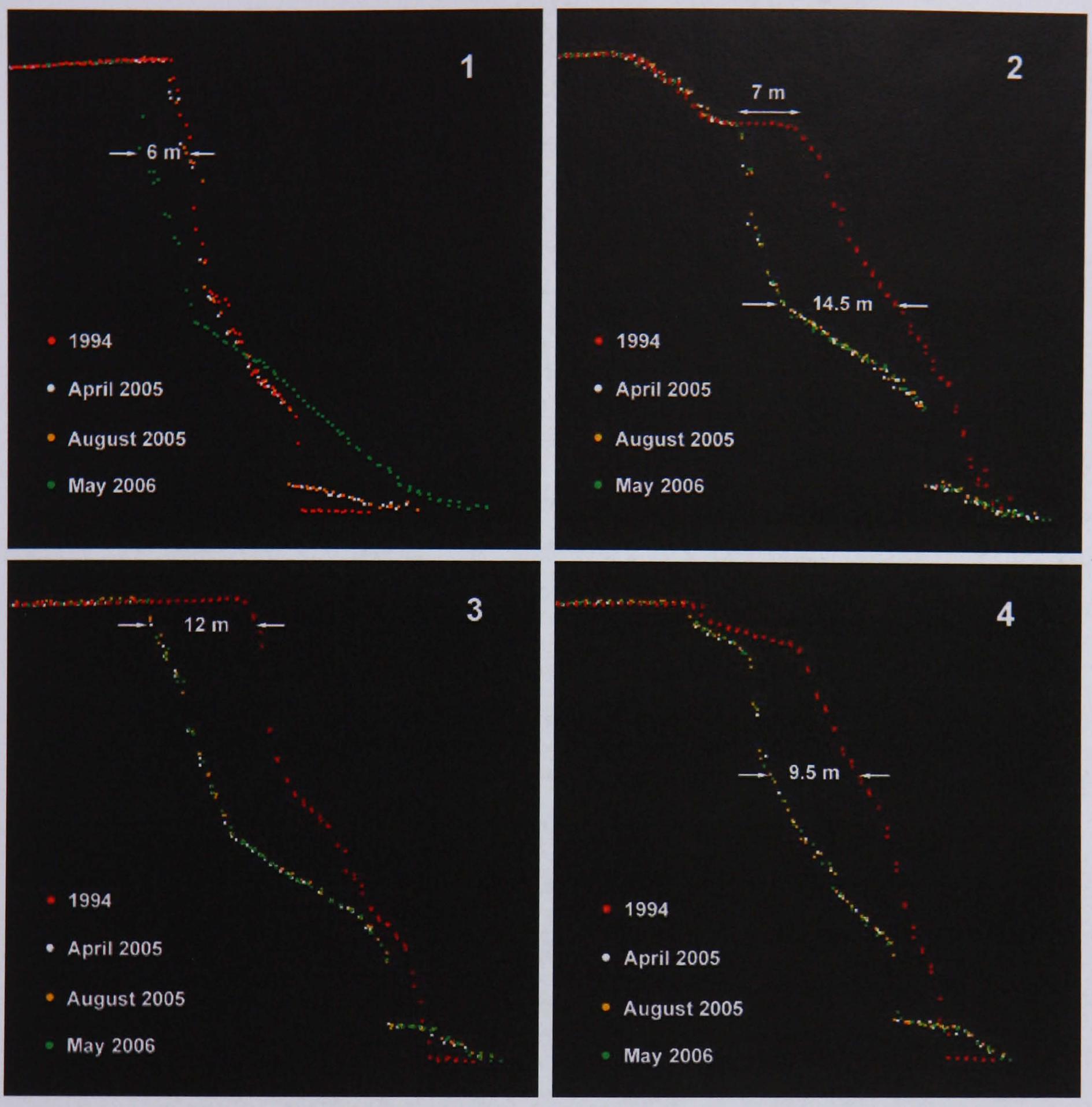

Figure 6.20 Profiles illustrating cliff-face change at selected locations.

cliff-face, although the lower portion of the cliff has also undergone erosion to a lesser extent. Interestingly, erosion has also affected the quarry, with 7 m of recession affecting the quarry ledge. This area of erosion is apparent in Figure 6.18 (i), and the more recent activity affecting the eastern end of the quarry workings (Figure 6.18, features C and D) suggests that this region may be relatively unstable. Profile 3 (Figure 6.20) reveals change to the cliff-face in the vicinity of the October 2000 cliff failure. However, it is unclear whether all of the material lost over the upper cliff in this area between March 1994 and April 2005 was associated with this single event. In any case, as Figure 6.20 (3) indicates, the upper cliff has again retreated in a near-parallel manner over this period, with 12 m of erosion at the cliff-top. The lower cliff is occupied by one of the small headlands, which appears more resistant to erosion. Profile 4 is located at

the extreme western end of the test site, close to the East Pier (Figure 6.19). Again, parallel retreat has occurred over the upper cliff between March 1994 and April 2005, with up to 9.5 m of recession (Figure 6.20).

These profiles would appear to indicate that for the period March 1994 to May 2006, the majority of geohazard activity has occurred over the middle and western section of Whitby East Cliff, with extended retreat of the upper cliff, corresponding to the geology of the Saltwick Formation. It is interesting to contrast the 1994 profile of the cliff-face to that of the more recent datasets. As Figure 6.20 illustrates, in 1994 the cliff-face was generally inclined at a consistent angle (approximately 64°), and could be considered as being of a single angular unit. However, more recently, differential erosion has altered the general profile, leading in some cases to the development of differing angular units over the upper and lower cliff-face. This is particularly evident in profiles 2 and 3. The lower cliff generally appears to be more resistant to erosion. The single inter-epoch period, March 1994 to April 2005, is insufficient to determine whether the rock armour has had any impact on reducing marine erosion of the cliff-toe. No clear evidence of geohazard activity affecting this zone could be identified between April 2005 and May 2006, but again, this period of monitoring is insufficient for any conclusions to be reached in this regard.

6.5.3.4 Volumetric Analysis of Change

As a final quantitative assessment of multi-temporal geohazard activity at Whitby East Cliff, volumetric change was determined for the periods March 1994–April 2005, April 2005–August 2005, and August 2005–May 2006. Again, *LSS* was used to perform this analysis, as described in Section 5.6.4.2. Thus far in Section 6.5.3, there has been evidence to suggest that geohazard activity may be more prolific over the upper cliff, in correspondence with the geology of the Saltwick Formation. This was investigated further here by calculating volumetric change separately for the upper and lower cliff, introducing a division which approximately corresponds to the boundary of the Whitby Mudstones group (lower cliff), and the Saltwick Formation (upper cliff), as indicated in Figure 6.21. Volumetric change was also calculated over the cliff-face as a whole, which equates to an area of approximately 14,000 m^2. The results of this analysis are presented in Figure 6.22.

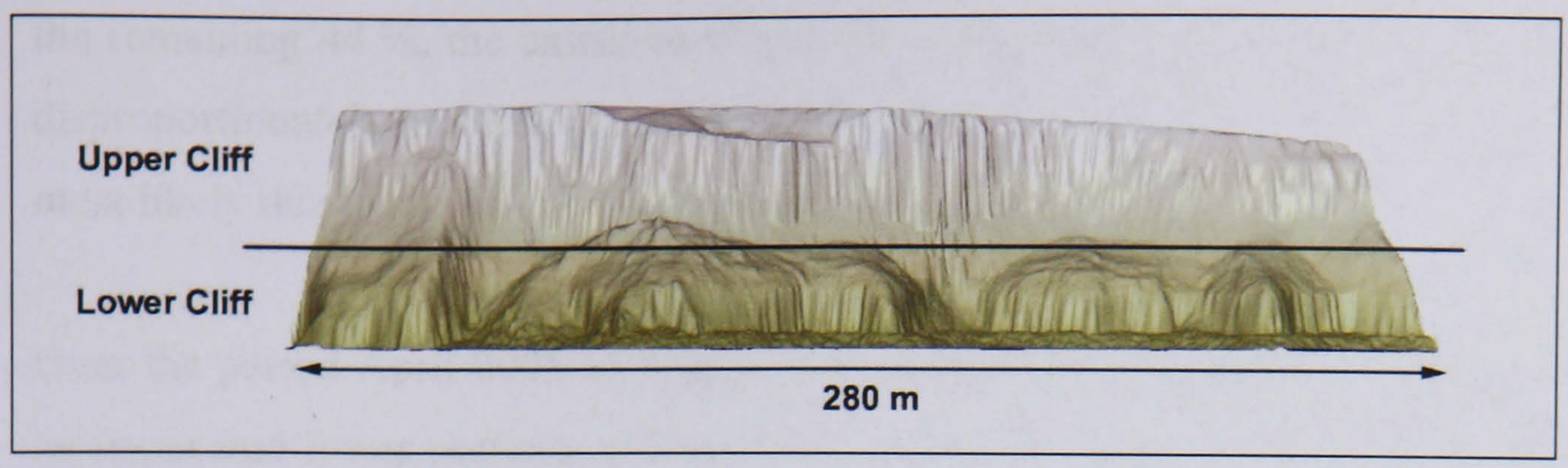

Figure 6.21 Division of upper and lower cliff for volumetric change analysis.

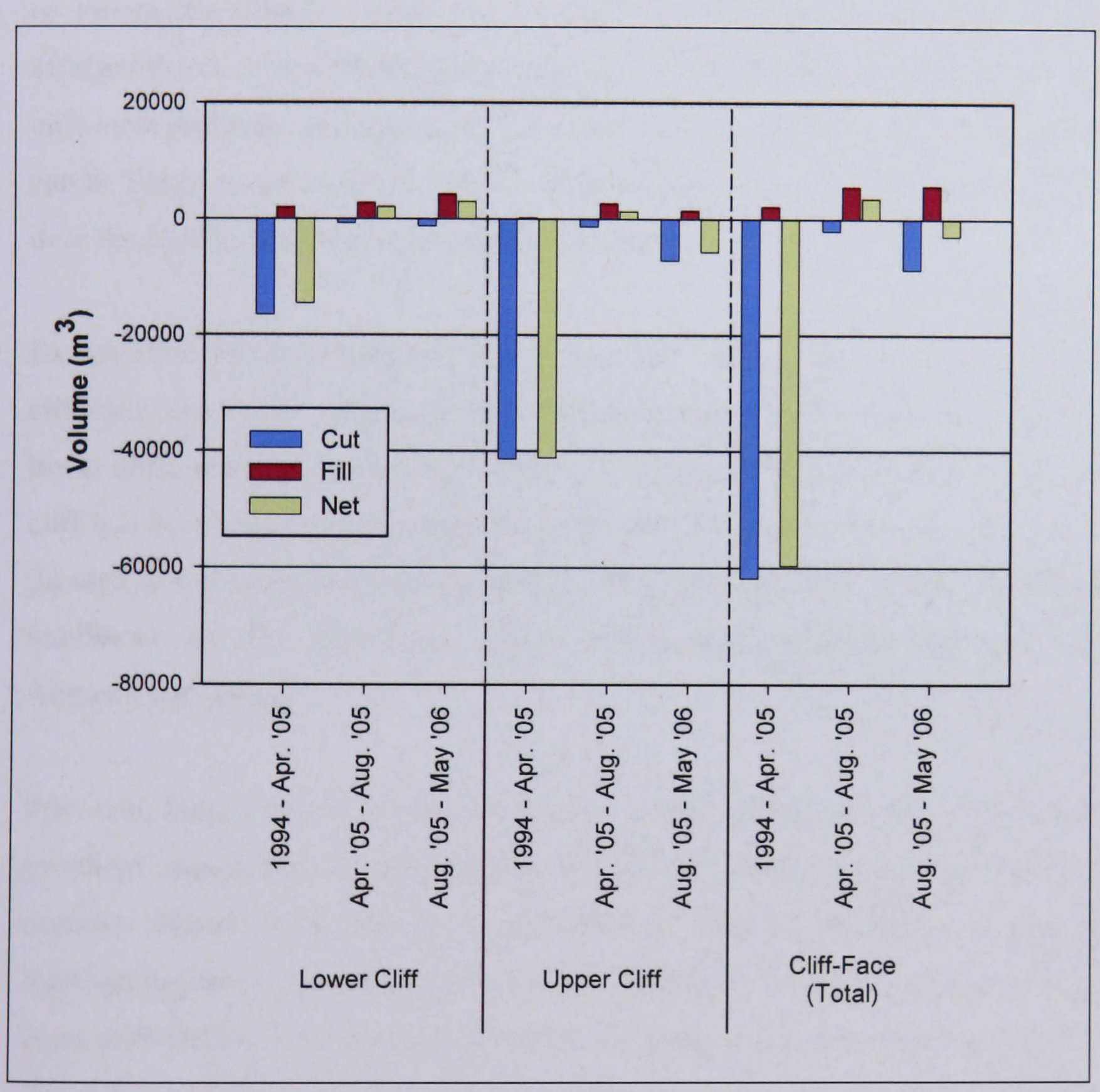

Figure 6.22 Inter-epoch volumetric change for lower cliff, upper cliff, and cliff-face as a whole.

As would be expected, the greatest volumetric change is associated with the longest inter-epoch period, 1994 to April 2005. In agreement with earlier analysis (e.g. Figure 6.16), this period is dominated by negative change, and it is evident that this has affected the upper cliff to a greater extent than the lower cliff. However, as the upper cliff occupies approximately 56 % of the total area, while the lower cliff accounts for

the remaining 44 %, the extent to which the upper cliff is affected would appear to be disproportionately greater. The fill volume (1999 m^3) associated with the lower cliff, is most likely due to the installation of rock armour in 2001.

Over the period April 2005 to August 2005, net positive change is recorded over both he upper and lower sections of the cliff-face. This is likely to be a direct reflection of the planimetric offset discussed in Section 6.5.3.1, and should therefore be considered as erroneous. The final inter-epoch period, August 2005 to May 2006 reveals a pattern of volumetric change which can be primarily attributed to the cliff failure which affected the eastern extreme of the cliff-face during this period. Net loss over the upper cliff most probably corresponds to the failed material, while net gain over the lower cliff can be linked to the associated debris accumulation zone. Overall, net loss has occurred over the cliff-face in its entirety during this period.

Examination of net volumetric change between March 1994 and May 2006, over the cliff-face as a whole, revealed that of the total material lost, 18 % originated from the lower cliff, while 82 % was derived from the upper cliff, thus confirming that the upper cliff has been more severely affected by geohazard activity. These values were derived through direct comparison of the March 1994 and May 2006 DEMs, and therefore are unaffected by the planimetric errors which have contaminated the April 2005–August 2005 dataset.

The cliff failure which occurred between August 2005 and May 2006 provided an excellent opportunity for targeted investigation of geohazard activity (Miller et al., in review). Figure 6.23 depicts an *LSS*-derived map of change over the cliff-face, highlighting areas of positive and negative difference. Before diverting attention to the main cliff failure, it is worth commenting on some anomalous features. These relate to the patterns of change associated with the region of rock armour at the foot of the cliff, and the lower edge of the abandoned quarry workings at the cliff-top. These features are not well suited to analysis of change in the direct normal to the cliff, and consequently, the resultant multi-temporal differences in these regions are somewhat misleading. The main cliff failure is highlighted in Figure 6.23. It can be seen that this has affected the full extent of the cliff, with the area of failure extending both downwards and laterally

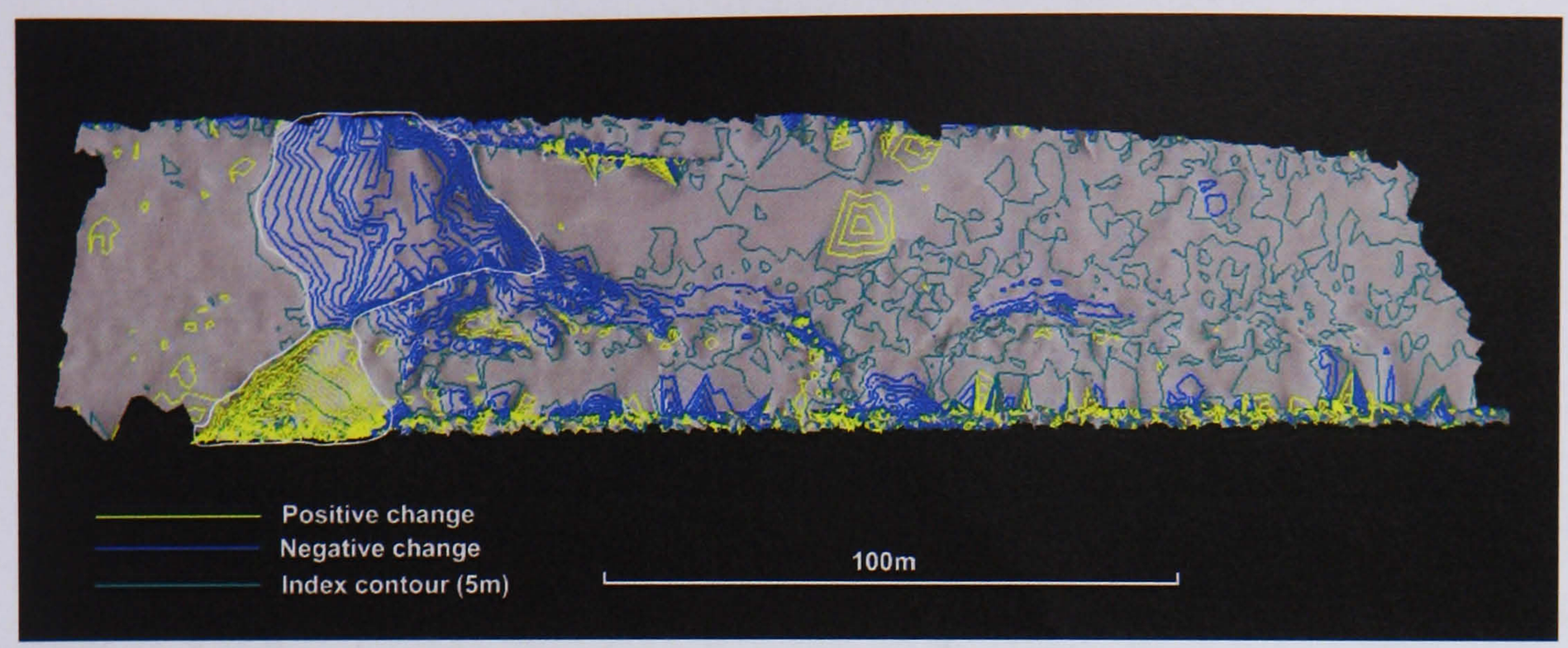

Figure 6.23 Map of cliff-face change, August 2005-May 2006, with primary failure area outlined (Miller et al., in review).

across the upper-cliff to the top of the small headland, while the failed material appears to have accumulated in a cone extending over the lower cliff to the cliff-toe. A field visit to the site in March 2007 verified this geohazard feature, with the failed material depicted in Figure 6.24. Larger blocks are evident around the base of the debris pile. These likely originated from the uppermost section of the cliff, immediately below the glacial till cap of the cliff-top (Figure 6.25).

Volumetric analysis of change, confined to the highlighted extents of the failure and debris area (Figure 6.23), was performed in *LSS*. This revealed that 6,198 m^3 of material was lost from the cliff-face, while 2,645 m^3 was deposited, resulting in a net loss of 3,553 m^3. This would indicate that a considerable portion of the failed material has been removed through marine erosion of the cliff-toe. This is certainly possible, as this failure occurred just outside the section of cliff-toe protected by rock armour. This is supported by the observations of Rosser et al. (2005), who conclude that failed material is rapidly removed from the cliff-toe by wave action.

Figure 6.24 Debris from cliff failure highlighted in Figure 6.23.

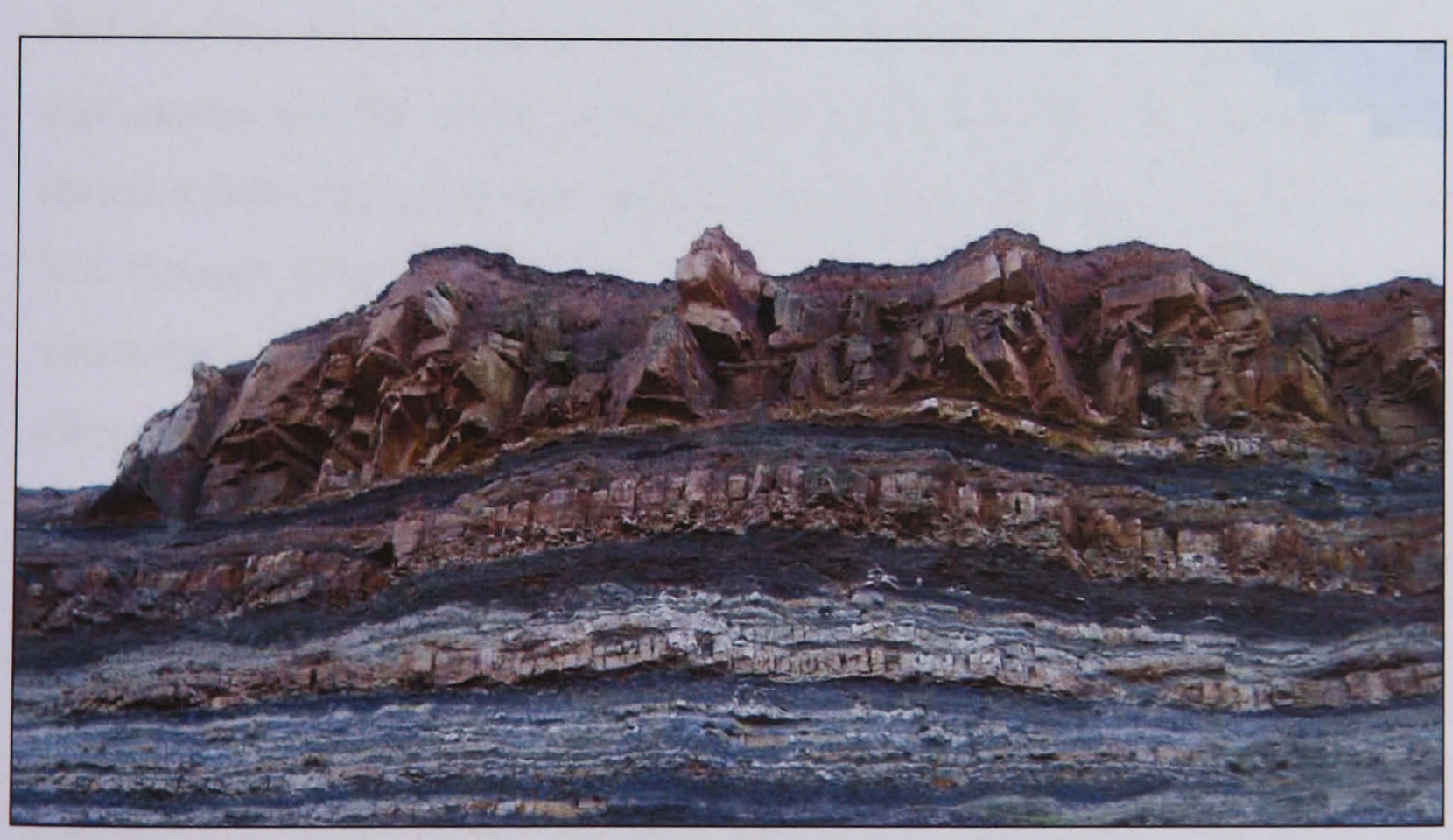

Figure 6.25 Large sandstone blocks jutting from the cliff-top.

6.5.3.5 Rates of Change

Total volumetric change between March 1994 and May 2006 (as discussed in Section 6.5.3.4), was further analysed in order to determine rates of change (in the direction approximately normal to the cliff-face). Results are detailed in Table 6-9. Unfortunately, confidence limits could not be determined, due to the lack of information regarding the planimetric quality of the multi-temporal DEMs (refer to Section 6.5.2.2).

Period	Region	Total Area (m^2)	Net Volumetric Change (m^3)	Change per m^2 (m)	Annual Change per m^2 (ma^{-1})
Mar. '94 - May '06	Upper Cliff	7666	-45791	-5.97	-0.50
	Lower Cliff	5650	-9841	-1.74	-0.15
	Cliff-Face Total	13951	-59326	-4.25	-0.35

Table 6-9 Rates of change across Whitby East Cliff, March 1994-May 2006, derived from volumetric analysis.

The results show that over the twelve year period 1994-2006 there is a marked contrast between the annual rates of change over the upper and lower cliff areas, with values of -0.50 ma^{-1} and -0.15 ma^{-1} respectively. This further underlines the higher rates of erosion over the upper cliff-face, and substantiates the existence of the modified angular cliff profiles which were identified and discussed in Section 6.5.3.3. One possible explanation for the lower erosion rate associated with the lower cliff is that failed material from the upper cliff may provide a ready source of replenishment to material lost through marine erosion and failure. Close inspection of Table 6-9 reveals that summation of net volumetric change over the upper and lower cliff results in a discrepancy of -3,694 m^3 when compared to total volumetric change, computed over the cliff-face as a whole. This is most likely due to the fact that slightly different boundaries will have been determined for the different cliff-face regions, and this will have affected the resultant volumetric calculations.

LSS was also used to calculate level differences between the March 1994 and May 2006 DEMs, in the same manner as described in Section 6.5.3.1, with determination of change over the upper cliff, lower cliff, and cliff-face as a whole. This facilitated derivation of the mean annual rates of change for these regions (Table 6-10) thus

enabling direct comparison with the corresponding values determined through volumetric analysis (Table 6-9). The lack of planimetric quality information again precluded the calculation of confidence limits, which was regrettable but unavoidable. In accordance with the findings presented in Section 6.5.3.4 in relation to volumetric analysis, the results emphasise the disparity between erosion over the upper and lower cliff-face. The rates of change presented in Table 6-10 are consistently lower than those reported in Table 6-9, although the same general trend is evident. This disparity is most likely due to the different strategies adopted in calculating the rates of change. The values detailed in Table 6-10 are likely to be more reliable, as these were derived directly from the raw elevation change calculations. The mean annual rate of retreat over this twelve year period was -0.216 ma^{-1} (Table 6-10). Rates of retreat over Whitby East Cliff are discussed further in Section 6.5.4.2.

Period	Region	Mean Change (m)	Mean Annual Change (ma^{-1})
Mar. '94 - May '06	Upper Cliff	-4.531	-0.378
	Lower Cliff	-0.674	-0.056
	Cliff-Face Total	-2.598	-0.216

Table 6-10 Rates of change across Whitby East Cliff, March 1994-May 2006, derived from level differences.

6.5.4 Changes to Cliff Edge Position 1986 – 2006

6.5.4.1 Introduction

As discussed in Section 1.1.3.6, determination of rates of cliff-top retreat or shoreline change have traditionally played an important role in coastal monitoring, particularly where historical datasets are concerned. Although such an approach may be suitable for analysis of dynamic beach and sediment environments, it may be misleading in the case of cliffed terrain. Bray and Hooke (1997) caution against relying upon the cliff edge as the exclusive indicator of change, as this can mask differential rates of retreat across the cliff-face as a whole. In addition, this approach generally contributes little towards enhancing understanding of the underlying processes.

However, analysis of changes to cliff-top position may prove useful in supplement to more comprehensive monitoring of the coastal zone, as this approach provides a tangible indication of the direct effects of coastal change. Furthermore, such information is particularly valuable at Whitby, given the existing cliff-top infrastructure, and concerns for the continuing threat to the historic Abbey site. Therefore, the position of the cliff-edge was extracted from the multi-temporal DEMs spanning the twenty-year period March 1986 to May 2006. The 1986 dataset was deemed reliable for this purpose, following the manual editing performed in *SocetSet* in order to incorporate breaklines representing the position of the cliff edge (Section 6.3.2.2). Consequently, this concluding analysis section focuses on assessment of change over this period.

6.5.4.2 Analysis of Cliff-Edge Change

The extracted positions of the cliff edge were imported to *ArcGIS* for visualisation (Figure 6.26). It is apparent that over this twenty-year period, most of the cliff-top experienced some recession. At the western end, the area indicated at A is that which was affected by the October 2000 cliff failure, with the cliff edge retreating by around 11 m between March 1994 and April 2005. To the east, erosion has also affected the former quarry workings. Most recently, a large section of cliff-top was lost due to the cliff failure discussed at the end of the previous section (occurring between August 2005 and May 2006), resulting in a 5 m retreat of the cliff edge (B). Intermittent retreat on a lesser scale has also occurred over the area adjacent to the coastguard station.

Examination of alterations to the cliff edge position over this twenty-year period indicates that Whitby East Cliff is actively retreating, and that most parts of the cliff-top have been affected. Analysis of the cliff-edge position between March 1986 and May 2006 indicates that the cliff-top is retreating at an approximate rate of -0.38 ma^{-1}. This corresponds almost exactly with the value of -0.378 ma^{-1} reported in Section 6.5.3.5 in relation to retreat over the upper cliff. However, as discussed in Section 6.5.3.5, there is clear variability over the cliff-face, with the lower cliff eroding at a markedly lower rate of -0.056 ma^{-1} (refer to Section 6.5.3.5). This produced a mean retreat rate of -0.216 ma^{-1} for the cliff-face as a whole. Rosser et al. (2005) report a retreat rate of -0.18 ma^{-1} for the cliff-top over the period 1895-2003. While this is notably lower than the rate of -0.38 ma^{-1} determined through the analysis presented in this section, the

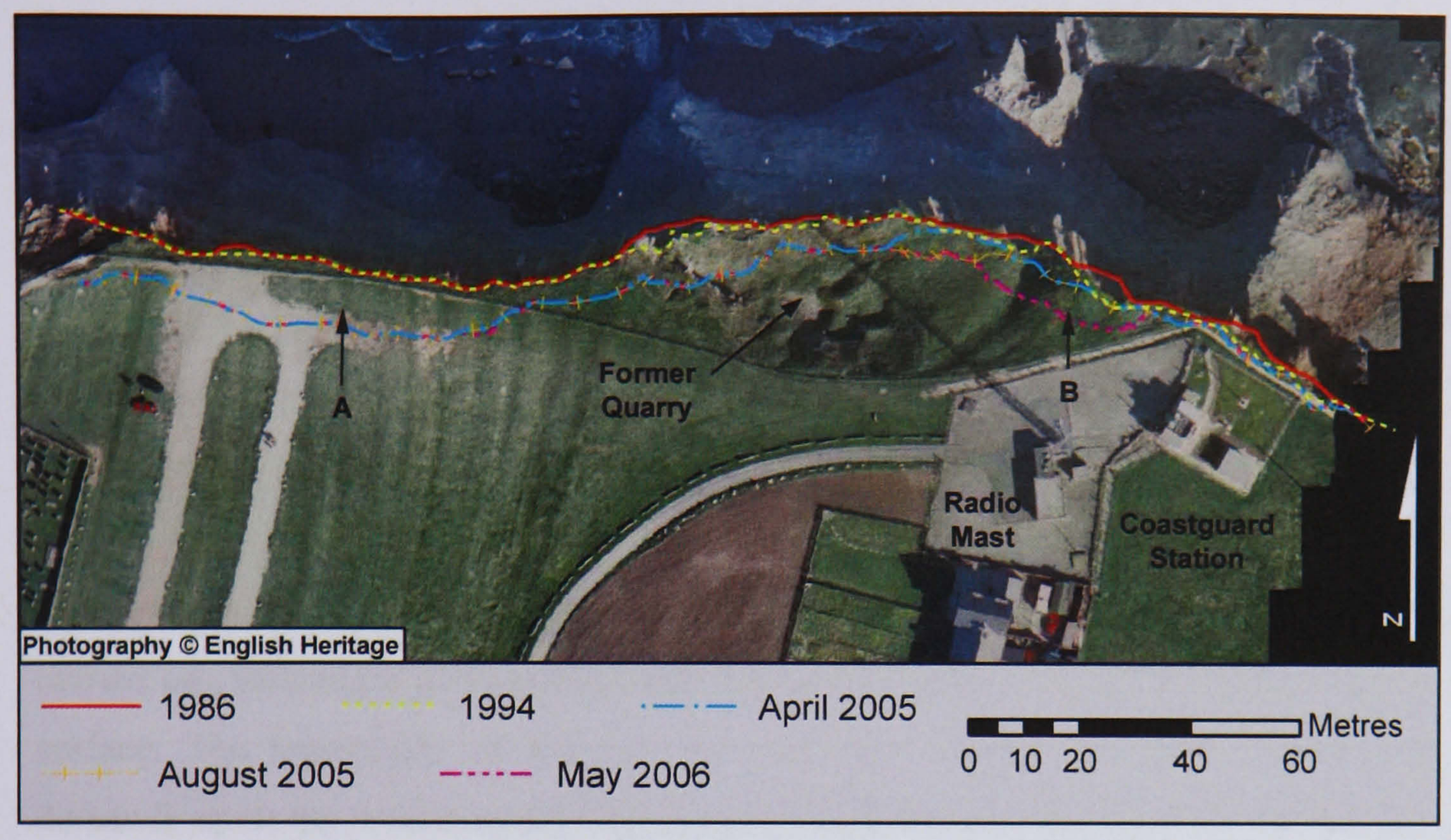

Figure 6.26 Cliff edge change at Whitby East Cliff, 1986-2006, with 1994 ortho-image as backdrop.

value reported by Rosser et al. (2005) may be more representative of the general, longer-term trend of retreat. This is supported by the close agreement of this value (-0.18 ma^{-1}, Rosser et al., 2005) with the value of -0.216 ma^{-1} determined in Section 6.5.3.5 for retreat over the cliff-face as a whole. It is possible that the cliff-edge retreat value of -0.38 ma^{-1} calculated here for the period 1986-2006, may be indicative of an increase in erosion over the upper cliff, or may represent a short-term fluctuation.

These findings serve to reinforce the variability of retreat over Whitby East Cliff. This is further highlighted through inspection of Figure 6.26, which reveals that over the eight year period, March 1986 to March 1994, extensive portions of the cliff-top (particularly at the western extreme) were stable, exhibiting little or no change. Likewise, there is a notable contrast between the 11 m of retreat affecting the western end of Whitby East Cliff over the total twenty-year period, and the mere 1.5 m which has occurred in places at the eastern extreme.

Consequently, while analysis of cliff-edge retreat confirms that Whitby East Cliff is actively eroding, and communicates the threat that this poses in the near future to the existing cliff-top infrastructure, it also demonstrates the limitations associated with adopting such an approach in isolation, particularly with regard to the spatial and temporal variability of cliff retreat. This will be discussed further in Section 7.2.3.

6.6 SUMMARY

While Chapter Five demonstrated the suitability of the integrated remote monitoring strategy for application to the soft cliff geohazard environment of Filey Bay, this chapter has investigated the transferability of this approach to the hard rocks of Whitby East Cliff. In the absence of terrestrial datasets, archival aerial photography and ALS have provided a basis for multi-temporal examination of geohazard activity through the robust surface matching strategy applied previously.

Following a check point-based assessment of DEM quality, surface matching was carried out, utilising a photogrammetrically-derived dataset from 1994 as the reference surface. The topography of the test site and the adjacent terrain placed particular demands upon the matching algorithm, enabling rigorous evaluation of transferability. Validation of the matching results has strongly reaffirmed the outcomes of Chapter Five, again demonstrating the value of surface matching as a technique for absolute orientation of DEMs, and highlighting the superiority of the robust algorithm over the un-weighted approach. Furthermore, the results have also illustrated that the robust algorithm is capable of reconciling surfaces where contamination through terrain change and outlier effects are minimal, thus demonstrating the more general applicability of this strategy.

Analysis of geohazard activity across the cliff-face over the periods March 1994-April 2005, April 2005-August 2005, and August 2005-May 2006 has been presented. This indicated that significant change has occurred over the total period, across most of the test site. The shorter-term monitoring periods enabled isolation and assessment of individual cliff failures. Further analysis has been presented through examination of cliff-normal profiles, enabling examination of change to the cliff-face profile at selected locations. Volumetric change analysis, and the derivation of rates of retreat, has confirmed that the upper cliff is eroding more rapidly than the lower cliff, most likely as a result of geological composition. As a final exercise, changes to the position of the cliff-edge have been investigated over the period 1986 to 2006. This has illustrated the temporal and spatial variability of retreat, reaffirming the potential pitfalls of over-reliance upon erosion rates derived from such analysis.

This chapter has demonstrated the successful transferability of the integrated remote monitoring approach in terms of application to a hard rock geohazard setting. However, the Whitby test site presented an extremely challenging environment, which has rigorously tested the surface matching algorithm, highlighting a number of important considerations. In addition, the topography of Whitby, particularly in relation to the near-vertical nature of the cliffs, has exposed a number of issues surrounding the application of both ALS and aerial photography. These issues will be discussed in greater detail, and in broader context in Chapter Seven.

CHAPTER 7

DISCUSSION AND CONCLUDING REMARKS

7.1 INTRODUCTION

This thesis has presented the development and implementation of an integrated remote monitoring strategy for coastal geohazards. The methodology, which incorporates airborne and terrestrial laser scanning, and archival aerial photography, has been detailed in Chapter Three. Chapter Four has presented the development and experimental testing of a robust surface matching algorithm which forms the core of the monitoring strategy. Chapters Five and Six have explored the implementation of this monitoring approach through application to soft-cliff and hard-rock environments respectively. This research has facilitated detailed assessment of a number of issues, which has enabled rigorous evaluation of the strengths and weaknesses of the monitoring approach and the associated techniques. This chapter discusses these findings, and introduces a number of recommendations for future research directions.

Firstly, the suitability of the selected techniques is considered with regard to issues of accuracy and effectiveness in relation to the processes under study. The performance of the robust surface matching algorithm is reviewed, and the success of the integrated monitoring approach, including issues of transferability, is assessed. A number of recommendations for future work are presented. Initially this focuses on further development of the robust surface matching software, and the suitability of this technique for application to alternative monitoring scenarios. The role of continuous monitoring is discussed, with particular reference to remote, autonomous GPS stations.

The potential of emerging techniques for coastal change monitoring is then reviewed, before considering upscaling of the current approach for monitoring of coastal change over large areas.

7.2 Discussion of Research Outcomes

7.2.1 Suitability of Techniques

7.2.1.1 Airborne Laser Scanning

Chapters Five and Six have demonstrated that ALS is capable of producing a consistent and continuous surface representation. Although it was initially anticipated that the ALS datasets may have suffered from occlusions in areas of steep slopes, in fact this was generally not the case. ALS was able to deliver excellent coverage of the Filey Bay test site, and the near-vertical cliffs at Whitby suffered from only minor occlusions in overhanging areas at the cliff-toe. However, spatial resolution was generally poorer at Whitby, due to the steepness of the cliffs.

The superiority of the ALS-generated DEMs over their photogrammetric counterparts was apparent at both Filey Bay and Whitby. This is primarily related to the fact that unlike photogrammetry, ALS is a direct sensing technique, and as such, is able to return a consistent representation of the terrain, unaffected by solar illumination. The photogrammetric datasets were affected by image matching problems (such as in the case of the 1986 Whitby dataset – refer to Section 6.3.2.2), and generally were observed to return noisier DEMs, particularly in areas of vegetation. These factors, coupled with the good coverage, meant that ALS was able to provide an excellent reference DEM for the surface matching at the Filey Bay test site.

Chapter Five demonstrated the effectiveness of ALS for geohazard monitoring in a soft-cliff coastal environment. Quality assessment of the ALS datasets at the four test areas indicated that vertical accuracy over the cliff-face was relatively good, with the majority of RMSE values below 0.300 m (Table 5-8). These values fall outside the manufacturer's specified vertical accuracy of $\pm$ 0.15 m, but as Hodgson and Bresnahan (2004) emphasise, such accuracies can generally only be expected to be achieved under

optimum conditions, such as flat terrain with minimal vegetation cover. Increased slope angle and vegetation cover are generally acknowledged as having a detrimental effect on ALS data quality (Hodgson and Bresnahan, 2004; Pfeifer et al., 2004; Göpfert and Heipke, 2006; Su and Bork, 2006), and the results presented in Section 5.5.3.2 support this. In ALS terms, the data acquired for this research can be considered as being of medium resolution (nominally 1 point/m^2). The results presented in Section 5.6 and Section 5.7 indicate that these datasets are particularly well-suited to soft-cliff geohazard monitoring, facilitating quantitative analysis of instability. ALS was also found to be valuable for monitoring of geohazard activity in the hard rock environment of Whitby. However, as will be discussed below, the current inadequacies in determining the complex ALS error budget, and addressing associated error-handling procedures, preclude the full potential of this technique from being exploited.

Although the research presented here has not explored the potential of ALS for monitoring over wider extents, the opportunity for this exists, and it is evident that ALS is a technique which facilitates rapid and effective acquisition over large areas. However, as a note of caution, the Filey Bay datasets, which involved acquisition at 1 point/m^2 over a coastal strip of approximately 10 km in length, resulted in an average of 22 million points (last pulse returns only) per epoch, and there are implications for the effective manipulation, analysis and management of datasets of this size.

As well as the advantages described above, a number of negative aspects were encountered in relation to ALS. However, it should be noted that these are broader issues, which are largely unrelated (in a direct sense) to the potential of this technique for coastal geohazard monitoring. Imagery is an inherent aspect of photogrammetry, and in addition to exploiting this for the derivation of metric information, it can also prove invaluable for interpretive purposes. However, the ALS datasets acquired for this research generally lacked corresponding imagery, which hampered interpretation. It is acknowledged however, that most commercial operators provide corresponding imagery as standard practice.

A further issue relates to the difficulties associated with acquiring airborne data at specific, scheduled times. Timely acquisition is normally an important requirement in terms of episodic monitoring. However, unfavourable weather conditions pose a major

impediment in this regard, and were partly responsible for the delays associated with the ALS datasets acquired for this research. This is a problem which is inherent to most airborne survey techniques, and which unfortunately has to be accepted, with schedules adjusted accordingly.

Chapters Five and Six also served to highlight the difficulties associated with assessing the planimetric quality of ALS datasets (refer to Section 5.4.1.2). This was particularly evident in Section 6.5.3.1, where ALS planimetric error led to indications that positive change had occurred over an extensive portion of the hard rock cliff-face at Whitby. As discussed in Section 2.5.4, ALS error sources are complex and numerous, and as Dowman (2004) observes, standardised procedures for calibration and quality assessment are lacking. As discussed in Section 5.4.1.2, planimetric quality is particularly difficult to assess. The target-based solution proposed by Csanyi and Toth (2007) holds much potential. However, an approach of this type requires data of a suitably high resolution (Dowman, 2004). For medium-to-low resolution datasets, such as those acquired for this research, the effectiveness of this strategy may be limited. Feature-based assessment of planimetric quality is possible, but this generally also requires data of a relatively high resolution, or necessitates the existence of corresponding imagery. The potential of surface matching for this task will be discussed briefly in Section 7.4.1.1.

Overall, this research has confirmed the potential of ALS in relation to coastal geohazard monitoring. ALS effectively overcomes the image matching difficulties associated with photogrammetry, and is capable of facilitating reliable analysis of coastal geohazard activity over both vegetated and un-vegetated areas. However, ALS is still maturing as a survey technique, particularly in the sense of calibration and quality assessment procedures, and continued research in relation to these aspects is urgently required.

7.2.1.2 Terrestrial Laser Scanning

Evaluation of TLS at the Filey Bay test site confirmed the value of this technique for coastal geohazard monitoring. The high resolution (up to 80 points/m^2) was found to provide an excellent complement to the ALS datasets, facilitating multi-scale

monitoring (as will be discussed further in Section 7.2.2.1). The high spatial resolution of TLS also highlights the potential of this technique for detailed analysis of micro-scale processes, and the possibilities for detecting pre-cursor failure activity.

TLS data collection demonstrated the benefits of this approach over traditional terrestrial techniques. The acquisition of such high data volumes is certainly not feasible through traditional land surveying techniques, and even the collection of a wireframe surface model through a kinematic GPS approach cannot compete with the spatial resolution of TLS. Furthermore, TLS offers faster acquisition, is less labour intensive than traditional land survey approaches, and with appropriate instrument selection, can offer completely remote data collection.

Although all three scanners used in the work incorporated digital cameras, the imagery was generally not useful for interpretive purposes, being of poor resolution (in the case of the Leica HDS2500), or being composed of multiple overlapping images, with adjacent areas of terrain affected by changing light conditions, and harsh shadows. However, while the resolution of the ALS datasets was too low to facilitate the use of intensity data for interpretation, the intensity information associated with the TLS datasets proved extremely useful. As Figure 7.1 illustrates, the point intensity information is almost as effective as a high resolution image, and allows detailed interpretation, with areas of bare earth and grass clearly visible. In this example (Figure 7.1) it is even possible to read the writing on a warning sign.

As was anticipated in Section 3.3.2, and evidenced in Section 5.7.2.1, the TLS datasets were considerably affected by occlusions due to the viewing perspective of this terrestrial technique. At Filey Bay, the main slope of the cliff generally gives way to a relatively flat area immediately above the cliff-toe, and these areas were worst affected, being obscured from the scanner position on the beach. As discussed in Section 5.5.3.2 the ALS datasets were found to be of a consistently higher accuracy than the corresponding TLS datasets for the four Filey Bay test areas. While the accuracy values associated with the ALS datasets were in the order of what would be anticipated given the dataset resolution, system specification, and nature of the terrain, the accuracy of the TLS datasets was notably poorer than expected (Table 5-7).

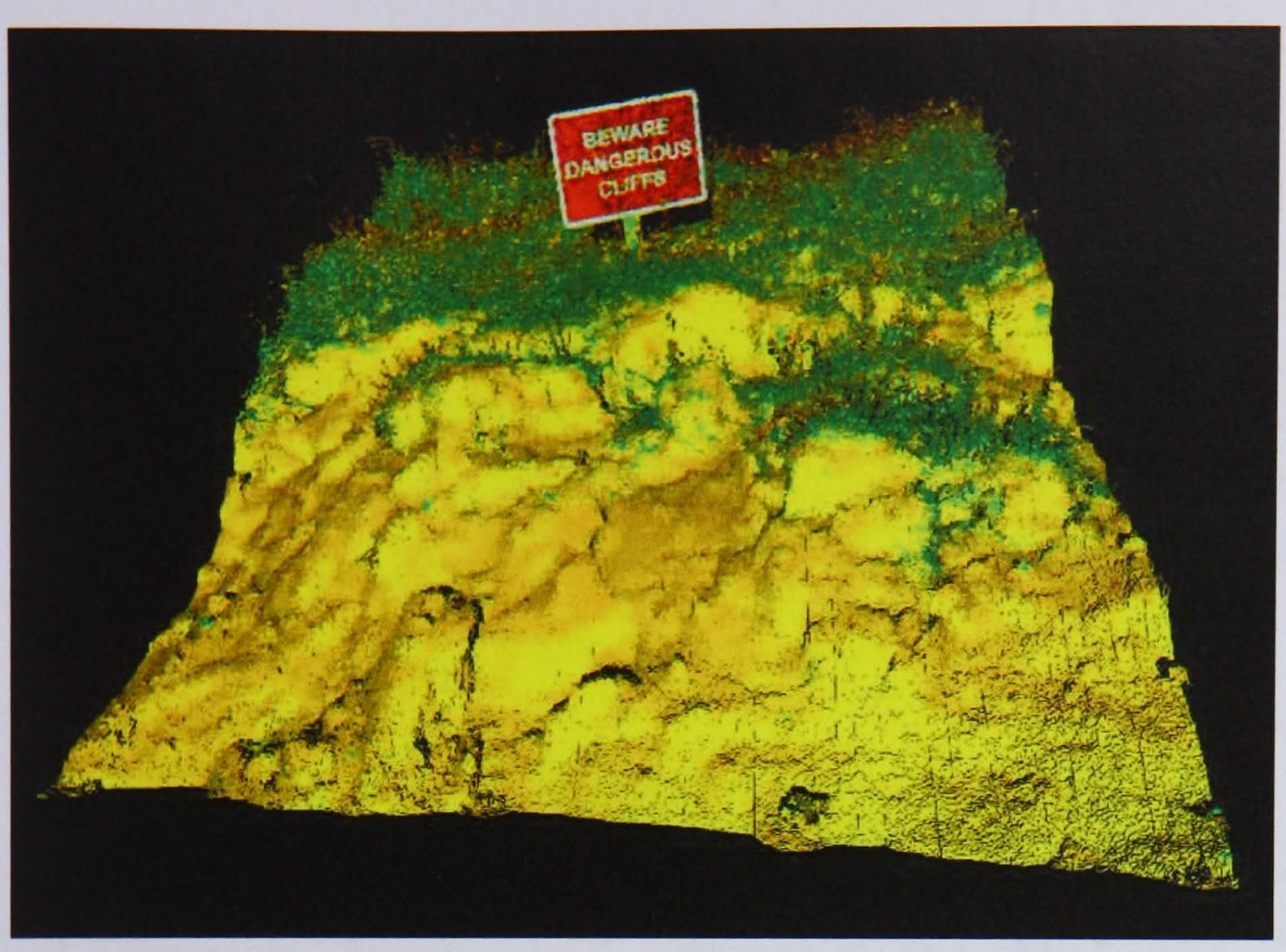

Figure 7.1 Scan of cliff area at Filey Bay (acquired with Leica HDS2500), rendered according to point intensity.

Occluded regions in the TLS datasets were most likely affected by weak surface triangulations, and indeed, following surface matching and merger with the ALS datasets, the resultant DEM was found to be of improved quality (Section 5.7.2.1). However, some of the TLS error may be attributable to the oblique scanning angle which may have resulted in poor penetration of vegetated areas, and in this regard, the vertical perspective of ALS may have been more successful in producing a faithful surface representation.

It is crucial to match TLS instrument specification to the monitoring requirements, and the constraints imposed by the coastal environment wherever possible. Section 5.5.2.1 discussed the differing characteristics of the three scanners used in this research, and it was emphasised that no one instrument could be identified as being optimal for the application at hand. Features such as scanner range, FOV, speed of acquisition, and georeferencing approach are particularly important for coastal geohazard monitoring, as it is desirable to employ remote monitoring, and ensure that surveys are completed as quickly as possible so as to optimise tidal windows. While power was not found to be an issue in relation to the scanners, it proved to be a limitation with regard to the user interface. Many scanners are controlled via a laptop computer, which generally may

offer only two to three hours of battery life. This presents a major difficulty for field-based TLS surveys. In this research, a portable generator had to be used to overcome power issues, but this is not a practical solution for field survey, especially where the site is remote, and the terrain hazardous. A further issue relates to the adverse weight and portability of current TLS systems. This remains an obstacle for the effective deployment of TLS, particularly in the rugged coastal environment. However, as TLS is increasingly embraced by the land surveying sector, it is likely that such issues will become less of a concern, and the general design, both in terms of ruggedness, and measurement integrity, is likely to improve.

Another issue associated with TLS is the significant amount of post-processing required in order to produce a digital terrain model, an issue emphasised by Bitelli et al. (2004). This includes registration of point clouds, removal of gross error points, and filtering to remove non-ground returns. In the case of the Filey Bay datasets, this latter aspect was found to be particularly time consuming, as the ground classification procedure is less straightforward than in the case of ALS datasets (refer to Section 5.5.2.2).

Overall, the results presented in this thesis confirm the potential of TLS for coastal geohazard monitoring. Furthermore, as TLS continues to mature, and as scanner design becomes increasingly refined, this technique is likely to be of growing relevance for a range of terrain monitoring applications.

7.2.1.3 Archival Aerial Photography

While ALS and TLS were utilised for present-day monitoring of geohazard activity, archival aerial photography facilitated historical assessment of change. Testing at both Filey Bay and Whitby East Cliff confirmed the value of this technique, which was effectively incorporated through the surface matching based registration approach.

DEMs derived from archival aerial imagery were found to provide an excellent source of metric change information, which facilitated analysis stretching back over a total of thirty-eight years to 1967, at the Filey Bay test site. In addition, the inherent image content associated with photogrammetry has proved to be important for interpretation of landscape change, and as evidenced in Section 5.6.4.1, was able to provide visual

confirmation of cliff failure and vegetation change. Although Filey Bay and Whitby presented distinctly different geohazard environments, the availability of historical datasets provided important information in relation to the legacy of geohazard activity at these locations. For example, analysis of the Filey Bay historical datasets highlighted the occurrence and development of a major landslide (refer to Section 5.6.4). This provided valuable context for assessment of the ALS and TLS datasets, which suggest that this feature remains active in present times (Section 5.7.3). Furthermore, the historical DEMs presented a useful indication of the magnitude and frequency of cliff failures at the two test sites. Potentially, such information could be used to further refine the frequency of episodic monitoring at these locations.

Photogrammetric processing of the 1986 Whitby dataset illustrated the image matching difficulties which may be encountered in coastal environments composed of steep cliff-faces, affected by regions of deep shadow. This is an inherent aspect of photogrammetry, but it is important to note that aerial photography is often the only source of three-dimensional metric terrain information for the last fifty to sixty years, and therefore remains an invaluable asset for historical monitoring studies. The Filey Bay datasets were generally unaffected by image matching difficulties, with the combination of topography and land cover resulting in good image texture.

In relation to the above discussion, it is important to assess the quality of DEMs derived from archival aerial photography. This is not always straightforward, especially if reliable check points cannot be acquired. In the surface matching approach utilised in this research, the adoption of a check *area*, as advocated by De Rose et al. (1998), Betts et al. (2003) and Schiefer and Gilbert (2007), proved useful for evaluating the quality of the historical photogrammetric DEMs (refer to Section 5.6.3.2). However, the use of check points is always preferable if these are available.

While this research has strongly advocated the benefits of archival photography for coastal geohazard monitoring, not all imagery is suitable for such purposes, and indeed much time was spent during the early stages of this research in sifting through and rejecting candidate imagery. This mainly relates to establishing whether or not the imagery is of metric quality. Some photogrammetric material may be unsuitable if scratched, over-exposed, or if solar illumination conditions are poor – for example, if

strong shadows are present. In the case of the NMR, some form of web-based search engine containing low resolution copies of the imagery and improved metadata could greatly assist in reducing the search time, and would place less demand upon NMR staff. However, with a collection of 2,000,000 vertical images, it has to be acknowledged that establishing such a system would necessitate a huge undertaking.

Other researchers have successfully utilised archival photogrammetric datasets for analysis of terrain change (e.g. Adams and Chandler, 2002; Casson et al., 2003; Walstra, 2006), and the research presented here, and summarised in Miller et al. (2007) and Miller et al. (in review), confirms that this material offers a highly effective source of metric change information. The searches carried out at the NMR, which represents only a single collection, highlighted the vast archive of vertical aerial photography available for the UK, and this offers tremendous potential for historical analysis of coastal change. However, in the case of the NMR, the process of gaining access to the material required for rigorous photogrammetric exploitation of the data was found to be a major barrier. This related to copyright restrictions (and a scarcity of details relating to copyright holders), a lack of camera calibration information, no provision for photogrammetric scanning, and a steadfast reticence to release film for external scanning. However, it should be highlighted that other collections, such as CUCAP (refer to Section 3.3.3.1), are well organised for photogrammetric access.

Despite these drawbacks, the value of archival aerial photography, and the opportunity that this offers for historical assessment of geohazard activity cannot be overstressed. The robust surface matching technique developed and implemented in this research further increases the potential of such datasets, as will be discussed in the following section.

7.2.1.4 Robust Surface Matching

The robust surface matching algorithm developed and implemented in this research has proven capable of facilitating reliable change detection, through robust registration of multi-temporal, multi-sensor datasets. The results presented in Chapters Five and Six demonstrated the effectiveness of surface matching for refining DEM registration.

Surface matching has also been found to be of value for elimination of systematic error, as discussed in Section 5.5.2.2, in relation to the epoch 1 TLS datasets.

The usefulness of surface matching for registration refinement and systematic error removal has also highlighted the capability of this technique for reducing general control requirements. This is highly relevant in coastal geohazard monitoring, as establishing control was found to be an extremely time-consuming procedure, and was greatly hampered by tidal restrictions. This particularly affected the TLS surveys (issues relating to archival aerial photography will be discussed later in this section). However, although control is an essential requirement for TLS, perhaps the absolute accuracy of such measurements need not be so high if surface matching can be employed for registration refinement at a later stage.

The development and implementation of the robust surface matching algorithm represents a key aspect of the research presented in this thesis. This technique underpins the integrated remote monitoring strategy, and is crucial for ensuring effective registration of datasets contaminated by change. Following successful testing with artificial datasets (refer to Section 4.4.4; Miller et al., 2006; Miller et al., 2007), Chapters Five and Six rigorously assessed the suitability of this technique for integration of topographic DEMs. Matching of historical DEMs containing regions of difference arising through geohazard activity, and vegetation and landscape change (Section 5.6), confirmed the effectiveness of this approach for registering surfaces contaminated by differences, and demonstrated the superiority of the robust algorithm over the un-weighted version. Furthermore, at the Whitby test site, the matching surfaces were largely unaffected by multi-temporal discrepancies, as the procedure was carried out over the relatively stable cliff-top area. This again provided strong confirmation that the robust algorithm was able to produce more accurate registration solutions (Section 6.5.2), and in doing so, highlighted the flexibility of this technique, indicating that it is well-suited for more general application to surfaces largely uncontaminated by change.

An important outcome of this research has been the success of surface matching as a technique for the absolute orientation of photogrammetrically-derived DEMs. The conventional approach to orienting such datasets requires the collection of suitable

GCPs in the field, and in the case of historical imagery, the difficulties associated with this are often highlighted as one of the main barriers to effective extraction of good quality metric data (e.g. Thieler and Danforth, 1994a; Dixon et al., 1998; Brown and Arbogast, 1999). In the course of carrying out this research, GCPs were obtained for the 1980 epoch of aerial photography at Filey Bay in order to facilitate production of a validation DEM. However, this exercise reaffirmed the difficulties associated with successfully executing this task; the landscape had changed considerably over the twenty-five year period, and the relatively featureless nature of the coastal terrain presented a major challenge. The surface matching technique removes the requirement for physical GCPs, instead deriving control directly from the geometry of the DEM surfaces. This not only eliminates the difficulties associated with the conventional approach, but is also likely to render the archival photogrammetric procedure a more cost-effective approach. As already discussed in Section 7.2.1.3, there exists a vast archive of historical aerial photography in the UK alone. Providing access restrictions can be overcome, and suitable care is taken in selecting data of an appropriate metric quality, robust surface matching offers tremendous potential for increased exploitation of this under-utilised resource, not only for coastal monitoring, but for more general analysis of terrain change.

In terms of the specific performance of the surface matching algorithm, the field testing highlighted a number of issues. While the algorithm was found to perform well at the Filey Bay test site, with no obvious problems encountered, Whitby presented a greater challenge. This was largely related to the nature of the topography, with near-vertical cliffs backed by a relatively flat cliff-top region. The least squares surface matching algorithm applied in this research is reliant upon minimisation of vertical surface differences. As discussed in Section 4.3.1, this strategy is generally well-suited to the matching of 2.5D topographic surfaces, as demonstrated through successful matching at Filey Bay. However, the Whitby test site presented extreme topography, in a surface matching sense.

Matching was carried out over the cliff-top area only, in order to eliminate the problematic vertical cliff-face (refer to Section 6.5.2.1). However, as discussed in Section 4.3.3, and emphasised by Rosenholm and Torlegård (1988) and Mitchell and Chadwick (1999), the algorithm requires strong surface gradients in order to determine

a reliable solution, and the flat cliff-top was not ideal in this regard. Re-introducing buildings to some of the DEMs was found to facilitate successful convergence, and check point-based analysis of the post-match surfaces indicated that strong solutions had been obtained with respect to the *z*-component (Section 6.5.2.2). However, it was not possible to evaluate the planimetric accuracy of the post-match DEMs, and it subsequently transpired that one of the ALS datasets (most likely the April 2005 DEM), was affected by a planimetric offset, resulting in the derivation of erroneous change over the cliff-face. Although it was suspected that the planimetric quality of the post-match surfaces generally represented an improvement over the original datasets, the matching solution was still relatively weak in this regard. This was most likely a direct consequence of the lack of strong surface gradients, resulting in the matching solution being weakly constrained in planimetric terms.

While it should be stressed that Whitby represents an extreme case in a more general sense, it can also be argued that in coastal terms, this topography is not so unusual. Therefore it must be concluded that the surface matching approach implemented here may be better suited to topography which exhibits strong surface gradients, such as that encountered at Filey Bay. Possible alternative matching strategies will be discussed in Section 7.4.1.1.

The robust surface matching algorithm has been essential for the effective reconciliation of disparate datasets in this research, and as a consequence, this technique has facilitated reliable evaluation of change over extended historical periods and shorter inter-epoch periods associated with more recent datasets. The algorithm has successfully handled DEMs derived from ALS, TLS and archival aerial photography, and in this respect offers much potential for applications involving DEMs arising from a range of alternative sensors. This research has convincingly demonstrated the value of surface matching as the linchpin of an organised monitoring framework, and highlighted its more general flexibility as an independent technique.

7.2.2 Integrated Remote Monitoring Strategy

7.2.2.1 Overall Performance Assessment

Thus far, this chapter has reviewed the performance of the individual components contributing to the monitoring approach. However, it is also important to consider the success of the monitoring strategy as a whole. The integrated approach – comprised of ALS, TLS, and archival aerial photography, combined through the robust surface matching technique – has been found to be highly suitable for quantitative assessment of coastal geohazard processes.

Contemporary monitoring has been successfully harmonised with historical analysis, enabling the identification of specific geohazard features, and evaluation of present-day behaviour in the context of historical development. This offers an opportunity for improved understanding of geohazard behaviour and evolution.

The integration of ALS and TLS datasets at Filey Bay delivered a synergistic DEM product in two respects. Firstly, occlusions in the individual datasets (particularly in the case of TLS) were successfully overcome, resulting in a superior surface representation (Section 5.7.2.1). Secondly, fusion of the TLS and ALS DEMs highlighted the benefits for multi-scale analysis of geohazard processes (Section 5.7.3). This latter aspect also emphasised the potential of the integrated approach for intensive monitoring of active pockets of geohazard activity, which could be applied in conjunction with wide-area monitoring at lower temporal frequencies. Although TLS data was not available for the Whitby test site, it is likely that the incorporation of such data would have strengthened monitoring efforts here. In particular, this would facilitate higher resolution monitoring of the cliff-face, both temporally and spatially. In turn, it is likely that this would enable the detection of lower magnitude rockfalls, providing greater insights into the development of such failures, as suggested by the findings of Rosser et al. (2005).

The techniques of ALS, TLS and archival photogrammetry are complementary in the sense that they are each capable of delivering relatively high resolution metric data which facilitates representation of the terrain as a continuous surface model. This is essential for subsequent quantitative analysis, and enables assessment of geohazard activity through a number of approaches, as will be discussed in Section 7.2.3.

The robust surface matching technique has played a central role in reconciling multi-temporal, multi-sensor datasets. This approach enables reliable change detection and analysis of geohazard processes. As already discussed in Section 7.2.1.4, the absolute orientation of the datasets utilised in this research was improved through the application of the robust matching software. If this facility had not been available, and the datasets had been compared directly (relying upon the conventional control measures), then the level of uncertainty associated with any analysis would likely have increased, making it more difficult to separate real terrain change from potential error, particularly over the more recent monitoring periods assessed through ALS and TLS.

The effectiveness of the integrated monitoring strategy can also be reviewed in relation to temporal resolution. The temporal frequency of historical datasets is generally difficult to control (Gorman et al., 1998), but it should be possible to optimise the effectiveness of present-day monitoring components. For the integrated ALS-TLS analysis carried out at Filey Bay, the monitoring interval was four months. Originally a six-month frequency was planned, but this was severely disrupted by the ALS delays, as discussed in Section 5.3.1. Clear evidence of change, related both to geohazard activity and vegetation growth, was present in both the ALS and TLS coverage (refer to Section 5.7.3). However, given the magnitude of this activity, monitoring at four-monthly intervals is unlikely to prove cost-effective through ALS (although this is partly dependant on the extents being monitored). With TLS facilitating effective analysis of these changes, and at a higher spatial resolution (Figure 5.30), it may be more efficient to carry out four-monthly monitoring of active regions such as this through TLS. ALS could then be incorporated for slightly longer-period monitoring, perhaps at intervals of six to twelve months. It should also be highlighted that geohazard activity at Filey Bay is likely to increase over the winter months, and therefore it may be necessary to adjust the frequency of monitoring on a seasonal basis, in order to accommodate such factors. It should be highlighted however, that monitoring during winter months is likely to be hampered to a greater extent by weather-related delays.

In terms of the Whitby test site, three epochs of ALS data were available (refer to Section 6.3.1), leading to four-month, and nine-month episodic monitoring intervals. As reported in Section 6.5.3.2, this facilitated detection of a number of failure events across the cliff-face (Figure 6.18). Although both the four- and nine- month monitoring periods

facilitated detection and analysis of relatively large magnitude failures, smaller magnitude failures were not revealed due to the spatial resolution of the technique, and the confidence with which change could be accurately determined. The results presented in Chapter Six would suggest that ALS monitoring at a frequency of four-months may be excessive, and again is unlikely to prove cost-effective, given that only minor change was detectable over the cliff-face during this period. The nine-month monitoring interval (or perhaps even a twelve-month interval) is likely to be more suitable, and ideally should be applied through an integrated approach incorporating higher-frequency TLS monitoring, which would facilitate detection of smaller magnitude cliff failures.

The outcomes of this research strongly indicate that the integrated strategy offers an efficient solution for coastal geohazard monitoring, particularly considering the complex nature of this environment, and the spatial and temporal variability of geohazard processes.

7.2.2.2 Assessment of Transferability

The integrated remote monitoring strategy was found to perform well in the soft-cliff geohazard environment of Filey Bay, facilitating effective quantification and evaluation of geohazard activity (Section 5.6; Section 5.7; Miller et al., 2007; Miller et al., in review). However, given the variability of coastal environments and associated geohazard processes, transferability testing was of crucial importance. This aspect was examined in Chapter Six, through application of the monitoring strategy to the hard rock test site at Whitby East Cliff.

The robust surface matching technique enabled successful reconciliation of both historical and present-day datasets at Whitby. In the case of the photogrammetrically-derived 1986 DEM, the surface matching algorithm was able to overcome a particularly poor initial orientation (including a scale deficiency), resulting in a marked improvement in the absolute orientation of this surface (Section 6.5.2.2). However, it must be acknowledged that the unfavourable topography of the cliff-top may have limited the effectiveness of the surface matching technique at Whitby. This aspect has already been discussed in Section 7.2.1.4, and will be examined further in Section

7.4.1.1 in relation to recommendations for future work. However, it should be highlighted that this issue appeared to have affected only one dataset. Furthermore, visual inspection of the pre-match surfaces indicated that the planimetric discrepancies were a pre-existing problem, and that the application of surface matching may have generally improved quality in this respect (refer to Section 6.5.3.1).

In assessing the specific performance of the robust algorithm, this was found to offer superior performance over the un-weighted algorithm, supporting the findings of the Filey Bay testing. This resulted in improved absolute orientation of the multi-temporal DEMs at Whitby, and in one case, the robust strategy was able to offer a solution where the un-weighted approach failed completely (refer to Section 6.5.2.2).

The incorporation of historical datasets again proved useful, enabling quantitative evaluation of cliff-face retreat over a twelve-year period. These datasets were also found to be valuable for assessment of recession rates over the twenty-year period, 1986-2006, which underlined the temporal and spatial variability of retreat. However, transferability testing at Whitby exposed the weaknesses of aerial photography in relation to image matching failure (as discussed in Section 7.2.1.3).

It is unfortunate that TLS could not be incorporated in the transferability testing. However, given the nature of the test site (near-vertical cliff-face), and the findings of Rosser et al. (2005), who explored the suitability of this technique for geohazard monitoring at Whitby East Cliff, it is likely that the incorporation of TLS would prove beneficial.

Taking a balanced view, transferability testing has been generally successful, and has confirmed the flexibility of the integrated monitoring strategy for application to alternative coastal environments. However, the case for integrated ALS-TLS monitoring has been strengthened through the deficiencies highlighted by the (unavoidable) omission of this technique at Whitby.

7.2.3 Implications in Relation to Geohazard Monitoring

The primary purpose of this research has been to develop strategies which improve the efficiency and effectiveness of coastal geohazard monitoring. Consequently, rigorous validation and assessment, in relation to the capabilities and limitations of the monitoring strategy and component techniques have been key issues throughout this research. However, it is also important to consider the implications of these results in relation to coastal geohazard monitoring, and examine the specific outputs which can be derived through the adoption of this strategy.

Traditional approaches to coastal change monitoring have tended to suffer from poor spatial resolution (Morton et al., 1993), and have often relied upon communicating change through the use of erosion rates alone. However, as discussed in Section 1.1.3.6 and highlighted through analysis in Section 6.5.4, this approach fails to disclose the spatial and temporal variability of geohazard activity across the cliff-face, and reveals very little in relation to underlying processes. In this research, the use of DEMs for episodic monitoring of coastal change has been shown to be an effective means of overcoming the poor spatial resolution of traditional approaches. In geomorphological terms, Lane et al. (1998) observe that multi-temporal DEM assessment provides a means of capturing '… the essential three-dimensionality of links between form and process'. Furthermore, the utilisation of DEMs offers excellent opportunities for effective visualisation of change (e.g. Section 5.6.4.1). This is not only important with regards to improved interpretation of terrain change, but also provides a mechanism for effective communication of such activity to non-experts.

Chapters Five and Six have highlighted the possibilities for quantitative analysis of geohazard activity in relation to the monitoring strategy implemented in this research. Analysis and visualisation of multi-temporal difference surfaces has proven to be an effective approach for assessing the spatial and temporal variability of geohazard activity. The value of historical datasets has already been stressed (Section 7.2.1.3), and cannot be over-emphasised. Historical analysis enabled the development of geohazard features to be tracked over time, and provided context for the subtle indications of instability detected in datasets relating to more recent inter-temporal periods (refer to Section 5.7.3). Investigation of historical datasets in this manner offers tremendous

potential, and exciting opportunities for improving understanding of geohazard processes in relation to their initiation, and development over time. Furthermore, historical assessment of cliff behaviour is generally useful for longer-term modelling of cliff-face evolution (Lee et al., 2002), which represents an important opportunity in relation to coastal planning and management.

DEM-based monitoring has also been shown to be valuable in facilitating volumetric assessment of change (refer to Section 5.6.4.2 and Section 6.5.3.4), which provides an effective means of communicating the scale and magnitude of geohazard processes. This also enables evaluation of the balance between deposition and erosion. The effects of the former are easily overlooked, but can play an active role in shaping coastal terrain, as evidenced in Section 5.6.4.2. Furthermore, the net volumetric change can reveal valuable information in relation to the intensity of marine erosion at a particular site, as demonstrated at Whitby (Section 6.5.3.4).

A major advantage of utilising continuous surface data (DEMs) is the ability to interrogate specific features or regions of interest, such as the landslide analysed in Section 5.6.4.2, or the cliff failure investigated in Section 6.5.3.4. In the case of the Whitby test site, this approach has also been shown to be of use in analysing suspected linkages between geological structure and differential rates of erosion (refer to Section 6.5.3.4).

Rates of retreat represent the conventional approach to quantification of coastal change, and are commonly utilised by coastal managers and those involved in policy development. Traditionally, rates of change are calculated through historical analysis of the back-scarp (cliff-edge) (Bray and Hooke, 1997; Lee and Clark, 2002). However, as discussed in Section 6.5.4.2, this approach may mask the spatial variability of geohazard activity, which generally acts across the cliff-face as a whole, and reveals little in relation to the underlying processes. Indeed, as Bray and Hooke (1997) emphasise, back-scarp retreat should not be utilised as the sole indicator of change, unless this is typical of retreat over the entire cliff-face. Section 5.6.4.3 and Section 6.5.3.5 highlighted further benefits of the multi-temporal difference surfaces, in relation to the derivation of rates of change. Unlike the cliff-top erosion rates, these relate to change across the cliff-face as a whole, and therefore, are likely to present a more

faithful indication of change and the intensity of geohazard activity. It would therefore be desirable to encourage coastal managers and planners to utilise such alternative strategies. However, cliff-edge retreat may still be of use, in a reduced capacity, for determining the threat that erosion may pose in the short-term, to cliff-top infrastructure. Other management decisions, such as assessing the requirement for coastal defences, would be better serviced by considering rates of change over the cliff-face as a whole.

Another issue which must be considered in relation to rates of retreat is the manner in which such values are calculated. At Filey Bay, change was evaluated in the vertical direction (along the *z*-axis). This was considered to be the most appropriate approach with regard to the nature of the geohazard processes operating at this site. However, coastal managers and planners are familiar with cliff-edge retreat, which is essentially a planimetric measure, and is conventionally measured in the direction normal to the back-scarp. This is similar to the strategy employed at Whitby (refer to Section 6.5.3.1), where change was assessed in the direction approximately normal to the near-vertical cliff-face – this being the dominant direction of retreat at this site. Hence the rates of retreat reported for the Whitby site are likely to be more meaningful to coastal managers and planners than the Filey Bay values. However, due to the variability of coastal topography and geohazard processes, it would be difficult to adopt a single, effective approach which could be applied to all coastal sites. It is important therefore to encourage coastal managers and planners to embrace the capabilities of emerging technology, such as ALS and TLS, in order to exploit the full range of possibilities that these offer in terms of visualisation, analysis and quantification of change, as reviewed earlier in this section.

Overall, it is evident from the review presented here, that the integrated remote monitoring strategy is capable of delivering a range of benefits in relation to the quantitative assessment of coastal geohazard processes. Such information is likely to be of value to a range of coastal scientists involved in monitoring and modelling coastal change, and ultimately should facilitate enhanced understanding of the underlying processes. Coastal managers and planners should also derive benefits from implementing these monitoring practices, as the assessment of change over the cliff-face as a whole would result in a greater appreciation for the temporal and spatial

variability of change. Analysis of current and historical behaviour is likely to provide relevant information in relation to the development of future coastal policy.

7.2.4 General Software Issues

Throughout the course of this research, a number of issues have arisen in relation to the limitations of existing data handling approaches. These largely relate to the inadequacies of the existing 2.5D data structure, which proliferates in terrain modelling. Essentially, through the 2.5D approach, height is considered as an attribute of x and y, so that each plan position can have only one corresponding height. However, this is not an accurate representation of reality, and although for many applications the existing approach is sufficient, problems may arise with features such as tunnels, bridges, caves, steep slopes and overhangs (Pfeifer, 2005). In these situations, a single x, y position may have an infinite number of corresponding z values. There is an increasing move towards provision of fully-3D geospatial data – TLS being a prime example. However, existing terrain modelling software packages are lagging behind, and very few are capable of handling fully-3D datasets.

This relates not only to the storage and representation of data, but also to the operations which can be performed. Analysis at the Whitby test site highlighted this problem. Due to the nature of retreat, the DEM surfaces were compared in the direction (approximately) normal to the cliff-face. However, most terrain analysis software packages assume that DEM-differencing requires comparison in the direction of the z-axis. This stems from the general definition of DEMs as being 2.5D surface models. This issue is known to inhibit analysis carried out by coastal geologists (Hobbs, 2007, personal communication). Addressing this issue is not straightforward, requiring essentially a revolutionary change to current terrain modelling concepts, and for some applications this may be unwarranted. However, this issue is being investigated, with a number of researchers proposing alternative data structures (e.g. Kraus and Otepka, 2005; Pfeifer, 2005).

The process of determining change in a single, consistent direction over the entire cliff-face also introduces inconsistencies to the change measurements. Where terrain is complex, with slopes of varying aspect and steepness, it is impossible to calculate

change in the normal direction at every location. This problem also affects the measurement of cliff-edge retreat, particularly where monitoring has been carried out over an extended period, as cliff-normal transect lines, defined at the start of the monitoring period may no longer be truly normal to the back-scarp, thus introducing random error (Pethick, 1996). This issue is particularly difficult to overcome given the capabilities of existing terrain modelling and analysis software, and must be considered when evaluating the results of multi-temporal change analysis.

7.3 Revisiting the Research Objectives

Following this in-depth discussion of the research outcomes, it is possible to evaluate the extent to which the initial research objectives have been achieved.

Objective One: assess existing and emerging geomatics techniques, both in isolation and combination, in relation to suitability for coastal geohazard monitoring.

This objective was addressed in Chapter Two, where a comprehensive literature review was presented. This evaluated the suitability of a number of geomatics techniques – both established and emerging – for the purposes of coastal geohazard monitoring. It was concluded that an integrated approach, as advocated by a number of researchers (e.g. Schenk and Csathó, 2002; Ruiz et al., 2004; Böhm and Haala, 2005), would offer the best solution, as this would allow the weaknesses of individual techniques to be overcome, while deriving synergy from their combined benefits.

Objective Two: develop a software-based solution, enabling the robust integration of multi-temporal, multi-sensor datasets in dynamic environments.

This second objective was tackled in Chapters Three and Four. Chapter Three developed and detailed the structure of the integrated remote monitoring strategy, providing justification for the selection of ALS, TLS, and archival aerial photography. The robust surface matching solution, identified as being highly appropriate for the effective reconciliation of these datasets, was developed in Chapter Four. This focussed on addressing the requirement for *robust* dataset registration, necessary in order to overcome regions of surface difference (outliers) brought about by multi-

temporal geohazard activity, differing surface representations (due to different acquisition techniques), and vegetation or other landscape change. The performance of the robust surface matching algorithm was validated through experimental testing. This confirmed its viability as the core element of a software-based monitoring strategy, facilitating the robust integration of topographic DEMs. The performance of the component techniques and the robust matching algorithm has been reviewed in detail in Section 7.2.1.

Objective Three: implement and evaluate the monitoring strategy through application to coastal test sites, examining issues of accuracy, effectiveness and transferability.

The monitoring strategy was implemented at coastal test sites located at Filey Bay, and Whitby, North Yorkshire, as described in Chapters Five and Six respectively. Integrated ALS-TLS analysis was presented for the Filey Bay site only (as explained in Section 6.3.1). Testing at both sites confirmed the effectiveness of the monitoring strategy, highlighting the valuable historical analysis which can be derived from the inclusion of archival photogrammetric datasets. The benefits of ALS and TLS were apparent, particularly when applied in an integrated fashion at the Filey Bay test site. Application to the Whitby test site facilitated evaluation of transferability issues. On the whole, this aspect was successful, but a number of issues, primarily relating to the challenging nature of the topography were highlighted, and have been discussed in Section 7.2.1.4 in relation to the surface matching technique. Overall, implementation of the monitoring strategy was highly successful.

Objective Four: undertake quantitative assessment of coastal geohazard activity, and through this determine the potential of the monitoring strategy in relation to enhancing understanding of coastal geohazard processes.

This final objective was addressed in Chapters Five and Six, where the implementation of the monitoring strategy at the Filey Bay and Whitby test sites enabled quantitative analysis of geohazard activity. Historical analysis enabled geohazard development to be traced over time, while more recent datasets revealed subtle signatures of instability. This information has shown considerable potential for contributing towards furthering understanding of geohazard processes, revealing

spatial and temporal connections between failure events. This aspect has been discussed in detail in Section 7.2.3.

7.4 Recommendations for Future Work and Outlook

7.4.1 Robust Surface Matching Development

7.4.1.1 Software Development

The value of the robust surface matching algorithm was successfully demonstrated in Chapters Five and Six, through application to the Filey Bay and Whitby test sites respectively. However, there is scope for refinement and further development.

Options could be investigated in relation to speeding up the performance of the algorithm. Although this is partly dependant upon the characteristics of the matching surfaces in relation to speed of convergence, the main control is the number of points on the reference surface, as the algorithm has to search through the triangle vertices file to determine the enclosing *S1* triangle for each *S2* point (refer to Section 4.3.3). This is the least efficient aspect of the algorithm (Buckley, 2003); all other operations, including the actual solution process, take only a fraction of the time. An alternative approach may be to investigate strategies for spatial indexing, which would limit the number of triangles to be searched on the *S1* reference surface. A quadtree-based approach may be one possibility. However, an alternative solution would be to reduce the extent over which matching is carried out. Gruen and Akça (2005) propose sub-patch matching, where the matching surface is reduced to a number of well-distributed sub-patches, allowing unnecessary point redundancy to be overcome, thus reducing the overall computational expense of the matching procedure.

Focussing on the robust aspects of the surface matching algorithm, it would be useful to evaluate the performance of alternative robust estimation functions. Due to time constraints, this was not possible within the current research. Tukey's Biweight function was selected for application here, as this is one of the most commonly utilised M-estimators, and is reported to offer good generic performance (Goodall, 1983). However, a number of alternative M-estimators exist, and may be worthy of investigation. Furthermore, the LMS-estimator has been advocated as a possible

alternative to M-estimators in the context of surface matching, and is reported to offer increased robustness (Li et al., 2001). However, incorporating the LMS-estimator in the existing algorithm is less straightforward than in the case of M-estimator functions.

During the course of this research it has been observed that in some cases – particularly where the datasets are noisy, or poorly constrained in terms of surface gradients – convergence may be slow or unconvincing, oscillations may occur in the parameter corrections, and ultimately the algorithm may fail to converge. This corresponds to the observations of Gruen and Akça (2005). In relation to these issues, the software could be further developed to include an optional graphical interface, which would allow information on convergence behaviour to be reported in real-time. This could enable parameter corrections to be visualised graphically over time (updated after each iteration), providing an indication of whether successful convergence is likely to be achieved. However, such information is only likely to be of use to expert users, and therefore would be best incorporated as an optional interface.

The Whitby test site highlighted a number of issues in relation to the performance of the surface matching algorithm. As explained in Section 6.5.2.1, matching was carried out over the cliff-top area only, as the algorithm would have been unable to handle the near-vertical cliffs. The least squares minimisation of *z*-differences is a matching approach which is well-suited to 2.5D surfaces (Mitchell and Chadwick, 1999), such as those generally encountered in terrain monitoring (e.g. the Filey Bay test site). However, the terrain at Whitby would be better dealt with through a fully-3D approach, due to the presence of strong vertical components. While an ICP-based strategy could be applied (refer to Section 4.2.1 for an overview of this strategy), this is computationally intensive (Sequeira et al., 1999) and relatively complex. Instead, the least squares surface matching variation proposed by Gruen and Akça (2005) (refer to Section 4.2.2 for a brief overview), may be more appropriate. Instead of minimising vertical surface differences, this approach minimises Euclidian distances between the surfaces, and through this, has been demonstrated as being capable of reconciling fully-3D surfaces (Gruen and Akça, 2005). It would be valuable to investigate the potential of this alternative strategy, and in theory, it should be possible to alter the existing functional model in order to implement and test this approach. This may offer increased general flexibility for handling of both 2.5D and fully-3D surfaces. Habib and Schenk (1999)

also recommend this minimisation approach, although their matching strategy is based upon the Hough transform (as introduced in Section 4.2.2).

This thesis has integrated ALS and TLS datasets through a robust surface matching technique. These surfaces were merged in a straightforward manner, resulting in the incorporation of all points from both surfaces. Pre-processing was carried out as an initial step in order to remove gross errors from both surfaces, and surface matching provided an effective means of removing residual systematic error. However, Schiewe (2000) highlights the importance of incorporating error treatment as part of the integration procedure. Gross error in the contributory surfaces has the potential to propagate into the merged DEM, and random error can have a degrading influence on the quality of the overall surface representation. This latter point is highlighted in Figure 7.2, which depicts an integrated ALS-TLS dataset over a flat beach area. This illustrates two effects. Firstly, the high resolution of the TLS datasets reveals the texture of the terrain, with ripples in the sand evident, particularly in the more southern TLS scan. However, this representation is inconsistent with the coarser ALS dataset, and the beach area, which is essentially flat, could be represented more efficiently through a much sparser combined dataset. Secondly, as highlighted by Buckley and Mitchell (2004), the combined effect of noise in both datasets results in a 'jagged' surface representation at the fine-scale, which is detrimental to the overall surface representation.

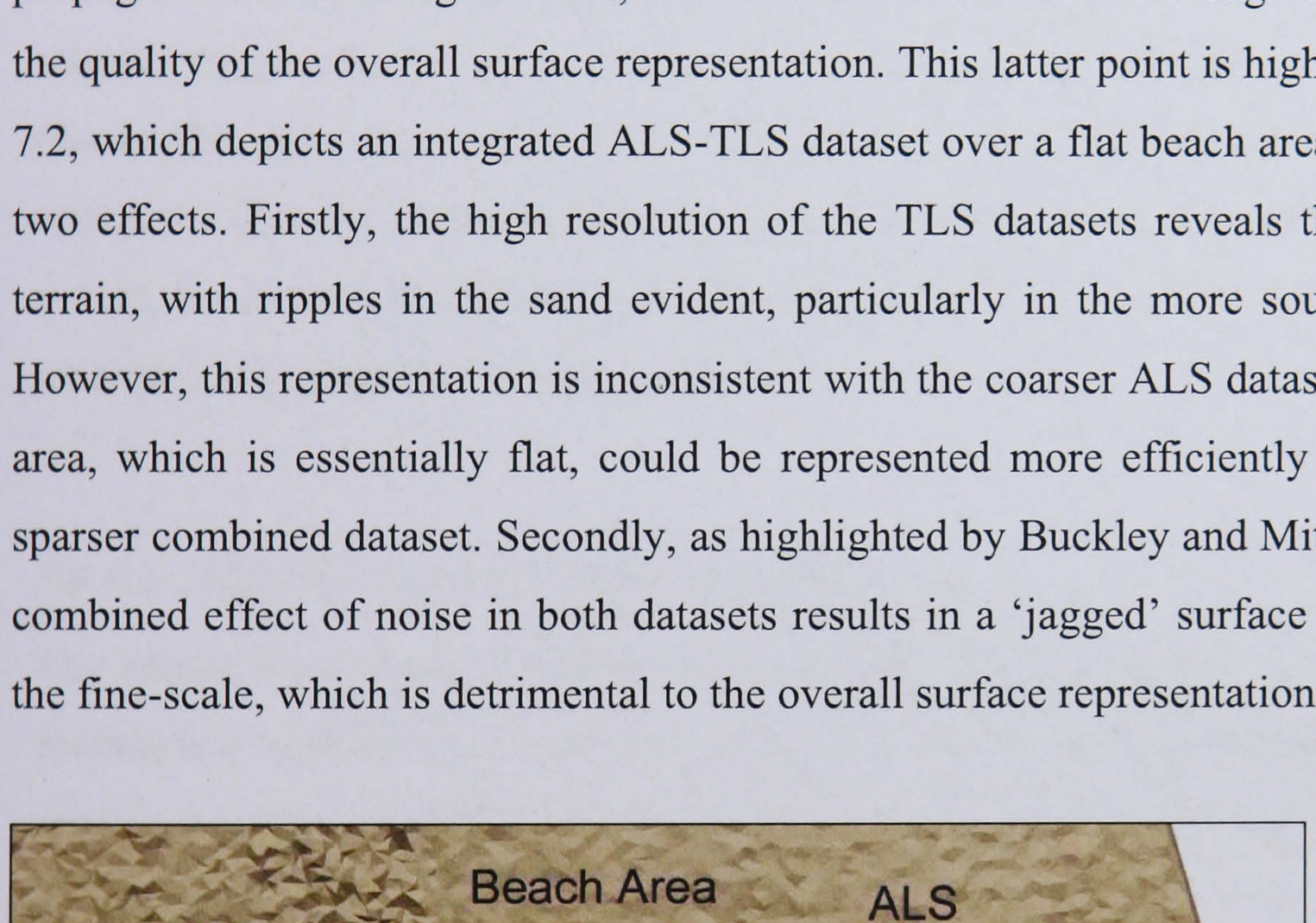

Figure 7.2 The detrimental influence of TLS sensor noise over a flat beach area, in an integrated ALS-TLS dataset.

These issues could be addressed through an intelligent dataset fusion strategy. Buckley and Mitchell (2004) propose a solution which relies upon least squares surface matching for initial removal of systematic error between the matching surfaces. Following this, the datasets are merged, with the removal of outliers, and point spacing is optimised through point culling driven by analysis of the local variability of surface gradients (Buckley and Mitchell, 2004). The existing surface matching software could be extended to incorporate such capabilities, thus increasing its general applicability.

Maas (2002) has highlighted the potential of least squares surface matching for identification and elimination of systematic error between overlapping ALS flightlines. Prior to any form of multi-sensor or multi-temporal dataset fusion, it is essential that internal systematic errors of this nature are adequately addressed. This problem was observed to have occurred in some of the datasets acquired for this research, but did not appear to directly affect the flightlines which provided coverage of the test areas. It would be extremely valuable to explore the potential of the least squares surface matching algorithm for such purposes.

7.4.1.2 Suitability for Alternative Applications

The robust least squares algorithm offers tremendous potential for alternative terrain monitoring applications, and this aspect is worthy of investigation. Although this represents a deviation from the coastal monitoring theme, this would enable the more general applicability of the robust surface matching software to be assessed, and may highlight valuable performance-related issues.

The robust algorithm is ideally-suited to applications which involve multi-temporal monitoring of dynamic environments, particularly where conventional control approaches are difficult to implement due to concerns related to cost and/or safety. Furthermore, as evidenced in the context of this research (refer to Section 5.6.3.1), some environments are relatively featureless, lacking suitable detail for control purposes.

In particular, robust surface matching may prove useful for applications related to glaciology and volcanology, which generally represent particularly dynamic, inaccessible and hazardous environments. Further geohazard applications exist in

mountainous regions, particularly in relation to the incorporation of archival photogrammetric datasets, which is a commonplace approach for historical analysis of mass movement processes (e.g. Casson et al., 2003; Chadwick et al., 2005; Brückl et al., 2006). This latter application is closely related to coastal geohazard monitoring, and the integrated ALS-TLS monitoring approach is likely to prove relevant, with a number of researchers already exploring the potential of TLS with respect to slope stability monitoring in mountainous environments (e.g. Ruiz et al., 2004; Scaioni et al., 2004; Abellán et al., 2006).

7.4.2 Upscaling to Wide-Area Monitoring of Coastal Change

The integrated remote monitoring strategy developed in this research has been implemented over relatively limited extents at two test sites. This was a necessary requirement in order to ensure comprehensive investigation of key aspects, and rigorous evaluation of the approach. However, the strategy offers considerable potential for upscaling, providing a means of assessing coastal geohazard activity and larger scale coastal change processes.

Both ALS and TLS are well-suited to this challenge. While ALS is capable of rapid data acquisition over large areas, TLS offers the capacity to focus intensive monitoring efforts on areas identified as being particularly unstable. However, one major advantage of the monitoring strategy developed here, is its generic nature, and the flexibility this offers. This relates to the fact that the robust surface matching technique, which acts as a mechanism for interlacing the different components, is not technique-specific. Surface matching is essentially a tool for DEM integration, and can be applied irrespective of the acquisition technique. Consequently, if alternative techniques were identified as being appropriate for monitoring over wider areas (e.g. possibly coarser resolution DEMs derived from satellite remote sensing), then these could be incorporated in the monitoring approach, instead of, or in complement to, existing techniques.

The potential of archival aerial photography in relation to wide-area monitoring of coastal change should not be overlooked. The robust surface matching technique offers an elegant and cost effective means of exploiting such datasets, and given the extensive coverage of many coastal regions, this offers an exciting opportunity for extended

analysis of coastal change, and substantial potential for enhancing understanding of larger-scale coastal processes.

There is considerable potential for automation, particularly in relation to the surface matching procedure, and subsequent change detection. Increased automation would be particularly valuable for larger-scale analysis of change. Surface matching and difference detection could be executed in a largely automated fashion, with users notified if change exceeded a certain threshold, in order to manually invoke TLS monitoring for example. Furthermore, if such an approach was incorporated in a GIS, change information could be combined with topographic parameters (such as slope and aspect), geological information, meteorological and hydrological data, and information on vegetation cover. Analysis of geohazard activity in conjunction with these variables would facilitate risk mapping, and is likely to reveal valuable insights into underlying failure mechanisms.

7.4.3 Emerging Techniques and Technology

There are a number of emerging techniques and technology which hold much promise for coastal change monitoring. Some of these are presently at a stage where they are ripe for investigation, and where such investigations may help to shape their continued development.

7.4.3.1 Continuous GNSS Monitoring

Section 2.3.4 briefly highlighted the potential of continuously-operating GNSS for geohazard monitoring. This is a technique which enables dedicated monitoring of discrete locations on a continuous basis, usually in an automated fashion (Miller et al., 2006). As discussed in Section 2.3.4, this technique is well-established for the monitoring of structures such as bridges and dams, and the monitoring of natural phenomenon such as crustal deformation and volcanoes. Recently however, increasing attention has been devoted to exploring the potential of continuously-operating GNSS for monitoring of geohazards, particularly landslides, in mountainous regions (e.g. Mora et al., 2003; Chadwick et al., 2005; Brückl et al., 2006).

Malet et al. (2002) examine the potential of continuous GNSS monitoring for assessing an earthflow in the French Alps. In their findings, they highlight some of the advantages this technique can offer over traditional methods, such as the provision of directly meaningful three-dimensional monitoring information in near real-time, which offers the potential for provision of an early warning system (Malet et al., 2002). A fully automated implementation of such an approach is presented by Brückl et al. (2006). However, due to the discrete nature of the measurements, the real value of this approach requires a network of receivers, strategically positioned over the region of instability. If the continuously-operating GNSS technique was incorporated within the episodic monitoring strategy developed in this research, this may facilitate improved analysis of particularly active geohazard locales, through real time monitoring (Miller et al., 2007). The increased temporal resolution would offer enhanced understanding of underlying failure mechanisms, and early warning of instability could initiate the episodic monitoring component in order to provide assessment at high spatial resolution (through TLS for example).

Although continuously-operating GNSS currently requires relatively high levels of investment, it is worthy of further investigation, as this is a technique which is likely to assume a role of increasing significance for a number of monitoring applications in the near future. Miniaturisation of components, and continued advancements in terms of power and communications are likely to result in this technique becoming more practical and affordable. Concepts such as Smart Dust give an indication of possibilities in the longer-term, where sensors can be miniaturised to the millimetre level, and 'scattered' over an area in large numbers to act as a dynamic sensor network with in-built power and communication capabilities (Warneke et al., 2001). In the more immediate future, the viability of continuous GNSS monitoring is increased through the provision of GNSS reference data from organisations such as OS. OS maintain a national network of continuously-operating reference stations (Active Network), from which observations are regularly downloaded and made available, free of charge, through the OS website with a latency of a few hours. Assuming the monitoring site is located within a reasonable distance of an OS active station, this removes the requirement to establish a reference station on stable ground, outside the geohazard area. Furthermore, the anticipated launch of new GNSS services, such as GALILEO,

and the re-emergence of GLONASS (refer to Section 2.3.1) is likely to drive GNSS-related developments and investment forward.

7.4.3.2 Unmanned Aerial Vehicles

A further technology which holds notable potential for coastal geohazard monitoring is that of Unmanned Aerial Vehicles (UAVs). The development of UAVs can be traced from military origins, where this technology has been established for some time. More recently, increasing research effort has been focussed on investigating the potential of this burgeoning technology for civilian applications, including earth observation. UAVs vary extensively in terms of capabilities, from long range, high altitude platforms operating from 3000 m or more, to micro and mini UAVs, which may acquire data from an altitude of less than 250 m, and offer a range of less than 10 km (Eisenbeiss, 2004). UAV-based remote monitoring offers the opportunity to combine existing techniques, such as photogrammetry, ALS and InSAR (e.g. Eisenbeiss, 2004; Nagai et al., 2004; NASA JPL, 2007), with platforms which offer increased flexibility and cost savings over piloted aircraft. This approach is likely to be particularly effective for coastal geohazard monitoring, where the use of UAVs may allow airborne data to be acquired at short notice (perhaps following a major cliff failure, or storm event). Where data can be gathered from low altitudes (below the cloud base), this raises the possibility for acquisition in overcast conditions.

7.4.3.3 Mobile Mapping Systems

Another technology which is developing at a fast pace is that of mobile mapping systems (MMS). These are typically composed of mapping sensors (such as digital cameras and laser scanners) which are combined with positioning sensors (often GPS-IMU technology), and mounted on a mobile platform in order to facilitate cost-effective dynamic mapping (Tao et al., 2001). These systems are often vehicle based (although many variations exist, and by definition, the term MMS could be applied to any moving platform), and have been widely investigation for mapping of urban environments (e.g. Manandhar and Shibasaki, 2001; Talaya et al., 2004). Although such systems cannot match the high spatial resolution of TLS, they provide a means of acquiring data rapidly over large extents, and are well-suited to corridor environments. Barber and Mills

(2007) recently investigated the potential of a waveform laser scanning MMS for coastal monitoring at Filey Bay. Although highlighting the ability of this system to rapidly scan the coastal cliffs at relatively high resolution, a notable weakness was found to be data occlusions caused by the oblique, terrestrial scanning perspective (Barber and Mills, 2007). This reaffirms the importance of the integrated airborne-terrestrial approach developed here. A particularly exciting development is that reported by Adams (2007), who details the initial development of a marine-based MMS for monitoring steep coastal cliffs. The current system configuration combines a standard TLS instrument with GPS-IMU sensors, mounted on an anchored platform such as a boat (Adams, 2007). Although there remain a number of challenges to be overcome with regards to optimising this technique, this development would appear to offer tremendous potential for monitoring inaccessible coastal geohazard sites.

7.4.3.4 Satellite Remote Sensing

While satellite remote sensing techniques cannot generally be considered as being emerging (at least not in the sense of the techniques presented thus far in Section 7.4.3), they continue to develop, and it is likely that they will play an increasingly important role in future coastal monitoring applications. As discussed in Section 2.7, sensors such as IKONOS and QuickBird are now able to provide imagery at sub-metre level resolution, which makes this technology increasingly suitable for coastal geohazard monitoring. Furthermore, InSAR is a well-established technique which continues to develop, and this may offer similar possibilities for wide area monitoring of change. However, ultimately, spaceborne techniques, like their airborne counterparts, are susceptible to poor weather conditions. While airborne sorties can be postponed until the weather improves, the same level of control does not exist for satellite sensors, and there is no guarantee that the next repeat pass will coincide with improved conditions. This is a problem which particularly affects high latitudes; however, for other regions of the world, satellite remote sensing techniques are already widely utilised for coastal monitoring, and the reliance upon such techniques is likely to further increase.

7.5 SUMMARY

In this concluding chapter, key research outcomes have been discussed at length. This has included a review of the suitability of the individual component techniques. As a direct sensing technique, ALS, has been found to be capable of producing a consistent, and reliable surface representation, providing a strong reference DEM for least squares surface matching. The high resolution of TLS data, associated with rapid acquisition, have been emphasised as being major assets over traditional land surveying approaches. Archival aerial photography has been highlighted as an excellent source of historical change information, providing context for present-day geohazard behaviour. The discussion on robust surface matching has emphasised the multiple benefits of this technique, including the reliable registration of multi-temporal, multi-sensor datasets, and the elimination of systematic error. This technique has been found to be particularly valuable for unlocking the potential of archival photogrammetric DEMs.

In discussing the general performance of the integrated monitoring strategy, the potential for multi-scale monitoring of geohazard activity has been emphasised, and issues relating to transferability have been discussed. The benefits of the monitoring strategy in direct relation to coastal geohazard activity have been debated, with a range of quantitative analysis strategies highlighted. In relation to more general software issues, the limitations of the existing 2.5D data structure, and the direct impact of this in the context of this research have been discussed.

Research objectives outlined in Chapter One have been re-evaluated in relation to the outcomes of the work presented in this thesis. Brief discussion has been devoted to highlighting how each objective has been successfully fulfilled. Following this, recommendations for future work have been presented. This has included discussion of possible strategies for improving the performance of the surface matching algorithm. In addition, the potential of the monitoring strategy in relation to upscaling for monitoring of large scale coastal change has been emphasised. Finally, emerging techniques and technology, including continuous GNSS monitoring, unmanned aerial vehicles, mobile mapping systems, and future developments in satellite remote sensing, have been briefly considered.

REFERENCES

Abellán, A., Vilaplana, J.M. and J., M., 2006. Application of a long-range terrestrial laser scanner to a detailed rockfall study at Vall de Núria (Eastern Pyrenees, Spain). *Engineering Geology*, 88(3-4): 136-148.

Achille, C., Fregonese, L., Monti, C. and Savi, C., 2005. Advanced methodologies for surface analysis: methods, comparison and monitoring of the mosaic surface floor of the St Mark's Basilica in Venice. *International Archives of Photogrammetry, Remote Sensing and Spatial Information Sciences,* 36(5/C34): 6 p.

Ackermann, F., 1999. Airborne laser scanning - present status and future expectations. *ISPRS Journal of Photogrammetry and Remote Sensing*, 54(2-3): 64-67.

Adams, D., 2007. Marine-based mobile mapping and survey systems. *Proceedings of 5th International Symposium on Mobile Mapping Technology (MMT'07); International Archives of Photogrammetry, Remote Sensing and Spatial Information Sciences*, Padua, Italy. 5 p.

Adams, J.C. and Chandler, J.H., 2002. Evaluation of LIDAR and medium scale photogrammetry for detecting soft-cliff coastal change. *The Photogrammetric Record*, 17(99): 405-418.

Adams, J.C., Smith, M.J. and Bingley, R.M., 2003. Development and integration of terrestrial cliff-face mapping techniques within regional coastal monitoring. *Proceedings of the Annual Conference of the Remote Sensing and Photogrammetry Society*, RSPSoc. Nottingham, UK. 8 p.

Afshar, M., Boroumand, M. and Studnicka, N., 2002. Archaeological scanning of Persepolis. Using 3D laser scanning for mapping of ancient sites in Iran. *GIM International*, 16(6): 12-15.

Aguilar, F.J., Agüera, F., Aguilar, M.A. and Carvajal, F., 2005. Effects of terrain morphology, sampling density, and interpolation methods on grid DEM accuracy. *Photogrammetric Engineering and Remote Sensing*, 71(7): 805-816.

Akça, D., 2003. Full automatic registration of laser scanner point clouds. *Proceedings of Optical 3-D Measurement Techniques VI*, Zurich, Switzerland. pp. 330-337.

Akel, N.A., Kremeike, K., Filin, S., Sester, M. and Doytsher, Y., 2005. Dense DTM generalisation aided by roads extracted from LiDAR data. *International Archives of Photogrammetry, Remote Sensing and Spatial Information Sciences*, 36(3/W19): 54-59.

Alba, M., Longoni, L., Papini, M., Roncoroni, F. and Scaioni, M., 2005. Feasibility and problems of TLS in modeling rock faces for hazard mapping. *International Archives of Photogrammetry, Remote Sensing and Spatial Information Sciences*, 36(3/W19): 156-161.

Allen, P.K., Troccoli, A., Smith, B., Murray, S., Stamos, I. and Leordeanu, M., 2003. New methods for digital modeling of historic sites. *IEEE Computer Graphics and Applications*, 23(6): 32-41.

Alshawabkeh, Y. and Haala, N., 2004. Integration of digital photogrammetry and laser scanning for heritage documentation. *International Archives of Photogrammetry, Remote Sensing and Spatial Information Sciences*, 35(B5): 6 p.

Angeli, M.-G., Pasuto, A. and Silvano, S., 2000. A critical review of landslide monitoring experiences. *Engineering Geology*, 55(3): 133-147.

Arnold, N.S., Rees, W.G., Devereux, B.J. and Amable, G.S., 2006. Evaluating the potential of high-resolution airborne LiDAR data in glaciology. *International Journal of Remote Sensing*, 27(6): 1233-1251.

Axelsson, P., 1999. Processing of laser scanner data - algorithms and applications. *ISPRS Journal of Photogrammetry and Remote Sensing*, 54(2-3): 138-147.

Bae, K.-H. and Lichti, D.D., 2004. Automated registration of unorganised point clouds from terrestrial laser scanners. *International Archives of Photogrammetry, Remote Sensing and Spatial Information Sciences*, 35(B5): 222-227.

BAE Systems, 2006. *SocetSet User's Manual, Version 5.3*. BAE Systems, 1061 p.

Baltsavias, E.P., 1999a. Airborne laser scanning: basic relations and formulas. *ISPRS Journal of Photogrammetry and Remote Sensing*, 54(2-3): 199-214.

Baltsavias, E.P., 1999b. A comparison between photogrammetry and laser scanning. *ISPRS Journal of Photogrammetry and Remote Sensing*, 54(2-3): 83-94.

Baltsavias, E.P., Favey, E., Bauder, A., Bösch, H. and Pateraki, M., 2001. Digital surface modelling by airborne laser scanning and digital photogrammetry for glacier monitoring. *The Photogrammetric Record*, 17(98): 243-273.

Bannister, A., Raymond, S. and Baker, R., 1998. *Surveying*, seventh ed. Longman, Harlow, 502 p.

Baptista, P., Bastos, L.C., Bernardes, C. and Dias, A., 2002. A GPS based system for monitoring sand movements - the Aveiro coastline case. *Proceedings of Littoral 2002*, Porto, Portugal. pp. 347-351.

Barber, D.M., 2003. *Terrestrial laser scanning for the metric survey of cultural heritage structures*, Newcastle University, Newcastle upon Tyne, 222 p.

Barber, D.M. and Mills, J.P., 2007. Vehicle based waveform laser scanning in a coastal environment. *Proceedings of 5th International Symposium on Mobile Mapping Technology (MMT'07); International Archives of Photogrammetry, Remote Sensing and Spatial Information Sciences*, Padua, Italy. 6 p.

Barringer, J.R.F. and Lilburne, L., 1997. An evaluation of digital elevation models for upgrading New Zealand Land Resource Inventory slope data. *Proceedings of GeoComputation '97 & SIRC '97*, Otago, New Zealand. pp. 15-22.

Basili, P., Capom, M., Bonafoni, S. and Mattioli, V., 2004. Integration of digital elevation data scanning 3D and interferometric SAR systems. *Proceedings of the IEEE International Geoscience and Remote Sensing Symposium (IGARSS) 2004*, IEEE. Anchorage, USA. pp. 2811-2814.

Bayram, B., Bayraktar, H., Helvaci, C. and Acar, U., 2004. Coastline change detection using Corona, SPOT and IRS 1D images. *International Archives of Photogrammetry, Remote Sensing and Spatial Information Sciences*, 35(B7): 437-441.

BBC, 2006. *Coast Series 2: Newcastle to Hull*. Open University, UK

BBC, 2007. http://www.bbc.co.uk/mediaselector/check/player/nol/newsid_6350000/newsid_6357800?redirect=6357879.stm&news=1&bbwm=1&nbram=1&nbwm=1&bbram=1 [Accessed: 13th February, 2007].

Behr, J.A., Hudnut, K.W. and King, N.E., 1998. Monitoring structural deformation at Pacoima Dam, California using continuous GPS. *Proceedings of the 11th International Technical Meeting of the Satellite Division of the Institute of Navigation (ION GPS-98)*, Nashville, USA. pp. 59-68.

Bellian, J.A., Kerans, C. and Jennette, D.C., 2005. Digital outcrop models: applications of terrestrial scanning lidar technology in stratigraphic modelling. *Journal of Sedimentary Research*, 75(2): 166-176.

Besl, P.J. and McKay, N.D., 1992. A method for registration of 3-D shapes. *IEEE Transactions on Pattern Analysis and Machine Intelligence*, 14(2): 239-256.

Betts, H.D., Trustrum, N.A. and De Rose, R.C., 2003. Geomorphic changes in a complex gully system measured from sequential digital elevation models, and implications for management. *Earth Surface Processes and Landforms*, 28(10): 1043-1058.

Bird, E.C.F., 2000. *Coastal Geomorphology - An Introduction*, John Wiley & Sons, Chichester, 322 p.

Bitelli, G., Dubbini, M. and Zanutta, A., 2004. Terrestrial laser scanning and digital photogrammetry techniques to monitor landslide bodies. *International Archives of Photogrammetry, Remote Sensing and Spatial Information Sciences*, 35(B5): 246-251.

Boehler, W., Bordas Vicent, M. and Marbs, A., 2003. Investigating laser scanner accuracy. *International Archives of Photogrammetry, Remote Sensing and Spatial Information Sciences*, 34(5/C15): 9 p.

Boehler, W., Heinz, G. and Marbs, A., 2001. The potential of non-contact close range laser scanners for cultural heritage recording. *International Archives of Photogrammetry, Remote Sensing and Spatial Information Sciences,* 34(5/C7): 8 p.

Boehler, W. and Marbs, A., 2002. 3D scanning instruments. *International Archives of Photogrammetry, Remote Sensing and Spatial Information Sciences,* 34(5): 9-12.

Böhm, J., 2005. Terrestrial laser scanning - a supplementary approach for 3D documentation and animation. *Proceedings of Photogrammetric Week '05*, Wichmann, Heidelberg. Stuttgart, Germany. pp. 263-271.

Böhm, J. and Haala, N., 2005. Efficient integration of aerial and terrestrial laser data for virtual city modeling using LASERMAPs. *International Archives of Photogrammetry, Remote Sensing and Spatial Information Sciences*, 36(3/W19): 192-197.

Bolstad, P.V. and Stowe, T., 1994. An evaluation of DEM accuracy: elevation, slope, and aspect. *Photogrammetric Engineering and Remote Sensing*, 60(11): 1327-1332.

Bornaz, L., Lingua, A. and Rinaudo, F., 2003. Terrestrial Laser Scanning: increasing automation for engineering and heritage applications. *GIM International*, 17(3): 12-15.

Bornaz, L. and Rinaudo. F., 2004. Terrestrial laser scanner data processing. *International Archives of Photogrammetry, Remote Sensing and Spatial Information Sciences*, 35(B5): 514-519.

Bray, M.J. and Hooke, J.M., 1997. Prediction of soft-cliff retreat with accelerating sea-level rise. *Journal of Coastal Research*, 13(2): 453-467.

Brock, J.C., Sallenger, A.H., Krabill, W.B., Swift, R.N. and Wright, C.W., 2001. Recognition of fiducial surfaces in LiDAR surveys of coastal topography. *Photogrammetric Engineering and Remote Sensing*, 67(11): 1245-1258.

Brown, D.G. and Arbogast, A.F., 1999. Digital photogrammetric change analysis as applied to active coastal dunes in Michigan. *Photogrammetric Engineering and Remote Sensing*, 65(4): 467-474.

Brückl, E., Brunner, F.K. and Kraus, K., 2006. Kinematics of a deep-seated landslide derived from photogrammetric, GPS and geophysical data. *Engineering Geology*, 88(3-4): 149-159.

Buckley, S.J., 2003. *A geomatics data fusion technique for change monitoring*. PhD Thesis, University of Newcastle upon Tyne, Newcastle upon Tyne, 258 p.

Buckley, S.J., Mills, J.P., Clarke, P.J., Edwards, S.J., Pethick, J. and Mitchell, H.L., 2002. Synergy of GPS, Photogrammetry and InSAR for coastal zone monitoring. *International Archives of Photogrammetry, Remote Sensing and Spatial Information Sciences*, 34(4): 6 p.

Buckley, S.J. and Mitchell, H.L., 2004. Integration, validation and point spacing optimisation of digital elevation models. *The Photogrammetric Record*, 19(108): 277-295.

Burrough, P.A. and McDonnell, R.A., 1998. *Principles of Geographical Information Systems*, Oxford University Press, Oxford, 333 p.

Camfield, F.E. and Morang, A., 1996. Defining and interpreting shoreline change. *Ocean and Coastal Management*, 32(3): 129-151.

Campbell, J.B., 2002. *Introduction to Remote Sensing*, third ed. Guilford, New York, 621 p.

Capra, L., Lugo-Hubp, J. and Borselli, L., 2003. Mass movements in tropical volcanic terrains: the case of Teziutlán (México). *Engineering Geology*, 69(3-4): 359-379.

Carmichael, O., Huber, D. and Hebert, M., 1999. Large data sets and confusing scenes in 3-D surface matching and recognition. *Proceedings of the Second International Conference on 3-D Digital Imaging and Modeling (3DIM'99)*, IEEE. Ottawa, Canada. pp. 358-367.

Casson, B., Delacourt, C., Baratoux, D. and Allemand, P., 2003. Seventeen years of the "La Clapière" landslide evolution analysed from ortho-rectified aerial photographs. *Engineering Geology*, 68(1): 123-139.

Chadwick, J., Dorsch, S., Glenn, N., Thackray, G. and Shilling, K., 2005. Application of multi-temporal high-resolution imagery and GPS in a study of the motion of a canyon rim landslide. *ISPRS Journal of Photogrammetry and Remote Sensing*, 59(4): 212-221.

Chandler, J., 1999. Effective application of automated digital photogrammetry for geomorphological research. *Earth Surface Processes and Landforms*, 24(1): 51-63.

Chandler, J.H. and Clark, J.S., 1992. The archival photogrammetric technique: further application and development. *The Photogrammetric Record*, 14(80): 241-247.

Chang, H.C., Ge, L., Rizos, C. and Milne, T., 2004. Validation of DEMs derived from radar interferometry, airborne laser scanning and photogrammetry by using GPS-RTK. *Proceedings of the IEEE International Geoscience and Remote Sensing Symposium (IGARSS) 2004*. IEEE. Anchorage, USA. pp. 2815-2818.

Chang, J.-C. and Slaymaker, O., 2002. Frequency and spatial distribution of landslides in a mountainous drainage basin: Western Foothills, Taiwan. *Catena*, 46(4): 285-307.

Chaplot, V., Darboux, F., Bourennane, H., Leguédois, S., Silvera, N. and Phachomphon, K., 2006. Accuracy of interpolation techniques for the derivation of digital elevation models in relation to landform types and data density. *Geomorphology*, 77(1-2): 126-141.

Charlier, R.H. and Bologa, A.S., 2003. Coastal zone under siege - is there realistic relief available? *Journal of Coastal Research*, 19(4): 884-889.

Charlton, M.E., Large, A.R.G. and Fuller, I.C., 2003. Application of airborne LiDAR in river environments: The River Coquet, Northumberland, UK. *Earth Surface Processes and Landforms*, 28(3): 299-306.

Chatterjee, R.S., Fruneau, B., Rundant, J.P., Roy, P.S., Frison, P.-L., Lakhera, R.C., Dadhwal, V.K. and Saha, R., 2006. Subsidence of Kolkata (Calcutta) City, India during the 1990s as observed from space by differential synthetic aperture radar interferometry (D-InSAR) technique. *Remote Sensing of Environment*, 102(1-2): 176-185.

Chave, A.D. and Thomson, D.J., 2003. A bounded influence regression estimator based on the statistics of the hat matrix. *Applied Statistics*, 52(3): 307-322.

Chen, Y. and Medioni, G., 1992. Object modelling by registration of multiple range images. *Image and Vision Computing*, 10(3): 145-155.

Clark, A.R. and Guest, S., 1991. The Whitby cliff stabilisation and coast protection scheme. *Proceedings of the International Conference on Slope Stability (Institute of Civil Engineers)*, Thomas Telford. Isle of Wight. pp. 283-290.

Clowes, M., 2007. Personal communication.

Coe, J.A., Ellis, W.L., Godt, J.W., Savage, W.Z., Savage, J.E., Michael, J.A., Kibler, J.D., Powers, P.S., Lidke, D.J. and Debray, S., 2003. Seasonal movement of the Slumgullion landslide determined from Global Positioning System surveys and field instrumentation, July 1998 - March 2002. *Engineering Geology*, 68(1-2): 67-101.

Coleman, D., Holland, P., Kaden, N., Klema, V. and Peters, S.C., 1980. A system of subroutines for iteratively reweighted least squares computations. *ACM Transactions on Mathematical Software*, 6(3): 327-336.

Collins, B.D. and Kayen, R., 2006. *Land-based LiDAR mapping - a new surveying technique to shed light on rapid topographic change*. USGS, 4 p.

Conforti, D., 2004. Mapping Mount Tinisa in Italy: merging airborne and TLS datasets. *GIM International*, 18(9): 41-43.

Cook, R.D. and Weisberg, S., 1982. *Residuals and Influence in Regression*, first ed. Chapman and Hall, New York, 230 p.

Cooper, M.A.R., 1998. Datums, coordinates and differences. In: Lane, S.N., Chandler, J.H., Richards, K.S. (Eds.), *Landform Monitoring, Modelling and Analysis*, John Wiley & Sons, Chichester, pp. 21-35.

Cooper, M.A.R. and Cross, P.A., 1988. Statistical concepts and their applications in photogrammetry and surveying. *Photogrammetric Record*, 12(71): 637-663.

Cooper, M.A.R. and Robson, S., 2001. Theory of close range photogrammetry. In: Atkinson, K.B. (Ed.), *Close Range Photogrammetry and Machine Vision*, first ed., Whittles, Latheronwheel, pp. 9-51.

Corsini, A., Pasuto, A., Soldati, M. and Zannoni, A., 2005. Field monitoring of the Corvara landslide (Dolomites, Italy) and its relevance for hazard assessment. *Geomorphology*, 66(1-4): 149-165.

Crombaghs, M., Oude Elberink, S., Brügelmann, R. and de Min, E., 2002. Assessing height precision of laser altimetry DEMs. *International Archives of Photogrammetry, Remote Sensing and Spatial Information Sciences*, 34(3A): 6 p.

Crosby, A., 1995. Chapter 2: Geology and physical environment. In: Barne, J.H., Robson, C.F., Kaznowska, S.S., Doody, J.P., Davidson, N.C. (Eds.), *Coasts and seas of the United Kingdom. Region 5 North-east England: Berwick-upon-Tweed to Filey Bay*, Joint Nature Conservation Committee, Peterborough, pp. 17-36.

Csanyi, N. and Toth, C.K., 2007. Improvement of Lidar data accuracy using Lidar-specific ground targets. *Photogrammetric Engineering and Remote Sensing*, 73(4): 385-396.

De Rose, R.C., Gomez, B., Marden, M. and Trustrum, N.A., 1998. Gully erosion in Mangatu Forest, New Zealand, estimated from digital elevation models. *Earth Surface Processes and Landforms*, 23(11): 1045-1053.

DEFRA, 2006a. *Consultation document: promoting an integrated approach to management of the coastal zone (ICZM) in England*. DEFRA, London, 41 p.

DEFRA, 2006b. *Shoreline Management Plan Guidance, Volume 1: Aims and Requirements*, DEFRA, London, 54 p.

Demir, N., Bayram, B., Alkis, Z., Helvaci, C., Çetin, I., Vögtle, T., Ringle, K. and Steinle, E., 2004. Laser scanning for terrestrial photogrammetry, alternative system or combined with traditional system? *International Archives of Photogrammetry, Remote Sensing and Spatial Information Sciences*, 35(B5): 5 p.

Desmet, P.J.J., 1997. Effects of interpolation errors on the analysis of DEMs. *Earth Surface Processes and Landforms*, 22(6): 563-580.

Dixon, L.F.J., Barker, R., Bray, M., Farres, P., Hooke, J., Inkpen, R., Merel, A., Payne, D. and Shelford, A., 1998. Analytical Photogrammetry for Geomorphological Research. In: Lane, S.N., Richards, K.S., Chandler, J.H. (Eds.), *Landform Monitoring, Modelling and Analysis*, John Wiley & Sons, Chichester, pp. 63-94.

Dorai, C., Weng, J. and Jain, A.K., 1997. Optimal registration of object views using range data. *IEEE Transactions on Pattern Analysis and Machine Intelligence*, 19(10): 1131-1138.

Dornbusch, U., Moses, C., Robinson, D. and Williams, R., 2005. Soft copy photogrammetry to measure shore platform erosion on decadal time scales. *Proceedings of CoastGIS 2005, 6th International Symposium on GIS and Computer Cartography for Coastal Zone Management*, Aberdeen, UK. pp. 72-84.

Dorninger, P. and Briese, C., 2005. Advanced geometric modeling of historical rooms. *International Archives of Photogrammetry, Remote Sensing and Spatial Information Sciences*, 36(5/C34): 6 p.

Dowman, I., 2004. Integration of LiDAR and IfSAR for mapping. *International Archives of Photogrammetry, Remote Sensing and Spatial Information Sciences*, 35(B2): 11 p.

Draper, N.R. and Smith, H., 1981. *Applied Regression Analysis*, second ed. John Wiley & Sons, New York, 709 p.

Draper, N.R. and Smith, H., 1998. *Applied Regression Analysis*, third ed. John Wiley & Sons, New York, 706 p.

East Riding of Yorkshire Council, 2005. http://www.eastriding.gov.uk/aspirelinks/coastal/3coastalmonitoring.pdf [Accessed: 5th October, 2006].

Ebner, H. and Strunz, G., 1988. Combined point determination using digital terrain models as control information. *International Archives of Photogrammetry, Remote Sensing and Spatial Information Sciences*, 27(B11): 578-587.

Eisenbeiss, H., 2004. A mini unmanned aerial vehicle (UAV): system overview and image acquisition. *International Archives of Photogrammetry, Remote Sensing and Spatial Information Sciences*, 36(5/W1): 7 p.

El-Ashry, M.T. (Ed.), 1977. *Air Photography and Coastal Problems*. Benchmark Papers in Geology, 38. Dowden, Hutchinson & Ross, Stroudsburg, Pennsylvania, 425 p.

El-Ashry, M.T. and Wanless, H.R., 1967. Shoreline features and their changes. *Photogrammetric Engineering*, 33(2): 184-189.

Elliot, M., Jones, N.V., Lewis, D.S., Pethick, J.S. and Symes, D.G., 1991. *Filey Bay Environmental Statement*, Institute of Estuarine and Coastal Studies, University of Hull, 131 p.

Elmqvist, M., 2002. Ground surface estimation from airborne laser scanner data using active shape models. *International Archives of Photogrammetry, Remote Sensing and Spatial Information Sciences*, 34(3A+B): 5 p.

Emery, K.O. and Kuhn, G.G., 1982. Sea cliffs: their processes, profiles and classification. *Geological Society of America Bulletin*, 93: 644-654.

English Heritage, 2003. *Coastal Defence and the Historic Environment*, English Heritage, 15 p.

English Nature, 2007. *Whitby - Saltwick SSSI Citation Document*. English Nature, 1 p.

Fabris, M. and Pesci, A., 2005. Automated DEM extraction in digital aerial photogrammetry: precisions and validation for mass movement monitoring. *Annals of Geophysics*, 48(6): 973-988.

Farina, P., Colombo, D., Fumagalli, A., Marks, F. and Moretti, S., 2006. Permanent Scatterers for landslide investigations: outcomes from the ESA-SLAM project. *Engineering Geology*. 88(3-4): 200-217.

Fernández, J., Yu, T.-T., Rodríguez-Velasco, G., González-Matesanz, J., Romero, R., Rodríguez, G., Quirós, R., Dalda, A., Aparicio, A. and Blanco, M.J., 2003. New geodetic monitoring system in the volcanic island of Tenerife, Canaries, Spain. Combination of InSAR and GPS techniques. *Journal of Volcanology and Geothermal Research*, 124(3-4): 241-253.

Ferretti, A., Prati, C. and Rocca, F., 2000. Nonlinear subsidence rate estimation using permanent scatterers in differential SAR interferometry. *IEEE Transactions on Geoscience and Remote Sensing*, 38(5): 2202-2212.

Ferretti, A., Prati, C. and Rocca, F., 2001. Permanent scatterers in SAR interferometry. *IEEE Transactions on Geoscience and Remote Sensing*, 39(1): 8-20.

Filin, S., 2005. Elimination of systematic errors from airborne laser scanning data. *Proceedings of International Geoscience and Remote Sensing Symposium*, IEEE. Seoul, South Korea. 4 p.

Filin, S. and Vosselman, G., 2004. Adjustment of airborne laser altimetry strips. *International Archives of Photogrammetry, Remote Sensing and Spatial Information Sciences*, 34(B3): 12-23.

Fisher, P., 1998. Improved modeling of elevation error with geostatistics. *GeoInformatica*, 2(3): 215-233.

Flood, M., 2001. LIDAR activities and research priorities in the commercial sector. *International Archives of Photogrammetry, Remote Sensing and Spatial Information Sciences*, 34(3/W4): 3-7.

Fox, J., 2002. *An R and S-PLUS Companion to Applied Regression*, Sage, London, 312 p.

Fraser, C.S., 2001. Network Design. In: Atkinson, K.B. (Ed.), *Close Range Photogrammetry and Machine Vision*, Whittles, Latheronwheel, pp. 256-281.

Fraser, C.S. and Riedel, B., 2000. Monitoring the thermal deformation of steel beams via vision metrology. *ISPRS Journal of Photogrammetry and Remote Sensing*, 55(4): 268-276.

French, J.R., 2003. Airborne LiDAR in support of geomorphological and hydraulic modelling. *Earth Surface Processes and Landforms*, 28(3): 321-335.

Fryer, J.G., 2001. Camera calibration. In: Atkinson, K.B. (Ed.), *Close Range Photogrammetry and Machine Vision*, Whittles, Latheronwheel, pp. 156-179.

Gamba, P., Dell'acqua, F. and Houshmand, B., 2003. Comparison and fusion of LIDAR and InSAR digital elevation models over urban areas. *International Journal of Remote Sensing*, 24(22): 4289-4300.

Gong, J., Li, Z., Zhu, Q., Sui, H. and Zhou, Y., 2000. Effects of various factors on the accuracy of DEMs: and intensive experimental investigation. *Photogrammetric Engineering and Remote Sensing*, 66(9): 1113-1117.

Gooch, M.J. and Chandler, J.H., 2001. Failure prediction in automatically generated digital elevation models. *Computers and Geosciences*, 27(8): 913-920.

Goodall, C., 1983. M-Estimators of Location: an Outline of the Theory. In: Hoaglin, D.C., Mosteller, F., Tukey, J.W. (Eds.), *Understanding Robust and Exploratory Data Analysis*, John Wiley & Sons, New York, pp. 339-403.

Göpfert, J. and Heipke, C., 2006. Assessment of LiDAR DTM accuracy in coastal vegetated areas. *International Archives of Photogrammetry, Remote Sensing and Spatial Information Sciences*, 36(B3): 79-85.

Gordon, S.J. and Lichti, D.D., 2004. Terrestrial laser scanners with a narrow field of view: the effect on 3D resection solutions. *Survey Review*, 37(292): 448-468.

Gordon, S.J., Lichti, D.D., Stewart, M.P. and Franke, J., 2004. Modelling point clouds for precise structural deformation measurement. *International Archives of Photogrammetry, Remote Sensing and Spatial Information Sciences*, 35(B5): 6 p.

Gorman, L., Morang, A. and Larson, R., 1998. Monitoring the coastal environment; Part IV: mapping, shoreline changes, and bathymetric analysis. *Journal of Coastal Research*, 14(1): 61-92.

Gruen, A., 2001. Least squares matching: a fundamental measurement algorithm. In: Atkinson, K.B. (Ed.), *Close Range Photogrammetry and Machine Vision*, Whittles, Latheronwheel, pp. 217-255.

Gruen, A. and Akça, D., 2005. Least squares 3D surface and curve matching. *ISPRS Journal of Photogrammetry and Remote Sensing*, 59(3): 151-174.

Guarnieri, A., Guidi, G., Tucci, G. and Vettore, A., 2003. Towards automatic modeling for cultural heritage applications. *International Archives of Photogrammetry, Remote Sensing and Spatial Information Sciences*, 34(5/W12): 176-181.

Gulyaev, S.A. and Buckeridge, J.S., 2004. Terrestrial methods for monitoring cliff erosion in an urban environment. *Journal of Coastal Research*, 20(3): 871-878.

Gutierrez, R., Neuenschwander, A. and Crawford, M., 2005. Development of laser waveform digitization for airborne LIDAR topographic mapping instrumentation. *Proceedings of International Geoscience and Remote Sensing Symposium*, IEEE. Seoul, South Korea. pp. 1154-1157.

Guzzetti, F., Carrara, A., Cardinali, M. and Reichenbach, P., 1999. Landslide hazard evaluation: a review of current techniques ad their application in a multi-scale study, Central Italy. *Geomorphology*, 31(1-4): 181-216.

Haala, N. and Brenner, C., 1999. Extraction of buildings and trees in urban environments. *ISPRS Journal of Photogrammetry and Remote Sensing*, 54(2-3): 130-137.

Habib, A. and Kelley, D., 2001. Automatic relative orientation of large scale imagery over urban areas using Modified Iterated Hough Transform. *ISPRS Journal of Photogrammetry and Remote Sensing*, 56(1): 29-41.

Habib, A. and Lee, Y.-R., 2001. Surface matching and change detection using a robust Modified Hough Transformation for robust parameter estimation. *The Photogrammetric Record*, 17(98): 303-315.

Habib, A. and Schenk, T., 1999. A new approach for matching surfaces from laser scanners and optical scanners. *International Archives of Photogrammetry, Remote Sensing and Spatial Information Sciences*, 32(3/W14): 55-61.

Hall, J.W., Meadowcroft, I.C., Lee, E.M. and van Gelder, P.H.A.J.M., 2002. Stochastic simulation of episodic soft coastal cliff recession. *Coastal Engineering*, 46(3): 159-174.

Hanssen, R.F., 2001. *Radar Interferometry*, Kluwer, Dordrecht, 308 p.

Hapke, C. and Richmond, B., 2000. Monitoring beach morphology changes using small- format aerial photography and digital softcopy photogrammetry. *Environmental Geosciences*, 7(1): 32-37.

Heiberger, R.M. and Becker, R.A., 1992. Design of an S function for robust regression using iteratively reweighted least squares. *Journal of Computational and Graphical Statistics*, 1(3): 181-196.

Heritage, G. and Hetherington, D., 2007. Towards a protocol for laser scanning in fluvial geomorphology. *Earth Surface Processes and Landforms*, 32(1): 66-74.

Hessami, M., Anctil, F. and Viau, A.A., 2001. Delaunay implementation to improve kriging computing efficiency. *Computers and Geosciences*, 27(2): 237-240.

Hill, C.D. and Sippel, K.D., 2002. Modern deformation monitoring: a multi sensor approach. *Proceedings of FIG XXII International Congress*, Washington, D.C., USA. 12 p.

Hoaglin, D.C., Mosteller, F. and Tukey, J.W., 1983. *Understanding Robust and Exploratory Data Analysis*, John Wiley & Sons, New York, 447 p.

Hoaglin, D.C. and Welsch, R.E., 1978. The Hat matrix in regression and ANOVA. *The American Statistician*, 32(1): 17-22.

Hobbs, P.R.N., 2007. Personal communication.

Hodgson, M.E. and Bresnahan, P., 2004. Accuracy of airborne lidar-derived elevation: empirical assessment and error budget. *Photogrammetric Engineering and Remote Sensing*, 70(3): 331-339.

Hofmann-Wellenhof, B., Lichtenegger, H. and Collins, J., 2001. *GPS Theory and Practice*, Springer, Vienna, 382 p.

Hsiao, K.H., Liu, J.K., Yu, M.F. and Tseng, Y.H., 2004. Change detection of landslide terrains using ground-based LiDAR data. *International Archives of Photogrammetry, Remote Sensing and Spatial Information Sciences*, 35(B7): 617-621.

Huang, Y.D., 2000. Evaluation of information loss in digital elevation models with digital photogrammetric systems. *Photogrammetric Record*, 16(95): 781-791.

Hudak, A.T., Lefsky, M.A., Cohen, W.B. and Berterretche, M., 2002. Integration of lidar and Landsat ETM+ data for estimating and mapping forest canopy height. *Remote Sensing of Environment*, 82(2-3): 397-416.

Hudnut, K.W., Borsa, A., Glennie, C. and Minster, J.-B., 2002. High-resolution topography along surface rupture of the 16 October 1999 Hector Mine, California, Earthquake (Mw 7.1) from airborne laser swath mapping. *Bulletin of the Seismological Society of America*, 92(4): 1570-1576.

Hug, C., Ullrich, A. and Grimm, A., 2004. Litemapper-5600 - a waveform digitizing LIDAR terrain and vegetation mapping system. *International Archives of Photogrammetry, Remote Sensing and Spatial Information Sciences*, 36(8/W2): 24-29.

Hugenholtz, C.H. and Wolfe, S.A., 2005. Recent stabilisation of active sand dunes on the Canadian prairies and relation to climate variations. *Geomorphology*, 68(1-2): 131-147.

Huising, E.J. and Gomes Pereira, L.M., 1998. Errors and accuracy estimates of laser data acquired by various laser scanning systems for topographic applications. *ISPRS Journal of Photogrammetry and Remote Sensing*, 53(5): 245-261.

Hunter, G., Pinkerton, H., Airey, R. and Calvari, S., 2003. The application of a long-range laser scanner for monitoring volcanic activity on Mount Etna. *Journal of Volcanology and Geothermal Research*, 123(1-2): 203-210.

IGOS, 2003. *IGOS Geohazards Theme Report*, Integrated Global Observing Strategy, 55 p.

IGS, 2007. http://igscb.jpl.nasa.gov/ [Accessed: 22nd June, 2007].

Irish, J.L. and Lillycrop, W.J., 1999. Scanning laser mapping of the coastal zone: the SHOALS system. *ISPRS Journal of Photogrammetry and Remote Sensing*, 54(2-3): 123-129.

James, T.D., Murray, T., Barrand, N.E. and Barr, S.L., 2006. Extracting photogrammetric ground control from lidar DEMs for change detection. *Photogrammetric Record*, 21(116): 312-328.

Jennings, S., Muldowney, L. and Wilmott, T., 2002. *Excavation and evaluation at Whitby, 2002: an archaeological response to coastal erosion*, Centre for Archaeology News (4), pp. 2-4.

Johnson, A.E. and Hebert, M., 1998. Surface matching for object recognition in complex three-dimensional scenes. *Image and Vision Computing*, 16(9-10): 635-651.

Johnson, A.E. and Hebert, M., 1999. Using spin images for efficient object recognition in cluttered 3D scenes. *IEEE Transactions on Pattern Analysis and Machine Intelligence*, 21(5): 433-449.

Jones, C., 1997. *Geographical Information Systems and Computer Cartography*, Longman, Harlow, 319 p.

Jones, L.D., 2006. Monitoring landslides in hazardous terrain using terrestrial LiDAR: an example from Montserrat. *Quarterly Journal of Engineering Geology and Hydrogeology*, 39(4): 371-373.

Jutzi, B. and Stilla, U., 2006. Characteristics of the measurement system of a full-waveform laser system. *International Archives of Photogrammetry, Remote Sensing and Spatial Information Sciences*, 36(1A): 6 p.

Kadobayashi, R., Kochi, N., Otani, H. and Furukawa, R., 2004. Comparison and evaluation of laser scanning and photogrammetry and their combined use for digital recording of cultural heritage. *International Archives of Photogrammetry, Remote Sensing and Spatial Information Sciences*, 35(B5): 401-406.

Karras, G.E. and Petsa, E., 1993. DEM matching and detection of deformation in close-range photogrammetry without control. *Photogrammetric Engineering and Remote Sensing*, 59(9): 1419-1424.

Katzenbeisser, R., 2003. About the calibration of LIDAR sensors. *ISPRS Journal of Photogrammetry and Remote Sensing*, 34(Part 3/W13): 59-64.

Kennie, T.J.M., 1990. Field data collection for terrain modelling. In: Petrie, G., Kennie, T.J.M. (Eds.), *Terrain Modelling in Surveying and Civil Engineering*, Whittles, Latheronwheel, pp. 4-16.

Kennie, T.J.M. and Petrie, G., 1990. Introduction to terrain modelling - application fields and terminology. In: Petrie, G., Kennie, T.J.M. (Eds.), *Terrain Modelling in Surveying and Civil Engineering*, Whittles, Latheronwheel, pp. 1-3.

Kidner, D.B., 2003. Higher-order interpolation of regular grid digital elevation models. *International Journal of Remote Sensing*, 24(14): 2981-2987.

Kienzle, S., 2004. The effect of DEM raster resolution on first order, second order and compound terrain derivatives. *Transactions in GIS*, 8(1): 83-111.

Klein, M. and Lichter, M., 2006. Monitoring changes in shoreline position adjacent to the Hadera power station, Israel. *Applied Geography*, 26(3-4): 210-226.

Knapen, A., Kitutu, M.G., Poesen, J., Breugelmans, W., Deckers, J. and Muwanga, A., 2006. Landslides in a densely populated county at the footslopes of Mount Elgon (Uganda): characteristics and causal factors. *Geomorphology*, 73(1-2): 149-165.

Komar, P.D., 1998. *Beach Processes and Sedimentation*, second ed. Prentice-Hall, New Jersey, 544 p.

Krabill, W.B., Wright, C.W., Swift, R.N., Frederick, E.B., Manizade, S.S., Yungel, J.K., Martin, C.F., Sonntag, J.G., Duffy, M., Hulslander, W. and Brock, J.C., 2000. Airborne laser mapping of Assateague National Seashore beach. *Photogrammetric Engineering and Remote Sensing*, 66(1): 65-71.

Kraus, K., 2000. *Photogrammetry, Volume 1: Fundamentals and Standard Processes*, 1, fourth ed. Dümmler, Bonn, 397 p.

Kraus, K. and Otepka, J., 2005. DTM modelling and visualization - the SCOP approach. *Proceedings of Photogrammetric Week '05*, Wichmann, Heidelberg. Stuttgart, Germany. pp. 241-252.

Kweon, I.S. and Kanade, T., 1992. High-resolution terrain map from multiple sensor data. *IEEE Transactions on Pattern Analysis and Machine Intelligence*, 14(2): 278-292.

Lane, S.N. and Chandler, J.H., 2003. Editorial: The generation of high quality topographic data for hydrology and geomorphology: New data sources, new applications and new problems. *Earth Surface Processes and Landforms*, 28(3): 229-230.

Lane, S.N., Chandler, J.H. and Richards, K.S., 1998. Landform Monitoring, Modelling and Analysis: Land *Form* in Geomorphological Research. In: Lane, S.N., Richards, K.S., Chandler, J.H. (Eds.), *Landform Monitoring, Modelling and Analysis*, John Wiley & Sons, Chichester, pp. 1-17.

Lane, S.N., James, T.D. and Crowell, M.D., 2000. Application of digital photogrammetry to complex topography for geomorphological research. *Photogrammetric Record*, 16(95): 793-821.

Langbein, J. and Bock, Y., 2004. High-rate real-time GPS network at Parkfield: utility for detecting fault slip and seismic displacements. *Geophysical Research Letters*, 31(15): 4 p.

Latypov, D., 2002. Estimating relative lidar accuracy information from overlapping flight lines. *ISPRS Journal of Photogrammetry and Remote Sensing*, 56(4): 236-245.

Lee, D.S. and Shan, J., 2003. Combining LiDAR elevation data and IKONOS multispectral imagery for coastal classification mapping. *Marine Geodesy*, 26(1-2): 117-127.

Lee, E.M. and Clark, A.R., 2002. *Investigation and Management of Soft Rock Cliffs*, Thomas Telford, London, 382 p.

Lee, E.M., Hall, J.W. and Meadowcroft, I.C., 2001. Coastal cliff recession: the use of probabilistic prediction methods. *Geomorphology*, 40(3-4): 253-269.

Lee, E.M., Meadowcroft, I.C., Hall, J.W. and Walkden, M., 2002. Coastal landslide activity: a probabilistic simulation model. *Bulletin of Engineering Geology and the Environment*, 61(4): 347-355.

Leica Geosystems, 2006. http://www.leica-geosystems.com/hds/en/lgs_5210.htm [Accessed: 26th February, 2007].

Leick, A., 2004. *GPS Satellite Surveying*, third ed. John Wiley & Sons, Hoboken, New Jersey, 435 p.

Lemmens, M., 2006. 3D laser scanner software. *GIM International*, 20(9): 49-53.

Lemmens, M., 2007. Airborne LiDAR sensors. *GIM International*, 21(2): 24-27.

Lennartz-Johansen, H. and Ellegaard, S., 2002. Analyzing Europe's largest suspension bridge. *Proceedings of FIG XXII International Congress*, Washington D.C., USA. 7 p.

Leung, K.W., 2003. Automatic real-time monitoring system (ARMS) - a robotic solution to slope monitoring. *Proceedings of 11th FIG Symposium on Deformation Measurements*, Santorini, Greece. 6 p.

Leva, D., Nico, G., Tarchi, D., Fortuny-Guasch, J. and Sieber, A.J., 2003. Temporal analysis of a landslide by means of a ground-based SAR interferometer. *IEEE Transactions on Geoscience and Remote Sensing*, 41(4): 754-752.

Li, R., Di, K. and Ruijin, M., 2003. 3-D shoreline extraction from IKONOS satellite imagery. *Marine Geodesy*, 26(1-2): 107-115.

Li, Z., 1988. On the measure of digital terrain model accuracy. *Photogrammetric Record*, 12(72): 873-877.

Li, Z., 1992. Variation of the accuracy of digital terrain models with sampling interval. *Photogrammetric Record*, 14(79): 113-128.

Li, Z., 1993. Mathematical models of the accuracy of digital terrain model surfaces linearly constructed from square gridded data. *Photogrammetric Record*, 14(82): 661-674.

Li, Z., Xu, Z., Cen, M. and Ding, X., 2001. Robust surface matching for automated detection of local deformations using Least-Median-of-Squares estimator. *Photogrammetric Engineering and Remote Sensing*, 67(11): 1283-1292.

Lichti, D.D. and Gordon, S.J., 2004. Error propagation in directly georeferenced terrestrial laser scanner point clouds for cultural heritage recording. *Proceedings of FIG Working Week*, Athens. Greece. 16 p.

Lichti, D.D., Gordon, S.J. and Tipdecho, T., 2005. Error models and propagation in directly georeferenced terrestrial laser scanner networks. *Journal of Surveying Engineering*, 131(4): 135-142.

Lillesand, T.M. and Kiefer, R.W., 2004. *Remote Sensing and Image Interpretation*, fifth ed. John Wiley & Sons, New York, 724 p.

Lim, K., Treitz, P., Wulder, M., St-Onge, B. and Flood, M., 2003. LiDAR remote sensing of forest structure. *Progress in Physical Geography*, 27(1): 88-106.

Lim, M., Petley, D., Rosser, N., Allison, R., Long, A. and Pybus, D., 2005. Combined digital photogrammetry and time-of-flight laser scanning for monitoring of cliff evolution. *Photogrammetric Record*, 20(110): 109-129.

Lindenbergh, R., Pfeifer, N. and Rabbani, T., 2005. Accuracy analysis of the Leica HDS3000 and feasibility of tunnel deformation monitoring. *International Archives of Photogrammetry, Remote Sensing and Spatial Information Sciences*, 36(3/W19): 24-29.

Lloyd, C.D. and Atkinson, P.M., 2002. Deriving DSMs from LiDAR data with kriging. *International Journal of Remote Sensing*, 23(12): 2519-2524.

Lohani, B., Mason, D.C., Scott, T.R. and Sreenivas, B., 2006. Extraction of tidal channel networks from aerial photographs alone and combined with laser altimetry. *International Journal of Remote Sensing*, 27(1): 5-25.

López, C., 2002. An experiment on the elevation accuracy improvement of photogrammetrically derived DEM. *International Journal of Geographical Information Systems*, 16(4): 361-375.

Lue, Y., 1997. One step towards a higher level of automation for softcopy photogrammetry Automatic Interior Orientation. *ISPRS Journal of Photogrammetry and Remote Sensing*, 52(3): 103-109.

Luzi, G., Pieraccini, M., Mecatti, D., Noferini, L., Macaluso, G., Galgaro, A. and Atzeni, C., 2006. Advances in ground-based microwave interferometry for landslide survey: a case study. *International Journal of Remote Sensing*, 27(12): 2331-2350.

Lyons, E., 2004. Personal communication.

Ma, B. and Ellis, R.E., 2003. Robust registration for computer-integrated orthopedic surgery: laboratory validation and clinical experience. *Medical Image Analysis*, 7(3): 237-250.

Maas, H.-G., 2000. Least-squares matching with airborne laserscanning data in a TIN structure. *International Archives of Photogrammetry, Remote Sensing and Spatial Information Sciences*, 33(3A): 548-555.

Maas, H.-G., 2002. Methods for measuring height and planimetry discrepancies in airborne laserscanner data. *Photogrammetric Engineering and Remote Sensing*, 68(9): 933-940.

Malet, J.-P., Maquaire, O. and Calais, E., 2002. The use of Global Positioning System techniques for the continuous monitoring of landslides: application to the Super-Sauze earthflow (Alpes-de-Haute-Provence, France). *Geomorphology*, 43(1-2): 33-54.

Manandhar, D. and Shibasaki, R., 2001. Vehicle-borne laser mapping system (VLMS) for 3-D urban GIS database. *Proceedings of 7th International Computers in Urban Planning and Urban Management Conference*, University of Hawaii at Manoa, Honolulu, Hawaii. pp. 2073-2075.

Mason, D.C., Davenport, I.J. and Flather, R.A., 1997. Interpolation of an intertidal digital elevation model from heighted shorelines: a case study in the Western Wash. *Estuarine, Coastal and Shelf Science*, 45(5): 599-612.

Masselink, G. and Hughes, M.G., 2003. *Introduction to Coastal Processes and Geomorphology*, Arnold, London, 354 p.

Massonnet, D., Briole, P. and Arnaud, A., 1995. Deflation of Mount Etna monitored by spaceborne radar interferometry. *Nature*, 375: 567-570.

McCullagh, M.J., 1988. Terrain and surface modelling systems: theory and practice. *Photogrammetric Record*, 12(72): 747-779.

McGlone, J.C. (Ed.), 2004. *Manual of Photogrammetry*. American Society for Photogrammetry and Remote Sensing, Bethesda, Maryland, 1151 p.

McIntosh, K. and Krupnik, A., 2002. Integration of laser-derived DSMs and matched image edges for generating an accurate surface model. *ISPRS Journal of Photogrammetry and Remote Sensing*, 56(3): 167-176.

McKean, J. and Roering, J., 2004. Objective landslide detection and surface morphology mapping using high-resolution airborne laser altimetry. *Geomorphology*, 57(3-4): 331-351.

Meisina, C., Zucca, F., Fossati, D., Ceriani, M. and Allievi, J., 2006. Ground deformation monitoring by using the Permanent Scatterers technique: the example of the Oltrepo Pavese (Lombardia, Italy). *Engineering Geology*, 88(3-4): 240-259.

Mikhail, E.M., Bethel, J.S. and McGlone, J.C., 2001. *Introduction to Modern Photogrammetry*, John Wiley & Sons, New York, 479 p.

Miller, P.E., Mills, J.P., Edwards, S.J., Bryan, P., Marsh, S. and Hobbs, P., 2006. Integrated remote monitoring for coastal geohazards and heritage sites. *Proceedings of Annual Conference of the American Society for Photogrammetry and Remote Sensing*, Reno, Nevada. 12 p.

Miller, P.E., Mills, J.P., Edwards, S.J., Bryan, P., Marsh, S., Hobbs, P. and Mitchell, H., 2007. A robust surface matching technique for integrated monitoring of coastal geohazards. *Marine Geodesy*, 30(1-2): 109-123.

Miller, P.E., Mills, J.P., Edwards, S.J., Bryan, P., Marsh, S. and Mitchell, H., in review. A robust surface matching technique for coastal geohazard assessment and management. *ISPRS Journal of Photogrammetry and Remote Sensing*.

Mills, J. and Barber, D., 2004. Geomatics techniques for structural surveying. *Journal of Surveying Engineering*, 130(2): 56-64.

Mills, J.P., Alhamlan, S., Abuoliat, A.S. and Horgan, J., 2006. Geometric validation of imagery and products from a high performance airborne digital sensor. *International Archives of Photogrammetry, Remote Sensing and Spatial Information Sciences*, 36(1B): 5 p.

Mills, J.P., Buckley, S.J. and Mitchell, H.L., 2003. Synergistic fusion of GPS and photogrammetrically generated elevation models. *Photogrammetric Engineering and Remote Sensing*, 69(4): 341-349.

Mills, J.P., Buckley, S.J., Mitchell, H.L., Clarke, P.J. and Edwards, S.J., 2005. A geomatics data integration technique for coastal change monitoring. *Earth Surface Processes and Landforms*, 30(6): 651-664.

Mirza, M.J. and Boyer, K., 1993. Performance evaluation of a class of M-estimators for surface parameter estimation in noisy range data. *IEEE Transactions on Robotics and Automation*, 9(1): 75-85.

Misra, P. and Enge, P., 2006. *Global Positioning System*, second ed. Ganga-Jamuna Press, Lincoln, Massachussetts, 569 p.

Mitasova, H., Overton, M.F., Harmon, R.S. and Berstein, D., 2004. Assessing coastal hazards using recent 3D evolution of beach geomorphology based on LiDAR and RTK-GPS surveys. *Proceedings of International Conference on Coastal Engineering*, Lisbon, Portugal. pp. 3162-3172.

Mitchell, H.L., 1994. A comprehensive system for automated body surface measurement. *International Archives of Photogrammetry, Remote Sensing and Spatial Information Sciences*, 30(5): 265-272.

Mitchell, H.L. and Chadwick, R.G., 1999. Digital photogrammetric concepts applied to surface deformation studies. *Geomatica*, 53(4): 405-414.

Moore, L.J., 2000. Shoreline mapping techniques. *Journal of Coastal Research*, 16(1): 111-124.

Moore, L.J. and Griggs, G.B., 2002. Long-term cliff retreat and erosion hotspots along the central shores of the Monterey Bay National Marine Sanctuary. *Marine Geology*, 181(1-3): 265-283.

Mora, P., Baldi, P., Casula, G., Fabris, M., Ghirotti, M., Mazzini, E. and Pesci, A., 2003. Global Positioning Systems and digital photogrammetry for the monitoring of mass movements: application to the Ca' di Malta landslide (northern Apennines, Italy). *Engineering Geology*, 68(1-2): 103-121.

Morton, R.A., Leach, M.P., Paine, J.G. and Cardoza, M.A., 1993. Monitoring beach changes using GPS surveying techniques. *Journal of Coastal Research*, 9(3): 702-720.

Nagai, M., Shibasaki, R., Manandhar, D. and Zhao, H., 2004. Development of digital surface model and feature extraction by integrating laser scanner and CCD sensor with IMU. *International Archives of Photogrammetry, Remote Sensing and Spatial Information Sciences*, 35(B5): 781-785.

Nagihara, S., Mulligan, K.R. and Xiong, W., 2004. Use of a three-dimensional laser scanner to digitally capture the topography of sand dunes in high spatial resolution. *Earth Surface Processes and Landforms*, 29(3): 391-398.

NASA JPL, 2003. http://solidearth.jpl.nasa.gov/PAGES/sea01.html [Accessed: 7th February, 2007].

NASA JPL, 2007. http://uavsar.jpl.nasa.gov/index.html [Accessed: 29th July, 2007].

National Research Council, 2004a. *A Geospatial Framework for the Coastal Zone*, National Research Council of the National Academies, Washington, D.C., 149 p.

National Research Council, 2004b. *Partnerships for Reducing Landslide Risk - Assessment of the National Landslide Hazards Mitigation Strategy*, National Research Council of the National Academies, Washington, D.C., 131 p.

National Tidal & Sea Level Facility, 2006. http://www.pol.ac.uk/ntslf/tides/datum.html [Accessed: 11th February, 2007].

Nayak, S., 2004. Role of remote sensing to integrated coastal zone management. *International Archives of Photogrammetry, Remote Sensing and Spatial Information Sciences*, 35(B7): 12 p.

NERC ARSF, 2006. http://arsf.nerc.ac.uk/instruments/altm.asp [Accessed: 12th March, 2007].

NERC ARSF, 2007. http://arsf.nerc.ac.uk/ [Accessed: 25th February, 2007].

Newman, A.V., Dixon, T.H. and Gourmelen, N., 2006. A four-dimensional viscoelastic deformation model for Long Valley Caldera, California, between 1995 and 2000. *Journal of Volcanology and Geothermal Research*, 150(1-3): 244-269.

Newton, I. and Mitchell, H.L., 2001. Medical Photogrammetry. In: Atkinson, K.B. (Ed.), *Close Range Photogrammetry and Machine Vision*, Whittles, Latheronwheel, pp. 303-327.

Niedermeier, A., Hoja, D. and Lehner, S., 2005. Topography and morphodynamics in the German Bight using SAR and optical remote sensing data. *Ocean Dynamics*, 55(2): 100-109.

Optech, 2006. http://www.optech.ca/i3dprodline-ilris3d.htm [Accessed: 10th January, 2007].

Ordnance Survey, 2007. http://www.ordnancesurvey.co.uk/oswebsite/gps/ [Accessed: 22nd June, 2007].

Pâquet, R., 2003. A method to predict accuracy of least squares surface matching for airborne laser scanning data sets. *Proceedings of the ISPRS working group III/3 workshop '3D reconstruction from airborne laserscanner and InSAR data'*, ISPRS. Dresden, Germany. 6 p.

Persson, Å., Söderman, U., Töpel, J. and Ahlberg, S., 2005. Visualization and analysis of full waveform airborne laser scanner data. *International Archives of Photogrammetry, Remote Sensing and Spatial Information Sciences*, 36(3/W19): 103-108.

Pethick, J., 1996. Coastal slope development: temporal and spatial periodicity in the Holderness cliff recession. In: Anderson, M.G., Brooks, S.M. (Eds.), *Advances in Hillslope Processes*, John Wiley & Sons, Chichester, pp. 897-917.

Pethick, J.S. and Crooks, S., 2000. Development of a coastal vulnerability index: a geomorphological perspective. *Environmental Conservation*, 27(4): 359-367.

Petley, D.N., Mantovani, F., Bulmer, M.H. and Zannoni, A., 2005. The use of surface monitoring data for the interpretation of landslide movement patterns. *Geomorphology*, 66(1-4): 133-147.

Petrie, G., 1990. Modelling, interpolation and contouring procedures. In: Petrie, G., Kennie, T.J.M. (Eds.), *Terrain Modelling in Surveying and Civil Engineering*, Whittles, Latheronwheel, pp. 112-127.

Pfeifer, N., 2005. A subdivision algorithm for smooth 3D terrain models. *ISPRS Journal of Photogrammetry and Remote Sensing*, 59(3): 115-127.

Pfeifer, N., Gorte, B. and Oude Elberink, S., 2004. Influences of vegetation on laser altimetry - analysis and correction approaches. *International Archives of Photogrammetry, Remote Sensing and Spatial Information Sciences*, 36(8/W2): 283-287.

Pilgrim, L.J., 1996a. Robust estimation applied to surface matching. *ISPRS Journal of Photogrammetry and Remote Sensing*, 51(5): 243-257.

Pilgrim, L.J., 1996b. Surface matching and difference detection without the aid of control points. *Survey Review*, 33(259): 291-304.

Planitz, B.M., Maeder, A.J. and Williams, J.A., 2005. The correspondence framework for 3D surface matching algorithms. *Computer Vision and Image Understanding*, 87(3): 347-383.

Point of Beginning, 2004. *3D Laser Scanning Hardware & Software Survey*, January. pp. 20-25.

Polischuk, G.M. and Revnivykh, S.G., 2004. Status and development of GLONASS. *Acta Astronautica*, 54(11-12): 949-955.

Poulton, C., 2004. *Disappearing Coasts*, Planet Earth, Summer 2004, pp. 26-27.

Press, W.H., Teukolsky, S.A., Vetterling, W.T. and Flannery, B.P., 1992. *Numerical Recipes in C: the Art of Scientific Computing*, Cambridge University Press, Cambridge, 994 p.

Prokop, A., 2006. *Determination of spatial snow depth distribution on slopes using terrestrial laser-scanner*. Geophysical Research Abstracts (EGU), 1 p.

Puglisi, G., Bonaccorso, A., Mattia, M., Aloisi, M., Bonforte, A., Campisi, O., Cantarero, M., Falzone, G., Puglisi, B. and Rossi, M., 2005. New integrated geodetic monitoring system at Stromboli volcano (Italy). *Engineering Geology*, 79(1-2): 13-31.

Pye, K. and Blott, S.J., 2006. Coastal processes and morphological change in the Dunwich-Sizewell area, Suffolk, UK. *Journal of Coastal Research*, 22(3): 453-473.

Raber, G.T., Jensen, J.R., Schill, S.R. and Schuckman, K., 2002. Creation of digital terrain models using an adaptive lidar vegetation point removal process. *Photogrammetric Engineering and Remote Sensing*, 68(12): 1307-1315.

Rawson, P.F. and Wright, J.K., 2000. Itinerary 2: Saltwick Bay to Whitby. In: Greensmith, J.T. (Ed.), *Geologists' Association Guide No. 34: The Yorkshire Coast*, third ed., Geologists' Association, 25-32.

Reshetyuk, Y., 2006. Calibration of terrestrial laser scanners Callidus 1.1, Leica HDS 3000 and Leica HDS 2500. *Survey Review*, 38(302): 703-713.

Riegl, 2006a. http://www.riegl.co.at/terrestrial_scanners/lpm-i800ha_/i800ha_all_.htm [Accessed: 26th February, 2007].

Riegl, 2006b. http://www.riegl.com/terrestrial_scanners/lpm-2k_/lpm_2k_all.htm [Accessed: 10th January, 2007].

Roberts, G.W., Brown, C. and Meng, X., 2005. Deflection monitoring of the Forth Road Bridge by GPS. *Proceedings of ION GNSS 18th International Technical Meeting of the Satellite Division*, Long Beach, USA. pp. 1016-1021.

Robinson, E., 2004. Coastal changes along the coast of Vere, Jamaica over the past two hundred years: data from maps and air photographs. *Quaternary International*, 120(1): 153-161.

Rosen, P.A., Hensley, S., Joughin, I.R., Madsen, S.N., Rodríguez, E. and Goldstein, R.M., 2000. Synthetic aperture radar interferometry. *Proceedings of the IEEE*, 88(3): 333-382.

Rosenholm, D. and Torlegård, K., 1988. Three-dimensional absolute orientation of stereo models using digital elevation models. *Photogrammetric Engineering and Remote Sensing*. 54(10): 1385-1389.

Rosin, M., Splieth, C., Hessler, M., Gärtner, M., Kordaß, B. and Kocher, T., 2002. Quantification of gingival edema using a new 3-D laser scanning method. *Journal of Clinical Periodontology*, 29(3): 240-246.

Rosser, N.J., Petley, D.N., Lim, M., Dunning, S.A. and Allison, R.J., 2005. Terrestrial laser scanning for monitoring the process of hard rock coastal cliff erosion. *Quarterly Journal of Engineering Geology and Hydrogeology*, 38(4): 363-375.

Roth, G., 1999. Registering two overlapping range images. *Proceedings of the Second International Conference on Recent Advances in 3-D Digital Imaging and Modeling (3DIM'99)*. Ottawa, Canada. pp. 191-200.

Rousseeuw, P.J. and Leroy, A.M., 1987. *Robust Regression and Outlier Detection*, John Wiley & Sons, New York, 329 p.

Rowlands, K.A., Jones, L.D. and Whitworth, M., 2003. Landslide Laser Scanning: a new look at an old problem. *Quarterly Journal of Engineering Geology and Hydrogeology*, 36(2): 155-157.

Ruckstuhl, A.F., Jacobsen, M.P., Field, R.W. and Dodd, J.A., 2001. Baseline subtraction using robust local regression estimation. *Journal of Quantitative Spectroscopy & Radiative Transfer*, 68(2): 179-193.

Ruiz, A., Kornuz, W., Talaya, J. and Colomer, J.L., 2004. Terrain modeling in an extremely steep mountain: a combination of airborne and terrestrial LiDAR. *International Archives of Photogrammetry, Remote Sensing and Spatial Information Sciences*, 35(B3): 4 p.

Runyan, K. and Griggs, G.B., 2003. The effects of armoring seacliffs on the natural sand supply to the beaches of California. *Journal of Coastal Research*, 19(2): 336-347.

Saadatseresht, M., Fraser, C.S., Samadzadegan, F. and Azizi, A., 2004. Visibility analysis in vision metrology network design. *Photogrammetric Record*, 19(107): 219-236.

Santala, J. and Joala, V., 2003. On the calibration of a ground-based laser scanner. *Proceedings of FIG Working Week 2003*, Paris, France. 7 p.

Saye, S.E., van der Wal, D., Pye, K. and Blott, S.J., 2005. Beach-dune morphological relationships and erosion/accretion: an investigation at five sites in England and Wales using LIDAR data. *Geomorphology*, 72(1-4): 128-155.

Scaioni, M., 2003. Independent model triangulation of terrestrial laser scanner data. *International Archives of Photogrammetry, Remote Sensing and Spatial Information Sciences*, 34(5/W12): 308-313.

Scaioni, M., Giussani, A., Roncoroni, F., Sgrenzaroli, M. and Vassena, G., 2004. Monitoring of geological sites by laser scanning techniques. *International Archives of Photogrammetry, Remote Sensing and Spatial Information Sciences*, 35(B7): 6 p.

Scarborough Borough Council, 2007. http://www.scarborough.gov.uk/default.aspx?page=9676 [Accessed: 25th June, 2007].

Schenk, T., 1999. *Digital Photogrammetry*, Volume 1, TerraScience, Laurelville, 428 p.

Schenk, T., 2001. Modeling and recovering systematic errors in airborne laser scanners. *Proceedings OEEPE Workshop on Airborne Laserscanning and Interferometric SAR for Detailed Digital Elevation Models*, Stockholm, Sweden. pp. 40-48.

Schenk, T. and Csathó, B., 2002. Fusion of LiDAR data and aerial imagery for a more complete surface description. *International Archives of Photogrammetry, Remote Sensing and Spatial Information Sciences*, 34(3A): 310-317.

Schenk, T., Seo, S. and Csathó, B., 2001. Accuracy study of airborne laser scanning data with photogrammetry. *International Archives of Photogrammetry, Remote Sensing and Spatial Information Sciences*, 34(3/W4): 113-118.

Schewchuk, J.R., 1996. Triangle: engineering a 2D quality mesh generator and Delaunay triangulator. *Lecture Notes in Computer Science*, 1148: 203-222.

Schiefer, E. and Gilbert, R., 2007. Reconstructing morphometric change in a proglacial landscape using historical aerial photography and automated DEM generation. *Geomorphology*, 88(1-2): 167-178.

Schiewe, J., 2000. Improving the integration of digital surface models. *International Archives of Photogrammetry, Remote Sensing and Spatial Information Sciences*, 33(B3): 807-814.

Schmid, T., Schack-Kirchner, H. and Hildebrand, E., 2004. A case study of terrestrial laser scanning in erosion research: calculation of roughness and volume balance at a logged forest site. *International Archives of Photogrammetry, Remote Sensing and Spatial Information Sciences*, 36(8/W2): 114-118.

Schneider, B., 2001. Phenomenon-based specification of the digital representation of terrain surfaces. *Transactions in GIS*, 5(1): 39-52.

Schulz, T. and Ingensand, H., 2004. Terrestrial laser scanning - investigations and applications for high precision scanning. *Proceedings of FIG Working Week*, Athens, Greece. 14 p.

Sequeira, V., Ng, K., Wolfart, E., Gonçalves, J.G.M. and Hogg, D., 1999. Automated reconstruction of 3D models from real environments. *ISPRS Journal of Photogrammetry and Remote Sensing*, 54(1): 1-22.

Seymour, R., Guza, R.T., O'Reilly, W. and Elgar, S., 2005. Rapid erosion of a small southern California beach fill. *Coastal Engineering*, 52: 151-158.

Sgrenzaroli, M., 2005. Cultural heritage 3D reconstruction using high resolution laser scanner: new frontiers data processing. *International Archives of Photogrammetry, Remote Sensing and Spatial Information Sciences,* 36(5/C34): 6 p.

Shearer, J.W., 1990. The accuracy of digital terrain models. In: Petrie, G., Kennie, T.J.M. (Eds.), *Terrain Modelling in Surveying and Civil Engineering*, Whittles, Latheronwheel, pp. 315-336.

Shi, W.Z., Li, Q.Q. and Zhu, C.Q., 2005. Estimating the propagation error of DEM from higher-order interpolation algorithms. *International Journal of Remote Sensing*, 26(14): 3069-3084.

Shrestha, R.L., Carter, W.E., Sartori, M., Luzum, B.J. and Slatton, K.C., 2005. Airborne laser swath mapping: quantifying changes in sandy beaches over time scales of weeks to years. *ISPRS Journal of Photogrammetry and Remote Sensing*, 59(4): 222-232.

Sidle, R.C., Ziegler, A.D., Negishi, J.N., Nik, A.R., Siew, R. and Turkelboom, F., 2006. Erosion processes in steep terrain - truths, myths, and uncertainties related to forest management in Southeast Asia. *Forest Ecology and Management*, 224(1-2): 199-225.

Sithole, G., 2005. *Segmentation and Classification of Airborne Laser Scanner Data*, 59, Netherlands Geodetic Commission, Delft, 184 p.

Sithole, G. and Vosselman, G., 2003. Comparison of filtering algorithms. *International Archives of Photogrammetry, Remote Sensing and Spatial Information Sciences*, 34(3/W13): 8 p.

Skaloud, J. and Lichti, D., 2006. Rigorous approach to bore-sight self-calibration in airborne laser scanning. *ISPRS Journal of Photogrammetry and Remote Sensing*, 61(1): 47-59.

Skidmore, A.K., 1989. A comparison of techniques for calculating gradient and aspect from a gridded digital elevation model. *International Journal of Geographical Information Systems*, 3(4): 323-334.

Smith, M.J. and Waldram, D.A., 1996. Automated digital terrain modelling of coastal zones. *International Archives of Photogrammetry, Remote Sensing and Spatial Information Sciences*, 31(B4): 919-924.

Smith, S.L., Holland, D.A. and Longley, P.A., 2003. Investigating the spatial structure of error in digital surface models derived from laser scanning data. *International Archives of Photogrammetry, Remote Sensing and Spatial Information Sciences*, 34(3/W13): 7 p.

Stylianidis, E., Patias, P., Tsioukas, V., Sechidis, L. and Georgiadis, C., 2003. A digital close-range photogrammetric technique for monitoring slope displacements. *Proceedings of 11th International FIG Symposium on Deformation Measurements*, Santorini Island, Greece. 6 p.

Su, J. and Bork, E., 2006. Influence of vegetation, slope, and LiDAR sampling angle on DEM accuracy. *Photogrammetric Engineering and Remote Sensing*, 72(11): 1265-1274.

Su, Y.Y., Hashash, Y.M.A. and Liu, L.Y., 2006. Integration of construction as-built data via laser scanning with geotechnical monitoring of urban excavation. *Journal of Construction Engineering and Management*, 132(12): 1234-1241.

Sunamura, T., 1992. *Geomorphology of rocky coasts*, John Wiley &Sons, Chichester, 302 p.

Symonds Group, 1998. http://www.symonds-group.com/uploaded_files/documents/61_1450_11.pdf [Accessed: 28th January, 2004].

Takagi, M., Asano, H. and Kikuchi, Y., 2002. Optimum spatial resolution of digital elevation model for topographic analysis. *International Archives of Photogrammetry, Remote Sensing and Spatial Information Sciences*, 34(4): 5 p.

Takase, Y., Sasaki, Y., Nakagawa, M., Shimizu, M., Yamada, O., Izumi, T. and Shibasaki. R., 2003. Reconstruction with laser scanning and 3D visualisation of Roman monuments in Tyre, Lebanon. *International Archives of Photogrammetry, Remote Sensing and Spatial Information Sciences*, 34(5/W12): 325-329.

Talaya, J., Alamus, R., Bosch, E., Serra, A., Kornus, W. and Baron, A., 2004. Integration of a terrestrial laser scanner with GPS/IMU orientation sensors. *International Archives of Photogrammetry, Remote Sensing and Spatial Information Sciences*, 35(B5): 6 p.

Tao, C.V., Chapman, M.A. and Chaplin, B.A., 2001. Automated processing of mobile mapping image sequences. *ISPRS Journal of Photogrammetry and Remote Sensing*, 55(5-6): 330-346.

Tao, C.V. and Hu, Y., 2002. Assessment of airborne LiDAR and imaging technology for pipeline mapping and safety applications. *International Archives of Photogrammetry, Remote Sensing and Spatial Information Sciences*, 34(1): 11 p.

Tarchi, D., Casagli, N., Fanti, R., Leva, D.D., Luzi, G., Pasuto, A., Pieraccini, M. and Silvano, S., 2003. Landslide monitoring by using ground-based SAR interferometry: an example of application to the Tessina landslide in Italy. *Engineering Geology*, 68(1-2): 15-30.

Thiel, K.-H. and Wehr, A., 2004. Performance capabilities of laser scanners - an overview and measurement principle analysis. *International Archives of Photogrammetry, Remote Sensing and Spatial Information Sciences*, 36(8/W2): 5 p.

Thieler, E.R. and Danforth, W.W., 1994a. Historical shoreline mapping (I): Improving techniques and reducing positioning errors. *Journal of Coastal Research*, 10(3): 549-563.

Thieler, E.R. and Danforth, W.W., 1994b. Historical shoreline mapping (II): application of the Digital Shoreline Mapping and Analysis Systems (DSMS/DSAS) to Shoreline Change Mapping in Peurto Rico. *Journal of Coastal Research*, 10(3): 600-620.

Thoma, D.P., Gupta, S.C., Bauer, M.E. and Kirchoff, C.E., 2005. Airborne laser scanning for riverbank erosion assessment. *Remote Sensing of Environment*, 95(4): 493-501.

Torlegård, K., Östman, A. and Lindgren, R., 1986. A comparative test of photogrammetrically sampled digital elevation models. *Photogrammetria*, 41(1): 1-16.

Tralli, D.M., Blom, R.G., Zlotnicki, V., Donnellan, A. and Evans, D.L., 2005. Satellite remote sensing of earthquake, volcano, flood, landslide and coastal inundation hazards. *ISPRS Journal of Photogrammetry and Remote Sensing*, 59(4): 185-198.

Trautenberg, H.L., Weber, T. and Schäfer, C., 2004. GALILEO system overview. *Acta Astronautica*, 55(3-9): 643-647.

Tucker, C., 2002. Testing and verification of the accuracy of 3D laser scanning data. *International Archives of Photogrammetry, Remote Sensing and Spatial Information Sciences*, 34(4): 6 p.

Ullrich, A., Schwarz, R. and Kager, H., 2003. Using hybrid multi-station adjustment for an integrated camera laser scanner system. *Civil Engineering Surveyor*, October 2003: 20-24.

Uren, J. and Price, W.F., 2006. *Surveying for engineers*, fourth ed. Palgrave MacMillan, Basingstoke, 824 p.

USGS, 2004. *Fact Sheet 2004-3072: Landslide Types and Processes*, USGS, 4 p.

Viles, H. and Spencer, T., 1995. *Coastal Problems - geomorphology, ecology and society at the coast*, Arnold, London, 350 p.

von Hansen, W., 2006. Robust automatic marker-free registration of terrestrial scan data. *International Archives of Photogrammetry, Remote Sensing and Spatial Information Sciences*, 36(3): 6 p.

Vosselman, G., 2002. On the estimation of planimetric offsets in laser altimetry data. *International Archives of Photogrammetry, Remote Sensing and Spatial Information Sciences*, 34(3A): 375-380.

Vosselman, G. and Maas, H.-G., 2001. Adjustment and filtering of raw laser altimetry data. *Proceedings of OEEPE Workshop on Airborne Laserscanning and Interferometric SAR for Detailed Digital Elevation Models*, Stockholm, Sweden. 11 p.

Wager, T.D., Keller, M.C., Lacey, S.C. and Jonides, J., 2005. Increased sensitivity in neuroimaging analyses using robust regression. *NeuroImage*, 26(1): 99-113.

Walstra, J., 2006. *Historical aerial photographs and digital photogrammetry for landslide assessment*. PhD Thesis, Loughborough University, Loughborough, 226 p.

Warneke, B., Last, M., Liebowitz, B. and Pister, K., 2001. Smart Dust: communicating with a cubic-millimeter computer. *Computer*, 34(1): 55-51.

Watt, P.J. and Donoghue, D.N.M., 2005. Measuring forest structure with terrestrial laser scanning. *International Journal of Remote Sensing*, 26(7): 1437-1446.

Wehr, A. and Lohr, U., 1999. Airborne laser scanning - an introduction and overview. *ISPRS Journal of Photogrammetry and Remote Sensing*, 54(2-3): 68-82.

White, K. and El Asmar, H.M., 1999. Monitoring changing position of coastlines using Thematic Mapper imagery, an example from the Nile Delta. *Geomorphology*, 29(1): 93-105.

Wise, S.M., 1998. The effect of GIS interpolation errors on the use of digital elevation models in geomorphology. In: Lane, S.N., Richards, K.S., Chandler, J.H. (Eds.), *Landform Monitoring, Modelling and Analysis*, John Wiley & Sons, Chichester, pp. 139-164.

Wolf, P.R. and Dewitt, B.A., 2000. *Elements of Photogrammetry with Applications in GIS*, third ed. McGraw-Hill, New York, 608 p.

Wolf, P.R. and Ghilani, C.D., 1997. *Adjustment Computations: Statistics and Least Squares in Surveying and GIS*, John Wiley & Sons, New York, 564 p.

World Bank, 1996. *Guidelines for Integrated Coastal Zone Management*, World Bank, Washington D.C., 16 p.

Wozencraft, J.M. and Lillycrop, W.J., 2002. Total shallow-water survey through airborne hydrography. *Proceedings of Oceanology International*, London, UK. 9 p.

Wright, J.K., 2000. Itinerary 8: Filey Brigg. In: Greensmith, J.T. (Ed.), *Geologists' Association Guide No.34: The Yorkshire Coast*, third ed., Geologists' Association, pp. 82-88.

Wunderlich, T.A., 2003. Terrestrial laser scanners - an important step towards construction information. *Proceedings of FIG Working Week 2003*, Paris, France. 11 p.

Würländer, R., Eder, K. and Geist, T., 2004. High quality DEMs for glacier monitoring - image matching versus laser scanning. *International Archives of Photogrammetry, Remote Sensing and Spatial Information Sciences*, 35(B7): 753-758.

Xu, C., Wang, H., Ge, L., Yonezawa, C. and Cheng, P., 2006. InSAR tropospheric delay mitigation by GPS observations: a case study in Tokyo area. *Journal of Atmospheric and Solar-Terrestrial Physics*, 68(6): 629-638.

Xu, Z. and Li, Z., 2000. Least median of squares matching for automated detection of surface differences. *International Archives of Photogrammetry, Remote Sensing and Spatial Information Sciences*, 33(B3/2): 1003-1007.

Zhang, D. and Hebert, M., 1999. Harmonic maps and their applications in surface matching. *Proceedings of IEEE Conference on Computer Vision and Pattern Recognition (CVPR'99)*, IEEE. Fort Collins, USA. pp. 524-530.

Zhao, H. and Shibasaki, R., 2001. A robust method for registering ground-based laser range images of urban outdoor objects. *Photogrammetric Engineering and Remote Sensing*, 67(10): 1143-1153.

Zhou, G., Song, C., Simmers, J. and Cheng, P., 2004. Urban 3D GIS from LiDAR and digital aerial images. *Computers and Geosciences*, 30(4): 345-353.

Zhu, C.Q., Shi, W.Z., Li, Q.Q., Wang, G.X., Cheung, T.C.K., Dai, E.F. and Shea, G.Y.K., 2005. Estimation of average DEM accuracy under linear interpolation considering random error at the nodes of TIN model. *International Journal of Remote Sensing*, 26(24): 5509-5523.